U.PORTO

FEUP FACULDADE DE ENGENHARIA
UNIVERSIDADE DO PORTO

Performance-based design of self-compacting concrete (SCC): a contribution to enchance SCC mixtures robustness

Sandra Conceição Barbosa Nunes

Dissertação apresentada à Faculdade de Engenharia da Universidade do Porto
para obtenção do grau de Doutor em Engenharia Civil

Outubro 2008

Orientador:

Doutor Joaquim Azevedo Figueiras

Co-orientadora:

Doutora Maria Joana Álvares Ribeiro de Sousa Coutinho

Membros do Júri:

Presidente

Doutor José Manuel Pinto Ferreira Lemos (por delegação Reitoral)

Vogais

Doutor Joost Walraven, Professor da Universidade Técnica de Delft, Países Baixos;

Doutor António Carlos Bettencourt Simões Ribeiro, Investigador Principal, Laboratório Nacional de Engenharia Civil;

Doutora Paula Manuela Lemos Pereira Milheiro de Oliveira, Professora Associada da Faculdade de Engenharia da Universidade do Porto;

Doutora Maria Joana Álvares Ribeiro de Sousa Coutinho, Professora Auxiliar da Faculdade de Engenharia da Universidade do Porto;

Doutor Joaquim Azevedo Figueiras, Professor Catedrático da Faculdade de Engenharia da Universidade do Porto.

Relatores (para a atribuição do Título de Doutoramento Europeu):

Doutor Joost Walraven, Professor da Universidade Técnica de Delft, Países Baixos;

Doutor Luís Agulló Fitté, Professor da Universidade Politécnica da Catalunha, Barcelona.

Tell me, and I forget.

Teach me, and I may remember.

Involve me, and I learn.

Abstract

Self-compacting concrete (SCC) can be distinguished by its ability to fill the form and consolidate under its own weight without any compaction energy. Placing SCC has minimal dependence on available workmanship on site; therefore, it has great potential to improve true quality of concrete in the final structure and to extend service life of modern structures. One of the main obstacles for a wider use of SCC is its sensitivity to small variations of the ingoing materials, mix-proportions and other external factors.

Many approaches to design SCC proceed by trial and error, using conventional single factor experiments, which can mask true effects on the response of concrete, such as interaction effects. A better approach to dealing with several factors is to conduct a factorial experiment. This is an experimental strategy in which factors are varied together, instead of one at a time. In the present work, a Central Composite Design was carried out to derive numerical models, relating mixture parameters to key properties of the cementitious materials (paste, mortar and concrete). These models were used to design and optimize mixtures and to simulate the effect of changes in mixture parameters.

This thesis provides scientific design tools to obtain optimized and more robust SCC mixtures. Interaction diagrams are suggested to represent the range of mortar mixture parameters where deformability and viscosity, adequate for SCC, coexist in a balanced manner. Six different types of cement were assessed in combination with limestone filler and a polycarboxylate type superplasticizer. The utility of interaction diagrams for quality control, tailor-made concrete mixtures and selection of constituent materials is highlighted. In addition, the target paste properties for different fine aggregate contents, were defined in terms of both empirical test results and rheological parameters, linking mortar and paste properties adequate for SCC.

A new methodology to compute a robustness measure based on data of typical materials weight deviations inherent of the production process at a specific production centre, is suggested. By applying this methodology it was found that it is possible to enhance robustness of SCC mixtures by only changing proportions of materials in the mixture. Minimizing superplasticizer dosage was found to be the most effective optimization criterion to enhance robustness of SCC mixtures. A more robust SCC enables the concrete supplier to provide better consistency in delivering SCC, reduces the need to

test and/or to adjust each batch, minimizes extra costs concerning quality control and contributes to a successful implementation of SCC at the production centre.

Resumo

O betão auto-compactável (BAC) distingue-se pela sua capacidade de preencher os espaços no interior da cofragem e consolidar apenas à custa do peso próprio, eliminando a necessidade de vibração. A colocação do BAC é menos dependente da qualidade da mão-de-obra, logo este material possui um enorme potencial para melhorar a qualidade final do betão na estrutura e prolongar o período de vida útil das estruturas modernas. Um dos maiores entraves a uma utilização mais generalizada do BAC é a sua sensibilidade a pequenas variações nas características dos materiais constituintes, nas proporções da mistura e noutros factores externos.

A maioria das abordagens no dimensionamento das composições do BAC adoptam um procedimento por tentativa-erro, com a introdução de variações num parâmetro de cada vez, o que não permite avaliar alguns efeitos significativos para a resposta, como é o caso dos efeitos de interacção. Uma abordagem mais correcta, quando estão envolvidos vários parâmetros, consiste em conduzir as experiências segundo um plano factorial. Neste procedimento experimental são introduzidas variações nos diversos parâmetros, simultaneamente, e não apenas em um de cada vez. No presente trabalho, o programa experimental foi desenvolvido segundo um Plano Factorial Aumentado que permitiu obter modelos numéricos para descrever as propriedades relevantes da pasta, argamassa e betão, em função dos parâmetros da mistura. Os modelos numéricos serviram para ajustar e optimizar as misturas e simular o efeito de variações nos parâmetros da mistura.

Esta dissertação apresenta ferramentas científicas para o dimensionamento de composições de betão tendo como objectivo final a optimização e o aumento da robustez do BAC. A gama de valores dos parâmetros da argamassa onde é possível encontrar um balanço entre deformabilidade e viscosidade adequado ao BAC foi definida e apresentada sob a forma de diagramas de interacção para seis tipos distintos de cimento. Estes cimentos foram estudados em combinação com fíler calcário e um superplastificante à base de policarboxilatos. Neste trabalho evidencia-se a utilidade destes diagramas de interacção para o controle de qualidade do BAC, a concepção de betões dimensionados à medida dos critérios de desempenho e para a selecção dos materiais constituintes. Para além disto, definiram-se as propriedades da pasta (com base em resultados de ensaios empíricos e ensaios reológicos) que conduzem a argamassas adequadas para um BAC, para diferentes conteúdos em agregado fino, estabelecendo assim a ligação entre as pro-

priedades que devem ser alcançadas ao nível da argamassa e da pasta destinadas ao BAC.

No âmbito do presente programa de doutoramento foi desenvolvida uma metodologia para a quantificação da robustez das composições de BAC, atendendo às condições específicas existentes no centro de produção do betão. Aplicando esta metodologia a diversas misturas demonstrou-se que a robustez pode ser melhorada através da selecção criteriosa das proporções na mistura. Nas condições do estudo aqui apresentado, o critério de optimização mais eficaz para o aumento da robustez consistiu em minimizar a dosagem de superplastificante. A utilização de composições robustas reduz o número de ensaios/ajustes por ciclo de produção e minimiza os custos extra com o controle de qualidade, contribuindo assim para o sucesso da implementação do BAC nos centros de produção existentes.

Résumé

Le béton autoplaçant (BAP) se distingue par sa capacité de remplir les espaces à l'intérieur du coffrage et durcir seulement par effet gravitaire, permettant ainsi d'éliminer la vibration. Puisque la mise en place du BAP est moins dépendante de la qualité de la main d'œuvre, ce matériel a un énorme potentiel pour améliorer la qualité finale du béton des structures et pour prolonger la vie utile des structures modernes. La sensibilité du BAP aux petites variations des caractéristiques des matériaux, des proportions des compositions ou à d'autres facteurs externes est un des plus grands inconvénients à son utilisation généralisée.

La plupart des abordages de formulation des compositions de BAP adoptent un processus d'essai-et-erreur, considérant l'introduction de petites variations d'un paramètre à la fois, ce qui ne permet pas d'évaluer certains effets importants sur la réponse, comme par exemple les effets d'interaction. Quand plusieurs paramètres sont en jeu, un abordage plus correct consiste à réaliser des expériences suivant un plan factoriel. Dans ce processus expérimental les variations des différents paramètres sont introduites simultanément et non considérant un paramètre à la fois. Dan le travail présenté, le programme expérimental a été développé suivant un plan factoriel augmenté, ce qui a permit d'obtenir des modèles numériques pour d'écrire les propriétés appropriés de la pâte, du mortier et du béton, en fonction des paramètres de la composition. Les modèles numériques ont été utilisés pour ajuster et optimiser les compositions et pour simuler l'effet de la variation des paramètres de la compositions.

Cette dissertation présente des outils scientifiques pour la formulation de compositions de béton ayant comme objectif final l'optimisation et l'augmentation de la robustesse du BAP. La gamme de valeurs des paramètres du mortier pour laquelle il est possible de trouver un équilibre entre la déformabilité et la viscosité adéquat pour le BAP a été définit et présentée par des diagrammes d'interaction adressant six différents types de ciment. Ces ciments ont été étudiés considérant leur combinaison avec du filler calcaire et un superplastifiant de type polycarboxylate. Ce travail souligne l'utilisation des diagrammes d'interaction pour contrôler la qualité du BAP, pour la conception de bétons formulés pour des critères de performances spécifiés sur mesure et pour la sélection des matériaux constituants. En outre, les propriétés de la pâte qui conduisent à des mortiers adéquats pour le BAP ont été définies (a partir de résultats obtenus d'essais empiriques

et d'essais rhéologiques), considérant différentes quantités de granulats fins. Ainsi, une liaison a été établie entre les propriétés qui doivent être obtenues pour la pâte et le mortier du BAP.

Dans le cadre du programme de doctorat ici présenté, un processus pour quantifier la robustesse des compositions de BAP a été développé, considérant les conditions spécifiques existantes au centre de production du béton. En appliquant ce processus à différentes compositions, il a été démontré que la robustesse peut être améliorée par la sélection soignée des proportions de la formulation. Dans les conditions de l'étude ici présentée, le critère d'optimisation le plus efficace pour élever le niveau de robustesse consiste à minimiser le dosage de superplastifiant. L'utilisation de compositions robustes réduit le nombre d'essais et d'ajustements par cycle de production et minimise les surplus de coûts associés au contrôle de qualité, soutenant de cette forme, le succès de l'implémentation du BAP dans les centres de production existants.

Acknowledgments

First of all, I would like to thank my supervisor Professor Joaquim Figueiras for giving me the opportunity to work on this innovative subject, for his support, for the fruitful discussions and valuable comments, as well as giving me the space to develop both my ideas and myself. I also would like to thank my co-supervisor Professor Joana Sousa Coutinho for her commitment to this research work and constant encouragement, support and friendship throughout the years. I am deeply indebted to Professor Paula Milheiro for sharing her profound knowledge in Statistics and research skills, which significantly contributed to the outcome of this work and, also, for the time and effort put into reading this thesis.

The research described in this thesis was conducted within the Laboratory for the Concrete Technology and Structural Behaviour of the Faculty of Civil Engineering of the University of Porto (LABEST/FEUP). This research was financed partially by AdI – Inovation Agency in the scope of a Portuguese research project "BACPOR" in direct co-operation with local industry, namely, Mota-Engil Engenharia, Sika and Maprel; and by FCT – Portuguese Foundation for Science and Technology under the scope of POCTI/ECM/61649/2004 research project. This research was also supported by FCT Research Grant SFRH/BD/25552/2005. Furthermore, the financial support of the Foundation Calouste de Gulbenkian and Foundation Luso-Americana to attend conferences; and the financial support of the Nuffic-Huygens Scholarship Programme (The Netherlands) is gratefully acknowledged. Collaboration and the supplying of materials by Mota-Engil Engenharia, Maprel, Cimpor, Sika and Comital is also gratefully acknowledged.

This work would not have been possible without the support of partners from industry, namely, Engineer Anibal Leite, Engineer António Rêgo Araújo and Engineer Raquel Magalhães (from Mota-Engil Engenharia), Engineer José David, Nídia Dias and Luís Guimarães (from Sika), António Mesquita, Engineer Catarina Coelho and Engineer João Pereira (from Cimpor) and Paulo Pinto (from Comital). I would like to thank the technical staff of LABEST/FEUP and the Department of Civil Engineering, especially, Paula Silva, Cecília Silva, Amândio Pinto, Claúdia Correia, Alberto Monteiro, Maria Vitória Freitas, Marta Poínhas Costa, Maria Teresa Pinto, Fernando Hora. Besides, I would like to thank all of my colleagues at LABEST/FEUP for the good work envi-

ronment, help with experiments and fruitful discussions, especially to Helena Figueiras, Ana Maria Proença, Carlos Félix, Américo Dimande, Helder Sousa, Miguel Azenha and Lino Maia. I am also very grateful for the collaboration and discussions with Professor José Carlos Lopes, Engineer Ricardo Santos and Engineer Rui Soares, which provided me with useful insights into rheology of cement suspensions; and with Professor José Inácio Martins and Engineer Sara Ferreira concerning the dispersing admixtures's mode of action . I am very grateful to all of my colleagues from Structures Section, for exempting me from lectures during a three years period so I could carry out this research work) and, in particular, the support given by the successive directors of the Structures Section, namely, Professor Álvaro Cunha, Professor Aníbal Costa, Professor Rui Faria and Professor António Adão da Fonseca. My appreciation goes to Professor Manuel Matos Fernandes and Professor Raimundo Delgado for the encouraging words throughout the years and many recommendation letters. I which to express greatest thanks to Cristina Costa, Xavier Romão, Filipe Magalhães and Miguel Castro who shared their views with me and whose advices and remarks contributed significantly to obtain the final result of this thesis.

I would like to thank Professor Joost Walraven for giving me the excellent opportunity to stay at the Delft University of Technology (TUDelft) in The Netherlands, and to work in the research project "Viscosity agents in SCC" as a member of his group, during a period of 4 months. Also, I would like to thank Engineer Steffen Grünewald for the conveying of knowledge, bibliography on SCC, interesting discussions and friendship. I address a sincere thanks to all colleagues at Department of Structural and Building Engineering of TUDelft, who also contributed for a pleasing stay in Delft.

Last but not least, I have to thank my parents and my sister for their endless love and support during all these years. I also would like to express my sincere gratitude to all my friends for their patience, constant help and encouragement.

Contents

List of Tables **xix**

List of Figures **xxv**

Notations and symbols **xxxv**

1. Introduction **1**

1.1. Scope of the research 1
1.2. Research objectives 4
1.3. Research strategy and outline of the thesis 5

2. Rheology of cement suspensions **9**

2.1. Introduction 9
2.2. Rheology 9
2.2.1. Introduction 9
2.2.2. Flow curve types 11
2.2.3. Rheological models 16
2.3. Rheological characterization 19
2.3.1. Measurement instruments 19
2.3.2. Rotational rheometers 20
2.3.3. Testing techniques 25
2.3.4. Measuring sequence setup 30
2.4. Fresh concrete, mortar and cement paste as particle suspensions 32
2.4.1. Factors influencing the rheology of suspensions 33
2.5. Concrete rheometeres 36
2.6. Rheology of SCC 37
2.6.1. Target area (Bingham parameters) 37
2.6.2. Thixotropy 38
2.6.3. Computational model of concrete flow 40

3. Cement-superplasticizer interactions **43**

3.1. Introduction 43
3.2. Portland cement hydration 43

3.2.1. Initial hydration (0-15 min) . . . 45
3.2.2. Dormant period (15 min-4 h) . . . 46
3.2.3. Acceleration period (4-8 h) . . . 46
3.2.4. Deceleration period (8-24 h) . . . 47
3.3. Physical interactions . . . 47
3.3.1. Derjaguin–Landau Verway–Overbeek (DLVO) theory . . . 47
3.3.2. Molecular structure of superplasticizers and mode of action . . . 49
3.4. Chemical interactions . . . 55
3.4.1. Preferential adsorption of Sp on specific surface sites (the role of ettringite) . . . 55
3.4.2. Polymer adsorption and absorption . . . 57
3.4.3. Influence of adding time . . . 58
3.4.4. The role of sulfate and alkalis . . . 59
3.4.5. Fluidity loss with time and influence of temperature . . . 61
3.4.6. Influence on hydration rate and hydration products . . . 62
3.5. Incorporation of viscosity agents . . . 62
3.6. Molecular structure of PC type superplasticizers . . . 65

4. SCC mix-design and properties 69
4.1. Introduction . . . 69
4.2. Fresh properties and empirical tests . . . 69
4.2.1. SCC fresh properties . . . 69
4.2.2. Standard (empirical) test methods . . . 70
4.2.3. Specifications for SCC . . . 76
4.3. Mix-design methods . . . 77
4.4. SCC mix-proportions . . . 79
4.4.1. Aggregates . . . 80
4.4.2. Paste volume . . . 80
4.4.3. Paste composition . . . 81
4.4.4. Typical values for SCC mix-proportions . . . 82
4.5. Hardened properties . . . 84
4.5.1. SCC .vs. conventional concrete . . . 84
4.5.2. Tailor-made SCC . . . 87
4.5.3. Concluding remarks . . . 89
4.6. Japanese SCC-designing method . . . 89
4.6.1. Mix-proportioning system . . . 89
4.6.2. Paste and mortar tests . . . 90
4.6.3. Concrete tests . . . 92
4.6.4. Modifications to this method . . . 92

4.6.5. Universal mixtures formulation . . . 93
4.7. Statistical design approach . . . 96
4.7.1. Introduction . . . 96
4.7.2. Experimental design, design factors and response variables . . . 96
4.7.3. Performing the experiments . . . 99
4.7.4. Statistical analysis of data . . . 100
4.7.5. Mixtures optimisation . . . 106
4.7.6. Comments on this approach . . . 107

5. Optimization of SCC mortar mixtures 109
5.1. Introduction . . . 109
5.2. Experimental programme . . . 109
5.2.1. Materials characterization . . . 109
5.2.2. Experimental plan . . . 110
5.2.3. Mixing sequence and testing methods . . . 112
5.3. Collected data, fitted models and mixtures optimization . . . 112
5.3.1. CEM I 42,5 R . . . 115
5.3.2. CEM I 52,5 R . . . 116
5.3.3. CEM II/A-L 42,5 R . . . 121
5.3.4. CEM II/B-L 32,5 N . . . 125
5.3.5. CEM IV/B (V) 32,5 N . . . 130
5.3.6. CEM II/B-L 32,5 R (BR) . . . 133
5.4. Discussion of results . . . 136
5.4.1. Main effects . . . 136
5.4.2. Interaction diagrams and number of optimized solutions . . . 138
5.4.3. Influence of cement type on mix proportions of SCC mortars . . . 139
5.4.4. Quality control . . . 141
5.4.5. Predicting capability of the models . . . 143
5.4.6. Cement/superplasticizer combination . . . 143
5.5. Concluding remarks . . . 145

6. Influence of cement variations on SCC mortar/paste properties 149
6.1. Introduction . . . 149
6.2. Cement production quality control . . . 149
6.2.1. Importance of cement variations for SCC robustness . . . 149
6.2.2. Control of cement properties . . . 151
6.2.3. Influence of cement parameters on concrete properties of mixtures without admixtures . . . 152
6.2.4. Influence of cement parameters on the properties of mixtures including a superplasticizer (polycarboxylate type) . . . 156

6.3. Experimental programme . . . 158
6.3.1. Materials characterization and mix proportions . . . 158
6.3.2. Mixing sequence and testing sequence . . . 158
6.3.3. Mortar test methods . . . 160
6.3.4. Paste test methods . . . 160
6.3.5. SCC-mortar properties variation with cement delivery . . . 164
6.3.6. SCC-paste properties variation with cement delivery . . . 165
6.3.7. Correlations . . . 168
6.4. SCC paste rheology . . . 176
6.4.1. Experimental programme . . . 177
6.4.2. Rheology vs. empirical test results . . . 177
6.4.3. Comparison of paste and mortar characteristics . . . 182
6.4.4. Comparison of paste and concrete characteristics . . . 186
6.5. Final remarks . . . 188

7. Evaluation of SCC mixtures robustness 191
7.1. Introduction . . . 191
7.2. Robustness definition . . . 191
7.3. Factors affecting properties during production . . . 193
7.3.1. Variability of constituent materials . . . 193
7.3.2. Inaccuracy in weighing of materials . . . 194
7.3.3. Mixing energy . . . 194
7.4. Strategies to increase SCC mixtures robustness . . . 195
7.4.1. Materials selection and mix-proportioning . . . 196
7.4.2. Quality control . . . 197
7.5. Robustness evaluation methods . . . 198
7.6. LABEST/FEUP robustness evaluation method . . . 198
7.6.1. Experimental programme . . . 199
7.6.2. Response models . . . 202
7.6.3. Robustness measure . . . 207
7.6.4. Comments on this method . . . 211
7.7. Application of LABEST/FEUP methodology to optimize SCC mixtures . 211
7.7.1. Experimental programme . . . 211
7.7.2. Response models . . . 214
7.7.3. Mixtures optimization . . . 217
7.8. Concluding remarks . . . 229

8. Conclusions and future perspectives 231
8.1. Conclusions . . . 231
8.2. Future perspectives . . . 234

Bibliography **237**

A. Paper:"Full-scale testing with SCC in Portugal" **253**

B. Characterization of SCC mixtures (POCI/ECM/61649/2004) **261**

B.1. Introduction 261
B.2. Materials characterization 261
B.3. Mixing sequence, mix proportions and test results 261
B.4. Robustness 263
B.5. Cost of materials by m^3 265
B.6. Mechanical properties 265
B.7. Temperature evolution, drying shrinkage and creep deformations 268
B.8. Transport properties 274

C. Fine materials characterization **279**

D. Analysis of Dflow model from paragraph 5.3.1 **291**

D.1. ANOVA tests 291
D.2. Model adequacy checking 291

E. Mix proportions and test results **301**

List of Tables

2.1. Typical values of viscosity for different materials and typical shear rate associated to different industrial processes (Chhabra and Richardson, 1999; Esping, 2007) . . . 11
2.2. Comparison of different measuring tools (Bohlin Instruments Ltd., 2004) 22

3.1. Main phases of Portland cement and their characteristics (Griesser, 2002; Jolicoeur and Simard, 1998; Moir, 2003) . . . 44
3.2. Types of VA and mode of action (Nawa et al., 1998; Phyfferoen and Lockwood, 1998) . . . 64
3.3. Summary of the effect of chemical structure parameters on the performance of superplasticizer . . . 68

4.1. Standardised test methods, assessed fresh property and consistency classes (ACM Centre, 2005) . . . 71
4.2. Mix proportions and test results of SCC mixtures developed within POCI/ECM/61649/2004 research project . . . 87
4.3. Hardening and hardened properties of SCC mixtures developed within POCI/ECM/61649/2004 research project . . . 88
4.4. β_p and E_p results for single powders and mixtures of powders . . . 91
4.5. Summary of selected statistical designs . . . 100
4.6. Analysis of variance test in multiple regression (Montgomery, 2001) . . . 104

5.1. Coded values for the variables used in the experimental design . . . 111
5.2. Values a_0 and Δa used in the transformation of coded values into absolute values of the variables in each experimental plan . . . 113
5.3. Correspondence between coded values and absolute variable values in each experimental plan . . . 113
5.4. Optimization constraints . . . 115
5.5. Statistics of the results for the total points and for central points (CEM I 42,5 R) . . . 116
5.6. Fitted numerical models for coded variables (CEM I 42,5 R) . . . 117
5.7. Statistics of the results for the total points and for central points (CEM I 52,5 R) . . . 120

5.8. Fitted numerical models for coded variables (CEM I 52,5 R) 120
5.9. Statistics of the results for the total points and for central points (CEM II/A-L 42,5 R) 123
5.10. Fitted numerical models for coded variables (CEM II/A-L 42,5 R) 124
5.11. Statistics of the results for the total points and for central points (CEM II/B-L 32,5 N) 127
5.12. Fitted numerical models for coded variables (CEM II/B-L 32,5 N) 128
5.13. Statistics of the results for the total points and for central points (CEM IV/B(V) 32,5 N) 131
5.14. Fitted numerical models for coded variables (CEM IV/B(V) 32,5 N) . . . 132
5.15. Statistics of the results for the total points and for central points (CEM II/B-L 32,5 R (BR)) 134
5.16. Fitted numerical models for coded variables (CEM II/B-L 32,5 R (BR)) . 135

6.1. Requirements for cements defined by NP EN 197-1 (Portugal. IPQ, 2001) 153
6.2. Optimized mixture parameters and mix proportions 159
6.3. Correlation matrix within cement characteristics and between cement characteristics and SCC mortar/paste test results, corresponding to CEM I 52,5 R 171
6.4. Correlation matrix within cement characteristics and between cement characteristics and SCC mortar/paste test results, corresponding to CEM I 42,5 R 172
6.5. Correlation matrix within cement characteristics and between cement characteristics and SCC mortar/paste test results, corresponding to CEM II/A-L 42,5 R 173
6.6. Correlation matrix within cement characteristics and between cement characteristics and SCC mortar/paste test results, corresponding to CEM II/B-L 32,5 N 174
6.7. Optimized mixture parameters and mix-proportions 178
6.8. Pastes selected for the study at the concrete level 187

7.1. Grading of aggregates (BACPOR, Maprel, Rio Maior) 199
7.2. Coded values for the factors used in the experimental design 200
7.3. Correspondence between coded values and actual parameter values . . . 201
7.4. Fitted numerical models (coded variables) 202
7.5. Coded values and test results from a previous study 203
7.6. Statistics of the results for the central points 203
7.7. Descriptive statistics of bootstrap samples 210
7.8. Grading of aggregates (POCI/ECM/61649/2004) 212
7.9. Coded values for the factors used in the experimental design 213

7.10. Correspondence between coded values and actual parameter values . . . 214
7.11. Fitted numerical models (coded values of variables) 215
7.12. Statistics of the results for the central points 216
7.13. Optimization constraints 220
7.14. SCC mix proportions, estimated test results for the target and changed mixtures (±5 and 10 l/m^3 of water) and computed robustness measures, for the mixtures obtained with optimization criteria A 222
7.15. SCC mix proportions, estimated test results for the target and changed mixtures (±5 and 10 l/m^3 of water) and computed robustness measures, for the mixtures obtained with optimization criteria B 223
7.16. SCC mix proportions, estimated test results for the target and changed mixtures (±5 and 10 l/m^3 of water) and computed robustness measures, for the mixtures obtained with optimization criteria C 224
7.17. SCC mix proportions, estimated test results for the target and changed mixtures (±5 and 10 l/m^3 of water) and computed robustness measures, for the mixtures obtained with optimization criteria D 225
7.18. SCC mix proportions, estimated test results for the target and changed mixtures (±5 and 10 l/m^3 of water) and computed robustness measures, for the mixtures obtained with optimization criteria E 226
7.19. SCC mix proportions, estimated test results for the target and changed mixtures (±5 and 10 l/m^3 of water) and computed robustness measures, for the mixtures obtained with optimization criteria F 227
7.20. Cost of materials 228

B.1. Testing plan for each of the mixtures studied 262
B.2. Grading of aggregates (POCI/ECM/61649/2004) 262
B.3. Mix proportions and fresh test results of SCC mixtures developed within POCI/ECM/61649/2004 research project 264
B.4. Test results for the target and changed mixtures (±10 l/m^3 of water) . . 264
B.5. Estimated cost of SCC mixtures 267
B.6. Compressive strength and specific gravity results 269
B.7. Modulus of elasticity test results and estimated values (Eurocode 2) . . . 270
B.8. Tensile strength test results and estimated values (Eurocode 2) 270
B.9. Apparent diffusion coefficient (D_{ns}) results 276
B.10. S, a_0 and R^2 values for each SCC mixture 276

C.1. Chemical characterization of CEM I 52,5R (Cimpor, Alhandra), for each cement delivery 280
C.2. Physical and mechanical characterization of CEM I 52,5R (Cimpor, Alhandra), for each cement delivery 281

C.3. Chemical characterization of CEM I 42,5R (Cimpor, Alhandra), for each cement delivery . . . 282
C.4. Physical and mechanical characterization of CEM I 42,5R (Cimpor, Alhandra), for each cement delivery . . . 283
C.5. Chemical characterization of CEM II/A-L 42,5R (Cimpor, Alhandra), for each cement delivery . . . 284
C.6. Physical and mechanical characterization of CEM II/A-L 42,5R (Cimpor, Alhandra), for each cement delivery . . . 285
C.7. Chemical characterization of CEM II/B-L 32,5N (Cimpor, Alhandra), for each cement delivery . . . 286
C.8. Physical and mechanical characterization of CEM II/B-L 32,5N (Cimpor, Alhandra), for each cement delivery . . . 287
C.9. Chemical characterization of CEM IV/B(V) 32,5 N, CEM II/B-L 32,5 R (BR) (Cimpor, Alhandra) and limestone filler (Micro 100, Comital) . . . 288
C.10. Physical and mechanical characterization of CEM IV/B(V) 32,5 N, CEM II/B-L 32,5 R (BR) (Cimpor, Alhandra) and limestone filler (Micro 100, Comital) . . . 289

D.1. ANOVA tests . . . 292
D.2. Model summary (coded and actual variables), colinearity statistics and Durbin-Watson statistic . . . 293
D.3. Residuals statistics . . . 294
D.4. Descriptive statistics of residuals . . . 295
D.5. Tests of normality on residuals . . . 298

E.1. Mix proportions and properties of fresh and hardened mortar specimens: CEM I 42,5 R (Cimpor-Alhandra) + V3000 . . . 302
E.2. Mix proportions and properties of fresh and hardened mortar specimens: CEM I 52,5 R (Cimpor-Alhandra) + V3000 . . . 303
E.3. Mix proportions and properties of fresh and hardened mortar specimens: CEM II/A-L 42,5 R (Cimpor-Alhandra) + V3000 . . . 304
E.4. Mix proportions and properties of fresh and hardened mortar specimens: CEM II/B-L 32,5 N (Cimpor-Alhandra) + V3000 . . . 305
E.5. Mix proportions and properties of fresh and hardened mortar specimens: CEM IV/B(V) 32,5 N (Cimpor-Alhandra) + V3000 . . . 306
E.6. Mix proportions and properties of fresh and hardened mortar specimens: CEM II/B-L 32,5 R (BR) (Cimpor^{b}) + V3000 . . . 307
E.7. Mix proportions and properties of fresh and hardened mortar specimens: CEM I 42,5 R (Secil-Maceira) + V3000 . . . 308

E.8. Mix proportions and properties of fresh and hardened mortar specimens: CEM I 42,5 R (Secil-Outão) + V3000 309
E.9. Mix proportions and properties of fresh and hardened mortar specimens: CEM I 42,5 R (Cimpor-Souselas) + V3000 310
E.10. Mix proportions and properties of fresh and hardened mortar specimens: CEM I 52,5 R (Cimpor-Alhandra) + V3005 311
E.11. Properties of mortars and corresponding pastes incorporating CEM I 52,5 R (Cimpor-Alhandra) from different deliveries 312
E.12. Properties of mortars and corresponding pastes incorporating CEM I 42,5 R (Cimpor-Alhandra) from different deliveries 313
E.13. Properties of mortars and corresponding pastes incorporating CEM II/A-L 42,5 R (Cimpor-Alhandra) from different deliveries 314
E.14. Properties of mortars and corresponding pastes incorporating CEM II/B-L 32,5 N (Cimpor-Alhandra) from different deliveries 315
E.15. Mix proportions and properties of fresh and hardened concrete specimens used in the experimental design (BACPOR, Maprel, Rio Maior) 316
E.16. Mix proportions and properties of fresh and hardened concrete specimens used in the experimental design (BACPOR, Maprel, Rio Maior) 317
E.17. Mix proportions and properties of fresh and hardened concrete specimens used in the experimental design (POCI/ECM/61649/2004) 318
E.18. Mix proportions and properties of fresh and hardened concrete specimens used in the experimental design (POCI/ECM/61649/2004) (cont.) 319

List of Figures

1.1. Structure of the thesis 7

2.1. Deformation of an ideal fluid exhibiting a Newtonian behaviour (Hackley and Ferraris, 2001) 10
2.2. Flow curve types (Saak, 2000) 12
2.3. Variation of shear stress with shear rate for time dependent fluid material (Chhabra and Richardson, 1999) 13
2.4. Shear-thinning and shear thickening behaviours of cement paste depending on the shear rate range(CEM I 42,5 R; limestone filler (Micro100); superplasticizer (Viscocrete 3000); w/c=0,35; wf/wc=0,39; Sp/p=1%; 25°C) 15
2.5. Flow curves for cement paste showing hysteresis when shear rate is increased and then decreased (CEM I 42,5 R; limestone filler (Micro100); superplasticizer (Viscocrete 3000) w/c=0,35; wf/wc=0,39; Sp/p=1%; 25°C) 15
2.6. Shear stepped and shear ramp modes in viscometry tests 16
2.7. Influence of cement hydration reactions on the evolution of flow curves of cement paste: (a) without conservation, at about $25°C$, and (b) with conservation, at about $0°C$ 17
2.8. Measurement methods and instruments (Hackley and Ferraris, 2001) . . . 20
2.9. Main parts in the rotational rheometer used in the present work (CVO-100, from Bohlin Instruments): (a) gap size indicator; (b) device to apply a constant torque (or rotation speed) to the tool and a device to determine the shear rate (or stress) response, respectively; (c) measurement tool; (d) thermostatic bath with temperature control 21
2.10. Measuring tools available for rotational rheometers: (a) concentric cylinder; (b) cone and plate; (c) parallel plate (Hackley and Ferraris, 2001) . . 23
2.11. Different configurations for concentric cylinders: (a) double gap; (b) cone and plate at the bottom; (c) hollow cavity at the bottom to trap air (Hackley and Ferraris, 2001) 24
2.12. Different configurations for vane geometries used in concrete rheometers: (a) two-point test (Tattersall); (b) IBB; (c) BML (Hackley and Ferraris, 2001) 24

2.13. Vapour hood incorporating a solvent trap 24
2.14. Rheological testing techniques (Bohlin Instruments Ltd, 1994) 25
2.15. Oscillatory shear strain out-of-phase with stress by a phase angle of δ . . 26
2.16. Evolution of storage and loss modulus of a cement paste as a function of hydration time (frequency=$1Hz$) 27
2.17. Applied shear strain and phase angle as a function of hydration time (frequency=$1Hz$) 28
2.18. Schematic time evolution of the stress for imposed shear rate experiments at different imposed rates and different definitions of yield stress, namely, static, dynamic and equilibrium (Møller et al., 2006) 29
2.19. (a) Equilibrium stress measurement of cement paste, and (b) evolution of peak and equilibrium flow curves for cement paste 30
2.20. Rotational rheometer (Bohlin CVO-100) used in this study 31
2.21. Testing sequence: first, pre-shear; second, waiting period; and, third, measuring period 31
2.22. (a) Up- and down-flow curves, and (b) fitted Bingham model to the down-curve data 32
2.23. Up- and down-flow curves showing almost zero enclosed area 33
2.24. Conceptual framework for rheology of concentrated suspensions (Koehler and Fowler, 2007) 34
2.25. Physical interpretation of the Bingham model (de Larrard, 1999) 35
2.26. Target area for SCC and corresponding slump flow (ACM Centre, 2005) 38
2.27. Sheared and resting zones when concrete is cast from the top (Ovarlez and Roussel, 2006) 39

3.1. Fluidity variation with superplasticizer type and producing plants (Hanehara and Yamada, 1999) 44
3.2. Heat of hydration of plain cement pastes incorporating different cement types determined by conduction calorimetry at 20 °C (Silva, 2007) 45
3.3. Normal and false setting (Hanehara and Yamada, 1999) 46
3.4. Ilustration of interfacial electric double layer formed on cement particle surface (Uchikawa et al., 1997b; Yoshioka et al., 1997) 48
3.5. (a) Energy balance according to DLVO theory and (b) illustration of interparticle potentials: A-stable dispersion, B-flocculated suspension, and C-coagulated suspension (Yang et al., 1997)) 49
3.6. Molecular units of: (a) LN, (b) SNF, (c) SMF, (d) PC (Dransfield, 2003) 50
3.7. Schematic illustration of (a) electrostatic repulsion and (b) steric stabilization 51

3.8. Zeta potential of different cement types and mineral additions, with and without superplasticizer. SP A is of LN type and SP B and C are of PC type (Nunes et al., 2008) 52
3.9. Bingham parameters of cement pastes incorporating Sp B and Sp C, with varying dosages of Sp (CEM I 52,5 R; limestone filler; w/c=0,35; w_f/w_c=0,39; 15 min) 53
3.10. Examples of total interparticle energy curves when the main dispersion mechanism is (a) electrostatic repulsion (described by DLVO theory) (b) steric hindrance (n is the number of ethylene oxide units in the graft chain)(Yoshioka et al., 1997) 54
3.11. Example of a PC type polymer molecule (Sika ViscoCrete®) adsorbed on cement grain surface 55
3.12. Effect of the partial substitution of cement by limestone filler on zeta potential results, in the presence of Sp B, for different cement types (Nunes et al., 2008) 56
3.13. Uneven polymer distribution on the surface of a cement grain (Plank and Hirsch, 2007) 57
3.14. Schematic interpretation of polymer adsorbed and absorbed (intercalated into hydrate phases) and situations of high and low reactivity of cement towards a superplasticizer (Flatt, 1999) 58
3.15. Adsorbed (or more correctly 'consumed') amounts of superplasticizers (PMS and BNS corresponds to SMF and SNF, respectively) on ettringite in case of direct and delayed adding time (Plank and Hirsch, 2007) . . . 59
3.16. Schematic interpretation of the influence of adding time on the amount of polymer consumed (Flatt, 1999) 60
3.17. Schematic interpretation of the influence of sulfate content (below the optimum dosage) on the amount of consumed polymer (Flatt, 1999) . . . 61
3.18. Target area of SCC mortars with and without a viscosity agent (Nawa et al., 1998) 63
3.19. Adsorbed amount of superplasticiser on the cement surface in the presence of adsorptive and non-adsorptive VAs (Nawa et al., 1998) 65
3.20. Schematic representation of PC type molecules with varying molecular structures (n is the number of ethylene oxide units; MCL is the main chain length; SCL is the side chain length) (Plank and Sachsenhauser, 2006) 66
3.21. Evolution of Bingham parameters with time of cement pastes incorporating Sp B ($(Sp/p)_{solid} = 0,25\%$) and Sp C ($(Sp/p)_{solid} = 0,175\%$) (CEM I 52,5 R; limestone filler; w/c=0,35; w_f/w_c=0,39; Temperature=20°C) . . 67

4.1. Abrams cone and plate used in the Slump flow test 72
4.2. Slump flow test carried out by a single operator, by using an Abrams cone fitted with a steel collar (photos taken at Stevin Laboratory, TUDelft, The Netherlands) 72
4.3. V-Funnel test 73
4.4. L-Box test 74
4.5. Sieve segregation test (photos taken at Stevin Laboratory, TUDelft, The Netherlands) 74
4.6. J-Ring test 75
4.7. Consistency class' specification of SCC for most common applications, adapted from (BIBM et al., 2005; Walraven, 2003) and Draft prEN 206-9 (CEN, 2007a) 77
4.8. Schematic representation of concrete as a suspension of aggregates in paste, taken from (Koehler and Fowler, 2007) 81
4.9. Box-plots of SCC mix-proportions of 68 case studies (Domone, 2006) . . 83
4.10. Box-plots of (a) w_w/w_p and (b) w_p of SCC mixtures not including VA (34 case studies) and including VA (34 case studies) (Domone, 2006) . . 83
4.11. (a) Mini-slump flow cone and (b) mini-V-funnel used in paste and mortar tests in the Japanese SCC-designing method (Okamura et al., 2000) . . 91
4.12. Box test 93
4.13. Central composite designs for (a) $k = 2$ and (b) $k = 3$ (Montgomery, 2001) 97
4.14. Number of runs (n_F) as a function of number of factors (k) and design type (two-level). Color coding: grey=complete factorial design; green=fractional design with resolution V or higher; yellow= fractional design with resolution IV; red=fractional design with resolution III (State-Ease Corporation, 2000) 99

5.1. Comparison of measured versus predicted values of Dflow (CEM I 42,5 R) 117
5.2. Comparison of measured versus predicted values of Tfunnel (CEM I 42,5 R) 118
5.3. Comparison of measured versus predicted values of fc,28 (CEM I 42,5 R) 118
5.4. Optimized mortars incorporating CEM I 42,5 R: (a) range of mixture variables and (b) estimated values of fc,28 (MPa) 119
5.5. Comparison of measured versus predicted values of Dflow (CEM I 52,5 R) 121
5.6. Comparison of measured versus predicted values of Tfunnel (CEM I 52,5 R) 122
5.7. Comparison of measured versus predicted values of fc,28 (CEM I 52,5 R) 122

5.8. Optimized mortars incorporating CEM I 52,5 R (a) range of mixture variables and (b) estimated values of fc,28 (MPa) 123
5.9. Comparison of measured versus predicted values of Dflow (CEM II/A-L 42,5 R) 125
5.10. Comparison of measured versus predicted values of Tfunnel (CEM II/A-L 42,5 R) 126
5.11. Comparison of measured versus predicted values of fc,28 (CEM II/A-L 42,5 R) 126
5.12. Optimized mortars incorporating CEM II/A-L 42,5 R (a) range of mixture variables and (b) estimated values of fc,28 (MPa) 127
5.13. Comparison of measured versus predicted values of Dflow (CEM II/B-L 32,5 N) 128
5.14. Comparison of measured versus predicted values of Tfunnel (CEM II/B-L 32,5 N) 129
5.15. Comparison of measured versus predicted values of fc,28 (CEM II/B-L 32,5 N) 129
5.16. Optimized mortars incorporating CEM II/B-L 32,5 N (a) range of mixture variables and (b) estimated values of fc,28 (MPa) 130
5.17. Comparison of measured versus predicted values of Dflow (CEM IV/B(V) 32,5 N) 131
5.18. Comparison of measured versus predicted values of Tfunnel (CEM IV/B(V) 32,5 N) 132
5.19. Comparison of measured versus predicted values of fc,28 (CEM IV/B(V) 32,5 N) 133
5.20. Optimized mortars incorporating CEM IV/B(V) 32,5 N (a) range of mixture variables and (b) estimated values of fc,28 (MPa) 134
5.21. Comparison of measured versus predicted values of Dflow (CEM II/B-L 32,5 R (BR)) 136
5.22. Comparison of measured versus predicted values of Tfunnel (CEM II/B-L 32,5 R (BR)) 137
5.23. Comparison of measured versus predicted values of fc,28 (CEM II/B-L 32,5 R (BR)) 137
5.24. Optimized mortars incorporating CEM II/B-L 32,5 R (BR) (a) range of mixture variables and (b) estimated values of fc,28 (MPa) 138
5.25. Range of optimized mixture variables (coded values) for different cement types 140
5.26. Variation of Sp/p with w/c for optimized mortars with V_s/V_m=0,45 . . . 141
5.27. Variation of V_w/V_p with w/c for optimized mortars with V_s/V_m=0,45 . . 142

5.28. Variation of estimated values of fc,28 (MPa) for optimized mortars with V_s/V_m=0,45 . . . 142
5.29. Measured versus predicted values of Dflow for CEM I 42,5 R from different sources . . . 144
5.30. Measured versus predicted values of Tfunnel for CEM I 42,5 R from different sources . . . 144
5.31. Measured versus predicted values of fc,28 for CEM I 42,5 R from different sources . . . 145
5.32. Range of optimized mixture variables for the combination of CEM I 52,5 R+ limestone filler+V3005: (a) contour plot of absolute values and (b) interaction diagram with coded values . . . 146

6.1. Flow table test results (Juvas et al., xxxx) . . . 150
6.2. (a) Flocculated cement particles and (b) deflocculated cement particles after superplasticizer addition . . . 151
6.3. Backscattered electrons image of CEM IV/B(V) 32,5 N particles . . . 155
6.4. Backscattered electrons image of CEM II/B-L 32,5 N particles . . . 156
6.5. Experimental set-up used in this study to measure temperature evolution of paste under semi-adiabatic conditions . . . 162
6.6. Typical evolution of temperature of cement paste (SCC) with time obtained from semi-adiabatic test . . . 162
6.7. (a) Typical evolution of shear stress with shear rate and (b) evolution of viscosity with shear rate of a cement paste . . . 163
6.8. Centrifuge (Centurion, model K240, series K2) used in the present study 164
6.9. Variation of (a) Dflow and (b) Tfunnel SCC-mortar results, with cement delivery . . . 165
6.10. Variation of (a) standard water demand results and (b) fc,28 SCC-mortar results, with cement delivery . . . 166
6.11. Variation of (a) Dflow and (b) Tfunnel SCC-paste results, with cement delivery . . . 167
6.12. Variation of (a) PD and (b) wfree SCC-paste results, with cement delivery 167
6.13. Variation of σ_0 and η_{pl} results of SCC-paste, with cement delivery . . . 168
6.14. Variation of standard (a) initial and (b) final setting times, with cement delivery . . . 169
6.15. Variation of (a) time to acceleration and (b) time at peak SCC-paste results, with cement delivery . . . 169
6.16. Variation of (a) initial temperature and (b) temperature at peak SCC-paste results, with cement delivery . . . 170
6.17. Variation of fc,28 SCC-paste results, with cement delivery . . . 170

6.18. Effects of (a) SO_3 and (b) $(Na_2O)_{equivalent}$ on Tfunnel of mortars incorporating CEM II/B-L 32,5 N . . . 175
6.19. Effect of residue 45 μm on (a) mortar Tfunnel and (b) paste Tflow of mixtures incorporating CEM II/A-L 42,5 R . . . 176
6.20. Relation between the viscosity at a shear rate of 50 $s^{-1}$and flow time of pastes ($\rho_{Spearman}$=0,902) . . . 179
6.21. α, r, H_0 and h dependant on cone geometry and filling volume (Roussel and Le Roy, 2005) . . . 180
6.22. Comparison between measured and predicted flow time . . . 180
6.23. Relation between the yield stress and flow diameter of pastes ($\rho_{Spearman}$= 0,902) . . . 181
6.24. Relation between yield stress and spread diameter calculated with Saak's model and Roussel's model (with both λ=0 and 0,005) for the mini-slump cone (Kantro) and experimental data collected in the present study . . . 182
6.25. Range of properties of the analysed pastes incorporating different cement types . . . 183
6.26. Range of properties of the analysed pastes, corresponding to different V_s/V_m . . . 184
6.27. Estimated responses of pastes corresponding to optimized mortar mixtures (CEM I 52,5 R+limestone filler+V3005) . . . 184
6.28. Relation between wfree and Tflow of SCC pastes ($\rho_{Spearman}$=0,986) . . . 185
6.29. Range of properties of the analysed pastes . . . 185
6.30. Range of rheological parameters of the analysed pastes . . . 186
6.31. Range of mix-proportions to obtain an SCC (of classes SF2, VF2 and PL2), incorporating Paste A and maintaining s_1/s=0,50 . . . 187
6.32. Range of mix-proportions to obtain an SCC (of classes SF2, VF2 and PL2), incorporating Paste B and maintaining s_1/s=0,50 . . . 188

7.1. Robustness of an industrial process (Aïtcin et al., 2001) . . . 192
7.2. Illustration of the effect of a viscosity agent on SCC robustness (Shindoh and Matsuoka, 2003) . . . 197
7.3. Comparison of measured versus predicted values of Dflow . . . 204
7.4. Comparison of measured versus predicted values of T50 . . . 205
7.5. Comparison of measured versus predicted values of Tfunnel . . . 205
7.6. Comparison of measured versus predicted values of H . . . 206
7.7. Comparison of measured versus predicted values of fc,28 . . . 206
7.8. Observed deviations of constituent materials during one week of concrete production in Maprel precast factory . . . 208
7.9. Bootstrap re-sampling to compute a robustness measure . . . 209

7.10. Comparison of measured versus predicted values of Dflow 217
7.11. Comparison of measured versus predicted values of T50 218
7.12. Comparison of measured versus predicted values of Tfunnel 218
7.13. Comparison of measured versus predicted values of H2/H1 219
7.14. Comparison of measured versus predicted values of fc,28 219
7.15. Sensitivity to variation in water content of mixes obtained with criteria A 221
7.16. Slope of regression lines of change in slump-flow against variation of water content 228
7.17. Robustness estimates of SCC mixes 229
7.18. Relation between robustness measure and slope of regression lines 230

B.1. Sensitivity of SCC mixtures to variation in water content 265
B.2. Distribution of aggregates in a cylinder specimen of Mix A with plus 10 l/m^3 266
B.3. Distribution of aggregates in a cylinder specimen of Mix B with plus 10 l/m^3 266
B.4. Distribution of aggregates in a cylinder specimen of Mix C with plus 10 l/m^3 267
B.5. Sensors installed inside the concrete prisms to monitor temperature and deformation 271
B.6. Mean temperature evolution on concrete prisms 271
B.7. Evolution of drying shrinkage deformations in comparison with Eurocode 2 rules 272
B.8. Systems used in concrete creep tests 273
B.9. Evolution of shrinkage, creep and (shrinkage+creep) deformations with time 273
B.10. Evolution of creep deformations with time in comparison with Eurocode 2 rules 274
B.11. Specimen and experimental set-up used in the resistance to chloride penetration test 275
B.12. Penetration depth of chloride ions (lighter part): (a) Mix A; (b) Mix B; (c) Mix C 275

D.1. (a) Standardized residuals and (b) studentized residuals - Dflow predicted values against residuals (left) and Dflow observed values against residuals (right) 295
D.2. Ustandardized residuals against each predictor variable 296
D.3. (a) Unstandardized residuals and (b) studentized residuals - Histogram (left) and box-plot (right) 297
D.4. Normal P-P plot of the standardized residuals of the regression 297

D.5. (a) Unstandardized residuals and (b) studentized residuals - Normal Q-Q plot (left) and detrended normal Q-Q plot (right) 298
D.6. Unstandardized residuals against run order 299
D.7. (a) Autocorrelation plot and (b) partial autocorrelation plot of unstandardized residuals 299

Notations and symbols

Capital roman letters

Aft	Alumino-ferrite trisulfate hydrate	[-]
ANOVA	Analysis of variance	[-]
CCD	Central Composite Design	[-]
C_3A	Tricalcium aluminate	[-]
C_4AF	Tetracalcium aluminoferrite	[-]
C_3S	Tricalcium silicate (Alite)	[-]
C_2S	Dicalcium silicate (Belite)	[-]
CEN	European Comittee for Standardization	[-]
C-S-H	Calcium silicate hydrate	[-]
Dflow	Spread flow diameter	[mm]
DLVO	Derjaguin–Landau Verway– Overbeek	[-]
EFNARC	European Federation for Specialist Construction Chemicals and Concrete Systems	[-]
FEUP	Faculty of Civil Engineering, Porto University, Portugal	[-]
H	Final concrete height of concrete in the Box test	[mm]
H2/H1	Ratio of the concrete heights in the front and back parts of the box in the L-box test	[-]
HR	Relative humidity of the environment	[%]
PD	Packing density of paste obtained from centrifuge test	[-]
LABEST	Laboratory for the Concrete Technology and Structural Behaviour	[-]
LN	Modified lignosulphonate	[-]
PC	Polycarboxilate ethers	[-]
SCC	Self-compacting concrete	[-]
SMF	Sulphonated melamine formaldehyde condensate	[-]
SNF	Sulphonated naphthalene formaldehyde condensate	[-]
Sp	Superplasticizer	[-]
Sp/p	Liquid superplasticizer to powders ratio (mass)	[%]
$(Sp/p)_{solid}$	Solid part of superplasticizer to powders ratio (mass)	[%]
T50	Time needed for concrete to reach the 50 cm diameter in the Slump-flow test	[s]
Tfunnel	Time taken for mortar/concrete to flow out of a V-shaped funnel	[s]
Tflow	Time taken for paste to flow out of Marsh cone	[s]
V_a	Air content (volume)	[m^3/m^3]

V_g	Coarse aggregate content (volume)	[m^3/m^3]
$V_{g,lim}$	Dry rodded coarse aggregate content (volume)	[m^3/m^3]
V_m	Mortar content (volume)	[m^3/m^3]
V_p	Powders content (volume)	[m^3/m^3]
V_{paste}	Paste content (volume)	[m^3/m^3]
V_s	Fine aggregate content (volume)	[m^3/m^3]
V_w	Water content (volume)	[m^3/m^3]
VA	Viscosity agent	[-]
V3000	Sika - Viscocrete 3000 superplasticizer	[-]
V3005	Sika - Viscocrete 3005 superplasticizer	[-]

Small roman letters

c.o.v.	Coefficient of variation	[%]
fc,28	Compressive strenght at 28 days	[kg/m^3]
s_i/s	Sand i to total sand ratio (mass)	[kg/m^3]
w_c	Cement content (mass)	[kg/m^3]
w_f	Filler content (mass)	[kg/m^3]
w_p	Powders content (mass)	[kg/m^3]
w_s	Fine aggregate content (mass)	[kg/m^3]
w_{si}	Sand i content (mass)	[kg/m^3]
w_{Sp}	Liquid superplasticizer content (mass)	[kg/m^3]
w_{free}	Free water content obtained from centrifuge test (mass)	[kg/m^3]
w_w	Water content (mass)	[kg/m^3]
w_{wc}	Corrected water content (mass)	[kg/m^3]
w/c	water to cement ratio (mass)	[-]

Small greek letters

γ	Shear deformation	[-]
$\dot{\gamma}$	Shear rate	[s^{-1}]
γ_{Sp}	Solid content of superplasticizer	[%]
η	Viscosity	[Pa.s]
η_{pl}	Plastic viscosity	[Pa.s]
σ	Shear stress	[Pa]

σ_0	Yield stress	[Pa]
ρ_w	Specific gravity of water	[kg/m^3]
ρ_c	Specific gravity of cement	[kg/m^3]
ρ_f	Specific gravity of filler	[kg/m^3]
ρ_g	Specific gravity of coarse aggregate	[kg/m^3]
ρ_{sdi}	Specific gravity of sand i	[kg/m^3]
$\rho_{Spearman}$	Spearman's correlation coefficient	[-]

1. Introduction

1.1. Scope of the research

Awareness of the ecological impact of construction industry and the need to address it in our modern society is becoming a factor of increasing importance. Cement and concrete industry faces challenges related to improving durability and enhancing performance while, at the same time, improving sustainability of production. The dominating influence of quality and efficiency of compaction on performance of a concrete structure, regardless of good quality of the initial mix, has been the main driving force for development of new admixtures and special types of concrete, like the case of self-compacting concrete (SCC). SCC is a new category of concrete which main characteristic is to fill the form and consolidate under its own weight without any compaction. Placing of SCC has minimal dependence on available workmanship on site; therefore, it has great potential to improve true quality of concrete in the final structure and to extend service life of modern structures.

After emergence of SCC in Japan in the early 1990's, under the leadership of Prof. Okamura (Okamura et al., 2000), there has been a growing interest in SCC technology among constructors and the construction industry in several countries. The main reason for this concern is the placing of concrete in heavy reinforced areas of difficult access where the quality of traditionally placed concrete is so much more dependent on the skill of workers. Furthermore, the use of this type of concrete should shorten the construction period, reduce manpower during placing, reduce damage on the concrete surface and increase freedom of structural and artistic design of concrete structures. Besides that, SCC technology has a profound beneficial effect on working conditions and noise levels in the areas surrounding construction sites. On the other hand, it promotes incorporation of industrial by-products in partial replacement of cement in the so-called eco-efficient concretes contributing to concrete technology sustainability (Petersson et al., 2001).

Precast industry is particularly suited for the use of SCC. In a precast factory, concrete elements with complex geometric shape and dense reinforcement are often produced. The production of such elements using traditional vibrated concrete can only be executed with great effort; very strong external vibrators have to be mounted and in some cases

casting has to be carried out in more than one step. When consolidation is incomplete the resulting concrete elements with defects have to be repaired, causing further delay and increase in cost. Vibration has also a harmful physical impact on workers. In a precast plant it is easier to install quality control systems because of the high degree of automation and repetition of similar processes. Besides, the production process is less influenced by weather conditions and transport time is shorter, so retaining fluidity of fresh concrete is not a problem. Often in precast industry, strength at early age becomes the dominant requirement due to the need to apply pre-stress or demoulding a few hours after casting. This leads to conventional concrete mixtures with very low water/cement ratio, including strong action superplasticizers and a cement content closer to that required for the powder-type SCC (Japan Society of Civil Engineers, 1998), thus minimizing the differences in the cost of materials between conventional and SCC mixtures. The higher material cost is easily overrun by increased productivity. For all of these reasons, many precast factories have fully converted to the use of SCC (Walraven, 2005).

In contrast, the introduction of SCC for in-situ production has been much slower. The main obstacles to a wider use of SCC by in-situ industry are the lack of agreement in terms of suitable test methods to identify and specify its key properties (Cussigh, 2007); the higher cost of materials, especially, for lower strength classes and powder-type SCCs; the variable conditions at the construction site; the more complicated control of materials' characteristics, mixing process and transportation and its impact on concrete properties (Walraven, 2005). In case of failure, the consequences for an in-situ application are much more severe than in the precast concrete industry, with demolition being the probable ultimate consequence. In the precast industry, unsuitable elements can be simply rejected with a lower economic impact.

SCC can be made from a wide range of materials but may be very sensitive to relatively small batch-to-batch changes, like variations in cement or mineral additions due to changes in the production process as well as changes in aggregate characteristics, which may lead to variability of performance (Walraven, 2005). Therefore, it is of great importance to have a robust mixture that is as insensitive as possible to small variations of the ingoing materials, composition and other external factors. Apart from regulation considerations, the growth of the SCC market share depends to a great extent on the robustness of the mixtures.

Mix-proportioning remains one of the most critical aspects in concrete production. Nowadays, more and more components are available to produce concrete: chemical admixtures and additions, several kinds of cements and aggregates (crushed, rounded, etc). But the design strategy for conventional concrete has generally been to propor-

tion the different grains to obtain a grading curve close to the "ideal" grading curve, which is supposed to produce the maximum packing density. The final optimization is achieved by trial and error. Iterative technological tests are of interest but costly and time consuming. To design SCC one cannot use the same "ideal" curves used for conventional concrete. Much more is demanded of SCC in its fresh state than of conventional vibrated concrete; it must (at least) show passing ability, filling ability and resistance to segregation (BIBM et al., 2005). Several mix design techniques have been followed in different countries, many of these proceed by trial and error (at paste, mortar or concrete levels) to optimize SCC. Some authors have proposed guidelines for SCC proportioning based on their own experience (Okamura et al., 2000; EFNARC, 2002; Petersson et al., 2001; Japan Society of Civil Engineers, 1998), which mainly consist of limiting the coarse aggregate volume and maximum aggregate size, using low water powder ratio and adding a superplasticizer. As these guidelines are general, they tend to be on the safe side and generally lead to high paste volumes, which are responsible for higher material costs and promote a tendency to higher shrinkage, creep and heat generation. Hence, a more scientific approach to mix-design is essential for dealing with constituent materials' specific properties to come up with an optimized concrete mixture for defined performance requirements.

The behaviour of highly flowable concretes, such as SCC, is getting closer to the behaviour of a suspension, which allows a multi-scale approach on mix-design (Flatt et al., 2006). The properties of the matrix (water, paste or mortar) and solid inclusions (fine materials, fine aggregate or coarse aggregate) can be used to predict the properties of a new material (paste, mortar or concrete, respectively). This type of approach is not possible with traditional concrete, since its behaviour is dominated by grain to grain contacts. For a more scientific approach, a rheometer can be used to study rheology of cement suspensions. Unlike measurements from empirical tests, rheological parameters are fundamental physical quantities, mutually independent and not dependent on operator or equipment.

The concrete producer of tomorrow will have to know how to play with all the different types of components offered by the cement and admixture producers to provide contractors with concrete that will be more economical, not in terms of the cost of 1 m^3, but in terms of performance, i.e., the cost of 1 MPa and/or 1 year of life cycle of a structure (Aïtcin, 2000). These challenges can only be met by application of advanced materials science and engineering.

1.2. Research objectives

The main objective of the current PhD research project is to contribute to the enhancement of SCC mixtures robustness or to reduce the sensitivity of mixtures to external sources of variability. This can be achieved by a well-balanced selection and control of materials as well as adequate proportioning in the concrete mixture. To accomplish this objective the current PhD research project aimed to develop: a more general scientific approach to SCC mix-design and a methodology to evaluate robustness of SCC mixtures.

The constituent materials for SCC are the same as those used in conventional concrete. The materials selection should try to improve robustness, making the concrete more tolerant to material variability. But for economic reasons materials' selection depends much on local availability so there is no fixed rule for the amount/type of aggregates, cement, additions and admixtures. Thus, a decisive factor for robustness of SCC mixtures is a clear understanding of the effect of each constituent material and of their interaction on SCC properties and an adequate mix-design method (more scientific). For example, trial and error methods are not adequate since they do not allow tailoring the mixtures to specific requirements and do not give indications on how to correct the mixture when variations in raw materials occur.

A more scientific and multi-scale approach on SCC mix-design was looked for, through the use of factorial experimental design, to mathematically model the influence of mixture parameters on relevant paste, mortar and concrete properties. In addition, more sophisticated experimental techniques, like the study of cement paste rheology (by using a rheometer), were introduced.

Since variability of most constituent materials can be translated by a change in water requirement, it is suggested that a variation of the target water content be tested and the respective changes in fresh state properties be evaluated for robustness checking (BIBM et al., 2005). But this approach seems too simplistic because it does not take into account the specific characteristics of the production centre, like the existing level of quality control, equipment performance, skills and knowledge of the personnel involved. Therefore, the current PhD project aimed to develop a methodology to compute a robustness measure, based on data of typical materials weight deviations, inherent of the production process, at a specific production centre. It intended to maximize the robustness of SCC mixtures based on mix-proportioning. Another objective of this work was to evaluate the influence of cement variations due to the production process, on fresh and hardened properties of mortar/paste mixes and its importance for SCC robustness.

Modelling of concrete properties should contribute to a rational concrete mix-design.

Numerical models should facilitate proportioning of optimized mixtures for defined requirements in both fresh and hardened states, including a robustness criterion. On the other hand, new concrete varieties can be considered concerning the type of application. Therefore, the present work should contribute to a more successful implementation of SCC in both precast and in-situ concrete industry. By shortening the gap between performance requirements and properties exhibited by the material in the real structure, a better use of existing resources will be possible, with consequent savings in materials consumption.

1.3. Research strategy and outline of the thesis

The current PhD research project was carried out in connection with two Portuguese research projects developed at the Faculty of Engineering of the University of Porto (FEUP), namely,

- BACPOR -"*Development of a Robust Technology for the Production, Transport and Placement of Self-compacting Concrete*" funded by Adi-Agência de Inovação and in co-operation with Grupo Mota-Engil, Sika and Maprel (from January 2003 to April 2005);
- FCT/POCTI/ECM/61649/2004 – "*A Scientific Mix-design Approach to Promote Sustainability in Concrete Construction*", funded by FCT-Fundação para a Ciência e Tecnologia with the collaboration of a Cimpor Indústrias de Cimento, SA and Cimpor-Tec, SA (from July 2005 to December 2007).

After the first years of research on SCC in Portugal, many mixtures were developed and tested in the laboratory but the experience of producing SCC on site was limited (Dias, 2002; Nunes, 2001; Oliveira, 2003). Accordingly, in 2003 the research project BACPOR was initiated at FEUP in direct co-operation with local industry, aiming to develop a robust technology to produce, transport and place self-compacting concrete using materials available in Portugal. Within BACPOR, different SCC mixtures were designed and completely characterized in the laboratory, and then applied to in-situ construction and precast industry. During full-scale tests, the adequacy of actual current processes involved in production, mixing, transport and placing was evaluated and the most critical issues concerning implementation of this technology were identified. In particular, the SCC mixtures optimized in the laboratory had to be adjusted during full-scale testing to attend to the differences in mixing efficiency; and it was observed that variations in cement due to changes in the production process and changes in aggregate type, e.g. from one sand pit to another, can cause significant variations of fresh properties. In addition, comparisons of hardened SCC and conventional concrete

properties both produced under actual conditions at the precast factory and on site were established. Further details on the investigation carried out within BACPOR research project can be found elsewhere (Figueiras, 2006; Nunes et al., 2005b, 2006, 2005c). Main conclusions obtained with full-scale testing are summarized in the paper presented in Appendix A.

The experience acquired during full-scale tests, especially with in-situ applications (Nunes et al., 2005b) highlighted the importance of a robust mixture for the successful implementation of SCC in the construction industry. As a consequence, within the BACPOR research project a methodology to assess the robustness for SCC was developed. This is presented in the first part of Chapter 7.

Following BACPOR, the research project POCI/ECM/61649/2004 was initiated, aiming to develop a more general scientific approach on concrete mix-design, which was found to be a requisite to design more robust concretes. This project included three main parts: experimental study, numerical modelling and optimization of mixtures. The study was carried out at the paste, mortar and concrete levels. Main results of this research project are presented in Chapters 5, 6 and 7. The main focus of this research work on SCC, was given by fresh concrete properties but further studies were carried out on properties in the hardened state, as those included in Appendix B.

The structure of the current thesis is schematically shown in Figure 1.1. In Chapters 2, 3 and 4 a literature review is presented, with reference to work developed in this PhD, providing theoretical background on the various subjects discussed in the following chapters. Chapter 2 presents an introduction to rheology of particle suspensions and factors affecting them, including description of flow behaviours, rheological models and main methods for measuring rheology of fresh cementitious materials. Chapter 3 discusses physical and chemical parameters affecting cement-superplasticizer interactions. In Chapter 4, both fresh and hardened properties of SCC are described along with an overview of existing mix-design methods. The Japanese SCC-designing method and the Experimental Design approach are described in further detail.

Chapter 5 describes experimental and numerical studies carried out for the design of mortar mixtures which are adequate for SCC. This was applied to six different types of cement in combination with limestone filler and a polycarboxylate type superplasticizer.

Chapter 6 describes a study dealing with the influence of different production dates of cement on fresh and hardened properties of mortar/paste mixes. It includes rheological characterization of cement pastes. In this chapter a link between material behaviour at different scales, namely paste, mortar and concrete, is established.

Chapter 7 discusses the concept of SCC mixtures robustness and describes the experimental and numerical studies involved in a new methodology to assess robustness of an SCC mixture developed under the current PhD research project.

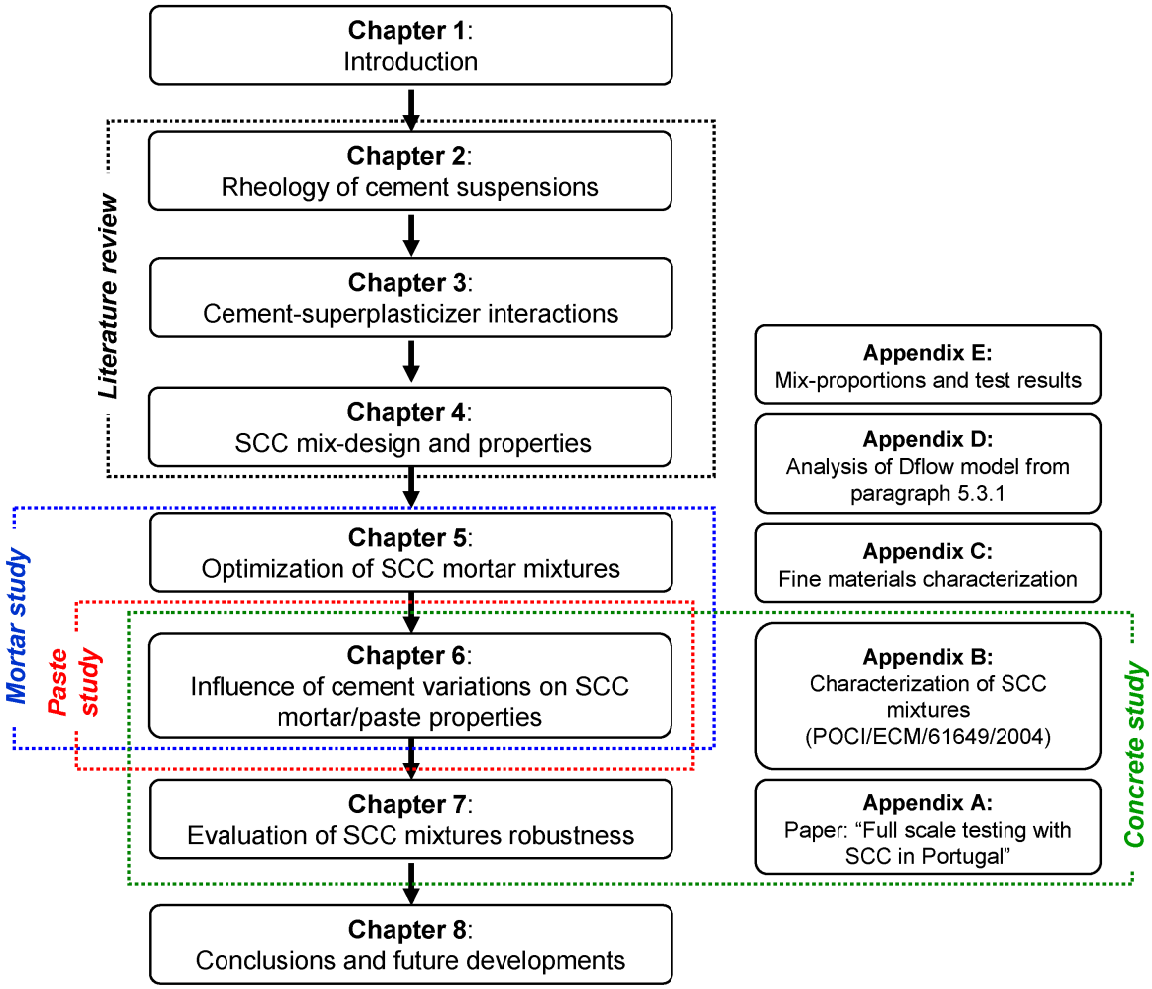


Figure 1.1.: Structure of the thesis

Finally, Chapter 8 presents the global conclusions and recommendations for future research to enhance robustness of SCC mixtures.

2. Rheology of cement suspensions

2.1. Introduction

The objective of this chapter is to present, through a literature review, an introduction to the rheology of particle suspensions and the factors affecting it. The flow behaviours, rheological models and main methods for measuring the rheology of fresh cementitious materials will be described.

This chapter describes as well, the equipment, testing technique, measuring tool and measurement sequence adopted for the rheological characterization of cement pastes, which is reported in Chapter 6.

2.2. Rheology

2.2.1. Introduction

Rheology is a well-established area of study for a wide range of materials. It is defined as the science of deformation and flow of matter and is normally applied to fluid materials or materials that exhibit a time-dependent response to stress (Struble, 2001; Esping, 2007). In the case of an ideal fluid, a linear relationship exists between the applied shear stress σ and shear rate $\dot{\gamma}$ defined as follows (Chhabra and Richardson, 1999)

$$\sigma = \eta\dot{\gamma} \tag{2.1}$$

where η is the viscosity (see Figure 2.1). Based on Figure 2.1, the shear stress and the shear rate are calculated from applied shear force F and the resulting shear deformation γ as follows

$$\sigma = \frac{F}{A} \tag{2.2}$$

$$\gamma = \frac{\Delta x}{y} = \tan\theta \tag{2.3}$$

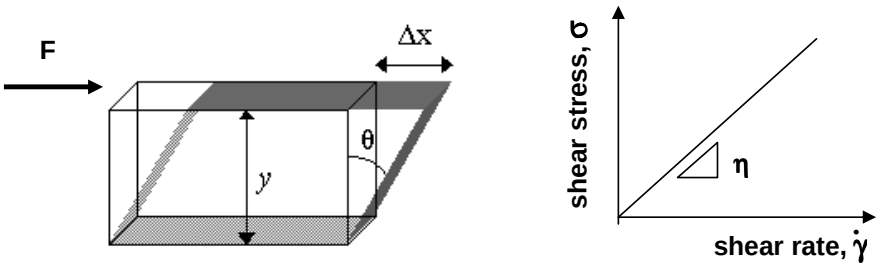


Figure 2.1.: Deformation of an ideal fluid exhibiting a Newtonian behaviour (Hackley and Ferraris, 2001)

$$\dot{\gamma} = \frac{\partial \gamma}{\partial t} \tag{2.4}$$

The simplest Newtonian behaviour described by equation (2.1) is analogous to the Hookean behaviour of an elastic solid. In an elastic solid material, shear strain is proportional to applied shear stress and if stress is removed, the solid material fully recovers the initial shape.

For many fluids, like polymers, paints, cosmetics, cement paste and concrete the relationship between shear stress and shear rate is non-linear (it can be shear-thinning or shear-thickening). Moreover, for some fluids, flow only initiates after a certain level of stress is surpassed (called the yield stress). These rheological behaviours, different from the Newtonian, will be further discussed in 2.2.2. Some materials also have a time dependence due to a flocculated microstructure, where the flow characteristics are influenced by the shear history of a material (it can be thixotropic or anti-thixotropic). This will be also discussed in 2.2.2.

As can be observed in Table 2.1 the viscosity of different materials varies in a wide range as well as the shear rate range associated to different industrial processes. Moreover, the viscosity may vary with applied shear rate, as in the case of non-Newtonian materials. Thus, to be able to characterize a fluid, a suitable instrument and measuring technique must be selected. In Section 2.3, a review of existing instruments, measuring tools and measuring techniques is presented. A mathematical model is often required to describe the rheological behaviour of a fluid and several theoretical models can be found in the literature. Those most often used for cementitious materials will also be presented in 2.2.3.

Table 2.1.: Typical values of viscosity for different materials and typical shear rate associated to different industrial processes (Chhabra and Richardson, 1999; Esping, 2007)

Material	approx. viscosity (Pa.s)	Process	shear rate range (s^{-1})
air	10^{-5}	sedimentation	10^{-1}- 10^{-3}
water	10^{-3}	levelling	10^{-1}- 10^{-2}
olive oil	10^{-1}	extruding	1- 10^{2}
mortar	1	pumping	1- 10^{3}
SCC	100	mixing/stirring	10^{1}- 10^{3}
molten glass	10^{15}	spraying	10^{4}- 10^{5}

2.2.2. Flow curve types

As shown in Figure 2.1 the plot of shear stress against shear rate (called flow curve or rheogram) for a Newtonian fluid is a straight line of slope η passing through the origin. The single constant η therefore completely characterises the flow behaviour of a Newtonian fluid at fixed temperature and pressure (Chhabra and Richardson, 1999). A non-Newtonian fluid is one whose flow curve is non-linear or does not pass through the origin, i.e. where the viscosity (shear stress divided by shear rate) is not constant at a given temperature and pressure but is dependent on flow conditions such as flow geometry, shear rate, shear history etc (Chhabra and Richardson, 1999).

Time independent flow behaviour

The non-newtonian fluids for which the shear rate at any point is determined only by the value of the shear stress at that point, at that instant, are known as time-independent. These fluids may be further subdivided into three types: shear-thinning (or pseudoplastic); shear-thickening (or dilatant); and viscoplastic. Qualitative flow curves for these types of fluid behaviour and corresponding variation of viscosity with shear rate are shown in Figure 2.2.

In all types of non-Newtonian behaviour the viscosity varies with shear rate, thus viscosity may be defined in many ways. The 'apparent viscosity' is the value of viscosity evaluated at some nominal average value of the shear rate (Hackley and Ferraris, 2001). When using an equipment with control of shear rate the term 'coefficient of viscosity' (or the abbreviated form 'viscosity') should be used to designate the ratio of shear stress to shear rate under simple steady shear (Hackley and Ferraris, 2001). The 'differential viscosity' can be considered as the slope of the shear stress-shear rate curve. The 'plastic viscosity', present in the Bingham model (see 2.2.3), corresponds to the differential viscosity determined in the linear portion of the flow curve (high shear rates zone) (Hackley and Ferraris, 2001).

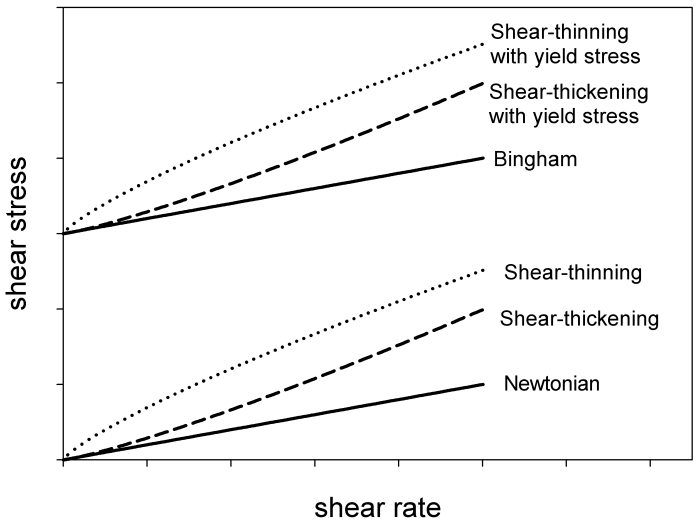


Figure 2.2.: Flow curve types (Saak, 2000)

Observing Figure 2.2, a material is said to be shear-thinning (or pseudoplastic) and shear- thickening (or dilatant) when the differential viscosity respectively decreases and increases with shear rate. The viscoplastic behaviour is characterized by the existence of a yield stress (σ_0), with the material behaving like a solid below the yield stress, but flowing like a viscous liquid when this stress is exceeded. This flow curve may be linear (Bingham behaviour) or non-linear (see Figure 2.2). The viscoplastic behaviour is found in flocculated suspensions, like cement paste (Saak, 2000; Hackley and Ferraris, 2001; Struble, 2001). A gel structure forms immediately after water is added to cement, due to a combination of colloidal interparticle forces and chemical reactions (Saak, 2000). But, the flocculated structure of fresh cement paste can be broken apart by applying a sufficiently high shear force (Saak, 2000). Some controversy exists about the real existence of 'yield stress' as a material property (Wallevik, 2003b; Møller et al., 2006; Esping, 2007). According to Wallevik (2003b), from the practical point of view, a yield stress value exists for high concentration coarse particle suspensions like fresh mortar and concrete, relative to the time and shear rate which is of interest for cement suspensions.

Time dependent fluid behaviour

In practice, viscosities may depend not only on the rate of shear but also on the time for which the fluid has been subjected to shearing. Time-dependent fluid behaviour may be further sub-divided into two categories: thixotropic and anti-thixotropic (Chhabra and Richardson, 1999).

The definition of thixotropy is a decrease of viscosity under shear stress, followed by gradual recovery when stress is removed (Wallevik, 2003b). If the flow curve is measured in a single experiment in which the shear rate is steadily increased at a constant

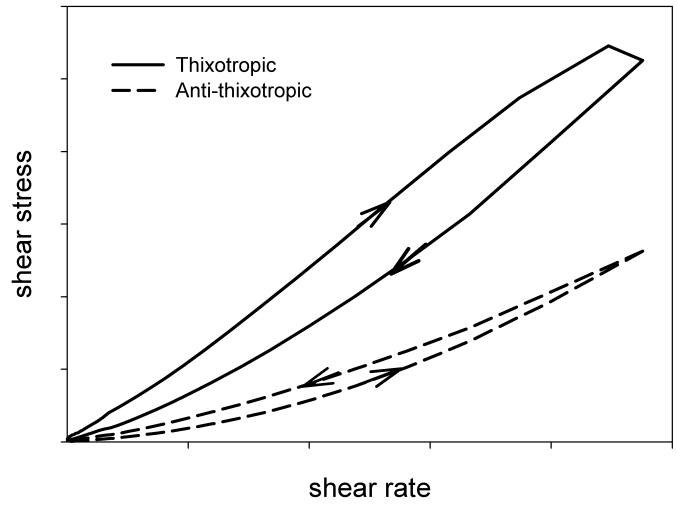


Figure 2.3.: Variation of shear stress with shear rate for time dependent fluid material (Chhabra and Richardson, 1999)

rate from zero to some maximum value and then decreased at the same rate to zero again, a hysteresis loop of the form shown in Figure 2.3 is obtained. The height, shape and enclosed area of the hysteresis loop depend on the duration of shearing, the rate of increase/decrease of shear rate and the past kinematic history of the sample. No hysteresis loop is observed for time-independent fluids, that is, the enclosed area of the loop is zero (Wallevik, 2003b). There are relatively few anti-thixotropic fluids (Chhabra and Richardson, 1999), that is, fluids for which the viscosity increases with time of shearing. Again, hysteresis effects are observed in the flow curve, but in this case, it is inverted, as compared with a thixotropic material (see Figure 2.3).

Cementitious materials generally show a thixotropic behaviour (Wallevik, 2003b; Roussel, 2005; Esping, 2007). This behaviour originates from the microstructure of the matrix system, due to coagulation and flocculation of suspended particles and the time taken to change this microstructure. As the suspension is sheared, the weak physical bonds among particles are ruptured, and the network among them breaks down into separate agglomerates, which can disintegrate further into smaller flocs whereas if the suspension is at rest the particles will start to coagulate or flocculate into agglomerates again.

Viscoelastic fluid behaviour

Many materials show both elastic and viscous effects under appropriate circumstances, meaning that the shear stress depends both on the shear strain and shear rate. In the absence of the time-dependent behaviour mentioned previously, these materials are said to be viscoelastic (Chhabra and Richardson, 1999). Flocculated suspensions show viscoelastic behaviour at low strains (below the yield stress) (Struble, 2001).

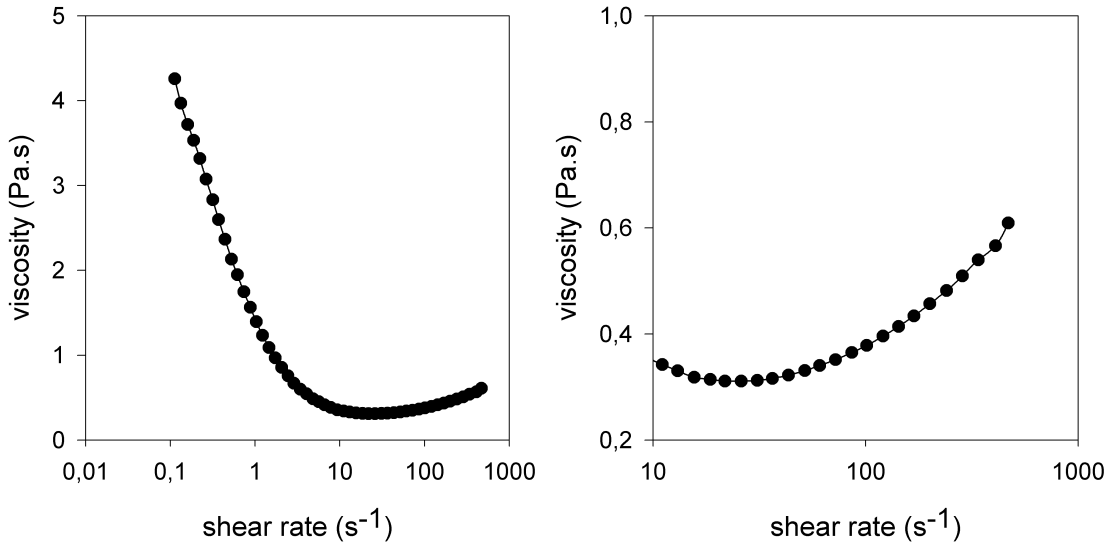
While static measuring techniques are appropriate to characterize both time-dependent and -independent fluid behaviours, dynamic measuring techniques (oscillatory tests) or creep/recovery tests are necessary to characterize completely the viscoelastic fluid behaviour, as it will be further detailed in 2.3.3.

Complexity of cement paste flow behaviour

As it was mentioned before the flocculated state of cement particles (especially, for colloidal particles, i.e. smaller than 1μm) is responsible for plastic behaviour, with the yield stress reflecting the forces holding particles together. Often this breakdown is not complete at the yield stress, so the suspension is still somewhat flocculated even though it flows, and this remaining flocculation is progressively disrupted as the shear rate is increased (Struble, 2001; Wallevik, 2003b). This can explain the shear thinning behaviour observed with cement paste, for a limited shear rate range (see Figure 2.4 (a)). But, it can also show shear thickening behaviour at higher shear rates, as can be observed in Figure 2.4 (b)). According to Wallevik (2003b) the upper limit of the shear rate range which is of interest to cement paste is as high as 60 to 80 s^{-1}.

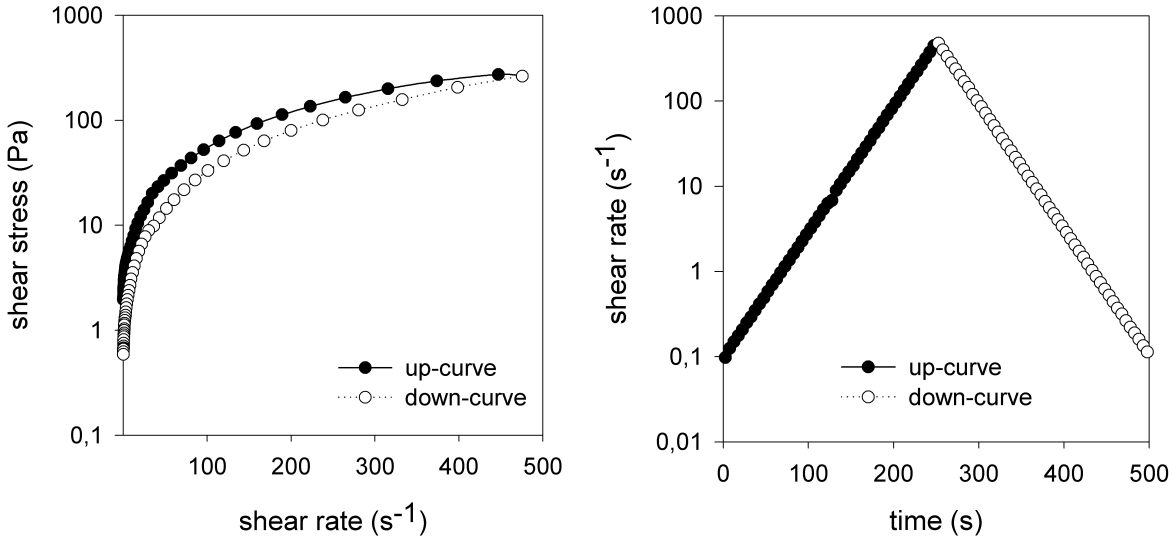
Another important aspect of cement paste is the extent to which hysteresis is observed between the stress of the up- and down curves in a shear ramp test. As can be observed in Figure 2.5 the stress in the up-curve is higher than the stress in the down-curve, for a given shear rate. This hysteresis reflects some lack of equilibrium between the microstructure and the shear rate, often because the material is undergoing some type of structural breakdown during shear (thixotropy). For this reason it is important to achieve full structural breakdown at each shear rate when calculating material parameters from a flow curve (for example, when adjusting the Bingham model). A way to achieve a complete structural breakdown during testing at each shear rate is to use the stepped shear test instead of a ramped test and to use only the down-curve data. A stepped shear test allows a waiting period for the equilibrium condition to be reached while the ramp shear test does not (see Figure 2.6). Furthermore, the time required to obtain equilibrium at each shear rate is shorter during the down part of the test because one is going from higher degree of dispersion to a lower one (Wallevik, 2003b). At low shear rates a suspension may be very slow to reach equilibrium. In the case of cement paste, it may not be possible to wait for such a long time, because of other time-dependent processes that are going on, like cement hydration. To be able to compare measurements in common references and minimize the influence of past shear history (due to mixing and handling of sample) it is advisable to pre-condition the sample before the start of the viscometry test (Saak, 2000; Esping, 2007).

Besides the reversible time-dependent behaviour (thixotropy), cementitious materials also show a time-dependent irreversible behaviour due to concurrent processes like the



(a) (b)

Figure 2.4.: Shear-thinning and shear thickening behaviours of cement paste depending on the shear rate range(CEM I 42,5 R; limestone filler (Micro100); superplasticizer (Viscocrete 3000); w/c=0,35; wf/wc=0,39; Sp/p=1%; 25°C)



(a) (b)

Figure 2.5.: Flow curves for cement paste showing hysteresis when shear rate is increased and then decreased (CEM I 42,5 R; limestone filler (Micro100); superplasticizer (Viscocrete 3000) w/c=0,35; wf/wc=0,39; Sp/p=1%; 25°C)

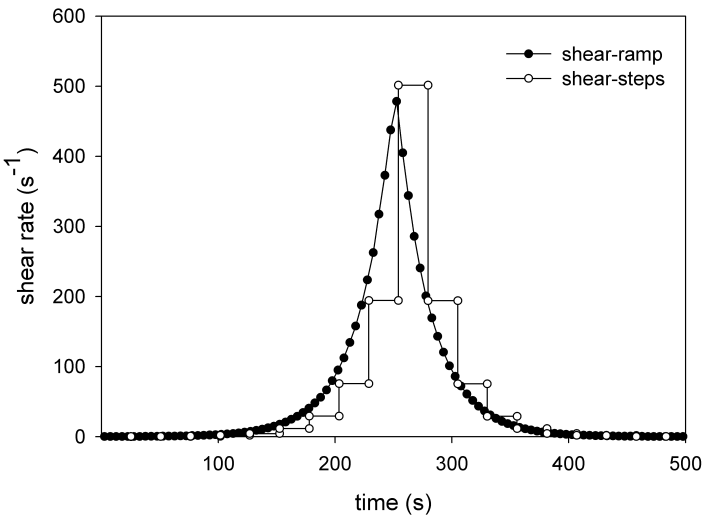
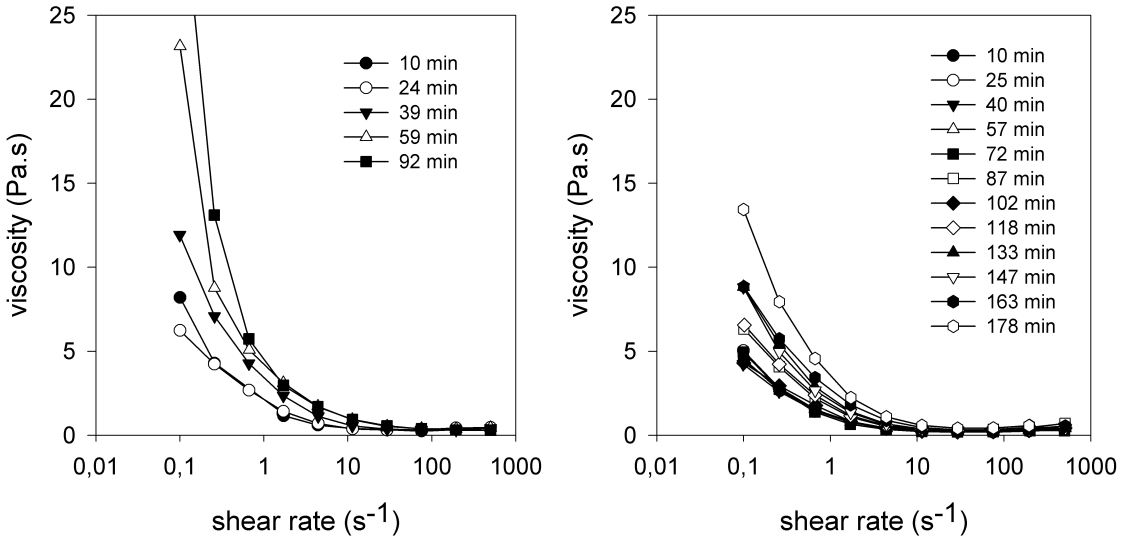


Figure 2.6.: Shear stepped and shear ramp modes in viscometry tests

growth of hydration products and water consumption during cement hydration, the loss of water by evaporation and the loss of dispersing efficiency of the superplasticizer (or other water reducing admixtures) (Esping, 2007; Struble, 2001). The influence of hydration progress on the flow behaviour of cement pastes is illustrated in Figure 2.7. In this figure the evolution of flow curves of cement paste samples stored in a closed recipient at room temperature (about $25°C$) and cement paste samples stored in a closed recipient at approximately $0°C$ is compared. The rheology of cement paste samples stored at $0°C$ show much less dependence on time than cement pastes stored at $25°C$. It is well-known that at $0°C$ temperature the hydration reactions stop, in practice. Since chemical reaction kinetic's have an exponential dependence on temperature, decreasing temperature slows down the pastes rheology evolution . It should be noted that, in this case, the observed increase of shear stress (and viscosity), for a given shear rate, with time is irreversible; and it should not be confused with thixotropy. Thixotropy effects were mitigated by appropriate pre-conditioning of samples and a shear stepped test.

2.2.3. Rheological models

Many mathematical expressions of varying complexity and form have been proposed in the literature to model non-Newtonian behaviour (Ferraris, 1999b; Hackley and Ferraris, 2001). Only a selection of the more widely used viscosity models for cementitious materials is presented here. To characterize the time-independent flow behaviours the Power-law, Bingham and Hershel-Buckley models can be used. These models are well suited for studying materials over a small shear rate range, under equilibrium steady flow conditions. To describe the time-dependent fluid behaviour (transient flow) of a



(a) (b)

Figure 2.7.: Influence of cement hydration reactions on the evolution of flow curves of cement paste: (a) without conservation, at about $25°C$, and (b) with conservation, at about $0°C$

suspension the "Coagulation Rate Theory", developed by Hattori and Izumi, can be used (Wallevik, 2003b), or a simpler model like the one proposed by Coussot et al. (2002).

Power-law (or Ostwald-de Waele)

The Power-law allows describing the general non-Newtonian behaviour in materials that show a negligible yield stress and a varying differential viscosity. The relationship between shear stress and shear rate is of the form

$$\sigma = k\dot{\gamma}^n \tag{2.5}$$

where k and n are two curve-fitting parameters. For shear-thinning fluids, n assumes a value between zero and one; while for shear-thickening n will be greater than one. When n equals one the equation (2.5) reduces to equation (2.1), which describes the Newtonian behaviour. The value of k can be viewed as the value of viscosity at unity shear rate.

Bingham

The Bingham relation describes the behaviour of viscoplastic fluids exhibiting yield stress. The ideal Bingham material is an elastic solid at low shear stress values and a

Newtonian fluid above a critical value called the Bingham yield stress. The relationship between shear stress and shear rate is of the form

$$\sigma = \sigma_0 + \eta_{pl}\dot{\gamma};\ \sigma \geq \sigma_0 \tag{2.6}$$

$$\dot{\gamma} = 0;\ \sigma < \sigma_0 \tag{2.7}$$

where σ_0 and η_{pl} are two curve fitting parameters, that can respectively be interpreted as yield stress and plastic viscosity. The Bingham model can describe the viscosity characteristics of a fluid with yield stress where viscosity is independent of shear rate, as shown in Figure 2.2.

Herschel-Bulckley

The Herschel-Bulkley model can be seen as a combination of the Bingham and Power-law models, to describe viscoplastic materials exhibiting a yield stress and a non-linear flow curve above the yield stress. The relationship between shear stress and shear rate is of the form

$$\sigma = \sigma_0 + \eta_{pl}\dot{\gamma^n};\ \sigma \geq \sigma_0 \tag{2.8}$$

$$\dot{\gamma} = 0;\ \sigma < \sigma_0 \tag{2.9}$$

where σ_0 , η_{pl} and n are the three curve fitting parameters. With the use of the third parameter, this model provides a somewhat better fit to some experimental data.

Hattori-Izumi

Hattori and Izumi developed the "Coagulation Rate Theory" which can be used as a mathematical tool to describe thixotropy (Wallevik, 2003b). According to this theory, the viscosity of a suspension as a function of time is given by

$$\eta = B_3 J_t^{2/3} = B_3 \left[n_3 \frac{U_0 \left(\dot{\gamma} H t^2 + 1\right) + Ht}{\left(Ht + 1\right)\left(\dot{\gamma} t + 1\right)} \right]^{2/3} \tag{2.10}$$

where B_3 is the friction coefficient between particles; n_3 is the number of particles; U_0

is the initial degree of dispersion and H is the coagulation rate constant (Wallevik, 2003b). The understanding of equation (2.10) and the concepts behind this theory is not straightforward; a further explanation is given in (Wallevik, 2003b). This model was applied and further developed in the numerical simulations carried out by Wallevik (2003a).

Coussot

Coussot et al. (2002) suggested a simple model where viscosity is an increasing function of λ, a parameter related to flocculation level inside the material, and is given by

$$\eta = \eta_0 \left(1 + \lambda^n\right) \tag{2.11}$$

where η_0 is viscosity at infinite shear rate when λ tends toward zero and n is a constant positive parameter. An evolution equation is added

$$\frac{d\lambda}{dt} = \frac{1}{\theta} - \alpha\dot{\gamma}\lambda \tag{2.12}$$

where $\frac{1}{\theta}$ is the flocculation term and the second term in equation (2.12) can be associated with the deflocculation rate (Coussot et al., 2002). This model has been used by Roussel to analyse rheological measurements obtained on cement pastes (Roussel, 2005).

2.3. Rheological characterization

2.3.1. Measurement instruments

There are essentially two methods for the rheometric measurements of fluids: the capillary and the rotational methods (see Figure 2.8). In capillary methods, the test fluid is made to flow through a narrow tube because of hydrostatic or applied pressure. In rotational methods the test fluid is continuously sheared between two surfaces, one or both of which are rotating (Hackley and Ferraris, 2001). Measurement instruments can be one of two types: a viscometer or a rheometer (see Figure 2.8). A viscometer is an instrument that principally allows measuring viscosity (or more precisely apparent viscosity); it is simpler in design and less expensive than rheometers. In opposition, a rheometer is an instrument used for the measurement of rheological properties over a varied and extended range of conditions. A rotational rheometer allows a sample to be

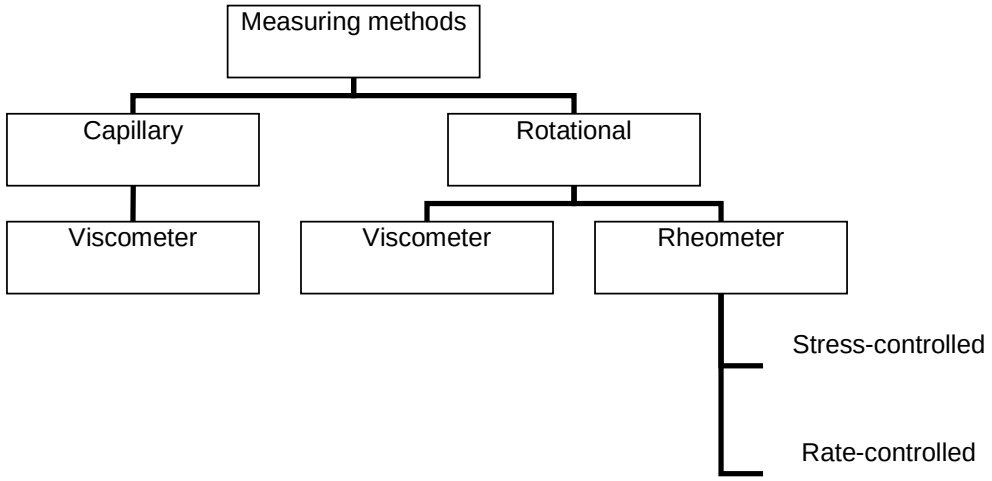


Figure 2.8.: Measurement methods and instruments (Hackley and Ferraris, 2001)

sheared for a defined period, under controlled shear stress (or shear rate) and under controlled temperature conditions. Rotational rheometers can also incorporate oscillatory and normal stress tests to characterize viscoelastic properties of samples (Hackley and Ferraris, 2001). For these reasons, rotational rheometers are better suited to characterize the complex non-Newtonian behaviour of cement pastes.

2.3.2. Rotational rheometers

Rotational rheometers are high-precision instruments that can be sub-divided into: shear rate-controlled and shear-stress controlled instruments. Some instruments have the capability of operating in either stress-controlled or shear-rate controlled modes. Instruments producing oscillatory strains are available, and a few commercial systems permit measurement of the normal stress. The rotational rheometer CVO-100, from Bohlin Instruments, used in the current work has all these facilities, except the normal stress measurement. The main parts of this type of instrument are presented in Figure 2.9. In stress-controlled measurements, a constant torque is applied to the measuring tool in order to generate rotation, and the resulting rotation speed is then determined. The rotation speed is then converted into a corresponding shear rate, based on the geometry of the measuring tool. In rate-controlled measurements, a constant rotation speed is maintained and the resulting torque generated by the sample is determined using a suitable stress-sensing device, such as a torsion spring or strain gauge (Hackley and Ferraris, 2001).



Figure 2.9.: Main parts in the rotational rheometer used in the present work (CVO-100, from Bohlin Instruments): (a) gap size indicator; (b) device to apply a constant torque (or rotation speed) to the tool and a device to determine the shear rate (or stress) response, respectively; (c) measurement tool; (d) thermostatic bath with temperature control

Measuring tools

In the rotational rheometers the fluid can be sheared between rotating cylinders, cone and plate or parallel plates, as shown in Figure 2.10. The main advantages and disadvantages associated with these measuring tools are summarized in Table 2.2. For non-Newtonian fluids, even a simple determination of a shear rate versus shear stress is far from being straightforward. Direct measurements of shear rate can only be determined directly if it is constant (or nearly so) through the measuring tool employed. Very narrow shearing gap measuring tools provide good approximations to this requirement. But, a shearing gap size is required to ensure adequate bulk measurements (a gap size approximately 10 to 100 times the size of the largest 'particle' size (Chhabra and Richardson, 1999); the gap size must be at least 10 times larger than the mean particles size (Bohlin Instruments Ltd, 1994)), and this may conflict with the gap size required to ensure near constant shear rate, within the gap. This restriction is more important for both concentric cylinders and cone and plate tools, since in the case of parallel plates, the gap size can be adjusted.

For cementitious materials, the concentric cylinders is the most commonly used measuring tool (Saak, 2000; Esping, 2007). Several configurations have been developed: 'cone' and 'hollow cavity' to overcome the end-effects due to shear flow at the bottom of the cylinder; 'double-gap' for low viscosity fluids (see Figure 2.11); 'vane' to

Table 2.2.: Comparison of different measuring tools (Bohlin Instruments Ltd., 2004)

Measuring tool	Referred to by	Advantages	Disadvantages
Concentric cylinder	diameter of the inner and outer cylinde	- more sensitive for low shear rate and low viscosities; - presented in several configurations (see Figure 2.11)	- larger sample volumes; - shear rate/stress varies slightly across the gap; - not so easy to clean; - larger mass and inertia, which can be problematic in oscillatory tests ; - not compatible with flat thermostat systems
Cone and plate	diameter and cone angle	- easy to clean; - small sample volume; - convenient for sample placement; - shear rate is constant throughout the sample; - gap size is fixed for each geometry type; - compatible with flat thermostat systems.	- sensitive to the gap size; - not adequate for temperature sweeps; - gap size is limited by the maximum particle size
Parallel plate	diameter of the the upper plate	- easy to clean; - small sample volume; - convenient for sample placement; - adjustable gap size; - compatible with flat thermostat systems	- shear rate varies across the sample;

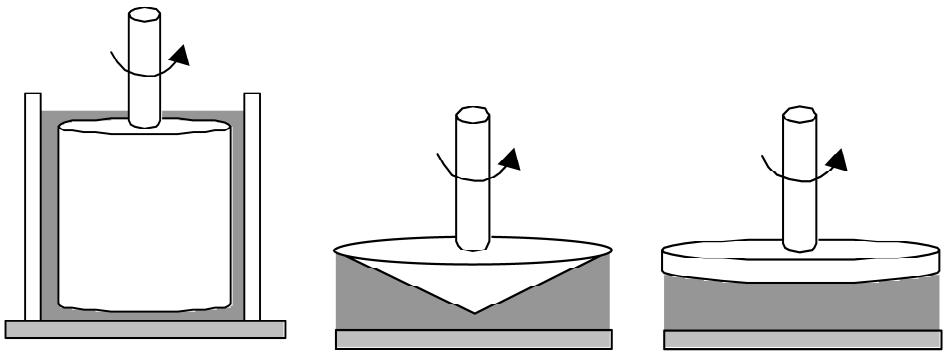


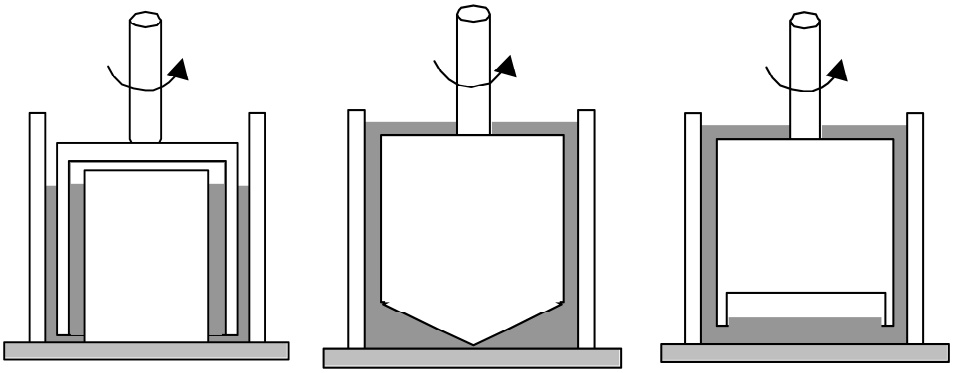
Figure 2.10.: Measuring tools available for rotational rheometers: (a) concentric cylinder; (b) cone and plate; (c) parallel plate (Hackley and Ferraris, 2001)

eliminate slippage[1] (see Figure 2.12) (Saak, 2000; Hackley and Ferraris, 2001; Esping, 2007). In addition, to prevent slippage the surface of the cylinder can also be sawn or otherwise roughened (Bohlin Instruments Ltd., 2004). A well-known commercial apparatus using this system is the BML rheometer for concrete (Wallevik, 2003b). The cone and plate tool is another widely used measuring tool. The small cone angle (generally, $\leq 4°$) ensures that the shear rate is constant throughout the shearing gap, this being of particular advantage when investigating time-dependent and non-Newtonian materials, because the entire sample experiences the same shear history (Chhabra and Richardson, 1999). In contrast to the cone and plate tool, with the parallel plates the shear rate varies radially and the gap height may be varied (Chhabra and Richardson, 1999). The large gap sizes available can be used to overcome the limitations encountered using the cone and plate, such as gap size as compared to maximum particle size. A well-known commercial apparatus using the rotating parallel-plates system is the BTRHEOM rheometer for concrete (Ferraris, 1999b).

Temperature control and moisture loss prevention

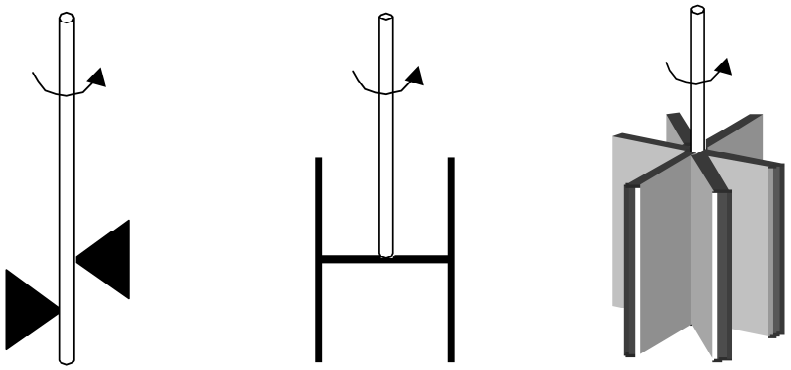
Temperature control is extremely important when making rheological measurements. In the CVO-100 rheometer (Bohlin Instruments) the temperature control units are mounted in a clamp on the base of the instrument as illustrated in Figure 2.9 (d); it provides temperature control by circulating water from a bath. When dealing with high concentration samples of low volume, even low moisture loss can also have a critical effect on measured rheological properties. To minimise moisture loss during rheological tests a vapour hood incorporating a solvent trap (filled with water) was employed (see Figure 2.13) (Bohlin Instruments Ltd., 2004).

[1] Formation of a water-rich layer near the smooth walls.



(a) (b) (c)

Figure 2.11.: Different configurations for concentric cylinders: (a) double gap; (b) cone and plate at the bottom; (c) hollow cavity at the bottom to trap air (Hackley and Ferraris, 2001)



(a) (b) (c)

Figure 2.12.: Different configurations for vane geometries used in concrete rheometers: (a) two-point test (Tattersall); (b) IBB; (c) BML (Hackley and Ferraris, 2001)

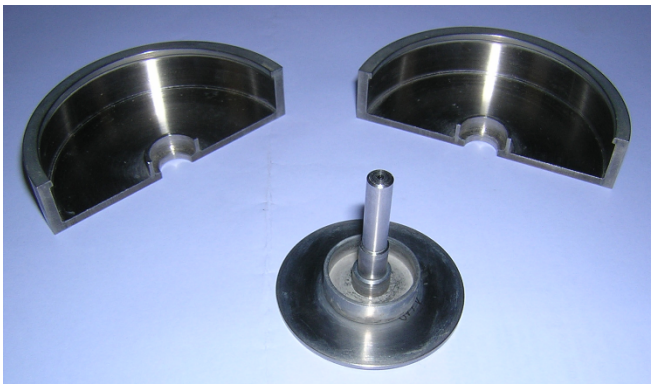


Figure 2.13.: Vapour hood incorporating a solvent trap

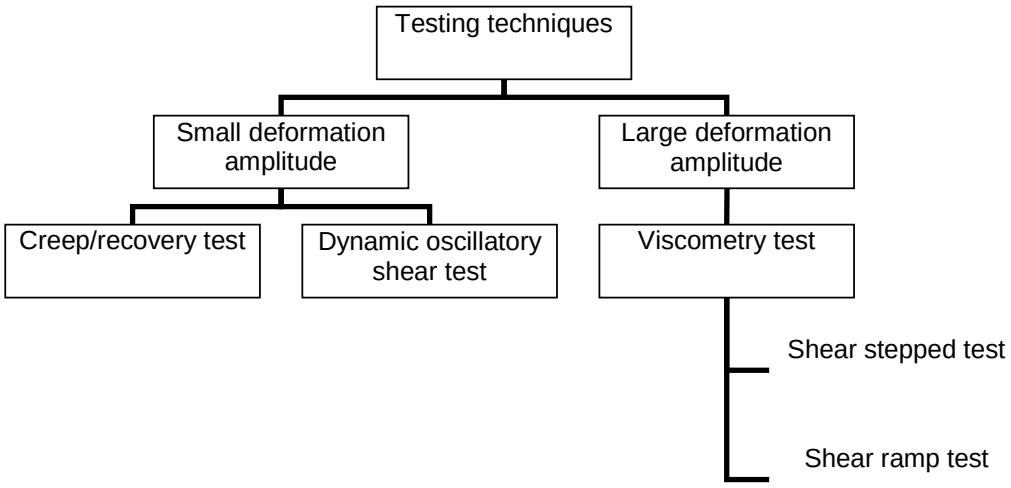


Figure 2.14.: Rheological testing techniques (Bohlin Instruments Ltd, 1994)

2.3.3. Testing techniques

Rheological testing techniques available in a rotational rheometer can be divided in two groups depending on the amplitude of shear strain rates applied during the test, namely, small and large amplitude deformation tests (see Figure 2.14). Both viscometry tests (shear stepped and shear ramp) can be used to characterize the flow behaviour of fluid materials, or to obtain flow curves like those presented in Figure 2.2. In a stepped shear test individual shear values are selected and each shear is applied for a given time, defined by the user; shear rate, shear stress and viscosity are recorded for each shear level. In opposition, in a ramp shear test a continuously increasing or decreasing shear is applied and measurements are taken at time intervals defined by the user. If one is interested in measuring the progressing changes in cement paste due to hydration, a viscometric test is not adequate because the shear rates necessary to cause flow are 'too high', thus breaking the fragile hydrated microstructure. In this case, creep/recovery or low-amplitude oscillatory tests can be used (Struble and Sun, 1995; Zhang, 2001). The deformations involved in these tests are small and kept within the linear viscoelastic region, so the structural build-up can be monitored over time without destroying the structure (Struble and Sun, 1995; Zhang, 2001).

In creep/recovery tests, a stress is applied for a time period (defined by the user) and resulting shear strain is measured. Since the change of strain will depend upon the applied stress, results are usually presented as 'creep compliance' ($J = shear\ strain/shear\ stess$) versus time. Recovery compliance is also measured when stress is removed. The creep/recovery behaviour for an elastic solid is quite distinct from that observed for a viscous fluid (Struble et al., 1998). In oscillatory shear test an oscillating shear stress (σ) (for example, a cosine wave) continuously excites the sample, thus the induced strain

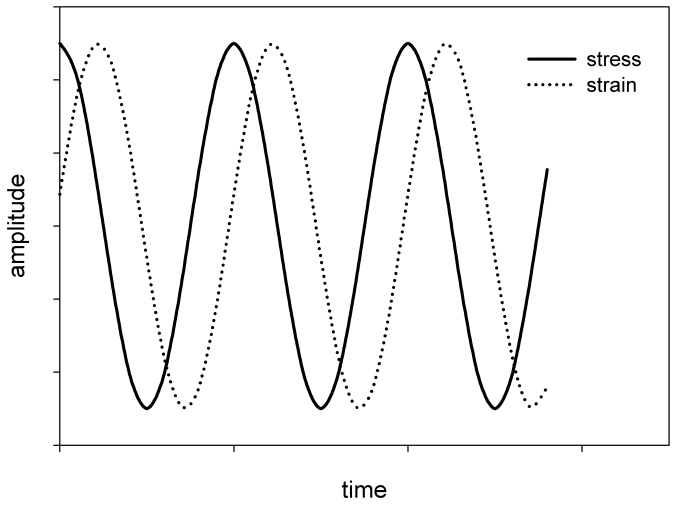


Figure 2.15.: Oscillatory shear strain out-of-phase with stress by a phase angle of δ

response (γ) will also follow a cosine wave equation as follows

$$\sigma = \sigma_0 \cos(wt) \tag{2.13}$$

$$\gamma = \gamma_0 \cos(wt - \delta) \tag{2.14}$$

where σ_0 is stress amplitude; γ_0 is strain amplitude; w is angular amplitude; t is time; and δ is the phase angle (Hackley and Ferraris, 2001)(see Figure 2.15). For an ideal solid, since strain is directly related to stress, it will be at a maximum when stress is maximum and zero when stress is zero, thus the phase angle will be $\delta = 0°$. If the material is purely viscous, it will be shear strain rate that is in phase with applied stress and not strain, the phase angle will be $\delta = 90°$. In this type of test the material rheological characteristics are described in terms of the shear storage modulus G' (representing the elastic response of the material), and the shear loss modulus G''(representing the irreversible viscous response) calculated as

$$G' = \frac{\sigma_0}{\gamma_0} \cos\delta \tag{2.15}$$

$$G'' = \frac{\sigma_0}{\gamma_0} \sin\delta \tag{2.16}$$

There have been relatively few studies examining viscoelastic properties of cement

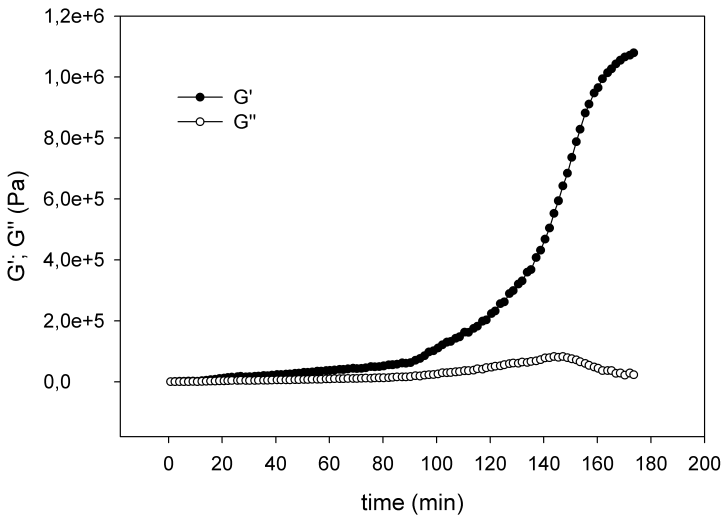


Figure 2.16.: Evolution of storage and loss modulus of a cement paste as a function of hydration time (frequency=$1Hz$)

pastes due primarily to equipment limitations. The major challenge in applying small amplitude oscillatory technique to the cement paste is how to get reliable data. The storage modulus of paste can get as high as 10^6 Pa and the critical strain is very low (10^{-4}) (Zhang et al., 2001)(see Figure 2.16). Small shear strain results in low sensitivity while a too large shear strain leads to a microstructural breakdown (Zhang et al., 2001)(see Figure 2.17). Accurate measurements require a torsion bar that is sensitive enough to measure such small strains while stiff enough to overcome the high modulus of the cement suspensions.

Most rheological testing on cement paste is to measure viscosity, yield stress and thixotropy. To accomplish it, several methods are suggested in the literature, based on different testing techniques.

Viscosity

For non-Newtonian fluids, like cement paste, a multipoint flow curve has to be measured. A single point result of viscosity does not describe this material completely. It is possible that two cement pastes with completely different rheological properties generate the same value of viscosity at a given value of shear rate if the flow curves intersect at this point. As stated before, to reach equilibrium conditions at each measurement the stepped shear test is preferred.

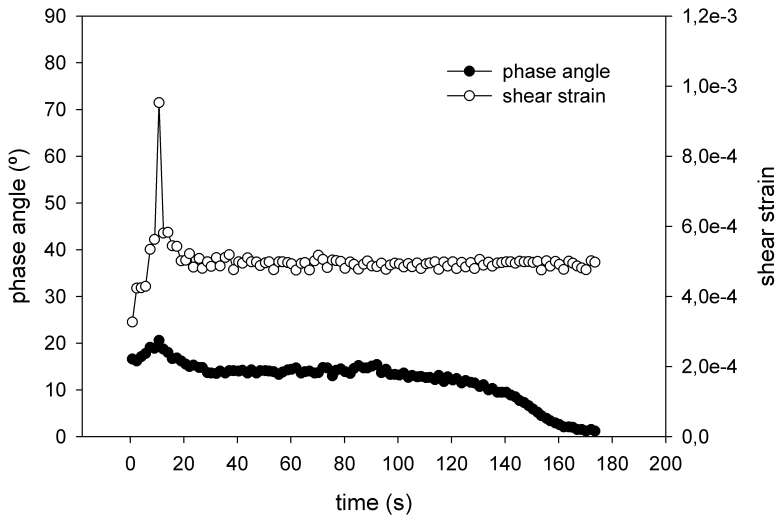


Figure 2.17.: Applied shear strain and phase angle as a function of hydration time (frequency=$1Hz$)

Yield stress

The most direct method for yield stress measurement is provided by stress-controlled rheometers; it involves applying a gradually increasing stress and monitoring the stress-time profile for an inflexion in the curve, i.e. the onset of flow. The development of viscoelastic effects is represented by the departure from linearity of the shear stress-time curve. From this curve, yield stress can be evaluated either from the point where the elastic response starts to diverge from its linearity (called static yield stress) or at the peak stress (called dynamic yield stress) (Saak, 2000) or the stress at the plateau beyond the peak (called equilibrium yield stress) (see Figure 2.18) (Møller et al., 2006). Struble et al. (1998) used multiple creep/recovery tests to determine changes in yield stress during hydration. This method is probably the most accurate way of characterizing the yield stress but it can be a very time consuming process (Møller et al., 2006).

Another possibility is an indirect determination of the yield stress, which involves the extrapolation of experimental shear stress versus shear rate data, from a flow curve, to zero shear rate. Often this is performed by fitting a suitable rheological model representing the fluid, where the yield stress corresponds to one of the model parameters (see paragraph 2.2.3). The yield stress measurement is very sensitive to the experimental procedure, the measuring tool, the occurrence of slippage and depends on the applied shear rate (Møller et al., 2006; Saak, 2000). Although it is often considered as a single fluid parameter, the yield stress as a true property of a suspension is a controversial issue (Wallevik, 2003b; Saak, 2000). Based on recent experimental findings, a model was suggested to describe a interplay between yield stress and thixotropy (see equation (2.11) and (2.12)) (Coussot et al., 2002; Møller et al., 2006). Thixotropy and yield

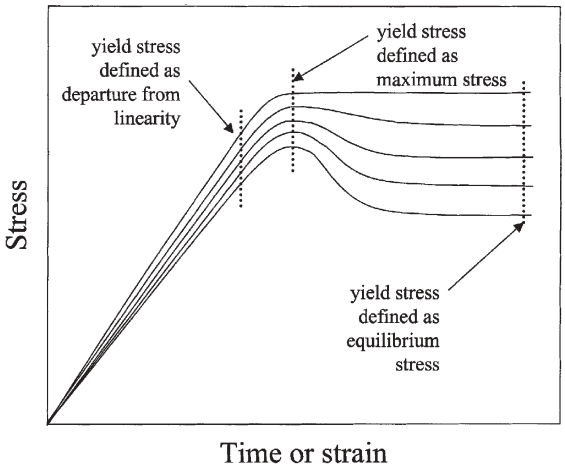


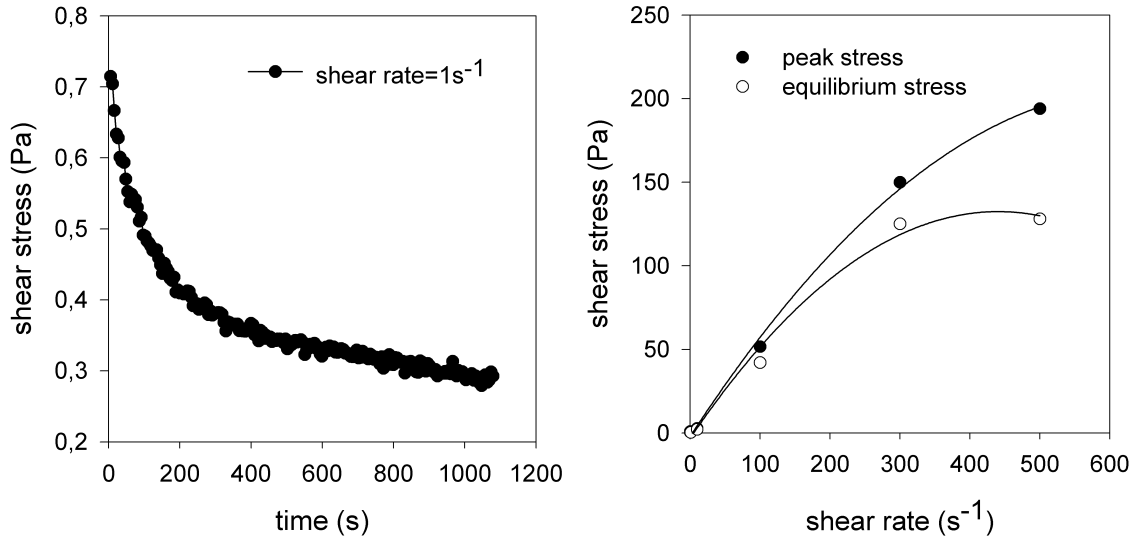
Figure 2.18.: Schematic time evolution of the stress for imposed shear rate experiments at different imposed rates and different definitions of yield stress, namely, static, dynamic and equilibrium (Møller et al., 2006)

stress are believed to be caused by the same fundamental physics, but are traditionally modelled as separate phenomena (Møller et al., 2006).

Thixotropy

The most common method used to quantify thixotropy is to determine the enclosed area between the up- and down-curves, obtained with a shear-ramp test (Saak, 2000; Wallevik, 2003b). In a shear-ramp test, shear stress (or shear rate) is ramped at a fixed speed up to a maximum value, then ramped back down at the same speed to the beginning (often called hysteresis loop) (see Figure 2.5). The test result depends on the shear history of the sample and on how rapidly the stress or shear rate was ramped.

Another possible approach consists in applying a constant shear stress (or rate) until a equilibrium state is reached. The equilibrium shear stress value represents the minimum stress that can be obtained at a given shear rate (see Figure 2.19 (a)). The difference between the peak stress (σ_{peak}) and equilibrium stress (σ_{eq}) is a measure of thixotropy. Using several samples at different shear rates, the equilibrium approach can be used to construct the peak as well as equilibrium flow curves (see Figure 2.19 (b)). This method is considered superior to the hysteresis loop approach but it has the disadvantage, for cement pastes, of requiring a large number of samples and tests to obtain the flow curves (Saak, 2000). Saak (2000) suggested a combined approach between equilibrium and hysteresis approaches to capture the general trend of peak an equilibrium stress flow curves while using only one test.



(a) (b)

Figure 2.19.: (a) Equilibrium stress measurement of cement paste, and (b) evolution of peak and equilibrium flow curves for cement paste

2.3.4. Measuring sequence setup

The measuring sequence setup of all rheological measurements refered to in Chapter 6 is presented in this section. Rheological characterization of cement pastes is carried out focused only on flow behaviour. Yield stress and plastic viscosity parameters were determined from flow curve data by using the Bingham model.

A rotational rheometer CVO-100, from Bohlin Instruments, was used. Data acquisition and control were performed with a PC-coupled to CVO-100 rheometer (see Figure 2.20). The measuring device consisted of a cone and plate geometry. The cone diameter was 40 mm with a cone angle of 4°, providing a gap of 150μm. A viscometry test (shear stepped), in shear rate control mode, was selected to obtain equilibrium flow curves. Before measurements a pre-conditioning procedure was applied. The temperature was controlled and kept constant at $25 \pm 0,1°C$ during all testing sequence. A pre-shear was applied to homogenize the sample during 45 seconds at a shear rate of $200\,s^{-1}$, followed by a resting period of 100 seconds (with no shear applied). During the measurements the rheometer was programmed to perform a 12-step logarithmic increase of shear rate ranging from $0,1\,to\,200\,s^{-1}$ and back again to complete a full cycle. Each measurement consisted of a delay and integration times. The shear rate was applied for the delay time (set equal to 10 s), but no information was recorded during this period. The average value of shear stress was measured for the integration time (set equal to 5 s) and the viscosity was then calculated as the ratio of average shear stress by imposed shear rate. The complete testing sequence as a function of time, including the pre-conditioning and

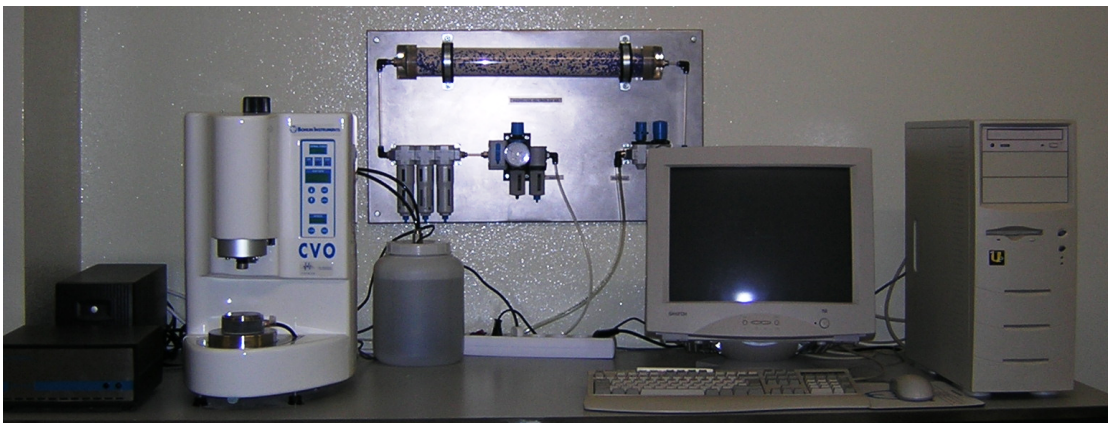


Figure 2.20.: Rotational rheometer (Bohlin CVO-100) used in this study

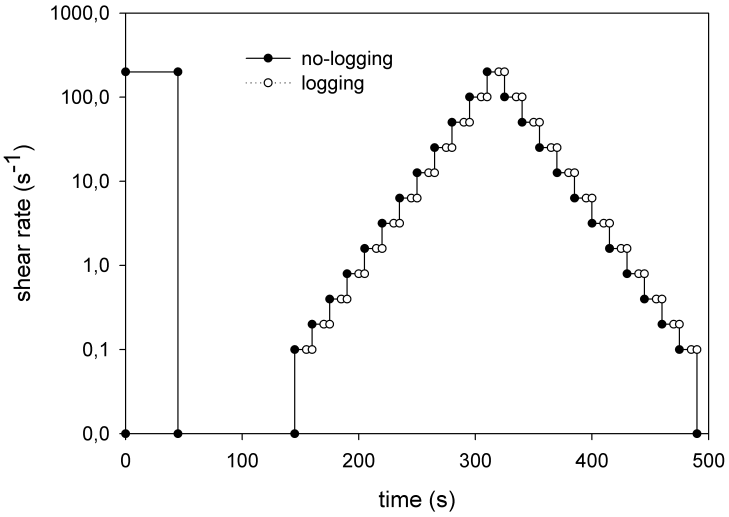
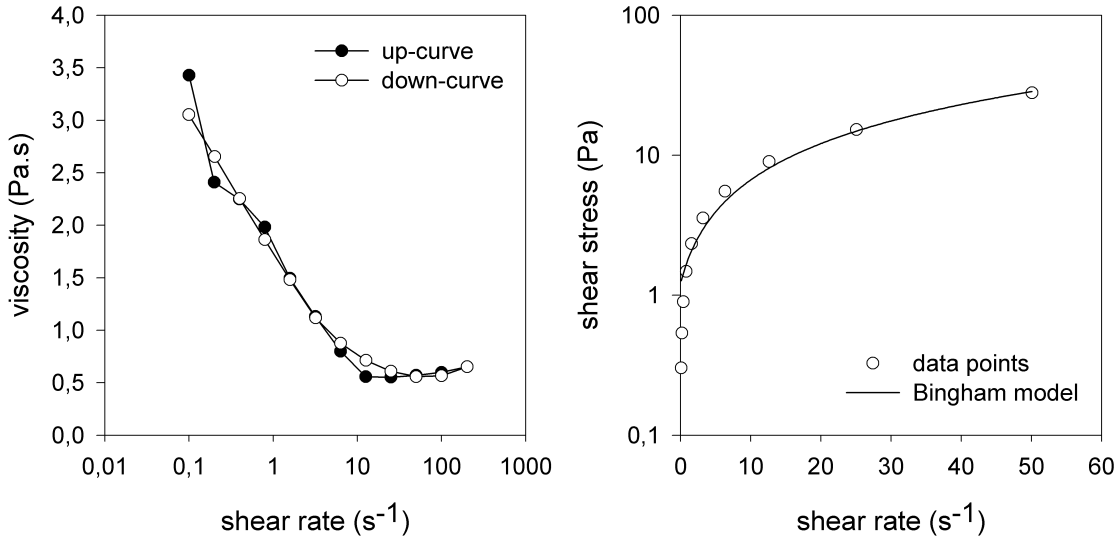


Figure 2.21.: Testing sequence: first, pre-shear; second, waiting period; and, third, measuring period

measuring parts, is presented in Figure 2.21.

The descending part of the obtained flow curves were fitted to the Bingham model (see equation (2.6)), as illustrated in Figure 2.22. Only data points corresponding to a shear-thinning behaviour were used; in some cases the last one or two data points were excluded because the material started to exhibit a shear thickening behaviour for these higher shear rates. The cement paste used as example in Figure 2.22 can be characterized by a yield stress of 1,218 Pa and a plastic viscosity of 0,545 Pa.s. The adjusted model parameters (yield stress and plastic viscosity) were taken as the rheological test results for the study presented in Chapter 6.

As can be observed in Figure 2.23, the area enclosed between the up- and down- curves is almost zero, meaning that the adopted measuring sequence was effective to eliminate the time-dependent effects, such as thixotropy. The selected measuring tool (cone and



(a) (b)

Figure 2.22.: (a) Up- and down-flow curves, and (b) fitted Bingham model to the down-curve data

plate; 4°/40 mm), which has the major advantage of imposing a constant shear rate through the sample, may be subject to some criticism. The corresponding gap size is of 150 μm allowing for a maximum 'particle size' of 15 μm, according to (Chhabra and Richardson, 1999). As can be observed in tables C.1 to C.10, in Appendix C, the coarser cements have particles of size as high as 90 μm. On the other hand, the mean particle size of studied cement pastes was around 15 μm or lower since limestone filler (finer than cement) was added to the mixtures, thus satisfying the requisite established in (Bohlin Instruments Ltd, 1994). Furthermore, a superplasticizer was always included preventing the formation of large flocculates. Concerning the selected rheological model, other authors suggested more complex models to characterize cement pastes behaviour (Yahia and Khayat, 2001a). In the present study, the Bingham model was selected for its simplicity (a low number of adjusting parameters) leading to rheological parameters which are in good agreement with empirical test results (see Chapter 6).

2.4. Fresh concrete, mortar and cement paste as particle suspensions

Fresh concrete, mortar and cement paste can be considered as different types of suspensions (Barnes et al., 1989; Struble, 2001; Walraven, 2003). A particle suspension consists of two phases, namely, the suspended particles and the suspending medium. Fresh concrete consists of particles with a broad range of sizes, shape, mass and surface

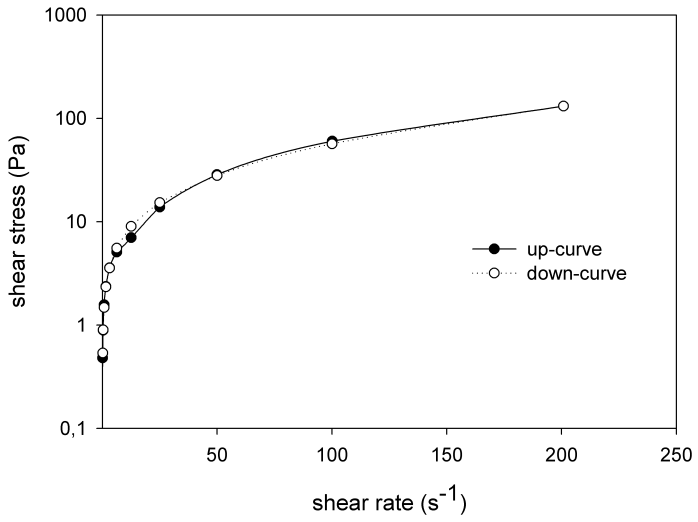


Figure 2.23.: Up- and down-flow curves showing almost zero enclosed area

texture suspended in water. This applies also to mortar and cement paste.

2.4.1. Factors influencing the rheology of suspensions

The rheological behaviour of suspensions is controlled mainly by the volume fraction of solid particles (concentration), the extent to which the particles are agglomerated or flocculated, particle shape characteristics and particle size distribution (Barnes et al., 1989; Struble, 2001).

In general, three types of forces act on particles in a suspension: colloidal, Brownian and viscous forces. Colloidal forces can cause a net attraction or repulsion between particles due to such a factors as van der Waals forces and electrostatic charges. This type of interactions between particles will be further discussed in Chapter 3. Brownian forces cause a rapid and random motion in very small particles (smaller than 1 μm) (Barnes et al., 1989; Struble, 2001). Brownian motion prevents settling of small particles even though they are more dense than the suspending fluid. The viscous forces are proportional to the velocity difference between particles and the surrounding medium. Thus, the suspension viscosity depends on the viscosity of the suspending medium (Barnes et al., 1989). When a suspension is at rest (or under very low shear rates) Brownian or colloidal forces dominate, for a given solids volume concentration below a critical value (ϕ_c) (Koehler and Fowler, 2007). A critical solids volume concentration is obtained when a network of contacting particles exists and friction forces become dominant. Maximum solids volume concentration (ϕ_m) is defined as the solids volume concentration at which particle interference makes flow impossible and the viscosity approaches infinity (see Figure 2.24). Suspensions with low solids volume fractions and low shear rates exhibit

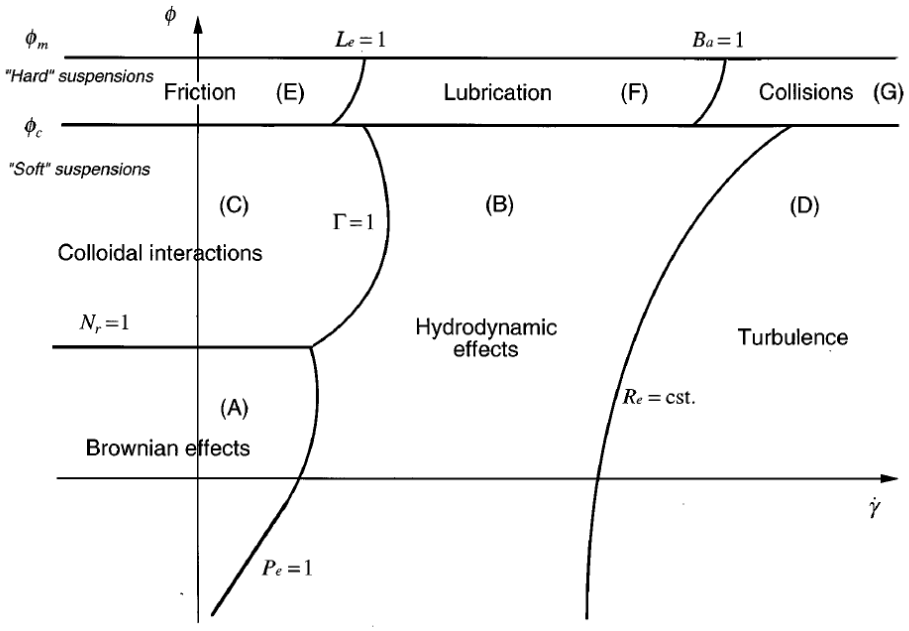


Figure 2.24.: Conceptual framework for rheology of concentrated suspensions (Koehler and Fowler, 2007)

shear-thinning behaviour and are dominated by Brownian motion. As the concentration is increased, colloidal interactions dominate at low shear rates and the suspension exhibits viscoelasticity, thixotropy, and yield stress (see Figure 2.24). If shear rate is increased from friction zone, the imposed velocity gradient imposes an orientation of the particle structure, a thin layer of fluid exists between particles which lubricates the contacts, then the viscosity is lowered (shear-thinning behaviour).

Colloidal particles forces dominate to a large extent the complex behaviour and time-dependent behaviour of cement paste. Some authors argue that rheology of fresh concrete is much simpler than for dilute cement paste, due to the large volume fraction of coarser particles (Wallevik, 2003b). For most sizes of aggregates, only viscous forces are relevant. Thus the following interpretation of the Bingham model parameters (see equation (2.6)) for mortar/concrete can be applied, as suggested by Ferraris and Larrard (1998) (see Figure 2.25):

- the term σ_0 is a contribution of the aggregate skeleton (results of friction between the particles) and is an increasing function of ϕ/ϕ_m and
- the term $\eta_{pl}\dot{\gamma}$ is a contribution of the suspending medium; where η_{pl} depends on the viscosity of the suspending fluid and is an increasing function of ϕ/ϕ_m.

Thus, the solid particles concentration relative to the maximum solid concentration (ϕ/ϕ_m) is a determining parameter for the rheology of mortar/concrete suspensions (de Larrard, 1999). It determines the number and nature of the contacts between particles just before initiating flow and the average distance between particles, during flow.

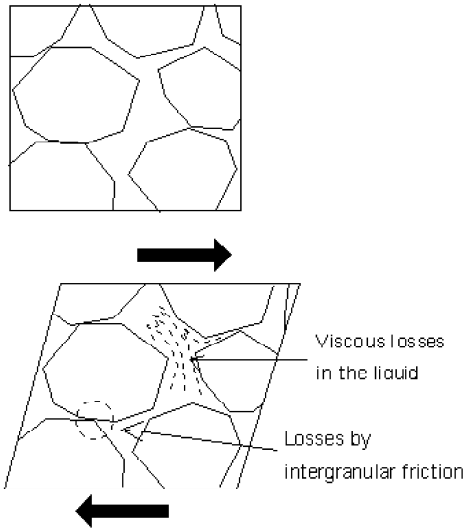


Figure 2.25.: Physical interpretation of the Bingham model (de Larrard, 1999)

An excess of fluid, beyond the minimum necessary to fill the pores, is necessary to reduce the friction between the particles. Thus, typical solid particles concentration in cement suspensions is significantly lower than ϕ_m. Besides, solid particles concentration is higher in concrete than in cement paste, is around 0,8 in the case of ordinary concretes, whereas, in the case of SCC, is around 0,6 (Roussel, 2006a). As a reference, the maximum packing fraction of monosized spheres is 0,74 in hexagonal structure and 0,52 in a cube structure. Mortar with water/cement/sand ratio 0,5/1/3 has $\phi_m \sim 0,75$ and high strength concrete can go up to 0,85 or higher (Wallevik, 2003b). Another important difference between cement paste and concrete is the range of strain rates. During placing, concrete is sheared at only about 1 to 10 s^{-1}; while cement paste (in concrete) experiences significantly higher shear rates (60 to 80 s^{-1}), because the cement paste is 'squeezed' between the aggregates (Wallevik, 2003b; Saak, 2000; Ferraris, 1999a). The shear rate applied to cement paste is around five times higher in the case of ordinary concrete and around two to three times higher in the case of SCC.

Various models can be found in the literature for the viscosity of suspensions. For low solids volume concentration ($\phi \leq 0,01$) suspensions of monosized spheres, Einstein suggested the following relationship

$$\eta = \eta_s \left(1 + 2,5\phi\right) \tag{2.17}$$

where η is the viscosity of the suspension and η_s is the viscosity of the suspending medium (Barnes et al., 1989). This equation clearly shows that particles increase viscosity of a suspending medium as a function of their concentration; but the effects of particle size and interaction between particles are not taken into account (Barnes et al.,

1989). For concentrated suspensions Krieger and Dougherty developed the following relationship

$$\eta = \eta_s \left(1 - \frac{\phi}{\phi_m}\right)^{-[\eta]\phi_m} \tag{2.18}$$

where ϕ_m is the maximum solids volume concentration and $[\eta]$ is called the intrinsic viscosity defined as

$$[\eta] = \lim_{\phi \to 0} \frac{\left(\frac{\eta}{\eta_s} - 1\right)}{\phi} \tag{2.19}$$

In Krieger and Dougherty relationship, the apparent viscosity is expressed as a function of solids volume concentration with additional parameters, namely, ϕ_m and $[\eta]$. $[\eta]$ accounts for particle shape characteristics while ϕ_m accounts for particle shape characteristics, degree of flocculation, and particle size distribution (Struble and Sun, 1995). A material with higher maximum solids fraction, due to favourable particle shape characteristics, particle size distribution, and lack of flocculation, results in lower relative viscosity at a given solids volume fraction (Barnes et al., 1989). The maximum solid fraction and intrinsic viscosity vary with shear stress and shear rate (Barnes et al., 1989; Struble and Sun, 1995). The Krieger-Dougherty equation has been applied successfully to cement paste (Struble and Sun, 1995; Vikan, 2005) and mortar (Toutou et al., 2005), but was not so adequate to model concrete (Toutou et al., 2005). For cement paste dispersed with superplasticizer, Struble and Sun (1995) estimated the intrinsic viscosity to be approximately 5 and maximum solids volume fraction to be approximately 0,7. Vikan estimates of maximum volume fractions of solids ranged from 0,5 to 0,6 and intrinsic viscosity at about 5 (Vikan, 2005). De Larrard (1999) found that plastic viscosity of mortar and concrete increases exponentially with normalized solid concentration (ϕ/ϕ_m).

2.5. Concrete rheometeres

Unlike mortar and cement paste, concrete requires specially designed rheometers. Designing a rheometer for testing fresh concrete presents considerable challenges. The suspension contains particles with a wide range of sizes (from less than 1 μm to 30 mm) (Esping, 2007). This wide range results from the heterogeneous concrete composition, which includes cement (5μm to 60μm), mineral fillers ($<$ 1 μm to 100 μm), fine aggregates (0,1 mm to 4 mm) and coarse aggregates (4 mm to 30 mm or higher in some special concretes). The larger particles tend to settle due to gravity and this segregation is aggravated during shear due to the thixotropic behaviour of cement paste. The

occurrence of slippage is also a common problem with concrete rheometers.

The smallest gap in the instrument should be 3 to 5 times the largest diameter of the coarse aggregate to obtain a representative sample and to avoid the interlocking of the aggregates that will prevent flow (Ferraris et al., 2001a). On the other hand, with concentric cylinders, the gap between the cylinders needs to be relatively small as compared to their diameters (the ratio of the radii of the two cylinders should be between 1 and 1,1) to provide a uniform shear rate (Ferraris et al., 2001a). As an example, a concrete with an aggregate maximum size of 10 mm, would require a gap size of 50 mm and an inner and outer cylinders with a radius of 0,5 m and 0,55 m, respectively. Such a 'wide-gap' rheometer was built by Coussot (CEMAGREF) and used for fresh concrete to validate the results obtained with a 'narrow-gap' rheometer (BTRHEOM) developed at the Laboratoire Central des Ponts et Chaussées (LCPC) (Ferraris et al., 2001a). Obviously, this type of instrument is unsuitable for field use because it would not be easily transported outside the laboratory.

To overcome some of these limitations, various rheometers with measuring tools consisting of a shaft with blades were developed after the "Two-point-test" workability apparatus designed by Tattersall. The original "Two-point test" was further modified and improved by Beaupré (IBB) and by Wallevik and Gjϕrv (BML) (see Figure 2.12). There is also a rheometer that uses the parallel plate measuring tool (BTRHEOM) that was developed by de Larrard et al. at LCPC. Further descriptions of these tests can be found elsewhere (Banfill et al., 2000).

2.6. Rheology of SCC

2.6.1. Target area (Bingham parameters)

As long as steady state flow is reached, the rheological behaviour of fresh concrete may be simply described using the Bingham or Herschel-Bulkley models (Roussel, 2005; Wallevik, 2003b). A wide range of SCC mixtures can be obtained. Wallevik (2003b) evaluated various SCC mixtures, from different countries, with the BML-rheometer, resulting in the area presented in Figure 2.26. SCCs exhibited almost no yield value, 0 to 60 Pa, and a wide range of plastic viscosity, 20 to more than 120 Pa.s (very variable between countries) (Wallevik, 2003b). The recommended combination of yield stress and plastic viscosity values for SCC by IBRI (ACM Centre, 2005) are represented by the inner area in Figure 2.26. The minimum slump flow values required to obtain SCC mixes with different plastic viscosities are also shown in Figure 2.26. The main difference between SCC and conventional concrete is the yield stress. The change in concrete yield stress is directly related to the paste rheology because of the dispersing

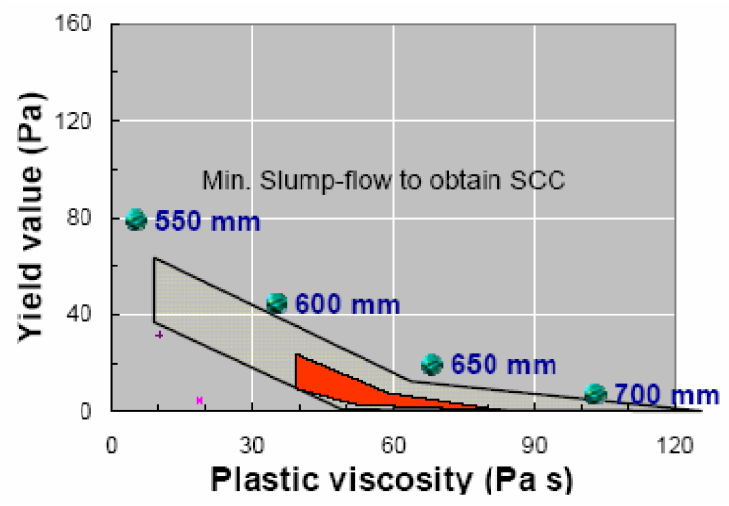


Figure 2.26.: Target area for SCC and corresponding slump flow (ACM Centre, 2005)

effect of superplasticizer, which acts on the paste level. The SCC plastic viscosity is not reduced to near zero because of the need for a sufficiently high paste viscosity to prevent segregation (in dynamic conditions) and the contribution of aggregates to increase solid particles concentration.

2.6.2. Thixotropy

Concrete contains thixotropic cement paste, therefore displays also a thixotropic behaviour (Roussel, 2005). Recent approaches to quantify thixotropic behaviour of SCC have focused on the flocculation at rest, because this has practical consequences on formwork pressure, multi-layer casting and stability of SCC. Over short timescales the reversible time-dependent effects (thixotropy) dominate while over larger time scales it is the hydration (irreversible) effects that dominate (Jarny et al., 2005). According to Roussel a Bingham model is sufficient to describe the steady state flow of fresh concrete and the yield stress at rest increases linearly as a function of time (Roussel, 2006a)(Roussel 2006), according to the following model

$$\sigma = (1 + \lambda)\,\sigma_0 + \eta_{pl}\dot{\gamma} \tag{2.20}$$

where the model parameters have the same meaning as presented in equations (2.6) and (2.11). The parameter λ evolves from an initial value of zero (just after mixing, maximum shearing phase) to a positive value according to equation (2.12). At rest (zero shear rate), the evolution of yield stress is given by

$$\sigma_0\,(t) = (1 + \lambda)\,\sigma_0 = \sigma_0 + A_{thix}t \tag{2.21}$$

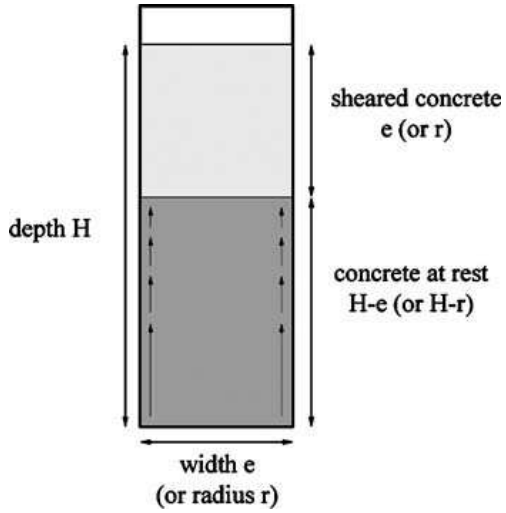


Figure 2.27.: Sheared and resting zones when concrete is cast from the top (Ovarlez and Roussel, 2006)

where A_{thix} is the flocculation rate of concrete that is fitted from experimental results; this parameter is of most interest for practical application of SCC (Roussel, 2007).

Formwork pressure

In the literature, contradictory values of lateral stresses in the formwork when casting with SCC can be found (Billberg, 2003). Initially, these differences were attributed to different casting rates, then it was concluded that the thixotropic behaviour of SCC plays also an important role (Billberg, 2003). The lateral stress is equal to the hydrostatic pressure when the casting rate is high or when the concrete is injected from the bottom of the formwork because the material is not able to flocculate and thus keeps on behaving as a fluid. The lateral stress does not reach the hydrostatic pressure when the material is cast from the top of the formwork slowly enough to flocculate and withstand the load of concrete cast above it. The lateral stress decreases quickly in the part where concrete is at rest (see Figure 2.27) because it builds up an internal structure (starts behaving as a solid) and has the ability to withstand the load from concrete cast above it, without increasing the lateral stress against the formwork (Ovarlez and Roussel, 2006). Ovarlez and Roussel proposed a model that physically links the consequences of thixotropy and the evolution of the lateral stress during and after casting; for further details on this model see (Ovarlez and Roussel, 2006).

Multi-layer casting

During placing, a layer of SCC has a short time to rest and flocculate before a second layer of concrete is cast above it. If it flocculates too much and its yield stress increases

above a critical value, then the two layers do not mix at all and, as vibrating is prohibited in the case of SCC, this creates a weak interface in the final structure. This can result in significant strength loss of hardened concrete (Roussel, 2007).

Stability of SCC

Due to density differences between the various concrete constituent materials, heterogeneities induced by gravity may occur in concrete, namely, bleeding and segregation (Roussel, 2006a). Bleeding concerns the water migration to the concrete surface, while segregation concerns the movement of coarser particles (upward or downward, depending on the density of particles relative to the density of the suspending medium). Segregation may occur in both static and dynamic conditions. In dynamic conditions other factors than gravity (the only present in static conditions) may induce segregation like the existence of obstacles or confined sections (Roussel, 2006a). The static segregation tendency in a given mixture depends on the yield stress of the suspending Bigham fluid and not on its plastic viscosity sections (Roussel, 2006a; Saak, 2000). During placing, the cement paste (inside the concrete) is deflocculated because of the high shear rates applied during the mixing and of the casting itself. This allows high deformability of concrete but, as soon as casting is over and before setting, gravity may induce sedimentation of the coarsest particles resulting in large heterogeneities of the hardened concrete, as it was observed during full-scale tests carried out during BACPOR research project (Nunes et al., 2005b). A thixotropic cement paste will, however, re-flocculate once at rest. Its yield stress will increase and could be sufficient to prevent the particles settling (Roussel, 2006a).

In conclusion, a thixotropic (high flocculation rate) or non-thixotropic (low flocculation rate) SCC mixture can be of interest depending on the application. A non-thixotropic SCC should be used in concrete slabs where the multi-layer casting problem is dominant and the segregation risk is reduced. In opposition, a thixotropic SCC should be used in the case of walls in order to minimize the lateral stresses in the formwork and segregation (Roussel, 2007). The substitution of cement with finer powders (higher surface area) such as silica fume or fly ash was found to increase flocculation rate (Roussel, 2007).

2.6.3. Computational model of concrete flow

To benefit from the full potential of SCC, numerical design of SCC mixtures with optimized performance relative to the geometry of the formwork, casting technique and configuration of reinforcement is needed (Gram et al., 2007; Roussel et al., 2007). Thus, recent studies are focusing on the development of computational tools to model fresh

concrete flow, based on its rheological parameters. Various types of software and simulation methods have been used:

- single fluid simulations (e.g. Computational Fluid Dynamics (Wallevik, 2003a; Roussel and Coussot, 2005; Thrane et al., 2005; Modigell et al., 2007; Waarde et al., 2007)
- numerical modelling of discrete particle flow (e.g. Distinct Element Method (Gram et al., 2007) and Dissipative Particle Dynamics (Martys and Ferraris, 2002) and
- numerical techniques allowing the modelling of particles suspended in a fluid (Roussel et al., 2007).

A general description of each of these computational techniques along with their advantages/disadvantages for the modelling of the flow of fresh concrete can be found in (Roussel et al., 2007).

3. Cement-superplasticizer interactions

3.1. Introduction

This chapter presents an overview of relevant literature on parameters affecting the cement-superplasticizer interactions.

Dispersion of cement particles is recognized as the main way by which superplasticizers improve the workability of concrete without increasing the water content (Björnström and Chandra, 2003; Flatt, 1999; Griesser, 2002). However, dispersion effect varies with type of cement, the production plant (for the same cement type) and type of superplasticizer (Flatt, 1999; Griesser, 2002; Hanehara and Yamada, 1999), as shown in Figure 3.1. Quantifying this effect is a difficult task and is further complicated by the ongoing hydration reactions of cement. Firstly, an overview of the basic chemical aspects of cement hydration is presented, after which the various physico-chemical concepts involved in cement-superplasticizer interactions are then reviewed. Finally, the influence of molecular structure parameters on the performance of polycarboxylate type superplasticizers is discussed more in detail, since this type of superplasticizer was used in the present work.

The present chapter provides theoretical background to discuss results presented in Chapters 5 and 6.

3.2. Portland cement hydration

Cement grains microcospically show a mosaic surface resulting from the different clinker phases, namely, C_3S, C_2S, C_3A, C_4AF (see Table 3.1) and gypsum. The first four minerals are formed during equilibrium conditions in the burning of cement clinker, while gypsum is added to the mill when clinker is ground to cement. The distribution of silicate and aluminate phases on the cement grain is determined by the milling process and the difference in resistance against fracture. Cement hydration starts as soon as water is added to the mix. The hydration of cement involves exothermic reactions, which may be measured by the heat generated as a function of time, using an isothermal calorimeter.

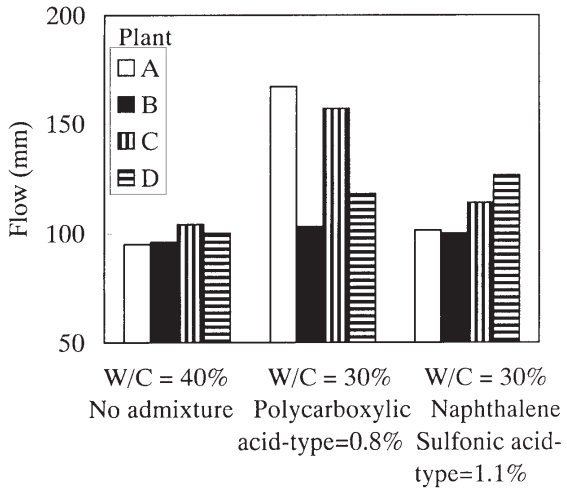


Figure 3.1.: Fluidity variation with superplasticizer type and producing plants (Hanehara and Yamada, 1999)

Table 3.1.: Main phases of Portland cement and their characteristics (Griesser, 2002; Jolicoeur and Simard, 1998; Moir, 2003)

Parameter	C_3S	C_2S	C_3A	C_4AF
Chemical formula	Ca_3SiO_5	Ca_2SiO_4	$Ca_3Al_2O_6$	$Ca_4Al_2Fe_2O_{10}$
Technical name	alite	belite	aluminate phase	ferrite phase
Typical range in clinker (%)	45 - 65	10 - 30	5 - 12	6 - 12
Reactivity	high	low	very high	low
Heat of hydration (J/g)	500	250	1340	420
Hydration product	C-S-H; CH	C-S-H; CH	ettringite; monosulfate	C_6AFH_{12}

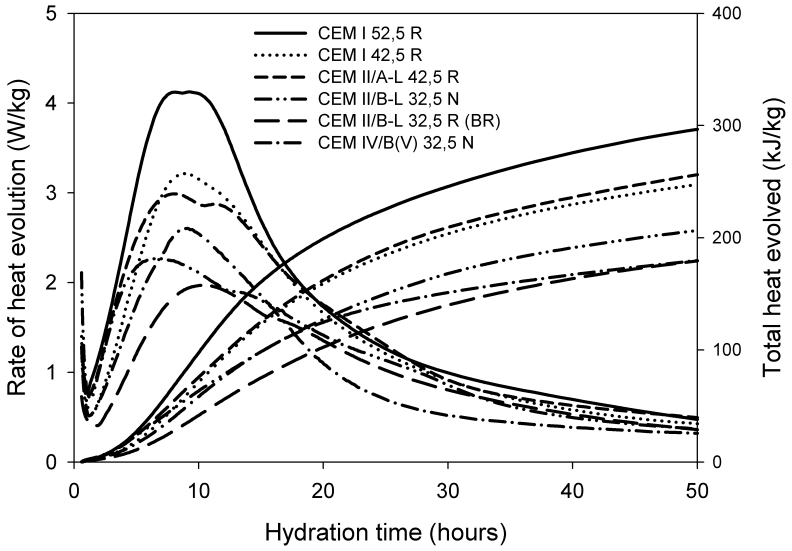


Figure 3.2.: Heat of hydration of plain cement pastes incorporating different cement types determined by conduction calorimetry at 20 °C (Silva, 2007)

The curves obtained for different cement types, supplied by Cimpor-Alhandra production center, used in the present work are presented in Figure 3.2. Four stages can be distinguished: an initial hydration period, a dormant period, acceleration and a deceleration period. With respect to fresh concrete properties (self-compactability) only the initial hydration and the dormant period are important (Griesser, 2002; Szecsy, 2005).

3.2.1. Initial hydration (0-15 min)

Water added to the mix absorbs into the outer part of the cement grain, dissolving easily soluble components like alkalis, calcium sulfate phases and free lime, which move out into the surrounding water (Griesser, 2002; Moir, 2003). Na^+, K^+, Ca^{2+}, SO_4^{2-} and OH^- ions enrich the pore water. An adequate supply of soluble calcium sulfate controls the C_3A hydration, thus preventing flash set. Ettringite is formed around the C_3A containing surfaces. However, if SO_4^{2-} concentration is too high, massive nucleation and growth of gypsum crystals may occur (false set). Contrary to flash set, false set is reversible, because the gypsum needles, which have developed a structure in the paste, can be broken and dispersed by re-mixing (see Figure 3.3). Thus, the cement manufacturer needs to optimize the level of readily soluble sulfate in the cement and match this to the reactivity of C_3A. As it will be explained later, this is the most important reaction for fluidity of cement paste. Considering the relative reactivities of aluminates and silicates, the initial gel products consist largely of aluminates though an amorphous calcium silicate hydrate known as C-S-H gel forms very rapidly on C_3S. C_3S reacts rapidly with water and the reaction is highly exothermic. The reaction rate

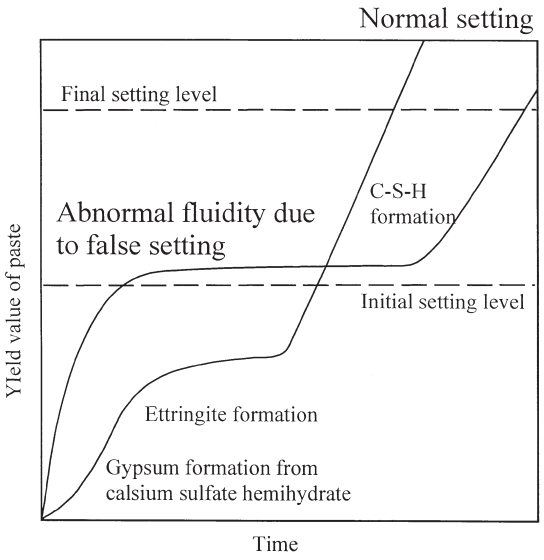


Figure 3.3.: Normal and false setting (Hanehara and Yamada, 1999)

of C_3S is higher than that of C_2S (Moir, 2003). Secondary gypsum may precipitate from the supersaturated pore water. After some minutes, the cement grains are coated with a protective layer of hydration products. At this stage the reactions appears to be suspended and the heat flux drastically decreases.

3.2.2. Dormant period (15 min-4 h)

The dormant period usually lasts several hours. This is of practical significance because it allows concrete to be placed. This period is characterized by a very low heat flow. Nevertheless, the surface gel layer (C-S-H phases) on the cement grains is thickening and the ettringite needles are slightly growing (Jolicoeur and Simard, 1998).

3.2.3. Acceleration period (4-8 h)

Near the end of the induction period, the rate of cement hydration reactions sharply increases. Several effects have been considered to explain the start of the acceleration period: disruption of the protective hydrates layer, nucleation and growth of C-S-H phases or portlandite, recrystallization of ettringite (Jolicoeur and Simard, 1998). During the acceleration period the suspension loses its plasticity and is converted into a stiff matrix, which is no longer castable. Cement paste setting is arbitrarily defined as the time when a pat of cement paste offers a certain resistance to penetration by a standard probe. The fast rise of temperature is controlled mainly by the intense hydration of C_3S associated with the formation of C-S-H phases and the precipitation of portlandite. C_3A and to a lesser extent C_4AF continue to hydrate. During the acceleration period

the calcium and sulfate ion concentration in the pore water are decreasing due to the ettringite formation.

3.2.4. Deceleration period (8-24 h)

This stage is characterized by hardening of the cement paste or concrete. In some cements, but not all, a small peak may be observed at the decreasing part of the curve (see CEM II/A-L 42,5 R curve in Figure 3.2). This seems to be associated with renewed ettringite formation (Moir, 2003). Due to lack of sulfate ions in the pore water, ettringite reacts with C_3A to form a phase with a lower content SO_3 content known as monosulfate (Moir, 2003). During the deceleration period the hydration reactions get more and more diffusion controlled. Pore volume decreases with increasing time and decreasing w/c ratio. Having completely hydrated, the cement mainly consists of C-S-H gel and portlandite (Moir, 2003). As can be observed in Figure 3.2, total heat of cement hydration (during the first 48 hours) is highest for finer cements with a high C_3S and C_3A contents. The extent of hydration is strongly influenced by cement fineness and the proportion of coarse particles. Cement grains which are coarser than approximately 30 μm will probably never fully hydrate (Moir, 2003).

3.3. Physical interactions

3.3.1. Derjaguin–Landau Verway–Overbeek (DLVO) theory

Most colloid suspensions (particles smaller than 10 μm) consist of particles with charged surfaces (Yang et al., 1997). Depending on the charge of the particles, a cementitious suspension can be in a dispersed or in a flocculated state. Particle charges can be either intrinsic or can result from interactions between two phases through dissolution, adsorption, or ionization of interfacial surface groups. The electrostatic field that arises from these charges is described by the double layer model (Yang et al., 1997; Uchikawa et al., 1997b) as shown in Figure 3.4. The inner, or Stern layer, consists of counter ions that are immobilized by the particles' surface. Outside the Stern layer region lies the diffuse layer, which is made up of ions that are repelled from the particle's surface due to the same sign charge. The boundary between the inner and diffuse layers is called the shear plane. The repelled ions in the diffuse layer give rise to an electrical potential that begins at the shear plane and decays with distance (see Figure 3.4). Zeta potential is defined as the potential difference between the shear plane and the end of the diffuse layer. This potential is taken as an approximation of the surface charge of the particle, since it is not possible to measure the surface potential of the particle

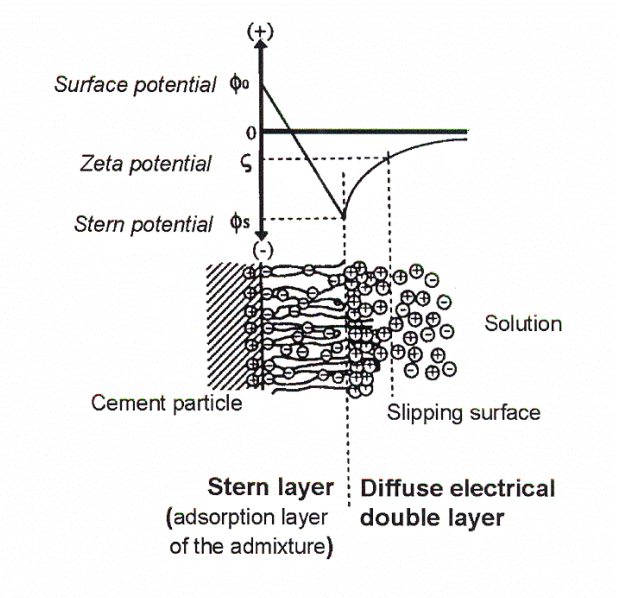


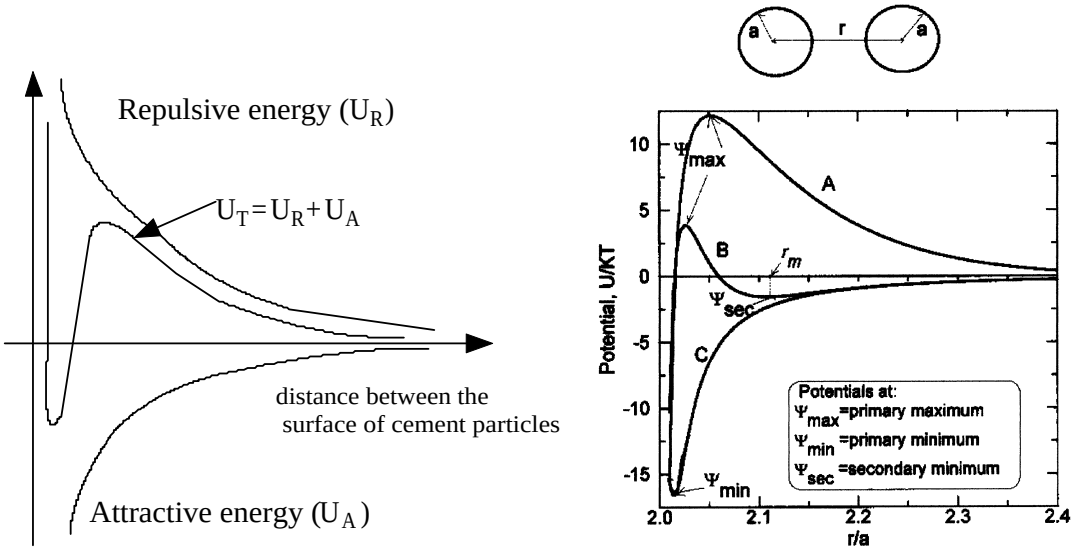
Figure 3.4.: Ilustration of interfacial electric double layer formed on cement particle surface (Uchikawa et al., 1997b; Yoshioka et al., 1997)

itself. Zeta potential can be obtained by measuring charged particles in suspension and observing their mobility under an electric field gradient.

From the potential zeta measurements and for a given particle size and ionic strength the total interaction potential can be computed as the sum of repulsive potential (i.e. electrostatic forces) and attractive potential (van der Waals) (see Figure 3.5 (a)),

$$U_T = U_R + U_A \tag{3.1}$$

For further details on the proposed models see (Yoshioka et al., 1997; Uchikawa et al., 1997a). Holding the zeta potential and particle size constant, while varying the ionic strength, produces the three basic types of total potential curves depicted in Figure 3.5 (b). Curve A occurs at low ionic strength and high surface potential and represents a stable dispersion in which the particles repel each other. The larger the primary maximum, ψ_{max}, the more stable the dispersion. Curve B represents a flocculated suspension in which particles achieve an equilibrium separation, r_m, dictated by the secondary minimum, ψ_{sec}. This occurs in systems of moderate ionic concentrations. As the ionic strength increases, it will eventually reach a critical value and ψ_{max} will disappear, resulting in a coagulated suspension, shown in curve C. Yang et al. (1997) showed that normal cement paste has an ionic strength that is above the critical concentration for coagulation and, according to the DLVO theory, should be coagulated with an interparticle potential, as depicted by curve C in Figure 3.5 (b). Because of the high ionic strength in the aqueous phase, the degree of flocculation or coagulation is not sensitive to the variation of the zeta potential, for zeta potentials between -20 mV



(a) (b)

Figure 3.5.: (a) Energy balance according to DLVO theory and (b) illustration of interparticle potentials: A-stable dispersion, B-flocculated suspension, and C-coagulated suspension (Yang et al., 1997))

and 20 mV (Yang et al., 1997). Furthermore, Yoshioka et al. (2002) found that without superplasticizer, the zeta-potentials of C_3S and C_2S were negative (- 5 mV). However, those of C_3A and C_4AF were positive from + 5 to + 10 mV. Therefore, accelerated coagulation of cement particles in a plain paste might occur due to their electrostatic potentials that are opposite to each other. Coagulated particles may retain water, which is no longer available to enhance fluidity and for the initial hydration reactions (Moir, 2003).

3.3.2. Molecular structure of superplasticizers and mode of action

As mentioned before, cement particles contain several mineral phases of different reactivity and their initial hydration will likely generate a surface with important variation in the surface charge density, both in size and magnitude. These localized surface charges promote flocculation of hydrating cement particles, but they can be effectively neutralized and separated by the anionic charge of the dispersing admixtures molecules which are adsorbed on the hydrating cement particles (Chandra and Bjornstrom, 2002).

A variety of dispersing admixtures has been developed and is currently available in the market. These can be divided in four basic groups according to their chemical structure as modified lignosulphonates (LN), sulphonated melamine formaldehyde condensate (SMF), sulphonated naphthalene formaldehyde condensate (SNF), and polycarboxilate ethers (PC) also called comb-polymers which contain sulphonic and carboxyl groups

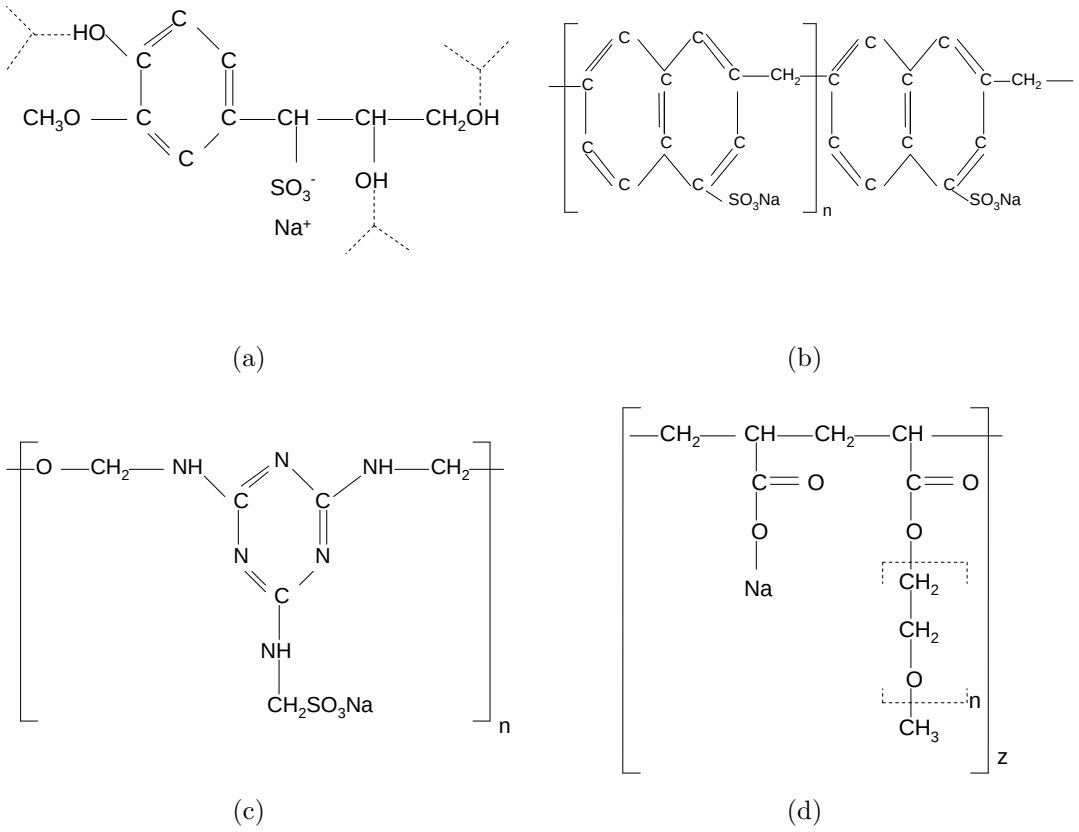
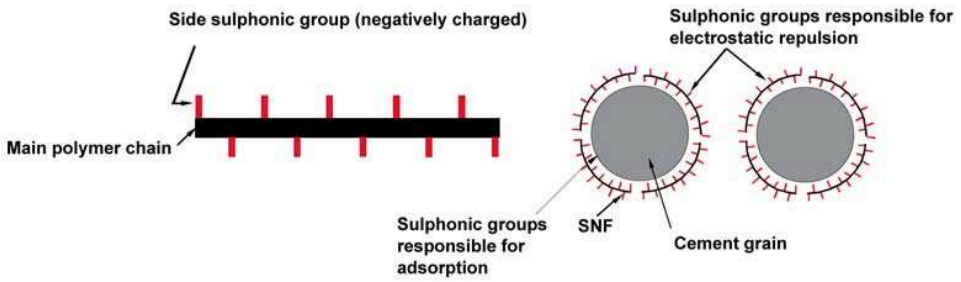


Figure 3.6.: Molecular units of: (a) LN, (b) SNF, (c) SMF, (d) PC (Dransfield, 2003)

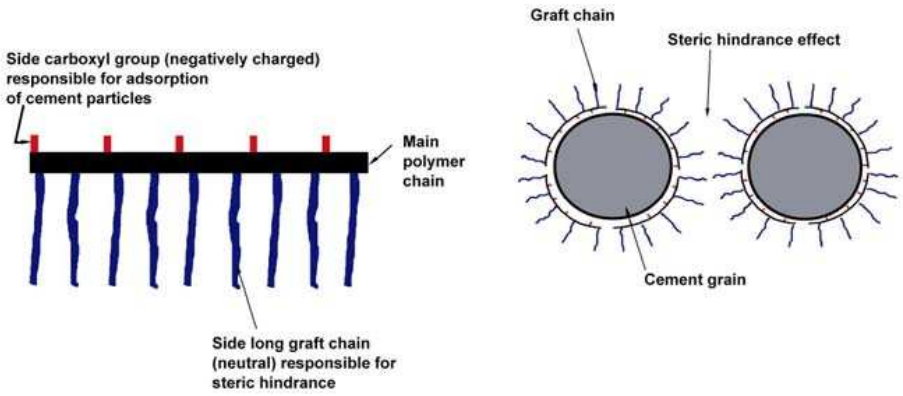
(Chandra and Bjornstrom, 2002; Dransfield, 2003). Figure 3.6 shows the simplified molecular units of each superplasticizer type. Apart from the superplasticizers of different basic groups, there can also be differences in superplasticizers from the same group depending upon their synthesis, which influences upon the molecular weight and chemical configuration, in particular in the case of PC type (Chandra and Bjornstrom, 2002; Dransfield, 2003).

The dispersion mechanism is dependent upon the type of superplasticizer adsorbed on the surface. Basically, there are two main types of dispersion mechanisms: electrostatic repulsion and steric hindrance (Björnström and Chandra, 2003). Some authors discuss other possible mechanisms, such as depletion effect and tribology effect (Roncero, 2000; Vikan, 2005).

The relatively high negative zeta potentials obtained when superplasticizers with a sulfonic group, like LN, SNF and SMF types, were used suggest that the dispersion mechanism of cement particles is mainly controlled by electrostatic repulsion between negatively charged particles (Björnström and Chandra, 2003). These molecules all carry SO_3Na groups, which in water dissociate into SO_3^- and Na^+. The SO_3^- remains attached to the admixture and carries a strong negative charge (Dransfield, 2003). Part



(a)



(b)

Figure 3.7.: Schematic illustration of (a) electrostatic repulsion and (b) steric stabilization

of this charge is used to attach the admixture to the cement but the remainder orientates out from the grain, forming the "Stern Layer" (see Figure 3.4), and repels the negative charges on admixture adsorbed onto adjacent cement grains, causing them to move and stay apart (see Figure 3.7 (a)). As well as observing the increased fluidity, the effect of these superplasticizers can be followed by looking at zeta potential measurements. Yoshioka et al. (2002) reported that in the presence of superplasticizer (Sp), all cement component minerals were negative in their potential and zeta potential values varied with the type of Sp. It was reported that the SNF and SMF superplasticizers with largest molecular weight gives the largest negative zeta potential (Björnström and Chandra, 2003). The LN, SNF and SMF have a lower molecular mass than the PC type and have no long side chains. The absence of long side chains provide the smaller sulfonated polymers with a higher charge density than PC polymer (Björnström and Chandra, 2003). As can be observed in Figure 3.8, the charge on the surface of particles from different cement types is positive before the Sp addition but then goes negative as the Sp adsorbs. Furthermore, the magnitude of the change in the charge varies with the type of Sp. It was much greater with Sp A, which is of LN type. Sp B and Sp C were

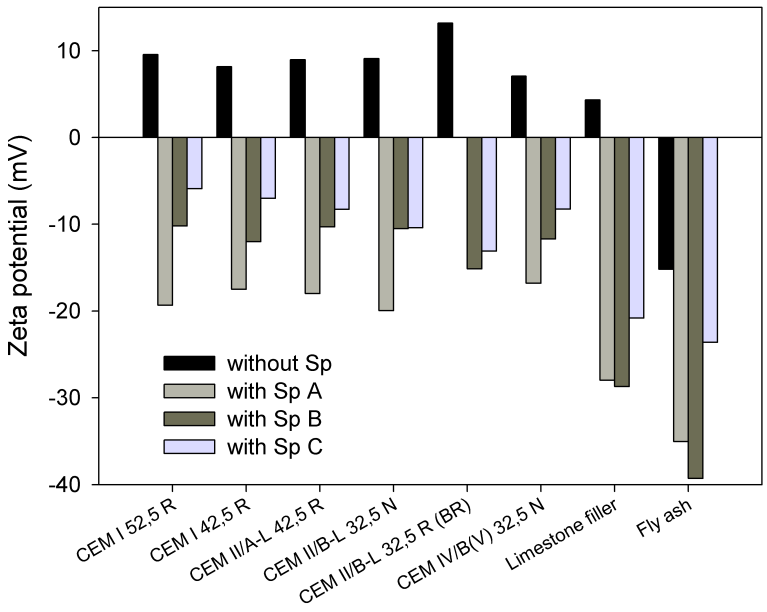


Figure 3.8.: Zeta potential of different cement types and mineral additions, with and without superplasticizer. SP A is of LN type and SP B and C are of PC type (Nunes et al., 2008)

both of PC type but with different molecular structures, based on different performance.

It should be pointed that the zeta potential results presented in Figure 3.8 does not necessarily correspond to the fluidities of cement paste and concrete. The measuring method of zeta potential used in this work was the electrophoretic method, which requires diluted concentration of particles in suspension because the migration speed of dispersed particles to which voltage is applied is directly observed (Nunes et al., 2008). This means it is unsuitable for practical cement paste with a w/c of 0,5 or less because it requires the concentration of particles of 1 %, in volume, or less but also it has shortcomings including poor reproducibility and low accuracy (Uchikawa et al., 1997b). In spite of these shortcomings, these zeta potential results can be used in comparative terms and are helpful to identify the mode of action of different superplasticizer types.

Based on DLVO theory, several authors suggested that the zeta-potential of cement must be less than -15 to -25 mV for stable dispersion (Uchikawa et al., 1997b; Yang et al., 1997; Yoshioka et al., 2002). Thus, based on the zeta potential results obtained with Sp A it can be expected that the electrostatic repulsion is the main repulsion mechanism of Sp A. In contrast, the zeta potentials obtained when using a PC superplasticizer types were always higher than -15 mV, in similar cement-based dispersions. Sp C led to even higher zeta potential values than Sp B for a superior performance. In Figure 3.9 it can be observed that the dispersing action of Sp C is stronger than Sp B leading to mixtures with lower yield stress and lower plastic viscosity, for the same dosage (Sp/p is the solid weight of superplasticizer by unit weight of powder materials). This

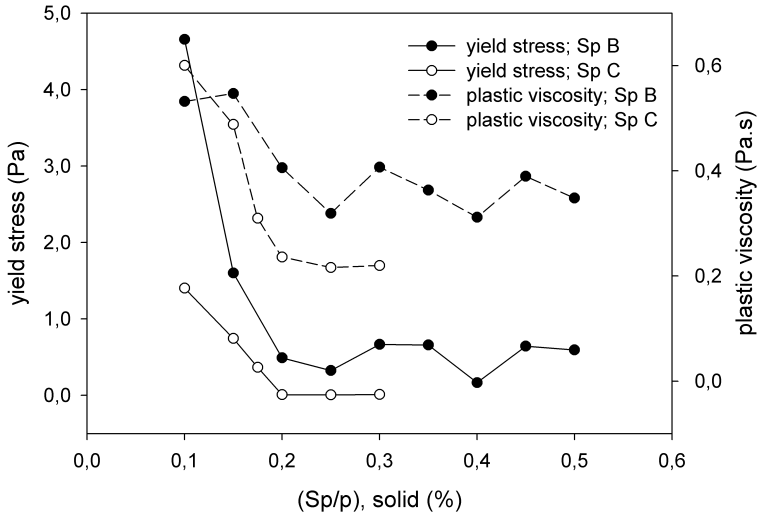
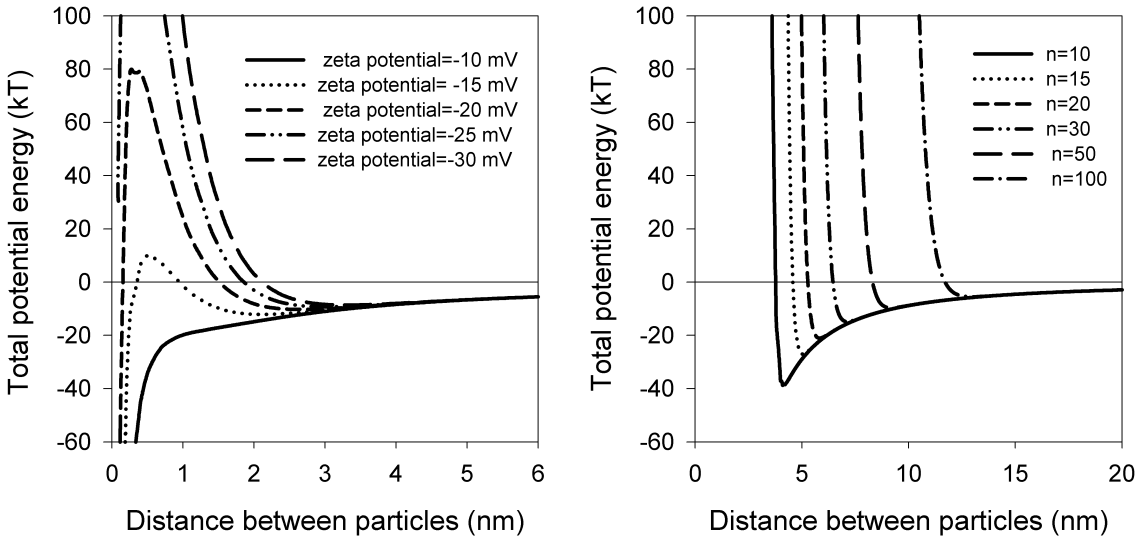


Figure 3.9.: Bingham parameters of cement pastes incorporating Sp B and Sp C, with varying dosages of Sp (CEM I 52,5 R; limestone filler; w/c=0,35; w_f/w_c=0,39; 15 min)

means the mechanism by which cement particles are dispersed can not be attributed to electrostatic repulsion, in the cases of Sp B and C. Uchikawa et al. (1997b) have utilized an atomic force microscope to measure the interactive force between the surface of the cement clinker and an adsorbed admixture, and compared this with the zeta potential measured by the electrokinetic sonic amplitude method. They concluded that steric hindrance played an important role in the dispersion of cement pastes, in the case of PC superplasticizer type. The molecules of PC type seem to bond chemically through their carboxyl (sulfonate and/or hydroxyl groups) which carries a moderate negative charge that is used to attach the admixture to the cement (Yoshioka et al., 1997). The long side chains (polyether groups) orientate away from the cement surface but will resist becoming entangled with the chains attached to an adjoining cement grain, thus keeping grains apart (Dransfield, 2003) (see Figure 3.7 (b)). Zeta potential values close to zero are reported in the literature in the case of PC type superplasticizers, depending on their molecular structure (Sakai et al., 2003).

The dispersion of cement particles through electrostatic repulsion that results from the adsorption of LN, SNF or SMF can be understood with the aid of DLVO theory (see Figure 3.10 (a)) (Neubauer et al., 1998; Yang et al., 1997). In the case of PC, the total interparticle potential energy (see Figure 3.10 (b)) can be calculated based on an assumed model for the adsorption of PC molecules, which accounts for long-range Van der Waals interactions (U_A), steric hindrance (U_S), and electrostatic stabilization (U_S) (Yoshioka et al., 1997), given by

$$U_T = U_R + U_A + U_S \tag{3.2}$$



(a) (b)

Figure 3.10.: Examples of total interparticle energy curves when the main dispersion mechanism is (a) electrostatic repulsion (described by DLVO theory) (b) steric hindrance (n is the number of ethylene oxide units in the graft chain)(Yoshioka et al., 1997)

In this equation ($U_R + U_A$) constitute the DLVO theory. The steric hindrance effect (U_S) was given by Evans and Napper (Yoshioka et al., 1997). According to this model, the PC molecules are assumed to be adsorbed on the cement particles, in the configuration shown in Figure 3.11, with the polyethylene oxide chain stretching into the solution. The existence of the main chain is neglected for the calculation of the steric hindrance effect. Input parameters for this model include the number of ethylene oxide units in the graft chain (value n in Figure 3.10 (b)), the effective chain length, the distance between two adjacent graft chains and the molecular weight of one graft chain. The problem, which is encountered in the application of these models very often, is the non-availability of the technical data of the Sp molecules.

Hesselink et al. (referred in (Yoshioka et al., 1997)) suggested that suspended particles coagulate when the minimum of the potential curve becomes smaller than approximately −5 kT. The particles that are in a weak flocculation have a tendency to disperse again, with the aid of mechanical energy, when the value increases above approximately −5 kT.

Superplasticizers may adsorb also on inert powders which are added to concrete, such as fly ash, limestone, silica fume and clays (Plank and Hirsch, 2007). The reason for this is electrostatic interaction between the admixtures and the charged surfaces of these powders. As can be observed in Figure 3.8, without superplasticizer, the measured zeta potential for limestone filler was positive while for fly ash it was negative. Other authors

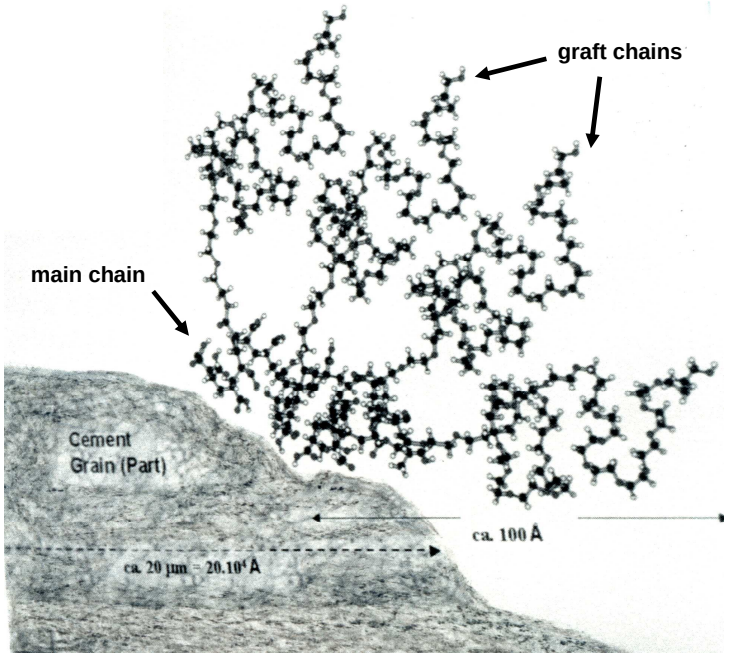


Figure 3.11.: Example of a PC type polymer molecule (Sika ViscoCrete®) adsorbed on cement grain surface

also found negative values for zeta potential of fly ash without superplasticizer (-15 and -21 mV) which became even more negative (-49 and -63 mV) in the presence of a SNF superplasticizer (Termkhajornkit and Nawa, 2004). The partial substitution of cement by limestone filler was found to be beneficial to reduce the potential zeta until a certain percentage, depending on cement type (see Figure 3.12). Thus, improved fluidity can be expected with the partial substitution of cement by limestone filler.

3.4. Chemical interactions

The physical interactions described above, involved in the deflocculation of cement particles when superplasticizers are added, play the most important role with regard to superplasticizer action, but also chemical interactions are suggested to explain changes on the behaviour of cement paste and concrete during the induction period (Flatt, 1999; Roncero, 2000).

3.4.1. Preferential adsorption of Sp on specific surface sites (the role of ettringite)

Previous studies of superplasticizer adsorption on the pure cement clinker phases revealed that much higher adsorption occurs on the aluminate and ferrite than on the

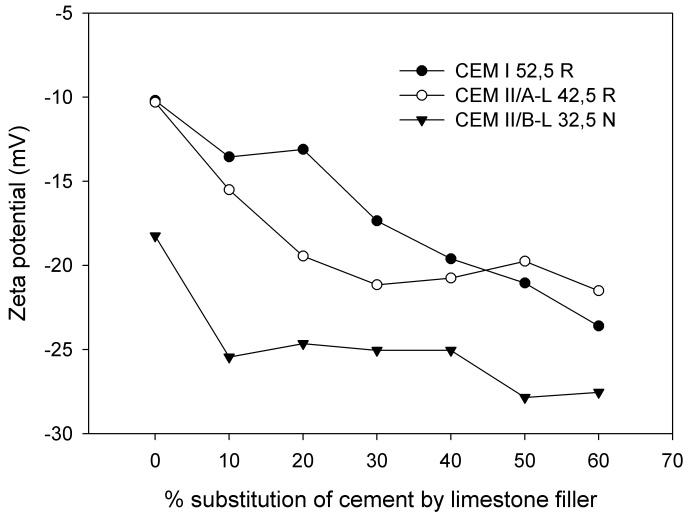


Figure 3.12.: Effect of the partial substitution of cement by limestone filler on zeta potential results, in the presence of Sp B, for different cement types (Nunes et al., 2008)

silicate phases, due to positive zeta potential values (Yoshioka et al., 2002). In a study carried out by Plank and Hirsch (2007) on early cement hydration phases, ettringite[1] and monosulfate[2] showed positive zeta potentials, + 4,15 and + 2,84, respectively, while syngenite[3], portlandite[4] and gypsum[5] showed zero or negative zeta potentials. The adsorbed amount of superplasticizer strongly depends on the existence of a positive zeta potential of the hydration phase. At comparable specific surface area, ettringite shows 2 to 4 times more polymer adsorbed per surface area than monosulfate and the adsorption of superplasticizers on portlandite and gypsum was negligible (Plank and Hirsch, 2007). This emphasizes the importance of ettringite for cement–superplasticizer interaction. Superplasticizers may also adsorb on C-S-H phases, however, the amount of polymer adsorbed per unit area is relatively small (Plank and Hirsch, 2007). Based on these results, Plank and Hirsch (2007) proposed a mosaic structure for the hydrating cement grains with uneven distribution of polymer molecules on its surface, concentrated on spots where ettringite crystallizes, as shown in Figure 3.13.

[1] $[Ca_6Al_2(OH)_{12}]\,(SO_4)_3 \cdot 26H_2O$=Aft (in order to reflect the variable composition of ettringite formed by mixtures of C_3A and C_4AF ettringite is often referred to as Aft, which stands for alumino-ferrite trisulfate hydrate)
[2] $[Ca_4Al_2(OH)_{12}]\,(SO_4) \cdot 6H_2O$=Afm
[3] $K_2SO_4 \cdot CaSO_4 \cdot H_2O$
[4] $Ca(OH)_2$
[5] $CaSO_4 \cdot 2H_2O$

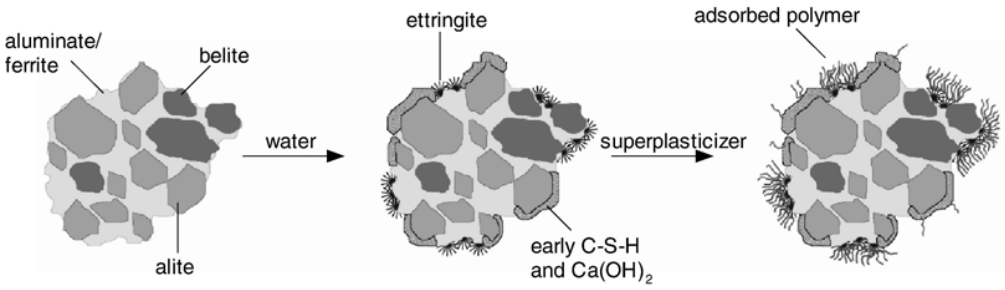


Figure 3.13.: Uneven polymer distribution on the surface of a cement grain (Plank and Hirsch, 2007)

3.4.2. Polymer adsorption and absorption

It has been shown that SNF and PC type superplasticizers (even those with a high density of very long side chains) not only adsorb on the surface of tricalcium aluminate, but also intercalate into its hydrate phase and form an organo-mineral compound (Plank et al., 2006). For this reason it is important to differentiate polymer consumption from polymer adsorption. The term polymer 'consumption' was suggested to group adsorption and absorption in the same term (Flatt and Houst, 2001) (see Figure 3.14). Thus, the superplasticizer added to a cement suspension can be divided into three parts: consumed by chemical reactions (during formation of Aft and C-S-H); adsorbed onto the hydrating cement particles (not integrated into organo-mineral products); remaining in the aqueous phase (Flatt and Houst, 2001).

The problem of polymer intercalation into hydrate phases is that this material is lost for adsorption and does not become effective as dispersing admixture. This can reflect in the required dosages and/or the dispersing effect as well as in the final properties of hydrated cement such as compressive strength (Plank et al., 2006). The amount of polymer, which is consumed by the early reactions, depends both on the polymer and the cement. Flatt and Houst (2001) introduced the concept of reactivity of a cement towards a superplasticizer, which is illustrated in Figure 3.14. In order to obtain the same fluidity, more superplasticizer was needed for cements having a high content of C_3A and/or a high cement fineness (Griesser, 2002). C_3A seems to have a stronger influence on fluidity compared to C_4AF (Griesser, 2002). Further, slight weathering of cement decreases hydration reactivity and superplasticizer dosage required for a given fluidity (Sakai et al., 2003). A very reactive cement would consume a lot of polymer by intercalation, therefore giving a lower workability at equal dosages. For economic reasons it is of interest to reduce the reactivity of cements.

In the next points, several ways to change the reactivity of cements towards a polymer will be discussed, considering different aspects related to cement and superplasticizer

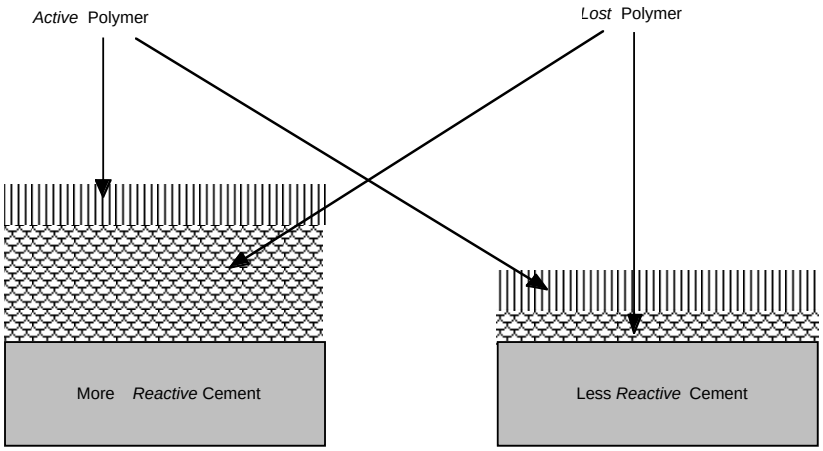


Figure 3.14.: Schematic interpretation of polymer adsorbed and absorbed (intercalated into hydrate phases) and situations of high and low reactivity of cement towards a superplasticizer (Flatt, 1999)

type.

3.4.3. Influence of adding time

It was found that delayed adding time of SNF and SMF type superplasticizers decreased the superplasticizer consumption compared to direct adding, or less superplasticizer was required for equal performance (fluidity) (Hanehara and Yamada, 1999). It was suggested that the superplasticizer should be added 2 minutes after water addition, which coincides with the beginning of the dormant stage (Roncero, 2000). Plank and Hirsch (2007) compared the consumed amounts for different superplasticizers when added at the beginning and after completion of ettringite crystallization. As can be seen in Figure 3.15, the consumed amounts of SMF and SNF are approximately 50% less with delayed adding time. Uchikawa et al. (1995) verified these findings by measuring the thickness of the hydrates formed on a polished clinker surface, which was dipped into an aqueous solution of SNF type superplasticizer, in both direct and delayed adding modes. In the case of direct adding the adsorbed hydrate layer thickness of C_3S and the interstitial phase was about 50 and 300 nm, respectively. At delayed adding time mode, the thickness of the adsorbed hydrates was 20 nm both for C_3S and the interstitial phase, and was compatible with the polymer size (referred in (Flatt, 1999)). It was also suggested that delayed adding time reduces the adsorption on C_3A and enhances the adsorption on silicate phases, which explains enhanced fluidity. According to Flatt (1999), in direct adding mode, a first layer of coprecipitate is formed, which might be expected to have dielectric properties similar to cement. Thus, the plane of origin for the van der Waals force would be shifted from the surface towards the basis of the polymer

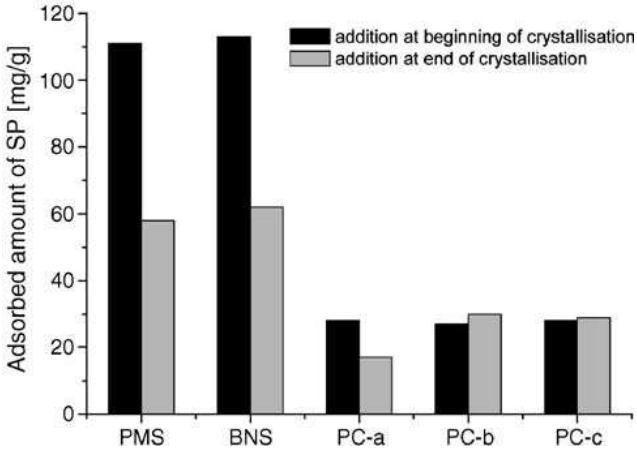


Figure 3.15.: Adsorbed (or more correctly 'consumed') amounts of superplasticizers (PMS and BNS corresponds to SMF and SNF, respectively) on ettringite in case of direct and delayed adding time (Plank and Hirsch, 2007)

layer. Provided enough polymers are added an ultimate layer might be able to adsorb and only this fraction of the polymer would be able of inducing electrostatic and steric repulsion (see Figure 3.16) (Flatt, 1999). In delayed adding time mode, most aluminates would form ettringite, before polymer is added.

As can be observed in Figure 3.15 the consumed amounts of PC is generally lower than the consumed amounts of SNF/SMF types, in both direct and delayed adding time modes. Furthermore, for PC type superplasticized cements both the consumption of superplasticizer molecules and the fluidity was found to be less influenced by delayed adding time (Plank and Hirsch, 2007). Similar results were reported by other authors (Hanehara and Yamada, 1999). This implies that less PC type superplasticizers intercalates into hydrate phases. This may be due to a reduced hydration activity caused by the superplasticizer molecules, due to the lower ionic activity compared to SMF and SNF type superplasticizers (Plank and Hirsch, 2007) or due to the larger size of PC molecules (Flatt, 1999).

3.4.4. The role of sulfate and alkalis

Various researchers reported the competition of SO_3 originating from SNF and SMF and sulfate ions present in the pore water for the same reactive sites on the hydrating cement surface, particularly on C_3A. It was found that the addition of soluble sulfates (K_2SO_4, Na_2SO_4, hemihydrate) reduced the consumed amount of SNF type superplasticizer (Griesser, 2002; Yamada et al., 2001b). If more sulphates are available, more ettringite will be formed and, consequently, fewer polymers are incorporated into hydrates, during the first minutes of cement hydration. As proposed by Flatt (1999) (see Figure 3.17), the consumption of polymer is decreased by higher availability of

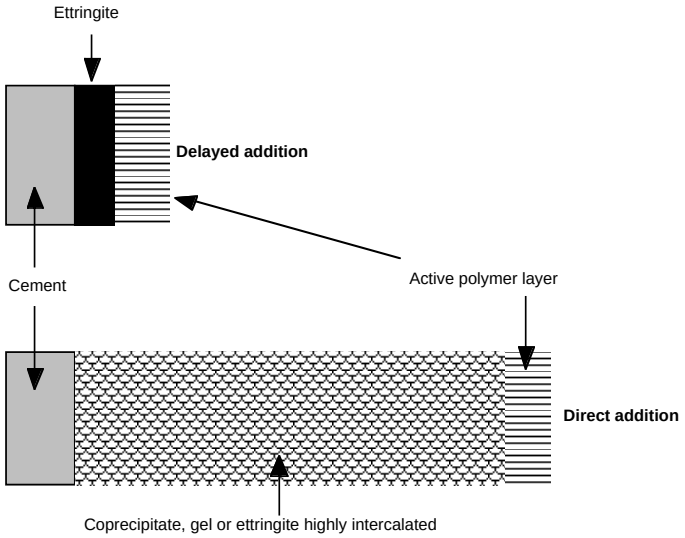


Figure 3.16.: Schematic interpretation of the influence of adding time on the amount of polymer consumed (Flatt, 1999)

sulfate ions, whether directly added or coming from the cement, because it minimizes the amount of polymer lost in organo-mineral products so that at equal dosage the superplasticizer efficiency is higher. Since the dissolved amount and the dissolution rate of alkali sulfates is considerably higher compared to the one of calcium sulfates, the former may significantly influence the rheological properties of superplasticized cement. The existence of optimum soluble alkali content was reported (Jiang et al., 1999; Vikan, 2005). Cements with less than the optimum soluble alkali content showed significant increases in fluidity when Na_2SO_4 was added while cements with more than the optimum soluble showed slightly decreased fluidity with the addition of Na_2SO_4. In the presence of SNF, the optimum soluble alkali content for high initial fluidity and low loss of fluidity with time was found to be in the order of 0,4-0,5% $(Na_2O)_{equivalent}$[6] (Jiang et al., 1999). It was suggested that an excessive amount of alkali sulfate compressed the electric double layer, which could explain the decrease in fluidity of cement paste (Zhang, 2001).

It should be noted that, depending on the clinker SO_3 content, alkalis in cement can be present as alkali sulphates (K_2SO_4 or Na_2SO_4) or these may enter into solid solution in the aluminates and silicate phases. The ratio of sulphur to total alkali determines the quantity of alkali sulphates in a clinker. When a clinker contains relatively large amounts of SO_3, a substantial fraction of alkalis goes into solution within a few minutes. In low SO_3 clinker, Na_2O and K_2O are incorporated preferentially into the C_3A phase, but also into C_2S phase of Portland clinker. Therefore, although the cements may have similar SO_3 content and total alkali contents, the amount of alkalis readily soluble in

[6] $(Na_2O)_{equivalent}$ is obtained from cement alkalis content as $(Na_2O + 0,66K_2O)$

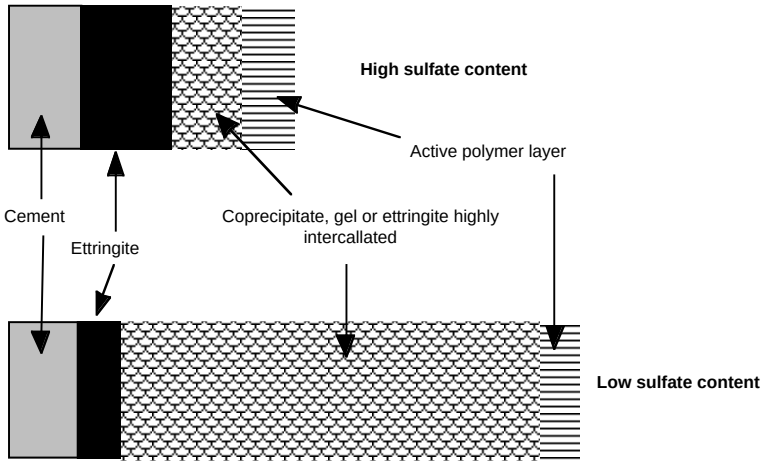


Figure 3.17.: Schematic interpretation of the influence of sulfate content (below the optimum dosage) on the amount of consumed polymer (Flatt, 1999)

them can vary widely (Jiang et al., 1999).

Various authors referred in (Hanehara and Yamada, 1999) found that alkaline sulphate in cement had the most significant effects on the dispersing action of PC type superplasticizers. The fluidity was lowered by increasing the amount of alkali sulfate. This was attributed mainly to the reduction of the amount of the admixture adsorbed on cement caused by adding the sulfate ions (Hanehara and Yamada, 1999; Yamada et al., 2001b). It was concluded that there is a competitive adsorption between the carboxylic group of the PC polymer and sulfate ions present in the pore water for the same reactive sites on the hydrating cement surface. Also, it was found that a high concentration of ions (sulfate or chloride ions) in the mixing water can shrink the side chains of PC polymer (responsible for the steric repulsion), thus reducing the dispersion action (Yamada et al., 2001b).

3.4.5. Fluidity loss with time and influence of temperature

Fluidity changes with elapsed time and temperature can also be discussed based on the concept of reactivity of cement towards a superplasticizer. With the progress of hydration, the surface area of cement particles increases, thus more polymer is consumed inducing loss of fluidity. On the other hand, sulfate ion concentration simultaneously decreases with elapsed time, which allows for higher adsorption of polymer molecules (if polymer molecules remain in the solution phase) inducing higher fluidity. Balance of these two effects determines the occurrence of fluidity retention, fluidity loss or fluidity gain. Thus, to realize good performance for fluidity retention, a suitable amount of

Sp must remain in the solution phase (Sakai et al., 2003). At lower temperatures, a smaller increase in specific surface of cement paste and a larger decrease in sulphate ion concentration reduce the reactivity, resulting in fluidity gain (Yamada et al., 1999). On the contrary, at higher temperatures, larger increases in specific surface of cement paste and smaller decreases in sulphate ion concentration result in higher reactivity, inducing fluidity loss (Yamada et al., 1999).

PC type superplasticizers maintain workability over a long time range. Sakai and Daimon (referred in (Flatt, 1999)) attribute this to the fact that the polyethylene side chains of the polymer molecules can stretch out and induce a steric effect while hydration layers grow from the surface.

3.4.6. Influence on hydration rate and hydration products

As may be expected, presence of organic admixtures which can interfere with nucleation and/or growth processes will influence hydration reaction rate, reaction products, or both. In general, all superplasticizers retard hydration of cement compared to a plain cement paste. Different mechanisms were proposed to explain inhibition of setting (set retardation): adsorbed superplasticizer molecules hinder diffusion of water and calcium ions at the cement-solution interface; formation of complex ions between Ca^{2+} and superplasticizer (decreasing the concentration of Ca^{2+} in the solution and decreasing the formation of portlandite); and the dispersive action of superplasticizers changes growth kinetics and morphology of hydrate phases (Roncero, 2000; Winnefeld et al., 2007). According to Winnefeld et al. (2007), retarding effect of PC type Sps is probably not caused by interaction with dissolved calcium ions, but due to changes in nucleation and growth kinetics of the hydrate phases.

Several authors reported changes in size and morphology of ettringite (Plank and Hirsch, 2007; Prince et al., 2003). In the presence of superplasticizers, the ettringite crystals are much smaller. In addition, the morphology changes from long and thin to short and compact needles. This was explained by preferential adsorption of superplasticizers on ettringite crystals inhibiting crystals growth (Plank and Hirsch, 2007).

3.5. Incorporation of viscosity agents

The incorporation of a viscosity agent in the concrete mixture can interfere in the cement-superplasticizer interactions. Viscosity agents (VA), also known as viscosity-modifying, viscosity-enhancing, anti-washout or stabiliser agents, are used in SCC applications to:

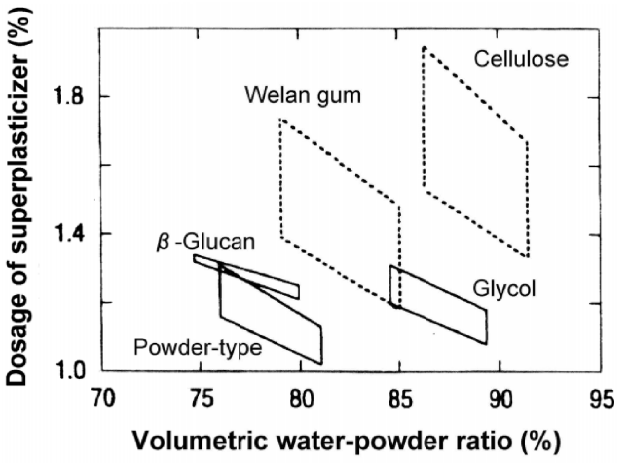


Figure 3.18.: Target area of SCC mortars with and without a viscosity agent (Nawa et al., 1998)

- enhance homogeneity of concrete (improve segregation resistance, reduce bleeding, decrease surface settlement, counteract blocking of aggregates near obstacles) (Grünewald and Walraven, 2004; Khayat, 1998; Phyfferoen and Lockwood, 1998);
- decrease sensitivity of SCC (mitigate the effects of variations in materials and proportions, like surface moisture content and grading of fine aggregate, but also effects of changes in concrete temperature) (Grünewald and Walraven, 2004; Khayat, 1998; Phyfferoen and Lockwood, 1998);
- design SCC mixtures which are not stable without a VA (to allow higher water/powder ratios, lower paste contents and the use of a wider range of materials such as gap-graded aggregates, manufactured sands, fibres and lightweight aggregates) (Grünewald and Walraven, 2004; Khayat, 1998; Phyfferoen and Lockwood, 1998) (see Figure 3.18).

Nawa et al. (1998) classified the VA's, used to enhance the cohesion and stability of cement-based materials, as presented in Table 3.2. Their mechanism of action varies largely depending on the type (see Table 3.2). These products are available either in powder- or in liquid-based form. Admixtures combining a superplasticizer and a VA have been developed, especially in products developed specifically for SCC applications. The advantage of these products is that no extra storage and dosing system for VA is required. But, for mixture optimization purposes it is better to add the SP and VA separately (Grünewald and Walraven, 2004).

According to Nawa et al. (1998) VAs may be broadly divided into two types: adsorptive and non-adsorptive. The functional group in the molecular structure of a VA is attracted to the cement surface in case of adsorptive type; while in the case of non-adsorptive type, it is attracted with water (Nawa et al., 1998). Consequently, adsorptive type VAs hinder the interaction of superplasticizers on cement surface. As can be observed in Figure 3.19,

Table 3.2.: Types of VA and mode of action (Nawa et al., 1998; Phyfferoen and Lockwood, 1998)

Type			Mode of action
Soluble in water	- cellulose-based polymers	adsorptive	- adsorb on the surface of cement particles and increase viscosity due to interparticle attraction forces;
	- acrylic-based polymers		
	- glycol-based polymers	non-adsorptive	- do not adsorb on the surface of cement particles but increase viscosity by action of linking between its own molecules;
Not soluble in water	- bio-polymers		- adsorb water, swell, and impart viscosity to the mixture
	- inorganic materials of high surface area		

the adsorbed amount of superplasticizer decreases with increasing adsorptive VA content. In this case, both yield stress and viscosity of cement paste will be affected with the introduction of VA. The increase in yield stress typically must be offset with additional water or superplasticizer (Yahia and Khayat, 2001b). On the other hand, mainly paste viscosity increases with the incorporation of non-adsorptive VAs. Most VAs used in concrete are adsorptive (Nawa, et al., 1998). Mixtures containing VA also exhibit enhanced shear-thinning and/or thixotropic behaviour (Grünewald and Walraven, 2005, 2004; Khayat, 1998; Lachemi et al., 2004). This is a result of association and intertwining of polymer chains (Khayat, 1998). According to Khayat (1998) the VA polymers themselves develop attractive forces (association) and thereby block the motion of water causing viscosity increase. The polymer chains can also intertwine especially at low shear rates and high concentrations, but break apart, stretch and orientate in the direction of flow at higher shear rates, hence resulting in shear-thinning behaviour. This shear-thinning and/or thixotropic behaviour ensures static stability (due to high viscosity at low shear rates) without interfering much with the required energy for processes like mixing, pumping and casting (due to lower viscosity at high shear rates).

Some incompatibilities were reported between cellulose derivatives and SNF superplasticizers (Khayat, 1998). SNF-type superplasticizers are compatible with acrylic-based VAs. SMF- type superplasticizers are compatible with cellulose-, acrylic- and glycol-based VAs. PC-type superplasticizers are compatible with cellulose- and glycol-based VA's (Grünewald and Walraven, 2004). Welan gum (a biopolymer commonly used in cement-based materials) is compatible with both SMF and SNF types of superplasticizer (Khayat, 1998).

Besides affecting rheology the incorporation of a VA can alter cement hydration and hardened concrete properties. The extent of these changes depend on the mixture composition, the type of superplasticizer, the type of VA, the required extra dosage of SP. Welan gum and cellulose derivative VAs may delay concrete setting times, while acrylic-based VAs generally do not affect setting time (Khayat, 1998). VAs can affect

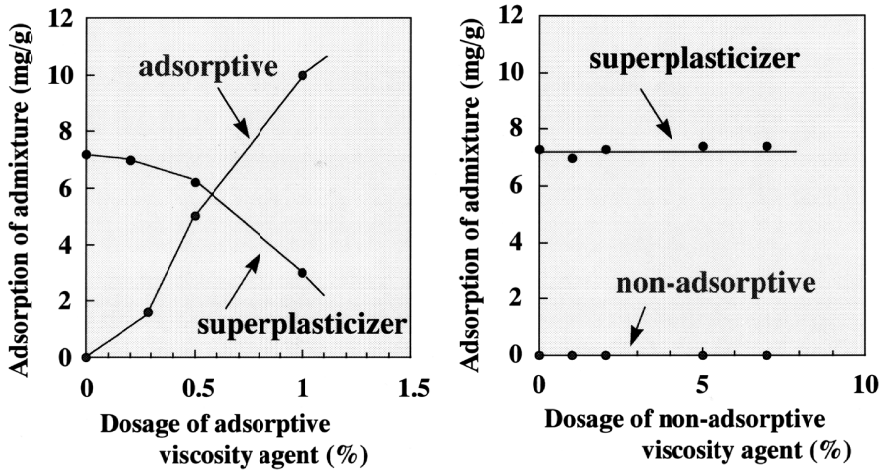


Figure 3.19.: Adsorbed amount of superplasticiser on the cement surface in the presence of adsorptive and non-adsorptive VAs (Nawa et al., 1998)

the air-void system of SCC, which can have consequences in terms of the quality of surface finishing, stiffness and strength of concrete and/or durability. In general, the interface zone between paste and aggregates and between paste and reinforcing bars is improved (Khayat, 1998). To sum up, when a VA is to be used, different types should be considered and their effects should be studied in conjunction with the superplasticizer, cement and other additions to come up with an optimized mixture that satisfies all performance requirements (Yahia and Khayat, 2001b).

3.6. Molecular structure of PC type superplasticizers

Nowadays, there is a wide use of PC type superplasticizers because of their superior performance in dispersing cement particles and maintaining fluidity in time, especially for high fluidity concretes like the case of self-compacting concrete. The polycarboxylate polymer is made up of a main chain and polyoxyethylene side chains (see Figure 3.11). These long side chains are responsible for the steric hindrance effect. It is believed that the adsorption of this kind of polymer on cement particles occurs via carboxylic (sulfonate and/or hydroxyl) groups from the main chain. A characteristic of this type of SP is that its chemical structure has the potential to be modified. The variations in type and length of the main and side chain of PC-type superplasticizers yield to a broad variety of new products with very variable properties (see Figure 3.20). Therefore, various PC type products are available in the market for specific applications. Sp B and Sp C, presented before, are good examples of this. Sp B is recommended for in-situ applications with prolonged transportation time while Sp C is more indicated for precast applications where enhanced fluidity and not too prolonged setting times are of

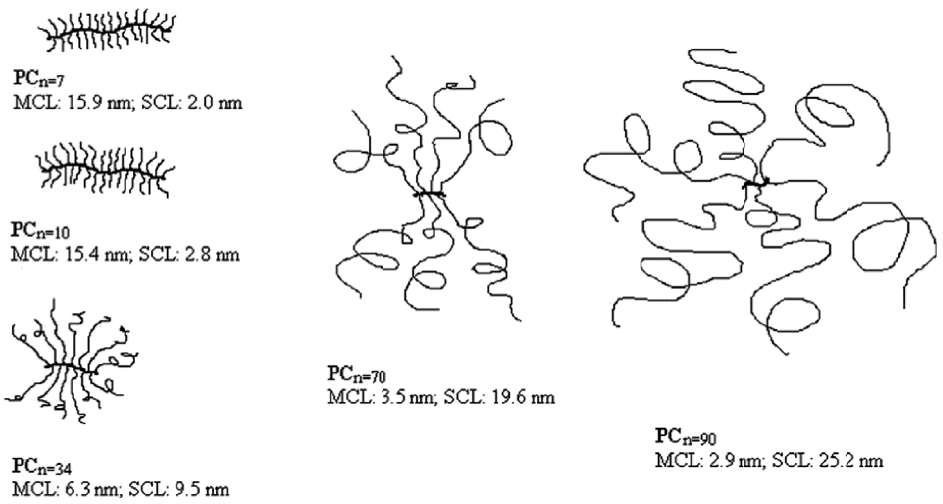


Figure 3.20.: Schematic representation of PC type molecules with varying molecular structures (n is the number of ethylene oxide units; MCL is the main chain length; SCL is the side chain length) (Plank and Sachsenhauser, 2006)

interest. The rheological results presented in Figure 3.9 confirm that Sp C has a stronger dispersing capability (resulting in lower yield stress and lower plastic viscosity, for the same dosage, in solid content); but cement pastes incorporating Sp C lose fluidity more rapidly than cement pastes incorporating Sp B (see Figure 3.21).

The influence of PC type molecular structure on the rheological properties of cementitious materials has been a subject of investigation. The main effects of chemical structure parameters on PC type superplasticizer performance are summarized in Table 3.3. It was found that the adsorption behaviour of Sp determines the rheology and setting of cement paste, mortar and concrete. Adsorption is related to the charge density of polymer. According to Winnefeld et al. (2007) the charge density of the polymer increases with decreasing side chain density and with decreasing side chain length, leading to an increasing amount of free carboxylic groups. Furthermore, polymer fractions with a high molecular weight adsorb preferentially on the cement particles. Various authors found that PC type superplasticizers with higher molecular weight adsorb stronger compared to polymers with lower molecular weight and same molecular architecture (Winnefeld et al., 2007). As can be observed in Table 3.3, there seems to be no agreement concerning the effect of side chain length. The minor effect of side chain length found by Winnefeld et al. (2007) was attributed to the conformation of the side chains, which is not stretched but more ‘‘mushroom’’-like especially in aqueous solutions with high ionic strengths.

The retarding effect seems to be determined by the coverage of the surface of the cement with PC polymer molecules. In the case of a PC polymer with long chains most of the

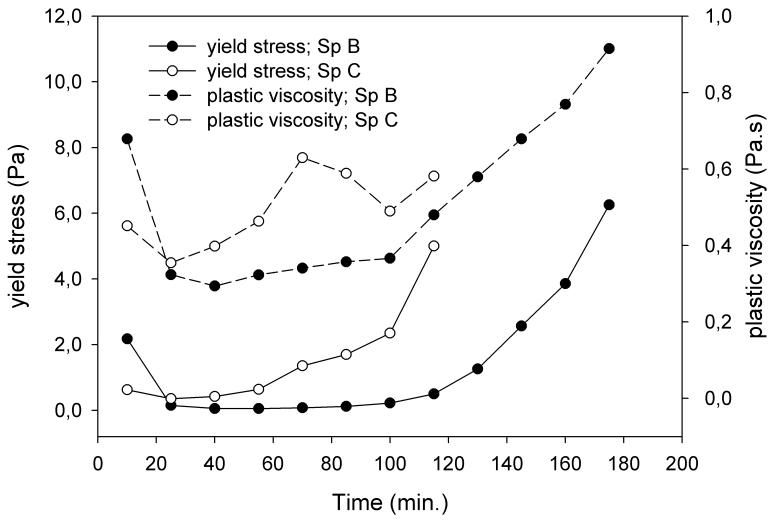


Figure 3.21.: Evolution of Bingham parameters with time of cement pastes incorporating Sp B ($(Sp/p)_{solid} = 0,25\%$) and Sp C ($(Sp/p)_{solid} = 0,175\%$) (CEM I 52,5 R; limestone filler; w/c=0,35; w_f/w_c=0,39; Temperature=20°C)

mass of the polymer is concentrated in the non-adsorbing backbone. Thus, the coverage of the surface of the cement is much less compared to a PC polymer with short side chains. A cement particle with a less covered surface should exhibit a faster setting (Winnefeld et al., 2007). Retardation increases also with PC dosage and the influence of PC dosage on retardation is more pronounced for shorter side chains and for lower side chain densities (Winnefeld et al., 2007). An increase of the molecular weight of PC had only a slight effect on setting times (Winnefeld et al., 2007). Other authors found that the setting time of cement paste depended on the ionic functional group concentration in the aqueous phase of the cement paste (Kirby and Lewis, 2004; Yamada et al., 2000). Winnefeld et al. (2007) also found that increasing side chain length and increasing side chain density of PC polymer lead to higher early strengths (16 h, 1 day).

Yamada et al. (2001a) suggested that the molecular structures with the longer main chain, the longer side chain and the higher COOH ratio are more resistant to variations in the SO_4^{2-} content of cement. Among these parameters, the ratio of carboxylic group in the trunk chain (COOH ratio) was found to be the most important factor (Yamada et al., 2001a). A higher tolerance for the fluctuation of sulfate ion concentration is of interest to improve mixtures robustness but it can be contradicting with other performance requirements, like fluidity retention.

Based on the effects discussed above one can speculate about the polymer structure differences between Sp B and Sp C that can be responsible for the higher fluidity, faster fluidity loss and shorter setting times of cement pastes incorporating Sp C. Compared to Sp B, Sp C probably has lower density of side chains (to increase the adsorption) and

Table 3.3.: Summary of the effect of chemical structure parameters on the performance of superplasticizer

	higher fluidity	less fluidity loss	shorter setting time	higher early strength
side chain length	longer[a] minor effect[b]	shorter[a]	longer[a, b]	longer[b]
main chain length	shorter[a]		longer[a]	
side chain density	lower[b]		higher [b]	higher[b]
ionic group content	higher[a]		lower[a, c]	
molecular weight	higher [b]		minor effect[b]	

according to: [a](Yamada et al., 2000); [b](Winnefeld et al., 2007);[c](Kirby and Lewis, 2004)

longer side chains (to reduce retardation) which are responsible for the faster fluidity loss.

4. SCC mix-design and properties

4.1. Introduction

SCC is defined primarily in terms of its fresh properties, therefore, the characterization and control of fresh properties are critical to ensure successful SCC performance. Fresh properties influence not only workability but also hardened properties like strength and durability. Furthermore, SCC is a complex material exhibiting several sensitive interactions between the constituent materials and further work is needed to better understand the effect of mixture parameters governing its fresh properties.

This chapter first describes the fresh properties that are relevant for the study and production of SCC and presents available empirical test methods, focusing mainly on those for which CEN is preparing standards. Specifications for SCC depending on application type are also considered. Then, the possible differences between hardened properties of SCC and conventional concrete and the applicability of currently existing design rules are discussed. After that, an overview of existing mix-design methods is given and the choice for the Experimental Design approach is justified. Finally, the Japanese SCC-designing method and the Experimental Design approach are described in further detail.

This chapter provides the mixtures formulation, the mix-design procedures and the test methods for the studies presented in Chapters 5, 6 and 7.

4.2. Fresh properties and empirical tests

4.2.1. SCC fresh properties

The key workability requirements for SCC are filling ability, passing ability and segregation resistance (BIBM et al., 2005; Concrete Society, 2005). The former describes the ability of concrete to flow under its own weight and completely fill formwork. Passing ability describes the ability of concrete to flow through confined conditions, such as the narrow openings between reinforcement bars. Segregation resistance (or stability)

describes the ability of concrete to remain homogeneous both during transport and placing (in dynamic conditions), and after placing until setting (in static conditions) (BIBM et al., 2005; Concrete Society, 2005). Additional information can be given about concrete mix viscosity, which is also important in understanding passing ability and segregation resistance, but is not essential for defining a fresh concrete as being self-compacting concrete.

Various test methods are available to measure these properties; however, no test method exists to measure all of these properties at once. Given that these properties are interrelated, most tests indirectly measure more than one property at a time, as will be presented in paragraph 4.2.2. Requirements for SCC workability can vary significantly depending on the application type - this will be discussed in paragraph in 4.2.3.

4.2.2. Standard (empirical) test methods

Traditional workability test methods like 'slump-test', 'flow table', 'Vebe' or 'degree of compactability' are not adequate for describing SCC fresh state properties. According to EN-206-1:2007 all SCCs fall into S5 class (slump) and F6 class (flow-table). None of these tests is able to distinguish the SCC mixtures in terms of filling ability, passing ability and segregation resistance. Thus, a wide range of test methods have been developed to measure and assess the fresh properties of SCC. Many of the existing tests were developed in commercial secrecy for specific applications and there had been no attempt to ensure that they were more generally applicable. Due to the lack of standardization of these test methods, the dimensions and details of tests found in literature can vary, influencing test results. Daczko (2003) lists dimensions of L-boxes, U-boxes, and J-rings reported by various researchers in literature. Furthermore, no agreement was reached on which test was the most suitable for general purposes. This hindered the increased use of SCC in general construction, since it was difficult to validate mix-designs and to write performance-based specifications. The establishment of a standardised test (or tests) was therefore an essential prerequisite to realise potential benefits of SCC and facilitate its widespread use in general construction.

Within the EU funded "Testing-SCC" project, 10 out of 23 potential tests were selected for detailed evaluation by a combination of laboratory tests, full-scale site trials and rheological studies (ACM Centre, 2005). From these results, a number of tests were identified as the most promising for use in the laboratory for mix design and development or in-site acceptance and quality-control. In addition, those tests were assessed for precision in a round-robin programme involving 23 laboratories throughout Europe in order to recommend the most suitable for CEN codification. One of the main conclusions of this project was that there is no single universal test, which can detect differences

Table 4.1.: Standardised test methods, assessed fresh property and consistency classes (ACM Centre, 2005)

Test	Test result	Fresh property	Consistency classes	
Slump-flow[a]	SF (mm)	primarily to assess filling ability	SF1	550 to 650
			SF2	660 to 750
			SF3	760 to 850
	t500 (s)	primarily to assess viscosity	VS1	≤2
			VS2	3 to 6
			VS3	> 6
V-funnel [a]	tv (s)	partially indicates filling ability and blocking	VF 1	< 9
			VF 2	9 to 25
L-box [b]	PA	primarily to assess passing ability	PL1	≥0,8 with 2 rebars
			PL2	≥0,8 with 3 rebars
J-ring[a]	BJ (mm)	primarily to assess passing ability	PJ1	≤10 with 12 rebars
			PJ2	≤10 with 16 rebars
	SFJ (mm)			
	T500J			
Sieve stability [a]	SR (%)	to assess segregation resistance	SR1	≤20
			SR2	≤15

[a] suitable for laboratory and site use; [b] suitable for laboratory use

between good and bad SCC mixes and is capable of measuring all three key properties (i.e. filling ability, passing ability and segregation resistance). Thus, a combination of tests might be required to fully characterize a mix. Based on the recommendations of The European project Group, the standards of five tests methods are being prepared by CEN, namely, Slump-flow, L-box, V-funnel, J-Ring and Sieve stability. These tests are listed in Table 4.1 along with the property(ies) assessed. These methods are widely used across Europe and for each of them specification classes were assigned, as shown in Table 4.1, (ACM Centre, 2005).

Slump flow test

Slump-flow test is a sensitive test that should normally be specified for all SCCs. It describes the flowing ability of a fresh mix in unconfined conditions. Test results are the slump-flow diameter (SF, expressed to the nearest 10 mm) and the time needed to reach the 500 mm diameter (t500, expressed to the nearest 0,5 s), which give an indication of filling ability and relative viscosity of SCC, respectively. Because the slump flow result can vary by changing the nature of the baseplate material, a metal surface has been specified; which should be moistened and without excess water (see Figure 4.1). This test can be performed by one single operator with the inclusion of a steel collar on the

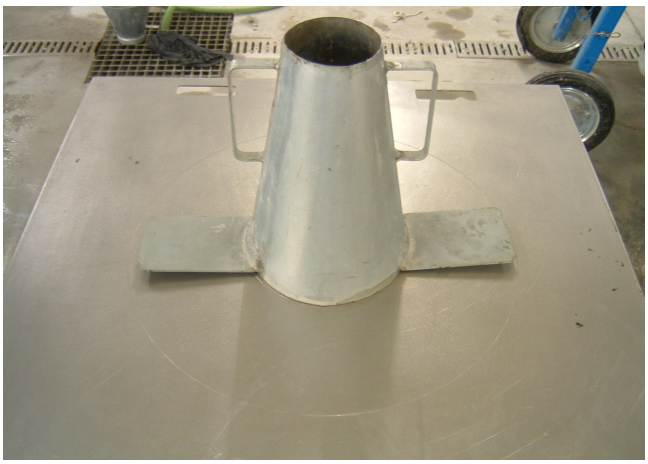


Figure 4.1.: Abrams cone and plate used in the Slump flow test



Figure 4.2.: Slump flow test carried out by a single operator, by using an Abrams cone fitted with a steel collar (photos taken at Stevin Laboratory, TUDelft, The Netherlands)

top of the Abrams cone, as illustrated in Figure 4.2. The Slump-flow test principle, apparatus, procedure, result computation and precision are further described in Draft prEN 12350-8 (CEN, 2007f).

V-Funnel test

The V-funnel test is used to assess the viscosity (and filling ability) of self-compacting concrete (see Figure 4.3). This test result is the time taken for the concrete to flow out of a V-shaped funnel (tv, expressed to the nearest 0,5 s). The V-funnel test principle, apparatus, procedure, result computation and precision are further described in Draft prEN 12350-9 (CEN, 2007d).



Figure 4.3.: V-Funnel test

L-Box test

The L-Box test is used to assess the passing ability of SCC through the gaps between vertical, smooth reinforcing bars (12 mm) (see Figure 4.4). There are two variations: the two-bar test (with a gap of 59 mm) and the three-bar test (with a gap of 41 mm) to simulate situations of lower and higher reinforcement density, respectively. The L-box can be made of steel or coated plywood. The ratio of the concrete heights in the front and back parts of the box is taken as the test result (PA, expressed to the nearest 0,05). The L-Box test principle, apparatus, procedure, result computation and precision are further described in Draft prEN 12350-10 (CEN, 2007c).

Sieve segregation test

The sieve segregation resistance test is used to assess the resistance of SCC to segregation. After sampling, the fresh concrete is allowed to stand for 15 min and any separation of bleed water is noted. The top part of the sample is then poured into a sieve with 5 mm square apertures (see Figure 4.5). After 2 min the weight of material which has passed through the sieve is recorded. The test result is the segregation ratio (SR, recorded to the nearest 1%), calculated as the proportion of the sample passing through the sieve. The sieve segregation test principle, apparatus, procedure, result computation and precision are further described in Draft prEN 12350-11 (CEN, 2007e)
.

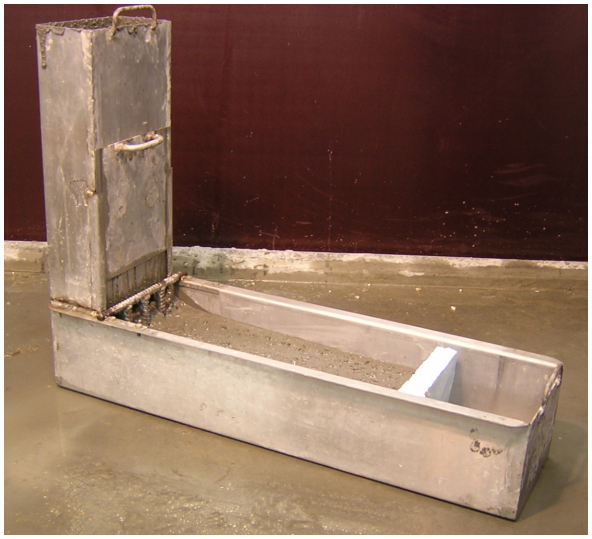


Figure 4.4.: L-Box test

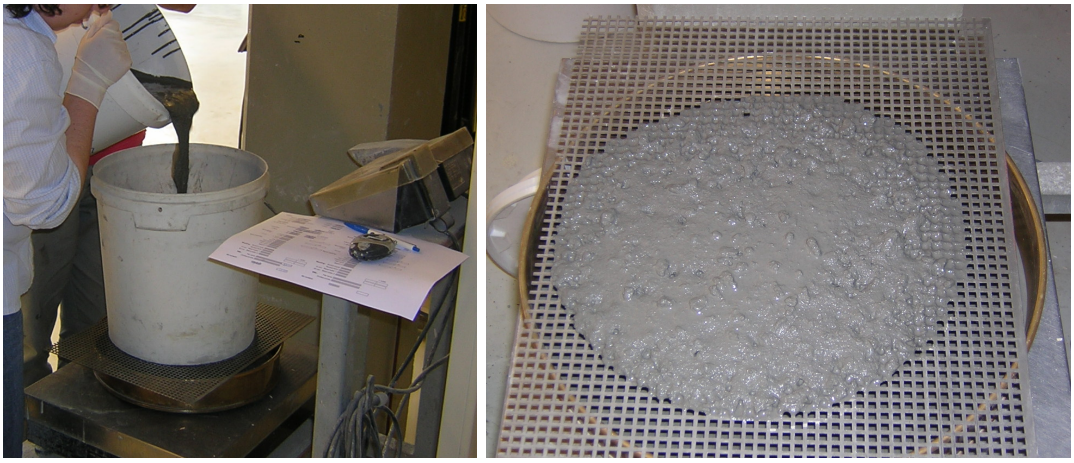


Figure 4.5.: Sieve segregation test (photos taken at Stevin Laboratory, TUDelft, The Netherlands)



Figure 4.6.: J-Ring test

J-Ring test

Similarly, to the L-Box test, the J-ring test is used to assess the passing ability of SCC through tight openings (see Figure 4.6). The bar spacings are the same as for the L-Box (59 and 41 mm), and 12 and 16 smooth bars are used. The narrow bar spacing simulates more congested reinforcement. The test result is given by the difference of concrete heights inside the ring and just outside the ring, also called the J-ring blocking step (BJ, recorded to the nearest millimetre). The J-Ring test principle, apparatus, procedure, result computation and precision are further described in DRAFT prEN 12350-12 (CEN, 2007b).

Correlation between empirical test results and rheological parameters

The empirical tests described above provide an index of workability that may or may not be related to more fundamental rheological parameters (for instance, the Bingham model parameters). Within the EU "Testing SCC" research project, the best correlations with the yield stress value were found with slump flow value (SF) and the L-box blocking ratio (PA) with R^2 equal to 0,76 and 0,73, respectively. The correlations of the yield value with the other test results were with R^2 below 0,4. T500 (from the slump flow test) and the V-funnel time (tv) showed the best correlation with plastic viscosity, with R^2 equal to 0,76 and about 0,6, respectively. The observed correlations of the plastic viscosity with slump flow and L-box blocking ratio were rather low (ACM Centre, 2005).

Furthermore, the empirical test results are related to each other to some degree, since they measure similar properties. Some relation was found between tv and T500 results and between PA and BJ results (Cussigh, 2007; ACM Centre, 2005). Table 4.1, indicates the property(ies) primarily assessed by each test method but the response of each test method may be affected by other properties of concrete being tested. For example, large V-funnel times can be originated by very viscous mixtures or blocking of aggregates near

the exit aperture with segregating mixtures. Summing up, the three key SCC properties (i.e. filling ability, passing ability and segregation resistance) are not independent (ACM Centre, 2005).

4.2.3. Specifications for SCC

Specification of fresh SCC properties (in terms of consistency classes or a target value) is strongly dependent on the specific application and/or site requirements, such as, confinement conditions, placing equipment, placing methods and finishing method (ACM Centre, 2005). Figure 4.7 exemplifies the classes to be specified in different SCC application types, based on BIBM et al. (2005); Walraven (2003) and Draft prEN 206-9 (CEN, 2007a). For all application types, a slump-flow class (SFi) will normally be specified, according to Figure 4.7 and Table 4.1. Where necessary, specific additional requirements can be used to fully describe the performance of an SCC mix, by specifying a viscosity class (VSi/VFi), a passing ability (PLi/PJi) class, a stability class (SRi) (according to Figure 4.7 and Table 4.1) and/or other technical requirements (for example, consistence retention time). A low viscosity SCC may be of interest where good surface finish is required, but it can be more prone to bleeding and segregation. In contrast, a viscous SCC tends to exhibit more thixotropy, which could be of interest to limit the lateral stresses in the formwork or to improve the static segregation resistance. Regarding passing ability, it is necessary to consider the smallest gap between reinforcement bars through which SCC has to flow to fill the formwork, here called flowing gap (fgap). The cover thickness of the reinforcement bars is not to be taken into account in the flowing gap computation. Draft prEN 206-9, Annex L, recommends classes PL1/PJ1 and PL2/PJ2 for typical housing and civil engineering structures, respectively, depending on the flowing gap (see Figure 4.7). If there is little (fgap>100 mm or thin slabs with fgap>80 mm) or no reinforcement, there may be no need to specify passing ability as a requirement. Stability becomes increasingly important for higher fluidity and SCC of lower viscosity. In Figure 4.7, SR1 and SR2 are indicated for horizontal and vertical applications depending on the flow distance (fdist) and flowing gap, according to the guidelines presented in Draft prEN 206-9, Annex L. For vertical applications, if the maximum flow distance (height) is higher than 5 m a SR lower than 10% is indicated in Draft prEN 206-9 (CEN, 2007a).

In addition to those in EN 206-1 (2000), Draft prEN 206-9 (CEN, 2007a) specifies requirements for the constituent materials of SCC, the properties of fresh and hardened SCC and their verification, the limitations for SCC composition, the specification of SCC, the factory production control procedures and the conformity criteria. Because some parts of ENV 13670 indicated the need for mechanical compaction, the reviewed document Draft prEN 13670 (CEN, 2008) has included specific clauses for SCC.

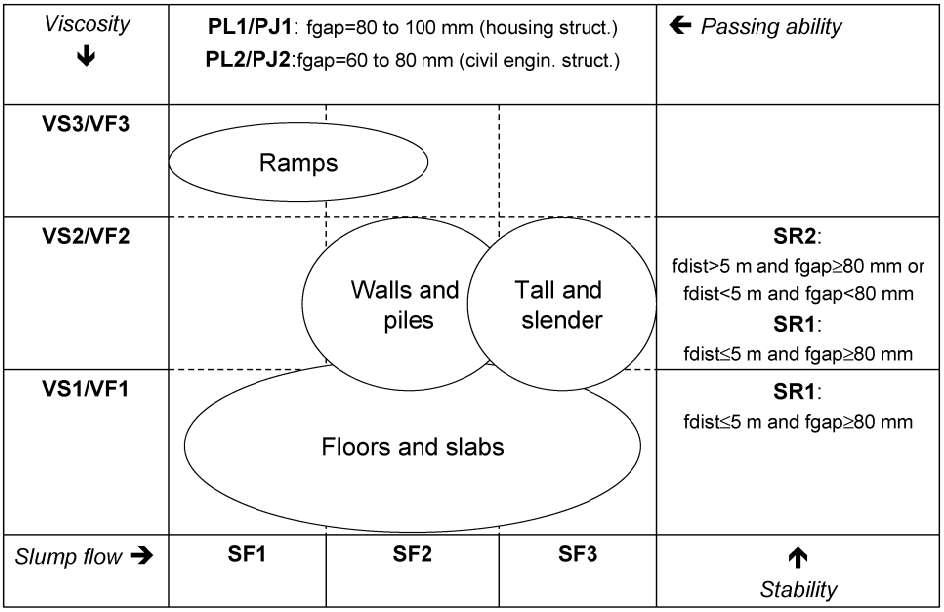


Figure 4.7.: Consistency class' specification of SCC for most common applications, adapted from (BIBM et al., 2005; Walraven, 2003) and Draft prEN 206-9 (CEN, 2007a)

4.3. Mix-design methods

A considerable number of mix-design methods have been developed independently by many academic institutions and construction industry companies (BIBM et al., 2005; Koehler and Fowler, 2007). Still, there is no standard method for SCC mix design. The methods vary widely in overall approach and in terms of complexity.

From early research on SCC in Japan, the Japanese proposed a SCC-designing method (Okamura et al., 2000), which has been followed and further developed by several researchers (Nunes et al., 2001; Takada et al., 1998). In this method, the coarse and fine aggregate contents are fixed and the paste composition is adjusted, based on tests carried out on the paste and mortar levels, to obtain a starting point for trial mixes on concrete. This method was suggested in Europe by EFNARC (2002) and in the US by the Precast/Prestressed Concrete Institute (Koehler and Fowler, 2007). The mixture parameters and test methods involved in this method were used in the present work, thus this mix-proportioning method is further described in Section 4.6.

Most methods consider SCC as a suspension of aggregates in paste. Thus, to proportion SCC three factors must be defined: the aggregates blend, paste volume, and paste composition. Some examples of test methods following this approach are: the Excess Paste Theory (Maeyama et al., 1998; Midorikawa et al., 2001; Oh et al., 1999), the Swedish CBI Method and modifications (Billberg, 2002; Bui and Montgomery, 1999;

Petersson and Billberg, 1999), the ACBM Paste Rheology Model (Saak, 2000), the Densified Mixture Design Algorithm Method (Chang, 2004), the Particle-Matrix Model (Smeplass and Mortsell, 2001), the ICAR Mixture Proportioning Procedure for SCC (Koehler and Fowler, 2007) and the methodology suggested by Gomes (2002) for high strength SCC. A common feature of these test methods is that the paste composition is designed independently to the rest of the mixture. Nevertheless, the strategies used to define the aggregates blend and to select the paste volume vary with each method. Besides, each method uses a different series of tests and has different target values for selecting the paste composition. In the final stage, paste volume, paste composition, and aggregate blend are combined for the preliminary trial concrete batch or batches.

Typically, a trial and error approach is followed in the final stage which consists in testing a first trial batch, evaluating the results, and then adjusting the mixture proportions, based on deducted relationships between the mixture parameters (Okamura et al., 2000) and existing knowledge or recommendations (BIBM et al., 2005) and, finally, retesting the adjusted mixture. This procedure is repeated until the required properties are achieved, which may involve carrying out a large and unpredictable number of trial batches. Besides, this optimization technique may not lead to a general solution of the problem. In contrast, Statistical Experimental Design is a more scientific and efficient approach for establishing an optimized mixture for a given constraint, while minimizing the number of experimental data points (Nehdi and Summer, 2002). Models established based on factorial design highlight not only the significance of the experimental variables but also that of their interactions. These models are valid for a wide range of mix proportioning and have a predictive capability for the responses of other points located within the experimental domain. This design approach was followed by other authors for many different purposes, namely, to design and optimize mixtures, to compare responses obtained from various test methods, to analyse the effect of changes in mixture parameters (to evaluate SCC mixture robustness) and to evaluate trade-offs between key mixture parameters and constituent materials (for example, superplasticizer and viscosity agent) (Bayramov et al., 2004; Khayat et al., 1999c,a, 2000; Nehdi and Summer, 2002; Nunes et al., 2006; Sonebi et al., 2007, 2005; Yahia and Khayat, 2001b).

A more scientific approach is also possible with the Compressible Packing Model developed by de Larrard (1999) for high performance concretes, which has been applied to SCC (Sedran and de Larrard, 1999; Sedran, 1999) and self-compacting fibre reinforced concrete (Grünewald, 2004). Concrete is seen as a suspension of solid particles in water. Proportioning is based on a packing model, to predict the packing density of the solid skeleton, which takes into account the packing process, the size distribution and shape of the particles and the degree of flocculation of finer particles. Equations are available for computing yield stress, plastic viscosity, a parameter representing filling/passing ability,

and a parameter representing segregation resistance (Sedran, 1999). Requirements for hardened properties can also be included (de Larrard, 1999). Therefore, initial trial proportions can be optimized numerically and must then be verified with laboratory trial batches.

In the first years of research on SCC at FEUP the Japanese SCC-designing method was applied with some modifications (Nunes et al., 2001, 2004, 2005a). This approach proceeds essentially by trial and error, using conventional single factor experiments resulting in mixes that might not be optimal in terms of aggregate and paste contents. Thus, within the present PhD research project, a more scientific mix-design method was searched for dealing with constituent materials specific properties and resulting in an optimized concrete mixture, for defined performance requirements. From the mix-design approaches described before, Experimental Factorial Design and the Compressible Packing Model were found to be the most satisfactory. In the author's opinion, the Compressible Packing Model, although a very interesting and valuable approach, was not selected in the present work because it presents, in practice, some barriers for general use. In particular, it requires the use of the model expressions detailed in (de Larrard, 1999) and the calculation of yield stress and plastic viscosity based on empirical measurements with the BTRHEOM, which is not available in most laboratories (it was not available at FEUP) and typically leads to higher results compared to other rheometers (Banfill et al., 2000). Conversely, the Experimental Factorial Design approach is a more universal and versatile approach. It has been widely used in other industries and does not require specific software. It is based on well-known statistical concepts and various commercial software and bibliography are available to help on these analyses. An additional advantage of this approach is that the researcher has some freedom to define the mixture parameters (it can be applied to paste, mortar or concrete) and the responses to be analysed (eg rheological parameters, empirical fresh test results, hardened concrete properties, etc.). This mix-design approach was followed in the work presented in Chapters 5 and 7 and is further described in Section 4.7.

4.4. SCC mix-proportions

The representation of an SCC mix as a suspension provides a consistent, fundamental framework for discussing the influence of mixture proportions on the key fresh SCC properties. As mentioned before, to proportion SCC the aggregates blend, paste volume and paste composition must be defined. The paste volume depends primarily on the aggregates blend characteristics and the paste composition depends both on aggregates blend characteristics and paste volume (Koehler and Fowler, 2007).

4.4.1. Aggregates

For a given application, the aggregates content should be maximized (which minimizes the paste volume) to reduce the cost of the material per m^3 and to improve hardened properties, without impairing self-compactability. The main factors determining aggregates content are: maximum size, particles size distribution, shape and angularity (Koehler and Fowler, 2007). When having more than one aggregate source (fine, intermediate or coarse) this must be considered. All of these factors will determine the maximum packing density of aggregates blend or the voids content of compacted aggregates. The selection of aggregates based on a minimum voids content criteria (or maximum packing density) is not necessarily the best criteria in all cases (Koehler and Fowler, 2007; de Larrard, 1999). For instance, an increase of maximum aggregate size may improve grading and reduce voids content but may not be possible due to passing ability and/or segregation resistance requirements. Thus, there is no universal optimal grading for SCC (Koehler and Fowler, 2007; de Larrard, 1999). In general, equidimensional, well-rounded aggregates are preferred, since they increase packing density and reduce interparticles friction. But, aggregates of all shape and angularity can be accommodated in SCC by increasing the paste volume (Koehler and Fowler, 2007; BIBM et al., 2005).

4.4.2. Paste volume

At concrete level, SCC can be seen as a suspension of aggregates in paste (see Figure 4.8), where the paste volume is set to be greater than the volume of voids between the compacted aggregates so that a thin layer of paste forms around the aggregate particles (excess paste) (Koehler and Fowler, 2007; Grünewald and Walraven, 2007). This excess paste increases fluidity and reduces aggregate inter-particle friction. If this layer is slightly too thin then frictional forces develop and destroy the self-compacting properties, regardless of the composition of the paste. If, however, it is slightly too thick, segregation of aggregates may occur. Thus, the required paste volume is determined by the packing density and surface area of aggregate to provide adequate spacing between aggregate particles (Koehler and Fowler, 2007; de Larrard, 1999). The minimum excess paste needed for concrete to flow can range from 8% for equidimensional, well-rounded aggregates to 16% for poorly shaped, angular aggregates (Koehler and Fowler, 2007). Additional paste can be used to increase the robustness of SCC mixtures (Koehler and Fowler, 2007), as it is demonstrated in Chapter 7.

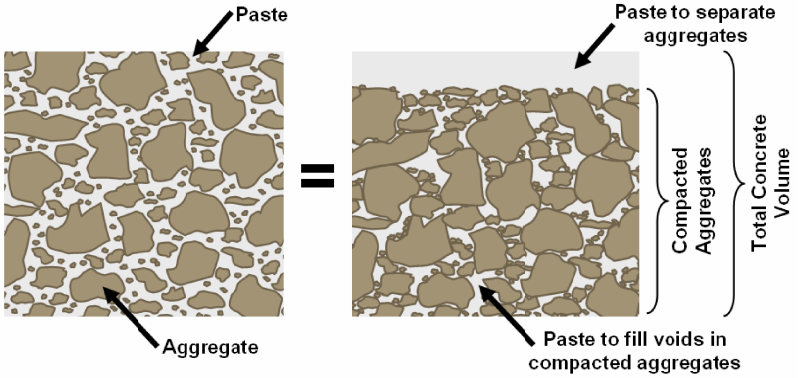


Figure 4.8.: Schematic representation of concrete as a suspension of aggregates in paste, taken from (Koehler and Fowler, 2007)

4.4.3. Paste composition

Once the paste volume is sufficient for a given aggregate blend, concrete workability can be further enhanced by adjusting the paste composition. At paste level, SCC paste can be seen as a suspension of powder particles in water (Grünewald and Walraven, 2007; Midorikawa et al., 2001). The optimum paste characteristics depend on the aggregates skeleton. A decrease of the excess paste to fill the aggregate skeleton can be compensated by an increase of the thickness of water around the powder grains and vice-versa (Grünewald and Walraven, 2007; Midorikawa et al., 2001). The rheological properties of the paste are adjusted and balanced by careful selection and proportioning of the cement and additions, by limiting the water/powder ratio and then by adding a superplasticiser and (optionally) a viscosity-modifying admixture (VA). Besides controlling workability, the paste composition has a large influence on early-age properties and long term hardened properties, including durability. Thus, in order to control temperature rise and thermal shrinkage cracking, as well as strength and durability, the fine powder content may contain a significant proportion of type I or II additions to keep the cement content at an acceptable level. Tests can be conducted on paste or mortar to evaluate the relative effects of various constituents; however, the final paste composition should be verified in concrete.

Depending on paste composition, SCC mixes may be classified into one of three types (Grünewald and Walraven, 2004):

- powder-type SCC, characterized by low water powder ratios and high superplasticizer dosages;
- VA-type SCC, characterized by high water powder ratios and a significant dosage of a VA;
- combination-type SCC, which is intermediate to the previous ones, i.e. moderately

low water powder ratios and small dosages of VA.

4.4.4. Typical values for SCC mix-proportions

Based on an analysis of 68 case studies from different countries, published between 1993 and 2003, performed by Domone (2006), typical values of SCC mix-proportions are presented in Figure 4.9, by using a box-plot[1] representation. In these 68 case studies 50% of the mixtures included VA, thus the results presented in Figure 4.9 are representative of all types of SCC. In most of the case studies maximum coarse aggregate sizes of 16 to 20 mm were used (Domone, 2006). Nearly all mixtures included some type of additions, with limestone powder being the most common one (Domone, 2006). The range of values presented in Figure 4.9 are, in general, in line with those provided by BIBM et al. (2005): a coarse aggregate content of 27 to 36 % (in volume); a paste content of 30 to 38% (in volume); powder content of 380 to 600 (kg/m^3). BIBM et al. (2005) added the following typical mix-proportion values: water powder ratio of 0,85 to 1,10 (in volume); a water content of 150 to 210 (kg/m^3); and a fine aggregate content of 48 to 55% of total aggregate weight. Observing Figure 4.9, it can be noticed that the size of the box and whiskers are smaller in the cases of V_g, V_{paste} and V_s/V_m when compared to w_w/w_p and w_p. This indicates that the mix-proportions related to the aggregate skeleton are more critical to attain self-compactability and there is a more wide range of solutions concerning paste composition (Domone, 2006).

By analysing the subset of mixes incorporating VA (34 case studies) and the subset of mixes without VA (34 case studies), some clear differences can be observed in terms of powder contents and water/powder ratio (see Figure 4.10). Since the differences between the median values are relatively small it can be concluded that most mixtures including VA are of the combination–type. These include only a small amount of VA, which is often added to reduce the sensitivity of the mix to variations of grading or moisture content of the aggregate (Domone, 2006). With further development of admixtures and the widespread use of VAs one can expect larger differences between mixtures with and without VA (Domone, 2006; Grünewald and Walraven, 2005).

Compared to conventional workability concrete, SCC will generally contain lower coarse aggregate contents, larger paste contents, lower water/powder ratios, higher superplasticizer dosages and sometimes a VA. Nevertheless, increasing the paste volume is not necessarily associated with increasing the cement or cementitious materials content (Concrete Society, 2005).

[1]The line within the box marks the median and the boundaries of the box closest and farthest to zero indicate the 25^{th} percentile and the 75^{th} percentile, respectively. The whiskers above and below the box indicate the 90^{th} and 10^{th} percentiles. In addition, the extreme and outlier points are plotted as empty circles and stars, respectively.

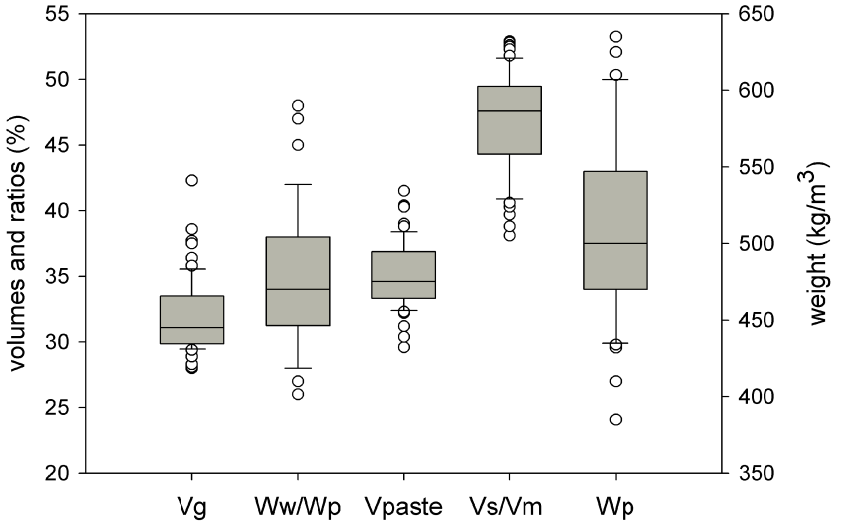
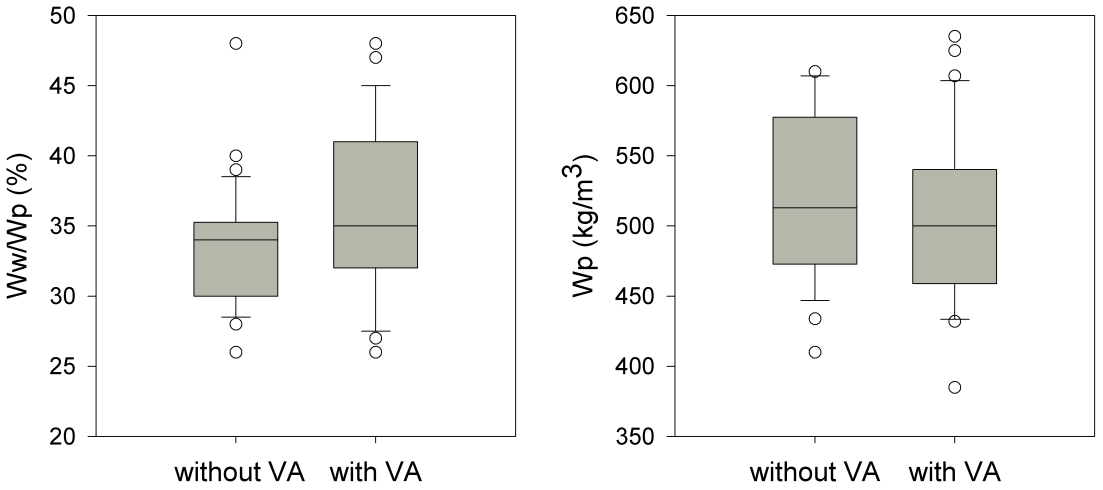


Figure 4.9.: Box-plots of SCC mix-proportions of 68 case studies (Domone, 2006)



(a) (b)

Figure 4.10.: Box-plots of (a) w_w/w_p and (b) w_p of SCC mixtures not including VA (34 case studies) and including VA (34 case studies) (Domone, 2006)

4.5. Hardened properties

In spite of SCC being made basically of the same constituent materials as conventional concrete, significant differences exist regarding their mix-proportions, as shown in the previous section, and also in the placing and compaction processes. Therefore, it is pertinent to discuss the possible differences between hardened properties of SCC and conventional concrete and the applicability of currently existing design rules. From the structural designers' point of view it is the hardened properties that are of paramount interest.

In the following sections, a short review of the influence of SCC mix proportions on the hardened properties is given, with reference to hardened properties data obtained during mix development and full-scale test studies carried out under BACPOR and POCI/ECM/61649/2004 research projects.

4.5.1. SCC .vs. conventional concrete

Considering hardened SCC and conventional vibrated concrete of similar strength, it can be assumed that properties are comparable and any differences lie in the scattering range for conventional concrete (BIBM et al., 2005; Walraven, 2005). Often, for SCC, similar or higher compressive strength, lower modulus of elasticity, higher splitting tensile strength, higher shrinkage and better bond to the reinforcement are reported (BIBM et al., 2005; Walraven, 2005). Similar trends were found when comparing properties of hardened SCC cast during full-scale tests in a precast factory and similar conventional concrete currently used in the same factory, within BACPOR research project (see paper included in Appendix A for further details).

Due to increased content and variety of fine materials (cement, limestone filler, fly ash, etc) and dispersing effect of superplasticizers an improved microstructure can be obtained, related to higher packing density of paste and reduced size and porosity of the interfacial transition zone (ITZ) (Klug and Holschemacher, 2003). This can explain improvements on compressive and tensile strengths of SCC (Klug and Holschemacher, 2003). In addition, SCC should exhibit slightly higher compressive strength as a result of the absence of vibration, which improves the bond between aggregate and paste (BIBM et al., 2005). It was found that limestone powders can also accelerate hydration, resulting in increased compressive strength up to 28 days (Domone, 2007; Klug and Holschemacher, 2003; Zhu and Gibbs, 2005). Limestone filler can react with C_3A forming carboaluminate and with C_3S accelerating the hydration of C_3S and modifying the Ca/Si ratio of C-S-H (Pera et al., 1999). Research has also shown that SO_4 ions in ettringite are replaced with carbonate ions when ground limestone filler is present (Pera

et al., 1999). Based on analysis and comparison of data from more than 70 case studies (Domone, 2007), the ratio of cylinder to cube strength varies from about 0,8 to 1,0 at strengths of about 30 to 90 MPa, respectively, which is generally higher than values used for conventional concrete. Reduction in modulus of elasticity of SCC could be expected due to lower content of coarse stiff aggregates. Elastic modulus of SCC can be up to 40% lower than that of conventional concrete at low compressive strength (20 MPa), but the difference reduces to less than 5% at high strengths (90-100 MPa) (Domone, 2007).

Based on database results from around the world (Klug and Holschemacher, 2003), drying shrinkage of SCC is 10 to 50% higher than that of conventional concrete (predicted by the CEB-FIP model code). Drying shrinkage of SCC may be higher than in conventionally placed concrete primarily due to higher paste volumes. The more highly refined pore structure of SCC (especially when reducing water-cementitious material ratio below 0,40, adding silica fume, increasing the cement fineness, etc) may also increase the risk of autogeneous shrinkage (Koehler and Fowler, 2007). Higher cementitious materials content and lower water-cementitious ratios can increase the susceptibility to thermal volume changes. The higher volume changes sometimes associated with SCC may not necessarily result in increased cracking risk due to higher tensile strength, lower modulus of elasticity, and higher creep.

Bond behaviour of reinforcement in concrete is strongly influenced by quality of the ITZ between the paste and embedded reinforcement (Valcuende and Parra). Furthermore, the position and orientation of a bar in the formwork has also a significant effect on its bond strength (the so-called top-bar effect). The top-bar effect arises from reduction of bond efficiency by formation of voids under horizontal bars which are perpendicular to the casting direction of concrete. Rising bleed water can be trapped under bars and plastic settlement of concrete can leave air voids under the bars which will impair the quality of concrete-steel interface in these zones. In spite of the limited number of studies on bond strength in SCC, in general it was found that bond strength is greater in SCC than conventional concrete (Valcuende and Parra). The differences between both types of concrete tend to even out as the strength of concrete increases (Valcuende and Parra). Consequently, Valcuende and Parra proposed a reduction of the anchorage length of reinforcement, dependent on concrete compressive strength, for the specific case of high viscosity powder-type SCC. SCC also tends to exhibit less variation of bond strength in height. In this respect, Valcuende and Parra also proposed a change to the factor that takes into account the top-bar effect for calculating the anchorage length of reinforcement. The improved bond behaviour of reinforcement in SCC is justified by SCC's filling ability, allowing the concrete to cover the reinforcement more effectively, and SCC's stability, minimizing bleeding, segregation and surface settlement (Valcuende

and Parra; Domone, 2007).

Transport properties of the near-surface concrete play a major role in durability of reinforced concrete (Neville, 1995; Sousa Coutinho, 2005). Usually, the more resistant concrete is to the ingress of aggressive agents (pure water or carrying ions, oxygen and carbon dioxide) the more durable it will be (Neville, 1995). The transport properties of concrete depend primarily on the paste volume, pore structure of the paste and ITZ between paste and aggregate particles (Zhu et al., 2001). Although SCC has higher paste volume, the pore structure of the bulk paste and the ITZ are often improved due to the low water-cementitious materials ratios and the use of additions, but not all additions have the same effect. Zhu et al. (2001) found that chloride diffusivity was very much dependent on the type of addition used in concrete. In summary, the permeability and diffusivity of SCC may be higher or lower than conventionally placed concrete depending on the mixture composition. So far, limited information is available in literature concerning all relevant durability issues, like carbonation, chloride penetration, frost resistance, sulfate attack, thaumasite formation and fire resistance. Concerning this subject, work is currently being carried out under RILEM Technical Committee TC 205-DSC: Durability of self-compacting concrete (Rilem Technical Committee, 2008).

Variation of in-situ properties within the structural elements and the relationship between the in-situ properties to those of standard specimens, made from samples of concrete taken at casting, are very important for both design and structural performance. In this respect, the use of SCC can eliminate defects due to vibration and assure a more uniform distribution of properties. Furthermore, the high segregation resistance of SCC can lead to enhanced homogeneity. Indeed, in one of the full-scale tests carried out within BACPOR research project, it was found that concrete strength measured at different locations of the box-culvert element disperses less than in a similar element with conventional concrete (see paper included in Appendix A for further details). Compaction resulting from external vibration is uneven depending on the distance to the vibration sources. To sum up, SCC provides potential for a superior level of homogeneity and durability for the structure. Nevertheless, mixes must have adequate filling and passing ability for the specific application and any tendency to segregation can have significant detrimental effects, as observed during “SCUT-IP5” full-scale tests carried out within BACPOR research project (see paper included in Appendix A for further details). In this case study, a significant reduction of strength and density of concrete cores, taken from high panels (height=5 m; length=1 m; thickness=0,20 m) casted with segregating SCC, was observed between the middle and the top of the panels (Nunes et al., 2005b).

Table 4.2.: Mix proportions and test results of SCC mixtures developed within POCI/ECM/61649/2004 research project

	Mix A CEM II/A-L 42,5 R	Mix B CEM I 52,5R	Mix C CEM IV/B(V) 32,5 N
Constituent materials (kg/m^3)			
cement	331	332	553
limestone filler	269	270	0
water	156	156	162
superplasticizer (V3000)	10,19[a]	11,45[b]	12,21
sand 1 (natural)		397	
sand 2 (natural)		369	
coarse aggregate		827	
Fresh test results			
Dflow (mm)	708	685	785
T50 (s)	2,4	2,4	2,4
Tfunnel (s)	13,7	15,7	10,4
H2/H1	> 0,80	> 0,80	> 0,80
ΔDflow/ΔWw[c]($mm/kg/m^3$)	6,9	9,6	8,5
Estimated cost (€/m^3)	55	60	65

[a] the equivalent to 0,624 kg/m^3 was discounted to account for the mixer effect;

[b] the equivalent to 0,700 kg/m^3 was discounted to account for the mixer effect;

[c] sensitivity of mixtures to changes in water content is taken here as an indicator of mixture robustness.

4.5.2. Tailor-made SCC

For a given application, SCC can often be designed to have equal or better hardened properties than conventional concrete by making use of the trade-offs associated with mixture parameters and type of materials. Although low water-powder ratios are usually dictated by workability requirements, the water-cement ratios can be varied much more widely depending on the quantities of fillers used, as it will be clarified in Chapter 5. The rate of development and ultimate values of strength, the elastic modulus, dimensional stability and transport properties depend on the amount and activity of these fillers (including those incorporated in cement). This was demonstrated in a study carried out within POCI/ECM/61649/2004 research project. As it is shown in Tables 4.2 and 4.3, different strategies for mixture proportioning may lead to SCC materials that have similar fresh state properties but have different behaviour when considering cost, sensitivity to water content variations, mechanical performance, early-age cracking risk and durability. In these three SCC mixtures, the aggregate skeleton was maintained and only paste composition was altered. A further detailed characterization of these SCC mixtures is given in Appendix B.

Table 4.3.: Hardening and hardened properties of SCC mixtures developed within POCI/ECM/61649/2004 research project

	Mix A	Mix B	Mix C
Mechanical properties at 10 days			
$f_{cm,cube}\,(MPa)$	$49,3$	$58,6$	$48,6$
$f_{cm,cylinder}\,(MPa)$	$43,4$	$51,2$	$42,2$
$f_{ctm}\,(MPa)$	$3,6$	$4,1$	$3,2$
$E_{cm}\,(GPa)$	$41,4$	$42,5$	$38,2$
Mechanical properties at 28 days			
$f_{cm,cube}\,(MPa)$	$50,6$	$62,7$	$58,4$
$f_{cm,cylinder}\,(MPa)$	$47,0$	$53,7$	$51,4$
$f_{ctm}\,(MPa)$	$3,8$	$4,1$	$3,5$
$E_{cm}\,(GPa)$	$42,0$	$44,0$	$40,8$
Temperature evolution			
Time to start increase	$4\,h\,20\,min$	$4\,h\,30\,min$	$7\,h\,10\,min$
Time to reach the peak temperature	$12\,h\,00\,min$	$11\,h\,35\,min$	$15\,h\,20\,min$
ΔTmáx. $(°C)$	$6,2$	$7,9$	$7,9$
Drying shrinkage deformations (mm/mm)			
7 days after demoulding	$43,7 \times 10^{-6}$	$72,3 \times 10^{-6}$	$86,4 \times 10^{-6}$
28 days after demoulding	$125,7 \times 10^{-6}$	$183,0 \times 10^{-6}$	$224,8 \times 10^{-6}$
205 days after demoulding	$238,3 \times 10^{-6}$	$297,6 \times 10^{-6}$	$349,5 \times 10^{-6}$
Creep strain deformations (mm/mm)			
10 days after loading	$194,8 \times 10^{-6}$	$183,5 \times 10^{-6}$	$167,9 \times 10^{-6}$
100 days after loading	$379,4 \times 10^{-6}$	$342,9 \times 10^{-6}$	$281,6 \times 10^{-6}$
170 days after loading	$424,1 \times 10^{-6}$	$374,1 \times 10^{-6}$	$321,2 \times 10^{-6}$
Transport properties			
$D_{ns}\,(m^2/s)$	$21,7 \times 10^{-12}$	$18,8 \times 10^{-12}$	$7,4 \times 10^{-12}$
Sorptivity $(g/(m^2/min^{0,5}))$	$73,29$	$49,53$	$45,71$

By comparing results in Tables 4.2 and 4.3, the most positive aspects of Mix A are lower cost, less sensitivity to water content changes, lower heat of hydration release and lower shrinkage deformations. The most positive aspects of Mix B are faster development of early mechanical properties, higher final strengths (28 days) and modulus of elasticity. Considering Mix C, the most positive aspects are that no additional silo is required for an extra addition, improved transport properties and lower creep deformations. Furthermore, the differences in strength observed at 28 days between Mix C and mixes A and B should be less pronounced at later ages.

4.5.3. Concluding remarks

In the view of the foregoing, SCC is seen as a concrete family that differs only when observed at fresh state. Hardened properties should be evaluated in the same manner as for conventionally placed concrete. The relationships between hardened properties and materials and mixture proportions for conventional concrete generally apply to SCC. Overall, analysis of data from test programmes carried out in the past few years has led to conclude that differences between SCC and conventional concrete of similar strength are small and covered by the safe assumptions in the tables and the formulae provided in the design codes (Domone, 2007; Klug and Holschemacher, 2003). No further revisions of existing standards were found to be necessary regarding SCC hardened properties (Eurocode 2)(Cussigh, 2007).

SCC is a wide family of mixes and there is no unique mix for a given application or set of performance requirements (Domone, 2006). Therefore, the need for a more scientific and efficient approach is emphasized in order to establish tailor-made mixtures that can achieve the desired properties such as filling ability, passing ability, segregation resistance, but also hardened properties, economy, and robustness.

4.6. Japanese SCC-designing method

4.6.1. Mix-proportioning system

According to the Japanese SCC-designing method, suggested by Okamura et al. (2000), the mix proportions are determined as follows:

1. air content is set at 2%, unless air entrainment is required when freeze-thaw resistant concrete is to be designed;
2. the coarse aggregate content in concrete, V_g, is limited to 50% of the dry rodded content ($V_{g,lim}$) excluding air volume;

3. the fine aggregate volume, V_s, corresponds to 40% of the mortar volume (V_m);
4. the water to powder volume ratio, V_w/V_p, is determined on the basis of paste and mortar tests;
5. the dosage of superplasticizer Sp/p (% of powder weight) is adjusted by a test on fresh concrete, to ensure self-compactability;
6. finally, tests are performed on trial batches of concrete to finalize the mixture proportions.

There are also some important conditions on applying this method (Takada et al., 1998):

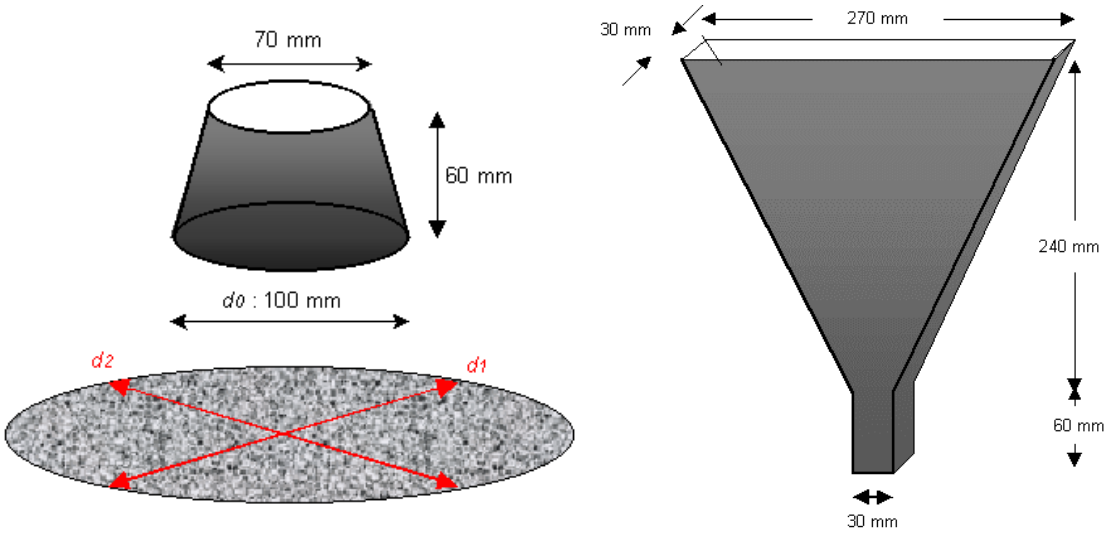
- the maximum aggregate size is 20 mm;
- the border size between fine and coarse aggregates is 5 mm;
- the particles finer than 0,09 mm are not considered as aggregate but as powder;
- Japanese moderate heat Portland cement is used as a standard powder material.

4.6.2. Paste and mortar tests

Physical properties of each powder materials composition can be estimated by a small set of flow tests on pastes (by using the mini-slump flow cone presented in Figure 4.11 (a)) with different water to powder volume ratios (for example, 1,1, 1,2, 1,3, and 1,4 by volume). Okamura et al. (2000) found that, for a paste made with any particular powder or powders composition, the relative flow area (G_p) given by

$$G_p = (d - 100)^2 - 1 \; with \; d = (d1 + d2)/2 \tag{4.1}$$

and the water powder ratio by volume (V_w/V_p) are linearly related. With the linear relation obtained by regression analysis of data, the water retaining ratio (β_p) and the deformation factor (E_p) can then be determined. The β_p is the water to powder volume ratio for which the deformation of the paste is zero; it can be thought as comprising the water adsorbed on the powder surface together with that required to fill the voids among the powder particles (Takada, et al., 1998). E_p is a measure of the sensitivity of the paste flow diameter to increasing water content (Domone and Hsi-Wen, 1997). Water demand of different powder types and powder compositions is compared in Table 4.4. Originally this test was carried out in pastes not including superplasticizer, Domone and Hsi-Wen (1997) showed that the addition of superplasticizer reduces both β_p and E_p values.



(a) (b)

Figure 4.11.: (a) Mini-slump flow cone and (b) mini-V-funnel used in paste and mortar tests in the Japanese SCC-designing method (Okamura et al., 2000)

Table 4.4.: β_p and E_p results for single powders and mixtures of powders

Powder/mixture[a]	β_p	E_p	Powder/mixture[b]	β_p	E_p
pc	1,08	0,061	100% pc	1,04	0,048
pfa	0,59	0,024	85% pc+15% lsp	0,98	0,052
ggbs	1,10	0,046	70% pc+30% lsp	0,93	0,053
lsp	0,77	0,037	60% pc+40% lsp	0,91	0,061
pc+1% Sp	0,86	0,034	60% pc+40% pfa	0,82	0,041

pc: Portland cement; pfa: pulverized fly ash; ggbs: ground granulated blast furnace slag; lsp: limestone powder; Sp: SNF based superplasticizer; [a](Domone and Hsi-Wen, 1997) ;[b](Nunes et al., 2004)

Mortar tests using the flow cone and the V-funnel (Figure 4.11) are suggested to evaluate interaction between fine materials, superplasticizer and fine aggregate particles (Okamura et al., 2000). These tests give a measure of deformability and viscosity through the calculation of the indexes G_m and R_m, respectively. The relative flow area (G_m) can be obtained from the measured flow diameters ($d1$ and $d2$) on the mortar flow test and the relative funnel speed (G_m) can be calculated from the measured time for mortar to flow out through the V-funnel (t), as follows:

$$G_m = (d/100)^2 - 1 \tag{4.2}$$

$$R_m = 10/t \tag{4.3}$$

Larger G_m values indicate higher deformability and smaller R_m values indicate higher viscosity. It was found that the adequate value of water/powder ratio (V_w/V_p) could be reached when $G_m = 5,0$ and $R_m = 1,0$, simultaneously, which corresponds to a slump flow diameter of 250 mm and a V-funnel time of 10 s (Okamura et al., 2000). To facilitate the search for the values of water/powder ratio and superplasticizer dosage to achieve appropriate deformability and viscosity, relationships between Sp/p and G_m/R_m and between V_w/V_p and $R_m/G_m^{0,4}$ were suggested (Okamura et al., 2000), reducing the number of trial mixes.

4.6.3. Concrete tests

According to the type of mixer, the dosage of superplasticizer Sp/p has to be adjusted with tests on fresh concrete, after mixing. Once initial mix proportions have been defined, self-compactability has to be tested by the Box (or U-box), slump flow and V-funnel tests (see paragraph 4.2.2) (Okamura et al., 2000). The Box test is recommended to assess passing ability. This test result is the final concrete height after passing through parallel bars (see Figure 4.12). As an alternative to this test the European "Testing SCC" project group recommended the L-box or J-ring tests for standardisation. A properly designed SCC should result in a slump-flow of 650 ± 50 mm and V-funnel time of 10 to 20 s (Takada et al., 1998).

4.6.4. Modifications to this method

The mix-proportioning system described above was recommended for robust, safe mixes, but subsequent developments have shown this to be conservative. During early investigation on SCC carried out in The Netherlands, the coarse aggregate content was

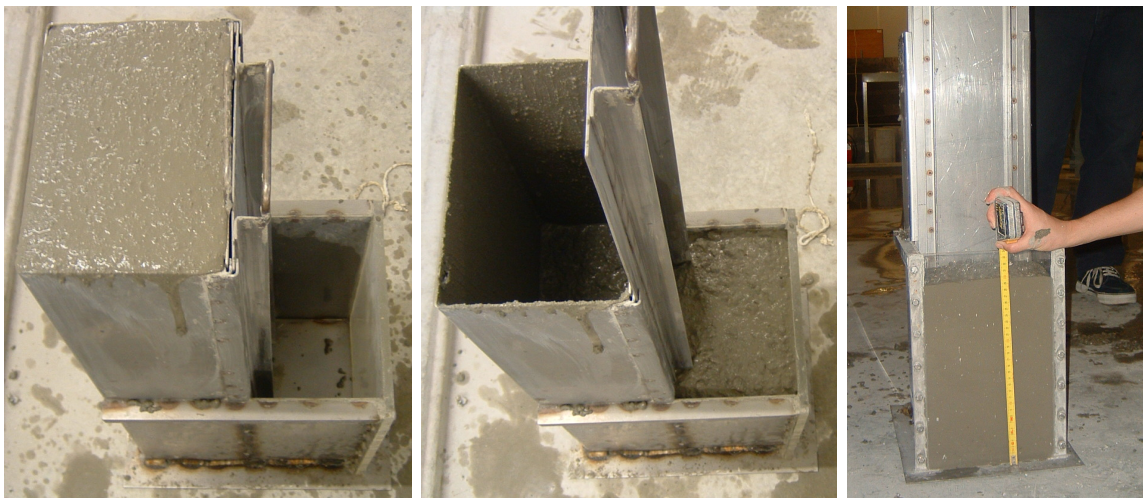


Figure 4.12.: Box test

successfully increased up to 60% of the dry rodded content, when using river aggregates and a maximum aggregate size of 16 mm (Takada et al., 1998). At this aggregate content, the required paste content was significantly lowered and therefore a more efficient mix was obtained.

Based on the experience acquired with the use of SCC in Europe until 2002, in the "European Guidelines and Specifications for Self-Compacting Concrete" published by EFNARC (2002) the Japanese SCC designing method was recommended with a number of modifications aimed at producing more efficient mixes, which are applicable to a wide range of materials used in Europe and to existing standards. The following modifications were introduced to the original Japanese SCC designing method:

- coarse aggregate content (defined as all particles larger than 4 mm) should be between 50 and 60% of the dry rodded content, depending on maximum aggregate size and shape of aggregates;
- fine aggregate content (defined as all particles larger than 0,125 mm and smaller than 4 mm) should be between 40–50 % of the mortar volume;
- a target mini-slump flow of 240 to 260 mm and a mini-V-funnel time of 7-11 s of mortar should be attained.

4.6.5. Universal mixtures formulation

Although the Japanese SCC-designing method was not followed in the present PhD research project, the recommended mixture variables and test methods (mortar tests) were found to be adequate to characterize SCC mixtures, at the mortar and concrete levels (see Chapters 5, 6 and 7).

SCC mix proportions can be established based on the following mixture variables: water to powder volume ratio (V_w/V_p); filler to cement weight ratio (w_f/w_c); superplasticizer to powder weight ratio (Sp/p); sand to mortar volume (V_s/V_m); solid volume ($V_{ap} = V_g/V_{g,lim}$), as suggested by Okamura et al. (2000). An additional variable must be considered when fine aggregate is a combination of two sands. In this work, weight ratio (s_1/s) sand 1 to total sand was used. When proportioning SCC, the volumetric composition of the mix is considered first, with subsequent conversion to proportions by weight, due to the need to overfill the voids between the aggregate skeleton (Concrete Society, 2005). The volumetric composition of concrete, by cubic meter, is given by

$$V_s + V_g + V_p + V_w + V_a = 1,0\,m^3 \tag{4.4}$$

From the absolute values of the mixture variables the paste/mortar/concrete mix proportions can be obtained using the following universal formulation:

First, for a given value of ($V_{ap} = V_g/V_{g,lim}$) and a defined air content (V_a), the coarse aggregate volume can be obtained from

$$V_g = \frac{V_g}{V_{g,lim}} \times V_{g,lim}(1 - V_a) \tag{4.5}$$

and from equation 4.4 and for a given value of (V_s/V_m), the mortar and sand volumes can be defined as

$$V_m = 1 - V_a - V_g \tag{4.6}$$

$$V_s = \frac{V_s}{V_m} \times V_m \tag{4.7}$$

Finally, for a given value of (V_w/V_p), the powder volume is obtained from

$$V_p = \frac{V_m - V_s}{1 + \frac{V_w}{V_p}} \tag{4.8}$$

From the (V_w/V_p) and (w/c) values the filler to cement weight ratio can be determined as follows

$$w_f/w_c = \left(\left(\frac{w/c}{\rho_w \times \frac{V_w}{V_p}} \right) - \frac{1}{\rho_c} \right) \times \rho_f \tag{4.9}$$

where ρ_w, ρ_c and ρ_f represent the specific gravity of water, cement and limestone filler (or any other addition), respectively. After determining the V_p and w_f/w_c the weight values of cement, limestone filler and water can be obtained as follows

$$w_c = \frac{V_p}{\frac{1}{\rho_c} + \frac{w_f/w_c}{\rho_f}} \tag{4.10}$$

$$w_f = (w_f/w_c) \times w_c \tag{4.11}$$

$$w_w = \frac{V_w}{V_p} \times V_p \times \rho_w \tag{4.12}$$

From the superplasticizer dosage (Sp/p) and the weight values of cement and filler the liquid weight of superplasticizer is given by

$$w_{Sp} = \frac{Sp}{p} \times (w_c + w_f) \tag{4.13}$$

Since aggregates were often made of a mixture of two sands and gravel, the dry aggregate contents can be obtained as follows

$$w_{gd} = V_g \times \rho_g \tag{4.14}$$

$$w_{sd} = \frac{V_s}{\frac{s_1/s}{\rho_{sd1}} + \frac{(1-s_1/s)}{\rho_{sd2}}} \tag{4.15}$$

$$w_{sd1} = (s_1/s) \times w_s\,;\; w_{sd2} = (1 - s_1/s) \times w_s \tag{4.16}$$

where ρ_g, ρ_{sd1} and ρ_{sd2} represent the specific gravity of coarse aggregate, sand 1 and sand 2, respectively. The water added to the mixture has to be corrected by subtracting the water content of the superplasticizer, adding the water needed for saturating the aggregates (when they are in a dry state) or subtracting the actual humidity of aggregates as follows

$$w_{wc} = w_w - w_{sp} \times (1 - \gamma_{Sp}) + \sum_i (w_{sdi} \times (A_{si} - H_{si})) + w_{gd} \times (A_g - H_g) \tag{4.17}$$

where γ_{Sp}, A and H represent the solid content of superplasticizer (%), the absorption coefficient of aggregates (%) and the humidity of aggregates (%), respectively.

When the aggregates are humid, the weights of the aggregates should also be corrected as:

$$w_{sdic} = w_{sdi} \times (1 + H_{si}) \tag{4.18}$$

$$w_{gdc} = w_{gd} \times (1 + H_g) \tag{4.19}$$

As it was mentioned before this is a universal formulation for concrete, mortar and paste. The particular case of mortar is obtained when V_{ap} equals zero; and the particular case of paste is obtained when both V_{ap} and V_s/V_m equal zero. This formulation was used to obtain the mix-proportions of all mixtures presented in Chapters 5, 6 and 7.

4.7. Statistical design approach

4.7.1. Introduction

In the concrete mix-design process, experimentation is always present to a larger or shorter extent, even with the more sophisticated and scientific mix-design methods. Statistical design approach refers to the process of planning the experiment so that appropriate data that can be analysed by statistical methods will be collected, resulting in sound conclusions and with a minimum number of experiments. Statistical design approach offers a valid basis for developing an empirical model that is an equation derived from data that expresses the relationship between the response and the important design factors. This empirical model can then be manipulated mathematically for various purposes (Montgomery, 2001).

In general, after formulating the problem, the statistical design approach involves the following procedure steps (Montgomery, 2001):

1. choice of factors (mixture variables), levels and ranges;
2. selection of the response variable(s);
3. choice of the experimental design;
4. performing the experiments;
5. statistical analysis of the data (fitting a model);
6. other computations with response models and conclusions.

The options made in each of these steps for the studies presented in Chapters 5 and 7, are discussed in the next sections.

4.7.2. Experimental design, design factors and response variables

Since some knowledge exists of both the materials to be used and SCC mix-proportions (see Section 4.4) the region to be investigated by the experimenter is relatively close

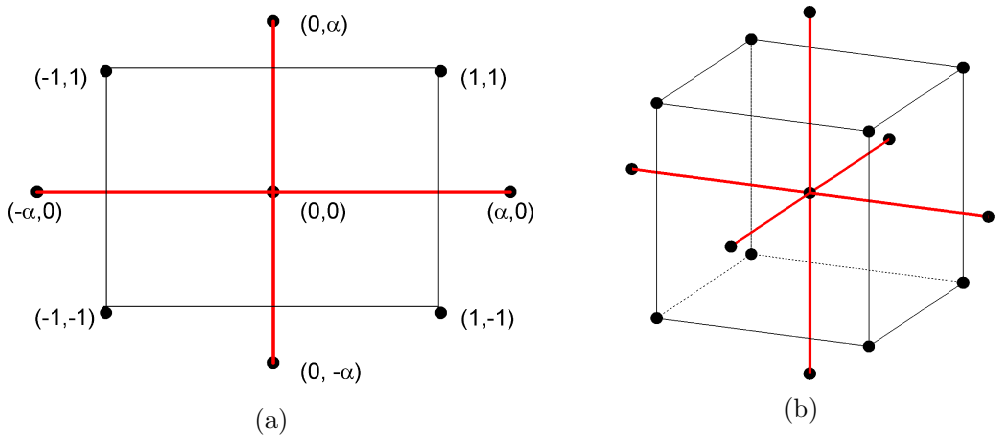


Figure 4.13.: Central composite designs for (a) $k = 2$ and (b) $k = 3$ (Montgomery, 2001)

to the optimum. In situations like this, a second order model is usually required to approximate the response because of curvature in the true response surface.

The most commonly used design for fitting a second order model is the *Central Composite Design* (CCD). The CCD is widely used in practice because it is relatively efficient with respect to the number of runs required. In general, a CCD consists of a 2^k factorial with n_F runs, $2k$ axial runs and n_c centre runs (Montgomery, 2001). Designs for $k = 2$ and $k = 3$ are shown in Figure 4.13.

The 2^k factorial part of the design is necessary to study the joint effect of the factors on a response. The effect of each of the k factors is evaluated at only two levels, the "high" and "low" levels of the factor coded +1 and -1, respectively (Figure 4.13). A complete replicate of such a design requires $n_F = 2^k$ runs. Unfortunately, with a 2^k factorial design one cannot estimate all the unknown parameters (the $\beta's$) in a second order model (see paragraph 4.7.4). A simple and highly effective solution to this problem is to increase the 2^k design with axial runs. Because the purpose of the model is to provide predictions of the response in the region of interest, it is important to have equal precision of estimation in all directions or a constant variance of the predicted response at points equally distant from the design centre. A design with this property is called *Rotatable* (Montgomery, 2001). The CCD may be made rotatable by proper choice of the axial spacing (α). The value of α for rotability depends on the number of points in the factorial part of the design (n_F) (Montgomery, 2001), being given by

$$\alpha = (n_F)^{1/4} \tag{4.20}$$

Replicate runs at the centre of the design (n_c runs) are added to give an estimate of the experimental error. Generally, 3 to 5 centre runs are recommended (Montgomery, 2001). The reason for adding replicate runs at the design centre is that center points

only affect the estimate of the model constant or the global response average.

There are many other designs that can be useful in practice, one of them is a small composite design, consisting of a fractional factorial design plus the usual axial and centre runs (Montgomery, 2001). As the number of factors in a 2^k factorial design increases, the number of runs required for a complete replicate of the design rapidly outgrows the resources (time and/or materials) of most experimenters (Figure 4.14). When k is large, if the experimenter can reasonably assure that certain high-order interactions are negligible, then a fractional factorial design $2^{(k-p)}$ involving fewer than the complete set of 2^k runs can be used to obtain information on the main effects and low-order interactions. The concept of design Resolution (indicated by a Roman numeral subscript in Figure 4.14) is a useful way to catalog fractional factorial designs according to the alias patterns they produce (Montgomery, 2001). In fractional factorial design two or more factors are called aliases when it is impossible to distinguish their effects. In Resolution III designs no main effects are aliased with any other main effects, but they are aliased with two-factor interactions and two-factor interactions may be aliased with each other. In Resolution IV designs no main effects are aliased with any other main effects or any other two-factor interaction, but two-factor interactions are aliased with each other. In Resolution V designs no main effect or two-factor interaction is aliased with any other main effect or two-factor interactions, but two-factor interactions are aliased with three-factor interactions. One should look for the highest possible resolution because it requires less restrictive assumptions regarding which interactions are negligible to obtain a unique interpretation of the data (Montgomery, 2001).

In many situations, the regular fractions presented in Figure 4.14 contain considerably more runs than are necessary to estimate the $p = 1 + k + k(k-1)/2$ parameters in the model containing up to two-factor interactions. For example, the smallest resolution V fraction with k=6 uses 32 runs (Figure 4.14) to estimate the 22 parameters in the model. Therefore, many authors have developed irregular fractions to provide resolution V designs using fewer runs (Oehlert and Whitcomb, 2002). Among examples of these irregular fractions are Jonh's 3/4 fractions (Jonh, 1961), Addelman' designs (Addelman, 1961) and minimum-run equireplicated[2] resolution V designs developed by Oehlert and Whitcomb (2002). These designs allowed to significantly reduce the number of experimental runs while still enabling estimate of the second-order model. For further details on the construction of these designs see (Oehlert and Whitcomb, 2002).

The selected statistical designs for the studies presented in Chapters 5 and 7 are indicated in Table 4.5, along with the selected factors (mixture parameters), response variables, α value, and total number of runs. Based on the Japanese SCC-designing method six parameters are required to completely define the concrete mixtures (air con-

[2]An equireplicated design is one in which each factor has an equal number of high and low levels.

n_F \ k	2	3	4	5	6	7	8	9	10	11	12
4	2^2	2^{3-1}_{III}									
8		2^3	2^{4-1}_{IV}	2^{5-2}_{II}	2^{6-3}_{III}	2^{7-4}_{III}					
16			2^4	2^{5-1}_{V}	2^{6-2}_{IV}	2^{7-3}_{IV}	2^{8-4}_{IV}	2^{9-5}_{III}	2^{10-6}_{III}	2^{11-7}_{III}	2^{12-8}_{III}
32				2^5	2^{6-1}_{VI}	2^{7-2}_{IV}	2^{8-3}_{IV}	2^{9-4}_{IV}	2^{10-5}_{IV}	2^{11-6}_{IV}	2^{12-7}_{IV}
64					2^6	2^{7-1}_{VII}	2^{8-2}_{V}	2^{9-3}_{IV}	2^{10-4}_{IV}	2^{11-5}_{IV}	2^{12-6}_{IV}
128						2^7	2^{8-1}_{VIII}	2^{9-2}_{VI}	2^{10-3}_{V}	2^{11-4}_{V}	2^{12-5}_{IV}
256							2^8	2^{9-1}_{IX}	2^{10-2}_{VI}	2^{11-3}_{VI}	2^{12-4}_{VI}
512								2^9	2^{10-1}_{X}	2^{11-2}_{VII}	2^{12-3}_{VI}

Figure 4.14.: Number of runs (n_F) as a function of number of factors (k) and design type (two-level). Color coding: grey=complete factorial design; green=fractional design with resolution V or higher; yellow= fractional design with resolution IV; red=fractional design with resolution III (State-Ease Corporation, 2000)

tent was fixed at 2%), while only four of these parameters are required to define mortar mixtures (see Table 4.5). A complete 2^4 factorial design was selected for the studies carried out at the mortar level (presented in Chapter 5). Since the studies at the concrete level involve a larger number of factors, only a fraction of the full factorial design was used to form the central composite design. A regular $2^{(5-1)}$ fractional factorial, with resolution V, was selected for the first study on concrete (presented in Chapter 7, Section 7.6) and one of the factors was kept constant, due to limitations of materials. A minimum-run equireplicated resolution V design (Oehlert and Whitcomb, 2002) was selected for the second study on concrete (presented in Chapter 7, Section 7.7). This allowed accommodation of all six mixture parameters as design factors. Further details on the ranges over which the factors were changed and the specific levels at which experimental runs were carried out, are given in Chapters 5 and 7.

4.7.3. Performing the experiments

Statistical methods in experimental design require that the observations (or errors) be independently distributed random variables (Montgomery, 2001). Thus, both the allocation of experimental materials and the order in which the individual runs are to be performed should be randomly determined. It is recommended to perform a few trial runs before conducting the experiment. This can be useful to check the adequacy of the selected range of mixture parameters, to check on the measurement system and to practice the overall experimental technique. During the experiment, it is also useful to

Table 4.5.: Summary of selected statistical designs

Reference	Experimental Design	Factors	Other Parameters	Responses
Chapter 5 (mortar mixtures)	CCD: 2^4 factorial design augmented with 8 axial runs plus 4 central runs	V_w/V_p; w/c; Sp/p; V_s/V_m	$\alpha = 2,0$ 28 runs	Slump flow test (Dflow); V-funnel test (Tfunnel); 28 days compressive strength test (fc,28)
Chapter 7 (concrete mixtures)	CCD: $2^{(5-1)}$ fractional factorial design (resolution V) augmented with 10 axial runs plus 4 central runs	V_w/V_p; w_f/w_c; Sp/p; s_1/s; $V_g/V_{g,lim}$	$\alpha = 2,0$ Vs/Vm was kept constant 30 runs	Slump flow test (Dflow, T50); V-funnel test (Tfunnel); Box-test (H); 28 days compressive strength test (fc,28)
Chapter 7 (concrete mixtures)	CCD: Minimum-run equireplicated resolution V design augmented with 12 axial runs plus 6 central runs	V_w/V_p; w_f/w_c; Sp/p; V_s/V_m; s_1/s; $V_g/V_{g,lim}$	$\alpha = 1,565$ 34 runs	Slump flow test (Dflow); V-funnel test (Tfunnel); L-box test (H2/H1); 28 days compressive strength test (fc,28)

spread the replicates of the centre point out in time (an exception to the randomization rule mentioned before); in this way the experimenter can get a rough check on the stability of the process during the experiment.

4.7.4. Statistical analysis of data

In this work commercial software *Design-Expert* (State-Ease Corporation, 2000) was used to analyse the results for each response variable, by examining summary plots of the data, fitting a model using regression analysis and analysis of variance (ANOVA), validating the model by examining the residuals for trends, outliers and other undesired features, and, finally, interpreting the model graphically.

Fitting a model

For each response variable, a quadratic model can be estimated from the central composite design data. The generic form of a second order model is:

$$y = \beta_0 + \sum_{i=1}^{k} \beta_i x_i + \sum_{i=1}^{k} \beta_{ii} x_i^2 + \sum_{i<j} \sum \beta_{ij} x_i x_j + \varepsilon \tag{4.21}$$

where y is the response; x_i are the independent variables; β_0 is the independent term; β_i, β_{ii} and β_{ij} are the coefficients of the independent variables and interactions, representing

their contribution to the response; ε is the random residual error term representing the effects of variables or higher order terms not considered in the model.

In general, any model that is linear in the parameters (the β values) can be regarded as a multiple linear regression model of the type

$$y = \beta_0 + \beta_1 x_1 + \beta_2 x_2 + \ldots + \beta_k x_k + \varepsilon \tag{4.22}$$

where x_i are called the predictor variables and the parameters β_j are called the regression coefficients. This applies to the second-order model in equation (4.21). The most common method of estimating the regression coefficients, in a multiple linear regression model, is to use a *Least Square Error* approach (LSE). From the $n > k$ observations collected on the response variable $y_1, y_2, \ldots, y_n$, for each observation x_{ij} on each of the predictor variable defined in the experimental design, the following n equations may be established

$$y_i = \beta_0 + \sum_{i=1}^{k} \beta_j x_{ij} + \varepsilon_i \quad i = 1, 2, \ldots, n \tag{4.23}$$

According to the LSE approach, the regression coefficients are estimated by minimizing the total sum of the squares of the errors (ε_i in equation (4.23)). Thus, the LSE estimators, $\hat{\beta}_0, \hat{\beta}_1, \ldots, \hat{\beta}_k$ must satisfy

$$\left.\frac{\partial(\sum_{i=1}^{n} \varepsilon_i^2)}{\partial \beta_j}\right|_{\hat{\beta}_0, \hat{\beta}_1, \ldots, \hat{\beta}_k} = 0, \quad j = 1, 2, \ldots, k \tag{4.24}$$

Finally, the fitted model is given by

$$\hat{y} = \hat{\beta}_0 + \sum_{j=1}^{k} \hat{\beta}_j x_j \tag{4.25}$$

In multiple linear regression analysis, a series of hypothesis-testing procedures are performed to evaluate the usefulness of the obtained model. *Student's t-test* is performed to identify non-significant terms and analysis of variance (ANOVA) is used to evaluate the regression model in several aspects (significance of regression, lack of fit and significance of each variable in the model).

Student's t-test

It may happen that, for some response variables, some of the terms in equation (4.25) may not be significant. The significance of each predictor variable on a given response can be evaluated using a Student's t-test (Montgomery, 2001). The hypotheses for testing the significance of any individual regression coefficient are

$$H_0 : \beta_j = 0$$
$$H_1 : \beta_j \neq 0$$

The test statistic for this test is

$$T_0 = \frac{\hat{\beta}_j}{se(\hat{\beta}_j)} \tag{4.26}$$

where the denominator is the standard error of the coefficient. H_0 is rejected (or the term in the model is significant) if when applying (4.26) to data one has $|T_0| > T_{\alpha/2,n-k-1}$, where $T_{\alpha/2,n-k-1}$ is a critical value calculated from a Student's t-distribution with parameter $(n-k-1)$. Alternatively, one can use the p-value approach to hypothesis testing and thus reject H_0 if the p-value for the statistic T_0 is less than the chosen significance level (α). This test procedure is equivalent to the *partial F test* on a single predictor variable, which will be exposed later.

When there are several candidate predictor variables in a regression model, one needs a search procedure together with an appropriate criterion to select the predictor variables that should be included in the model. The search proceeds in a stepwise manner, by either adding consecutive variables to the model (the so-called *Forward Elimination* method) or by removing variables from an initial set (the so-called *Backward Elimination* method). Since any regression coefficient depends on all the other predictor variables that are in the model, one can easily conclude that the final fitted model may differ slightly depending on the selected search method. In the present work, a step-by-step backward elimination was used to eliminate non-significant terms in the regression model (State-Ease Corporation, 2000), i.e. those terms associated with a p-value greater than the chosen significance level. In this study, the criteria used for the entry and removal of a variable in the model was $\alpha < 0{,}05$ and $\alpha > 0{,}10$, respectively.

ANOVA tests

The basic ANOVA test for significance of regression is to determine if there is a linear relationship between the response variable y and a subset of predictor variables. The appropriate hypotheses are:

$$H_0 : \beta_1 = \beta_2 = \ldots = \beta_k = 0$$
$$H_1 : \beta_j \neq 0 \; for \; at \; least \; one \; j$$

This test involves breaking the total deviation of the observations around the mean (SS_T) into two components: the deviations of the fitted values around the mean, known as regression sum of squares (SS_R); and the error sum of squares (SS_E), which represents the deviations of the observations around the regression fitted model. This test is usually summarized in an ANOVA table such as Table 4.6. This test consists on computing the value of the test statistic F_0 over the available data (see Table 4.6) and to reject H_0 if the value of F_0 exceeds $F_{\alpha,\,k,\,n-k-1}$, the critical value computed from a *Fisher-Snedecor* distribution with parameters (k) and ($n-k-1$) .

A measure of the amount of reduction in the variability of the response y obtained by using the regressor variables $x_1, x_2, \ldots, x_k$ in the model is given by the coefficient of multiple determination R^2 defined as

$$R^2 = \frac{SS_R}{SS_T} = 1 - \frac{SS_E}{SS_T} \tag{4.27}$$

Adding a variable to the model (whether it is statistically significant or not) will always increase R^2. For this reason an R^2_{adj} statistic is sometimes preferred, being defined as

$$R^2_{adj} = 1 - \frac{SS_E/(n-p)}{SS_T/(n-1)} \tag{4.28}$$

where $p = k + 1$ is the number of regression coefficients. Both measures are given for the models presented in Chapters 5 and 7.

As it was mentioned before, adding replicates of centre point to a factorial design allows obtaining an estimate of pure experimental error. This permits dividing the residual sum of squares (SS_E) into two components: the deviation due to pure error (SS_{PE}) and the deviation due to lack of fit (SS_{LOF}), computed as indicated in Table 4.6. In the expressions of SS_{PE} and SS_E, y_{ij} denotes the jth observation on the response at x_i , $i = 1, 2, \ldots, m$ and $j = 1, 2, \ldots, n_i$. Thus, there are $n = \sum_{i=1}^{m} n_i$ total observations. If there is a lack of fit, SS_{LOF} will dominate SS_E, compared with SS_{PE}. Therefore, the Lack of fit test procedure consists on computing the value of the test statistic F_0 on the available data (see Table 4.6) and deciding whether the hypothesis of the regression function to be linear should be rejected or not. If the value of F_0 exceeds $F_{\alpha,\,m-p,\,n-m}$, the critical value computed from a Fisher-Snedecor distribution with parameters ($m-p$, $n-m$).

The *partial F test* can be used to measure the contribution of the predictor variable x_j as if it was the last variable added to the model. It involves computing the "extra sum of squares" due to β_j, which is the increase in the regression sum of squares due to

Table 4.6.: Analysis of variance test in multiple regression (Montgomery, 2001)

Test for:	Source of variation	Sum of squares	Degrees of freedom	Mean square	F value
- significance of regression	regression	$SS_R = \sum_{i=1}^{n} (\hat{y}_i - \bar{y}_i)^2$	k	$MS_R = SS_R/k$	$F_0 = \frac{MS_R}{MS_E}$
	error or residual	$SS_E = \sum_{i=1}^{n} (y_i - \hat{y}_i)^2$	$n-k-1$	$MS_E = SS_E/(n-k-1)$	
	total	$SS_T = \sum_{i=1}^{n} (y_i - \bar{y}_i)^2$ $= SS_R + SS_E$	$n-1$		
- lack of fit	lack of fit	$SS_{LOF} = \sum_{i=1}^{m} n_i(\bar{y}_i - \hat{y}_i)^2$	$m-p$	$MS_{LOF} = SS_{LOF}/(m-p)$	$F_0 = \frac{MS_{LOF}}{MS_{PE}}$
	pure error	$SS_{PE} = \sum_{i=1}^{m} \sum_{j=1}^{n_i} (y_{ij} - \bar{y}_i)^2$	$n-m$	$MS_{PE} = SS_{PE}/(n-m)$	
	error or residual	$SS_E = \sum_{i=1}^{m} \sum_{j=1}^{n_i} (y_{ij} - \hat{y}_i)^2$	$n-p$		
- partial significance of each predictor variable	regression (reduced model)	$SS_R(\beta_j \mid \beta_0, \beta_1, \ldots, \beta_{j-1}, \beta_{j+1}, \ldots, \beta_k)$	1	$MS_R = SS_R/1$	$F_0 = \frac{MS_R}{MS_E}$
	error (full model)	$SS_E = \sum_{i=1}^{n} (y_i - \hat{y}_i)^2$	$n-k-1$	$MS_E = SS_E/(n-k-1)$	

adding x_j to a model that already includes $x_1, \ldots, x_{j-1}, x_{j+1}, \ldots, x_k$. This test consists on computing the value of F_0 over the available data (see Table 4.6) and to reject H_0 if the value of F_0 exceeds $F_{\alpha,1,n-p}$, the critical value computed from a Fisher-Snedecor distribution with parameters (1, $n-p$).

Alternatively, in all of these Fisher-tests one can use the p-value approach to hypothesis testing and thus reject H_0 if the p-value for the statistic F_0 regarding the available data is less than α.

Model adequacy checking

The hypothesis testing involved in regression analysis is based on the assumptions that the errors (ε_i) are independent and normally distributed with zero mean and constant variance. In order to assess these assumptions one can use graphical inspection and perform the Normal distribution fitting tests. In the present work the Normal probability plot of residuals were examined to check normality, the plots of residuals against predicted values and the plot of residual against values of the individual predictor variables were analysed to check the constancy of residual variance. In addition, the Lilliefors test for normality (a modification of Kolmogorov-Smirnov test of goodness of fit) and Shapiro-Wilk test for normality were performed. The Durbin-Watson test statistic was used to detect the presence of autocorrelation in the residuals from the regression analysis (Gunst and Mason, 1980). In addition, the randomness of residuals was evaluated by computing autocorrelations for data at varying time lags. Autocorrelations should be near zero for all time-lag separations, if not the randomness assumption fails. In case one or more of the autocorrelations will be significantly non-zero, an autoregressive model might be appropriate and a partial autocorrelation plot can be examined to help identify the order of the autoregressive model (Box et al., 1978).

If needed, a transformation of the response variable is often an effective method for stabilizing the response variance, making the distribution of the response variable closer to the normal distribution, and improving the fit of the model to the data. The selection of the form of the transformation can be made with the help of Box-Cox criteria which uses an estimate of λ for power transformations of the type $y* = y^{\lambda}$ or by trial–and–error (Montgomery, 2001). Besides the large family of power transformations, the $ln\, y$ and $log\, y$ can also be considered.

Another important issue is the detection of regression outliers. Regression outliers correspond to cases exhibiting a strong deviation from the fitted regression curve, which can have a harmful influence in the process of fitting the model to the data. Points with this characteristic are named leverage points. Identification of leverage points, for their eventual removal from the dataset, was carried out by analysing the Cook's distance.

If there are no outliers, these distances are of approximately equal amplitude and less than 1,0 (Montgomery, 2001).

The "best" regression models are those in which the predictor variables each correlate highly with the dependent variable but correlate at most only minimally with each other. The existence of high correlation between the predictor variables (multicollinearity) leads to imprecise determination coefficients, imprecise estimates and imprecise tests on the regression coefficients. Multicollinearity was assessed by using the so-called variance inflation factors (VIF), which are defined for each predictor variable as

$$VIF_k = (1 - r_k^2)^{-1} \tag{4.29}$$

where r_k^2 is the coefficient of multiple determination when x_k is regressed on the remaining variables in the model. An r_k^2 near 1, indicating higher correlation with the remaining variables will result in a large value of VIF. A VIF larger than 10 is usually taken as an indicator of multicollinearity.

An exemplification of test procedures for examining hypotheses about multiple linear regression models and techniques for checking model assumptions, described here, is given in Appendix D for the first model appearing in Chapter 5, paragraph 5.3.1.

4.7.5. Mixtures optimisation

Commercial software *Design-Expert* (State-Ease Corporation, 2000) also allows the simultaneous optimization of multiple responses obtained from the factorial experimental plan. Numerical optimization can optimize any combination of one or more goals. The allowable goals are to minimize or maximize a parameter, to target a specific level of a parameter, to keep a parameter within a specified range or none (the default goal is to keep the parameter within the low and high limits) (State-Ease Corporation, 2000). Each goal is assigned a weight (number between 1 and 5 with 5 being the most important and 1 the least important) and goals are combined in an overall desirability function. The optimization software searches for the greatest overall desirability. A value of one of the desirability function represents the ideal case. A zero indicates that one or more responses fall outside desirable limits. The goal seeking begins at a random starting point and proceeds up the steepest slope to a maximum. There may be two or more maxima because of curvature in the response surfaces and their combination into the desirability function. Starting from several points in the desiring space may be necessary to find the best local maximum.

Specific details on optimization criteria used in different studies are given in Chapters 5 and 7.

4.7.6. Comments on this approach

The experimental design approach provides a way to evaluate the effects of mixture proportions in a statistically sound manner with a minimum number of mixtures. The statistical concepts involved are well known and widely used in many industries. However, some prior knowledge is required to select the values of factors used in the experimental design such that all or most mixtures exhibit SCC or near-SCC flow characteristics.

In this approach deliberate laboratory testing is conducted with actual job materials to measure the response variables. Regression models can be fitted to the results of each measured response, which allow establishing final mixture proportions efficiently. As a rule, the resulting models are specific to only the materials and range of proportions considered. Nevertheless, the general relative trends found for a certain set of materials and proportions may remain consistent when a different set of materials is used.

5. Optimization of SCC mortar mixtures

5.1. Introduction

Since the mortar properties adequate for SCC were sufficiently well defined during the early development of SCC at the University of Tokyo (Okamura et al., 2000), initial tests are often carried out at mortar level. Not only mortar tests are easier to carry out, and less time consuming when compared to tests with concrete, but if target values are achieved at mortar level, the tests on concrete, although essential, may be reduced to a minimum (Okamura et al., 2000). This chapter presents the methodology used for the design of mortar mixtures which are adequate for SCC. This methodology was developed in three phases: first, the experimental phase conducted according to a central composite design; second, the statistical analysis and model fitting of data collected during the experimental phase and, third, the numerical optimization of mixture parameters using the models derived in the previous phase. This methodology was applied to six different types of cement in combination with limestone filler and a polycarboxylate type superplasticizer. Contour plots and interaction diagrams representing the range of mixture parameters where SCC can be found are presented for each cement type. These plots and diagrams can be useful to simplify the test protocol required to optimize a given SCC mixture.

This chapter provides reference mortar mixtures for the study on cement variations which is reported in Chapter 6.

5.2. Experimental programme

5.2.1. Materials characterization

Mortar mixes investigated in this study were prepared with cement (first delivery), a mineral additive, limestone filler (first delivery), reference sand conforming to CEN EN

196-1 and tap water. Six of the most currently used cement types in Portuguese construction industry were selected. The chemical and physical properties of the different cement types and limestone filler are presented in Tables C.1 to C.7 of Appendix C. The mean particle size of limestone filler was 4,5 μm. A polycarboxylate type superplasticizer (V3000) was used having a specific gravity of 1,05 and 18,5% solid content. Reference sand is a siliceous round natural sand (0,08-2 mm) with a specific gravity of 2,57 and an absorption value of 0,68%.

5.2.2. Experimental plan

Since curvature on the response surface of mortar properties was found by other authors (Nehdi and Summer, 2002), in the present study experiments were designed according to a central composite design adequate to fit a second order model (see paragraph 4.7.4). This design consisted of a 2^4 factorial statistical design (four factors at two levels) augmented with 8 axial runs plus 4 central runs to evaluate the experimental error. SCC mortar mix proportions were established based on the following variables x_i: water to powder volume ratio (V_w/V_p); water to cement weight ratio (w/c); superplasticizer to powder weight ratio (Sp/p); sand to mortar volume (V_s/V_m), as suggested by Okamura et al. (2000). The effect of each variable was evaluated at five different levels $-\alpha$, –1, 0, +1, $+\alpha$ as presented in Table 5.1 and the design was made rotatable by taking α equal to 2,0.

The absolute value of each variable corresponding to a given level in Table 5.1 depends on the variable itself and on the specific experimental plan. For a given variable and a given experimental plan the transformation of coded into absolute values is of the form:

$$a = a_0 + x \cdot \Delta a \tag{5.1}$$

with x being the coded variable measured with the step like units, a the absolute value in normal units, a_0 the absolute value of the variable at the centre of the design and Δa the variable variation (in absolute values) corresponding to a unit change in the coded variable.

In this work, experimental mixtures F8 and F9 (see Table 5.1) were first assessed and their results were analyzed before proceeding with the rest of the experimental plan, in an attempt to check the adequacy of the selected range of mixture parameters. Considering the combination of mixture levels in the F8 and F9 mixes, these should respectively lead to one of the most fluid mixtures and to one of the least fluid mixtures, of all mixtures in the experimental plan. Thus, it is desirable that the interval formed by the results obtained from F8 and F9 mixtures includes the target value for each mortar test which are a Dflow of 260 mm and a Tfunnel of 10 s, in the present work. When this is

Table 5.1.: Coded values for the variables used in the experimental design

Ref.	point type	V_w/V_p	w/c	Sp/p	V_s/V_m
Ci[a]	central	0	0	0	0
F1	factorial	-1	-1	-1	-1
F2		1	-1	-1	-1
F3		-1	1	-1	-1
F4		1	1	-1	-1
F5		-1	-1	1	-1
F6		1	-1	1	-1
F7		-1	1	1	-1
F8		1	1	1	-1
F9		-1	-1	-1	1
F10		1	-1	-1	1
F11		-1	1	-1	1
F12		1	1	-1	1
F13		-1	-1	1	1
F14		1	-1	1	1
F15		-1	1	1	1
F16		1	1	1	1
CC1	axial	2	0	0	0
CC2		-2	0	0	0
CC3		0	2	0	0
CC4		0	-2	0	0
CC5		0	0	2	0
CC6		0	0	-2	0
CC7		0	0	0	2
CC8		0	0	0	-2

[a] the central point was replicated four times (i=1 to 4)

not the case, the range of one or more variables should be changed, i.e. the values of a_0, Δa or both should be altered. In the present work, the plan was modified when changing from cement type CEM I 42,5 R to CEM II/B-L 32,5 N, CEM IV/B(V) 32,5 N and CEM II/B-L 32,5 R (BR). The values of a_0 and Δa adopted in each experimental plan, corresponding to the different cement types, are given in Table 5.2. Hence, the modelled experimental region in each experimental plan consisted of mixtures made with the variable ranges presented in Table 5.3.

5.2.3. Mixing sequence and testing methods

With the exception of F8 and F9, mixtures from the experimental plan were tested in a random order. The mixes were prepared in the laboratory in 1,4 l batches and mixed in a two-speed mixer complying to NP EN 196-1(Portugal. IPQ, 2006). The mixing sequence consisted of mixing sand and powder materials with 0,81 of the mixing water during 60 s, stopping the mixer to scrape material adhering to the bowl of the mixing bowl, mixing for another 60 s, adding the rest of the water with the superplasticizer, mixing for 60 s, stopping the mixer again to scrape material adhering to the bowl, mixing for another 30 s, stopping the mixer for 5 min (adequate for V3000 superplasticizer type) and finally mixing mortar during a further 30 s. The mixer was always set at low speed except in the last 30 s of the mixing sequence, when it was set as high speed. Mortar tests using the flow cone and the V-funnel, with the same internal dimensions as the Japanese equipment (see paragraph 4.6.2), were then carried out to characterize fresh state. After fresh mortar tests, three 70 mm cubes were moulded to evaluate 28 days compressive strength (fc,28). Mortar cubes were demoulded one day after casting and kept inside a chamber under controlled environmental conditions (Temperature=20°C and HR=95-98%) until testing age. The mortar flow test was used to assess deformability through the calculation of the flow diameter (Dflow) as the mean of two opposite diameters in the spread area. The V-funnel test was used to assess the viscosity and passing ability of the mortar. Test flow time was recorded (Tfunnel). Dflow, Tfunnel and fc,28 were the selected mortar properties to be analysed and modelled.

5.3. Collected data, fitted models and mixtures optimization

The mix proportions and test results of the 28 mixes prepared as described in paragraph 5.2.3 are summarized in Tables E.1, E.2, E.3, E.4, E.5 and E.6, of Appendix E, for the experimental plans incorporating CEM I 42,5 R, CEM I 52,5 R, CEM II/A-L 42,5 R, CEM II/A-L 32,5 N, CEM IV/B (V) 32,5 N and CEM II/B-L 32,5 R (BR),

Table 5.2.: Values a_0 and Δa used in the transformation of coded values into absolute values of the variables in each experimental plan

	V_w/V_p		w/c		Sp/p		V_s/V_m	
	a_0	Δa	a_0	Δa	a_0	Δa	a_0	Δa
CEM I 52,5 R	0,900		0,40		1,75%			
CEM I 42,5 R	0,900		0,40		1,75%			
CEM II/A-L 42,5 R	0,900	0,100	0,40	0,05	1,75%	0,25%	0,45	0,025
CEM II/B-L 32,5 N	0,850		0,40		1,75%			
CEM IV/B(V) 32,5N	0,800		0,42		1,75%			
CEM II/B-L 32,5R (BR)	0,700		0,38		1,25%			

Table 5.3.: Correspondence between coded values and absolute variable values in each experimental plan

variable	-2	-1	0	+1	+2
CEM I 42,5 R; CEM I 52,5 R; CEM II/A-L 42,5 R					
V_w/V_p	0,700	0,800	0,900	1,000	1,100
w/c	0,30	0,35	0,40	0,45	0,50
Sp/p	1,25%	1,50%	1,75%	2,00%	2,25%
V_s/V_m	0,400	0,425	0,450	0,475	0,500
CEM II/B-L 32,5 N					
V_w/V_p	0,650	0,750	0,850	0,950	1,050
w/c	0,30	0,35	0,40	0,45	0,50
Sp/p	1,25%	1,50%	1,75%	2,00%	2,25%
V_s/V_m	0,400	0,425	0,450	0,475	0,500
CEM IV/B(V) 32,5 N					
V_w/V_p	0,600	0,700	0,800	0,900	1,000
w/c	0,32	0,37	0,42	0,47	0,52
Sp/p	1,25%	1,50%	1,75%	2,00%	2,25%
V_s/V_m	0,4	0,425	0,45	0,475	0,5
CEM II/B-L 32,5 R (BR)					
V_w/V_p	0,500	0,600	0,700	0,800	0,900
w/c	0,28	0,33	0,38	0,43	0,48
Sp/p	0,75%	1,00%	1,25%	1,50%	1,75%
V_s/V_m	0,400	0,425	0,450	0,475	0,500

respectively. Statistics of the obtained results were computed for all data points and also for the central points only (see paragraphs 5.3.1 to 5.3.6). From these results it may be observed that with these experimental plans a wide range of mortars was covered. Moreover, the range of Dflow and Tfunnel results obtained is adequate since it includes both targets Dflow and Tfunnel. None of the mixes exhibited severe segregation. From the central points data it can be concluded that the highest experimental error is associated with the Tfunnel response variable, with exception of experimental plans including CEM IV/B (V) 32,5 N and CEM II/B-L 32,5 R (BR).

As explained in paragraph 4.7.4, for each response variable a quadratic model can be estimated from the central composite design data (see equation 4.21). The model parameters (β_0, β_j, β_{ij}) are estimated by means of a multilinear regression analysis. The estimates of the fitted models, including the residual error term, along with the regression coefficients, are given in the following paragraphs for each cement type. An analysis of variance showed that these models are significant when describing the effect of V_w/V_p, w/c, Sp/p and V_s/V_m on the modelled responses. The estimates of the model coefficients, obtained for the coded variables, give an indication of the relative significance of the various mixture variables on each response. A negative estimate means that the response variable will decrease if the given mixture variable increases. The most significant individual and interaction effects found on analysed responses are listed in paragraphs 5.3.1 to 5.3.6, for each cement type.

Residual analysis did not reveal obvious model inadequacies or indicate serious violations of the normality assumptions, except in the case of Tfunnel response. This problem was overcome after a variable transformation of the form $y^{-0,5}$. No evidence of autocorrelation or unstationarity was found in the residues.

In general, the estimated residual standard deviation does not exceeded the experimental error by far, so a good fitting can be expected. Three mixtures covering a wide range of proportioning and not used to derive the model (mixes 29 to 31 in Tables E.1 to E.6, in Appendix E) were selected to verify the ability of the proposed models to predict the responses. The four central point mixtures (mixes 1 to 4 in Tables E.1 to E.6, in Appendix E) were used along with these three mixtures to compare the measured-to-predicted values of each response variable. A plot of measured-to-predicted values of Dflow, Tfunnel and fc,28 are shown in paragraphs 5.3.1 to 5.3.6, for each experimental plan, with the prediction intervals corresponding to a 95% confidence level. One can observe that all points (including those not used to derive the models) fall within the limits of the prediction intervals. In addition, the ratio between predicted-to-measured values for Dflow, Tfunnel and fc,28 (central points and additional data) was not far from 1,0. Thus, one can expect the established models to be sufficiently accurate to predict the analysed fresh and hardened properties, with the possible exception of fc,28

Table 5.4.: Optimization constraints

Variable	Goal	Lower limit	Higher limit	Lower weight	Higher weight	Importance
V_w/V_p	is in range	-2,5	2,5	1	1	3
w/c	is equal to c_1 [a]	-2,5	2,5	1	1	3
Sp/p	is in range	-2,5	2,5	1	1	3
V_s/V_m	is equal to c_2 [b]	-2,5	2,5	1	1	3
Dflow (mm)	is target = 260	240	280	1	1	3
Tfunnel (s)	is target = 10	8	12	1	1	3

[a] c_1 varying from 0,3 to 0,5 by steps of 0,01; [b] c_2 varying from 0,4 to 0,5 by steps of 0,01

of mortars including CEM I 52,5 R (see paragraph 5.3.2). Nevertheless, this model will still be useful, explaining more than 50 % of the variations in the response.

After building the regression models that establish relationships between mix design variables and the responses, the numerical optimization technique was used to determine the range of mortar mixture parameters where deformability and viscosity coexist in a balanced manner, i.e. to determine the best mixtures which exhibit a spread flow of 260 mm and a flow time of 10 s. In the present work, a slightly higher target spread flow value was adopted when compared to the value recommended by the Japanese SCC-designing method, based on previous experience of the author and EFNARC (2002). The values of V_w/V_p and Sp/p that can lead to the best mixtures were searched for a given pair of (V_s/V_m; w/c) by using the constraints presented in Table 5.4. No restriction was established for the fc,28 response variable. Note that since the response models were expressed as a function of four independent variables, a multiple optimum will hardly occur. Because the error in predicting the responses increases with the distance from the centre of the modelled region, the use of the models was limited to an area bound by coded values + 2,5 to -2,5. Finally, the adjusted values of V_w/V_p and Sp/p and the estimated values of fc,28, for each pair of (V_s/V_m; w/c), were used to obtain the contour plots presented in paragraphs 5.3.1 to 5.3.6.

5.3.1. CEM I 42,5 R

The experimental plan corresponding to CEM I 42,5 R was carried out between the 18^{th} and 20^{th} of January 2006. A cement sample was taken from the first delivery of CEM I 42,5 R supplied by Cimpor, from the Alhandra production centre.

Statistics of the obtained results are presented in Table 5.5 for all data points and also for the central points only. The range of mortar properties covered with this experimental plan was: Dflow ranging from 197 to 336 mm, Tfunnel ranging from 2 to 12 s and

Table 5.5.: Statistics of the results for the total points and for central points (CEM I 42,5 R)

	N=28 total points			n_c=4 central points		
	Dflow (mm)	Tfunnel (s)	fc,28 (MPa)	Dflow (mm)	Tfunnel (s)	fc,28 (MPa)
Minimum	197	1,8	61,3	278	3,72	68,1
Maximum	336	11,7	79,2	283	4,1	72,7
Mean	275	4,9	72,5	280	4,0	70,9
Standard deviation	36	2,7	4,3	3	0,2	2,0
Coefficient of variation	13,1%	55,5%	6,0%	0,9%	4,9%	2,8%

fc,28 ranging from 61 to 79 MPa. The estimates of the fitted models, including the residual error term, along with the correlation coefficients, are given in Table 5.6. It can be observed that the estimated residual standard deviation (see Table 5.6) does not exceed the experimental error by far (see Table 5.5). The measured-to-predicted values of Dflow, Tfunnel and fc,28 are shown in Figures 5.1, 5.2 and 5.3, respectively, with the prediction intervals corresponding to a 95% confidence level. The ratio between predicted-to-measured values (central points and additional data) for Dflow, Tfunnel and fc,28 ranged between 1,00 and 1,05, 0,95 and 1,06, 0,97 and 1,06, respectively.

The results in Table 5.6 clearly show that w/c exhibit a great effect on all three measured responses, being only exceeded by the effect of V_w/V_p on (Tfunnel$^{-0,5}$) response. Besides w/c, the variable that most influenced Dflow was Sp/p. Significant interaction effects were found between V_w/V_p and w/c on all the analysed responses, and in the case of fc,28 response this effect was larger than the individual effects of V_w/V_p , Sp/p and V_s/V_m. This interaction effect is related to the filler content. Interaction effects between V_w/V_p and Sp/p and between w/c and V_s/V_m were also found to be significant on Dflow response. The quadratic term in w/c was significant for both Dflow and Tfunnel responses. The quadratic term in Sp/p was significant for both Dflow and fc,28 responses. The quadratic term in V_s/V_m was significant on fc,28 response.

The adjusted values of V_w/V_p and Sp/p for each pair of (V_s/V_m, w/c) in optimized mortars containing CEM I 42,5 R were used to obtain the contour plots presented in Figure 5.4 (a). The corresponding contour plot for estimated mortar compressive strength is presented in Figure 5.4 (b).

5.3.2. CEM I 52,5 R

The experimental plan corresponding to CEM I 52,5 R was carried out between the 16^{th} and 18^{th} of January 2006. A cement sample was taken from the first delivery of CEM I 52,5 R supplied by Cimpor, from the Alhandra production centre.

Table 5.6.: Fitted numerical models for coded variables (CEM I 42,5 R)

Response variable	Dflow (mm)	[Tfunnel (s)]$^{-0,5}$	fc,28 (MPa)
model terms estimate			
independent	282,67	0,504	70,862
V_w/V_p	11,16	0,093	-0,243
w/c	28,03	0,078	-3,543
Sp/p	18,51	0,022	1,014
V_s/V_m	-11,82	-0,045	0,054
$(V_w/V_p)\times(w/c)$	1,92	0,015	1,796
$(V_w/V_p)\times(Sp/p)$	-1,92	NS	NS
$(V_w/V_p)\times(V_s/V_m)$	NS	-0,006	NS
$(w/c)\times(V_s/V_m)$	2,11	NS	NS
$(w/c)^2$	-6,16	-0,009	NS
$(Sp/p)^2$	-2,41	NS	1,187
$(V_s/V_m)^2$	NS	NS	0,689
residual error, ε^a			
mean	0	0	0
standard deviation	3,072	0,011^b	1,734
R^2	0,993	0,992	0,839
R^2_{adj}	0,989	0,989	0,783

(NS) non-significant terms; ^{a}error term is a random and normally distributed variable; ^{b}corresponding value for Tfunnel is 0,27

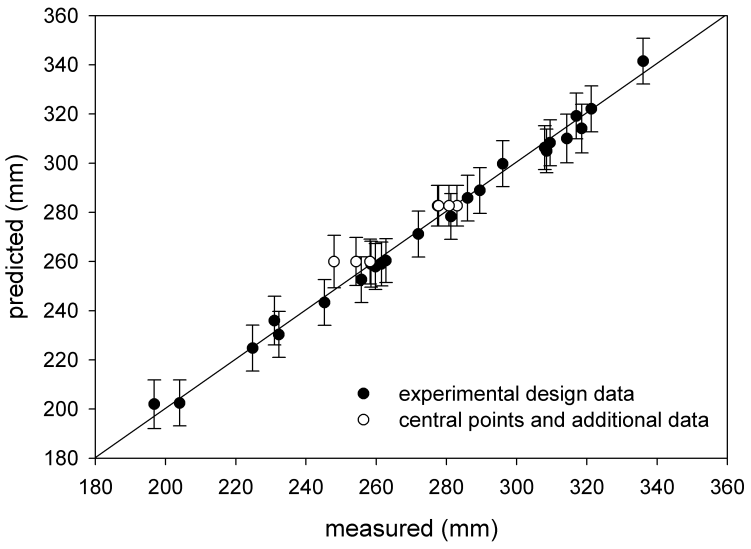


Figure 5.1.: Comparison of measured versus predicted values of Dflow (CEM I 42,5 R)

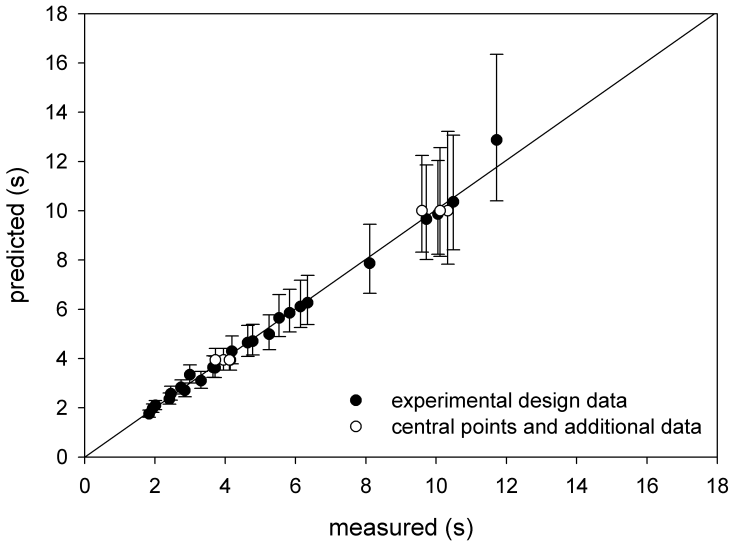


Figure 5.2.: Comparison of measured versus predicted values of Tfunnel (CEM I 42,5 R)

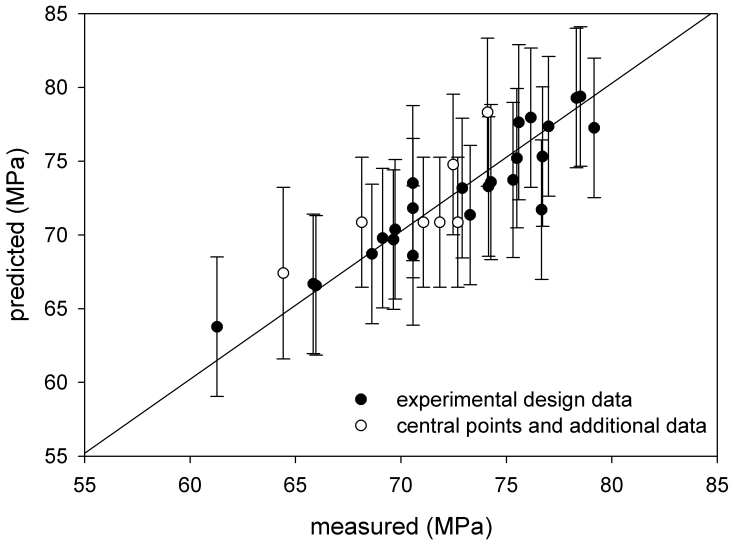
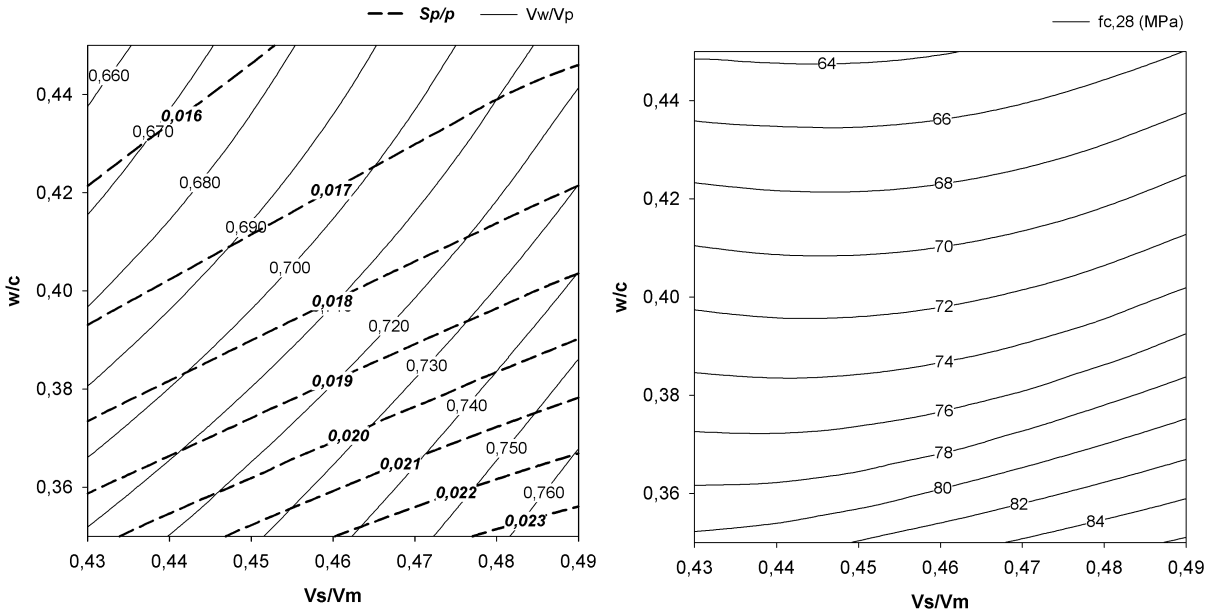


Figure 5.3.: Comparison of measured versus predicted values of fc,28 (CEM I 42,5 R)



(a) (b)

Figure 5.4.: Optimized mortars incorporating CEM I 42,5 R: (a) range of mixture variables and (b) estimated values of fc,28 (MPa)

Statistics of the obtained results are presented in Table 5.7 for all data points and for the central points only. The range of mortar properties covered with this experimental plan was: Dflow ranging from 168 to 311 mm, Tfunnel ranging from 2 to 16 s and fc,28 ranging from 67 to 87 MPa. The estimates of the fitted models, including the residual error term, along with the correlation coefficients, are given in Table 5.8. The estimated residual standard deviation (see Table 5.8) was always lower than the experimental error (see Table 5.7), except in the case of fc,28. Furthermore, the low regression coefficient of the fc,28 response indicates that the obtained model for fc,28 does not fully explains the variation in the response as a result of V_w/V_p, w/c, Sp/p and V_s/V_m variations. The measured-to-predicted values of Dflow, Tfunnel and fc,28 are shown in Figures 5.5, 5.6 and 5.7, respectively, with the prediction intervals corresponding to a 95% confidence level. The ratio between predicted-to-measured values (central points and additional data) for Dflow, Tfunnel and fc,28 ranged between 0,99 and 1,04, 0,96 and 1,08, 0,98 and 1,03, respectively. Due to the low regression coefficient of fc,28 response model the prediction intervals are expected to be large in the case of fc,28 as it is observed in Figure 5.7.

The results in Table 5.8 clearly show that w/c exhibit a great effect on all three measured responses, being only exceeded by the effect of V_w/V_p on (Tfunnel$^{-0,5}$) response. Besides w/c the variable that most influenced Dflow was Sp/p. Significant interaction effects were found between V_w/V_p and w/c on (Tfunnel$^{-0,5}$) and fc,28 responses. Interaction effects between w/c and Sp/p and between Sp/p and V_s/V_m were found to be significant

Table 5.7.: Statistics of the results for the total points and for central points (CEM I 52,5 R)

	N=28 total points			n_c=4 central points		
	Dflow (mm)	Tfunnel (s)	fc,28 (MPa)	Dflow (mm)	Tfunnel (s)	fc,28 (MPa)
Minimum	168	2,0	66,5	250	4,1	73,1
Maximum	311	15,9	86,6	256	4,6	76,8
Mean	251	5,8	75,5	253	4,4	75,5
Standard deviation	37	3,6	4,9	3	0,2	1,6
Coefficient of variation	14,8%	62,8%	6,5%	1,2%	5,4%	2,2%

Table 5.8.: Fitted numerical models for coded variables (CEM I 52,5 R)

Response variable	Dflow (mm)	$[\text{Tfunnel (s)}]^{-0,5}$	fc,28 (MPa)
model terms estimate			
independent	253,75	0,474	75,459
V_w/V_p	8,52	0,093	-0,283
w/c	32,54	0,083	-3,418
Sp/p	16,02	0,018	NS
V_s/V_m	-10,85	-0,044	-1,488
$(V_w/V_p)\times(w/c)$	NS	0,011	1,533
$(V_w/V_p)\times(V_s/V_m)$	NS	-0,008	NS
$(w/c)\times(Sp/p)$	-1,69	NS	NS
$(w/c)\times(V_s/V_m)$	NS	-0,006	NS
$(Sp/p)\times(V_s/V_m)$	2,13	NS	NS
$(V_w/V_p)^2$	1,22	0,004	NS
$(w/c)^2$	-4,59	-0,011	NS
residual error, ε^a			
mean	0	0	0
standard deviation	2,965	0,009[b]	3,149
R^2	0,994	0,995	0,582
R^2_{adj}	0,991	0,993	0,509

(NS) non-significant terms; [a]error term is a random and normally distributed variable; [b]corresponding value for Tfunnel is 0,19

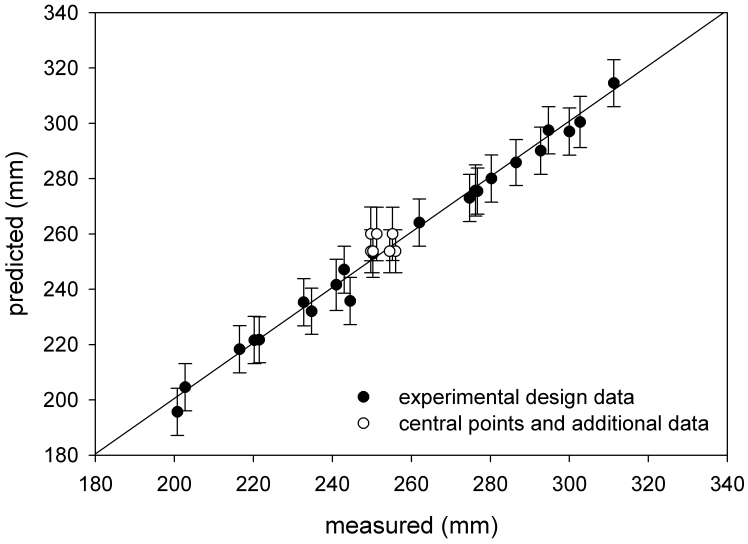


Figure 5.5.: Comparison of measured versus predicted values of Dflow (CEM I 52,5 R)

on Dflow response. Interaction effects between V_w/V_p and V_s/V_m and between w/c and V_s/V_m were also found to be significant on (Tfunnel$^{-0,5}$) response. The quadratic terms in w/c and V_w/V_p were found to be significant for both Dflow and (Tfunnel$^{-0,5}$) responses.

Contour plots representing the adjusted values of V_w/V_p and Sp/p for each pair of (V_s/V_m; w/c) in optimized mortars containing CEM I 52,5 R are presented in Figure 5.8 (a). The corresponding contour plot for estimated mortar compressive strength is presented in Figure 5.8 (b). A much lower number of optimized solutions was found with the current experimental plan compared to the previous one. This is shown by the reduced scale in both the x- and y-axis of Figure 5.8 (a).

5.3.3. CEM II/A-L 42,5 R

The experimental plan corresponding to CEM II/A-L 42,5 R was carried out between the 11^{th} and 13^{th} of January 2006. A cement sample was taken from the first delivery of CEM II/A-L 42,5 R supplied by Cimpor, from the Alhandra production centre.

Statistics of the obtained results are presented in Table 5.9 for all data points as well as for the central points only. The range of mortar properties covered with this experimental plan was: Dflow ranging from 215 to 349 mm, Tfunnel ranging from 2 to 10 s and fc,28 ranging from 62 to 86 MPa. The range of Dflow results obtained is adequate but the Tfunnel results were always below the target. The estimates of the fitted models, including the residual error term, along with the correlation coefficients, are given in Table 5.10. The estimated residual standard deviation (see Table 5.10) does not exceed the experimental error by far (see Table 5.9). The measured-to-predicted values

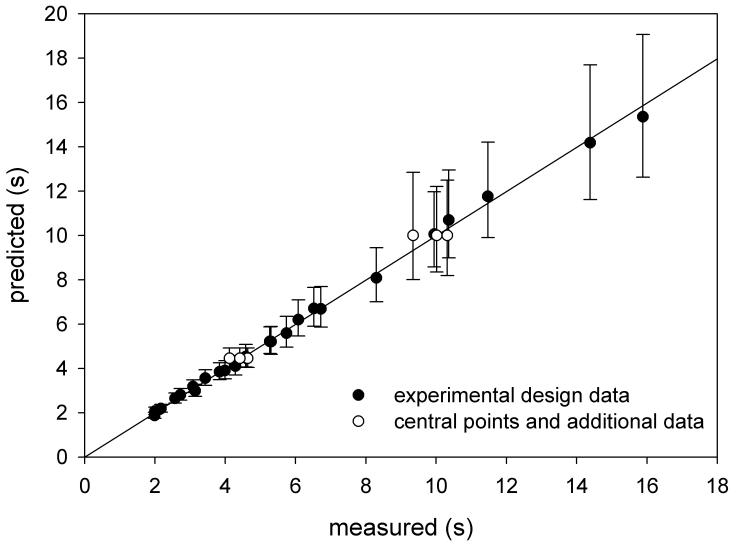


Figure 5.6.: Comparison of measured versus predicted values of Tfunnel (CEM I 52,5 R)

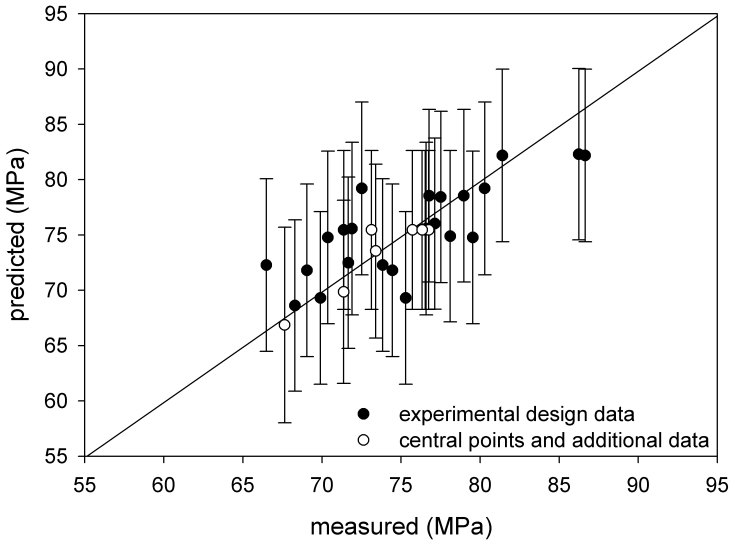


Figure 5.7.: Comparison of measured versus predicted values of fc,28 (CEM I 52,5 R)

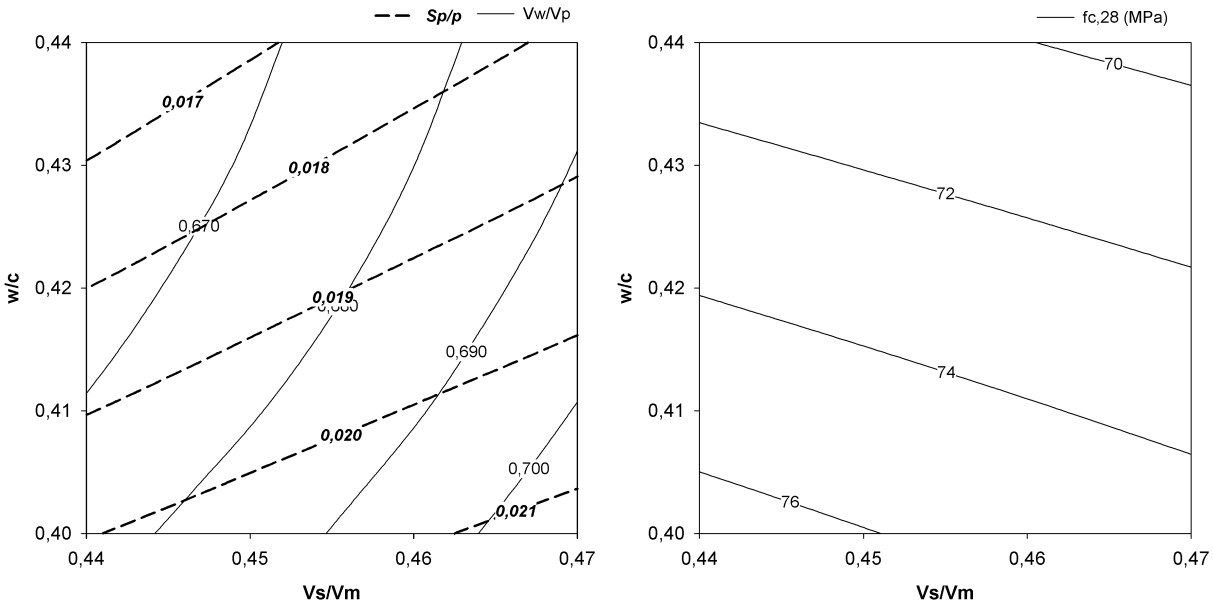


Figure 5.8.: Optimized mortars incorporating CEM I 52,5 R (a) range of mixture variables and (b) estimated values of fc,28 (MPa)

of Dflow, Tfunnel and fc,28 are shown in Figures 5.9, 5.10 and 5.11, respectively, with the prediction intervals corresponding to a 95% confidence level. The ratio between predicted-to-measured values (central points and additional data) for Dflow, Tfunnel and fc,28 ranged between 1,00 and 1,02, 0,94 and 1,17, 0,98 and 1,07, respectively.

The results in Table 5.10 clearly show that w/c exhibit a great effect on all three measured responses, being only exceeded by the effect of V_w/V_p on (Tfunnel$^{-0,5}$) response. Besides w/c, the variable that most influenced Dflow was Sp/p. A significant interaction effect was found between V_w/V_p and w/c on (Tfunnel$^{-0,5}$) and fc,28 responses. An interaction effect between V_w/V_p and V_s/V_m was also found to be significant on (Tfunnel$^{-0,5}$) response. A significant interaction effect between w/c and Sp/p was found on Dflow

Table 5.9.: Statistics of the results for the total points and for central points (CEM II/A-L 42,5 R)

	N=28 total points			n_c=4 central points		
	Dflow (mm)	Tfunnel (s)	fc,28 (MPa)	Dflow (mm)	Tfunnel (s)	fc,28 (MPa)
Minimum	215	1,7	62,5	286	3,3	72,8
Maximum	349	9,6	85,5	291	3,5	75,5
Mean	286	4,1	71,7	288	3,4	74,2
Standard deviation	32	2,2	5,4	2	0,1	1,1
Coefficient of variation	11,2%	52,7%	7,6%	0,8%	2,0%	1,5%

Table 5.10.: Fitted numerical models for coded variables (CEM II/A-L 42,5 R)

Response variable	Dflow (mm)	$[\text{Tfunnel (s)}]^{-0,5}$	fc,28 (MPa)
model terms estimate			
independent	290,80	0,551	74,144
V_w/V_p	10,26	0,101	1,062
w/c	25,24	0,067	-4,774
Sp/p	15,39	0,013	0,959
V_s/V_m	-11,97	-0,050	-1,058
$(V_w/V_p)\times(w/c)$	NS	0,009	-1,621
$(V_w/V_p)\times(V_s/V_m)$	NS	-0,009	NS
$(w/c)\times(Sp/p)$	-2,77	NS	NS
$(V_w/V_p)^2$	NS	-0,005	-1,111
$(w/c)^2$	-5,08	-0,013	NS
$(Sp/p)^2$	NS	NS	-1,012
$(V_s/V_m)^2$	NS	NS	-0,744
residual error, ε^a			
mean	0	0	0
standard deviation	2,998	$0,010^b$	1,607
R^2	0,991	0,993	0,909
R^2_{adj}	0,989	0,990	0,873

(NS) non-significant terms; [a]error term is a random and normally distributed variable; [b]corresponding value for Tfunnel is 0,19

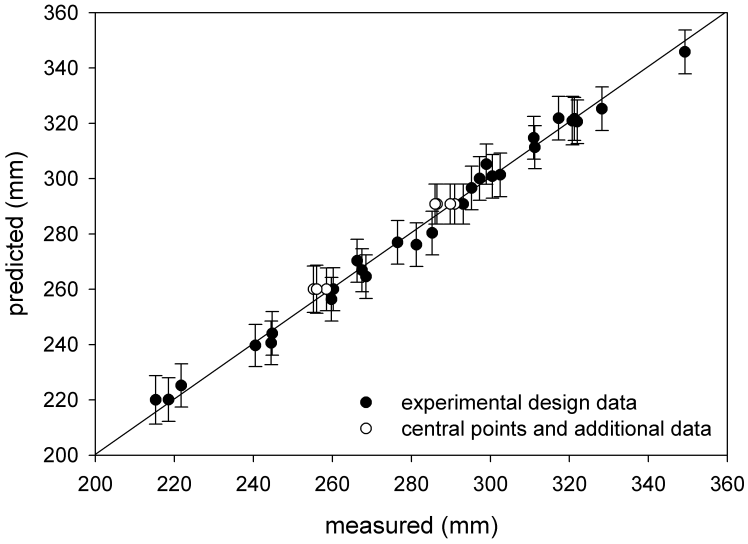


Figure 5.9.: Comparison of measured versus predicted values of Dflow (CEM II/A-L 42,5 R)

response. The quadratic term in w/c was significant for both Dflow and Tfunnel responses. The quadratic terms in Sp/p and V_s/V_m were also found to be significant on fc,28 response.

Contour plots representing the adjusted values of V_w/V_p and Sp/p for each pair of (V_s/V_m; w/c) in optimized mortars containing CEM II/A-L 42,5 R are presented in Figure 5.12 (a). The corresponding contour plot for estimated mortar compressive strength is presented in Figure 5.12 (b).

5.3.4. CEM II/B-L 32,5 N

The experimental plan corresponding to CEM II/B-L 32,5 N was carried out between the 23^{rd} and 25^{th} of January 2006. A cement sample was taken from the first delivery of CEM II/B-L 32,5 N supplied by Cimpor, from the Alhandra production centre.

Statistics of the obtained results are presented in Table 5.11 for all data points and for the central points only. The range of mortar properties covered with this experimental plan was: Dflow ranging from 224 to 346 mm, Tfunnel ranging from 2 to 12 seconds and fc,28 ranging from 47 to 80 MPa. The estimates of the fitted models, including the residual error term, along with the correlation coefficients, are given in Table 5.12. Again, the estimated residual standard deviation (see Table 5.12) does not exceed the experimental error by far (see Table 5.11). The measured-to-predicted values of Dflow, Tfunnel and fc,28 are shown in Figures 5.13, 5.14 and 5.15, respectively, with the prediction intervals corresponding to a 95% confidence level. The ratio between predicted-to-measured values (central points and additional data) for Dflow, Tfunnel and fc,28 ranged between

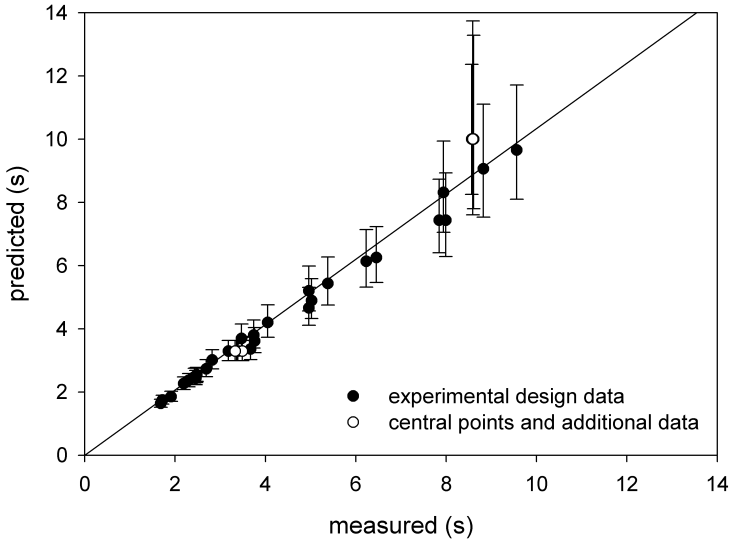


Figure 5.10.: Comparison of measured versus predicted values of Tfunnel (CEM II/A-L 42,5 R)

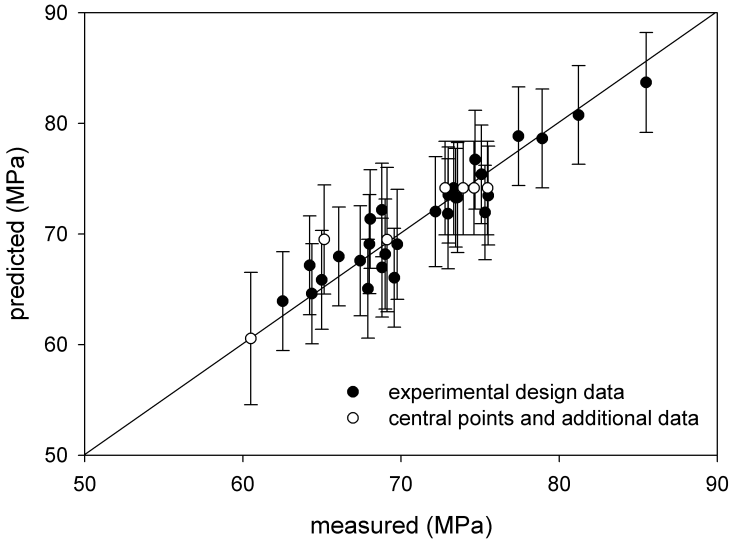
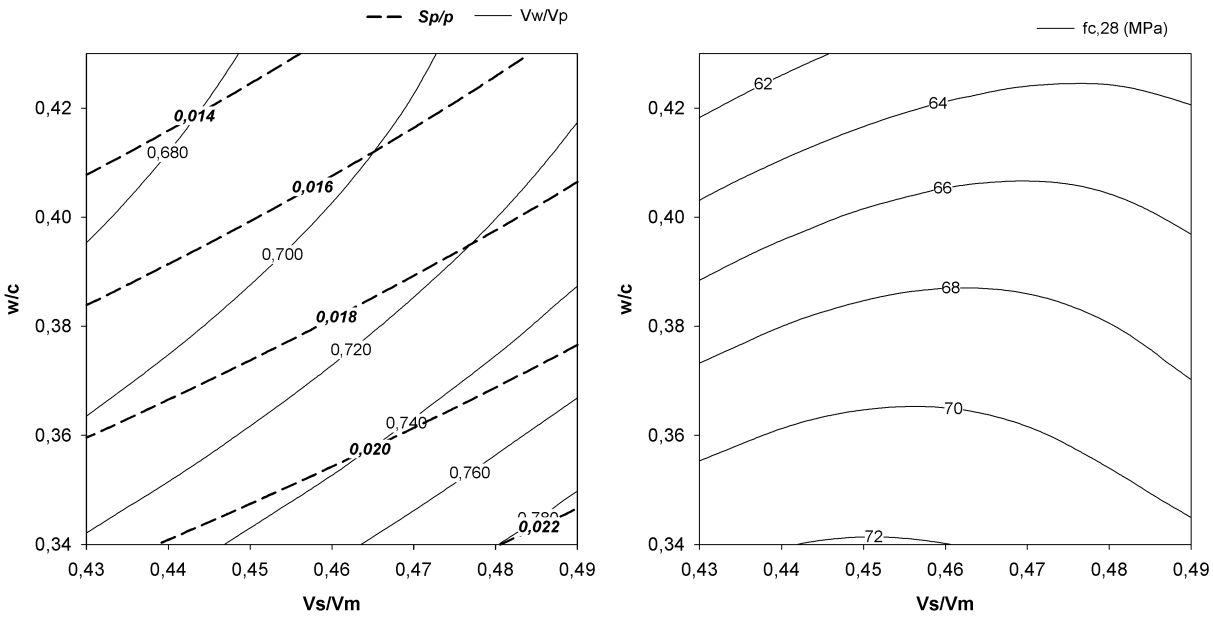


Figure 5.11.: Comparison of measured versus predicted values of fc,28 (CEM II/A-L 42,5 R)



(a) (b)

Figure 5.12.: Optimized mortars incorporating CEM II/A-L 42,5 R (a) range of mixture variables and (b) estimated values of fc,28 (MPa)

0,97 and 1,01, 0,94 and 1,19, 0,99 and 1,07, respectively.

The results in Table 5.15 again show that w/c exhibit a great effect on all three measured responses, being only exceeded by the effect of V_w/V_p on (Tfunnel$^{-0,5}$) response. Besides w/c the variable that most influenced Dflow was Sp/p. Significant interaction effects were found between V_w/V_p and Sp/p and between w/c and V_s/V_m on Dflow response. Significant interaction effects were found between V_w/V_p and w/c, V_w/V_p and V_s/V_m and between Sp/p and V_s/V_m on (Tfunnel$^{-0,5}$) response. The quadratic term in w/c was significant for both Dflow and fc,28 responses.

Contour plots representing the adjusted values of V_w/V_p and Sp/p for each pair of (V_s/V_m; w/c) and a contour plot for estimated mortar compressive strength are presented

Table 5.11.: Statistics of the results for the total points and for central points (CEM II/B-L 32,5 N)

	N=28 total points			n_c=4 central points		
	Dflow (mm)	Tfunnel (s)	fc,28 (MPa)	Dflow (mm)	Tfunnel (s)	fc,28 (MPa)
Minimum	224	1,9	47,3	295	4,1	59,7
Maximum	345	12,5	80,3	304	4,71	61,2
Mean	293	5,3	61,2	299	4,4	60,5
Standard deviation	28	2,9	7,9	4	0,3	0,8
Coefficient of variation	9,6%	54,0%	12,9%	1,3%	6,6%	1,2%

Table 5.12.: Fitted numerical models for coded variables (CEM II/B-L 32,5 N)

Response variable	Dflow (mm)	[Tfunnel (s)]$^{-0,5}$	fc,28 (MPa)
model terms estimate			
independent	295,12	0,476	60,406
V_w/V_p	10,30	0,103	-0,719
w/c	18,05	0,050	-8,057
Sp/p	17,39	0,019	0,675
V_s/V_m	-11,05	-0,045	NS
$(V_w/V_p)\times(w/c)$	NS	0,008	NS
$(V_w/V_p)\times(Sp/p)$	-2,30	NS	NS
$(V_w/V_p)\times(V_s/V_m)$	NS	-0,010	NS
$(w/c)\times(V_s/V_m)$	2,61	NS	NS
$(Sp/p)\times(V_s/V_m)$	NS	-0,006	NS
$(w/c)^2$	-2,56	NS	0,872
residual error, ε^a			
mean	0	0	0
standard deviation	4,379	0,010^b	1,684
R^2	0,976	0,992	0,954
R^2_{adj}	0,967	0,990	0,946

(NS) non-significant terms; ^{a}error term is a random and normally distributed variable; ^{b}corresponding value for Tfunnel is 0,41

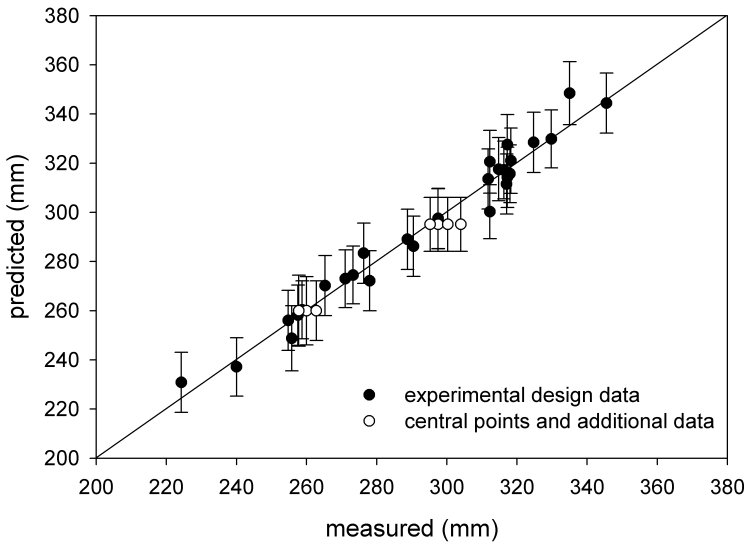


Figure 5.13.: Comparison of measured versus predicted values of Dflow (CEM II/B-L 32,5 N)

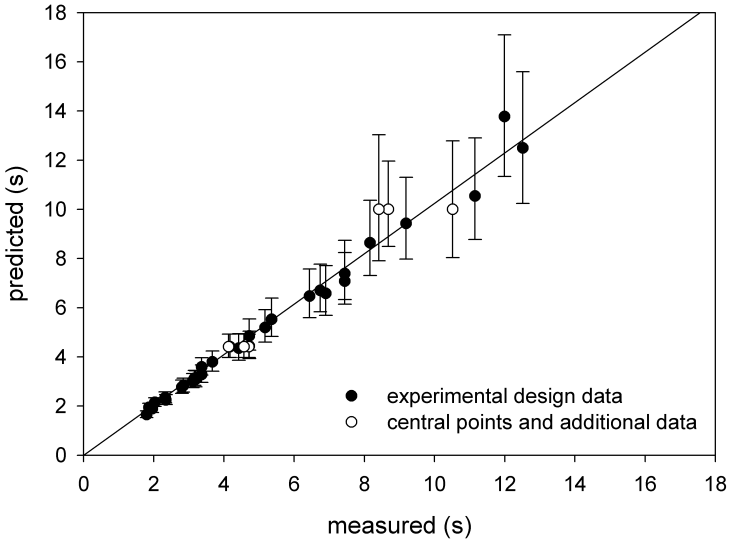


Figure 5.14.: Comparison of measured versus predicted values of Tfunnel (CEM II/B-L 32,5 N)

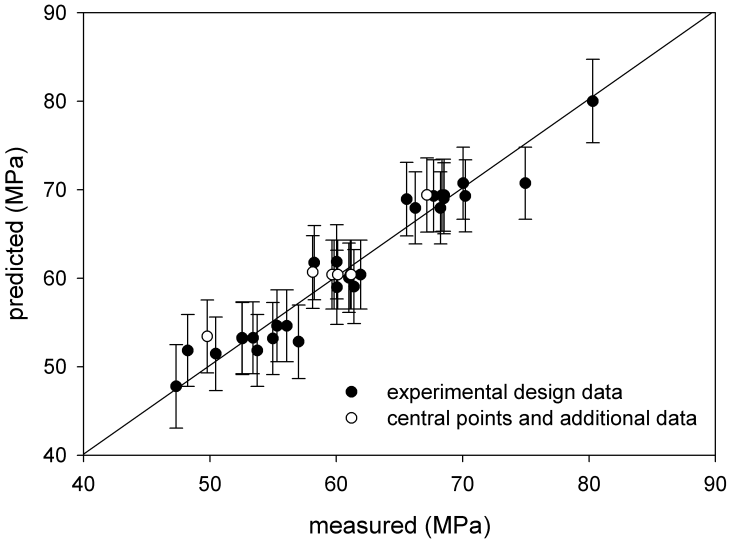
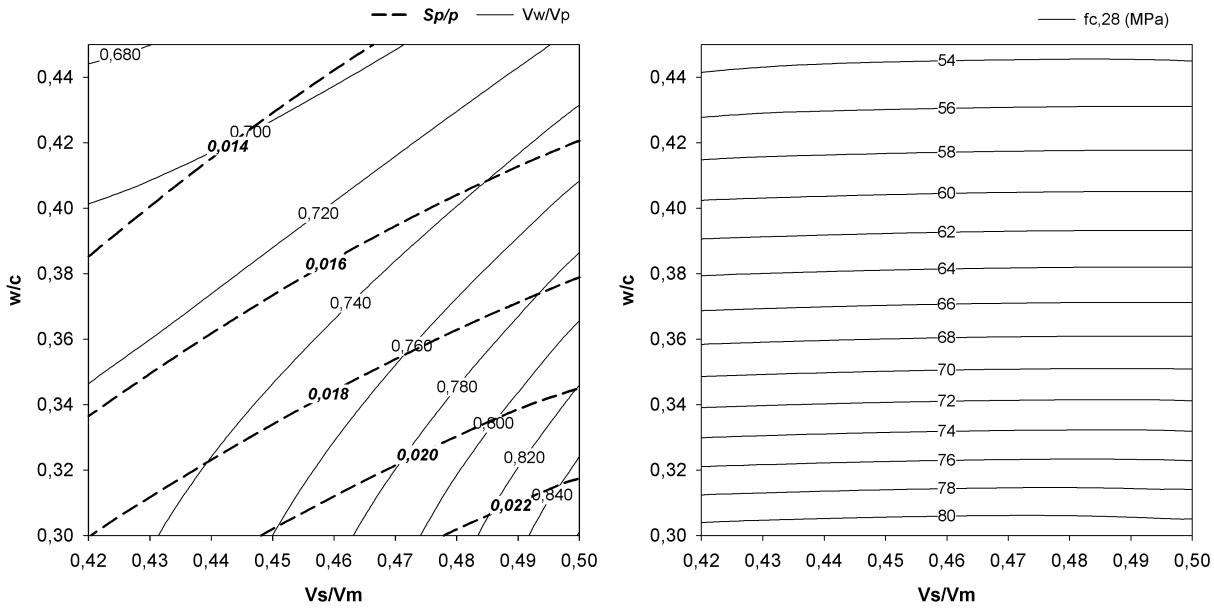


Figure 5.15.: Comparison of measured versus predicted values of fc,28 (CEM II/B-L 32,5 N)



(a) (b)

Figure 5.16.: Optimized mortars incorporating CEM II/B-L 32,5 N (a) range of mixture variables and (b) estimated values of fc,28 (MPa)

in Figure 5.16 (a) and (b), respectively, corresponding to optimized mortars containing CEM II/B-L 32,5 N. In the case of this cement type and the analyzed region, the contour lines for estimated mortar compressive strength are nearly horizontal due to the dominant effect of w/c in this response.

5.3.5. CEM IV/B (V) 32,5 N

The experimental plan corresponding to CEM IV/B(V) 32,5 N was carried out between the 25^{th} and 30^{th} of January 2006. A cement sample was taken from the first delivery of CEM IV/B(V) 32,5 N supplied by Cimpor, from the Alhandra production centre.

Statistics of the obtained results are presented in Table 5.13 for all data points and for the central points only. The range of mortar properties covered with this experimental plan was: Dflow ranging from 185 to 360 mm, Tfunnel ranging from 3 to 18 s and fc,28 ranging from 47 to 67 MPa. In this case the highest experimental error is associated with the fc,28 response instead of TFunnel response variable. The estimates of the fitted models, including the residual error term, along with the correlation coefficients, are given in Table 5.14. The estimated residual standard deviation (see Table 5.14) does not exceed the experimental error (see Table 5.13) except in the case of Tfunnel response, but the experimental error associated to Tfunnel was relatively low compared to previous experimental plans. The measured-to-predicted values of Dflow, Tfunnel and fc,28 are shown in Figures 5.17, 5.18 and 5.19, respectively, with the prediction

Table 5.13.: Statistics of the results for the total points and for central points (CEM IV/B(V) 32,5 N)

	N=28 total points			n_c=4 central points		
	Dflow (mm)	Tfunnel (s)	fc,28 (MPa)	Dflow (mm)	Tfunnel (s)	fc,28 (MPa)
Minimum	185	2,8	46,9	300	5,8	48,7
Maximum	360	18,0	66,6	312	6,1	57,0
Mean	290	7,4	57,0	308	6,0	53,9
Standard deviation	46	3,8	5,5	5	0,1	3,6
Coefficient of variation	15,8%	52,3%	9,6%	1,8%	2,3%	6,7%

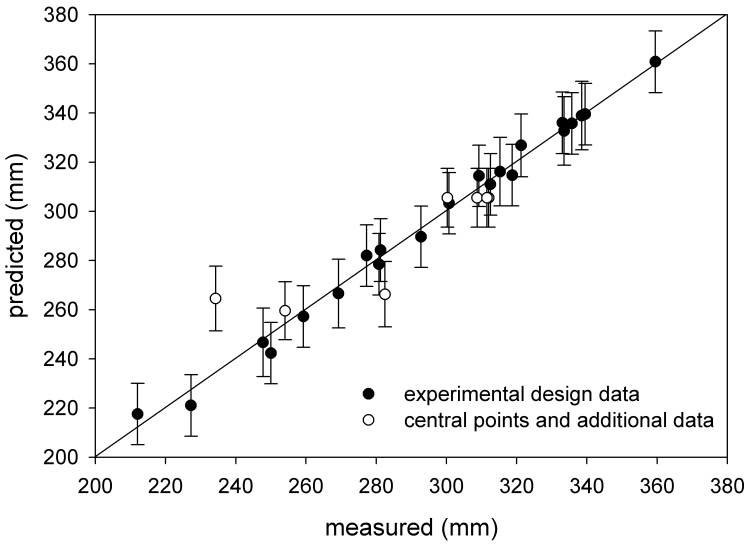


Figure 5.17.: Comparison of measured versus predicted values of Dflow (CEM IV/B(V) 32,5 N)

intervals corresponding to a 95% confidence level. The ratio between predicted-to-measured values (central points and additional data) for Dflow, Tfunnel and fc,28 ranged between 0,94 and 1,13, 0,87 and 1,19, 0,96 and 1,12 , respectively.

The results in Table 5.14 show that w/c exhibit a great effect on all three measured responses, being only exceeded by the effect of V_w/V_p on (Tfunnel$^{-0,5}$) response. Besides w/c, the variable that most influenced Dflow was Sp/p. A significant interaction effect was found between w/c and Sp/p on Dflow response. Significant interaction effects were found between V_w/V_p and w/c, V_w/V_p and V_s/V_m and w/c and V_s/V_m on (Tfunnel$^{-0,5}$). Only the interaction effect between V_w/V_p and Sp/p was found to be significant on fc,28 response. The quadratic term on V_w/V_p was significant for all responses. The quadratic term on w/c was significant for both Dflow and Tfunnel responses. The quadratic term on Sp/p was found to be significant for both Dflow and fc,28. The quadratic term on V_s/V_m was found to be significant for fc,28 response only.

Table 5.14.: Fitted numerical models for coded variables (CEM IV/B(V) 32,5 N)

Response variable	Dflow (mm)	[Tfunnel (s)]$^{-0,5}$	fc,28 (MPa)
model terms estimate			
independent	305,53	0,404	54,523
V_w/V_p	12,40	0,080	-0,626
w/c	37,73	0,055	-4,438
Sp/p	21,50	0,013	2,477
V_s/V_m	-10,65	-0,027	-1,020
$(V_w/V_p)\times(w/c)$	NS	0,013	NS
$(V_w/V_p)\times(Sp/p)$	NS	NS	1,131
$(V_w/V_p)\times(V_s/V_m)$	NS	-0,006	NS
$(w/c)\times(Sp/p)$	-8,97	NS	NS
$(w/c)\times(V_s/V_m)$	NS	-0,007	NS
$(V_w/V_p)^2$	-3,55	0,003	0,959
$(w/c)^2$	-10,52	-0,005	NS
$(Sp/p)^2$	-3,95	NS	0,994
$(V_s/V_m)^2$	NS	NS	0,974
residual error, ε^a			
mean	0	0	0
standard deviation	4,453	0,008^b	1,814
R^2	0,991	0,993	0,891
R^2_{adj}	0,987	0,989	0,845

(NS) non-significant terms; ^{a}error term is a random and normally distributed variable; ^{b}corresponding value for Tfunnel is 0,53

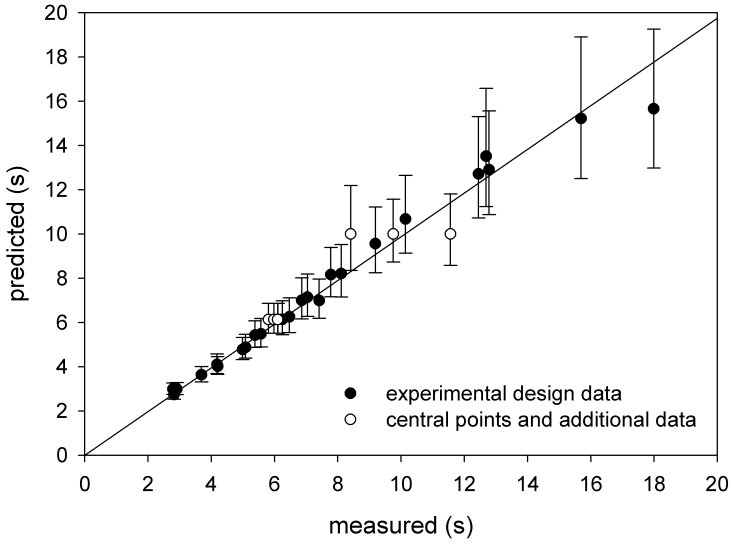


Figure 5.18.: Comparison of measured versus predicted values of Tfunnel (CEM IV/B(V) 32,5 N)

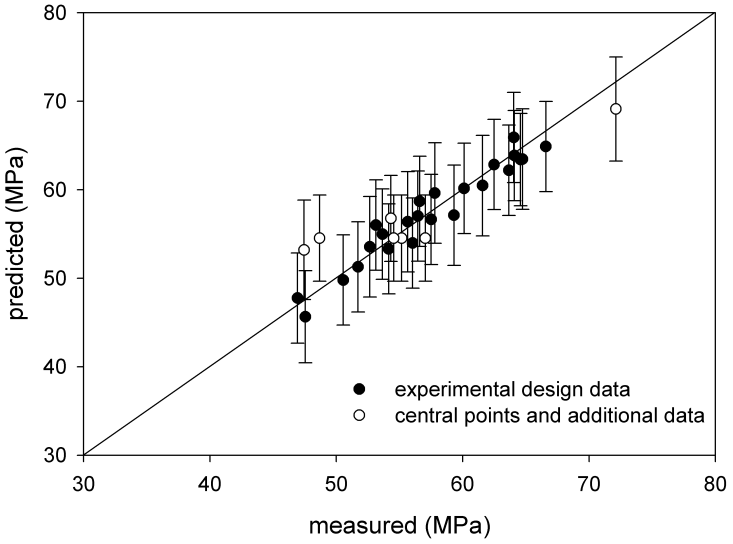


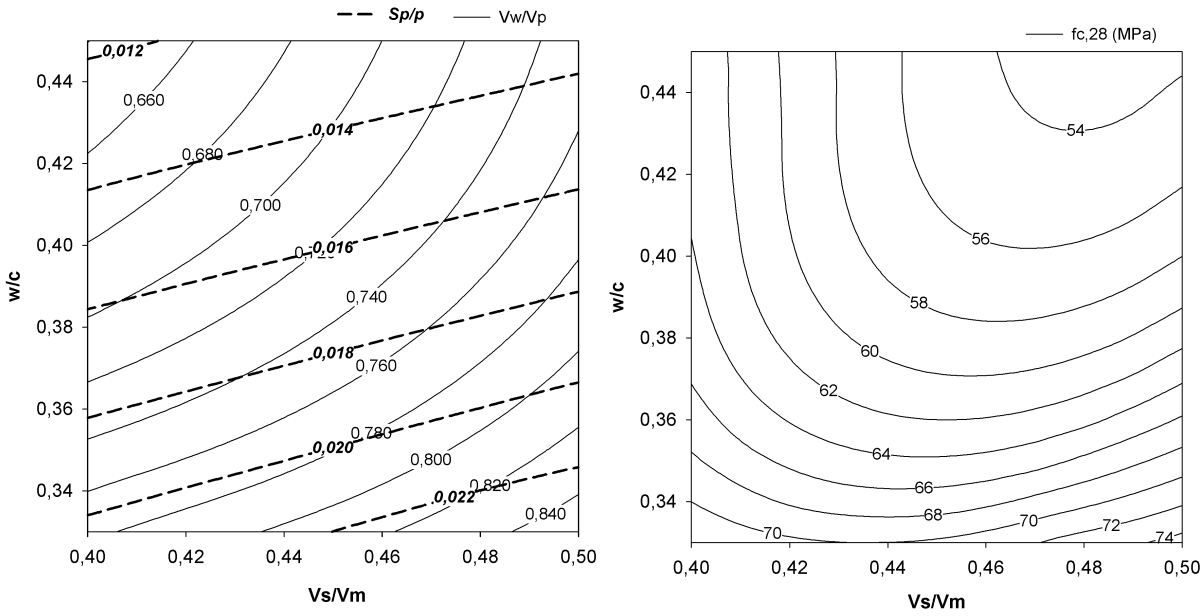
Figure 5.19.: Comparison of measured versus predicted values of fc,28 (CEM IV/B(V) 32,5 N)

Contour plots representing the adjusted values of V_w/V_p and Sp/p for each pair of $(V_s/V_m;\ w/c)$ in optimized mortars containing CEM IV/B(V) 32,5 N are presented in Figure 5.20 (a). The corresponding contour plot for estimated mortar compressive strength is presented in Figure 5.20 (b). By observing Figure 5.20 (b) a larger curvature is found in the contour lines compared to previous contour plots. This is in part due to the wider scale of variables in the x- and y-axis but also a change in cement type.

5.3.6. CEM II/B-L 32,5 R (BR)

The experimental plan corresponding to CEM II/B-L 32,5 R (BR), white cement, was carried out between the 18^{th} and 20^{th} of January 2006. A cement sample was taken from the first delivery of CEM II/B-L 32,5 R (BR) supplied by Cimpor, but produced by Secil.

Statistics of the obtained results are presented in Table 5.15 for all data points and for the central points only. The range of mortar properties covered with this experimental plan was: Dflow ranging from 184 to 340 mm, Tfunnel ranging from 2 to 22 s and fc,28 ranging from 52 to 87 MPa. From the central points data it can be concluded that the highest experimental error is associated with the fc,28 response variable. The estimates of the fitted models, including the residual error term, along with the correlation coefficients, are given in Table 5.16. The estimated residual standard deviation (see Table 5.16) does not exceed the experimental error by far (see Table 5.15). The measured-to-predicted values of Dflow, Tfunnel and fc,28 are shown in Figures 5.21, 5.22 and 5.23, respectively, with the prediction intervals corresponding to a 95% confidence level. The ratio between



(a) (b)

Figure 5.20.: Optimized mortars incorporating CEM IV/B(V) 32,5 N (a) range of mixture variables and (b) estimated values of fc,28 (MPa)

predicted-to-measured values (central points and additional data) for Dflow, Tfunnel and fc,28 ranged between 0,95 and 1,04, 0,87 and 1,19, 0,95 and 1,22 , respectively.

The results in Table 5.16 show that instead of w/c, Sp/p is the variable that most influenced Dflow of mortar mixtures incorporating CEM II/B-L 32,5 R (BR). Besides Sp/p the variable that most influenced Dflow was V_w/V_p. V_w/V_p and w/c exhibited the greatest effect on (Tfunnel$^{-0,5}$) and fc,28 responses, respectively. Significant interaction effects were found between w/c and Sp/p for all response variables. Significant interaction effects were found between V_w/V_p and w/c for both (Tfunnel$^{-0,5}$) and fc,28 responses. The interaction effect between V_w/V_p and Sp/p was also found significant for both Dflow and fc,28 responses. The interaction effect between V_w/V_p and V_s/V_m was

Table 5.15.: Statistics of the results for the total points and for central points (CEM II/B-L 32,5 R (BR))

	N=28 total points			n_c=4 central points		
	Dflow (mm)	Tfunnel (s)	fc,28 (MPa)	Dflow (mm)	Tfunnel (s)	fc,28 (MPa)
Minimum	184	1,89	52,1	308	5,72	66,6
Maximum	340	21,5	87,1	318	6,0	72,4
Mean	295	7,6	69,0	314	5,9	69,2
Standard deviation	36	4,7	9,0	5	0,2	2,4
Coefficient of variation	12,3%	62,0%	13,1%	1,6	2,6%	3,5%

Table 5.16.: Fitted numerical models for coded variables (CEM II/B-L 32,5 R (BR))

Response variable	Dflow (mm)	[Tfunnel (s)]$^{-0,5}$	fc,28 (MPa)
model terms estimate			
independent	309,82	0,40639	68,98
V_w/V_p	12,89	0,09618	-0,18
w/c	7,75	0,03239	-7,84
Sp/p	23,11	0,02087	4,16
V_s/V_m	-9,44	-0,02918	NS
$(V_w/V_p)\times(w/c)$	NS	0,01211	2,07
$(V_w/V_p)\times(Sp/p)$	-4,84	NS	1,37
$(V_w/V_p)\times(V_s/V_m)$	NS	-0,00688	NS
$(w/c)\times(Sp/p)$	-5,78	-0,00671	-1,46
$(V_w/V_p)^2$	-10,10	NS	NS
$(Sp/p)^2$	-5,97	NS	NS
residual error, ε^a			
mean	0	0	0
standard deviation	5,487	0,01028^b	2,63
R^2	0,966	0,989	0,918
R^2_{adj}	0,950	0,985	0,893

(NS) non-significant terms; ^{a}error term is a random and normally distributed variable; ^{b}corresponding value for Tfunnel is 0,53

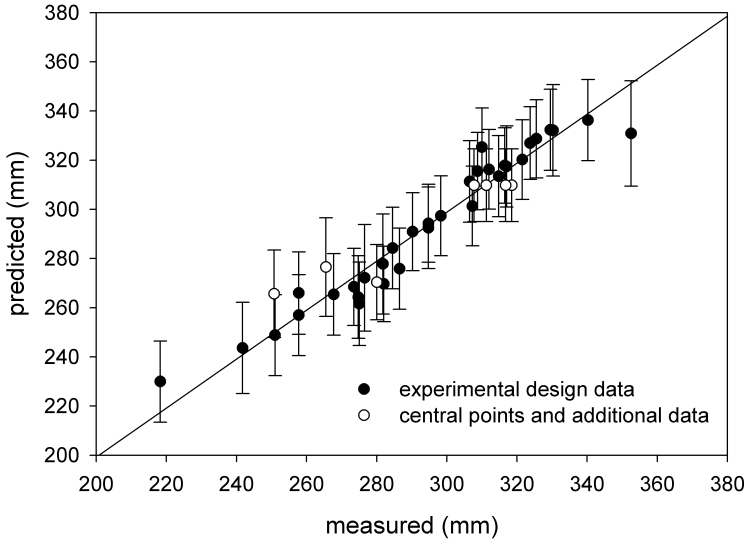


Figure 5.21.: Comparison of measured versus predicted values of Dflow (CEM II/B-L 32,5 R (BR))

significant for (Tfunnel$^{-0,5}$) response. Significant quadratic terms on V_w/V_p and Sp/p were found when modelling Dflow response.

Contour plots representing the adjusted values of V_w/V_p and Sp/p for each pair of (V_s/V_m; w/c) in optimized mortars containing CEM II/B-L 32,5 R (BR) are presented in Figure 5.24 (a). The corresponding contour plot for estimated mortar compressive strength is presented in Figure 5.24 (b).

5.4. Discussion of results

5.4.1. Main effects

In general, the main effects found in the models obtained for Dflow, (Tfunnel$^{-0,5}$) and fc,28 were the first order effects for all cement types. Considering only the first order effects, it was found that Dflow increases with V_w/V_p, w/c and Sp/p and decreases with an increase of V_s/V_m, independently of the cement type, as found by Okamura et al. (2000). On the contrary, Tfunnel increases with V_s/V_m and decreases with an increase of V_w/V_p, w/c or Sp/p, independently of the cement type, as also found by Okamura et al. (2000). As expected, fc,28 decreased with an increase of w/c or V_w/V_p, for all cement types. Moreover, it was found that fc,28 increases with Sp/p for all cement types, except in the case of CEM I 52,5 R. The influence of V_s/V_m on fc,28 response changed with the cement type.

The variables that influenced Dflow the most were w/c followed by Sp/p for all cement types, except CEM II/B-L 32,5 R (BR). In the case of this cement type, Dflow was more

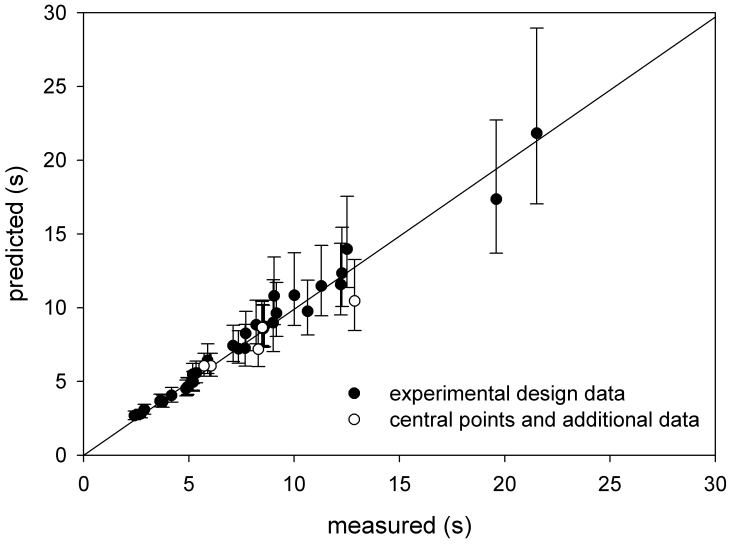


Figure 5.22.: Comparison of measured versus predicted values of Tfunnel (CEM II/B-L 32,5 R (BR))

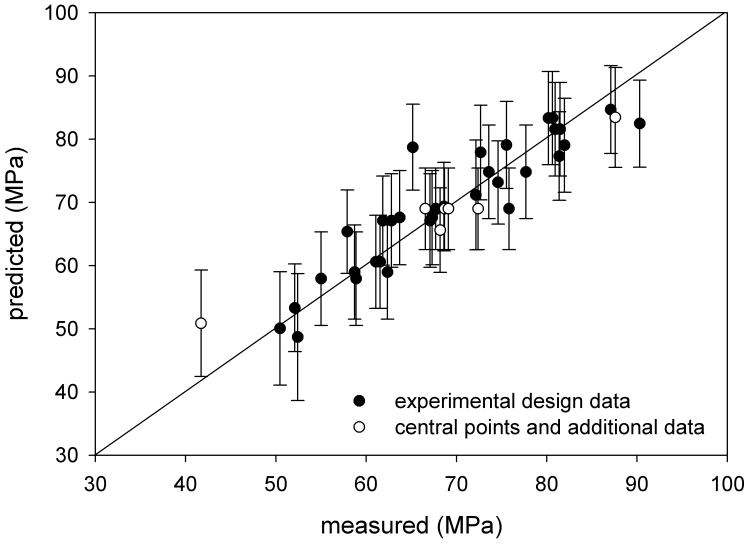
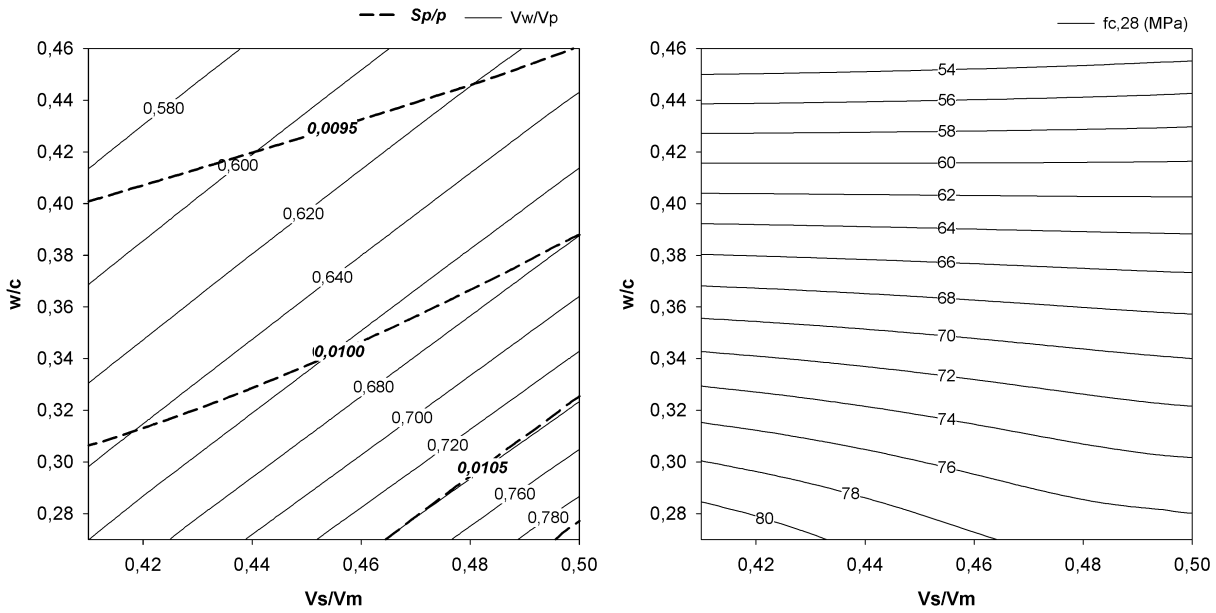


Figure 5.23.: Comparison of measured versus predicted values of fc,28 (CEM II/B-L 32,5 R (BR))



(a) (b)

Figure 5.24.: Optimized mortars incorporating CEM II/B-L 32,5 R (BR) (a) range of mixture variables and (b) estimated values of fc,28 (MPa)

influenced by Sp/p followed by V_w/V_p. The variables that influenced (Tfunnel$^{-0,5}$) the most were V_w/V_p followed by w/c , independent of the cement type. w/c was also found to be the most significant variable to explain fc,28 response, independent of the cement type.

Different interaction effects and other quadratic terms were found to be significant for the mortar responses, depending on the cement type. The quadratic term in w/c was significant for Dflow response of all cement types, except CEM II/B-L 32,5 R (BR).

5.4.2. Interaction diagrams and number of optimized solutions

The mixture parameters of optimized solutions can be represented in an interaction diagram like the one presented in Figure 5.25 as an alternative to the contour plots presented before. In this diagram all mixture parameters are presented in coded values and each circle corresponds to a level of the mixture variable. Each radial segment represents one of the optimized solutions and over this segment a dot is plotted for each mixture variable, using the correspondent marker. The distance of each dot to the centre is determined by the variable coded value. The interaction diagrams of the type presented in Figure 5.25 show a more global picture of the solutions highlighting other features of the optimization since they enable one:

- to rapidly distinguish which of the constituent materials combine well, in the sense that they favor the occurrence of a large range of optimized solutions, that can

be seen in the diagram by the emergence of a large amount of radial lines in the circle;

- to distinguish regions where the solutions get very close to the circular boundaries corresponding to levels -2 and +2, indicating that the limits of the factorial plan have been attained and one has depleted the set of solutions;
- to identify trends in V_w/V_p, w/c and Sp/p for a given constant level of V_s/V_m, by selecting successive arcs of filled dots and by following other marked curves in the corresponding sector;
- to identify situations of total or large incompatibility between cement and superplasticizer, in which case other superplasticizers should be tested.

By analyzing the diagrams in Figure 5.25 a common pattern is found for all cement types. In fact, both V_w/V_p and Sp/p increase when w/c is reduced for a given aggregate content (V_s/V_m), to maintain self-compactability properties. On the other hand, both Sp/p and V_w/V_p increase with aggregate content for a constant w/c ratio. The number of solutions found depends not only on the selected central point in each experimental plan but also on the interaction of the specific cement type with the limestone filler and the V3000 superplasticizer. This means that a different number of solutions can be found by changing the value a_0 for one or more of the independent variables. In the particular cases of CEM I 42,5 R, CEM I 52,5 R and CEM II/A-L 42,5 R (see Figure 5.25 (a) to (c)) one of the variables that clearly limited the number of solutions found was V_w/V_p, which reached a -2 value for each level of V_s/V_m. Thus, one can expect to find more solutions for higher values of w/c by reducing the absolute value of V_w/V_p, corresponding to the central point. CEM II/B-L 32,5 R (BR) can be distinguished by its very low values and small variation of Sp/p across the solutions range as compared to other cements (see Figure 5.24 (a) and Figure 5.25 (f)). This can be explained mainly by the differences in the chemical composition, namely, lower content of Al_2O_3 and Fe_2O_3 and lower alkalis content (see Table C.7 in Appendix C) which overcame the negative effect of a higher specific surface on fluidity (as discussed in Chapter 3).

5.4.3. Influence of cement type on mix proportions of SCC mortars

By analyzing only the solutions found for V_s/V_m=0,45, the main differences between different cement types are highlighted in Figures 5.26 to 5.28. In general, it can be observed from Figure 5.26 that the optimum superplasticizer dosage significantly changes with the cement type for each w/c ratio. CEM I 52,5 R required the highest dosage while a strong reduction in Sp/p was observed for CEM II/B-L 32,5 R (BR). Based on literature review (see Chapter 3), the required superplasticizer (PC type) dosage may

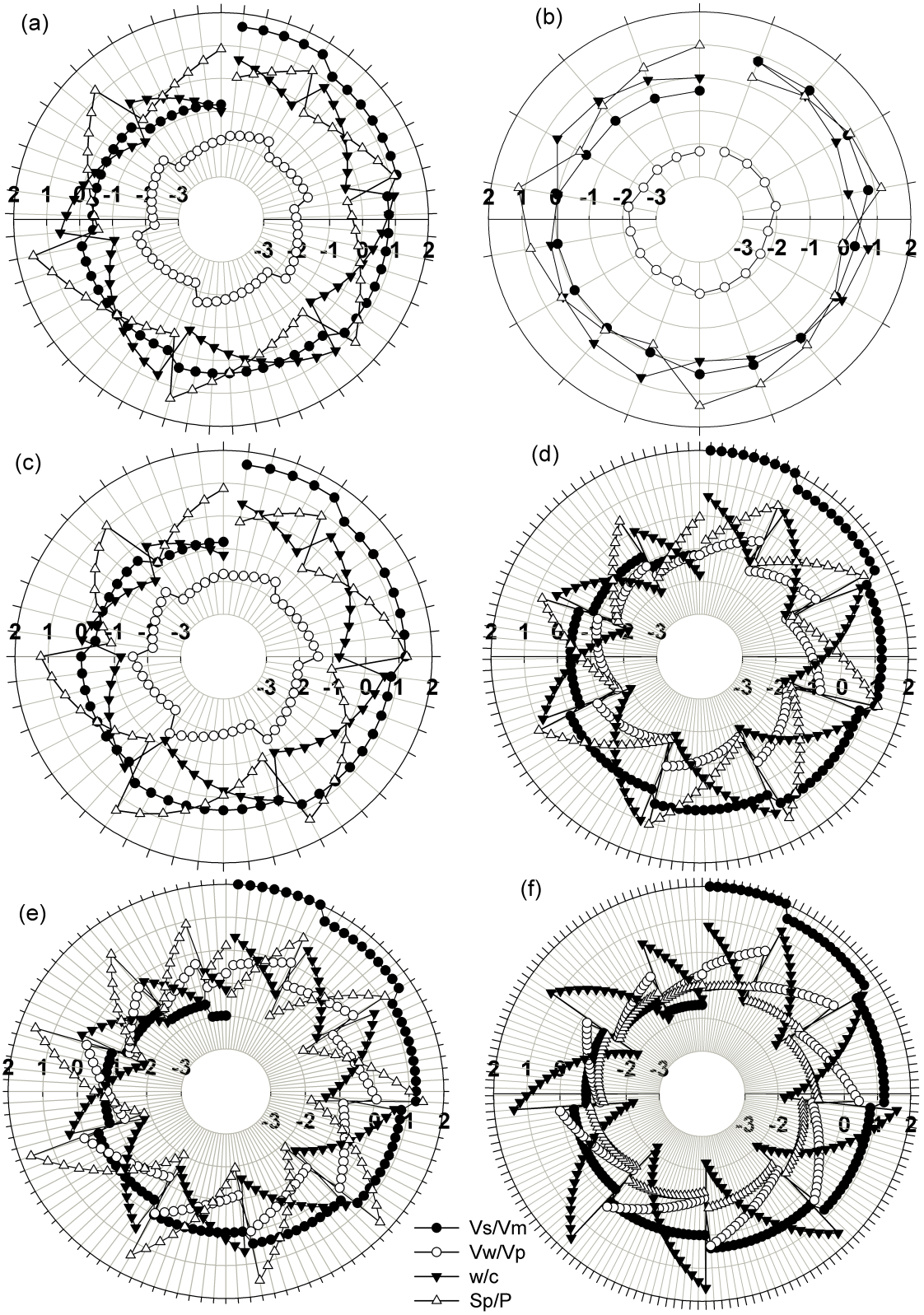


Figure 5.25.: Range of optimized mixture variables (coded values) for different cement types

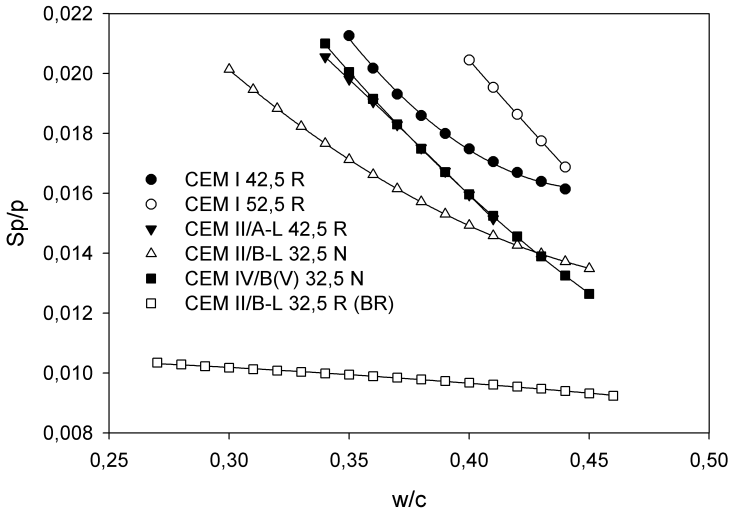


Figure 5.26.: Variation of Sp/p with w/c for optimized mortars with V_s/V_m=0,45

increase with C_3A content, surface area and alkali sulphate content in cement. Furthermore, the substitution of cement by limestone filler, until a certain dosage, reduces the required superplasticizer dosage. Unfortunately, one failed to obtain a complete characterization of cements for the first delivery (see Tables C.1 to C.10, in Appendix C) therefore a further discussion of the influence of cement characteristics on the required superplasticizer dosage can not be given here.

The values found for V_w/V_p are relatively close to each other for all cement types except for CEM II/B-L 32,5 R (BR) (see Figure 5.27). In general, values lower than the typical range of V_w/V_p suggested in (BIBM et al., 2005) [0,85; 1,10], were found to be adequate for the six Portuguese cement types tested in combination with superplasticizer V3000 and limestone filler. The estimated values of fc,28 (MPa) varied almost linearly with w/c but can differ significantly depending on the cement type, for a given w/c ratio (see Figure 5.28). This can be explained by different amounts and type of additions incorporated in each cement. As expected CEM I 52,5 R and CEM IV/B(V) 32,5 N led to the highest and the lowest compressive strength (28 days), respectively, for a given w/c ratio. The correction of w/c ratio to attain a certain target level of compressive strength with different cement types can also be estimated directly from Figure 5.28, with the possible exception of CEM I 52,5 (the fitted model explained only 58% of the variation in the response).

5.4.4. Quality control

The optimized mixtures presented above (incorporating reference sand) are useful to assess the workability and strength variations in different deliveries of cement, filler or

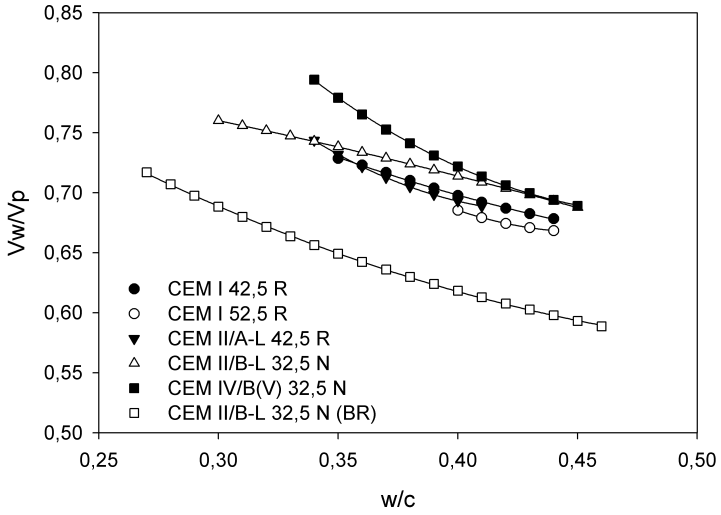


Figure 5.27.: Variation of V_w/V_p with w/c for optimized mortars with V_s/V_m=0,45

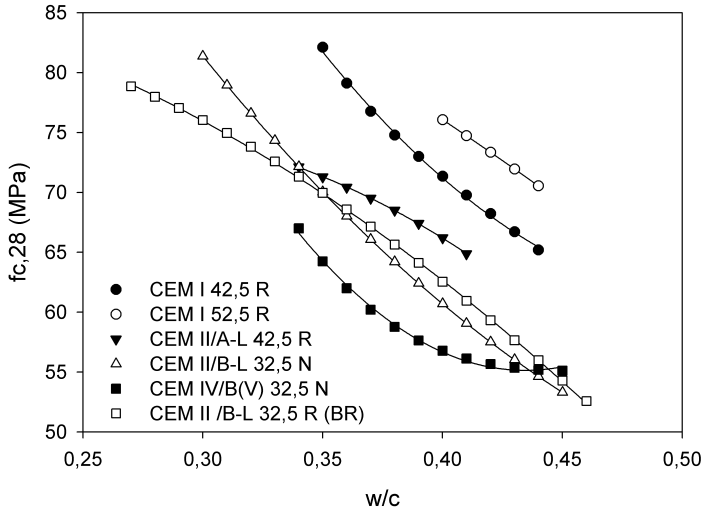


Figure 5.28.: Variation of estimated values of fc,28 (MPa) for optimized mortars with V_s/V_m=0,45

superplasticizer. A quality control plan should be established to monitor the extent to which optimized mortar properties meet specifications. The elimination of excessive deviations from target specifications and excessive variability around target specifications will contribute to enhance the robustness of SCC production process (BIBM et al., 2005). This procedure was adopted to assess the influence of different deliveries of cement on the workability and strength properties of SCC mortars and pastes, and is explained in Chapter 6.

5.4.5. Predicting capability of the models

According to Sonebi et al. (2005); Yahia and Khayat (2001b) the derived models can still be used to predict mortar properties when the material properties changes, such as cement source. To evaluate the effect of cement source on the accuracy of the models, mortars incorporating three new cements of type CEM I 42,5 R from a different factory or supplier, and maintaining the other constituent materials, were assessed. The mix proportions and test results of the 28 mixes prepared for the CEM I 42,5 R produced by Secil-Maceira, Secil-Outão and Cimpor-Souselas are summarized in Tables E.7, E.8 and E.9, respectively, in Appendix E. The scatter between the measured and the predicted (using the models derived to CEM I 42,5 R, Cimpor–Alhandra, presented in paragraph 5.3.1) values of mortar properties can be observed in Figures 5.29 to 5.31. From these figures it can be concluded that the models derived in section 5.3.1 are no longer adequate if the cement source is changed; and adjustments in the mixture parameters are required to maintain the mortar properties. But, since the relative influence of each variable on mortar responses do not significantly change with changes in material properties (as pointed in paragraphs 5.4.1 and 5.4.2) a limited number of tests should be enough to adjust mixture parameters.

5.4.6. Cement/superplasticizer combination

For both economical and technical reasons (as it will be demonstrated in Chapter 7) the combination of cement and superplasticizer which leads to lower dosages of superplasticizer should be preferred. From this point of view the combination of CEM I 52,5 R with V3000 was the least efficient from all the combinations studied in this work (see Figure 5.25). In cases like this, or even in cases of total incompatibility (a zero number of optimum solutions), other superplasticizers should be tested. By only changing the superplasticizer type from the same supplier, Viscocrete 3005 (V3005), a larger number of solutions could be found for mortars incorporating CEM I 52,5 R and for a wider range of superplasticizer dosages, as can be observed in Figures 5.32. V3005 is also a polycarboxylate type superplasticizer having a specific gravity of 1,05 and 25,5% solid

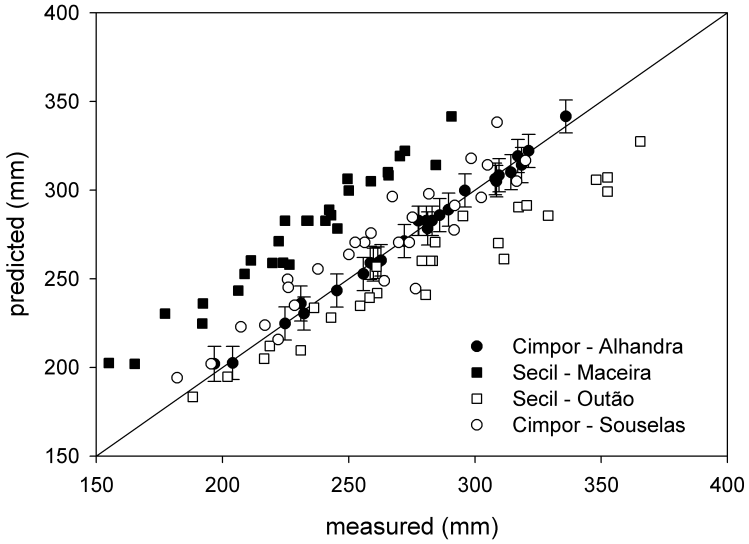


Figure 5.29.: Measured versus predicted values of Dflow for CEM I 42,5 R from different sources

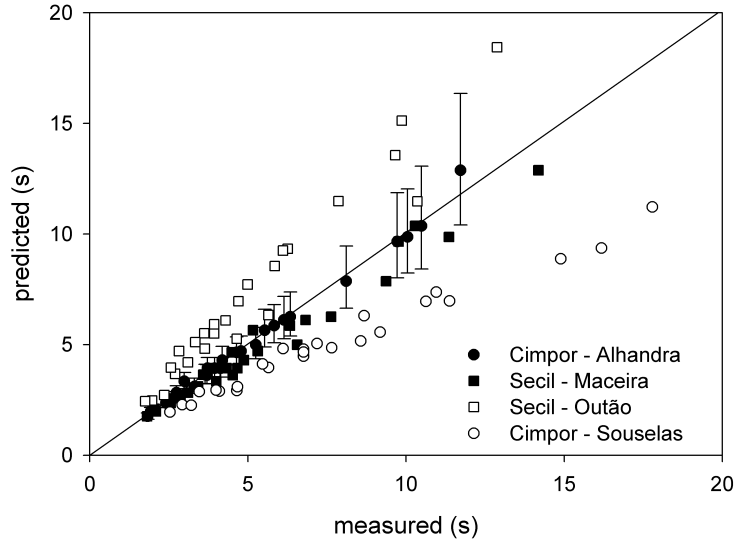


Figure 5.30.: Measured versus predicted values of Tfunnel for CEM I 42,5 R from different sources

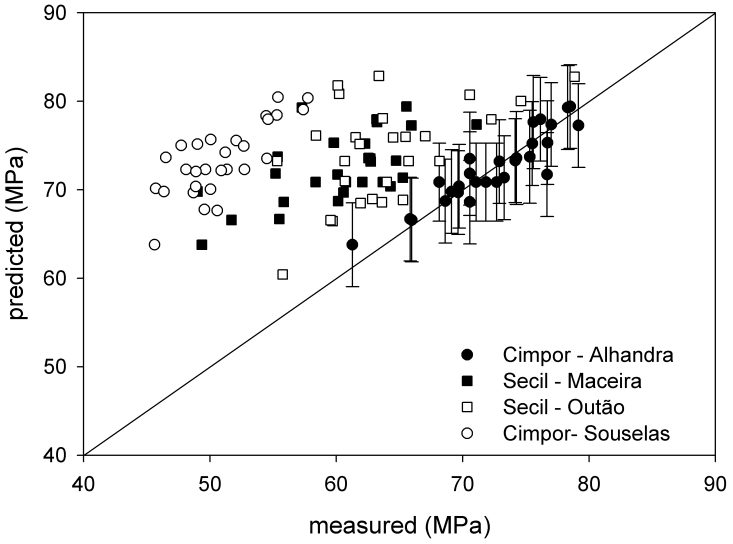


Figure 5.31.: Measured versus predicted values of fc,28 for CEM I 42,5 R from different sources

content. The mix proportions and test results of the 28 mixes prepared for CEM I 52,5 R (Cimpor-Alhandra) in combination with this superplasticizer (V3005), limestone filler and reference sand are summarized in Table E.10 of Appendix E.

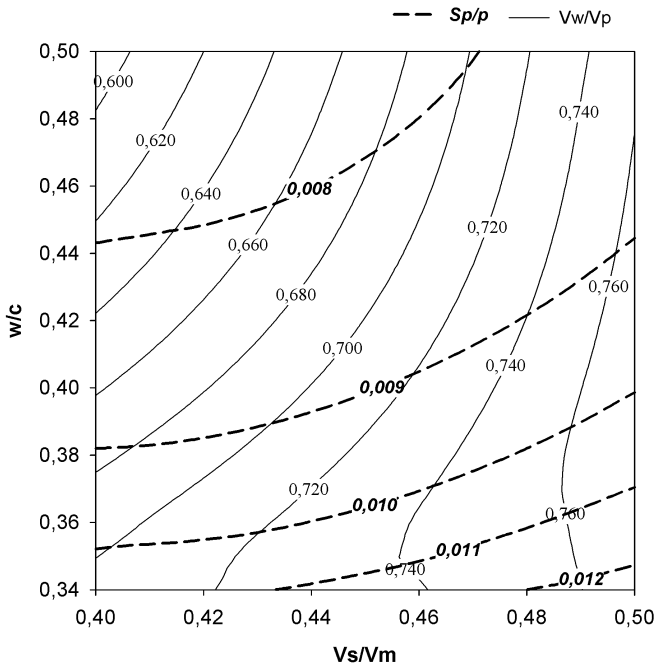
The approximation of the Sp/p contour lines in Figure 5.32, which can also be clearly observed in Figure 5.4 (a) in the case of V3000, indicates the saturation of superplasticizer's effect. Based on these figures, it can be concluded that the saturation dosage (Sp/p) of V3005 and V3000 superplasticizer types is around 1,1% and 2,2%, respectively.

5.5. Concluding remarks

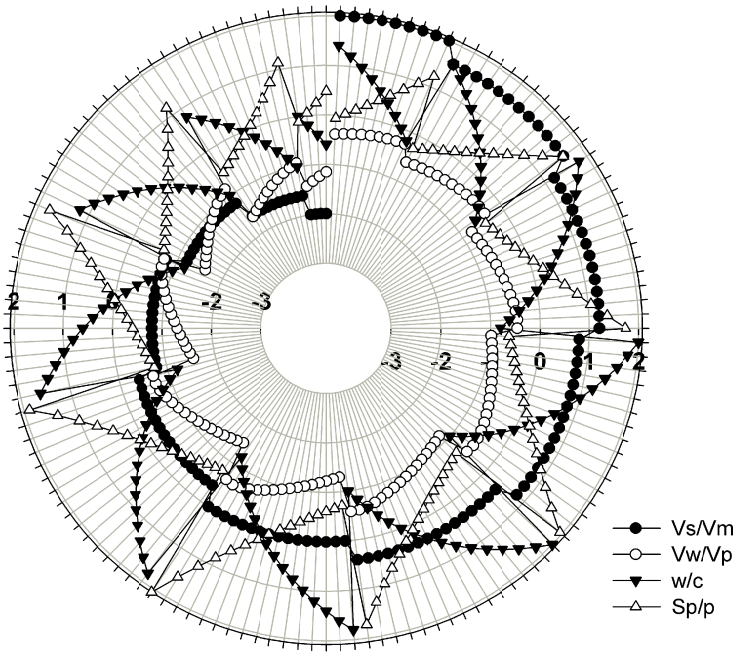
In this chapter a comprehensive procedure for the design of mortar mixtures which are adequate for SCC is provided. Six different types of cement, currently used by the Portuguese construction industry, were assessed in combination with limestone filler and a polycarboxylate type superplasticizer.

An experimental plan conducted according to a central composite design is useful to evaluate the effects of mixture parameters and their interactions on SCC mortar properties while reducing the number of trial batches needed to achieve balance among mixture variables. The mixture variables considered in the Japanese-method (Okamura et al., 2000) can be used as factors in the factorial design to characterize the behaviour of SCC mortar mixtures.

For a given combination of cement + limestone filler + superplasticizer (V3000) a large number of solutions could be found that lead to a spread flow of 260 mm and a flow



(a)



(b)

Figure 5.32.: Range of optimized mixture variables for the combination of CEM I 52,5 R+ limestone filler+V3005: (a) contour plot of absolute values and (b) interaction diagram with coded values

time of 10 s, in a wide range of w/c ratio and fine aggregate content. The number of solutions that were found depends on the interaction between constituent materials but also on the selected range of mixture parameters for the experimental plan.

Each type of cement has unique properties (physical and chemical) that will interact with other constituents, especially additions and admixtures, which reflects on the range of mixture levels of optimized mortar mixtures. Contour plots and interaction diagrams were suggested to represent the range of mixture levels where optimum solutions can be found. Values lower than the typical range of V_w/V_p suggested in (BIBM et al., 2005) [0,85; 1,10], were found to be adequate for the six Portuguese cement types tested in combination with superplasticizer (V3000) and limestone filler.

Information from the contour plots or interaction diagrams can simplify the test protocol required to optimize a given SCC mixture, namely, to select the combination of powder materials with admixtures. In particular, they are useful to compare the efficiency of different admixtures (superplasticizers, viscosity agents, or combination of both) and alternative additions. Optimized mortar mixtures can serve as reference mixtures in a quality control plan to detect variations in different deliveries of cement, filler or superplasticizer. The derived models can still be useful to predict mortar properties when the material properties change, such as the cement source.

The procedure presented in this chapter can easily be implemented in any concrete laboratory of a production centre since it involves mortar tests which are easy to carry out and involves simple and easy to construct test equipments. The variables considered in this work have by no means exhausted the range of factors that affect SCC mortar properties. For example, changes in environmental conditions like temperature and humidity, the evolution of properties over time, the mixing energy and stress history until the time of application, the incorporation of other additions or admixtures, can significantly change mortar properties, in both fresh and hardened states.

6. Influence of cement variations on SCC mortar/paste properties

6.1. Introduction

This chapter deals with the influence of different production dates of cement on fresh and hardened properties of mortar/paste mixes. The three main objectives of the current study are: first, to assess how large the fluctuations on fresh mortar/paste properties can become when a new delivery of cement is used; second, to identify the constituents in cement which might have caused the fluctuations in mortar/paste properties and, third, to verify if the different test results obtained on pastes correlate with each other, in particular, empirical and rheological test results.

6.2. Cement production quality control

6.2.1. Importance of cement variations for SCC robustness

According to BIBM et al. (2005) all cements which conform to EN 197-1 can be used for production of SCC. Generally, cement is seen as one of the constituent materials of concrete with less variation due to a stringent quality control during production. However, recent studies have shown that cement variations have a greater effect on workability and on early reactions of concrete than is generally thought (Juvas et al., xxxx; Wallevik et al., 2007). Kubens and Wallevik (2006) found that the effect of the production date of cement on rheology was only slight in mixtures without admixtures but more prominent in mixes containing dispersing admixtures. Yield stress results (or more precisely, G-yield result obtained from Con Tec Rheomixer) of blank, polycarboxylate ether and melamine mixes (7 samples), containing CEM I 52,5 R, had a coefficient of variation of 15%, 44% and 39%, respectively. These authors observed a similar trend for mixes containing other cements (three CEM I 42,5 R from different producers, and one CEM II/B-S 32,5 R) (Kubens and Wallevik, 2006). Juvas et al. (xxxx) found similar results (see Figure 6.1) when comparing the spread flow results of mortars without admixture,

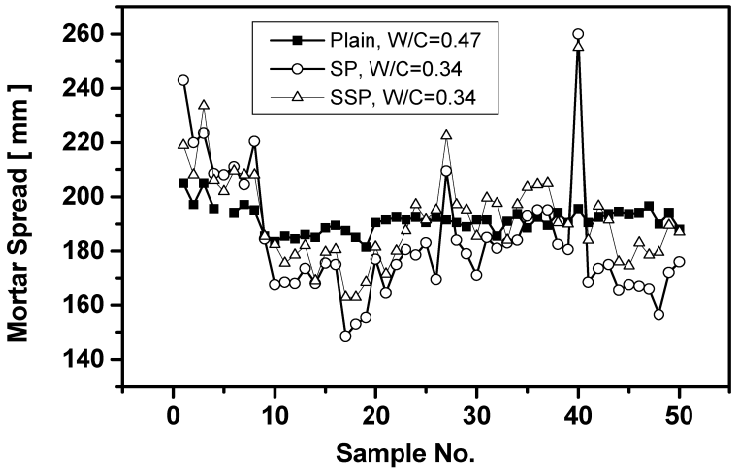


Figure 6.1.: Flow table test results (Juvas et al., xxxx)

containing a typical melamine plasticizer (SP) and a polycarboxylate plasticizer (SSP), from 50 samples of daily collected CEM I 52,5 R cement type. In Figure 6.1 larger variations are clearly observed with mixtures containing admixtures when compared to plain mixtures.

The rheology of plain mortar mixtures, with a water/cement ratio of about 0,50, is controlled largely by water (Aïtcin et al., 2001). In these mixtures, the cement grains are not uniformly dispersed throughout the water but tend to form small flocs which trap water within them (see Figure 6.2 (a)). By adding water these cement flocs are kept apart as a means of influencing the rheology of the paste (Aïtcin et al., 2001). Later in time, the first hydration products begin to interfere with the unrestricted movement of the cement flocs. Dispersing admixtures are used to both break up the flocs and to maintain the dispersion in a way that causes the cement particles to distribute more uniformly throughout the aqueous phase, reducing the yield stress value for a given water content and so increasing the fluidity of the mix. Not only has the fluidity increased, but more sites on the surface of the cement grains are available for interaction with superplasticizer and hydration (Dransfield, 2003). If water is removed from the system lowering the water/cement ratio to 0,3∼0,4, like in the case of mixtures mentioned above (Juvas et al., xxxx; Wallevik et al., 2007), the fluidity can be reduced back to what it was before the admixture addition. However, the average inter-grain distance will also reduce (see Figure 6.2 (b)), so less hydration will be necessary before the space between the cement grains is filled with hydration product to give setting and strength development (Dransfield, 2003). Finally, there will be less void space, not filled with any hydration product, resulting in fewer capillaries and therefore improved final strength and better durability (Dransfield, 2003). In conclusion, the mixtures containing superplasticizers are more complex systems and at low w/c ratios a small difference in the dispersion

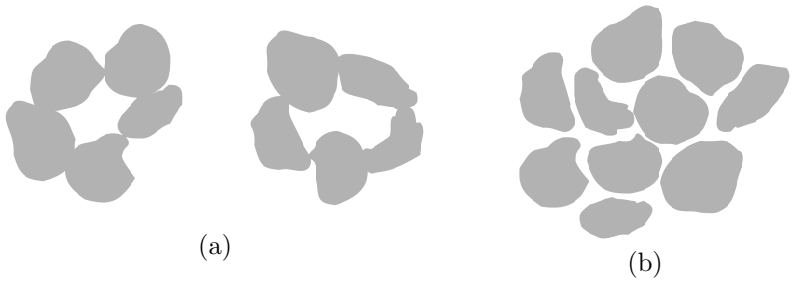


Figure 6.2.: (a) Flocculated cement particles and (b) deflocculated cement particles after superplasticizer addition

effect of the admixture changes the fluidity remarkably.

Wallevik et al. (2007) reported that the fluctuations observed in mortar, due to cement variations, can also be observed at the concrete level. It is suggested that the influence of cement variations on concrete properties can be more or less pronounced depending on cement content in the concrete mixture (Wallevik et al., 2007). In the case of self-compacting concrete, a high-range water reducer[1] must be incorporated and often mixtures have a higher content of cement when compared to conventional concrete mixtures. For these reasons, cement variations have became an important factor when discussing the robustness of SCC production.

6.2.2. Control of cement properties

The control of cement properties by the cement manufacturers is achieved first by control of raw mix chemistry, fineness and homogeneity; second, by control of clinker chemistry and degree of heat treatment and, finally, by control of cement fineness, SO_3 level and forms of SO_3 present (Newman and Choo, 2003). In general, the cement properties of greatest importance for customers are strength at 28 days, early strength, water demand, strength growth and alkali content. Besides, other aspects like interaction with admixtures and/or additions, heat of hydration, colour and flowability can be important to some particular applications. But above all, it is the consistency of performance in relation to these aspects that is of greatest importance to costumers (Newman and Choo, 2003).

The current Portuguese standard for common cements is NP EN 197-1 (Portugal. IPQ, 2001). In Table 6.1 the requirements imposed by NP EN 197-1 for the cement types used in this thesis (and most commonly used in Portugal) are summarized. Besides these requirements, NP EN 197-1 defines the permitted chemical composition of the individual constituents, the nature of minor additional constituents and the permitted

[1]Polycarboxylate type superplasticizers are the most used.

level of additives. NP EN 197-1 also describes the testing frequencies and the method of data analysis required to demonstrate compliance with EN 197-1.

None of the standard tests on cement (like setting or water demand) incorporate chemical admixtures, so these quality control results cannot give any information about cement/superplasticizer interaction (Wallevik et al., 2007). Moreover, Blaine fineness (the most observed single property of cement) is not a sufficient parameter for explaining the variations in the properties of fresh concrete mix or early age properties of concrete, especially with mixtures containing superplasticizers (Erdogdu, 2000; Juvas et al., xxxx; Kim et al., 2000). The two most commonly employed tests for studying cement/superplasticizer interaction are grout-based tests, namely, the mini-cone test (Aïtcin et al., 2001; Gomes, 2002; Roussel, 2006b; Roussel and Coussot, 2005; Schwartzentruber et al., 2006) and the Marsh flow test (de Larrard et al., 1997; Aïtcin et al., 2001; Gomes, 2002; Roussel and Le Roy, 2005; Schwartzentruber et al., 2006).

These grout-based tests are preferred to concrete tests because they are less demanding in terms of materials, energy, time and space. Juvas et al. (xxxx) suggested the use of the flow table test described in Punkki and Penttala (xxxx), and the semiadiabatic calorimeter to measure the uniformity of cement properties concerning workability and heat release at plant conditions. In order to get more accurate information from rheological properties a mortar/concrete viscometer (Kubens and Wallevik, 2006; Wallevik et al., 2007) or a paste rheometer can be used. However, these types of tests may not be suitable for the factory environment or construction site.

6.2.3. Influence of cement parameters on concrete properties of mixtures without admixtures

The standard cement properties of water demand (workability), setting time and strength development are determined mainly by (Newman and Choo, 2003):

- cement fineness (surface area and residue at 45 μm);
- loss on ignition (LOI);
- clinker alkalis and SO_3;
- clinker free lime;
- clinker compound composition (mainly, C_3S and C_3A);
- cement SO_3 and the forms of SO_3 present.

Table 6.1.: Requirements for cements defined by NP EN 197-1 (Portugal. IPQ, 2001)

Cement type	CEM I 52,5 R	CEM I 42,5 R	CEM II/A-L 42,5 R	CEM II/B-L 32, 5 N	CEM IV/ B(V) 32,5 N	CEM II/B-L 32,5 R (BR)
Composition:						
clinker (%)	95-100	95-100	80-94	65-79	45-64	65-79
Limestone filler, L (%)	–	–	6-20	21-35	–	21-35
Siliceous fly ash, V (%)	–	–	–	–	35-55	–
Minor addit. constit. (%)	0-5	0-5	0-5	0-5	0-5	0-5
Mechanical characteristics[a]:						
f_c,2 days (MPa)	≥30	≥20	≥20	–	–	≥10
f_c,7 days (MPa)	–	–	–	≥16	≥16	–
f_c,28 days (MPa)	≥52,5	≥42,5 ;≤62,5	≥42,5 ; ≤62,5	≥32,5 ; ≤52,5	≥32,5 ;≤52,5	≥32,5; ≤52,5
Physical characteristics [a]:						
Initial setting time (min)	≥45	≥60	≥ 60	≥ 75	≥75	≥ 75
Expansion (mm)	≤10	≤10	≤10	≤10	≤10	≤10
Chemical characteristics [a]:						
Loss on ignition (%)	≤5	≤5	–	–	–	–
Insoluble residue (%)	≤5	≤5	–	–	–	–
Sulphate, as SO_3 (%)	≤4	≤4	≤4	≤3,5	≤3,5	≤3,5
Chloride (%)	≤0,1	≤0,1	≤0,1	≤0,1	≤0,1	≤0,1
Pozzolanicity	–	–	–	–	satisfies the test	–
MgO				≤5% in clinker		

[a] specified in terms of characteristic values

Workability (water demand)

The key parameters to ensure satisfactory workability characteristics of mixtures without admixtures are an appropriate ratio of SO_3 to alkalis in the clinker and an appropriate level of dehydrated gypsum in the cement (Newman and Choo, 2003). Nevertheless, particle size distribution and specific surface area of cement also affect water demand (Hewlett, 2004).

The crystallization products formed after cooling of the clinker liquid depend on the relative levels of the two alkali oxides (Na_2O and K_2O) and the level of SO_3 in the clinker. The alkali oxides combine preferentially with SO_3, and if there is sufficient SO_3 these will crystallize to yield alkali sulfates. If there is insufficient SO_3 to combine with the alkali oxides then these may enter into solid solution in the aluminate and silicate phases. K_2O increases the reactivity of C_3A while Na_2O reduces it (Hewlett, 2004). Therefore, the quantity of readily soluble sulfate should be adjusted to the level of activity of C_3A in order to optimize fluidity (Hewlett, 2004). The solubility behaviour of sulfate depends on the form in which it is present in the cement. During cement mill (with temperatures in the range of 100 to 130 °C) the calcium sulfate dihydrate (gypsum) added to the mill undergoes dehydration first to hemihydrate and then to soluble anhydrite. The dehydrated forms of gypsum dissolve more rapidly than gypsum and this is beneficial in ensuring that sufficient Ca^{2+} and SO_4^{2-} ions are available in solution to control the initial reactivity of C_3A by forming a protective layer of ettringite. An insufficient supply of soluble calcium sulfate can result in a rapid loss of workability (flash set). If a too high level of dehydrated gypsum is present, then crystals of gypsum crystallize from solution causing false set (initial level of workability can be restored by re-mixing). Many natural gypsums contain a proportion of the mineral natural anhydrite, which is unaffected by milling temperature and dissolves slowly in the pore solution providing SO_4^{2-} ions necessary for strength optimization but having no potential to produce false set. Thus, the optimization of readily soluble sulfate is achieved by a combination of: control of cement total SO_3 level; controlling the level of natural anhydrite in the calcium sulfate used and controlling cement milling temperature.

Water demand increases significantly with the specific surface area of Portland cement (Hewlett, 2004). For equal specific surface area, cements with narrower particle size distribution have larger water demands due to higher volume of voids which need to be filled with water (Hewlett, 2004). The partial replacement of clinker by fly ash (as in the case of CEM IV/B(V) 32,5N presented in Table 6.1) should result in a reduction in water demand due to the spherical shape of particles which lubricate the mix, as can be observed in Figure 6.3. Limestone can have a positive influence on water demand (as in the cases of CEM II/A-L 42,5 R and CEM II/B-L 32,5 N presented in Table 6.1) because the fine limestone particles improve cement particle size distribution (see Figure 6.4),

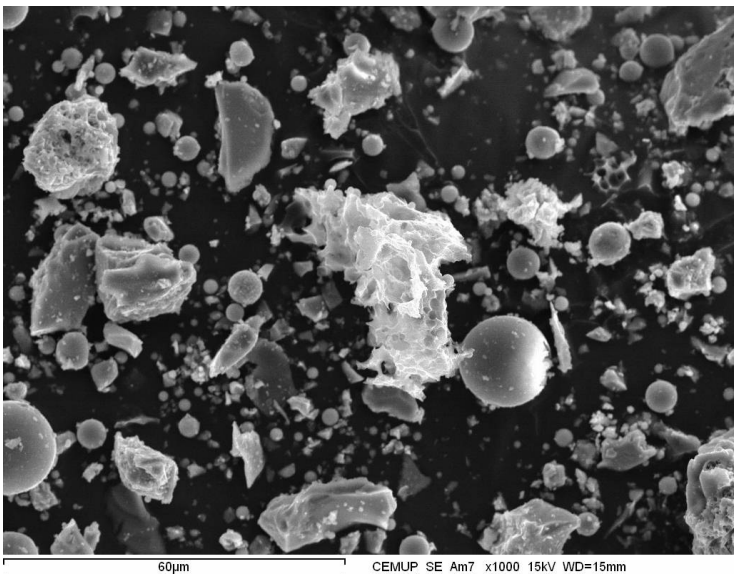


Figure 6.3.: Backscattered electrons image of CEM IV/B(V) 32,5 N particles

lowering the volume of voids which must be filled with water.

Setting time

Cement paste setting behaviour is determined mainly by clinker reactivity and by cement fineness (for a given water/cement ratio). The main factors, which tend to shorten setting time are increases in the levels of: clinker-free lime; cement fineness (surface area); C_3S content and C_3A content. Both fly ash and slag will increase setting time while a Portland limestone cement may have a slightly shorter setting time than the corresponding pure Portland cement (Newman and Choo, 2003; Pera et al., 1999).

Strength development

Late strength is only slightly dependent on cement fineness and for a given water/cement ratio it is determined mainly by the chemical composition of cement (Hewlett, 2004). While surface area is a good guide to the early rate of hydration of cement and thus early strengths, 45 μm residue is a more reliable guide to late strengths and, in particular, to 28 days strengths. For a given surface area, the lower the 45 μm residue the higher the 28 days strength (Newman and Choo, 2003). The pre-hydration of cement clinker represented by the increased loss on ignition (LOI) has a significant influence on strength development. However, the influence of LOI when cement contains a calcareous minor additional constituent is much less clear (Newman and Choo, 2003). Late strengths are normally maximized by low free lime level (as this maximizes combined silicate content) but low free lime levels are associated with low reactivity and extended setting times. The effect of C_3S is most pronounced at all ages whereas the contribution of

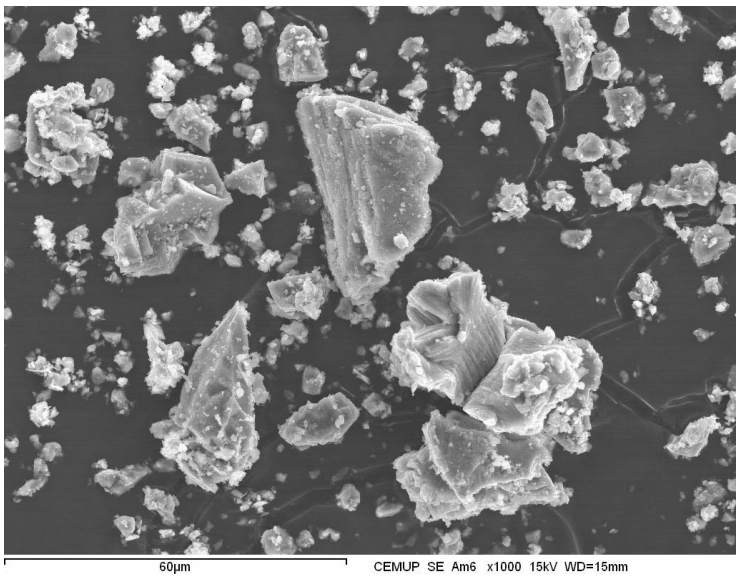


Figure 6.4.: Backscattered electrons image of CEM II/B-L 32,5 N particles

C_2S to strength becomes significant only at later ages. Soluble alkalis accelerate early strength development and depress late strengths (28 days) (Newman and Choo, 2003). Nevertheless, the alkalis present in the crystal lattice of clinker minerals appear to behave differently to those present in the form of soluble sulfates (Hewlett, 2004). The total SO_3 content of the cement also influences strength properties. With increasing SO_3 content the strength tends to increase up to an optimum value and then decreases with even higher SO_3 contents (Hewlett, 2004). The response of a cement to a change in cement SO_3 level is influenced by a number of factors, which include: the alkali content and in particular the alkali sulfate (soluble alkali) content; the C_3A level; the cement fineness. In most countries the opportunity to optimize cement SO_3 is restricted by the upper limits for SO_3 in the relevant standards.

6.2.4. Influence of cement parameters on the properties of mixtures including a superplasticizer (polycarboxylate type)

The presence of a superplasticizer affects workability greatly (reducing the water demand) but can also interfere with the nucleation and/or the growth processes, which can influence the hydration reaction rate and the reaction products (changing setting time and strength development). Due to the wide variability in the chemical and physical properties of cements, different cements behave in different ways in the presence of the same superplasticizer. Among the cement parameters which have been found to exert a major influence on the properties of superplasticized cement mixes (see Chapter 3), are:

- the physical characteristics of cements, such as specific surface area;

- the chemical characteristics of cements, such as its phase composition and the availability of quickly soluble SO_4^{2-} ions; the morphology of cement grains, especially the amount of C_3A at their surface; the quantity of soluble alkalis;

- the quantity of clinker substituted by a mineral addition in a blended cement.

Differences in performance of various cement-admixture combinations are typically more significant with lower water/powder ratios (Aïtcin et al., 2001). Since PC-type superplasticizer is used for concrete prepared with low water/powder ratios, as in the particular case of SCC, a small difference in the dispersion action of the admixture changes the fluidity remarkably.

In Chapter 3, the mode of action of different superplasticizers and their interaction with cement particles was discussed. The unique molecular structure of PC type superplasticizers contributes to their improved performance. The molecular structure of a PC type superplasticizer can be designed for a particular application by changing: the main chain length; side chain length; side chain density or type of chains (see Chapter 3, section 3.6). Consequently, these changes can affect the ability to reduce water, fluidity retention, setting time, and early strength development.

The initial reactivity of cement is critical for the performance of a PC type superplasticizer. Higher dosages of superplasticizer are required with an increase of cement fineness, an increase of C_3A phase at the surface of cement particles or an increase of quickly soluble SO_4^{2-} ions (especially, from alkali sulfate). The presence of sulfate ions in solution reduces the adsorption of PC polymers due to competitive adsorption on cement particles. Whereas an optimum sulfate ion concentration exists for SMF and SNF, the sulfate ion concentration should be minimized for PC type superplasticizers. Sulfates are supplied by both alkali sulfates and calcium sulfates. The type of calcium sulfate also matters, as dehydrated forms supply sulfate ions faster than gypsum.

As it was shown in Chapter 3, superplasticizer molecules may also adsorb on inert powders which are added in blended cements or directly into concrete, such as fly ash and limestone filler. In the particular case of limestone filler, it was demonstrated that substitution of cement clinker by limestone filler is beneficial in increasing the electrostatic repulsion effect of Sp.

Since many of these effects may occur simultaneously, it can be difficult to discover the main factors and interactions existing between the different components in a superplasticized cement suspension and this is further complicated by the ongoing hydration reactions of cement.

6.3. Experimental programme

In Chapter 5, SCC mortar mixes were optimized for different Portland cement types, namely, CEM I 52,5R, CEM I 42,5 R, CEM II/A-L 42,5 R and CEM II/B-L 32,5N, currently used in Portugal. To evaluate the range of workability and strength variations of SCC mortars/pastes due to different deliveries of cement (supplied from the same factory) four optimized mixes, corresponding to each cement type, were characterized in the fresh, hardening and hardened states for eight cement deliveries with different production dates. The testing programme included tests on SCC mortars, empirical and rheological tests on SCC pastes, experimental packing density and semi-adiabatic tests on SCC pastes. Besides, data of standard tests on cements, physical and chemical analysis of cements was obtained from the cement producer, for each cement delivery.

6.3.1. Materials characterization and mix proportions

The mortar mixes investigated in this study were prepared with cement, a mineral addition (limestone filler, first delivery), CEN standardized sand and tap water. The chemical and physical properties of the different cement types, for different deliveries, are presented in Tables C.1 to C.8 of Appendix C. The physical and chemical characterization of limestone filler used in this study (first delivery) is presented in Tables C.9 and C.10 of Appendix C. A polycarboxylate type superplasticizer (V3000) was used having a specific gravity of 1,05 and 18,5% solid content. Reference sand is siliceous round-grain natural sand (0,08-2 mm) with a specific gravity of 2,57 and an absorption value of 0,68%.

The mix proportions of mortar and paste, for each cement type, were established based on the mixture parameter values presented in Table 6.2. As can be observed in Table 6.2 the mortar mixtures exhibited the same V_s/V_m and w/c ratios, thus Sp/p and V_w/V_p had to be adjusted to attain similar mortar fresh properties (Dflow= 260 mm and Tfunnel=10 s), for each cement type (see Chapter 5). V_w/V_p values did not change significantly but Sp/p varied considerably with cement type.

6.3.2. Mixing sequence and testing sequence

The mortar and paste mixes were prepared in the laboratory in 1,4 and 1,25 litres batches, respectively, and mixed in a two-speed mixer complying to NP EN 196-1. The mixing sequence consisted of mixing sand and powder materials (or only powders, in the case of pastes) with 0,81 of the mixing water during 60 s, stopping the mixer to scrape material adhering to the mixing bowl, mixing for another 60 s, adding the rest of

Table 6.2.: Optimized mixture parameters and mix proportions

	CEM I 52,5R	CEM I 42,5R	CEM II/A-L 42,5R	CEM II/B-L 32,5N
Mixture parameters				
w/c	0,45	0,45	0,45	0,45
Sp/p	1,90%	1,72%	1,58%	1,49%
V_w/V_p	0,724	0,728	0,719	0,725
V_s/V_m	0,50	0,50	0,50	0,50
Mix proportions of mortar (kg/m^3)				
cement	466,5	468,3	464,6	466,9
limestone filler	378,3	374,5	376,9	361,0
water	205,6	207,7	206,9	208,8
superpl. (V3000)	16,1	14,5	13,3	12,4
standardized sand	1286	1286	1286	1286
Mix proportions of paste (kg/m^3)				
cement	932,9	936,6	929,2	933,9
limestone filler	756,6	749,0	753,9	722,0
water	393,6	397,8	396,4	400,1
superpl. (V3000)	32,1	29,0	26,6	24,7

the water with the superplasticizer, mixing for 60 s, stopping the mixer again to scrape material adhering to the bowl, mixing for another 30 s, stopping the mixer for 5 min and finally mixing mortar/paste during a further 30 s. The mixer was always set at low speed except in the last 30 s of the mixing sequence where it was set at high speed.

The mortar testing sequence was approximately the following:

0 h 00 min – start of mortar mixing procedure;

0 h 10 min – start of mortar flow test;

0 h 15 min – start of mortar V-funnel test;

0 h 17 min – moulding of three 70 mm cubes.

The paste testing sequence was approximately the following:

0 h 0 min – start of paste mixing procedure;

0 h 10 min – start of Marsh cone flow test;

0 h 20 min – start of paste flow test;

0 h 25 min – start of semi-adiabatic calorimeter test;

0 h 30 min – start of 1^{st} rheological test in the rheometer;

0 h 32 min – start of centrifuge test;

0 h 40 min – start of 2^{nd} rheological test in the rheometer;

0 h 42 min – moulding of three prismatic moulds (4×4×16 mm^3).

In general, for each cement delivery, SCC mortar and paste characterization tests were carried out in the same day to minimize the influence of environmental factors. During the waiting periods between tests the mortar/paste sample was covered with a humidified cloth to avoid the loss of water by evaporation. Just before the beginning of each test the mortar/paste sample was re-mixed by hand with a paddle (10 turns clockwise) to destroy any structuration formed during rest (thixotropy effects).

6.3.3. Mortar test methods

Mortar flow and V-funnel tests

Mortar tests using the flow cone and the V-funnel, with the same internal dimensions as the Japanese equipment, were carried out to characterize fresh state (see Chapter 4, section 4.6, for details on equipments and test procedures). The mortar flow test was used to assess deformability by calculating the flow diameter (Dflow, mortar) as the mean of two diameters of the spread area. The V-funnel test was used to assess the viscosity and passing ability of the mortar. Test flow time was recorded (Tfunnel, mortar).

Compressive strength at 28 days

After fresh mortar tests, three 70 mm cubes were moulded, without compaction, to evaluate 28 day compressive strength (fc,28, mortar). Mortar cubes were demoulded one day after casting and kept inside a chamber under controlled environmental conditions (Temperature=20°C and HR=95-98%) until testing age. Compressive strength at 28 days (fc,28, mortar) was taken as the mean of the three cubes' compressive strength.

6.3.4. Paste test methods

Marsh cone flow test

The Marsh cone flow test, including the geometry of testing apparatus, is described in NP EN 445 (Portugal. IPQ, 2002) as a method to determine the fluidity of injection grouts for rocks, soils or prestressed ducts. This test method is based on the measurement of the time taken for a certain volume of material to flow through the cone. In the present study, 1000 ml of paste were poured into the cone (with an opening of

10 mm in diameter) and the time taken for 500 ml to flow out was taken as the flow time. Paste flow time (Tflow) was given by mean of results obtained in two consecutive measurments. Flow time varies inversely with paste fluidity (Gomes, 2002; Roussel and Le Roy, 2005).

Paste flow test

The mini slump flow test was carried out to assess the deformability of paste. A truncated cone (with upper and lower diameters of 19 and 38 mm, respectively, and height of 57 mm) was used in this test, which is a smaller-scale version of the Abrams cone developed by Kantro (Gomes, 2002). After filling the cone with paste and levelling it, the cone was lifted and the paste flow diameter (Dflow, paste) was taken as the average of two diameters of the spread area.

Semi-adiabatic calorimeter test

The cement hydration reactions are exothermic. In this study, the heat of reaction of SCC pastes was measured with a simple semi-adiabatic calorimeter specially built for this study (see Figure 6.5) based on the calorimeter described in (Juvas et al., xxxx). It consists of a plastic box filled with insulation material forming four cavities in the centre where four cylindrical containers can be fitted. After filling these containers with cement paste, the box was closed. The insulation material surronding cement samples avoided rapid dissipation of heat to the environment. All tests were carried out in a chamber with controlled environmental conditions (Temperature=20±2°C and HR=50±5%). The temperature evolution of cement samples was continuously monitored, during 48 hours, through the installation of temperature sensors (PT100), outside the bottom part of each container, connected to an automatic acquisition system (datataker DT 515 Series 3) (see Figure 6.5). The mean value of three curves of temperature evolution with time was obtained for each cement sample. From this curve three points were distinguished (see white dots in Figure 6.6) and the following data was collected: the initial temperature of paste; the time to start of temperature raise; the time to reach maximum temperature and the value of maximum temperature.

Rheological tests (using a rheometer)

The viscosity and the yield stress as defined by the Bingham model were evaluated using a cone and plate rheometer (Bohlin CVO-100). The cone diameter was 40 mm with a cone angle of 4°. After placing the cement sample on the plate, the cone was lowered so that a gap of 150 μm between the cone and plate was achieved. The temperature of the

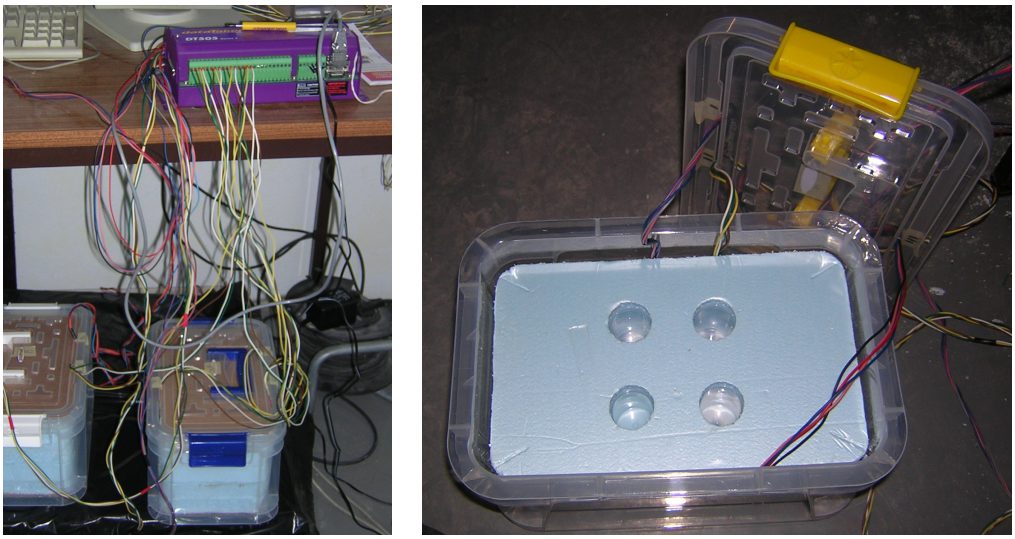


Figure 6.5.: Experimental set-up used in this study to measure temperature evolution of paste under semi-adiabatic conditions

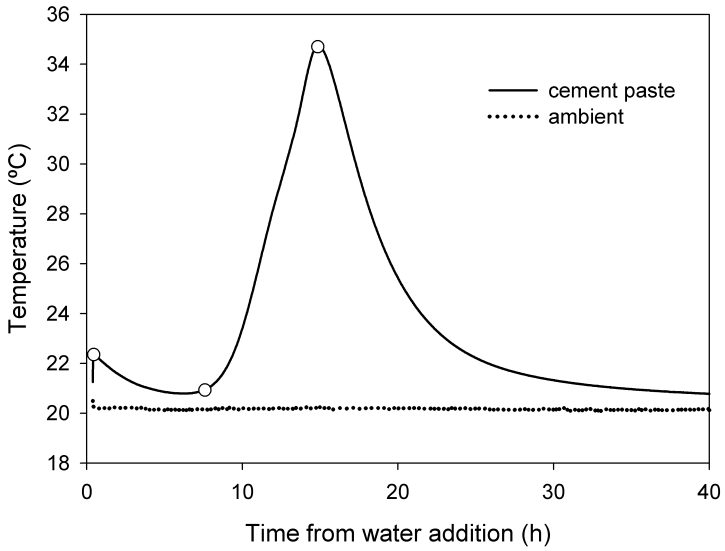
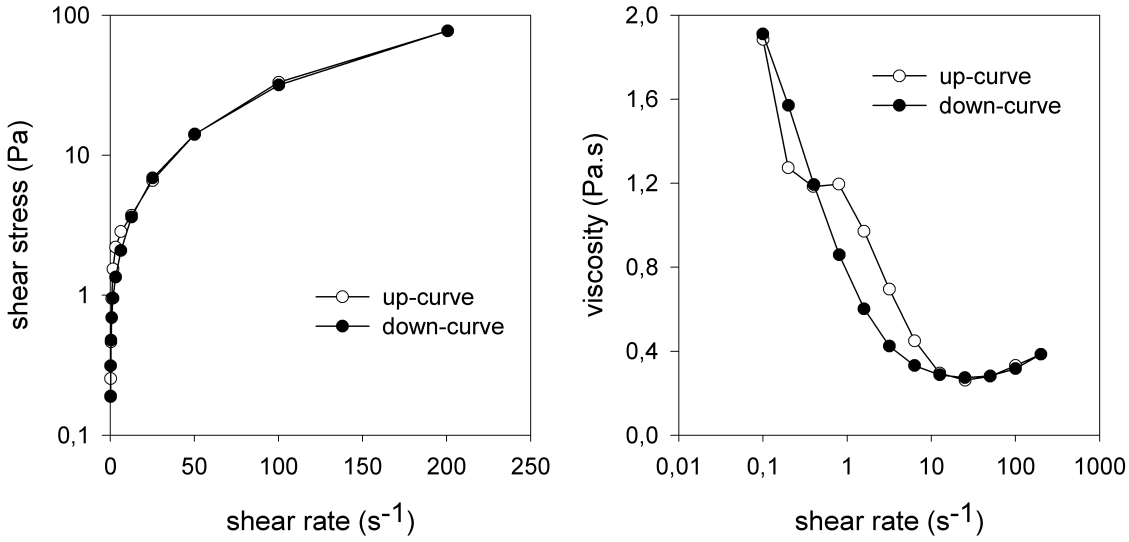


Figure 6.6.: Typical evolution of temperature of cement paste (SCC) with time obtained from semi-adiabatic test



(a) (b)

Figure 6.7.: (a) Typical evolution of shear stress with shear rate and (b) evolution of viscosity with shear rate of a cement paste

samples was set at 25 °C. Before measurements, a pre-shear procedure was applied to homogenize the sample, 45 s at a shear rate of 200 s^{-1}, followed by a resting period of 100 s. During the measurements (control shear rate mode) the rheometer was programmed to perform a 12-step increase of the shear rate ranging from 0,1 to 200 s^{-1} and back again to complete a full cycle. The Bingham model was adjusted to the point results of the down-curve (see Figure 6.7). For more details on rheology principles, rheological models and experimental procedure see Chapter 2.

Centrifuge test

A centrifuge (Centurion, model K240, series K2, see Figure 6.8) was used to compact the solids and to determine the free water of paste, which allowed calculating the packing density of the paste. The free water is defined as the water not restricted by particles, e.g. the water that can move around particles (Grünewald, 2004). About 30 min after the beginning of mixing, the four plastic containers (with 50 ml volume capacity) of the centrifuge were filled with paste (approximately 30 ml on each container). Then, centrifuging was carried out for 15 min at 3500 rpm. After that, the free water which rose up to the surface of the paste was removed with a pipette. The weight of the containers before and after centrifuging was determined. The free water content (w_{free}), in kg/m^3, was calculated from

$$w_{free} = \frac{w_{final} - w_{initial}}{30} \tag{6.1}$$

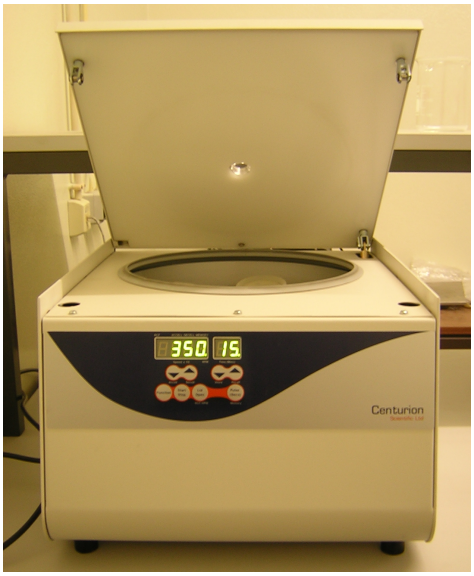


Figure 6.8.: Centrifuge (Centurion, model K240, series K2) used in the present study

where $w_{initial}$ and w_{final} are the weight of containers before and after removing the surplus of water, respectively. The mean value of results obtained with the four containers was taken as the test result. From this test result the packing density of paste (PD) can also be computed as

$$PD = \frac{V_{total} - V_w}{V_{total} - V_{wfree}} \tag{6.2}$$

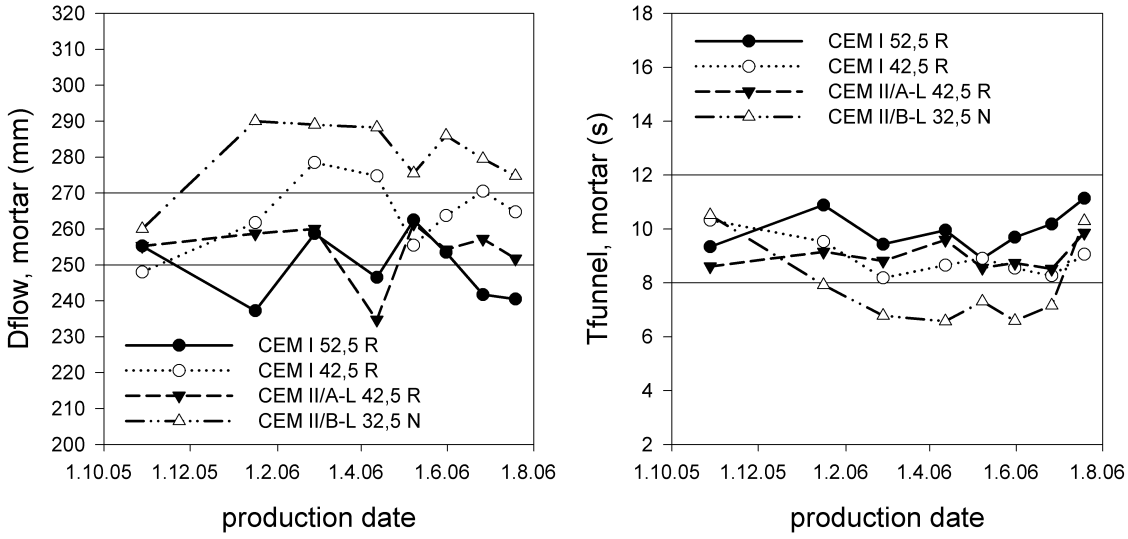
where V_{total}, V_w and V_{wfree} are the volume of the sample (30 ml); the total volume of water in the sample (obtained from the mix proportions) and the volume of free water in the sample which can be calculated from equation 6.1.

Tensile and compressive tests at 28 days

After fresh paste tests, three prismatic moulds (4×4×16 mm^3) were moulded, without compaction, to evaluate 28 day tensile and compressive strengths. Paste prisms were demoulded one day after casting and kept inside a chamber under controlled environmental conditions (Temperature=20°C and HR=95-98%) until testing age.

6.3.5. SCC-mortar properties variation with cement delivery

The effect of variations in cement delivery on SCC mortar fresh properties is presented in Figure 6.9, along with the established acceptance limits (see also Tables E.11 to E.14 of Appendix E). By using the quality controlled CEN sand, effects on rheology resulting from the sand were reduced to a minimum. The only parameter changing was



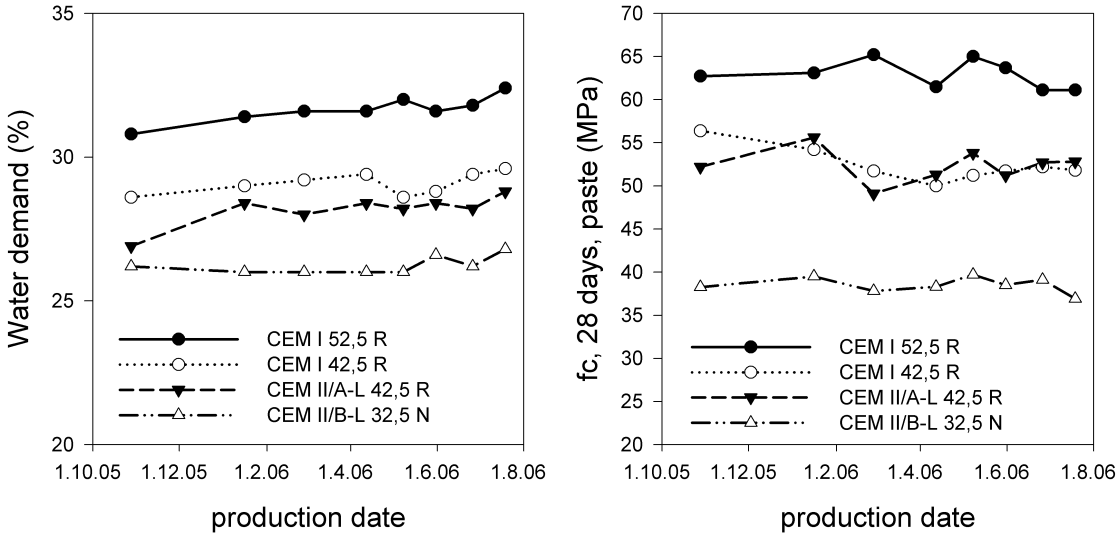
(a) (b)

Figure 6.9.: Variation of (a) Dflow and (b) Tfunnel SCC-mortar results, with cement delivery

cement depending on delivery. In general, a random variation of results was observed, falling within or without exceeding considerably by far the acceptance limits, except in the case of CEM II/B-32,5 N. Since the mix proportions were optimized for the first delivery and maintained constant from then on, in spite of the relatively small variation of results, beyond the second delivery all the results fell outside the acceptance limits. The observed variations of SCC fresh mortar properties could not be anticipated from results of the standard water demand test, as can be observed in Figure 6.10 (a), since this test does not take into account the effect of the superplasticizer. The problem with workability variations is that they can result in larger range of variation of the hardened state properties, due to the occurrence of segregation or lack of filling ability. This explains the variation of compressive strength results of SCC mortars, presented in Figure 6.10 (b) (c.o.v. varied from 5,4 to 8,6%). Again, these results could not be anticipated from standard compressive strength results (without superplasticizer), which exhibited a c.o.v. varying from 2,4 to 3,8%.

6.3.6. SCC-paste properties variation with cement delivery

As mentioned before, the paste phase from the optimized mortar mixtures was also characterized for each cement delivery, except for the first one (see Tables E.11 to E.14 of Appendix E). The results of SCC paste flow diameter and flow time are presented in Figure 6.11. These results present similar variation trend as to those of mortar flow and V-funnel tests (see Figure 6.9). In the case of pastes, the level of flow time results can be

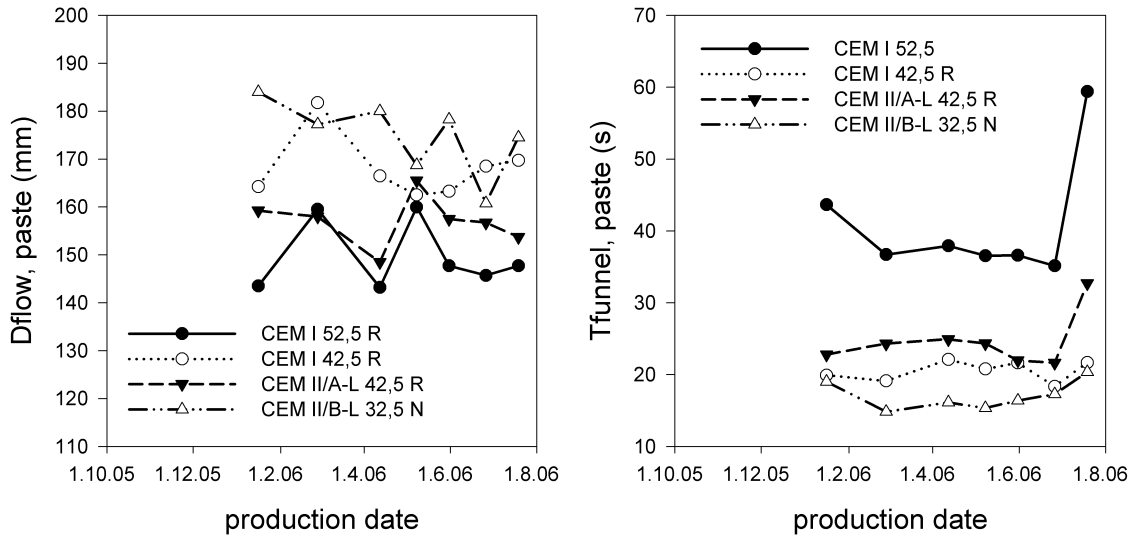


(a) (b)

Figure 6.10.: Variation of (a) standard water demand results and (b) fc,28 SCC-mortar results, with cement delivery

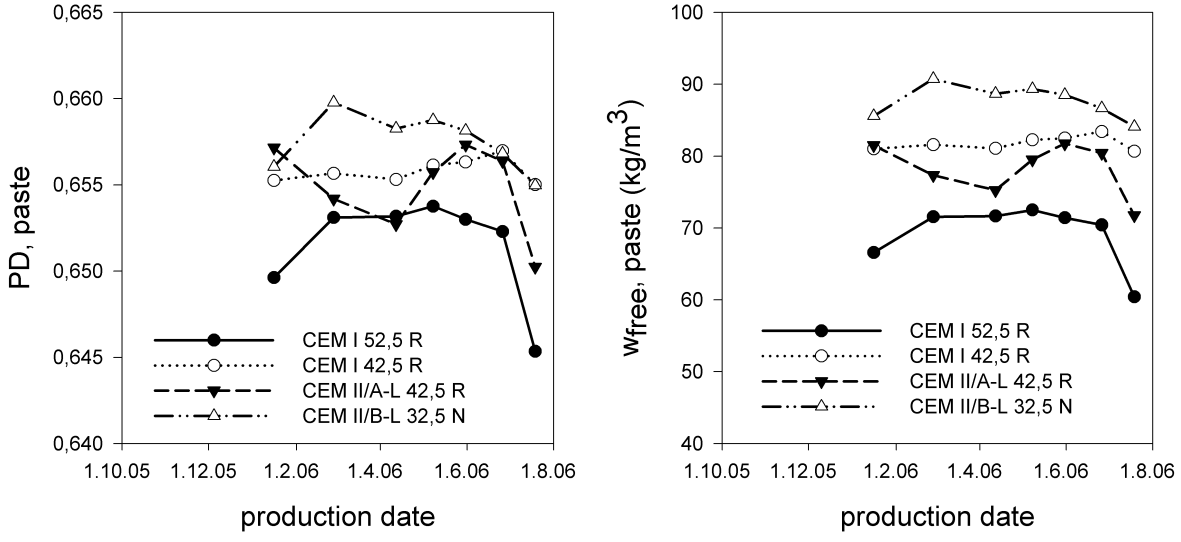
distinguished by cement type. A similar differentiation, by cement type, was observed in the results of free water content (see Figure 6.12). Higher free water contents are associated to lower flow times in the Marsh cone. The results of packing density of paste are related to the free water content (see section 6.3.4) but this differentiation by cement type is not so visible in the results of packing density. The variation of rheological parameters σ_0 and η_{pl} of SCC pastes are presented in Figure 6.13. In general, the mixtures containing CEM I 52,5 R and CEM II/B-L 32,5 N can be associated to the highest and the lowest values of both σ_0 and η_{pl}, respectively.

In Figure 6.14 the results of standard initial and final setting times are presented for each cement type and delivery. The results obtained with the semi-adiabatic calorimeter test are presented in Figures 6.15 and 6.16. In general, the time needed for the temperature to start increasing (related to initial setting time) was higher for CEM I 42,5 R followed by CEM I 52,5 R, CEM II/A-L 42,5 R and, finally, CEM II/B-L 32,5 N. Such an effect could not be expected from the initial setting time results. This was due to the retardation effect of the superplasticizer, especially for the highest dosages. A decreasing tendency is observed in the last four results (see Figure 6.15 (a)), for all cement types. This was probably due to the effect of the environment's temperature. The last four tests were carried out during summertime, thus the initial temperature of paste at the beginning of the semi-adiabatic calorimeter test was higher (see Figure 6.16 (a)) which accelerated the progress of initial hydration reactions. To overcome this problem the materials (including water) should be kept in a room with controlled environmental conditions during enough time to stabilize their temperature before mixing. Considering the time



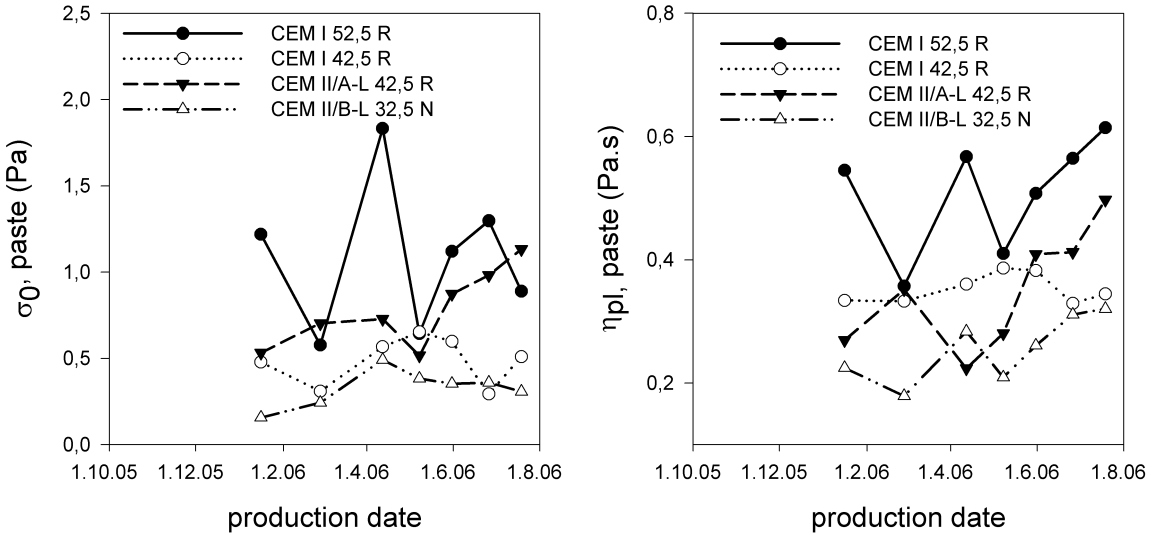
(a) (b)

Figure 6.11.: Variation of (a) Dflow and (b) Tfunnel SCC-paste results, with cement delivery



(a) (b)

Figure 6.12.: Variation of (a) PD and (b) wfree SCC-paste results, with cement delivery



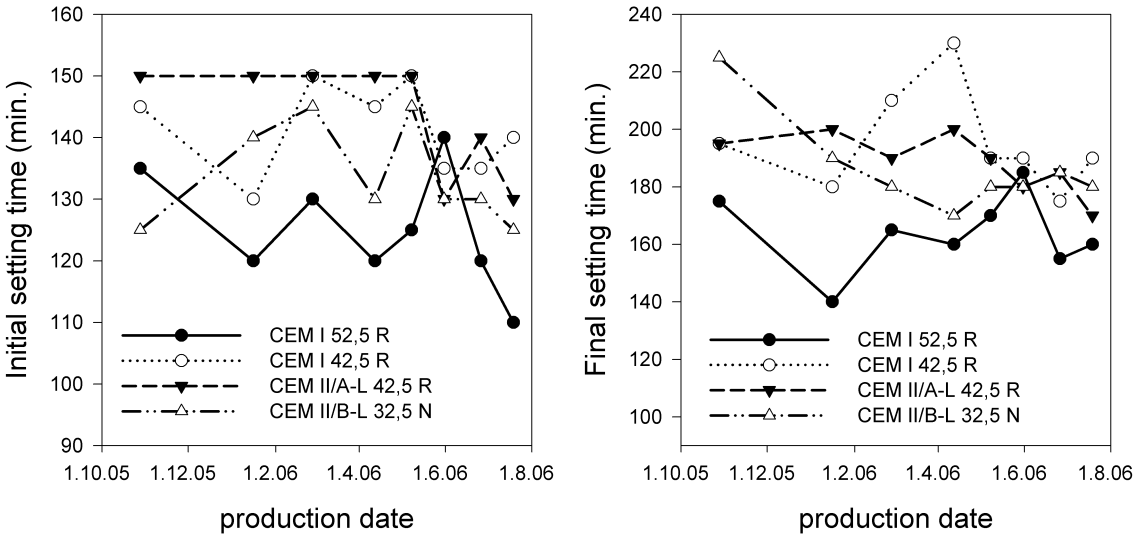
(a) (b)

Figure 6.13.: Variation of σ_0 and η_{pl} results of SCC-paste, with cement delivery

needed for SCC pastes to reach the peak temperature (related to final setting) no large differences were observed between cement types. The maximum temperature attained by SCC pastes (see Figure 6.16 (b)) can be clearly differentiated by the strength class of cement and seems to be associated with compressive strength of SCC pastes (see Figure 6.17). The results of paste tensile strength, at 28 days, are not presented here due to excessive variation of results within each test.

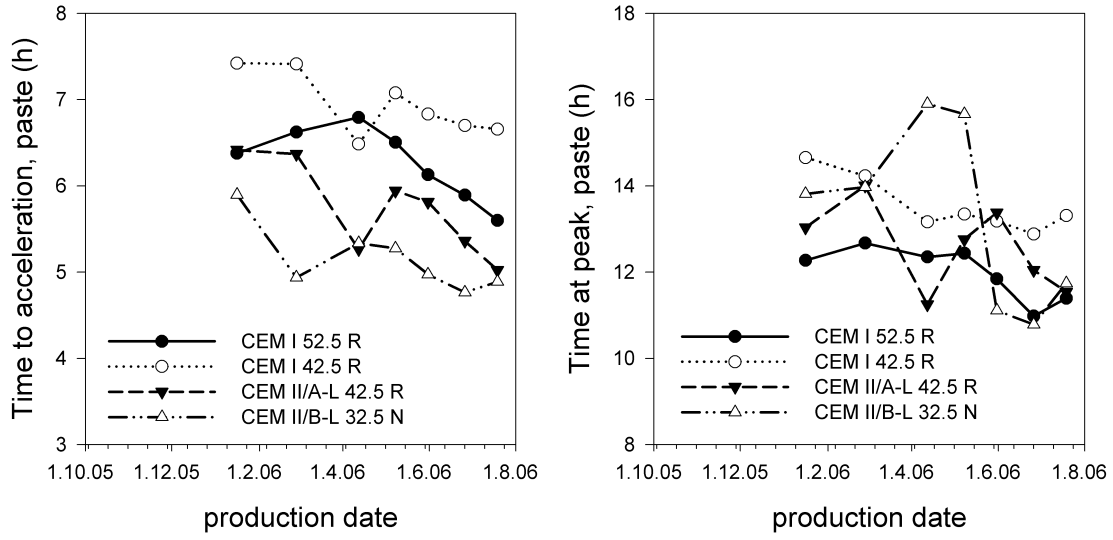
6.3.7. Correlations

A correlation analysis was performed using SPSS 15.0 commercial software. Spearman's correlation coefficient ($\rho_{Spearman}$) was used to discover whether there is any kind of association between two variables (dependent and explanatory). This is a non-parametric correlation coefficient which is preferred to Pearson's correlation coefficient because it works regardless of the distributions of the variables and is less affected by outliers (Sprent, 1993). The SCC mortar and paste test results were considered as dependent variables and various cement characteristics as explanatory variables. Selected explanatory variables were: loss on ignition; surface area (Blaine); residue in the 45 μm sieve; $(Na_2O)_{equivalent}$ content; SO_3 content; free CaO; C_3S, C_2S and C_3A contents of cement. The results are listed in Tables 6.3, 6.4, 6.5 and 6.6 for CEM I 52,5 R, CEM I 42,5 R, CEM II/A-L 42,5 R and CEM II/B-L 32,5 N, respectively. High absolute values of a correlation coefficient (that is values close to 1) only indicate that variables are associated with each other, not that one variable causes another. There are also negative relations but the important quality of these correlation coefficients is not their sign but



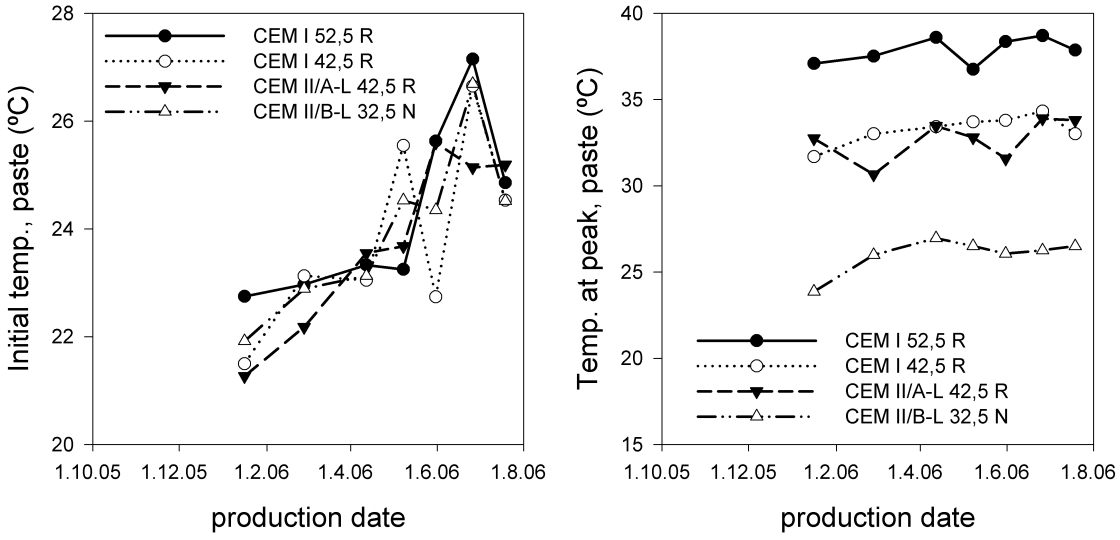
(a) (b)

Figure 6.14.: Variation of standard (a) initial and (b) final setting times, with cement delivery



(a) (b)

Figure 6.15.: Variation of (a) time to acceleration and (b) time at peak SCC-paste results, with cement delivery



(a) (b)

Figure 6.16.: Variation of (a) initial temperature and (b) temperature at peak SCC-paste results, with cement delivery

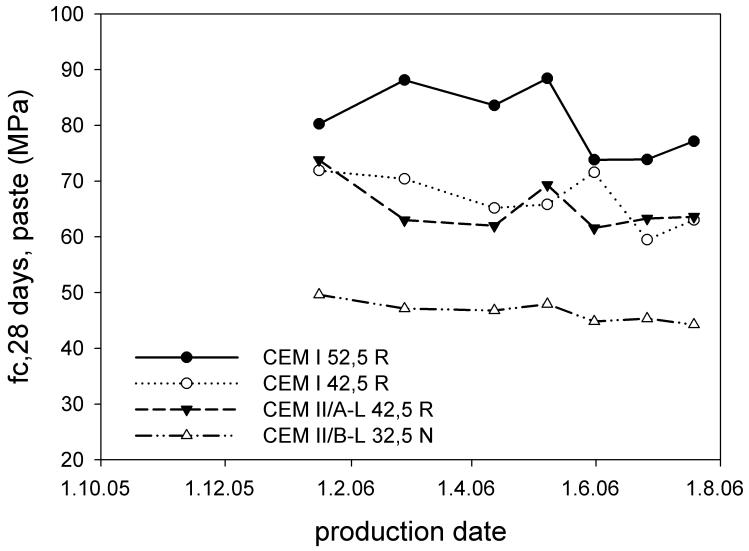


Figure 6.17.: Variation of fc,28 SCC-paste results, with cement delivery

Table 6.3.: Correlation matrix within cement characteristics and between cement characteristics and SCC mortar/paste test results, corresponding to CEM I 52,5 R

	LOI	SA (Blaine)	resid. 45μm	$(Na_2O)_{eq.}$	SO_3	free CaO	C_3S	C_2S	C_3A
LOI	1,000								
SA (Blaine)	-,571	1,000							
resid. 45μm	,084	,180	1,000						
$(Na_2O)_{eq.}$	-,214	,357	,060	1,000					
SO_3	-,690	,524	-,347	,357	1,000				
free CaO	-,301	,590	**,758**	,048	,133	1,000			
C_3S	-,321	,143	,018	-,107	-,429	-,164	1,000		
C_2S	,214	-,214	,072	,000	,286	,109	-,714	1,000	
C_3A	-,143	,071	,000	,143	,179	,436	-,357	-,179	1,000
Dflow[a]	-,310	,132	,220	-,229	-,667	,000	,577	,071	-,649
Tfunnel[a]	,167	-,084	-,268	,169	**,786**	-,205	-,505	-,143	,685
fc,28[a]	,357	,096	-,659	-,060	,095	-,024	-,468	,071	-,342
Dflow[b]	-,036	,345	,449	-,618	-,054	-,523	,355	-,252	-,164
Tflow[b]	,107	,288	-,593	-,360	,214	,109	**-,757**	,393	-,054
fc,28[b]	-,321	,703	-,445	-,108	-,643	,273	-,054	,750	-,667
PD[b]	-,321	,018	-,222	,126	**-,929**	,109	,523	,393	**-,775**
${w_{free}}^b$	-,321	,018	-,222	,126	**-,929**	,109	,523	,393	**-,775**
${\sigma_0}^b$	,071	-,595	-,185	,649	,000	,327	,036	,036	,252
${\eta_{pl}}^b$	,000	-,450	,000	,054	,429	-,218	-,108	-,071	,487
Temp. initial[b]	-,107	**-,847**	,704	,126	,357	-,600	,595	-,714	,505
Time acceler.[b]	-,036	,345	,449	-,618	-,054	-,523	,355	-,252	-,164
Time peak[b]	,107	,288	-,593	-,360	,214	,109	**-,757**	,393	-,054
Temp. peak [b]	-,321	,703	-,445	-,108	-,643	,273	-,054	,750	-,667

Note: correlation values typed **bold** and underlined are significant at the 0,01 level (2-tailed) and correlation values only typed **bold** are significant at the 0,05 level (2-tailed); [a]mortar test results;[b]paste test results

their absolute value.

High correlations between explanatory variables increase the difficulty of associating certain mortar/paste properties to cement properties because it is not clear how much of an effect should be attributed to each mortar/paste property. In this study, significant correlations were found between (free CaO) and (residue 45 μm) for all cement types, except CEM I 42,5 R. In the case of CEM II/A-L 42,5 R mixtures, a significant correlation was also found between (LOI) and (residue 45 μm). A significant correlation was found between (C_3A) and (C_2S) for the case of CEM I 42,5 R.

Considering CEM II/B-L 32,5 N mixture results, which exhibited the largest deviation from target, the SO_3 content of cement was the most relevant effect to explain the observed variations in mortar Tfunnel, paste Tflow, paste PD and w_{free} and max-

Table 6.4.: Correlation matrix within cement characteristics and between cement characteristics and SCC mortar/paste test results, corresponding to CEM I 42,5 R

	LOI	SA (Blaine)	resid. 45μm	$(Na_2O)_{eq.}$	SO_3	free CaO	C_3S	C_2S	C_3A
LOI	1,000								
SA (Blaine)	-,071	1,000							
resid. 45μm	,228	,144	1,000						
$(Na_2O)_{eq.}$	-,071	,190	-,192	1,000					
SO_3	,571	-,167	-,132	,476	1,000				
free CaO	,310	,143	,144	-,452	,071	1,000			
C_3S	-,414	-,288	-,054	,414	-,234	-,450	1,000		
C_2S	,296	,667	,037	-,630	-,482	,334	-,224	1,000	
C_3A	,036	-,429	,286	,571	,464	-,500	,000	**-,815**	1,000
Dflow[a]	,000	,167	,275	-,595	-,690	,143	-,559	,556	-,179
Tfunnel[a]	-,024	,190	-,204	**,762**	,476	-,548	,631	-,296	,250
fc,28[a]	-,214	,310	-,443	,310	,190	,286	,450	,222	-,714
Dflow[b]	,179	,571	,714	-,214	-,643	,071	-,054	,408	,000
Tflow[b]	,500	,000	-,429	,393	,571	-,500	-,288	,037	,250
fc,28[b]	,000	,000	-,464	-,357	-,071	,179	,288	,556	**-,821**
PD[b]	-,036	-,321	,143	-,464	,214	,750	-,468	-,259	,000
w_{free}[b]	-,036	-,321	,143	-,464	,214	,750	-,468	-,259	,000
σ_0[b]	,357	-,536	-,750	,393	**,821**	-,143	-,090	-,259	,107
η_{pl}[b]	,357	-,536	-,750	,393	**,821**	-,143	-,090	-,259	,107
Temp. initial[b]	-,107	-,321	,357	,357	,071	,107	-,018	-,704	,679
Time acceler.[b]	-,357	-,107	-,179	-,250	-,393	,286	,631	,259	-,679
Time peak[b]	-,179	,000	-,321	,107	-,357	-,107	**,775**	,334	-,571
Temp. peak [b]	,143	-,464	,179	-,143	,571	,357	-,577	-,556	,500

Note: correlation values typed **bold** and underlined are significant at the 0,01 level (2-tailed) and correlation values only typed **bold** are significant at the 0,05 level (2-tailed); [a]mortar test results;[b]paste test results

Table 6.5.: Correlation matrix within cement characteristics and between cement characteristics and SCC mortar/paste test results, corresponding to CEM II/A-L 42,5 R

	LOI	SA (Blaine)	resid. 45μm	$(Na_2O)_{eq.}$	SO_3	free CaO	C_3S	C_2S	C_3A
LOI	1,000								
SA (Blaine)	,635	1,000							
resid. 45μm	**-,790**	-,667	1,000						
$(Na_2O)_{eq.}$	-,228	,071	-,238	1,000					
SO_3	,467	,500	-,143	-,619	1,000				
free CaO	-,518	-,467	**,790**	-,395	,204	1,000			
C_3S	-,162	-,071	-,214	,714	-,571	-,739	1,000		
C_2S	,703	,321	-,536	-,071	,214	,036	-,536	1,000	
C_3A	-,200	-,018	,396	-,613	-,108	,145	-,198	-,270	1,000
Dflow[a]	-,407	,190	,214	,071	,310	,084	,250	-,643	-,054
Tfunnel[a]	**,838**	,595	-,667	-,024	,071	-,635	,107	,536	,108
fc,28[a]	,395	,643	-,357	,119	,214	-,419	,107	,107	,180
Dflow[b]	-,505	,179	,429	,107	,179	,252	,286	-,607	,108
Tflow[b]	,721	,750	**-,893**	,393	,107	-,468	-,036	,714	-,216
fc,28[b]	-,306	,393	-,036	,143	-,143	-,180	,250	-,429	,595
PD[b]	-,667	-,643	**,929**	-,393	-,179	,487	,107	-,607	,306
$w_{free}{}^b$	-,667	-,643	**,929**	-,393	-,179	,487	,107	-,607	,306
$\sigma_0{}^b$	,342	-,143	,000	-,643	,214	,234	-,714	,464	,270
$\eta_{pl}{}^b$	,090	,107	,286	**-,786**	,643	,631	**-,893**	,214	,378
Temp. initial[b]	,054	-,214	,321	-,679	,321	**,775**	**-,929**	,571	,126
Time acceler.[b]	-,396	,036	,393	,179	,036	-,072	,607	**-,786**	,036
Time peak[b]	-,144	,071	,536	-,250	,536	,306	,107	-,500	-,072
Temp. peak [b]	-,180	-,214	-,179	-,036	-,393	,018	-,321	,214	,324

Note: correlation values typed **bold** and underlined are significant at the 0,01 level (2-tailed) and correlation values only typed **bold** are significant at the 0,05 level (2-tailed); [a]mortar test results;[b]paste test results

Table 6.6.: Correlation matrix within cement characteristics and between cement characteristics and SCC mortar/paste test results, corresponding to CEM II/B-L 32,5 N

	LOI	SA (Blaine)	resid. 45μm	$(Na_2O)_{eq.}$	SO_3	free CaO	C_3S	C_2S	C_3A
LOI	1,000								
SA (Blaine)	-,571	1,000							
resid. 45μm	,084	,180	1,000						
$(Na_2O)_{eq.}$	-,214	,357	,060	1,000					
SO_3	-,690	,524	-,347	,357	1,000				
free CaO	-,301	,590	**,758**	,048	,133	1,000			
C_3S	-,321	,143	,018	-,107	-,429	-,164	1,000		
C_2S	,214	-,214	,072	,000	,286	,109	-,714	1,000	
C_3A	-,143	,071	,000	,143	,179	,436	-,357	-,179	1,000
Dflow[a]	,357	**-,881**	-,287	-,405	-,524	-,590	,179	-,321	,179
Tfunnel[a]	-,619	,524	-,252	**,738**	**,857**	,012	-,250	,286	-,036
fc,28[a]	-,071	-,190	,611	,405	-,333	,157	,357	-,250	-,071
Dflow[b]	,214	-,714	,180	,071	-,143	,000	-,393	,036	,643
Tflow[b]	-,643	,429	-,649	,071	**,893**	,109	-,429	,107	,571
fc,28[b]	,286	-,500	-,216	,571	-,286	**-,764**	,286	-,429	-,107
PD[b]	,643	-,429	,649	-,071	**-,893**	-,109	,429	-,107	-,571
w_{free}[b]	,643	-,429	,649	-,071	**-,893**	-,109	,429	-,107	-,571
σ_0[b]	,393	,536	,577	-,036	-,536	,600	,250	-,393	,107
η_{pl}[b]	-,571	,750	-,162	-,214	,500	,655	-,143	-,036	,536
Temp. initial[b]	-,107	**,893**	-,072	-,107	,179	,273	,179	-,107	-,321
Time acceler.[b]	,536	-,536	,126	,500	-,286	-,218	-,286	-,179	,500
Time peak[b]	,214	-,714	,180	,071	-,143	,000	-,393	,036	,643
Temp. peak [b]	-,643	,429	-,649	,071	**,893**	,109	-,429	,107	,571

Note: correlation values typed **bold** and underlined are significant at the 0,01 level (2-tailed) and correlation values only typed **bold** are significant at the 0,05 level (2-tailed); [a]mortar test results;[b]paste test results

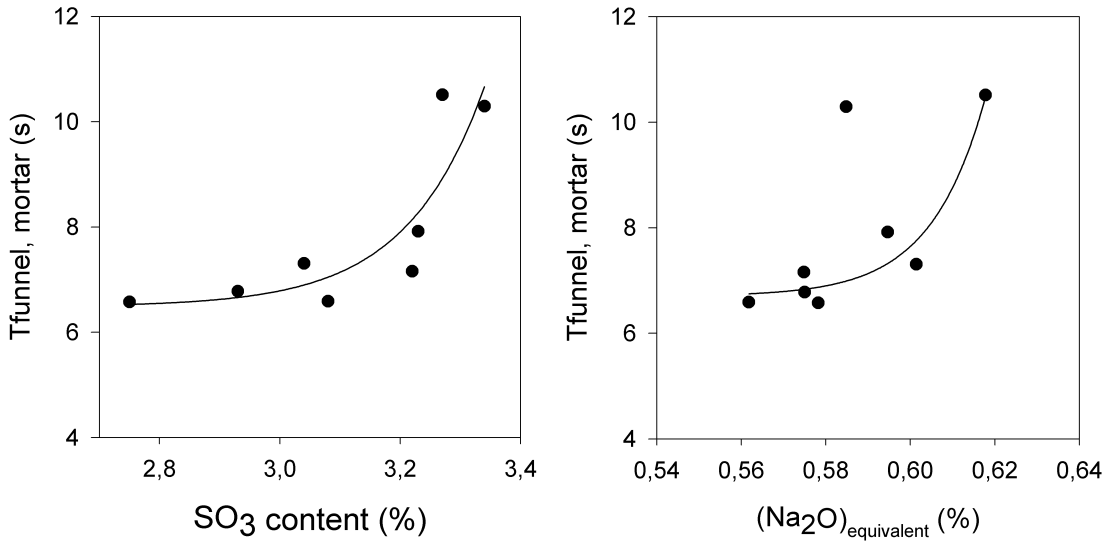
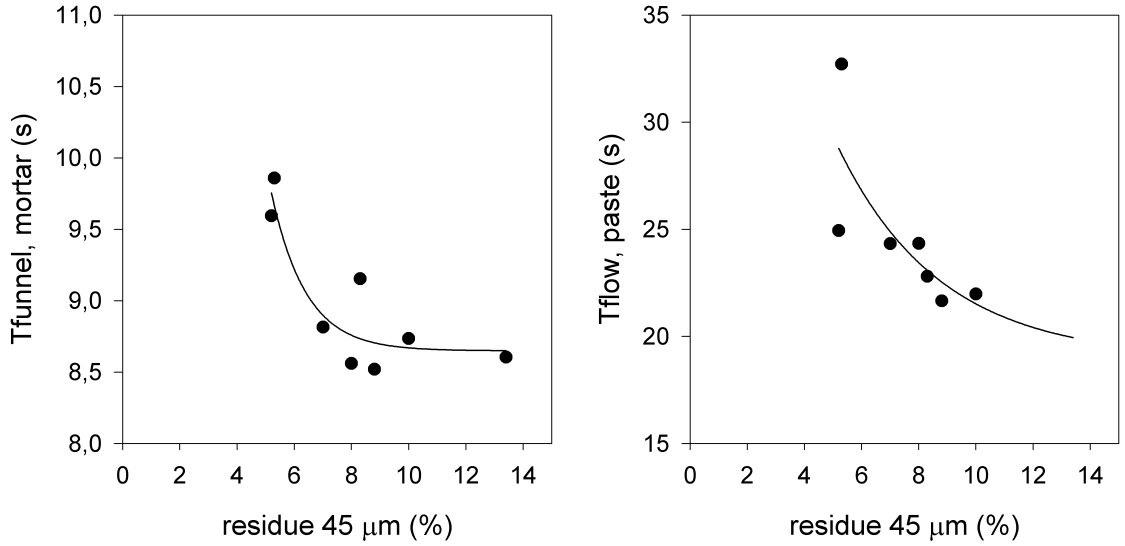


Figure 6.18.: Effects of (a) SO_3 and (b) $(Na_2O)_{equivalent}$ on Tfunnel of mortars incorporating CEM II/B-L 32,5 N

imum temperature of paste (see Table 6.6). A significant correlation was also found between mortar Tfunnel and $(Na_2O)_{equivalent}$ content of cement. The effect of surface area (Blaine) was significant to explain the variations of mortar Dflow and the temperature of paste in the beginning of the semi-adiabatic calorimeter test (see Table 6.6). Based on the experience of the cement producer, the specific surface area obtained by the Blaine method is not a good indicator of Type II cement fineness. In this case, the 50% percentile (D0,5) of the particle size distribution is a better indicator of cement fineness, but no significant correlation was found between (D0,5) and (Dflow, mortar) nor between (D0,5) and (Temp initial), for CEM II/B-L 32,5 N results ($\rho_{Spearman}$=0,048, $\rho_{Spearman}$=-0,286, respectively). Thus, only the effects of SO_3 and $(Na_2O)_{equivalent}$ contents were considered the most relevant for the observed variations, in the fresh state (see Figure 6.18). It can be observed that mortar Tfunnel increased with an increase of SO_3 and $(Na_2O)_{equivalent}$ contents in cement.

By analysing the correlation matrixes corresponding to CEM I 52,5 R and CEM I 42,5 R, the effects of SO_3 and/or $(Na_2O)_{equivalent}$ always appeared strongly associated to more than one fresh state SCC mortar/paste property (see Tables 6.3 and 6.4). In the case of CEM II/A-L 42,5 R, the effect of (residue 45 μm) seems to be the most significant to explain fresh state variations (see Table 6.5). Note that the LOI effect (associated to mortar Tfunnel) is also associated to (residue 45 μm) (see Table 6.5). As can be observed in Figure 6.19, an increase of residue in 45 μm sieve (an increase of coarser cement particles) increases fluidity of SCC mortar/paste.

Based on the literature review, the influences of SO_3 and/or $(Na_2O)_{equivalent}$ and of



(a) (b)

Figure 6.19.: Effect of residue 45 μm on (a) mortar Tfunnel and (b) paste Tflow of mixtures incorporating CEM II/A-L 42,5 R

the residue in 45 μm sieve could be expected (see section 6.2.4). An increase of SO_3 and/or $(Na_2O)_{equivalent}$ contents of cement can be associated to an increase of readily soluble sulfates in cement which reduce the dispersing action of PC type superplasticizer, lowering the amount of free water and, consequently, reducing fluidity (indicated by higher flow time results of mortar and paste). On the other hand, a reduction of residue in 45 μm sieve can be associated to a larger surface area of particles, thus a larger consumption of superplasticizer for the same dosage and, consequently, a lower dispersion effect and a reduction of fluidity.

6.4. SCC paste rheology

Rheology of cement paste largely dictates concrete rheology, given a specified aggregates skeleton (Ferraris et al., 2001b; Martys and Ferraris, 2002). The key role of the paste is clearly shown by the strong effect on concrete workability of the powder materials, water/powder ratio and of superplasticizer dosage. Furthermore, important phenomena in fresh concrete, like air entrapment and aggregates segregation are determined from paste rheology (along with the stabilising effect of smaller aggregate particles), which provides more or less freedom of motion to aggregates and air bubbles. In spite of importance of paste rheology, there is no generally accepted procedure for its study, and so direct comparison between different works and the definition of rheology-based acceptance criteria for SCC paste is often difficult.

Ultimately, it would be desirable to predict concrete behaviour from the paste characteristics. Tests on paste are easier to carry out and require less material. Although rheological tests require more expensive equipment and specific training, they allow a more fundamental and precise characterization of cement suspensions (see Chapter 2).

Since there is some consensus concerning target mortar properties for SCC (EFNARC, 2002; Okamura et al., 2000), in this study, mortar mixtures and corresponding paste mixtures were characterized in parallel, so that target SCC paste properties could be found. Furthermore, pastes were characterized by means of empirical and rheological (using a rheometer) tests. Thus, a relation between empirical test results and rheological tests could be defined, on the paste level. These relations may be of interest for industrial labs to transform empirical data, in arbitrary units, into relevant rheological parameters. Rheological parameters are intrinsic properties of the material while empirical test results are test geometry and material density dependant.

6.4.1. Experimental programme

The present experimental programme is an extension of the experimental programme described in section 6.3; optimized mortar mixtures with sand contents different from 0,5 and the corresponding paste mixtures were included in the study, in order to obtain a larger range of paste properties. The materials used were the same, and all cement deliveries were tested. The mix proportions of additional mortar and paste mixtures for each cement type were established based on the mixture parameter values presented in Table 6.7 and the respective paste test results are summarized in Tables E.11 to E.14 of Appendix E. Mixing and testing sequences were maintained (see section 6.3.2).

6.4.2. Rheology vs. empirical test results

In Figure 6.20 flow time results of pastes in the Marsh cone are plotted against the measured viscosity at 50 s^{-1} of shear rate, from the down-curve, measured at 35 minutes after the beginning of mixing. The corresponding Spearman's correlation coefficient was 0,902 (significant at the 0,01 level (two-tailed)) indicating that results of both tests are clearly related. However one notices that the scatter of both flow time and viscosity increased at increasing flow time. This was also found by other authors (Gomes, 2002; Grünewald and Walraven, 2005; Le Roy and Roussel, 2005). The correlation coefficient between flow time and viscosity decreased for lower shear rates. For example, the correlation coefficient between flow time and the viscosities measured at 12,6 $s^{-1}$and 1,6 s^{-1} was 0,858 and 0,853, respectively. At higher shear rates, the particles are 'fully' dispersed thus the results are less affected by time effects and shear history, which

Table 6.7.: Optimized mixture parameters and mix-proportions

	CEM I 52,5R		CEM I 42,5R		CEM II/A-L 42,5R		CEM II/B-L 32,5N	
Mixture parameters								
w/c	0,43	0,41	0,38	0,36	0,37	0,33	0,4	0,35
Sp/p	1,99%	2,05%	1,86%	1,89%	1,83%	1,89%	1,49%	1,41%
V_w/V_p	0,716	0,700	0,710	0,704	0,713	0,705	0,714	0,714
V_s/V_m	0,49	0,47	0,45	0,43	0,45	0,40	0,45	0,4
Mix proportions of mortar (kg/m^3)								
cement	494,8	532,5	601,1	654,3	618,5	751,9	572,7	714,1
limestone filler	373,0	379,3	346,4	335,0	323,1	288,8	349,3	300,3
water	207,3	211,3	221,9	227,8	222,7	239,1	225,8	245,3
superpl. (V3000)	17,2	18,7	17,6	18,7	17,2	19,6	13,8	14,3
standardized sand	1260	1209	1157	1106	1157	1029	1157	1029
Mix proportions of paste (kg/m^3)								
cement	970,1	1004,6	1092,9	1147,9	1124,6	1253,2	1041,3	1190,2
limestone filler	731,4	715,6	629,9	587,6	587,4	481,3	635,0	500,5
water	389,6	383,2	389,2	386,5	390,6	386,9	396,1	397,1
superpl. (V3000)	33,8	35,2	32,0	32,8	31,3	32,7	25,0	23,8

might explain the lower dispersion of results and the higher correlation coefficients. A similar relation was also found between flow time and plastic viscosity (Bingham model) ($\rho_{Spearman}$=0,894). The viscosity is almost equal to the plastic viscosity at high shear rates. However, at lower shear rates the viscosity is much higher than the plastic viscosity.

According to Roussel and Le Roy (2005) flow time is proportional to viscosity, but yield stress has to be taken into account to predict flow time of non-Newtonian fluids, like the case of cement pastes. The presence of yield stress increases the time needed for a certain amount to flow out of the cone (Roussel and Le Roy, 2005). The following relation between flow time and rheological parameters of paste was derived by (Roussel and Le Roy, 2005) and is given by

$$Tflow = \frac{a_v \mu_{pl}}{\rho - b_v \sigma_0} \tag{6.3}$$

where a_v and b_v are constants, depending on cone geometry and the observed flowing volume V, ρ is the material density, and η_{pl} and σ_0 are the plastic viscosity and yield stress, respectively. The constants a_v and b_v can either be calibrated using known materials or calculated using the following expressions

$$a_v = \frac{8V\tan(\alpha)\left[3h\left(H_0\tan(\alpha)+r\right)^3 + H_0 r\left(H_0^2\tan^2(\alpha)+3H_0 r\tan(\alpha)+3r^2\right)\right]}{\left[3\pi r^3\tan(\alpha)gr(h+H_0)\right]\left(H_0 tan(\alpha)+r\right)^3} \tag{6.4}$$

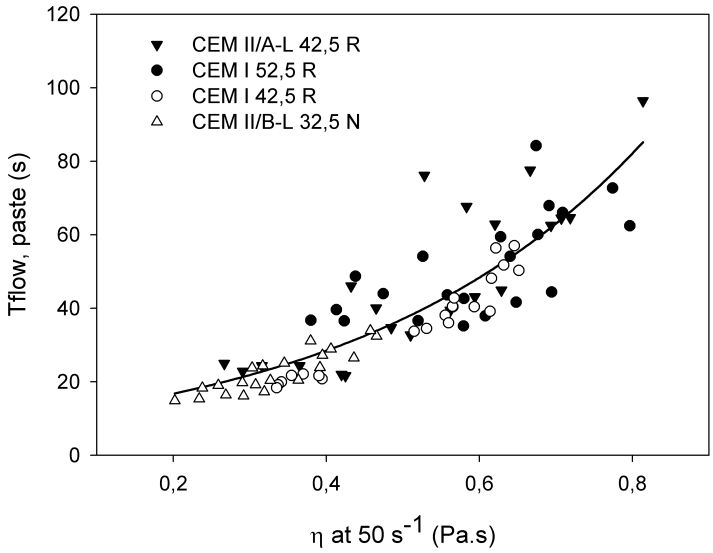


Figure 6.20.: Relation between the viscosity at a shear rate of 50 $s^{-1}$and flow time of pastes ($\rho_{Spearman}$=0,902)

$$b_v = \frac{\pi r^3 \left[8r \ln(H_0 \tan(\alpha) + r) - 8r \ln(r) + 8h \tan(\alpha)\right]}{3\pi r^3 \tan(\alpha) g r (h + H_0)} \tag{6.5}$$

where α, r, H_0 and h can be obtained from cone geometry and filling volume V, as indicated in Figure 6.21, and g is the gravitational constant (Roussel and Le Roy, 2005). a_v and b_v are very sensitive to r and h, which sometimes are difficult to measure, therefore estimation of these constants is sometimes preferred (Roussel and Le Roy, 2005). A comparison between measured flow time and predicted flow time using equation 6.3 is given in Figure 6.22, with a_v =154503 s^2/m^2 and b_v=25,5 s^2/m^2. From this figure it can be observed that up to a flow time approximately 50 s the model given by equation 6.3 adequately predicts the measured flow times. For flow times above 50 s data points start to deviate from the $y = x$ line. This may be due to differences in how yield stress is determined.

Several authors reported a relation between yield stress and slump, as well as, spread flow (of concrete, mortars or paste) (Flatt et al., 2006; Roussel and Coussot, 2005; Saak et al., 2004; Roussel et al., 2005). However, different relations can be found in the literature. A comparison between two models relating yield stress with spread radius and its range of validity is presented in (Flatt et al., 2006). Flatt et al. (2006) clarified that Saak's model (first developed by Murata) (Saak et al., 2004) and given by

$$\sigma_0 = \frac{\rho V g}{\sqrt{3}\pi R^2} \tag{6.6}$$

where ρ and V is the density and volume of the sample (assuming that the cone is

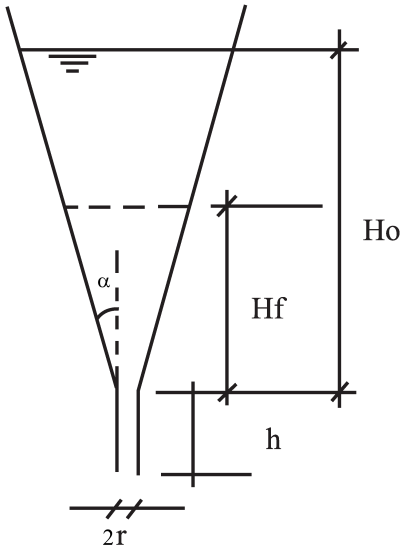


Figure 6.21.: α, r, H_0 and h dependant on cone geometry and filling volume (Roussel and Le Roy, 2005)

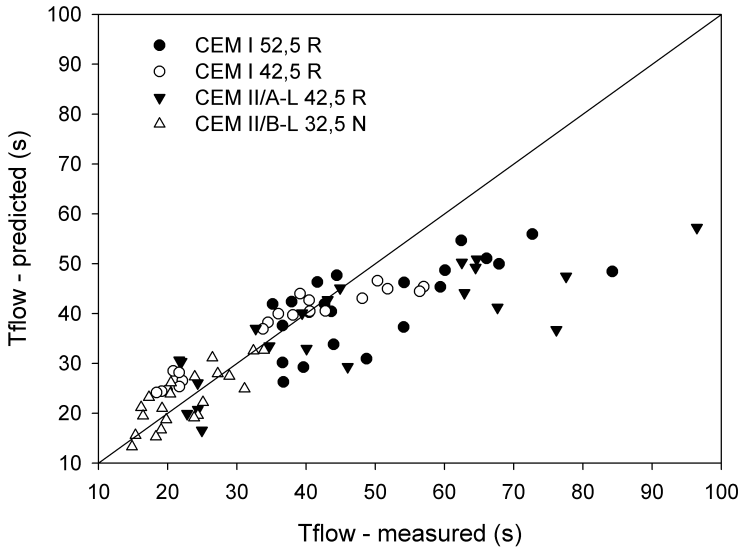


Figure 6.22.: Comparison between measured and predicted flow time

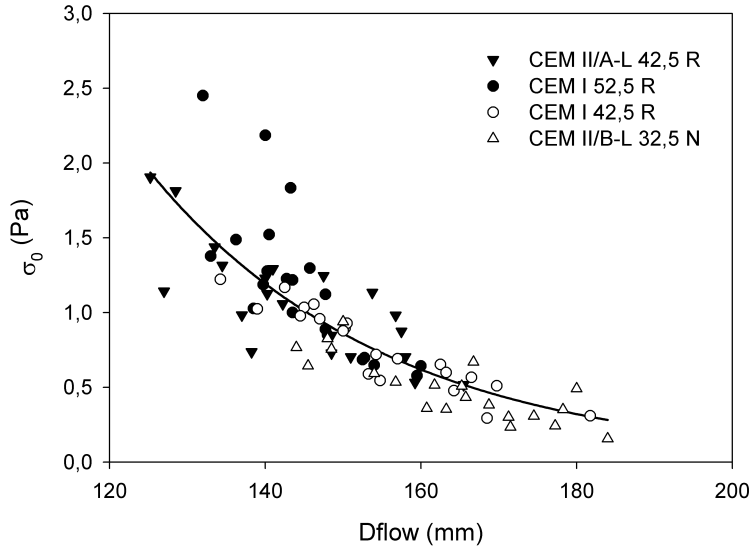


Figure 6.23.: Relation between the yield stress and flow diameter of pastes ($\rho_{Spearman}$= 0,902)

completely filled up), respectively, and R is the radius of the spread, performes well at low spread radius and not at large spread radius. In contrast, Roussel's model given by

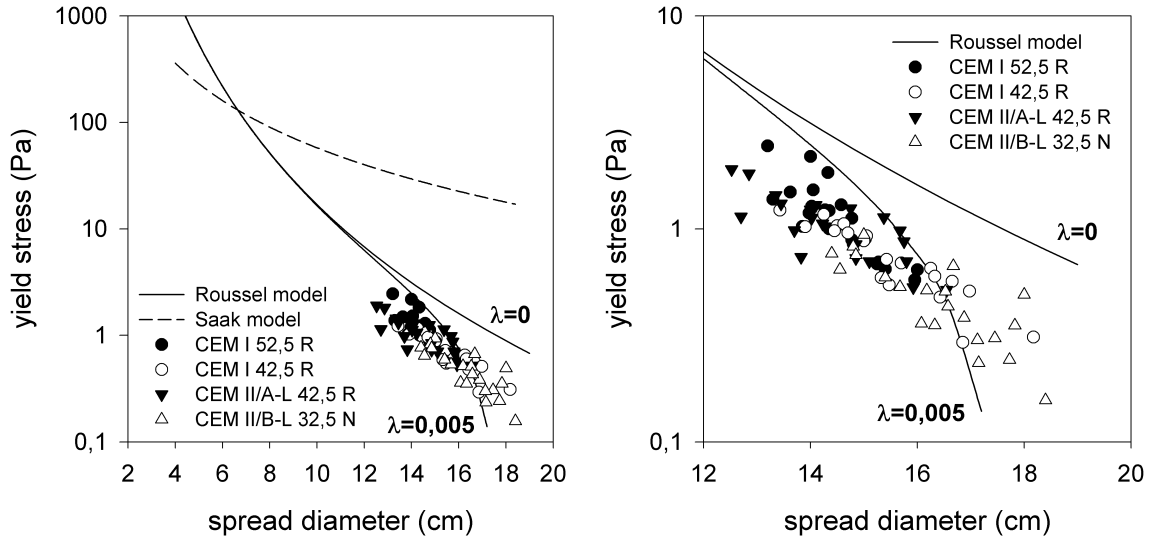
$$\sigma_0 = 1,747\rho V^2 R^{-5} - \lambda\frac{R^2}{V} \tag{6.7}$$

where ρ and V is the density and volume of the sample, respectively; R is the radius of the spread and λ is a constant (Roussel et al., 2005), was found to be more reliable for large spreads (Flatt et al., 2006). λ is a function of both unknown tested fluid surface tension and contact angle. A value of 0,005 was adopted by Roussel et al. (2005). In addition, an exponential function of the type of

$$\sigma_0 = a\exp(-bR) \tag{6.8}$$

where a and b are fitting parameters, was found to approximately fit experimental data over a wide range of diameters of interest (Flatt et al., 2006). The data collected in the present work supports this conclusion, as illustrated in Figure 6.23. In this figure mini-slump flow diameter results of pastes are plotted against the yield stress (Bingham model), for measurements carried out at 35 minutes after begining of the mixing. The corresponding Spearman's correlation coefficient was 0,902 (significant at the 0,01 level (two-tailed)).

The predictions of both Saak and Roussel models (with λ equal to 0 and 0,005) models according to equations 6.6 and 6.7 are given in Figure 6.24, for the range of spread diameters that can be obtained with Kantro's mini-slump cone. As can be observed in this



(a) (b)

Figure 6.24.: Relation between yield stress and spread diameter calculated with Saak's model and Roussel's model (with both λ=0 and 0,005) for the mini-slump cone (Kantro) and experimental data collected in the present study

figure the yield stress data collected in the present work is closer to the curve described by Roussel's model with surface tension effects included (λ=0,005). Nevertheless, this model failed to explain the relation between the spread diameter and yield stress results obtained in the current study. The divergence of data from Roussel's model can also be attributed to differences in how yield stress is determined.

6.4.3. Comparison of paste and mortar characteristics

The complete experimental programme included mortar mixtures with V_s/V_m ranging from 40 to 50%, w/c ratio ranging from 0,33 to 0,45, Sp/p ranging from 1,4% to 2%, and four different cement types. Mortar mix proportions were adjusted to attain similar fresh properties (Dflow= 260 mm and Tfunnel=10 s), for each cement type (see Table 6.2 and Table 6.7). In addition, changes in mortar/paste properties were introduced due to variations in cement, from different deliveries. Altogether, this resulted in a large range of paste properties, which correspond to 'good' or 'near-good' SCC mortars, as can be observed in Figure 6.25. The paste properties which led to mortar mixtures with Dflow=260±10 mm and Tfunnel=10±2 s, considered here as 'good' SCC mortars, are identified with a red dot in Figure 6.25. These are spread over the entire area except in the lower part on the right, for Dflow values higher than about 170 mm. Thus, one can conclude that there is a target area of paste properties which can lead to 'good' SCC mortars (exhibiting Dflow=260±10 mm and Tfunnel=10±2 s, simultaneously).

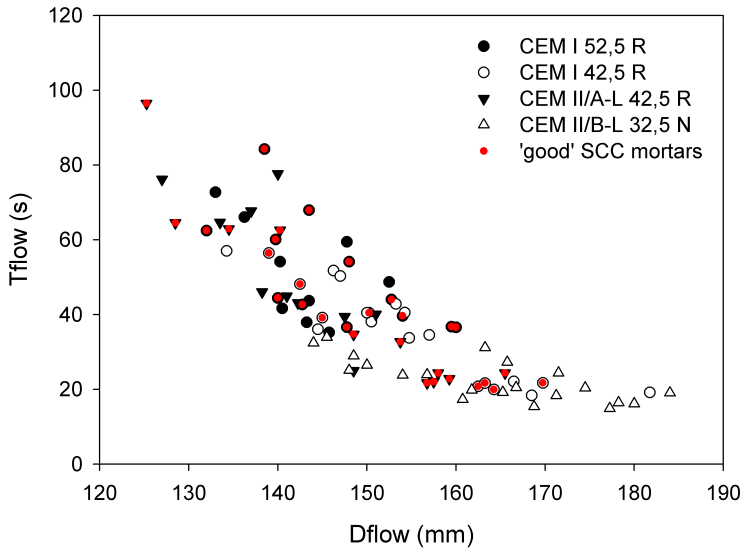


Figure 6.25.: Range of properties of the analysed pastes incorporating different cement types

In Figure 6.26 data points are distinguished in terms of fine aggregate content (V_s/V_m) instead of cement type. From this figure it can be clearly seen that target paste properties are related with aggregate content. Mortars with higher fine aggregate content (V_s/V_m) require more fluid pastes to be flowable, while mortars with lower fine aggregate content require more viscous pastes to be stable. This is in agreement with the estimated responses of pastes corresponding to optimized mortar mixtures, with varying aggregate content, shown in Figure 6.27. These mortar mixtures incorporated CEM I 52,5 R, limestone filler, superplasticizer V3005 and reference sand (see Chapter 5, paragraph 5.10.6). A central composite design was also carried out to mathematically model the influence of the three mixture parameters (w/c, V_w/V_p and Sp/p) and their coupled effects on Dflow and Tflow responses of paste mixtures.

Based on the target area defined in Figure 6.26 and on the mini-slump flow and Marsh flow tests the mixtures can be optimized first on the paste level to minimize the number of tests on the mortar/concrete levels. However, the variability of the flow time results and loss of fluidity with time increases with increasing paste viscosity, which is a major disadvantage of the Marsh flow test. This was also found by Gomes (2002) and Le Roy and Roussel (2005). In this study, a strong relation was found between flow time (Marsh cone) and free water (centrifuge test) results (see Figure 6.28) ($\rho_{Spearman}$=0,986; significant at the 0,01 level (two-tailed)). Therefore, the centrifuge test is a promising substitute test of the Marsh cone with the advantage of being equally precise for lower and higher fluidity pastes. The target area for the (Dflow, w_{free}) paste results is presented in Figure 6.29.

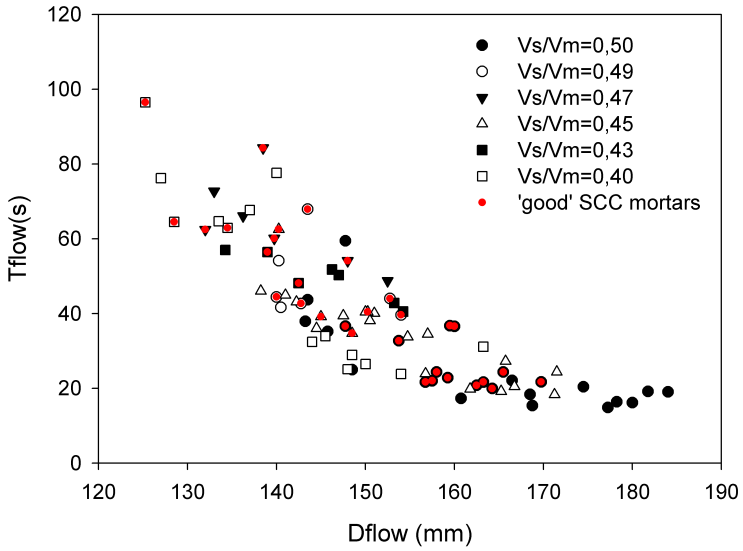


Figure 6.26.: Range of properties of the analysed pastes, corresponding to different V_s/V_m

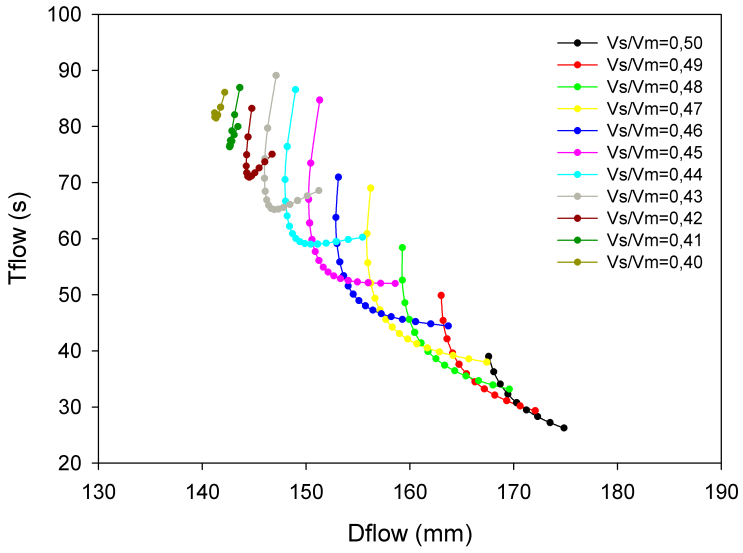


Figure 6.27.: Estimated responses of pastes corresponding to optimized mortar mixtures (CEM I 52,5 R+limestone filler+V3005)

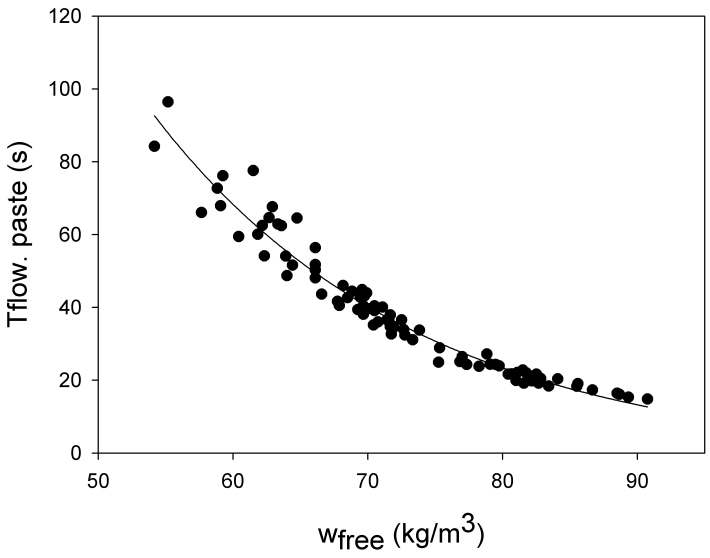


Figure 6.28.: Relation between wfree and Tflow of SCC pastes ($\rho_{Spearman}$=0,986)

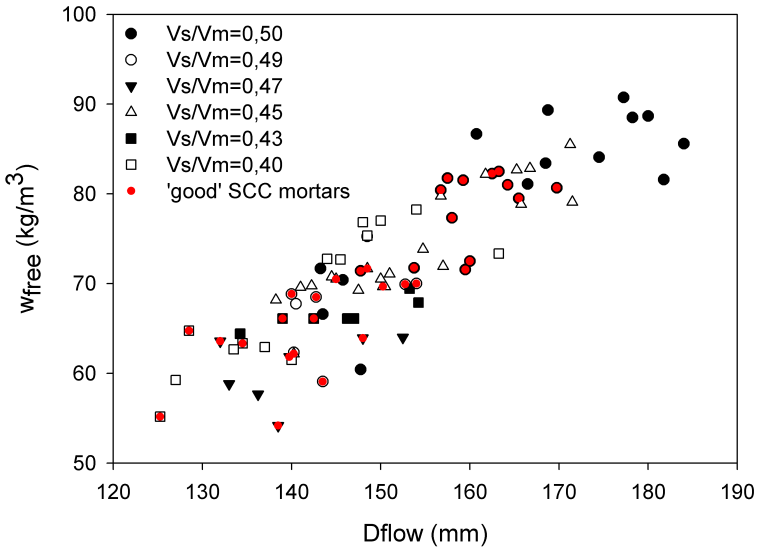


Figure 6.29.: Range of properties of the analysed pastes

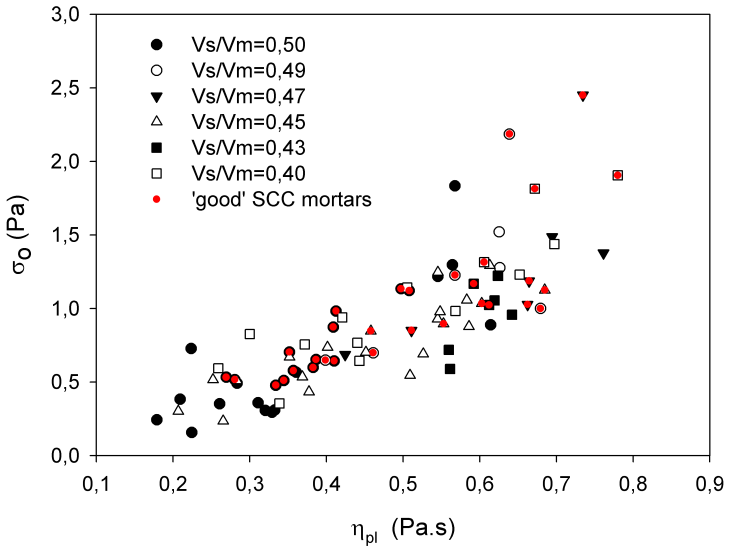


Figure 6.30.: Range of rheological parameters of the analysed pastes

In Figure 6.30 the range of rheological parameters values (Bingham model) obtained in this study are presented along with the identification of those which led to 'good' SCC mortars. 'Good' SCC mortars were found for pastes with a plastic viscosity ranging from about 0,3 to 0,8 Pa.s and a yield stress ranging from 0,5 to 2,5 Pa. It should be mentioned that the target areas defined in Figures 6.26, 6.29 and 6.30 will probably change if a different superplasticizer or a viscosity agent (admixture or a very fine material) is used (Grünewald and Walraven, 2005; Saak, 2000).

6.4.4. Comparison of paste and concrete characteristics

In order to understand the influence of paste characteristics in the final SCC mix-proportions, two different pastes, incorporating CEM II/A-L 42,5 R, were selected from Figure 6.26 for the studies carried out at the concrete level. The paste mix-proportions are given in Table 6.8 along with the respective test results. These mix-proportions were maintained at the concrete level and only the mixture parameters related with the aggregate skeleton were changed to adjust the mixtures, namely, V_s/V_m, $V_g/V_{g,lim}$ and s_1/s. A central composite design was carried out to mathematically model the influence of the three mixture parameters (V_s/V_m, $V_g/V_{g,lim}$ and s_1/s) and their coupled effects on Dflow, Tfunnel and H2/H1 responses of concrete mixtures. In Figures 6.31 and 6.32 the mix-proportions range to obtain an SCC of classes SF2, VF2 and PL2 are given for mixtures incorporating Paste A and B, respectively, while maintaining s_1/s=0,50. From these figures it can be clearly seen that the most fluid paste (A) led to mixtures with higher content of fine aggregate and lower coarse aggregate content (higher total surface area of aggregates); while the less fluid paste allowed incorporating higher content of

Table 6.8.: Pastes selected for the study at the concrete level

		Paste A	Paste B
Mix-proportions	w/c	0,45	0,37
	Sp/p	1,58%	1,83%
	V_w/V_p	0,719	0,713
Paste test results	Dflow (mm)	165,5	151,0
	Tflow (s)	24,4	40,0
	wfree (kg/m^3)	79,5	71,1
	η_{pl}(Pa.s)	0,28	0,45
	σ_0 (Pa)	0,52	0,70

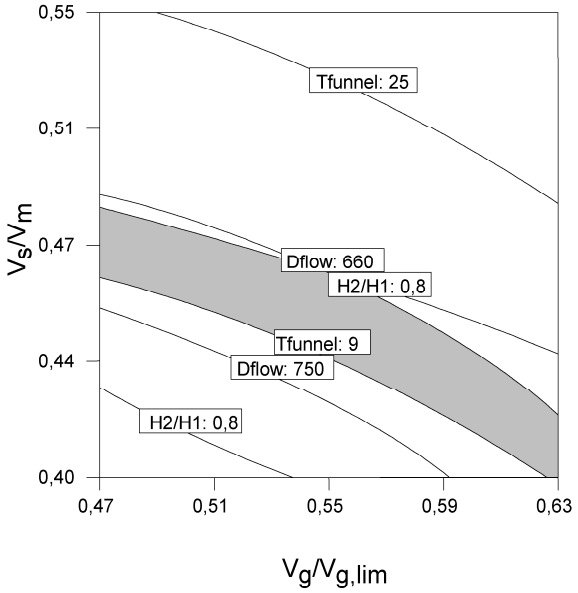


Figure 6.31.: Range of mix-proportions to obtain an SCC (of classes SF2, VF2 and PL2), incorporating Paste A and maintaining s_1/s=0,50

coarse aggregate together with lower fine aggregate content (lower total surface area of aggregates). It should be mentioned that in this study very favourable aggregates were used, namely, two natural rounded sands and limestone coarse aggregate (maximum size of 16 mm). The target areas presented in Figures 6.31 and 6.32 will probably change by changing aggregates type.

These conclusions are in agreement with the concept of "Concrete Equivalent Mortar" (CEM) introduced by Schwartzentruber and Catherine (2000). In this method, CEM mix proportions are calculated from the corresponding concrete mixture maintaining sand (particles smaller than 5 mm), cement, addition and superplasticizer types; water to cement ratio; superplasticizer to cement ratio; addition to cement ratio and surface of aggregates to cement ratio (using extra sand to replace particles of coarse aggregate larger than 5 mm) (Schwartzentruber and Catherine, 2000). A correlation was found

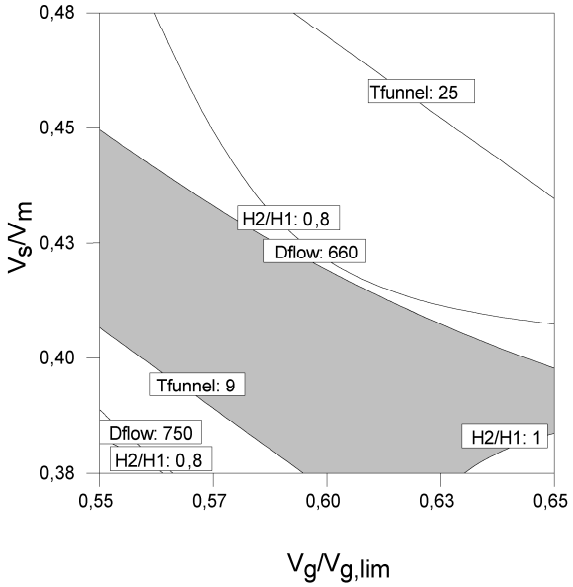


Figure 6.32.: Range of mix-proportions to obtain an SCC (of classes SF2, VF2 and PL2), incorporating Paste B and maintaining s_1/s=0,50

between workability of CEM and corresponding concrete, depending on aggregates used (Schwartzentruber and Catherine, 2000; Nachbaur et al., 2005). Therefore, fine aggregate content of CEM increases with surface area of aggregates in the concrete mixture. To obtain concrete from mortars studied in Chapter 5, instead of replacing part of the fine aggregate by coarse aggregate (as is the case of the CEM method) all fine aggregate (standard sand) must be replaced by current aggregates. In spite of that difference, one can conclude that optimized mortars with higher sand content correspond to concrete mixtures with higher total surface area of aggregates, i.e. richer in fine aggregate particles, and lower paste contents.

To sum up, content and distribution of aggregates (affecting the specific surface area) and paste characteristics must be known to predict behaviour of SCC mortars/concrete in the fresh state.

6.5. Final remarks

In the present study, different cement samples from the same production line were analysed. The only parameter changing was production date. It was shown that large deviations from target workability properties can occur depending only on cement delivery, as occurred for CEM II/B-L 32,5 N. Thus, cement variations and cement-superplasticizer interaction should be taken into account when discussing robustness of SCC mixtures. It is important to mention that the observed variations could have been different in the presence of another superplasticizer type.

This study highlighted the importance of an efficient quality control system to detect large deviations from target and hence implement corrective actions in order to maintain results in conformity with performance requirements. However, standard tests on cement like setting time and water demand are not adequate because they do not incorporate admixtures and do not give any indication about cement-superplasticizer interaction. It was demonstrated that analysing cement mortars with equivalent composition to the concrete mixture is effective for detecting workability variations and cement-superplasticizer compatibility problems. Effects of aggregate on test results are minimised by using standardised sand. Besides, mortar tests are simple, easy to carry out and require smaller amounts of material than concrete tests.

Based on obtained results, the mortar and paste flow tests and the centrifuge test are the most sensitive tests to detect the causes behind workability variations of SCC mixtures. The problem with cone flow tests is that they are not suitable for assessing pastes with low fluidity. Thus, the centrifuge test is a promising substitute test of the Marsh cone test with the advantage of being equally precise for lower and higher fluidity pastes.

Many factors influence fluidity and the hydration process of cement paste. Some of these factors may also have synergistic effects. This makes it difficult to point out one particular parameter, which is responsible for producing a certain property. A more 'robust' measure of association between two variables, the Spearman's correlation coefficient, was recommended here instead of a classical correlation coefficient. Moreover, the quality information presently available from the cement supplier is not detailed enough. Physical and chemical parameters from cement characterization are necessary for explaining the variation of early age properties of SCC mixtures. In this study, the SO_3 and/or $(Na_2O)_{equivalent}$ contents of cement and the residue in the 45 μm sieve were found to be associated to fluidity changes of SCC mortar/paste mixtures.

As expected, it was found that empirical test results correlate with the rheological parameters of pastes, namely, yield stress and plastic viscosity. Furthermore, the existing models for predicting the mini-slump flow diameter and the flow time of pastes were implemented and compared with experimental data. A reasonable approximation was found between measured and predicted values, but a better approximation could be expected if the same protocol to determine yield stress (mixing sequence, test equipment, tool geometry, testing sequence) had been followed.

The target paste properties, for different fine aggregate content, were defined in terms of both empirical test results and rheological parameters, linking mortar and paste properties that are adequate for SCC. The influence of paste characteristics on the final SCC mix proportions was discussed based on two experimental studies, carried out at concrete level, and on the "Concrete Equivalent Mortar" approach. It was concluded that optimized mortar mixtures with higher sand content (see Chapter 5) will lead to

SCC mixtures with higher total surface area of aggregates, i.e. richer in fine aggregate particles, and lower paste contents.

7. Evaluation of SCC mixtures robustness

7.1. Introduction

This chapter presents a methodology to assess robustness of SCC mixtures. This methodology (LABEST/FEUP methodology) was developed in three phases: first, the experimental phase conducted according to a central composite design; second, the statistical analysis and model fitting of data collected during the experimental phase and, third, the derived numerical models are used to compute a measure of the target SCC mix robustness based on simulations of mixture parameters. The proposed measure represents the probability that a SCC mix verifies the fulfillment of the acceptance criteria.

The LABEST/FEUP methodology was first developed under the scope of the research project BACPOR, during the full-scale tests phase of SCC production in Maprel precast factory, in Rio Maior, Portugal. Later, within the scope of the research project POCI/ECM/61649/2004 the LABEST/FEUP methodology was applied and compared with the results given by the methodology suggested in "The European Guidelines for Self-compacting Concrete" in order to validate it and to verify if it is possible to enhance robustness of SCC mixtures by only changing proportions of materials in the mixture.

7.2. Robustness definition

According to Aïtcin et al. (2001) an industrial process is robust if it allows for a large variation of variable(s) V while maintaining the property(ies) P inside the acceptance interval(s) (see Figure 7.1). Thus, from Figure 7.1, it can be said that Process A is more robust than Process B. To attain the same level of robustness with both processes, it would be necessary to reduce the range of the interval ΔV, in Process B, and this would only be accomplished by increasing the control on raw materials and/or through the modernization of existing equipments. In general, these improvements are difficult

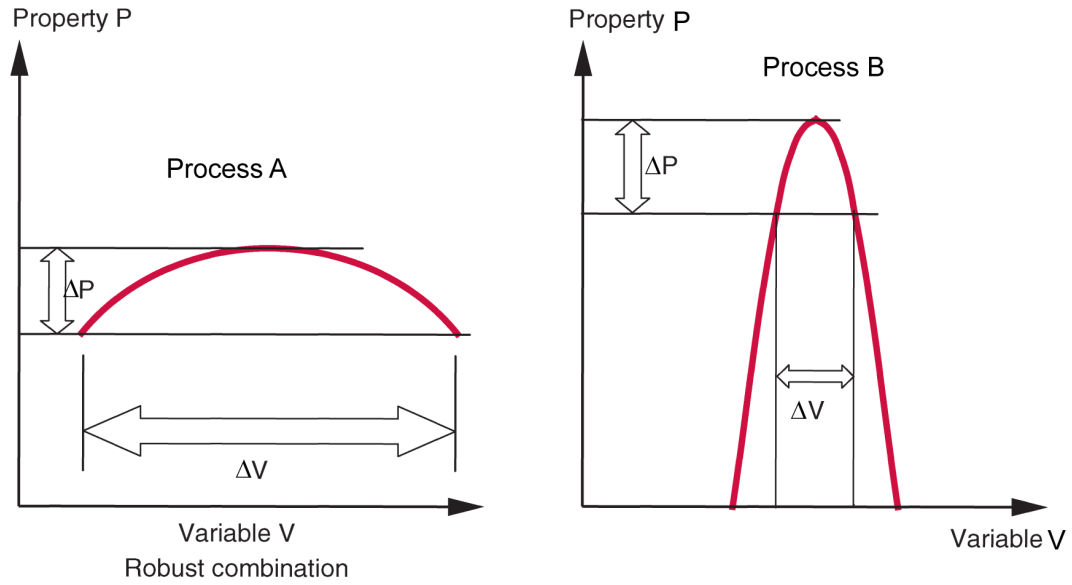


Figure 7.1.: Robustness of an industrial process (Aïtcin et al., 2001)

to implement and very expensive so industry systematically tends towards those combinations whose level of robustness is high enough to offset the relative lack of quality control (Aïtcin et al., 2001).

A critical factor in the SCC production process is its sensitivity to small batch-to-batch changes in one or more of the constituents, which may lead to variability of performance (BIBM et al., 2005; Bonen et al., 2007; Rigueira et al., 2006, 2007; Concrete Society, 2005). Thus, the concept of concrete "robustness" was introduced, which corresponds to the tolerance of SCC production, to the daily fluctuations of materials (BIBM et al., 2005). In "The European Guidelines for Self Compacting Concrete" (BIBM et al., 2005) the robustness of SCC is defined as the capacity of concrete to retain its fresh properties when small variations in the properties or quantities of the constituent materials occur.

It should be noted that the European definition of robustness (BIBM et al., 2005) differs from the one suggested by the American researchers (Bonen et al., 2007). According to the ACBM research team (Bonen et al., 2007), robustness is regarded as the ability of a given mixture to maintain both the fresh properties and uniformity pre- and post-casting of one batch or successive batches. This is a broader definition since it includes the ability of SCC to resist to changes in materials properties and mix proportions, due to batching inaccuracies, but also the ability to resist to changes during transport and placement (dynamic stability) and post placement (static stability). According to Bonen et al. (2007) robustness is a time dependent quality and it should be regarded according to the application.

The author's opinion is that, to make it clearer, the concepts of robustness (related to properties after mixing), dynamic stability (related to properties during transport and

casting) and static stability (related to properties from the end of casting to setting time) should be discussed separately. In the present work, the European definition was adopted and generalized as the capacity of concrete to retain its performance requirements, which is of interest for a specific application (fresh and hardened properties), when small variations in the properties or quantities of the constituent materials occur. Thus, the major concern in this study was the need to reduce intervention at the plant or job site to adjust the mixtures in successive batches.

7.3. Factors affecting properties during production

During production, there may be a number of factors that individually or collectively contribute to disturb the balance between SCC fresh state properties, namely, deformability, passing ability and resistance to segregation. Variations in the SCC properties can be attributed to variability of the constituent materials (Bonen et al., 2007), inaccuracy in the weighing of materials (Bonen et al., 2007) and changes in the mixing energy (Emborg, 2000; Takada, 2004). Changes in the environment conditions, like temperature and humidity were also found to affect the rheological properties of concrete (Sakai et al., 2003). After mixing, during the transport and casting processes rheological properties of SCC may also suffer significant changes due to time and temperature effects, shear history effect and thixotropy (Bonen et al., 2007; Roussel, 2007) but, as mentioned before, transport and casting stages are not covered by the definition of robustness adopted here.

7.3.1. Variability of constituent materials

As discussed in paragraph 4.4.2, SCC can be seen as a suspension of aggregates in paste and the required paste volume depends on the relative proportions of aggregates in the mixture, particle size distribution of each aggregate type, shape of aggregates, angularity and texture (de Larrard, 1999; Koehler and Fowler, 2007). Thus, a change in any of these aggregate characteristics may result in a deviation from the target volume of paste, by unit volume of concrete. The influence of fine aggregates on fresh properties of the SCC is significantly greater than that of coarse aggregate (BIBM et al., 2005), in particular the finer fractions (less than 0,125 mm and 0,09 mm, according to BIBM et al. (2005) and Okamura et al. (2000), respectively) which should be considered as fines accounting directly for the volume of paste. The coarse to fine aggregate ratio in the mix and the maximum size of aggregates are determining factors for the passing ability of SCC, for a given reinforcement spacing (BIBM et al., 2005; Billberg, 2002; Petersson and Billberg, 1999). Changes in the moisture content or water absorption of

aggregates will change the target rheological properties of paste and, consequently, of concrete. Moisture contents of fine aggregates normally are greater than those of coarse aggregates.

At paste level, SCC paste can be seen as a suspension of powder particles in water (Grünewald and Walraven, 2007). Therefore, changes in particle size distribution, shape and water absorption of fine materials may affect the water demand of SCC (BIBM et al., 2005). Wallevik et al. (2007) found that changes in cement induced by the production process can have a significant effect on workability and reactions of concrete, especially with superplasticized mixes. Factors such as fineness, sulfate content, alkalis and C_3A content may have a significant effect (BIBM et al., 2005; Moir, 2003; Vikan et al., 2007). The influence of cement variations, due to the production process, on paste/mortar properties was assessed and was discussed more in detail in Chapter 6. Admixtures will normally be very consistent from batch to batch (BIBM et al., 2005), although care must be taken to keep an uniform concentration of the product inside the storage tank as well as to consider the effects of seasonal temperature variations. Chemistry and age of recycled water and solids from slurry may affect workability of SCC (Rilem Technical Committee, 2006).

A change of the type or source of supply of any of the constituent materials is likely to make a significant change to concrete properties, as it was shown in Chapter 5 for the cases of a change in the superplasticizer type (same manufacturer) and cement source (same type).

7.3.2. Inaccuracy in weighing of materials

Deviations in mix proportions can occur due to inaccuracy of weighing equipment which can affect workability of SCC (Bonen et al., 2007) and, generally, larger errors are introduced when batching small load sizes. Normal weighing tolerances regulated by national and international standards are in general acceptable for production of SCC (Rilem Technical Committee, 2006). Accuracy of admixture dosing equipment may vary depending on the type of dosing equipment and its set-up (Rilem Technical Committee, 2006). The variation of viscosity of liquid admixtures, due to changes in surrounding temperature, can also influence the accuracy of dosing of those admixtures.

7.3.3. Mixing energy

SCC is also less tolerant to changes in the mixing protocol than conventional concrete because it contains a higher amount of fines which depend on the mixing energy to be efficiently dispersed (Rilem Technical Committee, 2006). A suitable mixing protocol

is to be established for each individual plant during the initial full-scale tests (Rilem Technical Committee, 2006). The main influencing factors of mixing efficiency are: the concrete mixture itself (type of constituent materials and mix-proportions), the loading sequence, mixing sequence, mixing speed, mixing time, type of mixer, batching volume and cleanliness of the mixer before loading.

SCC typically requires a longer mixing time or mixing energy than conventional concrete (Chopin et al., 2004; Rilem Technical Committee, 2006), but it is possible to reduce the mixing times by increasing the mixing speeds or by changing the configuration of the paddles in the mixer. Admixture manufacturers recommend that the superplasticizer should be diluted in water before adding to the concrete, allowing a better dispersion of the relatively small quantity of admixture within the mass of concrete (Rilem Technical Committee, 2006). The instant of addition of the superplasticizer may also affect fluidity, depending on the superplasticizer type, as discussed in Chapter 3. Takada (2004) investigated the effects of the mixer type on fresh properties of SCC and concluded that forced pan mixers have a higher mixing efficiency than drum mixers. Furthermore, it was shown that the type of superplasticizer used influences the necessary mixing time and mixing intensity (Takada, 2004). Chopin et al. (2004) studied the effects of mixing time by varying the quantity of powder, use of limestone filler, and various types and contents of silica fume and superplasticizer. These authors showed that the mixing time could be reduced by increasing the fine particle content (with constant w/c), increasing the total water amount, increasing maximum solid content of aggregates (for constant total aggregate content) and replacing part of the cement by silica fume (Chopin et al., 2004). For better consistency, the volume of the SCC mix should be as near to the maximum mixer capacity as possible. The mixer should be clean but not dry. Mixing conventional concrete before mixing SCC may create some inconsistency in properties of SCC, especially if incompatible admixtures have been used before mixing SCC (Rilem Technical Committee, 2006).

7.4. Strategies to increase SCC mixtures robustness

Observing Figure 7.1, one can easily conclude that robustness can be increased by reducing the range of the interval ΔV, which in the case of the SCC production process can be accomplished by reducing constituent materials variations and deviations from target mix proportions through more quality control and/or modernization of existing equipments. Another way to increase robustness is to change from a curve of the type of Process B to one of the type of Process A (see Figure 7.1), which can be achieved by a well-balanced selection and proportioning of constituent materials.

7.4.1. Materials selection and mix-proportioning

The constituent materials for SCC are the same as those used in conventional concrete, conforming to NP EN 206-1 (Portugal. IPQ, 2007), and should satisfy the requirements for individual constituents covered by specific European standards (BIBM et al., 2005). According to BIBM et al. (2005), material selection should try to improve robustness, making concrete less sensitive to material variability. But, for economic reasons, materials selection depends much on local availability so there is no fixed rule for the amount of aggregates, cement, additions and admixtures. Thus, a decisive factor for robustness of SCC mixtures is a clear understanding of the effect of each constituent material and of their interaction on SCC properties and an adequate mix-design method (scientific).

Some indications can be found in the literature to increase robustness of SCC mixtures through materials selection and mix-proportioning. Bonen et al. (2007) point that the desired flow properties should be maximized by materials selection rather than increasing superplasticizer content or water content. Khayat et al. (1999b) showed that the use of coarse aggregate and sand combinations that enable increase in packing density can reduce superplasticizer demand and plastic viscosity of SCC. Hwang and Khayat found concrete-equivalent mortars, including naphthalene-based superplasticizer, to be less sensitive to variations in water content (or more robust) than similar mixtures including polycarboxylate-based superplasticizer (ACBM, 2007). The type of binder was also shown to affect robustness (ACBM, 2007). There is some consensus that the introduction of a viscosity-modifying agent (VA) is effective to minimize the effect of variations in moisture content, fines in the sand or its grain size distribution, making SCC more robust and less sensitive to small variations in the proportions and condition of other constituents (BIBM et al., 2005) (see Figure 7.2). A VA is an admixture which is able to modify cohesion of the mixture without significantly altering its fluidity. Sakata et al. (referred by (Bonen et al., 2007)) reported that in SCC made with low water/powder ratio of 0,33 (powder containing limestone filler), the incorporation of a small concentration of Welan Gum of 50 g/m^3 can reduce variability in slump flow of SCC due to changes in cement Blaine (318 to 342 m^2/kg), fineness modulus of sand (2,08 to 3,06), and temperature of fresh concrete (10 to 30°C). But according to Khayat et al. (1999c) SCC made with a low content of VA and a relatively low water content can represent greater robustness than SCC made with a low binder content and a higher dosage of VA. In the former mixtures, VA is used to reduce variation in rheology due to some small changes in the materials properties, while yield stress and viscosity values are mainly controlled by low w/c and aggregate/cement. The latter mixtures are less robust because any small changes in VA content compromise viscosity and can lead to excessive bleeding and segregation. This means that VA should not be regarded as a way of avoiding the need for a good mix design and careful selection of other SCC

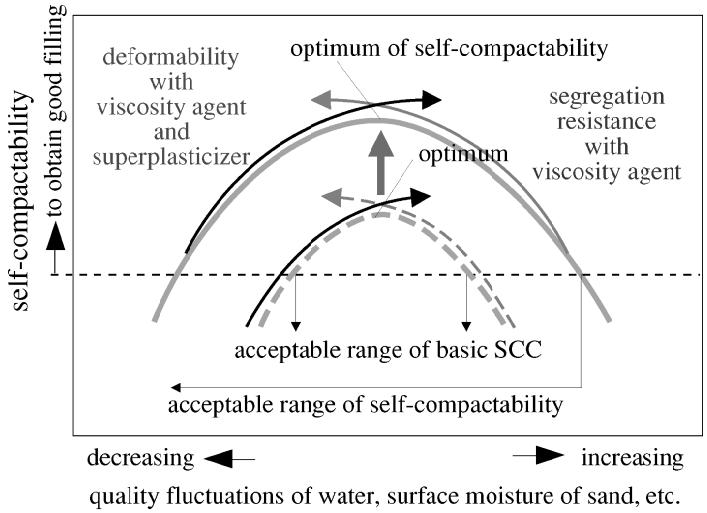


Figure 7.2.: Illustration of the effect of a viscosity agent on SCC robustness (Shindoh and Matsuoka, 2003)

constituents.

7.4.2. Quality control

Experience shows that SCC can be successfully produced in a consistent and continuous way only at a properly equipped concrete mixing plant under an established and reliable quality assurance system (Rilem Technical Committee, 2006). It is recommended (and it is a requirement in some EU member countries) that the producer is qualified according to ISO 9001 or equivalent (BIBM et al., 2005). Depending on the mixture's robustness, the control of the constituent materials needs to be increased and the tolerable variations restricted, so that daily production of SCC is within the conformity criteria without the need to test and/or adjust every batch.

In general, it is recommended that the aggregates are evaluated each production day prior to commencing batching. Thereafter, visual checks should be carried out on each delivery of aggregate; any noticeable change should be evaluated prior to accepting or rejecting the delivery. The moisture content of aggregates should be continuously monitored and the mix adjusted to account for any variation. When new batches of cement, addition or admixture are delivered, additional performance tests may be necessary to monitor any significant changes or interactions between constituents. Batching equipment should be regularly checked for its accuracy. An investment in modernization of existing equipment, increasing its accuracy, will eventually produce more economical SCC.

It is important that all personnel who will be involved in the production and delivery of SCC receive adequate training prior to production from a person with previous ex-

perience of self-compacting concrete. This training may include observing trial batches being produced and tested.

7.5. Robustness evaluation methods

In "The European Guidelines for Self-Compacting Concrete" the robustness checking is recognized as an important step in the SCC design process (BIBM et al., 2005). Since variability of most constituent materials can be translated by a change in water requirement, it is suggested by BIBM et al. (2005) that compositions with plus and minus 5 to 10 litres of the target water content be tested and the respective changes in fresh state properties be measured. A robust SCC should tolerate these deviations, i.e. should maintain its fresh properties inside the specified limits (BIBM et al., 2005).

Hwang and Khayat (referred in (Bonen et al., 2007)) suggested determining an index of mixtures' robustness, the minimum water content (MWC), by testing concrete-equivalent mortars. MWC was determined as the increase in w/c that can lead to a unit change of flow diameter. Combinations of materials leading to higher values of MWC, that can result in a lower degree of increase of flow diameter after a given increase of w/c, are the most robust combinations. Nachbaur et al. (2005) also suggested the extension of "concrete equivalent mortar" method (Schwartzentruber and Catherine, 2000) to SCC, to predict the SCC mixture properties based on results obtained in equivalent mortars reducing, this way, the amount of concrete batches needed to complete the mixture proportioning optimization. Grünewald and Walraven (2007) introduced a variation of ± 10 l/m^3 on reference pastes and concluded that the information obtained from the mini-slump test is not very accurate to identify the robustness of SCC mixtures from the paste test alone.

These approaches, based only on a change in water content, seem too simplistic because they do not take into account the specific characteristics of the production centre, like the existing level of quality control, equipment performance, skills and knowledge of the personnel involved. Therefore, in the present study a methodology was developed to compute a robustness measure based on data of typical materials' weight deviations inherent to the production process, at a specific production centre. This methodology is presented in the next section.

7.6. LABEST/FEUP robustness evaluation method

The present study was developed under the scope of the research project BACPOR, during the full-scale tests phase of SCC production in Maprel precast factory, in Rio

Table 7.1.: Grading of aggregates (BACPOR, Maprel, Rio Maior)

Sieve size (mm)	0,074	0,150	0,297	0,59	1,18	2,38	4,75	6,30	9,5	12,5
sand 1	0,0	5,3	19,2	48,1	81,5	98,9	100	100	100	100
sand 2	0,9	4,5	14,7	38,7	66,6	88,1	99,9	100	100	100
coarse aggregate	0,0	0,11	0,5	0,7	1,0	2,3	20,7	46,3	90,5	100

Maior, Portugal. The objective of this study was to evaluate the robustness of the target SCC mix composition, to be applied during full-scale tests, based on information of daily fluctuations inherent from the production process at Maprel precast factory. The corresponding experimental plan was carried out between 8^{th} and 14^{th} of March 2005.

7.6.1. Experimental programme

Materials characterization

Crushed calcareous aggregate (1-12 mm), a siliceous natural fine sand (sand 1) with a fineness modulus of 2,47 and natural coarse sand (sand 2) with a fineness modulus of 2,87 were used (see Table 7.1). The specific gravity of the coarse aggregate, sand 1 and sand 2 were 2,61, 2,54 and 2,54, and absorption values were 1,31%, 1,10% and 0,96%, respectively, according to NP EN 1097-6 (Portugal. IPQ, 2004). In this study SCC mix was prepared with Portland cement (CEM I 52,5 R) and a mineral addition (limestone filler), with a specific gravity of 3,12 and 2,70, respectively. A polycarboxylate type superplasticizer was used having a specific gravity of 1,05 and 20,2% solid content.

Experimental design

A $2^{(5-1)}$ fractional factorial statistical design (Montgomery, 2001), corresponding to five parameters at two levels, was used to establish models that describe key SCC properties. Since the central point in the factorial design applied in this study corresponds to a SCC mixture optimized in a previous study (Nunes et al., 2005c), the analysed region is relatively close to the optimum. In this situation a second order model is usually required to approximate the response because of the curvature that may be present in the true response surface. For this reason the factorial design (2^4=16 runs) was augmented with 10 axial runs plus 4 central runs, resulting in a central composite design that can be used to fit a second-order model (Montgomery, 2001).

SCC mix proportions can be established based on the following parameters: water to powder volume ratio (V_w/V_p); filler to cement weight ratio (w_f/w_c); superplasticizer to

Table 7.2.: Coded values for the factors used in the experimental design

Ref.	point type	V_w/V_p	w_f/w_c	Sp/p	s_1/s	$V_g/V_{g,lim}$
Ci[a]	central	0	0	0	0	0
F1	factorial	-1	-1	-1	-1	1
F2		1	-1	-1	-1	-1
F3		-1	1	-1	-1	-1
F4		1	1	-1	-1	1
F5		-1	-1	1	-1	-1
F6		1	-1	1	-1	1
F7		-1	1	1	-1	1
F8		1	1	1	-1	-1
F9		-1	-1	-1	1	-1
F10		1	-1	-1	1	1
F11		-1	1	-1	1	1
F12		1	1	-1	1	-1
F13		-1	-1	1	1	1
F14		1	-1	1	1	-1
F15		-1	1	1	1	-1
F16		1	1	1	1	1
CC1	axial	2	0	0	0	0
CC2		-2	0	0	0	0
CC3		0	2	0	0	0
CC4		0	-2	0	0	0
CC5		0	0	2	0	0
CC6		0	0	-2	0	0
CC7		0	0	0	2	0
CC8		0	0	0	-2	0
CC9		0	0	0	0	2
CC10		0	0	0	0	-2

[a] the central point was replicated four times (i=1 to 4)

powder weight ratio (Sp/p); sand to mortar volume (V_s/V_m); solid volume ($V_g/V_{g,lim}$), as suggested by Okamura et al. (2000). An additional parameter must be considered when fine aggregate is a combination of two sands. In this work weight ratio (s_1/s) sand 1 to total sand was used, resulting in five factors used in the modelling: V_w/V_p; w_f/w_c; Sp/p; s_1/s and $V_g/V_{g,lim}$. The volumetric ratio V_s/V_m was kept constant and equal to 0,462. The effect of each factor was evaluated at five different levels $-\alpha$, –1, 0, +1, $+\alpha$ as presented in Table 7.2 and the design was made rotatable by taking α equal to 2,0. Actual parameter values, at each level, are given in Table 7.3.

Table 7.3.: Correspondence between coded values and actual parameter values

mixture parameter	-2	-1	0	+1	+2
V_w/V_p	0,727	0,791	0,855	0,919	0,983
w_f/w_c	0,432	0,470	0,508	0,546	0,584
Sp/p	0,020	0,021	0,023	0,025	0,026
s_1/s	0,598	0,673	0,748	0,823	0,897

Mixing sequence, testing methods and test results

Mixtures from the experimental plan were tested in a random order. The mixes were prepared in the laboratory in 25 litres batches and mixed in an open pan mixer. The mixing sequence consisted of mixing both sands and coarse aggregate with ¼ of the mixing water during 2½ minutes, waiting for 2½ minutes for absorption, adding powder materials, followed by the rest of the water with the superplasticizer and finally mixing concrete during a further 8 minutes. Slump-flow, V-funnel and Box tests were then carried out to characterize fresh state. Details on equipment used for testing fresh concrete and on test procedures can be found in (BIBM et al., 2005). After tests on fresh concrete, three standard 150 mm cubes were moulded to evaluate 28 days compressive strength (fc,28). Concrete cubes were demoulded one day after casting and kept inside a chamber under controlled environmental conditions (Temperature=20°C and HR=95-98%) until a compressive strength test was carried out at 28 days concrete age. The Slump-flow test was used to evaluate deformation capacity, viscosity and resistance to segregation of SCC (by visual observation). From this test, final slump flow diameter (Dflow) and time necessary for concrete to reach a 50 cm diameter (T50) were recorded. The V-funnel test was used to assess viscosity and passing ability of SCC. Test flow time was recorded (Tfunnel). The Box test was used to assess the ability of concrete to pass through tight openings between reinforcing bars and filling ability; filling height was recorded (H). Dflow, T50, Tfunnel, H and fc,28 were the selected concrete properties to be analysed and modelled.

The mix proportions and test results of the 30 mixes prepared as described above are summarized in Tables E.15 and E.16 in Appendix E. From these results it may be observed that with this experimental plan a wide range of SCCs was covered with Dflow ranging from 505 to 750 mm, T50 ranging from 1,47 to 6,31 s, Tfunnel ranging from 6,59 to 28,47 s and fc,28 ranging from 52,20 to 75,31 MPa. All mixes exhibited a filling height in the Box-test higher than 300 mm, meaning that blocking is not a critical aspect in the analysed region; this can be attributed to low maximum aggregate size and low coarse aggregate content. None of the mixes exhibited severe segregation.

Table 7.4.: Fitted numerical models (coded variables)

Response variable	Dflow (mm)	T50 (s)	[Tfunnel (s)]$^{-0,5}$	H (mm)	fc,28 (MPa)
model terms estimate					
independent	650,53	2,936	0,304	333,36	63,00
V_w/V_p	58,67	-1,291	0,054	8,12	-3,29
w_f/w_c	8,21	-0,110	0,006	NS	-1,11
Sp/p	23,5	-0,355	NS	2,79	1,25
s_1/s	NS	-0,035	0,004	NS	1,26
$V_g/V_{g,lim}$	-8,46	0,220	NS	-3,54	-0,67
$(w_f/w_c)\times(s_1/s)$	NS	0,344	-0,009	NS	NS
$(Sp/p)\times(V_g/V_{g,lim})$	10,44	-0,451	NS	3,44	-1,24
$(V_w/V_p)^2$	-6,95	0,316	NS	-3,95	NS
$(V_g/V_{g,lim})^2$	NS	NS	NS	NS	-1,46
residual error, ε^a					
mean	0	0	0	0	0
standard deviation	13,188	0,468	0,015[b]	5,023	2,248
R^2	0,953	0,865	0,921	0,787	0,759
R^2_{adj}	0,941	0,811	0,909	0,743	0,682

(NS) non-significant terms; [a]error term is a random and normally distributed variable; [b]corresponding value for Tfunnel is 4,30

7.6.2. Response models

In this work, commercial software (Design-Expert) (State-Ease Corporation, 2000) was used to analyse results for each response variable by examining summary plots of the data, fitting a model using regression analysis and ANOVA, validating the model by examining the residuals for trends and outliers and interpreting the model graphically.

Fitted models

The estimates of the fitted models, including the residual error term, along with the correlation coefficients, are given in Table 7.4. An analysis of variance showed that these models are significant when describing the effect of V_w/V_p, w_f/w_c, Sp/p, s_1/s and $V_g/V_{g,lim}$ on the modelled responses. Residual analysis did not reveal any obvious model inadequacies or indicate serious violations of the normality assumptions, except in the case of Tfunnel. This problem was overcome after a variable transformation of the type $1/\sqrt{y}$, as indicated in Table 7.4.

Table 7.5.: Coded values and test results from a previous study

V_w/V_p	w_f/w_c	Sp/p	s_1/s	$V_g/V_{g,lim}$	Date	Dflow (mm)	T50 (s)	Tfunnel (s)	H (mm)	fc,28 (MPa)
0	0	0	0	0	14-02-2005	645,0	2,78	10,07	335	69,03
0	0	0	0	0	14-02-2005	630,0	3,10	10,69	320	69,17
0	0	0	0	0	14-02-2005	683,0	2,59	9,44	322	–
0	0	0	0	0	15-02-2005	670,0	2,72	10,09	318	62,82
1	0	0	0	0	15-02-2005	705,0	2,57	7,85	340	65,20
-1	0	0	0	0	15-02-2005	610,0	3,97	13,47	330	68,90
0	0	-1	0	0	15-02-2005	645,0	2,47	10,43	332	61,85
0	0	1	0	0	15-02-2005	697,5	2,66	10,72	325	66,03

Table 7.6.: Statistics of the results for the central points

Central points (n=8)	Dflow (mm)	T50 (s)	Tfunnel (s)	H (mm)	fc,28 (MPa)
mean	656	2,8	10,1	328	64,6
standard deviation	17	0,2	0,6	9	3,2
coefficient of variation	2,6%	8,1%	5,7%	2,8%	5,0%
estimated error[a]	±11,6	±0,15	±0,40	±6,3	±2,4

[a] corresponding to a 95% confidence level

Accuracy of the proposed models

Even though the majority of the fitted models exhibited relatively high correlation coefficients (see R^2 and R^2_{adj} in Table 7.4) their accuracy must be verified. The results of four central points included in the experimental design, together with four additional central runs from a previous study (see data in Table 7.5) were analysed in order to estimate the experimental error. The corresponding mean value, standard deviation, coefficient of variation and estimated error (95% confidence interval) are presented in Table 7.6. The lowest coefficient of variation (2,6%) was associated to Dflow and the highest one (8,1%) was associated to T50. As can be observed in Table E.15 from Appendix E and Table 7.5 replicate runs of central points were spread out in time to get a rough check on the stability of the process during the experimental programme. The accuracy of the derived models can be assessed by comparing the residual standard deviation (see Table 7.4) and the standard deviation calculated from the central points (see Table 7.6)(Montgomery, 2001). A good fit can be expected when the residual standard deviation does not exceed the experimental error by far. In this study, the standard deviation measured on the central points was always higher or close to the residual standard deviation, except in the case of T50.

The accuracy of the proposed models was also analysed by comparing predicted-to-

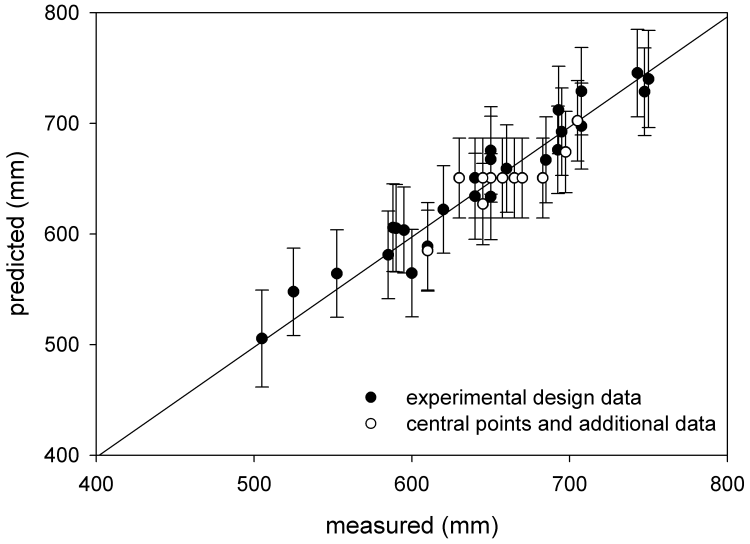


Figure 7.3.: Comparison of measured versus predicted values of Dflow

measured values obtained with the eight mixtures presented in Table 7.5. The ratio between predicted-to-measured values for Dflow, T50, Tfunnel, H and fc,28 ranged between 0,95 and 1,03, 0,76 and 1,33, 0,99 and 1,18, 0,97 and 1,05, 0,91 and 1,02, respectively. Again, these values indicate good accuracy for the established models except in the case of T50. The predicted-to-measured values of Dflow, T50, Tfunnel, H and fc,28 are shown in Figures 7.3 to 7.7, respectively, with the prediction intervals corresponding to a 95% confidence level. In these figures the black dots represent the experimental design results and the white dots represent results obtained in a previous study (not used to derive the numerical models). One can observe that all points fall within or very close to the limits of the prediction intervals. Thus, one can expect the established models to be sufficiently accurate to predict the analysed fresh and hardened properties.

Individual and interaction effects

Since statistical models were established in coded variables, the estimates of the model coefficients presented in Table 7.4 give an indication of the relative significance of the various mixture parameters on each response. Naturally a negative coefficient means that the response variable will decrease if the given mixture parameter increases. The results in Table 7.4 clearly show that V_w/V_p exhibit the greatest effect on all five measured responses. The variables Sp/p and $V_g/V_{g,lim}$ also influence SCC properties. Significant interaction effects were found between w_f/w_c and s_1/s on both T50 and (Tfunnel$^{-0,5}$) responses and between Sp/p and $V_g/V_{g,lim}$ on all the analyzed responses except (Tfunnel$^{-0,5}$). The quadratic term in V_w/V_p was significant for Dflow, T50 and H responses. The quadratic term in $V_g/V_{g,lim}$ was significant for the fc,28 response.

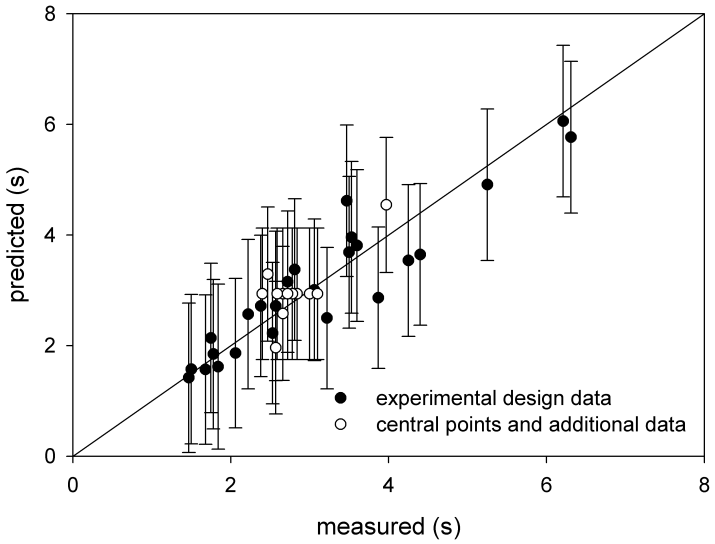


Figure 7.4.: Comparison of measured versus predicted values of T50

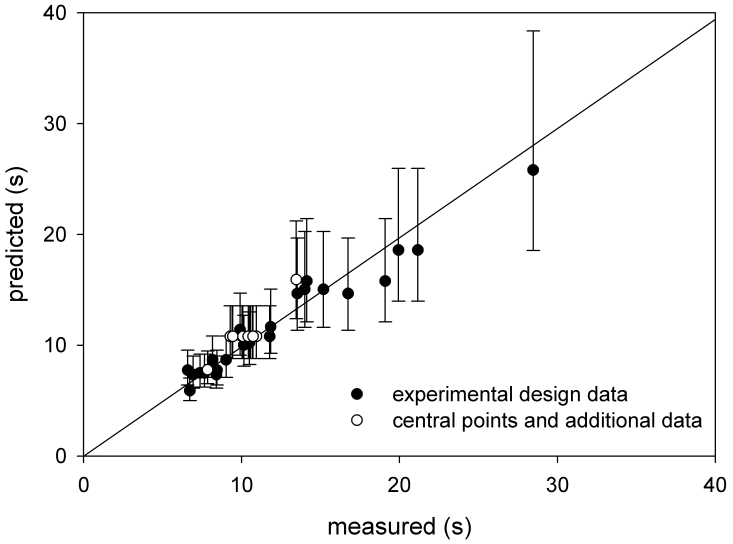


Figure 7.5.: Comparison of measured versus predicted values of Tfunnel

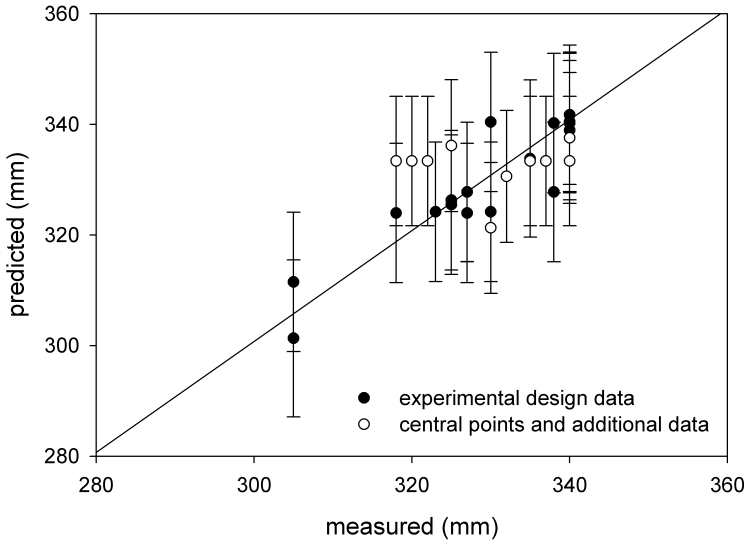


Figure 7.6.: Comparison of measured versus predicted values of H

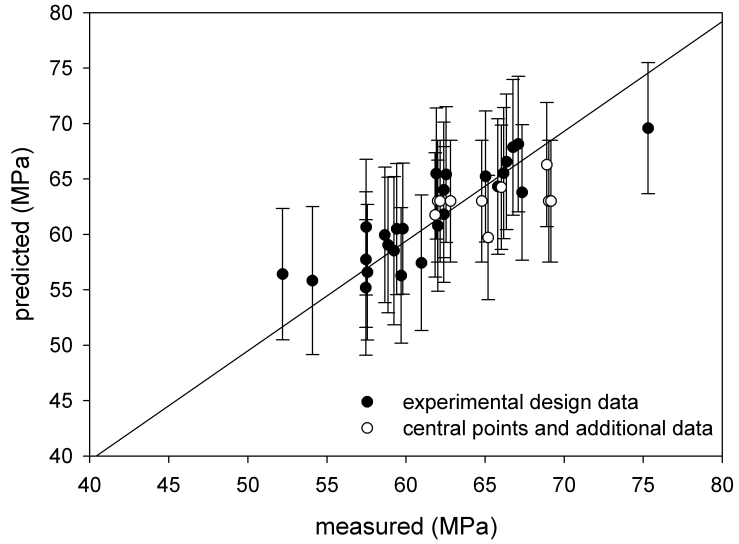


Figure 7.7.: Comparison of measured versus predicted values of fc,28

7.6.3. Robustness measure

When adapting Figure 7.1 to the case of concrete production process, a large number of independent variables (X_i, $i = 1, \ldots, n$) influence concrete properties (Y_i, $i = 1, \ldots, n$) and a considerable amount of concrete properties must be assessed to verify the fulfilment of the performance criteria. In the present study, as mentioned before, five independent variables were considered, namely, $X_1 = V_w/V_p$, $X_2 = w_f/w_c$, $X_3 = Sp/p$, $X_4 = s_1/s$ and $X_5 = V_g/V_{g,lim}$. Based on these variables numerical models were derived to describe Y_1=Dflow, Y_2=T50, Y_3=Tfunnel, Y_4=H and Y_5=fc,28, which are the dependent variables. Once the acceptance limits for each dependent variable are established, if the typical fluctuations of V_w/V_p, w_f/w_c, Sp/p, s_1/s and $V_g/V_{g,lim}$ associated to the production process have a known distribution one can consider the probability that the performance criteria is fulfilled, given by

$$p = P\left(\bigcap_{i=1}^{5} R_{inf}^{i} < Y_i < R_{sup}^{i}\right) \tag{7.1}$$

as a measure of robustness of the SCC mix. Since this probability cannot be computed exactly, one can use the frequency of accepted intervals computed on a large sample

$$f = \frac{number\ of\ occurences\ of\ the\ event\ "\left(\bigcap_{i=1}^{5} R_{inf}^{i} < Y_i < R_{sup}^{i}\right)"}{sample\ size} \tag{7.2}$$

to estimate 7.1, that is, to estimate robustness of the SCC mix under study. As it will be explained later in this section, applying bootstrap resampling techniques enables improvement of this estimate and evaluating how accurately a statistic calculated from the observed data estimates the corresponding quantity for the whole population (Efron and Tibshirani, 1993).

Constituent materials variations

Since this study was carried out prior to the industrial application of SCC at Maprel precast factory there was no available data of daily fluctuations concerning SCC production. Therefore, records of target and measured weight values of each constituent material corresponding to 1,5 m^3 batches of conventional concrete (C45/55) were used. These batches were all produced at Maprel precast factory during one week using the same materials that were used for the experimental factorial plan. A total of 132 observations were collected. Figure 7.8 presents the observed deviations of the constituent materials. The deviations were calculated dividing the difference between the target and the measured values by the target value. Absolute deviations for aggregates were added up and presented as “aggregates”. For the superplasticizer, no deviations were

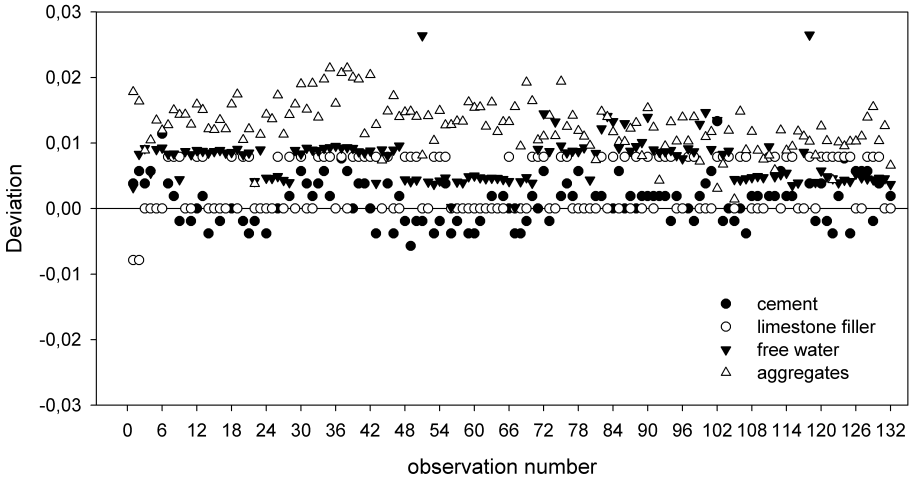


Figure 7.8.: Observed deviations of constituent materials during one week of concrete production in Maprel precast factory

recorded. It may be observed from Figure 7.8 that deviations respect the limits imposed in the NP EN 206-1 (Portugal. IPQ, 2007). Some deviations remained a constant sign (positive in the cases of water, sand 1 and coarse aggregate and negative in the case of sand 2) along the production process when both positive and negative deviations would be expected to occur randomly.

Bootstrap re-sampling

A bootstrap sample is obtained by randomly sampling n times, with replacement, from the original N data points. The sampling process consists of randomly generating j_1, $j_2, \ldots,$ j_n integers, each of which equals any value between 1 and N with probability $1/N$. These integers determine which members of the original data set are selected to be in the random sample. This process allows a simple member to appear once, more than once or never. For each bootstrap sample (of size n) the statistic of interest can be evaluated and it is called a bootstrap replication. This process is repeated many times to generate B bootstrap samples and respective bootstrap replications. Then the sample of the bootstrap replications (size B) is used to assess the accuracy of the computed statistic, for example, to construct confidence intervals (Efron and Tibshirani, 1993). Applying the first percentile method (Efron and Tibshirani, 1993) the 100(1-α)% confidence interval for the true value of the unknown parameter of the population is then given by the two values that include the central 100(1-α)% of this distribution. For example a 95% confidence interval is given by the 2,5% and 97,5 % percentiles of the generated distribution. Details on this statistical method are reported in (Efron and

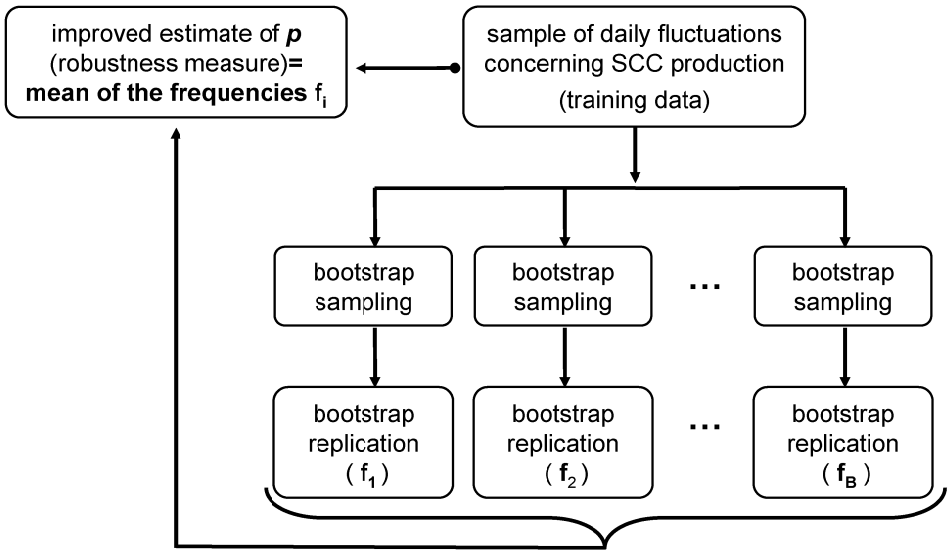


Figure 7.9.: Bootstrap re-sampling to compute a robustness measure

Tibshirani, 1993).

In the present study the quantity to be estimated is the probability p given in equation (7.1) and the frequency of accepted intervals given in equation (7.2) is computed for each bootstrap sample. An improved estimate of p, i.e. the robustness measure, is given by the mean of the frequencies obtained in the B replications (see Figure 7.9).

Implementation, results and discussion

In this work, as previously mentioned, $N = 132$ independent data points were observed, consisting of target and measured weight values of each constituent material. From this data, a large number of independent bootstrap samples ($B = 2000$) were generated, each one of size $n = 100$. For each re-sampled point in the bootstrap sample, the target and measured values of independent variables ($X_1 = V_w/V_p$; $X_2 = w_f/w_c$; $X_3 = Sp/p$; $X_4 = s_1/s$ and $X_5 = V_g/V_{g,lim}$) were calculated from the weight values of each constituent material. Then, the corresponding deviation ΔX_i from the target value in each independent variable was calculated

$$\Delta X_i = X_i^{measured} - X_i^{target} \tag{7.3}$$

These deviations where added to the values of the independent variables of the target SCC mix (corresponding to the central point in the factorial design, X_i^0) to simulate the variations associated to the production process

$$X_i = X_i^0 + \Delta X_i \tag{7.4}$$

Table 7.7.: Descriptive statistics of bootstrap samples

	p_1	p_2	p_3	p_4	p_5	p
number of bootstrap replications (B)	2000	2000	2000	2000	2000	2000
mean	0,965	0,965	0,918	1	0,864	0,739
median	0,970	0,970	0,920	1	0,870	0,740
mode	0,970	0,970	0,920	1	0,860	0,740
std. error of mean	$3{,}99\times 10^{-4}$	$4{,}06\times 10^{-4}$	$6{,}21\times 10^{-4}$	0	$7{,}63\times 10^{-4}$	$9{,}76\times 10^{-4}$
minimum	0,900	0,880	0,800	1	0,730	0,590
maximum	1,000	1,000	0,990	1	0,960	0,890
std. deviation	0,018	0,018	0,028	0	0,034	0,044
percentile 2,5%	0,930	0,930	0,860	1	0,790	0,650
percentile 97,5%	0,990	0,990	0,970	1	0,930	0,820

Finally, concrete properties (Y_1=Dflow; Y_2=T50; Y_3=Tfunnel; Y_4=H and Y_5=fc,28) could be estimated using the derived numerical models presented in Table 7.4. The statistic presented in equation (7.2) (a frequency) was computed for each bootstrap sample, as an estimate of the target SCC mixture robustness. Besides this frequency, individual frequencies were also computed as estimates of

$$p_i = P\left(R^i_{inf} < Y_i < R^i_{sup}\right),\ i = 1\ to\ 5 \tag{7.5}$$

with the purpose of evaluating the contribution of each concrete property to robustness. The acceptance intervals considered for Y_1, Y_2, Y_3, Y_4 and Y_5 were [600;680] (mm), [2; 5] (s), [8; 12] (s), [300; ∞] (mm) and [60; 70] (MPa), respectively.

A statistical analysis using commercial software (*SPSS*) was carried out on the samples of p_i and p that resulted from running the 2000 bootstrap replications (Table 7.7). As observed before with the experimental plan results, the values of the filling height (Y_4) were always higher than 300 mm, so estimates of p_4 were always equal to 1,0. The obtained estimate of the SCC mixture robustness was 0,74 with a 95% confidence interval of [0,650; 0,820] (see Table 7.7). In other words, a robustness value of 0,74 means that the target SCC mix, when produced at Maprel precast factory, is expected to fail to satisfy all the acceptance criteria about once in every 4 batches. From Table 7.7 we can also notice that SCC compressive strength is the property that exhibited more sensitivity regarding to the introduced variations in the constituent materials and it is the one that contributed the most to reduce the robustness estimate.

7.6.4. Comments on this method

The variations considered in this work have by no means exhausted the range of factors that affect SCC mixtures' robustness. For example, changes in environment conditions like temperature and humidity, changes in the mixing energy and sequence, the evolution of concrete properties through time, the variations in material characteristics from different suppliers, can significantly change SCC fresh and hardened properties.

When starting the study an important step is an adequate definition of independent variables, of relevant concrete properties to be analysed and of the respective acceptance limits, since these decisions will affect the final value of robustness. It is also important to collect relevant data about constituent material variations, inherent to the production with SCC, which will then be used to simulate variations of SCC mix proportions. In case a large sample of typical constituent material variations is available bootstrap re-sampling may be discarded, since it will not improve significantly the robustness estimate. But, in general, this is not the case during the initial full-scale tests stage when alternative SCC mixtures are still being considered and the robustness evaluation is included in the decision-making process.

7.7. Application of LABEST/FEUP methodology to optimize SCC mixtures

Within the scope of the research project POCI/ECM/61649/2004 the methodology presented in the previous section was applied and compared to the results given by the methodology suggested in "The European Guidelines for Self-compacting Concrete". The objective of this study was to validate the LABEST/FEUP methodology and to verify if it is possible to enhance robustness of SCC mixtures by only changing proportions of materials in the mixture. The corresponding experimental plan was carried out between 16^{th} and 25^{th} October 2006.

7.7.1. Experimental programme

Materials characterization

Crushed granite aggregate (1-16 mm), a siliceous natural fine sand (sand 1) with a fineness modulus of 2,33 and natural coarse sand (sand 2) with a fineness modulus of 3,54 were used (see Table 7.8). The specific gravity of the coarse aggregate, sand 1 and sand 2 were 2,60, 2,49 and 2,59, and absorption values were 1,11%, 0,25% and 0,50%, respectively, according to EN 1097-6 (Portugal. IPQ, 2004). In this study SCC

Table 7.8.: Grading of aggregates (POCI/ECM/61649/2004)

Sieve size (mm)	0,063	0,125	0,25	0,5	1,0	2,0	4,0	8,0	16,0
sand 1	0,5	1,2	21,5	58,6	88,2	97,7	99,5	100	100
sand 2	0,5	1,1	2,6	8,7	48,2	86,7	98,5	100	100
coarse aggregate	0,1	0,3	0,5	0,7	1,0	1,5	2,8	25,0	100

mix was prepared with Portland cement CEM II/A-L 42,5 R, from the fifth delivery supplied by Cimpor-Alhandra, (see Tables C.5 and C.6 in Appendix C for more detailed characterization) and a mineral addition (limestone filler), with a specific gravity of 3,07 and 2,70, respectively. A polycarboxylate type superplasticizer (Viscocrete 3000) was used having a specific gravity of 1,05 and 18,5% solid content.

Experimental design

A central composite design (a minimum-run equireplicated resolution V design augmented with 12 axial runs plus 6 central runs) was carried out to mathematically model the influence of mixture parameters and their coupled effects on deformability, passing and filling abilities and compressive strength of SCC mixtures. The six mixture parameters used in the modelling were: water to cement weight ratio (w/c); superplasticizer to powder weight ratio (Sp/p); water to powder volume ratio (V_w/V_p); sand to mortar volume (V_s/V_m); sand 1 to total sand weight ratio (s_1/s) and solid volume ($V_g/V_{g,lim}$). The effect of each factor was evaluated at five different levels $-\alpha$, –1, 0, +1, $+\alpha$, as presented in Table 7.9, where the α value was taken equal to 1,565. Actual parameter values, at each level, are given in Table 7.10.

Mixing sequence, testing methods and test results

Mixtures from the experimental plan were also tested in a random order. The mixes were prepared in the laboratory in 18 litres batches and mixed in an open pan mixer. The mixing sequence was maintained (see paragraph 7.6.1). Slump-flow, V-funnel and L-box tests were then carried out to characterize fresh state. Details on equipment used for testing fresh concrete and on test procedures can be found in (BIBM et al., 2005). After fresh concrete tests, four standard 150 mm cubes were moulded to evaluate 28 days compressive strength (fc,28). Concrete cubes were demoulded one day after casting and kept inside a chamber under controlled environmental conditions (Temperature=20°C and HR=95-98%) until a compressive strength test was carried out at 28 days concrete age. The final flow diameter (Dflow), flow time (Tfunnel), height ratio (H2/H1) from slump-flow, V-funnel and L-box tests, respectively, along with the average compressive

Table 7.9.: Coded values for the factors used in the experimental design

Ref.	point type	w/c	Sp/p	V_w/V_p	V_s/V_m	s_1/s	$V_g/V_{g,lim}$
Ci[a]	central	0	0	0	0	0	0
F1	factorial	-1	-1	1	1	-1	1
F2		1	1	-1	-1	-1	-1
F3		-1	-1	-1	-1	1	-1
F4		1	1	1	1	-1	-1
F5		-1	1	-1	1	-1	1
F6		1	1	1	-1	-1	1
F7		1	-1	-1	1	-1	1
F8		-1	1	-1	1	1	-1
F9		1	-1	1	-1	-1	-1
F10		1	-1	1	1	1	1
F11		1	-1	-1	1	1	-1
F12		1	1	-1	1	1	1
F13		-1	1	-1	-1	1	1
F14		1	1	1	-1	-1	-1
F15		-1	-1	1	1	1	-1
F16		1	-1	-1	-1	1	1
F17		-1	1	1	-1	-1	-1
F18		-1	-1	-1	-1	-1	1
F19		-1	-1	-1	1	-1	-1
F20		-1	1	1	1	1	1
F21		1	1	1	-1	1	-1
F22		-1	-1	1	-1	1	1
CC1	axial	-1,565	0	0	0	0	0
CC2		1,565	0	0	0	0	0
CC3		0	-1,565	0	0	0	0
CC4		0	1,565	0	0	0	0
CC5		0	0	-1,565	0	0	0
CC6		0	0	1,565	0	0	0
CC7		0	0	0	-1,565	0	0
CC8		0	0	0	1,565	0	0
CC9		0	0	0	0	-1,565	0
CC10		0	0	0	0	1,565	0
CC11		0	0	0	0	0	-1,565
CC12		0	0	0	0	0	1,565

[a] the central point was replicated six times to estimate degree of experimental error

Table 7.10.: Correspondence between coded values and actual parameter values

mixture parameter	-1,565	-1	0	+1	+1,565
w/c	0,340	0,375	0,438	0,500	0,535
Sp/p	0,014	0,015	0,018	0,020	0,021
V_w/V_p	0,687	0,710	0,750	0,790	0,813
V_s/V_m	0,384	0,400	0,428	0,455	0,471
s_1/s	0,422	0,450	0,500	0,550	0,578
$V_g/V_{g,lim}$	0,497	0,520	0,560	0,600	0,623

strength measured on cubes at 28 days concrete age (fc,28) were the selected concrete properties to be analysed and modelled.

The mix proportions and test results of the 40 mixes prepared as described above are summarized in Tables E.17 and E.18, in Appendix E. With the present experimental plan a wide range of SCCs was covered with Dflow ranging from 448 to 875 mm, T50 ranging from 0,63 to ∞, Tfunnel ranging from 4,9 to 35,6 s, H2/H1 ranging from 0 to 0,96 and fc,28 ranging from 47,8 to 68,9 MPa. When a large number of variables is included in the experimental plan the range of response results is expected to increase, as well as the probability of finding unsatisfactory mixtures or outliers. This is the case of the present study as compared to the previous study, presented in section 7.6.

7.7.2. Response models

In this work commercial software (Design-Expert) (State-Ease Corporation, 2000) was also used to analyse the results for each response variable by examining summary plots of the data, fitting a model using regression analysis and ANOVA, validating the model by examining the residuals for trends and outliers and interpreting the model graphically.

Fitted models

The estimates of the fitted models, including the residual error term, along with the correlation coefficients, are given in Table 7.11. An analysis of variance showed that these models are significant when describing the effect of w/c, Sp/p, V_w/V_p, V_s/V_m, s_1/s and $V_g/V_{g,lim}$ on the modelled responses. The estimates of the model coefficients presented in Table 7.11 give an indication of the relative significance of the various mixture parameters on each response. Residual analysis did not reveal any obvious model inadequacies or indicate serious violations of the normality assumptions, in the case of Dflow and fc,28 responses. This was not the case with T50, Tfunnel and H2/H1. This problem was overcome after variable transformation, as indicated in Table 7.11.

Table 7.11.: Fitted numerical models (coded values of variables)

Response variable	Dflow (mm)	$[T50(s)]^{-0,5}$	$[Tfunnel\ (s)]^{-0,5}$	$[H2/H1(mm)+0,01]^{1,98}$	fc,28 (MPa)
model terms estimate					
independent	728,25	0,865	0,308	0,742	57,21
w/c	64,07	0,149	0,033	0,126	-4,41
Sp/p	37,59	0,061	0,011	0,068	1,80
V_w/V_p	18,55	0,114	0,031	0,044	-1,02
V_s/V_m	-51,80	-0,158	-0,046	-0,146	-0,97
s_1/s	7,41	0,050	NS	0,042	NS
$V_g/V_{g,lim}$	-31,61	-0,064	-0,032	-0,153	1,76
$(w/c)\times(Sp/p)$	NS	NS	NS	-0,052	NS
$(w/c)\times(V_w/V_p)$	NS	NS	NS	-0,063	NS
$(w/c)\times(V_s/V_m)$	14,55	0,055	NS	0,068	NS
$(Sp/p)\times(V_s/V_m)$	NS	NS	NS	0,028	NS
$(Sp/p)\times(V_g/V_{g,lim})$	NS	NS	NS	NS	-0,81
$(V_w/V_p)\times(V_s/V_m)$	15,63	0,053	NS	0,035	NS
$(V_w/V_p)\times(s_1/s)$	-11,12	NS	NS	NS	NS
$(V_s/V_m)\times(s_1/s)$	10,18	NS	NS	NS	NS
$(Sp/p)^2$	-21,67	-0,064	-0,006	-0,050	-1,45
$(V_w/V_p)^2$	NS	NS	NS	NS	1,28
$(V_s/V_m)^2$	-21,16	NS	NS	-0,068	-1,37
$(V_g/V_{g,lim})^2$	-11,98	-0,063	-0,008	-0,054	NS
residual error, ε^a					
mean	0	0	0	0	0
standard deviation	18,89	$0,112^b$	$0,011^b$	$0,055^b$	1,58
R^2	0,963	0,831	0,976	0,951	0,892
R^2_{adj}	0,943	0,771	0,971	0,921	0,859

(NS) non-significant terms; ^{a}error term is a random and normally distributed variable;^{b}corresponding value for T50, Tfunnel and H2/H1 is 0,85 (excluding the two 10^6 observation values), 1,29 and 0,053, respectively.

Table 7.12.: Statistics of the results for the central points

Central points (n=8)	Dflow (mm)	T50 (s)	Tfunnel (s)	H2/H1	fc,28 (MPa)
mean	735	1,5	10,5	0,86	58
standard deviation	25	0,23	0,2	0,03	2
coefficient of variation	3,4%	15,7%	2,1%	3,6%	4,1%
estimated error[a]	±20,14	±0,19	±0,17	±0,02	±1,90

[a] corresponding to a 95% confidence level

Notice that a diameter of 50 cm was not reached in the slump flow test for mixtures number 5 and 15 (see Table E.17, in Appendix E), thus the respective result of T50 was ∞. For these cases, a very high value (10^6) was adopted as the T50 result in the modelling data. Notice also that the observation number 6 (see Table E.17 in Appendix E) was excluded because this mixture exhibited severe segregation, leading to separation of constituent materials. The value of 68,93 in the variable fc,28 was identified as an outlier and excluded from the data used to adjust the model.

Accuracy of the proposed models

All fitted models presented relatively high correlation coefficients (see $R^2$and R^2_{adj} Table 7.11). The results of six central points included in the experimental design (see data in Table B.17 from Appendix B) were analysed in order to estimate the experimental error. The corresponding mean value, standard deviation, coefficient of variation and estimated error (95% confidence interval) are presented in Table 7.12. The lowest coefficient of variation (2,1%) was associated to Tfunnel and the highest one (15,7%) was associated to T50. As can be observed in Table E.16 of Appendix E, replicate runs of central points were spread out in time to get a rough check on the stability of the process during the experimental programme. In this study, the standard deviation measured on the central points was always higher or close to the residual standard deviation, except in the case of Tfunnel and T50. In this study, the experimental error associated to Tfunnel was abnormally low, as compared to the previous study (see paragraph 7.6.2), so a good fit can be also expected from the Tunnel model in the present situation. In the case of T50, the obtained experimental error was similar to the previous study (see section 7.6.2) so there is not much confidence on this model.

The accuracy of the proposed models was also analysed by comparing predicted-to-measured values obtained with the six central point mixtures. The ratio between predicted-to-measured values for Dflow, T50, Tfunnel, H2/H1 and fc,28 ranged between 0,93 and 1,04; 0,75 and 1,15; 0,97 and 1,02; 0,95 and 1,05; 0,94 and 1,04; respectively. Again, these values indicate good accuracy for the established models except in the case

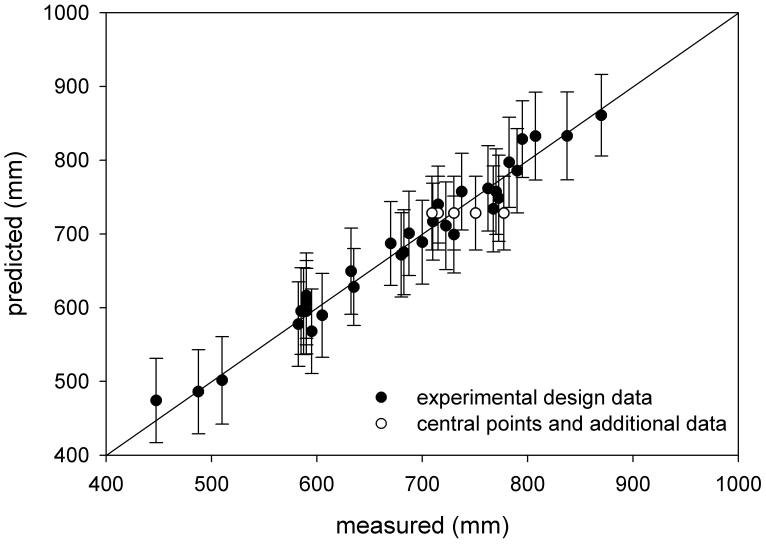


Figure 7.10.: Comparison of measured versus predicted values of Dflow

of T50. The predicted-to-measured values of Dflow, T50, Tfunnel, H2/H1 and fc,28 are shown in Figures 7.10 to 7.14, respectively, with the prediction intervals corresponding to a 95% confidence level. In these figures as before the black dots represent the experimental design results and the white dots represent central points. One can observe that all points fall within or very close to the limits of the prediction intervals. Thus, one can expect the established models to be sufficiently accurate to predict the analysed fresh and hardened properties, except in the case of T50.

Individual and interaction effects

The significant individual and interaction effects may change when the set of independent variables included in the plan is changed. In this study the variable V_s/V_m was also included in the experimental plan and w/c was used instead of w_f/w_c as compared to the previous study (see section 7.6). The results in Table 7.11 show that V_s/V_m and w/c exhibit a great effect on all responses concerning the fresh state of concrete. The variable $V_g/V_{g,lim}$ had a high effect also on T50, Tfunnel and fc,28 responses. As expected w/c had the highest effect on fc,28 response followed by Sp/p. Significant interaction and quadratic effects were also found to be significant as presented in Table 7.11.

7.7.3. Mixtures optimization

After building the regression models that establish relationships between mix design variables and the responses, the numerical optimization technique was used to determine the mixture parameters to satisfy different economic criteria, while maintaining

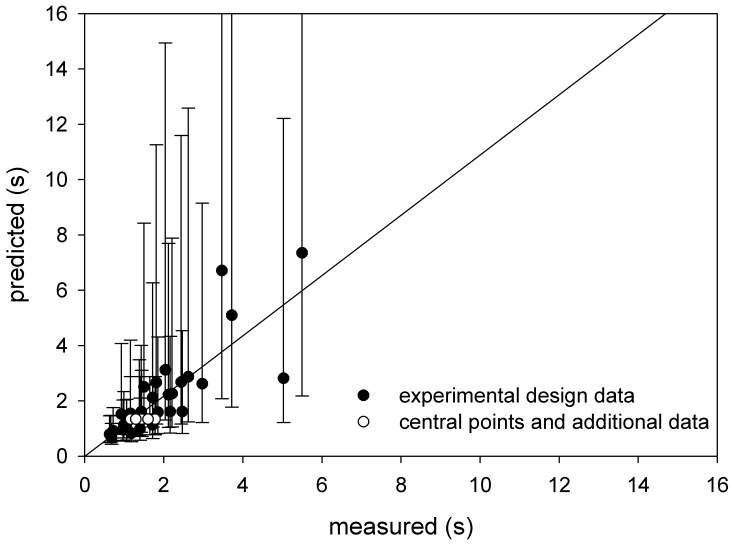


Figure 7.11.: Comparison of measured versus predicted values of T50

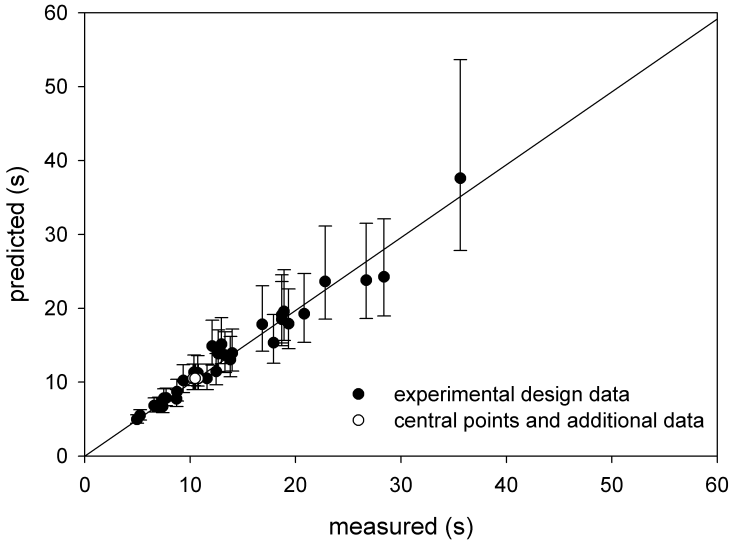


Figure 7.12.: Comparison of measured versus predicted values of Tfunnel

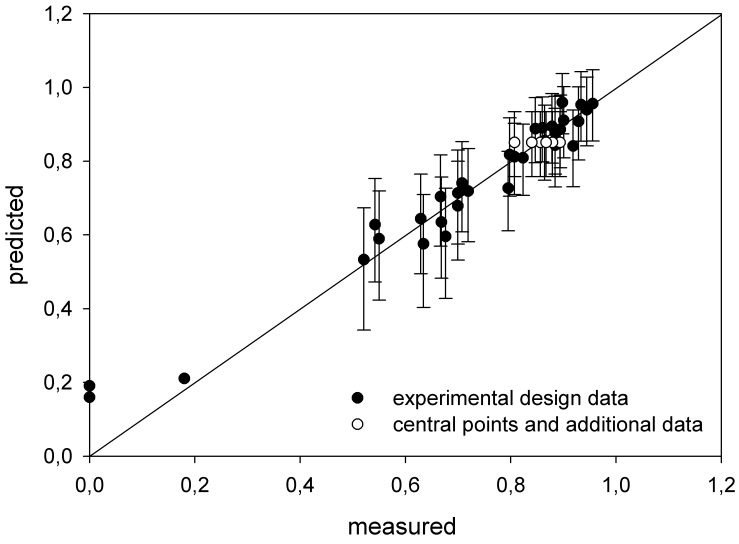


Figure 7.13.: Comparison of measured versus predicted values of H2/H1

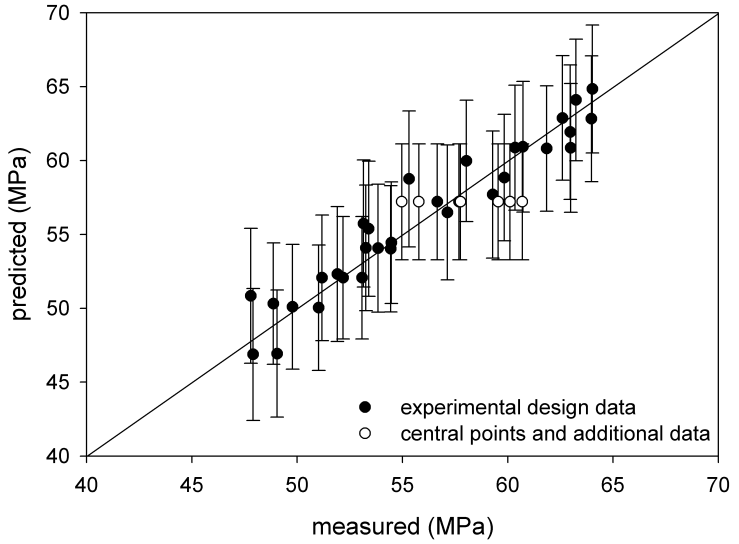


Figure 7.14.: Comparison of measured versus predicted values of fc,28

Table 7.13.: Optimization constraints

	Criteria					
Variable	A	B	C	D	E	F
w/c	equal to c^a					
Sp/p	is in range	*minimize*	*minimize*	is in range	*minimize*	*minimize*
V_w/V_p	is in range	is in range	is in range	is in range	*maximize*	*maximize*
V_s/V_m	is in range	is in range	*maximize*	is in range	*maximize*	is in range
s_1/s	is in range	is in range	is in range	is in range	is in range	is in range
$V_g/V_{g,lim}$	is in range	is in range	*maximize*	*maximize*	*maximize*	is in range
V_{paste}	*minimize*	none	none	none	none	*minimize*
Dflow	target is 680 mm					
Tfunnel	target is 10 s					
H2/H1	is in range [0,83; 1,0]					

[a] c was set equal to 0,40, 0,45 and 0,50;

Range of variables (coded values) was set as [-2,0; 2,0], respectively;

Lower and higher weight values of constraints were both set equal to 1;

Importance was set equal to 3 for all constraints

self-compactability, by using the constraints presented in Table 7.13. The volume of paste, per m^3, was computed from mixture parameter values as follows

$$V_{paste} = 1 - V_g - V_s \tag{7.6}$$

where V_g and V_s are the volumes of coarse and fine aggregates, respectively (see Chapter 4, section 4.6.5). For all mixtures, target slump-flow was 680 mm, target V-funnel time was 10 s and target H2/H1≥0,83. Three different water/cement ratios were studied, namely, 0,4, 0,45 and 0,50. No restriction was established for the fc,28 response variable. The obtained mix proportions and corresponding estimated SCC properties are presented in Tables 7.14 to 7.19, corresponding to criteria A to F, respectively. The estimated total cost of each mixture is also presented, based on local prices used in the typical Portuguese market by October 2006 (see Table 7.20).

Changes in both fresh and hardened concrete properties of all mix compositions with ±5 and 10 l/m^3 of the target water, as suggested in (BIBM et al., 2005), were estimated using the numerical models presented in Table 7.11. Results are also presented in Tables 7.14 to 7.19, corresponding to criteria A to F, respectively. A ±5 l/m^3 water change corresponds approximately to the limit imposed by NP EN 206-1 (Portugal. IPQ, 2007) for the water content variation (±3%).

As can be observed in Figure 7.15 an almost linear relation exists between the variation of concrete water content and the change in slump flow diameter. Therefore, the slope

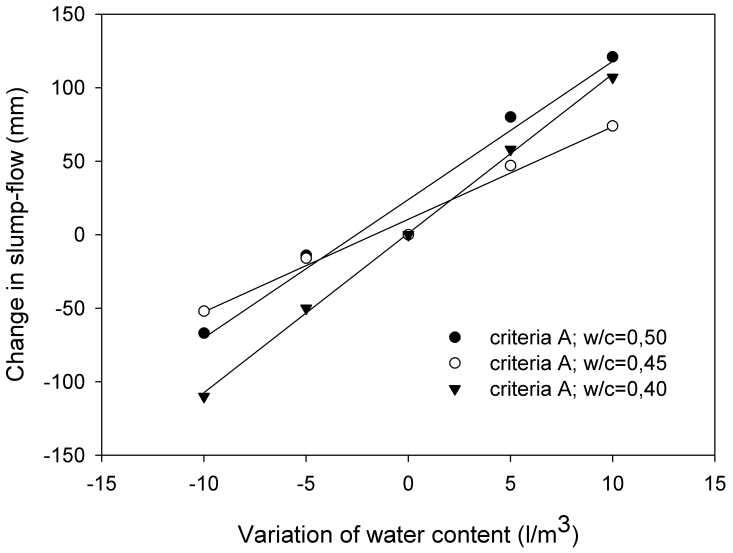


Figure 7.15.: Sensitivity to variation in water content of mixes obtained with criteria A

of these lines can be taken as an indicator of mixes' sensitivity to variation in water content (Concrete Society, 2005). Steeper slopes indicate mixtures more sensitive to variation in water content. Obtained slope values are presented in Figure 7.16 for each studied mixture. Based on these results, in terms of fresh state, it can be concluded that criteria B led to SCC mixtures less sensitive to changes in water content.

SCC mixtures robustness was also assessed by using FEUP/LABEST methodology (see Section 7.6 for a description), that is by measuring the probability that the properties of a mix fall inside the acceptance intervals. In this study, the acceptance intervals $[R^i_{inf}; R^i_{inf}]$ considered for Y_1=Dflow Y_2=Tfunnel, Y_3=H2/H1 and Y_4=fc,28 were [650;710] (mm), [8; 12] (s), [0,8; 1,0] and [target-5; target +5] (MPa), respectively. The frequency of acceptance (equation (7.2)) computed on a large sample of simulated mixes was used to estimate robustness of each SCC mix under study. Simulations were carried out based on data of daily fluctuations inherent from the production process at Maprel precast factory (see section 7.6.3). The computed estimates for the robustness of the mixes obtained with criteria A to F is given in the bottom of Tables 7.14 to 7.19, respectively, along with the associated 95% confidence intervals (see also Figure 7.17). Besides the robustness measure, estimates of individual probabilities are also given in Tables 7.14 to 7.19. By analysing these individual probabilities (p_1 to p_5), it can be concluded that, in general, the slump flow diameter and blocking ratio failed to satisfy the acceptance criteria more frequently, thus contributing more to reduce the robustness (p).

Based on both methodologies results (see Figures 7.16 and 7.17), minimizing the super-plasticizer dosage (and consequently increasing the paste volume to keep adequate fresh

Table 7.14.: SCC mix proportions, estimated test results for the target and changed mixtures (±5 and 10 l/m^3 of water) and computed robustness measures, for the mixtures obtained with optimization criteria A

Mixture parameters															
X_1: w/c	0 ,50					0,45					0,40				
X_2:Sp/p	1,39%					1,45%					2,13%				
X_3:V_w/V_p	0,751					0,752					0,807				
X_4:V_s/V_m	0,436					0,430					0,455				
X_5: s_1/s	0,426					0,494					0,446				
X_6: $V_g/V_{g,lim}$	0,536					0,515					0,518				
Constituent materials (kg/m^3)															
cement	329,0					376,1					419,8				
limestone filler	302,4					276,5					192,8				
water	168,9					172,6					168,6				
superpl. (V3000)	8,79					9,46					13,07				
sand 1	321,2					373,0					356,6				
sand 2	433,1					382,2					442,1				
coarse agg.	772,7					742,5					746,5				
Cost of materials (€/m^3)	51,6					54,2					57,4				
Sensitivity to variation in water content															
Added water (l/m^3)	+10	+5	0	-5	-10	+10	+5	0	-5	-10	+10	+5	0	-5	-10
Y_1: Dflow (mm)	801	760	680	666	613	754	727	680	664	628	787	738	680	630	570
Y_2: Tfunnel (s)	6,1	7,2	10,0	10,7	13,4	6,5	7,6	10,0	11,0	13,6	6,8	8,1	10,0	12,0	15,2
Y_3: H2/H1	0,88	0,88	0,83	0,81	0,75	0,90	0,88	0,83	0,80	0,73	0,92	0,89	0,83	0,77	0,67
Y_4: fc,28 (MPa)	43,7	43,4	45,0	45,2	47,3	47,7	47,5	48,8	49,3	51,4	61,8	59,2	57,4	56,6	56,7
LABEST/FEUP methodology															
	p_1	p_2	p_3	p_4	p	p_1	p_2	p_3	p_4	p	p_1	p_2	p_3	p_4	p
robustness	0,83	0,99	0,86	1,00	**0,71**	0,86	0,99	0,88	1,00	**0,75**	0,80	0,99	0,92	1,00	**0,73**
percentile 2,5%	0,75	0,97	0,79	0,99	0,62	0,80	0,98	0,81	0,99	0,66	0,72	0,97	0,87	0,98	0,64
percentile 97,5%	0,90	1,00	0,92	1,00	0,79	0,93	1,00	0,94	1,00	0,83	0,88	1,00	0,97	1,00	0,82

Table 7.15.: SCC mix proportions, estimated test results for the target and changed mixtures (±5 and 10 l/m^3 of water) and computed robustness measures, for the mixtures obtained with optimization criteria B

Mixture parameters															
X_1: w/c	0,50					0,45					0,40				
X_2:Sp/p	1,36%					1,39%					1,51%				
X_3:V_w/V_p	0,707					0,712					0,734				
X_4:V_s/V_m	0,420					0,407					0,410				
X_5: s_1/s	0,452					0,504					0,489				
X_6: $V_g/V_{g,lim}$	0,510					0,516					0,506				
Constituent materials (kg/m^3)															
cement	333,7					378,7					435,2				
limestone filler	344,2					313,5					257,7				
water	170,4					173,5					176,4				
superpl. (V3000)	9,24					9,60					10,47				
sand 1	335,0					359,9					354,2				
sand 2	406,0					353,7					370,7				
coarse agg.	735,3					744,1					729,3				
Cost of materials (€/m^3)	53,0					55,1					57,9				
Sensitivity to variation in water content															
Added water (l/m^3)	+10	+5	0	-5	-10	+10	+5	0	-5	-10	+10	+5	0	-5	-10
Y_1: Dflow (mm)	758	730	680	665	628	718	705	680	670	648	721	706	680	666	642
Y_2: Tfunnel (s)	6,5	7,6	10,0	10,9	13,5	6,6	7,7	10,0	11,0	13,5	6,8	7,9	9,9	11,1	13,6
Y_3: H2/H1	0,95	0,94	0,91	0,89	0,84	0,91	0,90	0,87	0,85	0,79	0,90	0,88	0,83	0,80	0,73
Y_4: fc,28 (MPa)	39,5	41,2	45,5	46,6	50,4	44,1	45,7	49,6	50,9	54,6	51,0	51,8	54,0	55,4	58,2
LABEST/FEUP methodology															
	p_1	p_2	p_3	p_4	p	p_1	p_2	p_3	p_4	p	p_1	p_2	p_3	p_4	p
robustness	0,86	0,99	1,00	1,00	**0,85**	0,88	0,99	0,98	1,00	**0,86**	0,88	0,99	0,88	1,00	**0,77**
percentile 2,5%	0,78	0,97	0,99	0,98	0,77	0,82	0,97	0,96	0,98	0,79	0,81	0,97	0,82	0,99	0,68
percentile 97,5%	0,92	1,00	1,00	1,00	0,92	0,94	1,00	1,00	1,00	0,92	0,94	1,00	0,94	1,00	0,85

Table 7.16.: SCC mix proportions, estimated test results for the target and changed mixtures (±5 and 10 l/m^3 of water) and computed robustness measures, for the mixtures obtained with optimization criteria C

Mixture parameters															
X_1: w/c	0,50					0,45					0,40				
X_2:Sp/p	1,38%					1,44%					1,59%				
X_3:V_w/V_p	0,743					0,737					0,746				
X_4:V_s/V_m	0,427					0,420					0,421				
X_5: s_1/s	0,416					0,458					0,478				
X_6: $V_g/V_{g,lim}$	0,550					0,528					0,510				
Constituent materials (kg/m^3)															
cement	328,8					374,7					429,5				
limestone filler	307,9					288,1					244,4				
water	168,9					172,1					174,0				
superpl. (V3000)	8,79					9,55					10,72				
sand 1	303,9					333,8					354,3				
sand 2	426,1					395,5					387,6				
coarse agg.	793,0					761,8					735,8				
Cost of materials (€/m^3)	51,7					54,4					57,5				
Sensitivity to variation in water content															
Added water (l/m^3)	+10	+5	0	-5	-10	+10	+5	0	-5	-10	+10	+5	0	-5	-10
Y_1: Dflow (mm)	792	754	680	668	619	754	728	680	665	629	746	723	687	667	634
Y_2: Tfunnel (s)	6,1	7,2	10,0	10,7	13,4	6,4	7,6	10,0	10,9	13,6	6,8	8,0	10,1	11,5	14,1
Y_3: H2/H1	0,86	0,86	0,83	0,81	0,76	0,89	0,88	0,83	0,81	0,74	0,91	0,89	0,83	0,79	0,72
Y_4: fc,28 (MPa)	44,2	44,2	46,5	46,7	49,2	47,5	48,0	50,3	51,1	53,8	53,8	54,0	55,6	56,6	59,0
LABEST/FEUP methodology															
	p_1	p_2	p_3	p_4	p	p_1	p_2	p_3	p_4	p	p_1	p_2	p_3	p_4	p
robustness	0,84	0,99	0,83	1,00	**0,69**	0,86	0,99	0,86	1,00	**0,73**	0,80	0,99	0,90	1,00	**0,71**
percentile 2,5%	0,77	0,97	0,75	0,99	0,60	0,79	0,97	0,79	0,99	0,65	0,72	0,98	0,83	0,99	0,63
percentile 97,5%	0,91	1,00	0,90	1,00	0,78	0,93	1,00	0,92	1,00	0,82	0,88	1,00	0,95	1,00	0,80

Table 7.17.: SCC mix proportions, estimated test results for the target and changed mixtures (±5 and 10 l/m^3 of water) and computed robustness measures, for the mixtures obtained with optimization criteria D

Mixture parameters															
X_1: w/c	0,50					0,45					0,40				
X_2:Sp/p	1,38%					1,44%					2,14%				
X_3:V_w/V_p	0,734					0,722					0,800				
X_4:V_s/V_m	0,418					0,410					0,452				
X_5: s_1/s	0,404					0,435					0,450				
X_6: $V_g/V_{g,lim}$	0,559					0,536					0,527				
Constituent materials (kg/m^3)															
cement	328,7					374,1					417,2				
limestone filler	315,8					300,3					196,6				
water	168,8					171,8					167,7				
superpl. (V3000)	8,92					9,69					13,12				
sand 1	287,3					308,1					354,0				
sand 2	423,6					400,6					432,8				
coarse agg.	805,7					772,9					759,7				
Cost of materials (€/m^3)	51,9					54,7					57,4				
Sensitivity to variation in water content															
Added water (l/m^3)	+10	+5	0	-5	-10	+10	+5	0	-5	-10	+10	+5	0	-5	-10
Y_1: Dflow (mm)	784	749	680	668	623	749	724	680	666	631	784	738	681	633	576
Y_2: Tfunnel (s)	6,1	7,2	10,0	10,7	13,4	6,5	7,6	10,0	11,0	13,6	6,9	8,2	10,2	12,4	15,7
Y_3: H2/H1	0,85	0,85	0,83	0,81	0,77	0,88	0,87	0,83	0,81	0,75	0,92	0,89	0,83	0,77	0,67
Y_4: fc,28 (MPa)	44,2	44,8	47,8	48,2	51,0	47,0	48,1	51,5	52,5	55,8	61,2	59,0	57,5	57,0	57,4
LABEST/FEUP methodology															
	p_1	p_2	p_3	p_4	p	p_1	p_2	p_3	p_4	p	p_1	p_2	p_3	p_4	p
robustness	0,85	0,99	0,82	1,00	**0,69**	0,86	0,99	0,85	1,00	**0,73**	0,80	0,99	0,91	1,00	**0,72**
percentile 2,5%	0,77	0,97	0,74	0,99	0,60	0,79	0,97	0,78	0,98	0,64	0,72	0,98	0,86	0,98	0,63
percentile 97,5%	0,92	1,00	0,89	1,00	0,78	0,93	1,00	0,91	1,00	0,81	0,88	1,00	0,96	1,00	0,81

Table 7.18.: SCC mix proportions, estimated test results for the target and changed mixtures (±5 and 10 l/m^3 of water) and computed robustness measures, for the mixtures obtained with optimization criteria E

Mixture parameters															
X_1: w/c	0,50					0,45					0,40				
X_2:Sp/p	1,38%					1,45%					1,61%				
X_3:V_w/V_p	0,748					0,744					0,760				
X_4:V_s/V_m	0,432					0,425					0,428				
X_5: s_1/s	0,422					0,476					0,484				
X_6: $V_g/V_{g,lim}$	0,543					0,525					0,507				
Constituent materials (kg/m^3)															
cement	328,9					374,3					430,2				
limestone filler	304,1					282,4					233,0				
water	168,9					171,9					174,4				
superpl. (V3000)	8,76					9,50					10,67				
sand 1	313,9					352,1					365,5				
sand 2	429,1					387,7					389,7				
coarse agg.	783,0					756,6					731,5				
Cost of materials (€/m^3)	51,6					54,2					57,3				
Sensitivity to variation in water content															
Added water (l/m^3)	+10	+5	0	-5	-10	+10	+5	0	-5	-10	+10	+5	0	-5	-10
Y_1: Dflow (mm)	797	757	680	667	616	754	727	680	665	628	751	725	685	664	629
Y_2: Tfunnel (s)	6,1	7,2	10,0	10,7	13,4	6,5	7,6	10,1	11,1	13,7	6,7	7,9	10,0	11,3	13,9
Y_3: H2/H1	0,87	0,87	0,83	0,81	0,75	0,90	0,88	0,83	0,80	0,74	0,92	0,89	0,83	0,79	0,71
Y_4: fc,28 (MPa)	44,0	43,9	45,7	45,9	48,1	47,7	47,9	49,8	50,5	52,9	55,0	54,5	55,3	55,9	57,8
LABEST/FEUP methodology															
	p_1	p_2	p_3	p_4	p	p_1	p_2	p_3	p_4	p	p_1	p_2	p_3	p_4	p
robustness	0,84	0,99	0,84	1,00	**0,70**	0,86	0,99	0,87	1,00	**0,75**	0,81	0,99	0,90	1,00	**0,73**
percentile 2,5%	0,76	0,97	0,77	0,99	0,61	0,79	0,98	0,80	0,99	0,66	0,73	0,97	0,84	0,99	0,64
percentile 97,5%	0,91	1,00	0,91	1,00	0,78	0,93	1,00	0,93	1,00	0,83	0,89	1,00	0,95	1,00	0,81

Table 7.19.: SCC mix proportions, estimated test results for the target and changed mixtures (±5 and 10 l/m^3 of water) and computed robustness measures, for the mixtures obtained with optimization criteria F

Mixture parameters															
X_1: w/c	0,50					0,45					0,40				
X_2:Sp/p	1,42%					1,46%					1,97%				
X_3:V_w/V_p	0,756					0,757					0,794				
X_4:V_s/V_m	0,445					0,434					0,455				
X_5: s_1/s	0,442					0,511					0,487				
X_6: $V_g/V_{g,lim}$	0,515					0,507					0,498				
Constituent materials (kg/m^3)															
cement	330,2					377,1					422,7				
limestone filler	299,6					273,3					203,1				
water	169,1					172,9					170,1				
superpl. (V3000)	8,92					9,47					12,34				
sand 1	345,5					391,4					394,3				
sand 2	437,0					375,0					415,5				
coarse agg.	743,6					731,6					718,3				
Cost of materials (€/m^3)	51,8					54,2					57,3				
Sensitivity to variation in water content															
Added water (l/m^3)	+10	+5	0	-5	-10	+10	+5	0	-5	-10	+10	+5	0	-5	-10
Y_1: Dflow (mm)	805	761	680	662	607	752	726	680	664	628	773	732	680	639	586
Y_2: Tfunnel (s)	6,2	7,3	10,0	10,8	13,5	6,5	7,6	10,0	11,0	13,6	7,0	8,3	10,2	12,1	15,2
Y_3: H2/H1	0,90	0,88	0,83	0,81	0,74	0,91	0,89	0,83	0,80	0,73	0,94	0,90	0,83	0,76	0,66
Y_4: fc,28 (MPa)	42,8	42,2	43,3	43,5	45,3	47,6	47,2	48,2	48,6	50,5	60,0	58,0	56,7	56,4	56,9
LABEST/FEUP methodology															
	p_1	p_2	p_3	p_4	p	p_1	p_2	p_3	p_4	p	p_1	p_2	p_3	p_4	p
robustness	0,82	0,99	0,86	1,00	**0,70**	0,86	0,99	0,88	1,00	**0,76**	0,82	1,00	0,92	1,00	**0,75**
percentile 2,5%	0,75	0,97	0,79	0,99	0,61	0,79	0,97	0,82	0,99	0,67	0,74	0,98	0,87	0,98	0,66
percentile 97,5%	0,89	1,00	0,93	1,00	0,79	0,93	1,00	0,94	1,00	0,84	0,89	1,00	0,97	1,00	0,83

Table 7.20.: Cost of materials

Cement (CEM II/A-L 42,5R)	69 €/ton
Limestone filler	30 €/ton
Superplasticizer	0,6 €/kg
Sand 1 (natural)	10 €/ton
Sand 2 (natural)	12 €/ton
Coarse aggregate	9 €/ton

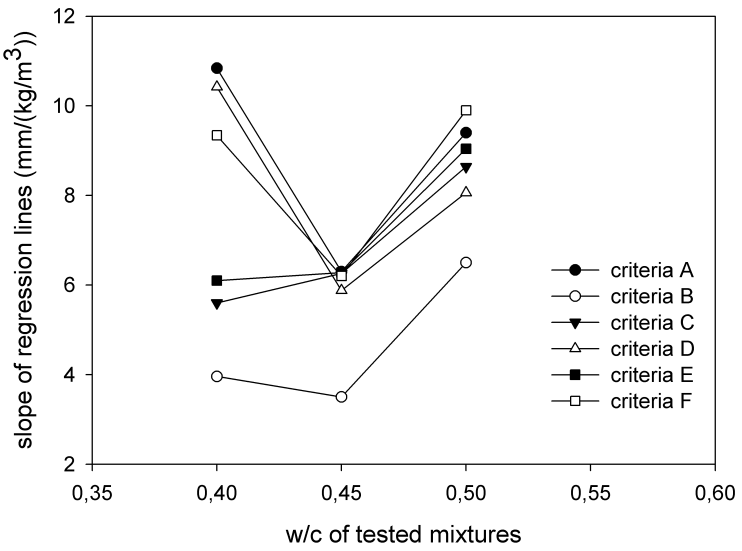


Figure 7.16.: Slope of regression lines of change in slump-flow against variation of water content

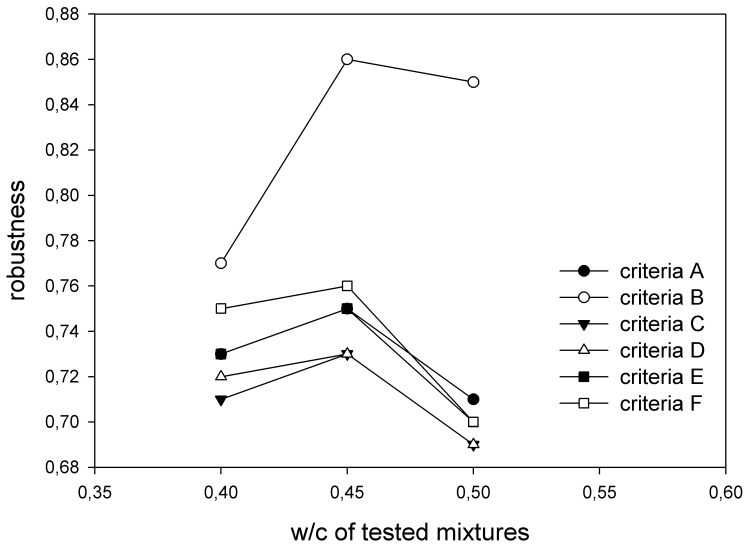


Figure 7.17.: Robustness estimates of SCC mixes

properties) seems to be the most effective optimization criteria to enhance robustness of SCC mixtures. Therefore, after selecting the w/c ratio, based on strength requirements, SCC mix obtained with criteria B should be selected when produced at Maprel precast factory. In spite of both methodologies having led to the same conclusion, no strong correlation was found between the robustness measure (FEUP/LABEST methodology) and the sensitivity to variation in water content (see Figure 7.18). The corresponding Spearman's correlation coefficient was 0,488 (significant at the 0,05 level (two-tailed)).

7.8. Concluding remarks

In this chapter the importance of a robust SCC mixture for the successful introduction of SCC in concrete industry was highlighted. The strategies to increase robustness and the existing methodologies to assess SCC mixtures' robustness were presented and discussed and a new methodology was suggested.

As it was found in the studies carried out at mortar level (see Chapter 5), an experimental plan conducted according to a factorial design is useful to establish numerical models relating mixture parameters with the SCC properties of interest. The mixture parameters considered in the Japanese-method can be used as factors in the factorial design to characterize the behaviour of SCC mixtures. Data collected during the experimental plan can be used to establish numerical models relating mixture parameters with the SCC properties of interest. Nevertheless, when a large number of variables is included in the experimental plan the range of response results is expected to increase, as well as the probability of finding unsatisfactory mixtures or outliers.

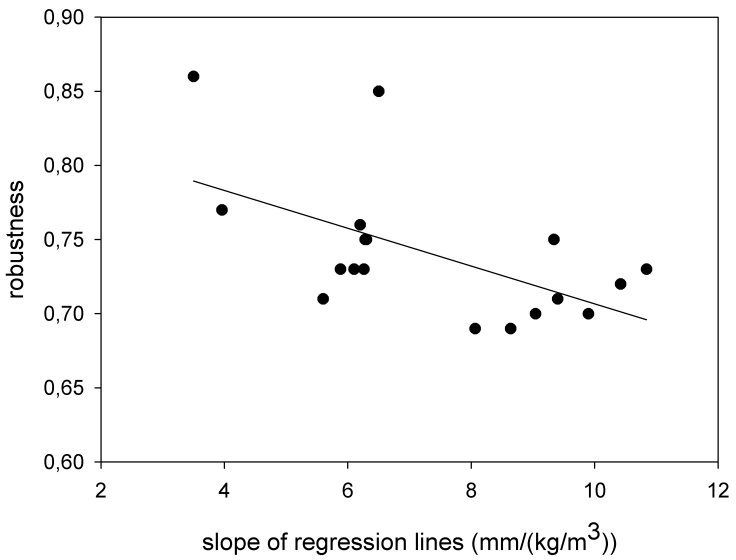


Figure 7.18.: Relation between robustness measure and slope of regression lines

Numerical simulations can replace trial batches in estimating the variability of each SCC mixture to changes only in water content, as recommended in "The European Guidelines for Self-compacting Concrete". Or, as suggested by LABEST/FEUP methodology, using data of typical material weight deviations inherent to the production process, variations of SCC target mix composition can be simulated, the derived numerical models can be applied to estimate SCC concrete properties and a measure of SCC robustness can be obtained. Applying the bootstrap technique to the original data sample, the robustness value can be accurately estimated and the accuracy of this estimate can be assessed. The number and type of selected independent variables and relevant concrete properties to be analyzed, as well as the respective acceptance limits affect the final value of robustness. The methodology presented in this work is particularly useful to evaluate and compare robustness of different SCC mixtures and to assist the concrete producer in selecting mixes.

SCC mixtures exhibiting similar fresh state properties, compressive strength and cost of materials, per m^3, were distinguished in terms of robustness. Minimizing the superplasticizer dosage, and consequently increasing the paste volume to keep adequate fresh properties, was found to be the most effective optimization criteria to enhance robustness of SCC mixtures under the conditions described in this study. A more robust SCC enables the concrete supplier to provide better consistency in delivering SCC, reduces the need to test and/or adjust each batch, minimizes extra costs with quality control and contributes to a successful implementation of SCC at the production centre.

8. Conclusions and future perspectives

8.1. Conclusions

The present PhD research project has been oriented mainly towards obtaining more robust SCC mixtures. The most critical factors for SCC robustness are mix-proportioning and SCC sensitivity to constituent materials production and mix-proportions variations. The present thesis summarises the various studies carried out at paste, mortar and concrete levels; and provides scientific design tools to obtain an optimized SCC. A methodology was developed to compute a robustness measure based on data of typical materials weight deviations inherent to the production process at a specific production centre. This methodology is particularly useful to evaluate and compare robustness of different SCC mixtures and to assist the concrete producer in selecting mixes. Concerning sensitivity to constituent materials' production, the influence of different production dates of cement on fresh and hardened properties of mortar/paste mixes and the influence of cement-superplasticizer interactions was discussed. A more robust SCC enables the concrete supplier to provide better consistency in delivering SCC, reduces the need to test and/or adjust each batch, minimizes extra costs with quality control and contributes to a successful implementation of SCC at the production centre.

From the experimental studies and result analyses the following conclusions can be drawn:

Mix-design method and mix-proportions

- An experimental plan conducted according to a central composite design is useful to evaluate the effects of mixture parameters and their interactions on SCC paste/mortar/concrete properties while reducing the number of trial batches needed to achieve balance among mixture variables.
- The mixture variables considered in the Japanese-method can be used as factors in the factorial design to characterize the behaviour of SCC paste/mortar/concrete mixtures.

- Data collected during the experimental plan can be used to establish numerical models relating mixture parameters with the SCC properties of interest. Nevertheless, when a large number of variables is included in the experimental plan, the range of response results is expected to increase, as well as the probability of finding unsatisfactory mixtures or outliers.
- For a given combination of cement + addition + superplasticizer, in general, a large number of mortar solutions can be found that lead to a spread flow of 260 mm and a flow time of 10 s, in a wide range of w/c ratio and fine aggregate content. The number of solutions that were found depends on the interaction between constituent materials but also on the selected range of mixture parameters for the experimental plan.
- Each type of cement has unique properties (physical and chemical) that will interact with other constituents, especially additions and admixtures, which reflect on the range of mixture levels of optimized mortar/concrete mixtures. Contour plots and interaction diagrams were suggested to represent the range of mixture levels where optimum solutions can be found. Values lower than the typical range of V_w/V_p suggested in (BIBM et al., 2005) [0,85; 1,10], were found to be adequate for six Portuguese cement types tested in combination with superplasticizer (V3000) and limestone filler.
- Information from the contour plots or interaction diagrams can simplify the test protocol required to optimize a given SCC mixture, namely, to select the combination of powder materials with admixtures. In particular, they are useful to compare the efficiency of different admixtures (superplasticizers, viscosity agents, or combination of both) and alternative mineral additives.
- The target paste properties, for different fine aggregate contents, were defined in terms of both empirical test results and rheological parameters, linking mortar and paste properties that are adequate for SCC. Target paste properties are related to aggregate content. Mortars with higher fine aggregate content required more fluid pastes to be flowable, while mortars with lower fine aggregate content require more viscous pastes to be stable.
- It was found that optimized mortar mixtures with higher sand content will lead to SCC mixtures with higher total surface area of aggregates, i.e. richer in fine aggregate particles and lower paste contents. In general, this is of interest for both economic and material performance reasons.
- As expected, it was found that empirical test results correlate with the rheological parameters of pastes, namely, yield stress and plastic viscosity. Furthermore, existing models for predicting mini-slump flow diameter and flow time of pastes were

implemented and compared with experimental data. A reasonable approximation was found between measured and predicted values, but a better approximation could be expected if the same protocol to determine yield stress (mixing sequence, test equipment, tool geometry, testing sequence) had been followed.

- Variables considered in this work have by no means exhausted the range of factors that affect SCC properties. For example, changes in environmental conditions like temperature and humidity, evolution of properties with time, mixing energy and stress history until the time of application, incorporation of other additions or admixtures can significantly change mortar properties, in both fresh and hardened states.

Robustness of SCC mixtures

Sensitivity to cement variations

- Large deviations from target mortar workability properties can occur depending only on cement delivery (as occurred in the case of CEM II/B-L 32,5 N) or cement source (cement producer or production centre). Thus, cement variations and cement-superplasticizer interaction should be taken into account when discussing robustness of SCC mixtures.
- It is important to have an efficient quality control system to detect large deviations from the target and hence implement corrective actions in order to maintain results in conformity with performance requirements. However, standard tests on cement like setting time and water demand are not adequate because they do not incorporate admixtures and do not give any indication about cement-superplasticizer interaction. It was demonstrated that analysing cement mortars with equivalent composition to the concrete mixture is effective to detect workability variations and cement-superplasticizer compatibility problems. Effects of fine aggregate on test results were minimised by using standardised sand.
- Parameters from cement characterization are necessary for explaining variation of early age properties of SCC mixtures, namely: physical characteristics of cements, such as specific surface area; chemical characteristics of cements, such as their phase composition and the availability of quickly soluble SO_4^{2-} ions; morphology of cement grains, especially the amount of C_3A at their surface; quantity of soluble alkalis; quantity of clinker substituted by a mineral addition in a blended cement. In this study, the SO_3 and/or $(Na_2O)_{equivalent}$ contents of cement and the residue in 45 μm sieve were found to be associated to fluidity changes of SCC mortar/paste mixtures. Nevertheless, sometimes the quality information available from the cement supplier is not detailed enough.

Sensitivity to mix-proportions variations

- Using data of typical material weight deviations inherent to the production process, variations of SCC target mix composition can be simulated, the derived numerical models can be applied to estimate SCC concrete properties and a measure of SCC robustness can be obtained. The proposed measure represents the probability that a SCC mix verifies the fulfillment of the acceptance criteria.
- Applying the bootstrap technique to the original data sample, the robustness value can be accurately estimated and the accuracy of this estimate can be assessed.
- The number and type of selected independent variables and relevant concrete properties to be analyzed, as well as the respective acceptance limits, affect the final value of robustness.
- SCC mixtures exhibiting similar fresh state properties, compressive strength and cost of materials, per m^3, were distinguished in terms of robustness. Minimizing the superplasticizer dosage, and consequently increasing the paste volume to keep adequate fresh properties, was found to be the most effective optimization criteria to enhance robustness of SCC mixtures under the conditions described in the study presented in Chapter 7. In spite of both FEUP/LABEST and EFNARC methodologies' having led to this same conclusion, no strong correlation was found between robustness measure and sensitivity to variation in water content.

8.2. Future perspectives

Self-compacting concrete was a revolutionary step ahead in improving material quality and efficiency of the construction industry. In the next years, the European market share of SCC is expected to increase with the standardization of test methods, specifications and use of SCC depending on application types. Apart from these regulation considerations, the growth of the SCC market share depends much on the enhancement of SCC mixtures robustness, especially for in-situ applications. To that end the research described in this thesis can be extended by conducting the following additional research:

- To evaluate improvement of the robustness measure (obtained with the methodology described in Chapter 7) by the inclusion of different types of VAs, in combination-type SCC mixtures (i.e. moderately low water powder ratios and small dosages of VA).
- To evaluate robustness of VA-type SCC mixtures (i.e. high water powder ratios and a significant dosage of a VA) and compare it with that of powder-type and combination-type SCC mixtures.

- To evaluate improvement of the robustness measure by incorporation of other supplementary materials of high specific gravity and/or specific surface area.

Obviously, the incorporation of viscosity agents and other supplementary materials has also an impact on other SCC characteristics like cost, fluidity evolution with time, thixotropy, mechanical properties, deformational stability, microstructure and durability, which should also be investigated. In order to better characterize the effect of these products a segregation test should be carried out along with other SCC fresh state characterization tests.

In addition, further full-scale testing should be conducted to relate the robustness measure with the real number of failed mixtures at the production centre and to verify the LABEST/FEUP methodology with a wider range of materials and applications.

Concerning the mix design method, in a multi-scale approach, an extensive study was carried out at paste level (or mortar incorporating standardised sand) by using different cement types and deliveries. Similar research is needed with a wide range of aggregates to better understand their influence on the final SCC mix proportions, as well as fresh and hardened properties. Besides, it would be interesting to investigate the relation between packing density and SCC mixture robustness. Since target SCC-paste properties were defined in terms of both empirical test results and rheological parameters more benefit should be taken, in future, from the studies carried on the paste level, in particular, the rheological tests.

Bibliography

ACBM. Self consolidating concrete.A white paper by researchers at The Center of Advanced Cement Based Materials (ACBM). Technical report, University of Illinois, 2007.

ACM Centre. Measurement of properties of fresh self-compacting concrete. Final Report (EU Project G6RD-CT-2001-00580, "Testing-SCC"). Technical report, University of Paisley, 2005.

S. Addelman. Fractions of the 2n factorial experiments. *Technometrics*, 3(4):319–321, 1961.

P.-C. Aïtcin. Cements of yesterday and today. concrete of tomorrow. *Cement and Concrete Research*, 30(9):1349–1359, 2000.

P.-C. Aïtcin, S. Jiang, and B.-G. Kim. Cement/superplasticizer interaction. The case of polysulfonates. *Bulletin des Laboratoire des Ponts et Chaussées*, July-August(233): 89–99, 2001.

P. Banfill, D. Beaupré, F. Chapdelaine, F. d. Larrard, L. Nachbaur, T. Sedran, O. Wallevik, and J. E. Wallevik. Comparison of concrete rheometers. International tests at LCPC (Nantes, France) in October, 2000. Technical report, National Institute of Standards and Technology, 2000.

H. A. Barnes, J. F. Hutton, and K. Walters. *An introduction to rheology.* Rheology Series ; 3). Elsevier Science B. V., Amsterdam, 1989.

F. Bayramov, C. Tasdemir, and M. A. Tasdemir. Optimisation of steel fibre reinforced concretes by means of statistical response surface method. *Cement and Concrete Composites*, 26(6):665–675, 2004.

BIBM, CEMBUREAU, EFCA, EFNARC, and ERMCO. The European Guidelines for Self-compacting Concrete. Specification, Production and Use, 2005.

P. Billberg. Mix design model for self-compacting concrete. In *1st North American Conference on the Design and Use of Self-Consolidating Concrete*, pages 65–70, Illinois, North America, 2002. Center for Advanced Cement-based Materials.

P. Billberg. Form pressure generated by self-compacting concrete. In O. Wallevik and I. Nielsson, editors, *3rd International Symposium on Self-Compacting Concrete*, pages 271–280, Reykjavik, Iceland, 2003. RILEM publications S.A.R.L.

J. Björnström and S. Chandra. Effect of superplasticizers on the rheological properties of cements. *Materials and Structures*, 36(10):685–692, 2003.

Bohlin Instruments Ltd. *A basic introduction to rheology.* 1994.

Bohlin Instruments Ltd. *User manual for Bohlin rheometers.* 2004.

D. Bonen, Y. Deshpande, J. Olek, L. Shen, L. Struble, D. Lange, and K. Khayat. Robustness of self-consolidating concrete. In *5th RILEM International Symposium on Self-Compacting Concrete*, pages 33–42, Ghent, Belgium, 2007. RILEM.

G. E. P. Box, W. G. Hunter, and J. S. Hunter. *Statistics for experimenters. An introduction to design, data analysis, and model building.* Wiley Series in probability and mathematical statistics. John Wiley & Sons, New York, 1978.

V. K. Bui and D. Montgomery. Mixture proportioning method for self-compacting high performance concrete with minimum paste volume. In A. Skarendahl and O. Petersson, editors, *1st International Rilem Symposium on SCC*, R, pages 373–384, Stockholm, Sweden, 1999. Rilem publications S.A.R.L.

CEB. CEB-FIP model code 1990. Design code, 1998.

CEN. Eurocódigo 2. Projecto de estruturas de betão (NP ENV 1992-1-1): Parte 1-1. Regras gerais e regras para edifícios, 2004.

CEN. Execution of concrete structures (DRAFT prEN 13670), 2008.

CEN. Concrete: Part 9: Additional Rules for Self-compacting Concrete (SCC), 2007a.

CEN. Testing fresh concrete (DRAFT prEN 12350-12): Part 12: Self-compacting concrete - J-ring test, 2007b.

CEN. Testing fresh concrete (DRAFT prEN 12350-10): Part 10: Self-compacting concrete - L-box test, 2007c.

CEN. Testing fresh concrete (DRAFT prEN 12350-9): Part 9: Self-compacting concrete - V-funnel test, 2007d.

CEN. Testing fresh concrete (DRAFT prEN 12350-11): Part 11: Self-compacting concrete - sieve segregation test, 2007e.

CEN. Testing fresh concrete (DRAFT prEN 12350-8): Part 8: Self-compacting concrete - Slump-flow test, 2007f.

S. Chandra and J. Bjornstrom. Influence of cement and superplasticizers type and dosage on the fluidity of cement mortars-Part I. *Cement and Concrete Research*, 32 (10):1605–1611, 2002.

P.-K. Chang. An approach to optimizing mix design for properties of high-performance concrete. *Cement and Concrete Research*, 34(4):623–629, 2004.

R. Chhabra and J. Richardson. *Non-newtonian flow in the process industries. Fundamentals and engineering applications*. Butterworth-Heinemann, Oxford, 1999.

D. Chopin, F. de Larrard, and B. Cazacliu. Why do HPC and SCC require a longer mixing time? *Cement and Concrete Research*, 34(12):2237–2243, 2004.

Concrete Society. *Self-compacting concrete a review Concrete Society Technical Report nº 62*. Concrete Society, Camberley, Surrey, 2005.

P. Coussot, Q. D. Nguyen, H. T. Huynh, and D. Bonn. Viscosity bifurcation in thixotropic, yielding fluids. *J. Rheol.*, 46(3):573–589, 2002.

F. Cussigh. A set of European standards for SCC. In G. D. Schutter and V. Boel, editors, *5th International RILEM Symposium on Self-Compacting Concrete-SCC2007*, volume 1, pages 1041–1047, Ghent, Belgium, 2007. RILEM Publications S.A.R. L.

J. A. Daczko. A comparison of passing ability test methods for self-consolidating concrete. In O. Wallevik and I. Nielsson, editors, *3rd International Symposium on Self-Compacting Concrete*, pages 335–344, Reykjavik, Iceland, 2003. RILEM publications S.A.R.L.

F. de Larrard. *Concrete mixture proportioning. A scientific approach*. Modern concrete technology series. E & FN Spon, London, 1999.

F. de Larrard, F. Bosc, C. Catherine, and F. Deflorenne. The AFREM method for the mix-design of high performance concrete. *Materials and Structures*, 30(7):439–446, 1997.

N. C. Dias. *Betão auto-compactável branco*. Tese de mestrado, Faculdade de Ciências e Tecnologia da Universidade de Coimbra, Portugal, 2002.

P. Domone and C. Hsi-Wen. Testing of binders for high performance concrete. *Cement and Concrete Research*, 27(8):1141–1147, 1997.

P. L. Domone. Self-compacting concrete. An analysis of 11 years of case studies. *Cement and Concrete Composites*, 28(2):197–208, 2006.

P. L. Domone. A review of the hardened mechanical properties of self-compacting concrete. *Cement and Concrete Composites*, 29(1):1–12, 2007.

J. Dransfield. Admixtures for concrete, mortar and grout. In J. NEWMAN and B. S. CHOO, editors, *Advanced Concrete Technology: Constituent Materials*, volume 1. Elsevier, Oxford, 2003.

EFNARC. Specification and guidelines for self-compacting concrete, 2002.

B. Efron and R. J. Tibshirani. *An introduction to Bootstrap*. New York, 1993.

M. Emborg. Final Report of Task 8.1: Mixing and transport. Brite EuRam Project BRPR-CT96-0366. Technical report, Betongindustri AB, 2000-06-30 2000.

S. Erdogdu. Compatibility of superplasticizers with cements different in composition. *Cement and Concrete Research*, 30(5):767–773, 2000.

O. Esping. *Early age properties of self-compacting concrete. Effects of fine aggregate and limestone filler*. Phd thesis, Chalmers University of Technology, 2007.

C. Ferraris, F. d. Larrard, and N. Martys. Fresh concrete rheology. Recent developments. In S. Mindess and J. Skalny, editors, *Materials Science of Concrete VI*, pages 215–241, Westerville, OH, 2001a.

C. F. Ferraris. Measurement of the rheological properties of cement paste. A new approach. In J. G. Cabrera and R. R. Rivera Villareal, editors, *RILEM International Symposium on The Role of Admixtures in High Performance Concrete*, pages 333–342, Monterrey, 1999a. RILEM Publications S.A.R. L.

C. F. Ferraris. Measurment of the rheological properties of high performance concrete. State of the art report. *Journal of Research of the National Institute of Standards and Technology*, 104(5):461–478, 1999b.

C. F. Ferraris and F. d. Larrard. Testing and modelling of fresh concrete rheology. Technical report, National Institute of Standards and Technology Internal Report 6094, 1998.

C. F. Ferraris, K. H. Obla, and R. Hill. The influence of mineral admixtures on the rheology of cement paste and concrete. *Cement and Concrete Research*, 31(2):245–255, 2001b.

H. Figueiras. *Estudo e desenvolvimento experimental de composições de betão auto-compactável. Aferição das suas características mecânicas e durabilidade*. Tese de mestrado, Faculdade de Engenharia da Universidade do Porto, 2006.

Finland. Nordisk Innovations Center. Concrete, mortar and cement-based repair materials. Chloride migration coefficient from non-steady-state migration experiments (NT BUILD 492), 1999.

R. J. Flatt. *Interparticle forces and superplasticizers in cement suspensions*. Phd thesis, École Polytechnique Fédérale de Lausanne, 1999.

R. J. Flatt and Y. F. Houst. A simplified view on chemical effects perturbing the action of superplasticizers. *Cement and Concrete Research*, 31(8):1169–1176, 2001.

R. J. Flatt, D. Larosa, and N. Roussel. Linking yield stress measurements. Spread test versus Viskomat. *Cement and Concrete Research*, 36(1):99–109, 2006.

P. Gomes. *Optimization and characterization of high-strength self-compacting concrete*. Phd thesis, Universitat Politécnica de Catalunya, 2002.

A. Gram, A. Farhang, and J. Silfwerbrand. Computer-aided modelling and simulation of self-compacting concrete flow. In G. D. Schutter and V. Boel, editors, *5th International RILEM Symposium on Self-Compacting Concrete-SCC2007*, volume 1, pages 455–460, Ghent, Belgium, 2007. RILEM Publications S.A.R. L.

A. Griesser. *Cement-superplasticizer interactions at ambient temperatures. Rheology, phase composition, pore water and heat of hydrationof cementitious systems.* Phd thesis, Swiss Federal Institute of Technology, 2002.

S. Grünewald. *Performance-based design of self-compacting fibre reinforced concrete.* Phd thesis, Delft University of Technology, 2004.

S. Grünewald and J. C. Walraven. Viscosity agents in self-compacting concrete. A state-of-the-art. Technical report, Delft University of Technology, 2004.

S. Grünewald and J. C. Walraven. Self-compacting concrete with viscosity agents in the fresh state. Technical report, Delft University of Technology, 2005.

S. Grünewald and J. C. Walraven. Characteristics and influence of paste on the behaviour of self-compacting concrete in the fresh state. In G. D. Schutter and V. Boel, editors, *5th International RILEM Symposium on Self-Compacting Concrete-SCC2007*, volume 1, pages 137–142, Ghent, Belgium, 2007. RILEM Publications S.A.R. L.

R. F. Gunst and R. L. Mason. *Regression analysis and its application. A data-oriented approach.* Marcel Dekker, Inc., New York, 1980.

V. A. Hackley and C. F. Ferraris. Guide to rheological nomenclature for liquid-based particle systems. *National Institute of Standards and Technology, U.S. Department of Commerce*, Special Publication 946, 2001.

S. Hanehara and K. Yamada. Interaction between cement and chemical admixture from the point of cement hydration, absorption behaviour of admixture, and paste rheology. *Cement and Concrete Research*, 29(8):1159–1165, 1999.

P. C. Hewlett. *Lea's chemistry of cement and concrete.* Elsevier, Amsterdam [etc.], 4th ed edition, 2004.

Japan Society of Civil Engineers. Recommendation for construction of self-compacting concrete. In *International Workshop on SCC*, pages 417–437, Japan, 1998.

S. Jarny, N. Roussel, S. Rodts, F. Bertrand, R. Le Roy, and P. Coussot. Rheological behavior of cement pastes from MRI velocimetry. *Cement and Concrete Research*, 35 (10):1873–1881, 2005.

S. Jiang, B.-G. Kim, and P.-C. Aitcin. Importance of adequate soluble alkali content to ensure cement/superplasticizer compatibility. *Cement and Concrete Research*, 29(1): 71–78, 1999.

C. Jolicoeur and M.-A. Simard. Chemical admixture-cement interactions. Phenomenology and physico-chemical concepts. *Cement and Concrete Composites*, 20(2-3):87–101, 1998.

P. W. M. Jonh. Three-quarter replicates of 24 and 25 designs. *Biometrics*, 17(2): 319–321, 1961.

K. Juvas, A. Käppi, K. Salo, and E. Nordenswan. The effects of cement variations on concrete workability. *Nordic Concrete Research*, Publication 26, xxxx.

K. Khayat, A. Ghezal, and M. Hadriche. Factorial design model for proportioning self-consolidating concrete. *Materials and Structures*, 32(9):679–686, 1999a.

K. Khayat, C. HU, and H. Monty. Stability of self-consolidating concrete, advantages, and potential applications. In A. Skarendahl and O. Petersson, editors, *1st International Rilem Symposium on SCC*, pages 143–152, Stockholm, Sweden, 1999b. Rilem publications S.A.R.L.

K. Khayat, A. Ghezal, and M. Hadriche. Utility of statistical models in proportioning self-consolidating concrete. *Materials and Structures*, 33(5):338–344, 2000.

K. H. Khayat. Viscosity-enhancing admixtures for cement-based materials. An overview. *Cement and Concrete Composites*, 20(2-3):171–188, 1998.

K. H. Khayat, A. Ghezal, and M. S. Hadriche. Utility of statistical models in proportioning self-consolidating concrete. In A. Skarendahl and O. Petersson, editors, *1st International Rilem Symposium on SCC*, pages 345–360, Stockholm, Sweden, 1999c. Rilem publications S.A.R.L.

B.-G. Kim, S. Jiang, C. Jolicoeur, and P.-C. Aitcin. The adsorption behavior of PNS superplasticizer and its relation to fluidity of cement paste. *Cement and Concrete Research*, 30(6):887–893, 2000.

G. H. Kirby and J. A. Lewis. Comb polymer architecture affects on the rheological property evolution of concentrated cement suspensions. *Journal of the American Ceramic Society*, 87(9):1643–1652, 2004.

Y. Klug and K. Holschemacher. Comparison of the hardened properties of self compacting and normal vibrated concrete. In O. Wallevik and I. Nielsson, editors, *3rd International Symposium on Self-Compacting Concrete*, pages 596–605, Reykjavik, Iceland, 2003. RILEM publications S.A.R.L.

E. P. Koehler and D. W. Fowler. Aggregates in Self-Compacting Concrete - Final Report , ICAR Project 108. Aggregates in Self-Consolidating Concrete, 2007.

S. Kubens and O. Wallevik. Interaction of cement and admixtures. The influence of cement deliveries on rheological properties. In *16. iBausil*, Weimar, Germany, 2006.

M. Lachemi, K. M. A. Hossain, V. Lambros, P.-C. Nkinamubanzi, and N. Bouzoubaâ. Performance of new viscosity modifying admixtures in enhancing the rheological properties of cement paste. *Cement and Concrete Research*, 34:185–193, 2004.

R. Le Roy and N. Roussel. The marsh cone as a viscometer. Theoretical analysis and practical limits. *Materials and Structures*, 38(1):25–30, 2005.

A. Maeyama, K. Maruyama, T. Midorikawa, and N. Sakata. Characterization of powder for self-compacting concrete. In *International Workshop on Self-Compacting Concrete*, pages 191–200, Japan, 1998.

N. Martys and C. F. Ferraris. Simulation of SCC flow. In *1st North American Conference on the Design and Use of Self-Consolidating Concrete*, pages 21–26, Illinois, North America, 2002. Center for Advanced Cement-based Materials.

T. Midorikawa, G. I. Pelova, and J. C. Walraven. Application of "The water layer model" to self-compacting mortar with different size distribution of fine aggregate. In K. Ozawa and M. Ouchi, editors, *2nd International Symposium on SCC*, pages 237–246, Tokyo, Japan, 2001. COMS Engineering Corporation.

M. Modigell, K. Vasilic, W. Brameshuber, and S. Uebachs. Modelling and simulation of the behaviour of self-compacting concrete. In G. D. Schutter and V. Boel, editors, *5th International RILEM Symposium on Self-compacting Concrete- SCC2007*, volume 1, pages 387–392, Ghent, Belgium, 2007. RILEM Publications S.A.R.L.

G. Moir. Cements. In J. Newman and B. S. Choo, editors, *Advanced Concrete Technology: Constituent Materials*, volume 1. Elsevier, Oxford, 2003.

P. C. F. Møller, J. Mewis, and D. Bonn. Yield stress and thixotropy. On the difficulty of measuring yield stresses in practice. *Soft Matter*, 2:274–283, 2006.

D. C. Montgomery. *Design and analysis of experiments*. New York, 5th ed. edition, 2001.

L. Nachbaur, V. Waller, O. Hadda, and M. Vachon. Extension of concrete equivalent mortar (CEM) to self-compacting concrete. In S. P. Shah, editor, *2nd North American Conference on the Design and Use of Self-Consolidating (SCC) and the 4th International RILEM Symposium on Self-Compacting Concrete*, volume 2, pages 1235–1241, Chicago, 2005. Hanley Wood.

T. Nawa, T. Izumi, and Y. Edamatsu. State-of-the-art report on materials and design of self-compacting concrete. In *International Workshop on SCC*, pages 160–190, Japan, 1998.

M. Nehdi and J. Summer. Optimization of ternary cementitious mortar blends using factorial experimental plans. *Materials and Structures*, 35(8):495–503, 2002.

C. M. Neubauer, M. Yang, and H. M. Jennings. Interparticle potential and sedimentation behavior of cement suspensions. Effects of admixtures. *Advanced Cement Based Materials*, 8(1):17–27, 1998.

A. M. Neville. *Properties of concrete*. Harlow : Addinson Wesley Longman, 4th ed edition, 1995. Addison Wesley Longman LimitedEdinburgh GateHarlowEssex CM20 2JEEngland.

J. Newman and B. S. Choo. *Advanced concrete technology.Constituent materials*. Wiley, New York, 2003.

S. Nunes. *Betão auto-compactável. Tecnologia e propriedades*. Tese de mestrado, Faculdade de Engenharia da Universidade do Porto, 2001.

S. Nunes, J. Figueiras, and J. S. Coutinho. Experimental study and numerical modelling of self-compacting concrete. In J. Walraven, J. Blaauwendraad, T. Scarpas, and B. Snijder, editors, *5th International PhD Symposium in Civil Engineering*, volume 2, pages 857–865, Delft, The Netherlands, 2004. Hanley Wood.

S. Nunes, H. Figueiras, J. S. Coutinho, and J. Figueiras. Método para definição da composição de betão autocompactável. Self-compacting concrete mix-design method. *e-Mat - Revista de Ciência e Tecnologia de Materiais de Construção Civil*, 2(1):1–11, 2005a.

S. Nunes, H. Figueiras, J. S. Coutinho, and J. Figueiras. SCC implementation in the Portuguese industry. In S. P. Shah, editor, *The 2nd North American Conference on the Design and Use of Self-Consolidating (SCC) and the 4th International RILEM Symposium on Self-Compacting Concrete*, volume 2, pages 1165–1171, Chicago, 2005b. Hanley Wood.

S. Nunes, H. Figueiras, A. M. Proença, R. Magalhães, A. Leite, R. Santos, J. Sousa Coutinho, and J. Figueiras. Desenvolvimento de uma tecnologia robusta para o fabrico, transporte e aplicação do betão auto-compactável. Relatório final do projecto de investigação BACPOR. Technical report, LABEST/FEUP, Departamento de Engenharia Civil da Universidade do Porto, 2005c.

S. Nunes, H. Figueiras, P. Milheiro Oliveira, J. S. Coutinho, and J. Figueiras. A methodology to assess robustness of SCC mixtures. *Cement and Concrete Research*, 36(12): 2115–2122, 2006.

S. Nunes, S. Costa, P. Milheiro Oliveira, J. Sousa Coutinho, and J. Figueiras. Uma abordagem científica no dimensionamento de composições de betão para promover a sustentabilidade na construção. Relatório final do projecto de investigação POCTI/ECM/61649/2004. Technical report, LABEST/FEUP, Departamento de Engenharia Civil da Universidade do Porto, 2008.

S. B. Nunes, J. S. Coutinho, J. Sampaio, and J. A. Figueiras. Laboratory tests on SCC with portuguese materials. In K. Ozawa and M. Ouchi, editors, *2nd International Symposium on SCC*, pages 393–402, Tokyo, Japan, 2001. COMS Engineering Corporation.

G. Oehlert and P. Whitcomb. Small efficient equireplicated resolution v fractions of 2k designs and their application to central composite designs, 2002.

S. G. Oh, T. Noguchi, and F. Tomosawa. Toward mix design for rheology of self-compacting concrete. In A. S. Petersson and O., editors, *1st International Rilem Symposium on SCC*, pages 361–372, Stockholm, Sweden, 1999. Rilem publications S.A.R.L.

H. Okamura, K. Ozawa, and M. Ouchi. Self-compacting concrete. *Structural Concrete: Journal of FIB*, 1(1):3–17, 2000.

M. Oliveira. *Desenvolvimento de um betão auto-compactável sem fíler e económico*. Tese mestrado, Faculdade de Ciências e Tecnologia da Universidade de Coimbra, Portugal, 2003.

G. Ovarlez and N. Roussel. A physical model for the prediction of lateral stress exerted by self-compacting concrete on formwork. *Materials and Structures*, 39(2):269–279, 2006.

J. Pera, S. Husson, and B. Guilhot. Influence of finely ground limestone on cement hydration. *Cement and Concrete Composites*, 21(2):99–105, 1999.

O. Petersson and P. Billberg. Investigation on blocking of self-compacting concrete with different maximum aggregate size and use of viscosity agent instead of filler. In A. S. Petersson and O., editors, *1st International Rilem Symposium on SCC*, pages 333–344, Stockholm, Sweden, 1999. Rilem publications S.A.R.L.

O. Petersson, r. Skarendahl, and R. T. C. 174-SCC. *Self-compacting concrete.State-of-the-Art report*, volume 1 of *RILEM ; Report 23*. Cachan : RILEM Publications, France, 2001.

A. Phyfferoen and B. Lockwood. Biopolymers in self-compacting concrete. In *International Workshop on SCC*, pages 211–217, Japan, 1998.

J. Plank and C. Hirsch. Impact of zeta potential of early cement hydration phases on superplasticizer adsorption. *Cement and Concrete Research*, 37(4):537–542, 2007.

J. Plank and B. Sachsenhauser. Impact of molecular structure on zeta potential and adsorbed conformation of a-allyl-?-methoxypolyethylene glycol - maleic anhydride superplasticizers. *Journal of Advanced Concrete Technology*, 4(2):233–239, 2006.

J. Plank, H. Keller, P. R. Andres, and Z. Dai. Novel organo-mineral phases obtained

by intercalation of maleic anhydride-allyl ether copolymers into layered calcium aluminum hydrates. *Inorganica Chimica Acta*, 359(15):4901–4908, 2006.

Portugal. IPQ. Cimento : NP EN 197-1 2001. Parte 1, Composição, especificações e critérios de conformidade para cimentos correntes, 2001.

Portugal. IPQ. Caldas de injecção para armaduras de pré-esforço métodos de ensaio NP EN 445 2000, 2002.

Portugal. IPQ. Ensaios do betão endurecido NP EN 12390-4: 2003 Parte 4 resitência a compressão, 2003a.

Portugal. IPQ. Ensaios do betão endurecido NP EN 12390-6: 2003 Parte 6 resitência a tracção por compressão de provetes, 2003b.

Portugal. IPQ. Ensaios das propriedades mecânicas e físicas dos agregados NP EN 1097-6 2003 Parte 6 determinação da massa volúmica e da absorção de água, 2004.

Portugal. IPQ. Métodos de ensaio de cimentos NP EN 196-1: 2006 Parte 1 determinação das resistências mecânicas, 2006.

Portugal. IPQ. Betão NP EN 206-1: 2007 Parte 1 especificação, desempenho, produção e conformidade, 2007.

Portugal. LNEC. Betões. Determinação do módulo de elasticidade em compressão, 1993a.

Portugal. LNEC. Betões. Determinação da fluência em compressão, 1993b.

Portugal. LNEC. Betões. Determinação do coeficiente de difusão dos cloretos por ensaio de migração em regime não estacionário, 2004.

Portugal.LNEC. Betões. Determinação da retracção e da expansão, 1993.

W. Prince, M. Espagne, and P. C. Aitcin. Ettringite formation. A crucial step in cement superplasticizer compatibility. *Cement and Concrete Research*, 33(5):635–641, 2003.

J. Punkki and V. Penttala. Water requirement of cement, W180. A practical test method. *Nordic Concrete Research*, Publication 27, xxxx.

J. Rigueira, E. G. Taengua, M. Bonilla, and P. Serna. A study on the robustness of a SCC dosage. In *Fédération Internationale du Béton. Proceedings of the 2nd International Congress*, Naples, Italy, 2006.

J. Rigueira, E. Taengua, and P. Serna. Robustness of SCC dosages and its implications on large-scale production. In G. D. Schutter and V. Boel, editors, *5th International RILEM Symposium on Self-Compacting Concrete-SCC2007*, volume 1, pages 95–101, Ghent, Belgium, 2007. RILEM Publications S.A.R. L.

RILEM TC 116-PCD. Test for gas permeablity of concrete. A. Preconditioning of concrete test specimens for the measurement of gas permeability and capillary absorption of water. *Materials and Structures*, 32(3):174–176, 1999a.

RILEM TC 116-PCD. Test for gas permeablity of concrete. C. Determination of the capillary absorption of water of hardened concrete. *Materials and Structures*, 32(3): 178–179, 1999b.

Rilem Technical Committee. Final report of RILEM TC 188-CSC 'Casting of self compacting concrete'. *Materials and Structures*, 39(10):937–954, 2006.

Rilem Technical Committee. Final report of RILEM TC 205-DSC: durability of self-compacting concrete. *Materials and Structures*, 41(2):225–233, 2008.

J. Roncero. *Effect of superplasticizer on the behavior of concrete in the fresh and hardened states. Implications for high performance concretes.* Phd thesis, Universitat Politécnica de Catalunya, 2000.

N. Roussel. Steady and transient flow behaviour of fresh cement pastes. *Cement and Concrete Research*, 35(9):1656–1664, 2005.

N. Roussel. A thixotropy model for fresh fluid concretes. Theory, validation and applications. *Cement and Concrete Research*, 36(10):1797–1806, 2006a.

N. Roussel. Correlation between Yield Stress and Slump. Comparison between numerical simulations and concrete rheometers results. *Materials and Structures*, 39(4):501–509, 2006b.

N. Roussel. A thixotropy model for fresh fluid concretes. Theory and applications. In G. D. Schutter and V. Boel, editors, *5th International RILEM Symposium on Self-compacting Concrete- SCC2007*, volume 1, pages 267–272, Ghent, Belgium, 2007. RILEM Publications S.A.R.L.

N. Roussel and P. Coussot. "Fifty-cent rheometer" for yield stress measurements. From slump to spreading flow. *Journal of Rheology*, 49(3), 2005.

N. Roussel and R. Le Roy. The marsh cone: a test or a rheological apparatus? *Cement and Concrete Research*, 35(5):823–830, 2005.

N. Roussel, C. Stefani, and R. Leroy. From mini-cone test to Abrams cone test. Measurement of cement-based materials yield stress using slump tests. *Cement and Concrete Research*, 35(5):817–822, 2005.

N. Roussel, M. R. Geiker, F. Dufour, L. N. Thrane, and P. Szabo. Computational modeling of concrete flow. General overview. *Cement and Concrete Research*, 37(9): 1298–1307, 2007.

A. W. Saak. *Characterization and modelling of the rheology of cement paste. With applications toward self-flowing materials.* Phd thesis, Northwestern University, 2000.

A. W. Saak, H. M. Jennings, and S. P. Shah. A generalized approach for the determination of yield stress by slump and slump flow. *Cement and Concrete Research*, 34 (3):363–371, 2004.

E. Sakai, K. Yamada, and A. Ohta. Molecular structure and dispersion-adsorption mechanisms of comb-type superplasticizers used in Japan. *Journal of Advanced Concrete Technology*, 1(1):16–25, 2003.

A. Schwartzentruber and C. Catherine. La méthode du mortier de béton équivalent (MBE). Un nouvel outil d'aide à la formulation des bétons adjuvantés. *Materials and Structures*, 33(8):475–482, 2000.

L. D. Schwartzentruber, R. Le Roy, and J. Cordin. Rheological behaviour of fresh cement pastes formulated from a Self Compacting Concrete (SCC). *Cement and Concrete Research*, 36(7):1203–1213, 2006.

T. Sedran. *Rheologie et rheometrie des betons. Application aux betons autonivelans.* Phd thesis, Laboratoire Central des Ponts et Chaussées, 1999.

T. Sedran and F. de Larrard. Optimization of self-compacting concrete thanks to packing model. In A. Skarendahl and O. Petersson, editors, *1st International Rilem Symposium on SCC*, pages 321–332, Stockholm, Sweden, 1999. Rilem publications S.A.R.L.

T. Shindoh and Y. Matsuoka. Development of combination-type self-compacting concrete and evaluation test methods. *Journal of Advanced Concrete Technology*, 1(1): 26–36, 2003.

L. M. G. d. Silva. *Caracterização das propriedades termo-mecânicas do betão nas primeiras idades para aplicação estrutural.* Tese mestrado, Faculdade de Engenharia da Universidade do Porto, 2007.

S. Smeplass and E. Mortsell. The particle matrix model applied on SCC. In K. O. &. M. Ouchi, editor, *2nd International Symposium on SCC*, pages 267–276, Tokyo, Japan, 2001. COMS Engineering Corporation.

M. Sonebi, P. J. M. Bartos, W. Zhu, J. Gibbs, and A. Tamini. Final Report of Task 4. Properties of Hardened Concrete, Rational production and Improved Working Environment Trough Using Self Compacting Concrete. Brite Euram Project BRPR-CT96-0366, 2000.

M. Sonebi, L. Svermova, and P. Bartos. Statistical modelling of cement slurries for self-compacting SIFCON containing silica fume. *Materials and Structures*, 38(1):79–86, 2005.

M. Sonebi, S. Grünewald, and J. Walraven. Filling ability and passing ability of self-consolidating concrete. *ACI Materials Journal*, 104(2):162–170, 2007.

J. Sousa Coutinho. The combined benefits of CPF and RHA in improving the durability of concrete structures. *Cement and Concrete Composites*, 25(1):51–59, 2003.

J. Sousa Coutinho. *Melhoria da durabilidade dos betões por tratamento da cofragem*. 2005.

P. Sprent. *Applied nonparametric statistical methods*. London, 2nd ed. edition, 1993.

State-Ease Corporation. Design-expert software: Version 6 user´s guide, 2000.

L. Struble. Rheology. In Ramachandran and Beaudoin, editors, *Handbook of Analytical Techniques in Concrete Science and Technology*, pages 333–367. Noyes, Park Ridge NJ, 2001.

L. Struble and G.-K. Sun. Viscosity of Portland cement paste as a function of concentration. *Advanced Cement Based Materials*, 2:62–69, 1995.

L. Struble, R. Szecsy, W.-G. Lei, and G. K. Suun. Rheology of cement paste and concrete. *Cement, Concrete and Aggregates*, 20(2):269–277, 1998.

R. Szecsy. Integration and application of self-compacting concrete as a technology into other types of performance concrete. In S. P. Shah, editor, *The 2nd North American Conference on the Design and use of Self-compacting Concrete and the 4th International RILEM Symposium on Self-compacting Concrete*, volume 2, pages 1173–1177, Chicago, 2005. Hanley Wood.

K. Takada. *Influence of admixtures and mixing efficiency on the properties of self-compacting concrete. The birth of self-compacting concrete in the Netherlands*. Phd thesis, Delft University of Technology, 2004.

K. Takada, G. I. Pelova, and J. C. Walraven. Self-compacting concrete produced by Japanese method with Dutch materials. In *12th European Ready Mixed Concrete Congress*, volume 2, pages 775–785, Portugal, 1998.

P. Termkhajornkit and T. Nawa. The fluidity of fly ash-cement paste containing naphthalene sulfonate superplasticizer. *Cement and Concrete Research*, 34(6):1017–1024, 2004.

L. N. Thrane, C. Pade, P. Szabo, M. Geiker, and H. Stang. Simulation and verification of flow in test methods. In S. P. Shah, editor, *The 2nd North American Conference on the Design and Use of Self-Consolidating Concrete and the 4th International RILEM Symposium on Self-Compacting Concrete*, volume 1, pages 551–556, Chicago, 2005. Hanley Wood.

Z. Toutou, N. Roussel, C. Lanos, Y. Mélinge, P. Monnet, A. Pantet, and R. L. Roy. Rhéologie des suspensions à matrice cimentaire : approche expérimentale multi-échelle. *Revue Européenne de Génie Civil*, 9(3):309–320, 2005.

H. Uchikawa, D. Sawaki, and S. Hanehara. Influence of kind and added timing of organic admixture on the composition, structure and property of fresh cement paste. *Cement and Concrete Research*, 25(2):353–364, 1995.

H. Uchikawa, S. Hanehara, and D. Sawaki. A reply to the discussion by Susanta Chatterji of the paper "the role of steric repulsive force in the dispersion of cement particles in fresh paste prepared with organic admixture". *Cement and Concrete Research*, 27(9): 1453–1455, 1997a.

H. Uchikawa, S. Hanehara, and D. Sawaki. The role of steric repulsive force in the dispersion of cement particles in fresh paste prepared with organic admixture. *Cement and Concrete Research*, 27(1):37–50, 1997b.

M. Valcuende and C. Parra. Bond behaviour of reinforcement in self-compacting concretes. *Construction and Building Materials*, In Press, Corrected Proof.

H. Vikan. *Rheology and reactivity of cementitious binders with superplasticizers*. Phd thesis, Norwegian University of Science and Technology, 2005.

H. Vikan, H. Justnes, F. Winnefeld, and R. Figi. Correlating cement characteristics with rheology of paste. *Cement and Concrete Research*, 37(11):1502–1511, 2007.

F. v. Waarde, E. A. B. Koenders, J. A. L. a. Nijeholt, and J. C. Walraven. Theoretical and practical investigations on SCC formwork. In G. D. Schutter and V. Boel, editors, *5th International RILEM Symposium on Self-Compacting Concrete- SCC 2007*, volume 1, pages 417–422, Ghent, Belgium, 2007. RILEM Publications S.A.R.L.

J. E. Wallevik. *Rheology of particle suspensions. Fresh concrete, mortar and cement paste with various types of lignosulfonates*. Phd thesis, The Norwegian University of Science and Technology, 2003a.

O. Wallevik. Rheology of cement suspensions, 2003b.

O. H. Wallevik, S. Kubens, and F. Müller. Influence of cement-admixture interaction on the stability of production properties of SCC. In G. D. Schutter and V. Boel, editors, *5th International RILEM Symposium on Self-Compacting Concrete-SCC2007*, volume 1, pages 211–216, Ghent, Belgium, 2007. RILEM Publications S.A.R. L.

J. Walraven. Structural aspects of self compacting concrete. In O. Wallevik and I. Nielsson, editors, *3rd International Symposium on Self-Compacting Concrete*, pages 15–22, Reykjavik, Iceland, 2003. RILEM publications S.A.R.L.

J. Walraven. Self-compacting concrete. Challenge for designer and researcher. In S. P. Shah, editor, *The 2nd North American Conference on the Design and Use of Self-Consolidating (SCC) and the 4th International RILEM Symposium on Self-Compacting Concrete*, volume 1, pages 431–446, Chicago, 2005. Hanley Wood.

F. Winnefeld, S. Becker, J. Pakusch, and T. Gotz. Effects of the molecular architecture of comb-shaped superplasticizers on their performance in cementitious systems. *Cement and Concrete Composites*, 29(4):251–262, 2007.

A. Yahia and K. H. Khayat. Analytical models for estimating yield stress of high-performance pseudoplastic grout. *Cement and Concrete Research*, 31(5):731–738, 2001a.

A. Yahia and K. H. Khayat. Experiment design to evaluate interaction of high-range water-reducer and antiwashout admixture in high-performance cement grout. *Cement and Concrete Research*, 31(5):749–757, 2001b.

K. Yamada, T. Yanagisawa, and S. Hanehara. Influence of temperature on the dispersibility of polycarboxylate type superplasticizer for highly fluid concrete. In A. Skarendhal and O. Petersson, editors, *1st RILEM Symposium on Self-Compacting Concrete*, volume 1, pages 437–448, Stockholm, 1999. RILEM Publications.

K. Yamada, T. Takahashi, S. Hanehara, and M. Matsuhisa. Effects of the chemical structure on the properties of polycarboxylate-type superplasticizer. *Cement and Concrete Research*, 30(2):197–207, 2000.

K. Yamada, S. Ogawa, and S. Hanehara. Controlling of the adsorption and dispersing force of polycarboxylate-type superplasticizer by sulfate ion concentration in aqueous phase. *Cement and Concrete Research*, 31(3):375–383, 2001a.

K. Yamada, S. Ogawa, and T. Takahashi. Improvement of the compatibility between cement and superplasticizer by optimizing the chemical structure of the polycarboxylate-type superplasticizer. In K. Ozawa and M. Ouchi, editors, *2nd International Symposium on Self-Compacting Concrete*, volume 1, pages 159–168, Tokyo, 2001b. COMS Engineerin Corporation.

M. Yang, C. M. Neubauer, and H. M. Jennings. Interparticle potential and sedimentation behavior of cement suspensions. Review and results from paste. *Advanced Cement Based Materials*, 5(1):1–7, 1997.

K. Yoshioka, E. Sakai, M. Daimon, and A. Kitahara. Role of steric hindrance in the performance of superplasticizers for concrete. *Journal of the American Ceramic Society*, 80(10):2667–2671, 1997.

K. Yoshioka, E.-i. Tazawa, K. Kawai, and T. Enohata. Adsorption characteristics of superplasticizers on cement component minerals. *Cement and Concrete Research*, 32 (10):1507–1513, 2002.

H. Zhang. *Using dynamic rheology to explore the microstructure and stiffening of cementitious mixtures*. Phd thesis, University of Illinois, 2001.

T. Zhang, S. Shang, F. Yin, A. Aishah, A. Salmiah, and T. L. Ooi. Adsorptive behavior of surfactants on surface of Portland cement. *Cement and Concrete Research*, 31(7): 1009–1015, 2001.

W. Zhu and J. C. Gibbs. Use of different limestone and chalk powders in self-compacting concrete. *Cement and Concrete Research*, 35(8):1457–1462, 2005.

W. Zhu, J. Quinn, and P. J. M. Bartos. Transport properties and durability of self-compacting concrete. In K. Ozawa and M. Ouchi, editors, *2nd International Symposium on SCC*, pages 451–458, Tokyo, Japan, 2001. COMS Engineering Corporation.

A. Paper:"Full-scale testing with SCC in Portugal"

In the current appendix, a paper describing full-scale tests carried out within the research project BACPOR is included.

Industry-related research on modern concrete technology

Full-scale testing with SCC in Portugal

This paper discusses a research project "BACPOR", in direct co-operation with Portuguese industry, aimed to develop a robust technology to produce, transport and place self-compacting concrete using materials available in Portugal. Within "BACPOR" different SCC mixes were designed and completely characterized in the laboratory, and then applied to "in-situ" construction and the precast industry. The adequacy of actual current processes involved in production, mixing, transport and placing was evaluated throughout full-scale testing and the most critical issues were identified concerning implementation of this technology in the Portuguese construction industry.

Sandra Nunes, Helena Figueiras,
Joana Sousa Coutinho, Joaquim Figueiras,
LABEST, Portugal

With the disappearance of trans-national barriers and subsequent economic globalization, the construction companies must become more competitive, not only incorporating new technologies, but also by using new management methodologies that will enable an increase in productivity. In Portugal, specialized labour is becoming scarce and development of the SCC technology nationally will empower use of available workmanship, without impairing quality of the final product. It will also attract younger people to this sector who are looking for their first job.

Although SCC is the most probable substitute for conventional concrete a significant investment has to be made in terms of know-how, production procedures and quality control, and training of personnel for the sustained application of this emerging technology in Portugal. In this context, the Portuguese research project "BACPOR" was carried out in direct co-operation with local industry. This project comprised three main components: laboratory study, full-scale tests and pilot industrial applications, for both "in-situ" construction and precast industry. This paper will focus mainly on the full-scale testing results.

Why is SCC so interesting for the Portuguese industry?

There has been a growing interest on SCC technology among the main Portuguese constructors and the construction industry. The main reasons for this interest concern the placing of concrete in heavy reinforced areas of difficult access where quality of traditionally placed concrete is to a great extent dependent on the skill of workers. Furthermore, the use of this type of concrete should shorten the construction period, reduce manpower during placing, reduce damage on the surface of the construction, increase durability, improve working conditions and increase the freedom of structural and artistic design of concrete structures.

The precast industry is especially suited for the use of SCC. In precast factories, concrete elements with a complex geometric shape and dense reinforcement are often produced. The production of such elements using traditional vibrated concrete can only be executed with great effort; very strong external vibrators have to be mounted and in some cases casting has to be carried out in more than one step.

When consolidation is incomplete the resulting concrete elements with defects have to be repaired, causing further delay and increase in cost. Vibration has also harmful physical impact on workers.

SCC requires a reliable control of material characteristics, mixing process and transportation [1]. In a precast plant it is easier to install quality control systems because of the high degree of automation and repetition of similar processes. Besides, the production process is less influenced by weather conditions and transport time is shorter, therefore, retaining fluidity of fresh concrete is not a problem.

Co-operation with construction industry

The Portuguese research project "BACPOR" was carried out at the Faculty of Engineering, University of Porto (FEUP) in direct co-operation with local industry. Within this research project, many different SCC mixtures were designed and completely characterized in the laboratory; three of them were selected to carry out full-scale tests under actual conditions on site (**Table 1**). Performance requirements were established for each mix. Selected constituent materials for each industrial application are also presented in **Table 1**. These include both natural and crushed aggregates, calcareous and granitic aggregates, with different grading. Powder materials included different types of cement, limestone filler and fly ash. Superplasticizers available in the Portuguese market were also used. Selected constituent materials are representative of the most currently used materials by the Portuguese construction industry.
The full-scale tests were intended to evaluate adequacy of actual current production, mixing, transport and placing processes and to identify which changes had to be introduced. A large characterization of SCC properties both in the fresh and hardened state was carried out to evaluate technology robustness and to verify the fulfillment of performance criteria.

Precast industry application – beam element

SCC versus conventional concrete

The mix-design method used for this work was based on the Japanese SCC-design-

ing method and previous work carried out at FEUP. The numerous possible combinations of materials for SCC means that a large number of variables need to be adjusted (cement, mineral additions, superplasticisers, viscosity agents, aggregates). Their interaction is therefore often difficult to predict with sufficient accuracy. After the characterization of individual components, testing was carried out on the paste, mortar and concrete levels to optimize the mixture. This is described in detail in [2].

Slump-flow, V-funnel and Box tests were carried out to adjust the SCC mix proportions. The Slump-flow test is used to evaluate deformation capacity, viscosity and also resistance to segregation of SCC by visual observation. This test records the final slump flow diameter (D_{flow}) and the time necessary for concrete to reach a 50cm diameter (T_{50}). The V-funnel test is usec to assess viscosity and passing ability of SCC. This test records flow time (T_{funnel}). With the Box test it is possible to assess ability of concrete to pass through tight openings between reinforcing bars and filling ability. This test measures the filling height (H). Details of the equipment usec for testing fresh concrete and test procedures used can be found in [1], [3].

Final SCC mix proportions are presented in **Table 2** together with mix proportions of a conventional concrete used in the same precast application. The main differences between the SCC and the conventional concrete mix proportions are the coarse aggregate, powder materials and superplasticizer. These differences are responsible for the higher cost in materials. Based on fresh concrete test results (D_{flow} = 652 mm; T_{50} = 3.0 sec.; T_{funnel} = 9.7 sec.; H = 340 mm) this SCC mixture, producec under actual conditions in the "Maprel-Nelas" precast factory, exhibited good deformability and good segregation resistance without blocking.



Sandra Nunes, PhD candidate and Assistant of the Department of Civil Engineering, Faculty of Engineering, University of Porto (FEUP), where she obtained her MSc degree in 2002 on the subject of self-compacting concrete. Her scientific areas of interest are self-compacting concrete technology; modelling of concrete properties and concrete structures analysis

snunes@fe.up.pt



Helena Figueiras, MSc student of Civil Engineering, Faculty of Engineering, University of Porto (FEUP) where she obtained her graduation in Civil Engineering in 2003. Her scientific areas of interest are self-compacting concrete; concrete durability and health monitoring of structures.

helena.figueiras@fe.up.pt



Joana Sousa Coutinho, Assistant Professor of Civil Engineering, Faculty of Engineering, University of Porto (FEUP) where she obtained her PhD in Civil Eng. on durability of concrete. Prof. for Construction Materials since 1998 and New Materials since 2001. Member of COST 521 – Corrosion of steel in reinforced concrete structures, until 2002, presently member of CT104 – Concrete, CT 105 – cement, CT12 – Steel . Expert for CT154- Aggregates. Researcher in cement replacements such as RHA (rice husk ash), metakaolin, biomass ash. Researcher on different types of concrete and durability.

jcouti@fe.up.pt



Joaquim Figueiras, Full Professor of the Department of Civil Engineering, Faculty of Engineering, University of Porto (FEUP), Chair of Concrete Structures Courses; Director of Structural Laboratory (LABEST) of Faculty of Engineering. His scientific areas of interest are modelling of constitutive relationships for the non-linear analysis of structural concrete and advanced materials; experimental and numerical analysis of concrete structures; behaviour and design for structural rehabilitation and health monitoring of structures.

jafig@fe.up.pt

Characterization	Beam element	Box-culvert	Wall panel
Type of application	precast industry	precast industry	cast in-situ
Fluidity retention	----------	----------	at least, 1 hour
Strength class	C45/55	C45/55	C35/45
Initial strengths*	≥ 45MPa, at 36 hours	≥ 35 MPa, at 72 hours	≥ 36 MPa, at 48 hours
Constituent materials			
Cement	CEM I 52.5 R	CEM I 52.5 R	CEM I 42.5 R
Mineral addition	limestone filler	limestone filler	fly ash
Fine aggregate 1	natural sand	natural sand	natural sand
Fine aggregate 2	crushed granite	natural sand	crushed granite
Coarse aggregate	crushed granite	crushed limestone	crushed granite

Table 1:
Type of application, performance requirements and constituent materials

**Cube (150x150x150 mm³) compressive strength*

Constituent materials	SCC (kg/m³)	Conventional concrete (kg/m³)
Cement	380	380
Limestone filler	114	0
Sand 1	534	375
Sand 2	375	592
Coarse aggregate	704	832
Water	175	168
Superplasticizer (liquid)	9.9	6.0
Material cost	112%	100%

Table 2:
Mix proportions of SCC mixtures and conventional concrete

Table 3 shows the development of compressive strength, tensile splitting strength and Young's modulus for both the SCC mix and the conventional concrete. Water absorption by capillary tests and chloride migration tests were carried out to assess concrete durability, according to RILEM recommendations on permeability of concrete [4] and NT BUILD 492 [5], respectively. The compressive strength and tensile splitting strength of the examined SCC was generally higher compared to conventional concrete both of class C50/60. Young's modulus was lower for SCC, probably due to lower coarse aggregate content. SCC and conventional concrete showed similar resistance to fluid ingress, although conventional concrete has a lower water/cement ratio. This may be attributed to the improved cement dispersion caused by the superplasticizer.

Full scale testing was carried out in winter, at the "Maprel-Nelas" precast factory under normal working conditions. A 2.5m length beam element with highly dense reinforcement was selected for full-scale tests (**Figure 1**). In this factory no extra silo was available to store the limestone filler, therefore it had to be added manually to the mixer. Due to the existing formwork configuration, used for conventional concrete, casting was carried out in two steps, first the bottom part and then the sides, with a waiting period inbetween until the concrete set. This interruption of concrete supply resulted in a lift line on vertical surfaces as well as possible bonding problems between layers, as shown in **Figure 2**. The motor vehicle used to transport concrete from the mixer to the casting area included an endless screw which drove concrete upwards from the tank and then discharged it into the formwork.

This system is not the most adequate since concrete drops from a high distance and therefore air is entrapped during the fall. SCC filled up the entire mould surrounding the reinforcement, but in some parts a few air bubbles were visible.



Formwork system (on the left) and reinforcement of a beam element (on the right)

Type of test	Age (days)	SCC	Conventional concrete
Compressive strength*	1	27,9 MPa	-------
	4	51,8 MPa	-------
	7	54,8 MPa	53,2 MPa
	14	67,5 MPa	-------
	28	69,2 MPa	66,2 MPa
Compressive strength**	7	55,6 MPa	-------
	28	60,4 MPa	63,0 MPa
Tensile splitting strength**	7	4,3 MPa	3,7 MPa
	28	4,6 MPa	-------
Young's modulus**	7	32,9 GPa	32,3 GPa
	28	35,9 GPa	37,6 GPa
Water absorption by capillarity*	28	0,143 mm/$h^{0.5}$	0,170 mm/$h^{0.5}$
Apparent diffusion coefficient***	28	1,14x10^{-7} cm^2/s	1,37x10^{-7} cm^2/s

Table 3:
Mechanical properties and durability tests results (average values)

** tests on cubes (150x150x150 mm^3);*
*** tests on cylinders*
(diameter = 150 mm; height = 300 mm);
**** tests on drilled cores*
(diameter = 100 mm; height = 50 mm)



Lift line in the beam element cast with SCC

Precast industry application – box-culvert

Mix, transport and installation

As presented in **Table 1**, the objective of Project 2 was to design a SCC mix to be applied in the "Maprel-Rio Maior" precast industry. One of the elements selected for full scale testing was a box-culvert (length = 2.5 m; height =1.15 m; width = 2.32 m; wall thickness = 0.15 - 0.20 m) (**Figure 3**). To enable the drilling of cores from the box-culvert for further testing, three zones with no reinforcement were planned, one in the centre of each wall and the third on the slab, as shown in **Figure 3**. Similar elements were cast with both SCC and conventional concrete.



Reinforcement in the box-culvert selected for full-scale tests

Full scale testing was carried out in winter under normal working conditions. The paddle-mixer in the factory had a maximum capacity of two cubic metres. The mixing procedure used was the same as for conventional concrete but with increased mixing time. Considering the higher mixing efficiency at the factory compared to mixing in the laboratory and taking into account possible misestimates of aggregate moisture, the water content and superplasticizer dosage were both reduced so as to produce concrete less prone to segregation.

The motor vehicle used to transport concrete from the mixer to the casting area is shown in **Figure 4**. This system presented several limitations, the discharge height permitted was smaller than the elevation required for larger box-culvert moulds which are also handled in this factory. Conversely, if the mould is smaller, concrete drops from a high distance and air is entrapped during the fall. Another relevant limitation concerns the capacity of the tank which is smaller than the maximum capacity of the mixer. This can delay the production of SCC since no waiting period for vibration is required as for when using conventional concrete.



Motor-vehicle used to transport and cast concrete

Conventional concrete elements were externally vibrated and since vibration is non existent in the production of SCC elements work on site was far lighter and noise levels were reduced. The environment on site was improved considerably with the use of SCC leading to a very positive attitude among workers and engineers.

In-situ compressive strength

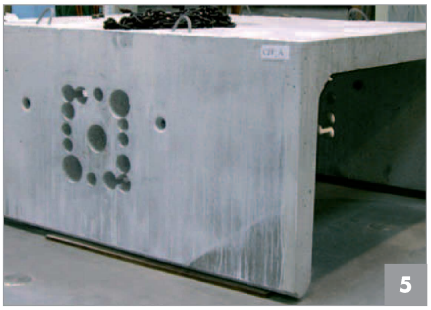
The in-situ compressive strength at about 60 days was obtained from cores drilled from different parts of the box-culverts such as the central areas of the walls and slab (**Figure 5**). Cores drilled from the walls were loaded perpendicular to the casting direction whereas slab cores were loaded parallel to casting direction. The diameter of these cores was 94 mm and

the height/diameter ratio (h/d) of cores varied between 1.58 and 1.72.

Core strength was converted to the strength of corresponding standard cylinders (d = 150mm; h = 300mm) using the relations presented by Mansur [6], depending on the level of strength ranging from 20 to 100 MPa. Converted values from the mean compressive strength as well as the specific gravity results for both SCC and conventional concrete box-culvert elements are presented in **Table 4**. Compressive strength and specific gravity results were consistent throughout the SCC box-culvert whereas for the conventional concrete box-culvert compressive strength and specific gravity decreased considerably in the slab. SCC therefore led to a more homogeneous and isotropic material along the box-culvert.

Concrete property	location	SCC	CONV
Compressive strength (MPa)	wall-A	67,8	67,3
	wall-B	69,7	66,3
	slab part	70,7	58,1
Specific gravity (kg/m³)	wall-A	2339	2380
	wall-B	2329	2346
	slab part	2305	2289

Table 4: Converted compressive strength of cores (60 days) and specific gravity



Box-culvert element and location of test cores in the lateral wall-A

In-situ industry application – wall panel

This full-scale test was performed during winter and the outdoor temperature at the "SCUT-IP5" construction site was around 11.5 °C. The mixing procedure was the same as for normal concrete but mixing time was increased for SCC. Formwork was prepared to cast three similar panels (**Figure 6**) with the following dimensions: height = 5 m; length = 1 m; thickness = 0.20 m.

The same SCC mix previously designed during the laboratory study phase was used. This mix when produced for full-scale testing at the construction site exhibited segregation with blocking of aggregates in the V-funnel and Box tests, immediately after mixing. The slump-flow diameter measured was 680mm. Variation of workability was observed during the whole



Casting of a panel using a skip (on the left); pumping SCC into a panel (on the right)

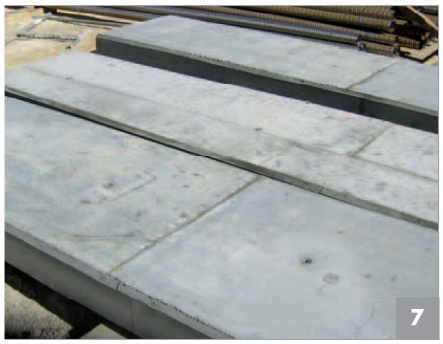
production chain. After 1 hour transportation to the casting site in a concrete truck, an increase of fluidity was observed, slump-flow diameter increased to 740 mm and a mortar rim around the spread was observed. Despite severe segregation this batch was used to cast two of the three panels. Before casting these SCC panels, a first panel had been cast with conventional vibrated concrete using a skip; this panel was completely filled within 15 minutes. Then a panel was cast with SCC discharged with a skip and the fill was completed within 8 minutes. Finally SCC was pumped into the third panel and only 2 minutes were necessary to completely fill this panel. SCC has a lower viscosity than conventional concrete, thus a greater flow rate when pumped. As a consequence, the measured pumping pressure was 20% lower, reducing wear and tear on the pumps.

Large differences in behavior were observed between the mixes when produced in the laboratory and on site. Possible causes for these differences were: efficiency of the mixing; consistency variations over time; materials weighing errors; mis-determinations for humidity content in the aggregates and variation of materials characteristics.

Also, the 19 mm coarse aggregate contained particles with a longer dimension in one direction (up to 40mm), low amounts of material was retained on the 2.36 mm sieve, and the high amounts of superplasticizer used may have made this mixture more prone to segregation.

As can be observed in **Figure 7** segregated SCC mixtures were experienced, however a good surface finish, without voids was achieved. Cores were drilled at different heights from each panel, with and without reinforcement. When comparing cores H3 and H1, in **Figure 8**, taken from the top and the bottom of the panel, respectively, different amounts of coarse aggregate can be observed which clearly confirms the occurrence of segregation. Based on the compressive strength and concrete density results of cores taken from the panels cast with both the skip and the pump, it was concluded that: segregation was more pronounced in the panel with pumped SCC. A significant reduction of strength and density was observed between the middle and the top of the panels and this difference was more pronounced when concrete was pumped.

No significant decrease of strength and concrete density was observed between the bottom and middle parts of the "skip" panel.



Finish of cast panels

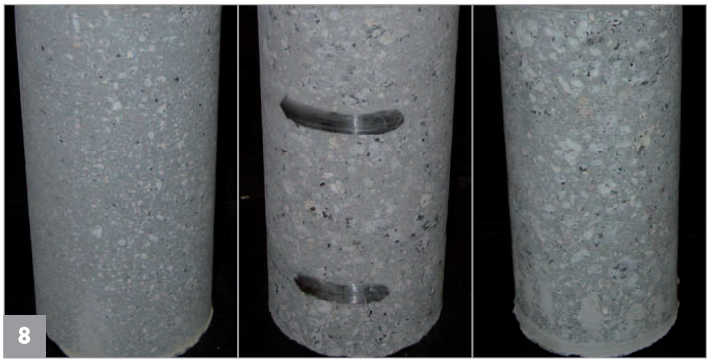
Discussion and concluding remarks

Until now many mix designs were developed and tested in the laboratory but the experience of producing SCC on site, in Portugal, is limited. Within the "BACPOR" project, which covered a wide range of applications and materials, the SCC mixes optimized in the laboratory had to be adjusted during full-scale testing to attend to the differences in the mixing efficiency and achieve high segregation resistance and sufficient deformability of fresh concrete. It has also been observed that variations in cement or mineral additions due to changes in the production process and changes in aggregate type, e.g. from one sand pit to another, can cause significant variations of the fresh properties. Therefore, it is of great importance to have a robust mixture that is as insensitive as possible for small variations of the ingoing materials and to be as consistent as possible over time.

Production capacity and casting capacity on site should be balanced off so as to ensure that SCC is placed without breaks in supply and within flowability retention time. Discontinued SCC production will affect filling ability and may result in unwanted lift lines on vertical surfaces as well as possible bonding problems between layers. Full-scale tests carried out at both Portuguese precast factories demonstrated that SCC has to be placed in one continuous pour; installations and equipment set for conventional concrete must be therefore adjusted. It is also recommended that workers involved should be specially trained.

Despite the difficulty in achieving all of the desired qualities on site, as occurred during "SCUT-IP5" full-scale testing, it was proved that the use of SCC has the potential to provide initial savings because of the reduction in labor required to place the concrete, especially when it is pumped.

Considering hardened SCC and conventional vibrated concrete of similar strength, it can be assumed that properties are comparable and any differences lie in the scattering range for conventional concrete; often lower modulus of elasticity, higher splitting tensile strength, higher



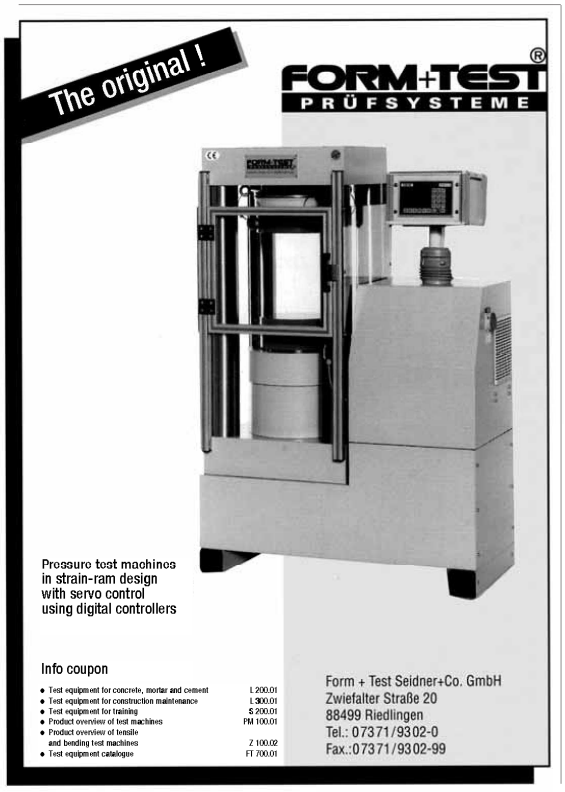
Cores drilled from panels cast with SCC at different heights: top (on the left); middle (on the middle); bottom (on the right)

shrinkage and better bond with the reinforcement are reported [1]. Besides, it is possible to compensate for the lower aggregate content (or higher paste content) in the SCC mixtures with a more dense paste to get similar or improved concrete properties.

It was found that concrete strength measured at different locations of the box-culvert element spreads less than in a similar element with conventional concrete. Compaction resulting from external vibration is uneven depending on the confinement and distance to the vibration sources. Properly proportioned, produced and placed SCC is generally more compact and homogeneous than equivalent vibrated concrete, which enhances the strength and durability performance of concrete structures made of SCC mixtures.

Acknowledgements

This research work was financed by AdI-Innovation Agency and carried out under the scope of a Portuguese research project "BACPOR" in direct co-operation with local industry, namely, Mota-Engil Engenharia, Sika and Maprel.



References

[1] EFNARC. The European Guidelines for Self-com-pacting Concrete. (Erhältlich bei: www.efnarc.org)

[2] Nunes S. Experimental study and numerical modelling of self-compacting concrete. In: Walraven J, Blaauwendraad J, Scarpas T, Snidjer B, editors. Tagungsband 5th International PhD Symposium in Civil Engineering. Delft, Niederlande. 2004. p. 857-865.

[3] Nunes S, Figueiras H, Coutinho JS, Figueiras J. Relatório de Execução Material, 4º Semestre de Actividades, Consórcio BACPOR. 2005. (in Portugiesisch)

[4] RILEM TC116-PCD. Permeability of concrete as a criterion of its durability, C: Determination of the capillary absorption of water of hardened concrete. Materials and Structures 1999; 32:178-179. T BUILD 492. Concrete, mortar and cementbased materials: Chloride migration coefficient from non-steady-state migration experiments. NORDTEST. 1999.

[6] Mansur MA, ASCE M, Islam MM. Interpretation of concrete strength for non-standard specimens. Journal of Materials in Civil Engineering 2002; 151-155.

B. Characterization of SCC mixtures (POCI/ECM/61649/2004)

B.1. Introduction

The current appendix gives a more detailed characterization of three SCC mixtures developed within POCI/ECM/61649/2004 research project, referred in Chapter 4. The tests, reference standards, testing age and number and type of specimens used to characterize each of the SCC mixtures studied, are detailed in Table B.1.

B.2. Materials characterization

Crushed calcareous aggregate (1-16 mm), a siliceous natural fine sand (sand 1) with a fineness modulus of 2,33 and natural coarse sand (sand 2) with a fineness modulus of 3,54 were used (see Table B.2). The specific gravity of the coarse aggregate, sand 1 and sand 2 were 2,59, 2,49 and 2,59, and absorption values were 1,54%, 0,25% and 0,50% , respectively. In this study SCC mixes were prepared with cements CEM II/A-L 42,5 R (fifth delivery), CEM I 52,5 R (fifth delivery) and CEM IV/B(V) 32,5 N (second delivery), all supplied by Cimpor-Alhandra, and a mineral addition (limestone filler, second delivery), with a specific gravity of 3,04, 3,11, 2,76 and 2,70, respectively. A more detailed characterization of fine materials is given in Appendix A. A polycarboxylate type superplasticizer (Viscocrete 3000) was used having a specific gravity of 1,05 and 18,5% solid content.

B.3. Mixing sequence, mix proportions and test results

Mixes were prepared in the laboratory in two batches of 85 l each and mixed in an tilting gravity mixer. The mixing sequence consisted of mixing both sands and coarse aggregate with one quarter of the mixing water during 2,5 min, waiting for 2,5 min for absorption, adding of the powder materials, followed by the rest of the water with

Table B.1.: Testing plan for each of the mixtures studied

Test	Reference standard/ recommendation	Testing age	Number of specimens
Slump-flow	(BIBM et al., 2005)	after mixing	–
V-funnel	(BIBM et al., 2005)	after mixing	–
L-box	(BIBM et al., 2005)	after mixing	–
Robustness	(BIBM et al., 2005)	after mixing	–
Compressive strength	(Portugal. IPQ, 2003a)	7 days [a] 28 days	4 cubes, 3 cylinders 3 cubes , 3 cylinders
Elasticity modulus	(Portugal. LNEC, 1993a)	7 days [a] 28 days	3 cylinders 3 cylinders
Tensile splitting strength	(Portugal. IPQ, 2003b)	7 days [a] 28 days	3 cylinders 3 cylinders
Shrinkage	(Portugal.LNEC, 1993)	continuous reading	2 prisms
Creep	(Portugal. LNEC, 1993b)	continuous reading	2 prisms
Resistance to chloride penetration	(Portugal. LNEC, 2004)	28 days	3 cubes⇒ 6discs (Ø=0,10m; h=0,05m)
Water absorption by capillarity	(RILEM TC 116-PCD, 1999a,b) (adapted)	28 days [b]	3 cubes ⇒6 slices

specimen dimensions: cube (0,15×0,15×0,15 m^3; cylinder (Ø=0,15 m; h=0,30 m);
prism (0,15×0,15×0,55 m^3);[a]tests were carried out at 10 days of concrete age;
[b]tests were carried out at 135 days of concrete age.

Table B.2.: Grading of aggregates (POCI/ECM/61649/2004)

Sieve size (mm)	0,063	0,125	0,25	0,5	1,0	2,0	4,0	8,0	16,0
sand 1	0,5	1,2	21,5	58,6	88,2	97,7	99,5	100	100
sand 2	0,5	1,1	2,6	8,7	48,2	86,7	98,5	100	100
coarse aggregate	0,1	0,1	0,1	0,1	0,2	0,2	1,1	34,7	100

the superplasticizer and finally mixing concrete during a further 8 min. Slump-flow, V-funnel and L-box tests were then carried out to characterize fresh state. Final SCC mix proportions are presented in Table B.3 along with test results on fresh concrete. Since a different mixer (an open pan mixer) and batch volume (25 l) were used during the mix development phase a correction of superplasticizer dosage was necessary to account for the higher mixing efficiency of the tilting gravity mixer, as indicated in Table B.3. All mixtures exhibited good deformability, without blocking, and enough viscosity to avoid segregation.

After testing fresh concrete, 13 cubes and 12 cylinders were moulded to assess concrete hardened properties. These specimens were demoulded one day after casting and kept inside a chamber under controlled environmental conditions (Temperature=20°C and HR=95-98%) until testing at the specified ages (see Table B.1).

B.4. Robustness

In *The European Guidelines for Self-Compacting Concrete* it is suggested that compositions with plus and minus 5 to 10 l of the target water content, be tested and the respective changes in fresh state properties be measured in order to check robustness of SCC mixtures. A robust SCC should tolerate these deviations, i.e. should maintain its fresh properties inside the specified limits (BIBM et al., 2005). A change in water content of ± 5 l/m^3 corresponds approximately to the limit imposed by NP EN 206-1 (Portugal. IPQ, 2007) for the water content variation ($\pm 3\%$). In the present study changes in water content of plus and minus 10 l/m^3 were introduced and mixtures were tested in the fresh and hardened states (compressive strength was assessed at 77 days). Test results are shown in Table B.4. The results from reference mixtures differ from those presented in Table B.3 because these batches were prepared in a different mixer (an open pan mixer) adequate for smaller batch volumes, which is less efficient.

The changes in slump flow diameter due to the variation in water content of each mixture are plotted in Figure B.1 along with the fitted data lines. The gradient (ΔDflow/ΔWw) gives the sensitivity of the mixture to variation in water content, which can be used as an indicator of SCC mixtures robustness (BIBM et al., 2005; Concrete Society, 2005). Mixtures with steeper gradients are more sensitive to variation in water content and, therefore, one can expect them to be less robust. The gradient corresponding to mixes A, B and C was 6,9, 9,6 and 8,5 mm/(kg/m^3), respectively.

Considering mixes with plus 10 l/m^3 the major concern is stability, but as can be observed in Figures B.2 to B.4 none of the mixtures exhibited severe segregation; aggregates are well distributed along the height of the cylinder specimens. This refers only to

Table B.3.: Mix proportions and fresh test results of SCC mixtures developed within POCI/ECM/61649/2004 research project

	Mix A CEM II/A-L 42,5 R	Mix B CEM I 52,5R	Mix C CEM IV/B(V) 32,5 N
Mix proportions			
w/c	0,45	0,45	0,28
Sp/p	1,70%	1,90%	2,21%
V_w/V_p	0,719	0,724	0,784
V_s/V_m		0,459	
s_1/s		0,519	
$V_g/V_{g,lim}$		0,553	
V_a		0,022	
Constituent materials (kg/m^3)			
cement	331	332	553
limestone filler	269	270	0
water	156	156	162
superplasticizer (V3000)	10,19[a]	11,45[b]	12,21
sand 1 (natural)		397	
sand 2 (natural)		369	
coarse aggregate		827	
Fresh test results			
Dflow (mm)	708	685	785
T50 (s)	2,4	2,4	2,41
Tfunnel (s)	13,7	15,7	10,4
H2/H1	$>$ 0,80	$>$ 0,80	$>$ 0,80

[a] the equivalent to 0,624 kg/m^3 was discounted to account for the mixer effect;

[b] the equivalent to 0,700 kg/m^3 was discounted to account for the mixer effect;

Table B.4.: Test results for the target and changed mixtures (±10 l/m^3 of water)

added	Mix A			Mix B			Mix C		
water (l/m^3)	-10	0	+10	-10	0	+10	-10	0	+10
Dflow (mm)	612	682	750	570	680	762	578	625	748
T50 (s)	3,8	2,3	1,2	6,2	2,8	1,4	4,2	3,4	1,5
Tfunnel (s)	17,9	10,9	7,6	21,7	11,2	7,9	14,0	12,8	6,5
H2/H1	0,73	0,86	0,89	0,68	0,85	0,94	0,60	0,78	0,85
f_{cm}(77days)(MPa)	60,4	55,2[a]	50,4	65,4	61,3[a]	59,8	66,4	65,9[a]	58,6

[a] these values were estimated from the measured f_{cm}(28 days) according to Eurocode 2 relationships

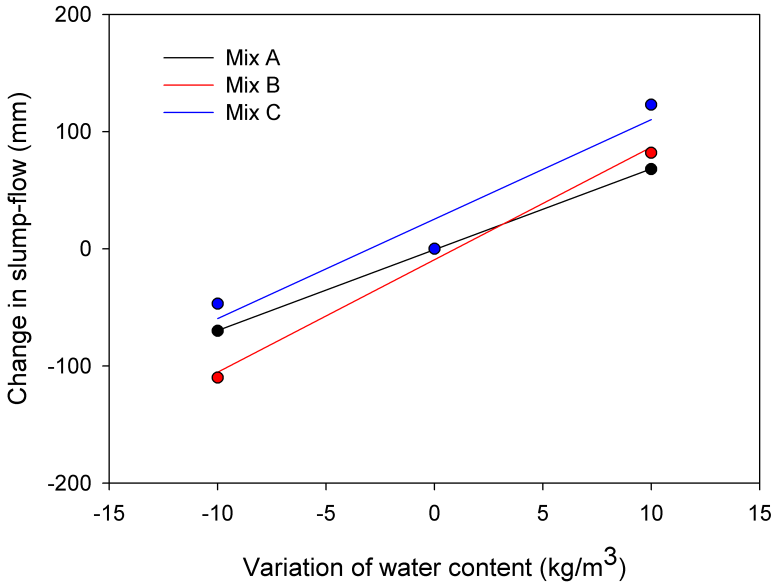


Figure B.1.: Sensitivity of SCC mixtures to variation in water content

static stability, depending on casting conditions and application type, dynamic stability should also be assessed. Considering mixes with minus 10 l/m^3, the major concerns are the lack of filling ability and/or passing ability and surface finish. Based on the obtained test results, the mixes with minus 10 l/m^3 would not be adequate for applications with highly congested reinforcement or when a good surface finish is required.

B.5. Cost of materials by m^3

Table B.5 presents the pricing of SCC mixtures based on the cost of materials only (without water). The cost was based on local prices used in the typical Portuguese market by June 2007. In these mixtures, the fine materials were responsible for more than 60% of the total cost, while aggregates were responsible for about 25% of the total cost. The remaining 15% represent the cost of the superplasticizer.

B.6. Mechanical properties

Development of compressive strength, Young's modulus and tensile splitting strength for each SCC mixture is shown in Tables B.6, B.7 and B.8, respectively, where the mean value is presented along with the coefficient of variation (c.o.v.). Compressive strength is the most important mechanical property for most applications. Therefore, in national and international codes concrete is classified on the basis of its compressive strength



Figure B.2.: Distribution of aggregates in a cylinder specimen of Mix A with plus 10 l/m^3



Figure B.3.: Distribution of aggregates in a cylinder specimen of Mix B with plus 10 l/m^3



Figure B.4.: Distribution of aggregates in a cylinder specimen of Mix C with plus 10 l/m^3

Table B.5.: Estimated cost of SCC mixtures

	Mix A	Mix B	Mix C
cement	CEM II/A-L 42,5 R 76 €/ton	CEM I 52,5R 89 €/ton	CEM IV/B(V) 32,5 N 75 €/ton
limestone filler		30 €/ton	
superplasticizer (V3000)		0,6 €/kg	
sand 1 (natural)		10 €/ton	
sand 2 (natural)		12 €/ton	
coarse aggregate		9 €/ton	
Estimated cost (€/m^3)	55	60	65

and relations between compressive strength and other mechanical properties relevant for structural design are given in (CEB, 1998; CEN, 2004). In Tables B.7 and B.8, estimates of the modulus of elasticity and tensile strength based on the obtained values of $f_{cm,cyl}$(28 days) and according to Eurocode 2 relationships (derived for conventional concrete) are presented and compared with the test results. In general, results of SCC mixtures were higher than the estimated values. These differences were larger for mixtures incorporating limestone filler (mixes A and B). Results from Table B.6 also indicate a lower dependency on the specimen geometry than expected for conventional concrete in the same strength class ($f_{c,cyl}/f_{c,cube} \backsimeq 0{,}8$).

B.7. Temperature evolution, drying shrinkage and creep deformations

Mixes A, B and C were prepared in the laboratory in 13/06/2006, 20/06/2006 and 27/06/2006, respectively. Immediately after mixing, the four prisms were moulded inside a chamber with controlled environmental conditions (Temperature=20±2°C and HR=50±5%), to determine temperature evolution and shrinkage deformations. After casting, the moulds were covered with a plastic film to avoid humidity loss. The temperature evolution and deformation of concrete was continuously monitored through the installation of temperature sensors (PT100) and electric resistance sensors (350 Ohms at 24°C from Vishay), respectively, installed in the centre of the prism (see Figure B.5). These sensors were then connected to an automatic acquisition system (datataker DT 515 Series 3) to allow continuous monitoring of temperature and deformation in each prism. The mean of four curves of temperature evolution during the first three days is given in Figure B.6. From these results it can be expected that mixes A and B have similar initial setting time (related to the time needed to start increasing temperature) which is significantly lower than the initial setting time of mix C. The lowest and highest final setting times (related to the time needed to reach the peak temperature) can be expected with mixes B and C, which could be expected since a CEM I and CEM IV were used in mixes B and C, respectively. Similar maximum temperature variations were observed with mixes C and B, which can be explained by the combination of strength class of cement and water/cement ratio used in each of the mixtures.

The prisms were demoulded three days after casting, accelerating the drying of prisms, and kept inside the chamber with controlled environmental conditions. The mean of two curves of shrinkage deformation evolution with time is given in Figure B.7, for each mixture. Zeroing was done at the time when the peak temperature was reached, because it is believed that sufficient adherence has developed between the sensor and the surrounding concrete by this time. A hump is observed in each curve around 160

Table B.6.: Compressive strength and specific gravity results

Mix	Age of testing	Specimen	ρ (kg/m^3)	f_{ci} (MPa)	f_{cm} (MPa)	c.o.v.	$\frac{f_{cm,cyl}}{f_{cm,cube}}$
A	10 days	*cube* 1	2392	47,97	49,3	3,2%	0,88
		cube 2	2424	50,38			
		cube 3	2420	51,00			
		cube 4	2383	47,95			
		cylinder 1	2365	43,82	43,5[a]	2,0%	
		cylinder 2	2357	42,44			
		cylinder 3	2344	44,10			
	28 days	*cube* 5	2408	52,58	50,6	3,7%	0,93
		cube 6	2413	48,81			
		cube 7	2381	50,43			
		cylinder 4	2378	46,65	47,0	1,4%	
		cylinder 5	2377	46,70			
		cylinder 6	2386	47,81			
B	10 days	*cube* 1	2452	57,46	58,6	2,8%	0,87
		cube 2	2477	60,95			
		cube 3	2444	58,25			
		cube 4	2438	57,55			
		cylinder 1	2386	51,83	51,2[a]	1,2%	
		cylinder 2	2380	51,22			
		cylinder 3	2382	50,57			
	28 days	*cube* 5	2444	64,25	62,7	2,7%	0,86
		cube 6	2412	63,03			
		cube 7	2411	60,88			
		cylinder 4	2386	55,05	53,7	8,4%	
		cylinder 5	2380	57,35			
		cylinder 6	2382	48,66			
C	10 days	*cube* 1	2294	41,98	48,6	9,5%	0,87
		cube 2	–	52,80			
		cube 3	–	49,78			
		cube 4	2315	49,86			
		cylinder 1	2272	42,53	42,2[a]	2,4%	
		cylinder 2	2291	43,02			
		cylinder 3	2270	41,08			
	28 days	*cube* 5	2331	–	58,4	-	0,88
		cube 6	2347	62,06			
		cube 7	2292	54,64			
		cylinder 4	2288	53,11	51,4	4,5%	
		cylinder 5	2273	52,18			
		cylinder 6	2286	48,76			

[a] $f_{cm,cyl}$(10 days) was estimated from $f_{cm,cyl}$(28 days) results by using the hardening law indicated in Eurocode 2. Estimated $f_{cm,cyl}$(10 days) values were 41,1, 46,9 and 43,3 for mixes A, B and C, respectively.

Table B.7.: Modulus of elasticity test results and estimated values (Eurocode 2)

Mix	Age of testing	Specimen	E_{ci} (GPa)	E_{cm} (GPa)	c.o.v.	$E_{cm}(EC2)^a$ (GPa)	$E_{cm}/E_{cm}(EC2)$
A	10 days	*cylinder* 1	44, 24	41, 4	6, 0%	33, 6	1, 23
		cylinder 2	40, 42				
		cylinder 3	39, 56				
	28 days	*cylinder* 4	37, 57	42, 0	9, 3%	33, 6	1, 20
		cylinder 5	43, 72				
		cylinder 6	44, 82				
B	10 days	*cylinder* 1	43, 76	42, 5	9,7%	35, 0	1, 21
		cylinder 2	37, 87				
		cylinder 3	45, 81				
	28 days	*cylinder* 4	41, 74	44, 0	4, 5%	36, 4	1, 21
		cylinder 5	45, 01				
		cylinder 6	45, 25				
C	10 days	*cylinder* 1	38, 48	38, 2	1, 0%	34, 2	1, 12
		cylinder 2	38, 28				
		cylinder 3	37, 75				
	28 days	*cylinder* 4	44, 61	40, 8	–	36, 0	1, 13
		cylinder 5	36, 97				
		cylinder 6	–				

[a] E_{cm} was estimated from $f_{cm,cyl}$ values, at 28 days, (Table B.6) by using the relations indicated in Eurocode 2.

Table B.8.: Tensile strength test results and estimated values (Eurocode 2)

Mix	Age of testing	Specimen	$f_{ct,spi}$ (MPa)	f_{ctm} (MPa)	c.o.v.	$f_{ctm}(EC2)^a$ (MPa)	$f_{ctm}/f_{ctm}(EC2)$
A	10 days	*cylinder* 7	3, 72	3, 6	7, 5%	3, 0	1, 19
		cylinder 8	3, 94				
		cylinder 9	4, 31				
	28 days	*cylinder* 10	4, 38	3, 8	7, 0%	3, 5	1, 10
		cylinder 11	4, 43				
		cylinder 12	3, 89				
B	10 days	*cylinder* 7	4, 13	4, 1	9,2%	3, 4	1, 21
		cylinder 8	4, 46				
		cylinder 9	4, 95				
	28 days	*cylinder* 10	4, 24	4, 1	–	3, 8	1,07
		cylinder 11	4, 85				
		cylinder 12	–				
C	10 days	*cylinder* 7	3, 45	3, 2	–	3, 1	1, 04
		cylinder 8	3, 76				
		cylinder 9	–				
	28 days	*cylinder* 10	3, 54	3, 5	9, 5%	3, 7	0, 95
		cylinder 11	4, 28				
		cylinder 12	3, 97				

[a] f_{ctm} was estimated from $f_{cm,cyl}$ values, at 28 days, (Table B.6) by using the relations indicated in Eurocode 2.

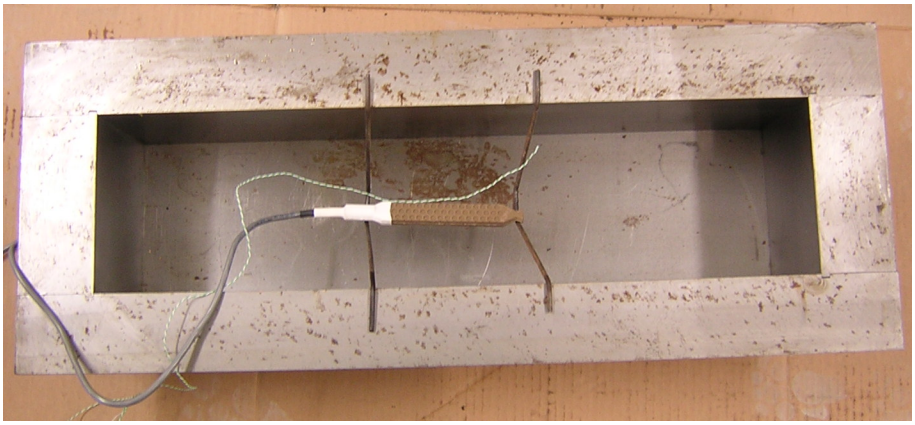


Figure B.5.: Sensors installed inside the concrete prisms to monitor temperature and deformation

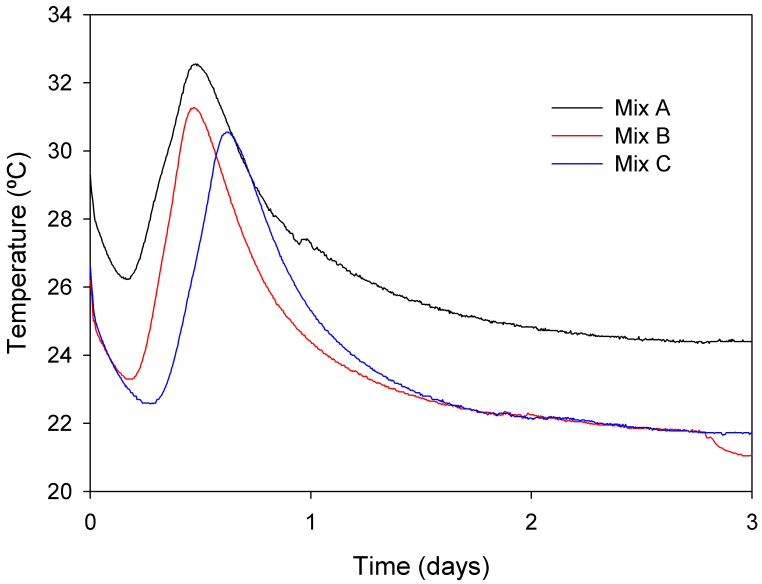


Figure B.6.: Mean temperature evolution on concrete prisms

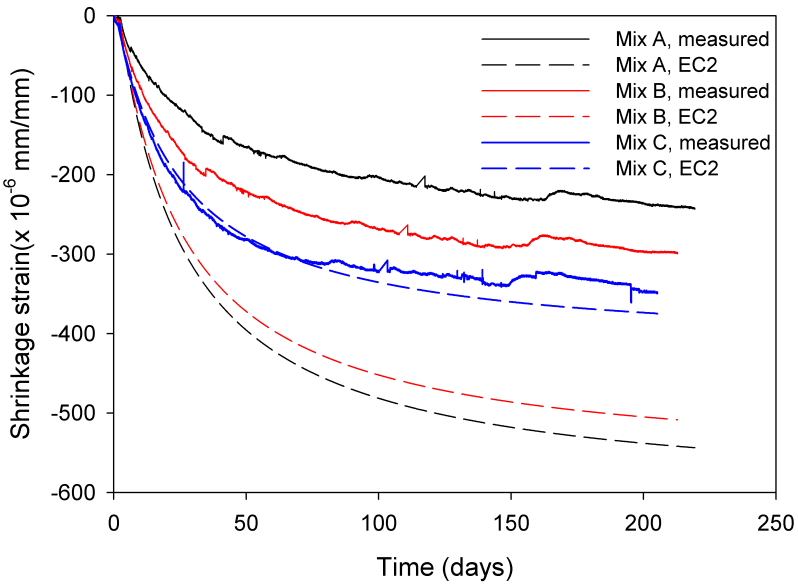


Figure B.7.: Evolution of drying shrinkage deformations in comparison with Eurocode 2 rules

days. This was due to a change in the environment's humidity as a consequence of an accidental infiltration of water in the chamber. The evolution of drying shrinkage deformation as estimated by Eurocode 2 relationships is also plotted in Figure B.7, starting at the demoulding time for each mixture. A good agreement was found between the measured shrinkage deformations and those estimated by Eurocode 2 in the case of Mix C, but much smaller shrinkage deformations were observed in the case of mixes B and C. A possible explanation for these differences is the addition of filler with fineness larger than cement, which is responsible for a denser microstructure, thereby affecting shrinkage positively.

Two of the four prisms were used to carry out creep tests. Loading age was 41, 37 and 34 days for mixes A, B and C, respectively. By using the creep systems illustrated in Figure B.8 the same load was applied for both prisms. The creep load stress was 28%, 26% and 27% of cylinders compressive strength, at 28 days. The mean of two curves of (shrinkage+creep) deformations evolution with time, after loading, is given in Figure B.9, for each mixture. The mean evolution of shrinkage deformations as measured from shrinkage prisms is also plotted in Figure B.9. Thus, the creep deformation part was obtained by subtracting these two curves (see Figure B.9). The mean curve of creep deformation evolution with time (after loading) is repeated in Figure B.10 in comparison with the creep evolution curves as given by Eurocode 2. For all SCC mixtures the observed creep deformations were lower than the Eurocode 2 prediction; the differences were more pronounced in the case of Mix A.

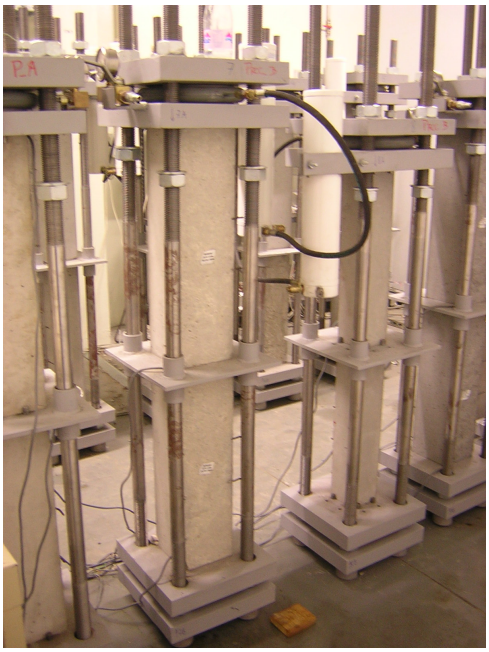


Figure B.8.: Systems used in concrete creep tests

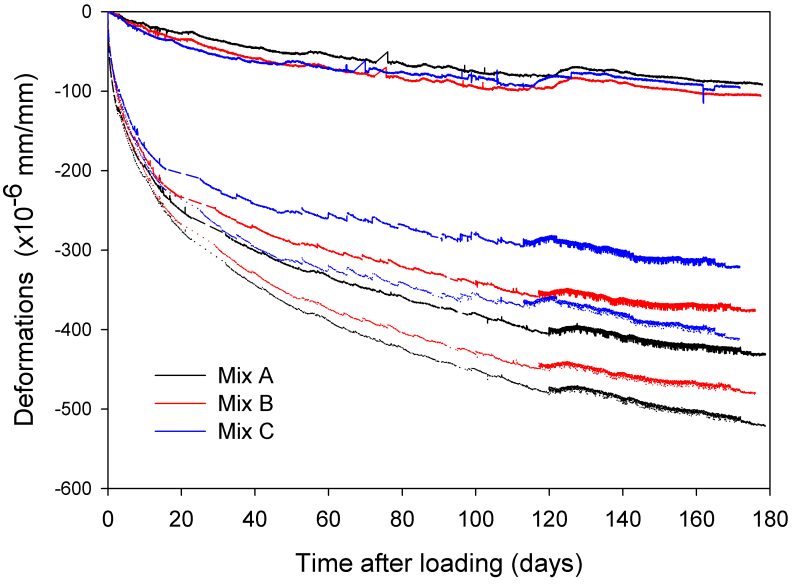


Figure B.9.: Evolution of shrinkage, creep and (shrinkage+creep) deformations with time

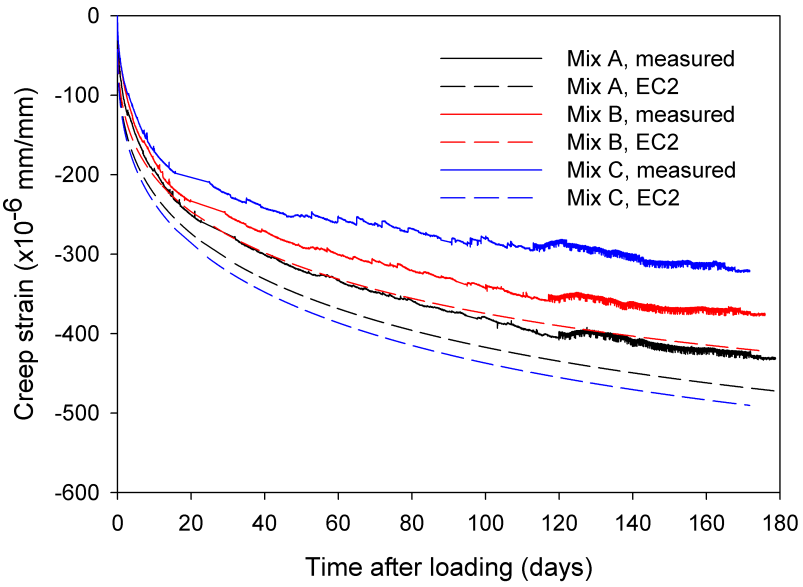
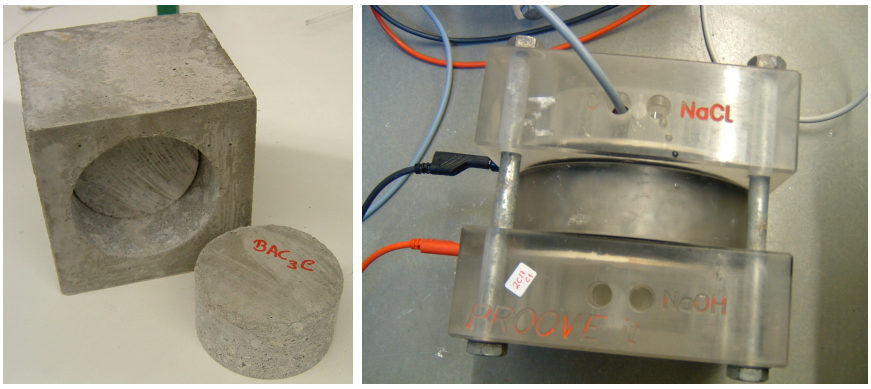


Figure B.10.: Evolution of creep deformations with time in comparison with Eurocode 2 rules

B.8. Transport properties

Transport properties of the near-surface concrete, which play a major role in durability of reinforced concrete, are controlled by three mechanisms, namely, capillary absorption, permeability and diffusion (Neville, 1995; Sousa Coutinho, 2003). In the present study water absorption by capillarity and a chloride migration test were carried out to assess concrete durability.

Resistance to chloride penetration was assessed following the Portuguese standard LNEC E463 (Portugal. LNEC, 2004) which is based in the NORDTEST method (Finland. Nordisk Innovations Center, 1999). Cube specimens (28 day old) were used and cores of approximately 100 mm diameter were drilled out and sawn in three parts; the top 50 mm discs corresponding to moulded faces A and B were used for this test (see Figure B.11 (a)). The conditioning of the concrete disc specimens consisted of: 1 hour air drying; 3 hours vacuum (pressure <600 mm Hg); 1 hour of additional vacuum with specimens under deaerated water, followed by 18 hours of soaking in saturated calcium hydroxide solution. The NORDTEST method is a non-steady state migration method based on a theoretical relation between diffusion and migration, which enables the calculation of the apparent chloride diffusion coefficient from an accelerated test. It is based on measuring the depth of colour change of a silver nitrate solution sprayed on the specimens previously submitted to a migration test (disc specimens were submitted to an electrical current corresponding to a potential difference of 30 V, during 24 hours) (see Figure B.11 (b)). Results of this test are presented in Figure B.12 and Table B.9.



(a) (b)

Figure B.11.: Specimen and experimental set-up used in the resistance to chloride penetration test



(a) (b) (c)

Figure B.12.: Penetration depth of chloride ions (lighter part): (a) Mix A; (b) Mix B; (c) Mix C

Test results show that Mix A is less resistant to chloride ingress. Mix B exhibited slightly improved behaviour when compared to Mix A. A significant reduction in the apparent diffusion coefficient (D_{ns}) was found with Mix C.

To consider ability of near-surface concrete to absorb and transmit water by capillary action the RILEM TC116-PCD recommendation was adopted with some modifications (Sonebi et al., 2000; RILEM TC 116-PCD, 1999a,b). The moulded side faces of 150 mm cube specimens were tested, instead of the moulded bottom face of 150 mm cube specimens used in the RILEM recommendation. These specimens (thickness=50 mm) were allowed to dry in a ventilated heater at 40±5°C until constant mass. After cooling, the specimens were prepared and tested according to the RILEM recommendation. The uptake of water by capillary absorption was measured through the weight gain of each specimen at time intervals of 10 min, 0,5 h, 1 h, 4 h, 18 h and 24 hours of contact water

Table B.9.: Apparent diffusion coefficient (D_{ns}) results

Specimen	$D_{ns} \times 10^{-12}$ (m^2/s)		
	Mix A	Mix B	Mix C
cube 8 – face A	20,44	18,08	2,07[a]
cube 8 – face B	22,53	18,32	6,38
cube 9 – face A	20,82	19,86	7,07
cube 9 – face B	21,07	19,21	6,63
cube 10 – face A	23,28	19,06	8,59
cube 10 – face B	22,04	18,38	8,20
average	21,7	18,8	7,4
c.o.v.	5,1%	3,6%	13,2%

[a] this value was excluded because it is an outlier

Table B.10.: S, a_0 and R^2 values for each SCC mixture

Specimen	Mix A			Mix B			Mix C		
	S	a_0	R^2	S	a_0	R^2	S	a_0	R^2
cube 11, face A	72,44	29,02	0,996	48,49	81,05	0,979	48,92	90,86	0,982
cube 11, face B	78,97	27,09	0,997	34,33[a]	67,59	0,990	46,56	91,38	0,983
cube 12, face A	65,56	113,31	0,993	48,85	77,95	0,987	47,52	63,70	0,990
cube 12, face B	76,13	93,64	0,995	36,76[a]	92,63	0,993	45,50	56,73	0,992
cube 13, face A	73,46	90,23	0,995	51,25	81,35	0,988	42,87	105,90	0,985
cube 13, face B	73,20	140,32	0,996	34,43[a]	84,73	0,995	42,87	107,02	0,983
average	73,29			42,35			45,71		
c.o.v.	6,1%			18,8%			5,4%		

(Sonebi et al., 2000). The absorption of water into concrete under capillary action is dependent on the square-root of time and may be modelled by the following equation (Sousa Coutinho, 2003)

$$A = a_0 + St^{0.5} \tag{B.1}$$

where A (g/m^2) is the water absorption by unit area since the moment the specimen was dipped in a few millimeters of water, S is the *Sorptivity* of the material, t is the elapsed time and a_0 (g/m^2) is the water absorbed initially by pores in contact with water. Testing each specimen led to the model parameters and correlation coefficients presented in Table B.10. Results show that the rate of capillary absorption, indicated by the *Sorptivity* parameter is higher for Mix A. A slightly lower mean *Sorptivity* value was found for Mix B compared to Mix C. But, it should be noted that Mix B test results exhibited an abnormal high c.o.v., if one excludes the test results marked with ([a]) in Table B.10 the average S value would be 49,53, in the worst scenario.

In summary, both water absorption by capillarity and a chloride migration tests indicate that mixes C and A will perform better and poorly, respectively, in terms of durability. Mix B test results were closer to Mix A in terms of resistance to chloride ingress, but closer to Mix C in terms of water absorption by capillarity. Such results suggest that the near-surface concrete is denser and more resistant to fluid ingress in the Mix C, due primarily to the lower water/cement ratio. The pores network of near-surface concrete of Mix B seems not to differ significantly from Mix C. This can be explained by the combination of a finer cement with limestone filler in Mix B. In spite of that, Mix B does not exhibit a resistance to chloride ingress similar to Mix C. This can be explained by the different chloride binding capacity of mixtures including limestone filler (mixes A and B) and fly ash (Mix C).

C. Fine materials characterization

In the current appendix, chemical, physical and mechanical properties of fine materials used in the present PhD research project is presented including different deliveries of cement and limestone filler. The information presented in Tables C.1 to C.10 was provided by the respective suppliers, with exception to the size distribution results identified with (^{a}), obtained from tests carried out at LABEST/FEUP by using laser light diffraction technique (Mastersizer 2000 with Hydro2000S acessory, from Malvern) (Nunes et al., 2008).

Table C.1.: Chemical characterization of CEM I 52,5R (Cimpor, Alhandra), for each cement delivery

Delivery	1^{st}	2^{nd}	3^{rd}	4^{th}	5^{th}	6^{th}	7^{th}	8^{th}
Date of collection	28-10-2005	16-01-2006	27-02-2006	12-04-2006	08-05-2006	31-05-2006	26-06-2006	19-07-2006
Chemical characteristics								
LOI (%)	1,92	2,25	1,64	1,65	2,13	2,15	1,91	2,1
SiO_2 (%)	18,71	18,84	18,80	18,87	18,98	18,78	18,97	19,01
Al_2O_3 (%)	5,47	5,43	5,51	5,55	5,43	5,6	5,6	5,51
Fe_2O_3 (%)	3,05	2,87	3,40	3,42	3,57	3,58	3,53	3,57
Total CaO (%)	63,96	63,6	63,40	64,38	64,03	63,54	63,43	63,85
MgO (%)	1,8	2,05	1,68	1,77	1,6	1,72	1,64	1,54
SO_3 (%)	3,25	3,38	3,32	3,29	3,31	3,35	3,49	3,61
K_2O (%)	1,05	1,05	1,05	1,06	1,03	1,05	1,08	0,94
Na_2O (%)	0,09	0,1	0,10	0,10	0,09	0,09	0,12	0,13
Free CaO (%)	2,67	2,3	1,51	1,51	1,12	1,12	1,23	1,02
Insoluble residue, Na_2CO_3 (%)	0,64	0,78	0,70	–	0,99	0,84	1,02	0,86
Cl^- (%)	0,02	0,02	0,01	–	0,02	0,01	0,01	0,01
S^{2-} (%)	–	–	–	–	–	0,11	–	–
$(Na_2O)_{equivalent}$ (%)	0,78	0,79	0,79	0,80	0,77	0,78	0,83	0,75
Mineral composition								
C_3S (%)	–	65,4	65,8	66,2	67,5	67,1	67,1	66,1
C_2S (%)	–	7,9	8,9	10,5	7,8	7,0	7,4	7,5
C_4AF (%)	–	7,9	9,4	9,6	8,9	9,0	8,8	8,5
C_3A (%)	–	8,2	6,9	6,9	7,6	7,7	8,5	8,4
Gypsum (%)	–	4,6	4,1	4,2	4,0	4,6	4,6	5,1
Calcite (%)	–	2,4	1,1	0,8	1,9	2,0	1,9	1,9
Mineral additions								
Limestone filler - L (%)	–	3,80	2,5	–	3,4	3,3	2,9	3,6

Table C.2.: Physical and mechanical characterization of CEM I 52,5R (Cimpor, Alhandra), for each cement delivery

Delivery	1^{st}	2^{nd}	3^{rd}	4^{th}	5^{th}	6^{th}	7^{th}	8^{th}
Date of collection	28-10-2005	16-01-2006	27-02-2006	12-04-2006	08-05-2006	31-05-2006	26-06-2006	19-07-2006
Physical characteristics								
Specific gravity (g/cm^3)	3,13	3,13	3,11	3,13	3,11	3,11	3,13	3,08
Surface area, *Blaine* (cm^2/g)	3830	4120	4220	3820	3880	3770	3820	3870
Residue, 90 μm (%)	0,1	–	–	–	–	–	–	–
Residue, 45 μm (%)	2,8	1,4	1,5	1,2	1,7	1,7	1,8	1,7
Residue, 32 μm (%)	–	4,7	4,4	4,0	5,9	6,6	6,1	5,4
Residue, 90 μm (%)[a]	0,0	0,0	0,0	0,0	0,0	0,0	0,0	0,0
Residue, 45 μm (%)[a]	6,9	5,1	5,4	5,3	6,2	5,9	6,9	5,4
Residue, 32 μm (%)[a]	18,7	15,6	15,9	16,0	17,3	16,6	17,8	15,5
Mean size (μm)[a]	15,0	13,6	14,0	14,1	14,5	14,0	14,5	13,5
Mechanical characteristics								
f_{ctm}(2 days) (MPa)	6,2	6,5	6,3	6,0	6,2	6,4	6,6	6,5
f_{ctm}(7 days) (MPa)	8,0	7,5	7,8	7,9	7,4	8,1	7,2	8,1
f_{ctm}(28 days) (MPa)	7,1	8,4	8,3	8,4	8,8	9,2	8,3	9,1
f_{cm}(2 days) (MPa)	38,9	40,2	42,5	41,0	38,4	40,6	40,1	41,6
f_{cm}(7 days) (MPa)	54,3	53,0	52,7	53,0	51,5	53,4	50,9	52,0
f_{cm}(28 days) (MPa)	62,7	63,1	65,2	61,5	65,0	63,7	61,1	61,1
Normal consistency								
Water demand (%)	30,8	31,4	31,6	31,6	32,0	31,6	31,8	32,4
Initial setting time (min)	135	120	130	120	125	140	120	110
Final setting time (min)	175	140	165	160	170	185	155	160
Expansion (mm)	1,5	1,5	1,0	1,0	1,0	1,0	0,5	1,0
Hidration heat 3 days (cal/g)	77	81	72	82	86	86	77	74
Hidration heat 7 days (cal/g)	85	95	77	84	91	89	79	80
Hidration heat 28 days (cal/g)	94	105	82	97	95	95	87	95

Table C.3.: Chemical characterization of CEM I 42,5R (Cimpor, Alhandra), for each cement delivery

Delivery	1^{st}	2^{nd}	3^{rd}	4^{th}	5^{th}	6^{th}	7^{th}	8^{th}
Date of collection	28-10-2005	16-01-2006	27-02-2006	12-04-2006	08-05-2006	31-05-2006	26-06-2006	19-07-2006
Chemical characteristics								
LOI (%)	2,72	2,26	2,67	2,64	2,60	2,93	2,49	2,81
SiO_2 (%)	18,76	19,10	18,80	18,98	18,26	19,05	19,03	18,82
Al_2O_3 (%)	5,31	5,50	5,42	5,51	5,47	5,48	5,52	5,40
Fe_2O_3 (%)	3,23	3,17	3,36	3,45	3,32	3,34	3,44	3,15
Total CaO (%)	63,19	63,87	64,31	64,33	63,89	63,87	63,96	64,06
MgO (%)	1,71	2,08	1,73	1,53	1,86	1,70	1,58	1,61
SO_3 (%)	3,04	2,68	2,67	2,72	2,75	2,76	2,69	2,74
K_2O (%)	1,14	1,04	1,02	1,04	1,08	1,01	1,03	1,07
Na_2O (%)	0,11	0,09	0,09	0,10	0,09	0,08	0,09	0,09
Free CaO (%)	1,38	1,06	1,46	1,18	1,29	1,40	1,34	0,95
Insoluble residue, Na_2CO_3 (%)	0,62	–	–	–	–	0,76	–	–
Cl^- (%)	0,03	0,01	0,01	–	–	0,02	–	–
S^{2-} (%)	–	–	–	–	–	0,06	–	–
$(Na_2O)_{equivalent}$ (%)	0,86	0,78	0,76	0,79	0,80	0,75	0,77	0,80
Mineral composition								
C_3S (%)	–	63,2	61,4	60,1	62,0	60,5	61,2	62,0
C_2S (%)	–	10,7	11,2	10,7	9,6	10,7	9,8	10,2
C_4AF (%)	–	9,2	9,6	9,4	9,3	9,1	9,9	8,2
C_3A (%)	–	6,6	6,1	7,2	7,6	6,9	8,0	8,5
Gypsum (%)	–	3,9	5,5	6,3	4,5	5,1	4,7	4,9
Calcite (%)	–	3,8	4,1	3,9	4,6	4,7	3,5	3,7
Mineral additions								
Limestone filler - L (%)	–	–	–	5,0	–	4,9	–	4,8

Table C.4.: Physical and mechanical characterization of CEM I 42,5R (Cimpor, Alhandra), for each cement delivery

Delivery	1^{st}	2^{nd}	3^{rd}	4^{th}	5^{th}	6^{th}	7^{th}	8^{th}
Date of collection	28-10-2005	16-01-2006	27-02-2006	12-04-2006	08-05-2006	31-05-2006	26-06-2006	19-07-2006
Physical characteristics								
Specific gravity (g/cm^3)	3,16	3,13	3,14	3,13	3,13	3,11	3,14	3,11
Surface area, *Blaine* (cm^2/g)	3270	3190	3220	3230	2950	3150	3180	3160
Residue, 90 μm (%)	0,8	1,1	1,2	0,9	0,7	0,9	1,1	1,1
Residue, 45 μm (%)	13,0	12,5	13,0	11,0	10,6	12,7	13,7	13,5
Residue, 32 μm (%)	–	–	–	–	–	–	–	–
Residue, 90 μm (%)[a]	2,1	2,1	2,4	2,0	1,4	1,7	2,0	1,9
Residue, 45 μm (%)[a]	16,9	21,1	21,3	17,9	18,8	19,2	20,6	20,5
Residue, 32 μm (%)[a]	29,3	35,7	35,8	31,2	33,1	33,5	34,9	35,0
Mean size (μm)[a]	18,10	22,44	22,38	19,38	20,87	21,15	21,61	21,91
Mechanical characteristics								
f_{ctm}(2 days) (MPa)	5,8	4,5	5,0	5,4	4,9	5,3	4,8	5,0
f_{ctm}(7 days) (MPa)	7,6	6,5	6,6	7,2	6,8	7,5	6,6	6,8
f_{ctm}(28 days) (MPa)	8,4	8,1	8,0	8,9	8,4	8,4	8,3	8,3
f_{cm}(2 days) (MPa)	31,4	27,6	28,9	29,6	29,4	28,4	27,9	28,7
f_{cm}(7 days) (MPa)	46,9	39,1	41,0	40,3	40,6	40,6	40,5	40,2
f_{cm}(28 days) (MPa)	56,4	54,2	51,7	50,0	51,2	51,7	52,2	51,8
Normal consistency								
Water demand (%)	28,6	29,0	29,2	29,4	28,6	28,8	29,4	29,6
Initial setting time (min)	145	130	150	145	150	135	135	140
Final setting time (min)	195	180	210	230	190	190	175	190
Expansion (mm)	0	1,0	0,5	1,0	1,0	1,0	1,0	1,5
Hidration heat 3 days (cal/g)	73	58	64	68	66	72	63	65
Hidration heat 7 days (cal/g)	76	74	77	79	73	71	79	78
Hidration heat 28 days (cal/g)	82	72	77	81	84	83	83	79

Table C.5.: Chemical characterization of CEM II/A-L 42,5R (Cimpor, Alhandra), for each cement delivery

Delivery	1^{st}	2^{nd}	3^{rd}	4^{th}	5^{th}	6^{th}	7^{th}	8^{th}
Date of collection	28-10-2005	16-01-2006	27-02-2006	12-04-2006	08-05-2006	31-05-2006	26-06-2006	19-07-2006
Chemical characteristics								
LOI (%)	5,82	6,41	6,69	6,69	6,39	6,65	6,35	7,55
SiO_2 (%)	17,41	17,26	16,73	17,22	16,82	16,99	17,19	16,82
Al_2O_3 (%)	5,03	5,02	4,85	5,17	5,11	5,03	5,07	4,93
Fe_2O_3 (%)	2,98	2,87	3,00	3,11	3,11	3,04	3,14	2,89
Total CaO (%)	62,26	62,76	62,15	62,18	62,31	62,09	62,09	61,82
MgO (%)	1,7	1,69	1,71	1,72	1,78	1,81	1,49	1,43
SO_3 (%)	2,84	3,06	3,69	2,73	3,20	3,23	3,13	3,37
K_2O (%)	1,00	0,95	0,92	1,02	1,00	0,88	0,93	0,84
Na_2O (%)	0,09	0,09	0,11	0,08	0,08	0,08	0,09	0,11
Free CaO (%)	1,15	0,90	0,95	0,84	1,12	1,34	1,12	1,01
Insoluble residue, Na_2CO_3 (%)	–	–	1,07	–	1,35	0,89	1,16	1,33
Cl^- (%)	0,02	0,01	0,01	–	0,02	0,01	0,02	0,01
S^{2-} (%)	–	–	–	–	–	0,08	–	–
$(Na_2O)_{equivalent}$ (%)	0,75	0,72	0,72	0,75	0,74	0,66	0,70	0,66
Mineral composition								
C_3S (%)	–	58,2	56,2	56,4	55,6	54,6	54,8	53,1
C_2S (%)	–	5,7	10,3	10,8	10,4	10,7	9,9	11,3
C_4AF (%)	–	8,8	9,5	8,6	9,0	8,2	9,1	7,9
C_3A (%)	–	7,7	6,1	6,1	6,3	6,6	7,4	7,5
Gypsum (%)	–	6,1	6,1	4,9	5,4	5,3	6,0	6,1
Calcite (%)	–	10,7	10,0	10,1	10,2	10,9	10,4	12,2
Mineral additions								
Limestone filler - L (%)	–	12,5	13,2	12,7	12,5	12,6	12,3	14,4

Table C.6.: Physical and mechanical characterization of CEM II/A-L 42,5R (Cimpor, Alhandra), for each cement delivery

Delivery	1^{st}	2^{nd}	3^{rd}	4^{th}	5^{th}	6^{th}	7^{th}	8^{th}
Date of collection	28-10-2005	16-01-2006	27-02-2006	12-04-2006	08-05-2006	31-05-2006	26-06-2006	19-07-2006
Physical characteristics								
Specific gravity (g/cm^3)	3,11	3,10	3,10	3,04	3,04	3,07	3,04	3,08
Surface area, *Blaine* (cm^2/g)	3710	3760	3840	3750	3830	3670	3620	3930
Residue, 90 μm (%)	0,8	0,5	0,5	0,4	0,6	1,2	0,9	0,5
Residue, 45 μm (%)	13,4	8,3	7,0	5,2	8,0	10,0	8,8	5,3
Residue, 32 μm (%)	–	–	–	–	–	–	–	–
Residue, 90 μm (%)^a	1,2	0,9	0,9	0,5	1,1	1,5	2,5	0,4
Residue, 45 μm (%)^a	16,2	14,4	14,1	10,5	13,6	15,1	18,1	9,9
Residue, 32 μm (%)^a	29,1	26,8	26,6	21,7	25,5	27,4	30,5	20,6
Mean size (μm)^a	17,92	16,61	16,69	14,78	16,18	16,99	18,19	13,80
Mechanical characteristics								
f_{ctm}(2 days) (MPa)	5,27	5,50	5,50	5,80	5,30	5,30	5,30	5,90
f_{ctm}(7 days) (MPa)	7,40	7,30	6,90	7,00	7,50	7,60	7,00	7,50
f_{ctm}(28 days) (MPa)	7,47	9,00	7,80	8,20	8,40	8,10	8,60	8,70
f_{cm}(2 days) (MPa)	29,28	31,60	30,60	29,90	30,50	28,90	30,00	31,50
f_{cm}(7 days) (MPa)	43,63	44,50	41,10	40,30	41,10	41,10	41,80	42,30
f_{cm}(28 days) (MPa)	52,20	55,60	49,10	51,30	53,80	51,20	52,70	52,80
Normal consistency								
Water demand (%)	26,9	28,4	28,0	28,4	28,2	28,4	28,2	28,8
Initial setting time (min)	150	150	150	150	150	130	140	130
Final setting time (min)	195	200	190	200	190	180	185	170
Expansion (mm)	0,5	0,5	0,0	0,5	0,0	0,0	0,0	1,0
Hidration heat 3 days (cal/g)	65	66	69	70	75	76	66	77
Hidration heat 7 days (cal/g)	68	70	74	80	77	83	75	84
Hidration heat 28 days (cal/g)	84	85	78	83	88	92	85	92

Table C.7.: Chemical characterization of CEM II/B-L 32,5N (Cimpor, Alhandra), for each cement delivery

Delivery	1^{st}	2^{nd}	3^{rd}	4^{th}	5^{th}	6^{th}	7^{th}	8^{th}
Date of collection	28-10-2005	16-01-2006	27-02-2006	12-04-2006	08-05-2006	31-05-2006	26-06-2006	19-07-2006
Chemical characteristics								
LOI (%)	12,74	13,91	14,25	14,31	14,54	14,39	13,87	13,88
SiO_2 (%)	14,35	14,29	12,88	12,82	12,74	13,75	13,50	13,60
Al_2O_3 (%)	4,20	4,21	4,00	4,12	4,17	4,20	4,14	4,11
Fe_2O_3 (%)	2,54	2,12	2,28	2,20	2,31	2,27	2,34	2,23
Total CaO (%)	58,87	60,35	60,47	60,74	59,75	60,23	59,86	60,07
MgO (%)	1,36	1,52	1,41	1,24	1,47	1,48	1,34	1,43
SO_3 (%)	3,27	3,23	2,93	2,75	3,04	3,08	3,22	3,34
K_2O (%)	0,83	0,81	0,75	0,77	0,79	0,73	0,78	0,78
Na_2O (%)	0,07	0,06	0,08	0,07	0,08	0,08	0,06	0,07
Free CaO (%)	1,24	0,62	0,73	1,18	0,73	0,95	0,78	0,95
Insoluble residue, Na_2CO_3 (%)	–	–	–	–	–	1,75	–	–
Cl^- (%)	0,02	0,01	0,01	–	–	0,02	–	–
S^{2-} (%)	–	–	–	–	–	0,06	–	–
$(Na_2O)_{equivalent}$ (%)	0,62	0,59	0,58	0,58	0,60	0,56	0,57	0,58
Mineral composition								
C_3S (%)	–	44,2	44,7	44,5	44,4	43,2	46,1	43,3
C_2S (%)	–	6,6	7,5	6,4	6,8	8,1	6,2	10,5
C_4AF (%)	–	6,9	7,3	6,9	6,6	6,4	7,5	7,0
C_3A (%)	–	6,5	5,3	7,9	5,6	6,0	5,7	6,1
Gypsum (%)	–	8,4	6,5	6,6	7,2	6,6	7,6	6,1
Calcite (%)	–	24,4	25,9	25,2	26,3	26,7	24,3	23,4
Mineral additions								
Limestone filler - L (%)	–	–	–	2,6	–	2,3	–	–

Table C.8.: Physical and mechanical characterization of CEM II/B-L 32,5N (Cimpor, Alhandra), for each cement delivery

Delivery	1^{st}	2^{nd}	3^{rd}	4^{th}	5^{th}	6^{th}	7^{th}	8^{th}
Date of collection	28-10-2005	16-01-2006	27-02-2006	12-04-2006	08-05-2006	31-05-2006	26-06-2006	19-07-2006
Physical characteristics								
Specific gravity (g/cm^3)	3,02	2,98	3,00	2,97	2,99	2,97	2,99	2,99
Surface area, *Blaine* (cm^2/g)	4230	3850	3750	3990	4060	3920	4190	4070
Residue, 90 μm (%)	1,6	1,8	2,2	2,6	2,0	2,1	2,0	2,2
Residue, 45 μm (%)	16,3	12,9	14,0	15,5	13,7	14,3	13,3	13,3
Residue, 32 μm (%)	–	–	–	–	–	–	–	–
Residue, 90 μm (%)[a]	2,6	3,2	2,7	3,1	2,7	3,6	2,8	2,6
Residue, 45 μm (%)[a]	18,4	19,3	18,3	18,8	18,2	20,0	18,2	17,9
Residue, 32 μm (%)[a]	30,2	30,9	29,8	30,0	29,7	31,6	29,5	29,3
Mean size (μm)[a]	17,18	17,13	16,27	16,01	16,30	17,44	16,03	15,92
Mechanical characteristics								
f_{ctm}(2 days) (MPa)	4,1	3,4	3,5	4,0	3,7	3,4	3,3	3,1
f_{ctm}(7 days) (MPa)	5,7	5,3	5,1	5,0	5,2	5,9	5,4	4,9
f_{ctm}(28 days) (MPa)	6,8	6,8	6,2	6,9	6,9	6,7	7,0	6,4
f_{cm}(2 days) (MPa)	21,2	18,3	17,7	17,6	19,8	19,0	16,9	16,4
f_{cm}(7 days) (MPa)	32,1	29,0	27,9	28,3	30,3	29,2	28,7	27,2
f_{cm}(28 days) (MPa)	38,3	39,5	37,8	38,3	39,7	38,5	39,1	36,9
Normal consistency								
Water demand (%)	26,2	26,0	26,0	26,0	26,0	26,6	26,2	26,8
Initial setting time (min)	125	140	145	130	145	130	130	125
Final setting time (min)	225	190	180	170	180	180	185	180
Expansion (mm)	0,5	1,0	0	0	0,5	0	0	1,0
Hidration heat 3 days (cal/g)	–	71	–	–	–	–	–	–
Hidration heat 7 days (cal/g)	–	79	–	–	–	–	–	–
Hidration heat 28 days (cal/g)	–	77	–	–	–	–	–	–

Table C.9.: Chemical characterization of CEM IV/B(V) 32,5 N, CEM II/B-L 32,5 R (BR) (Cimpor, Alhandra) and limestone filler (Micro 100, Comital)

Material type	CEM IV/B (V) 32,5 N		CEM II/B-L 32,5 R (BR)	Limestone filler	
Delivery	1^{st}	2^{nd}	1^{st}	1^{st}	2^{nd}
Date of collection	28-10-2005	08-05-2006	02-05-2006	–	02-05-2006
Chemical characteristics					
LOI (%)	2,58	3,02	10,71	43,10	43,91
SiO_2 (%)	30,95	31,73	17,63	–	0,18
Al_2O_3 (%)	12,90	12,67	2,24	< 0,4	0,04
Fe_2O_3 (%)	4,85	6,88	0,39	0,04	0,04
Total CaO (%)	41,60	39,85	64,88	–	54,96
$CaCO_3$(%)	–	–	–	99,0	–
MgO (%)	1,78	1,69	0,59	–	0,1
SO_3 (%)	1,41	2,00	2,94	–	–
K_2O (%)	1,28	1,06	0,21	–	–
Na_2O (%)	0,41	0,27	–	–	–
Free CaO (%)	1,43	0,84	1,88	–	–
Insoluble residue, Na_2CO_3 (%)	–	29,54	–	–	–
Cl^- (%)	0,03	–	0,04	–	–
S^{2-} (%)	–	–	–	–	–
$(Na_2O)_{equivalent}$ (%)	1,25	0,97	–	–	–
Mineral additions					
Limestone filler - L (%)			–		
Siliceous fly ash, V (%)	–	36,9			

Table C.10.: Physical and mechanical characterization of CEM IV/B(V) 32,5 N, CEM II/B-L 32,5 R (BR) (Cimpor, Alhandra) and limestone filler (Micro 100, Comital)

Material type	CEM IV/B (V) 32,5 N		CEM II/B-L 32,5 R (BR)	Limestone filler	
Delivery	1^{st}	2^{nd}	1^{st}	1^{st}	2^{nd}
Date of collection	28-10-2005	08-05-2006	02-05-2006	–	02-05-2006
Physical characteristics					
Specific gravity (g/cm^3)	2,81	2,76	2,95	2,70	2,73
Surface area, *Blaine* (cm^2/g)	3830	3630	4620	5150	5430
Residue, 90 μm (%)	0,2	0,7	0		
Residue, 45 μm (%)	4,0	4,6	1,7		
Residue, 32 μm (%)	–	–	–		
Residue, 90 μm (%)^a	1,2	1,6	0,0	7,9	9,8
Residue, 45 μm (%)^a	10,6	12,0	5,2	23,7	26,3
Residue, 32 μm (%)^a	21,9	23,0	14,3	30,8	33,7
Mean size (μm)^a	15,48	15,18	10,56	8,21	9,95
Mechanical characteristics					
f_{ctm}(2 days) (MPa)	3,6	3,4	4,3		
f_{ctm}(7 days) (MPa)	5,3	5,2	6,4		
f_{ctm}(28 days) (MPa)	6,3	7,8	7,7		
f_{cm}(2 days) (MPa)	17,5	17,3	22,9		
f_{cm}(7 days) (MPa)	28,3	28,3	35,5		
f_{cm}(28 days) (MPa)	39,7	38,3	44,7		
Normal consistency					
Water demand (%)	31,4	31,6	27,6		
Initial setting time (min)	145	180	130		
Final setting time (min)	280	220	195		
Expansion (mm)	0	1,0	0,5		
Hidration heat 3 days (cal/g)	–	57	84		
Hidration heat 7 days (cal/g)	–	61	86		
Hidration heat 28 days (cal/g)	–	71	95		

D. Analysis of Dflow model from paragraph 5.3.1

In the current appendix test procedures for examining hypotheses about multiple linear regression models and techniques for checking model assumptions, discussed in Chapter 4 (paragraph 4.7.4), are exemplified for the first model appearing in Chapter 5 (paragraph 5.3.1), that is Dflow model for mortars incorporating CEM I 42,5R (supplied by Cimpor-Alhandra).

D.1. ANOVA tests

The ANOVA results derived from the current data set is shown in Table D.1. The model F statistic of 272,12 turns out to be extremely large. There is only a 0,01% chance that a statistic that large could occur due to noise. The lack of fit F-statistic of 2,27 implies that the lack of fit is not significant relative to the pure error. There is a 27,24% chance that a lack of fit F-statistic that large could occur exclusively due to noise. Table D.1 also shows that only significant terms were included in the model, that is those with a p-value lower than 0,10.

The estimated model coefficients (coded and actual variables), including the respective standard error, along with the correlation coefficients, are given Table D.2. The values of both R^2 and R^2_{adj} close to 1,0 indicate that a large proportion of the variability of Dflow response is explained by the obtained regression model.

D.2. Model adequacy checking

Examining residuals is one of the most important tasks in regression analysis. Usually, three types of residuals are analysed, namely, unstandardized residuals, standardized residuals and studentized residuals (Gunst and Mason, 1980). These transformed residuals have different properties and each can be useful in detecting different undesirable patterns that can result from the tentative of adjusting a model to the data. Table D.3

Table D.1.: ANOVA tests

Test for:	Source of variation	Sum of squares	Degrees of freedom	Mean square	F value	p-value
- significance of regression	regression	34677,24	9	3853,03	272,12	$< 0{,}0001$ [a]
	error or residual	254,87	18	14,16		
	total	34932,11	27			
- lack of fit	lack of fit	234,24	15	15,62	2,27	0,2724
	pure error	20,62	3	6,88		
- partial significance of each predictor variable	V_w/V_p	2987,09	1	2987,09	210,96	$< 0{,}0001$
	w/c	18858,02	1	18858,02	1331,84	$< 0{,}0001$
	Sp/p	8223,25	1	8223,25	580,76	$< 0{,}0001$
	V_s/V_m	3354,75	1	3354,75	236,93	$< 0{,}0001$
	$(V_w/V_p)\times(w/c)$	59,10	1	59,10	4,17	0,0560
	$(V_w/V_p)\times(Sp/p)$	59,10	1	59,10	4,17	0,0560
	$(w/c)\times(V_s/V_m)$	71,19	1	71,19	5,03	0,0378
	$(w/c)^2$	1012,19	1	1012,19	71,49	$< 0{,}0001$
	$(Sp/p)^2$	155,00	1	155,00	10,95	0,0039
	error (full model)	254,87	18	14,16		

[a] predictors: V_w/V_p; w/c; Sp/p; V_s/V_m; $(V_w/V_p)\times(w/c)$;$(V_w/V_p)\times(Sp/p)$;$(w/c)\times(V_s/V_m)$;$(w/c)^2$; $(Sp/p)^2$

Table D.2.: Model summary (coded and actual variables), colinearity statistics and Durbin-Watson statistic

	coded variables		actual variables	
	coefficient estimate	standard error	coefficient estimate	VIF
independent	282,669	1,190	-150,137	1,000
V_w/V_p	11,156	0,768	92,344	1,000
w/c	28,031	0,768	1426,812	1,000
Sp/p	18,510	0,768	27824,167	1,000
V_s/V_m	-11,823	0,768	-1147,917	1,000
$(V_w/V_p)\times(w/c)$	1,922	0,941	384,375	1,000
$(V_w/V_p)\times(Sp/p)$	-1,922	0,941	-7687,500	1,000
$(w/c)\times(V_s/V_m)$	2,109	0,941	1687,500	1,000
$(w/c)^2$	-6,161	0,729	-2464,375	1,029
$(Sp/p)^2$	-2,411	0,729	-385750,00	1,029
R	R^2	R^2_{adj}	std error of the estimate	
,996	,993	,989	3,763	
Durbin-Watson			2,086	

sumarizes residuals statistics. If the errors are normally distributed, then approximately 95% of the standardized residuals shall fall in the interval (-2,+2). This is the case for our current data set (see Table D.3 and Figure D.1 (a)). In the current study residual plots were utilized for checking for the presence of patterns in the data, namely,

- to detect trends and extreme measurements, such as outliers;
- to identify potential problems, such as changes in the variance of the residuals;
- and to assess compliance with model assumptions, such as the shape of the error distribution (normality assumption).

Therefore, a plot of residuals against predicted and observed response and a plot of residuals against each predictor variable are given in Figures D.1 and D.2, respectively. The histogram and box-plot of residuals are presented in Figure D.3 and normality plots of residuals are shown in Figures D.4 and D.5. In addition, Table D.4 provides descriptive statistics of the residuals, where the values of the skewness and kurtosis are of particular interest, and Table D.5 presents the statistics of Kolmogorov-Smirnov and Shapiro-Wilk normality tests. Random order of residuals observed in Figure D.6 and Durbin-Watson test statistic (see Table D.2) show no evidence of autocorrelation in the residuals. This conclusion is supported by autocorrelation plots of residuals presented in Figure D.7. Based on VIF results (Table D.2) there is no evidence of multicollinearity among the predictor variables. Based on the maximum value of the Cook distance measure ($<$ 1,0, see Table D.3) there is no evidence of the existence of influential observations. Analysis of all of these plots and test statistics did not reveal obvious model inadequacies or

Table D.3.: Residuals statistics

	Minimum	Maximum	Mean	Std. Deviation	N
Predicted value	201,96	341,50	275,32	35,84	28
Std. predicted value	-2,047	1,847	,000	1,000	28
Std. error of predicted value	1,190	2,833	2,198	,484	28
Adjusted predicted value	201,479	345,055	275,238	35,294	28
Residual	-5,508	4,412	,00000	3,072	28
Standardized residual	-1,464	1,173	,000	,816	28
Studentized residual	-2,104	1,781	,011	1,075	28
Deleted residual	-12,029	10,183	,0834	5,510	28
Studentized deleted residual	-2,355	1,907	-,009	1,136	28
Mahal. distance	1,736	14,336	8,679	3,644	28
Cook's distance	,000	,579	,095	,168	28
Centered leverage value	,064	,531	,321	,135	28

indicate serious violations of the normality assumptions.

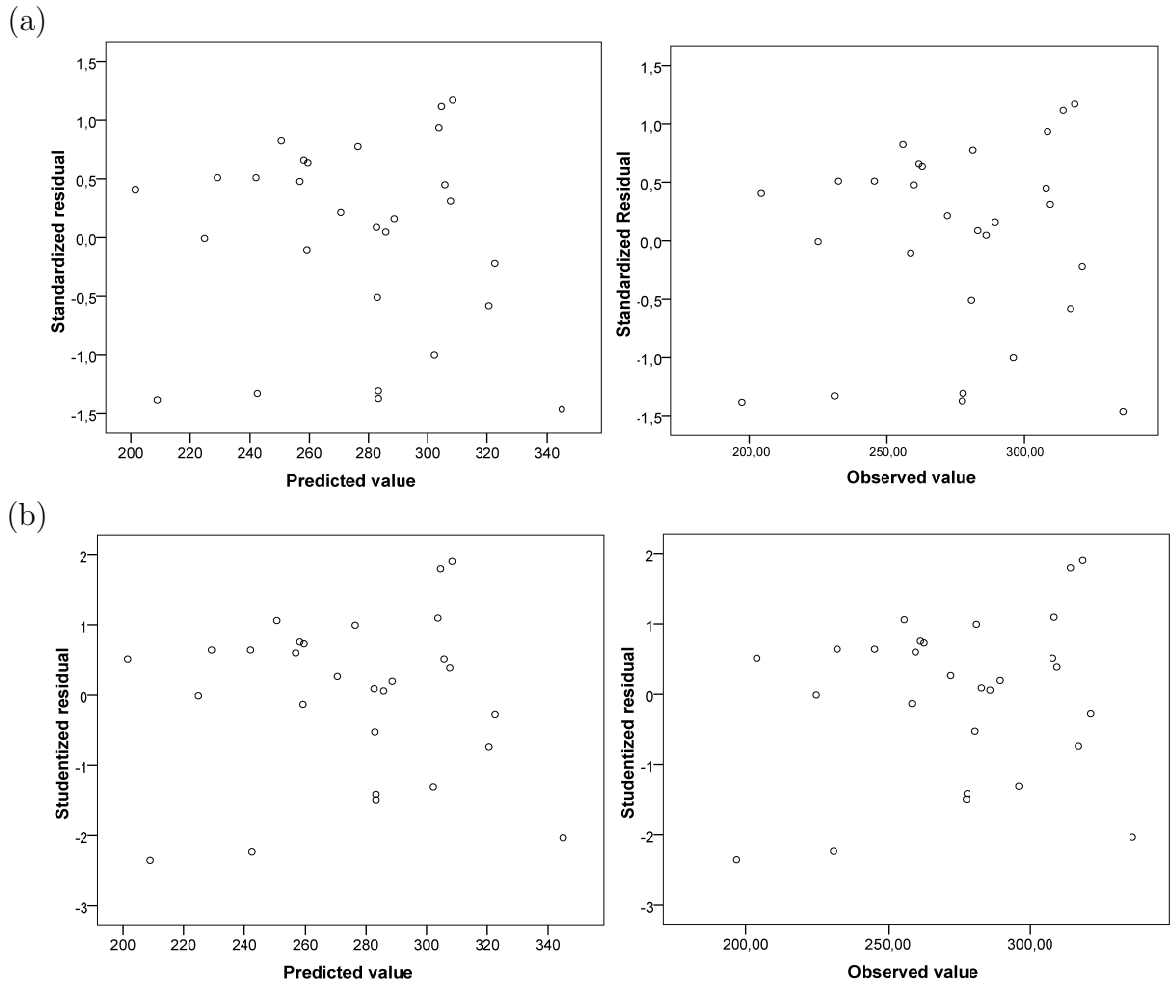


Figure D.1.: (a) Standardized residuals and (b) studentized residuals - Dflow predicted values against residuals (left) and Dflow observed values against residuals (right)

Table D.4.: Descriptive statistics of residuals

		unstandardized		studentized	
		Statistic	Std. Error	Statistic	Std. Error
Mean		,000000	,581	,011	,203
95% Confid. Interval for Mean	Lower Bound	-1,191		-,406	
	Upper Bound	1,191		,427	
5% Trimmed Mean		,0595		,030	
Median		,700		,238	
Variance		9,440		1,155	
Std. Deviation		3,072		1,075	
Minimum		-5,508		-2,104	
Maximum		4,412		1,781	
Range		9,921		1,416	
Interquartile Range		4,402		1,416	
Skewness		-,612	,441	-,563	,441
Kurtosis		-,790	,858	-,454	,858

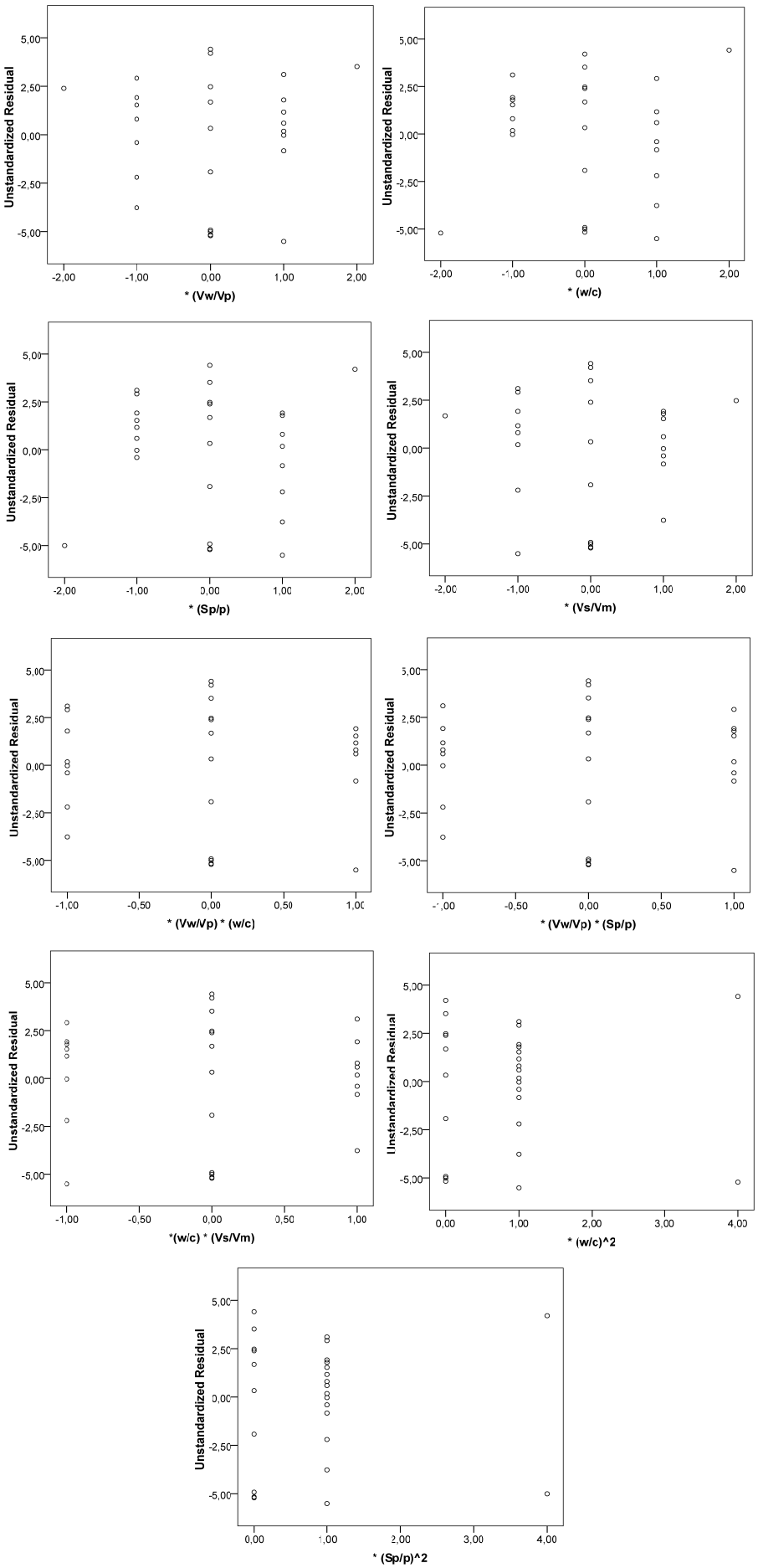


Figure D.2.: Ustandardized residuals against each predictor variable

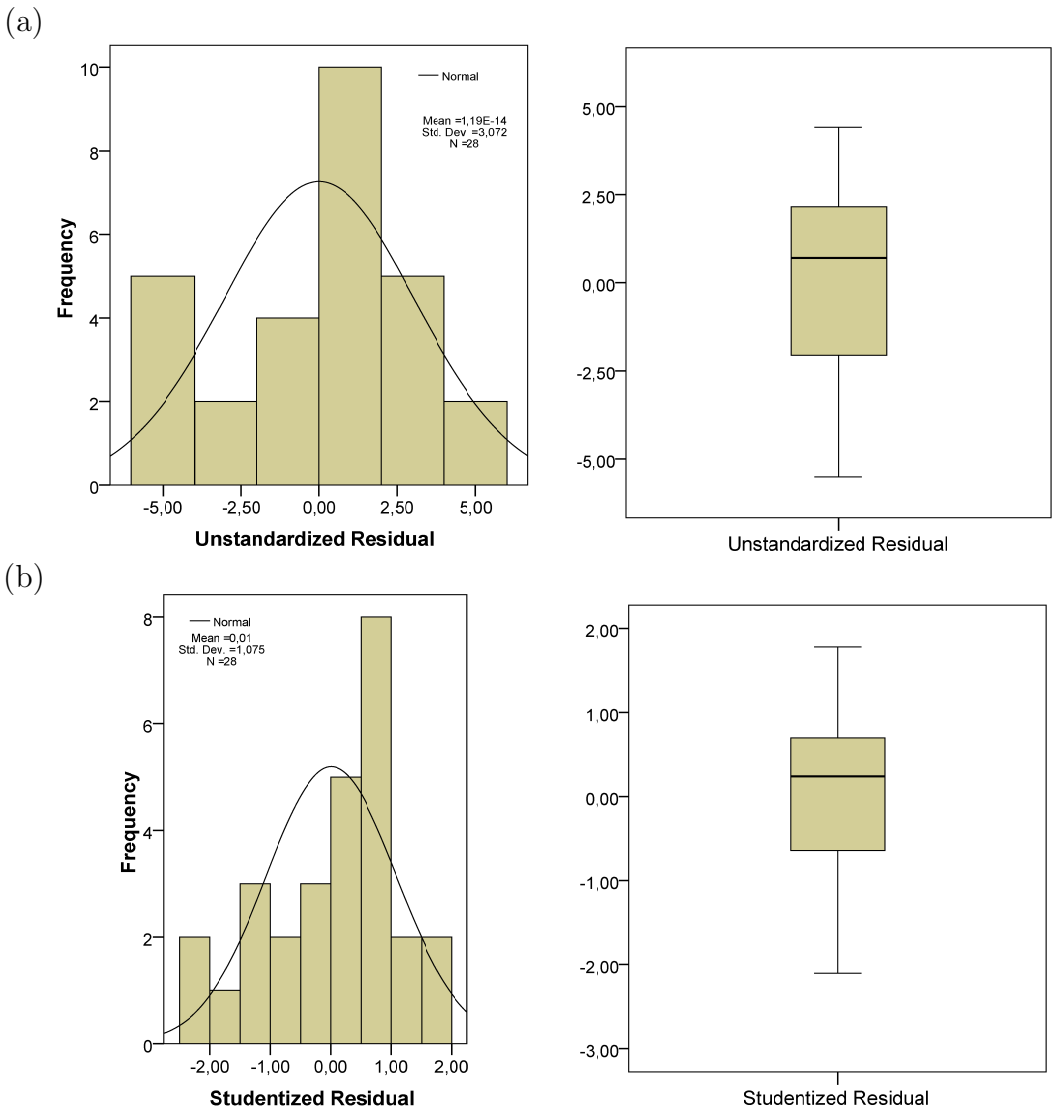


Figure D.3.: (a) Unstandardized residuals and (b) studentized residuals - Histogram (left) and box-plot (right)

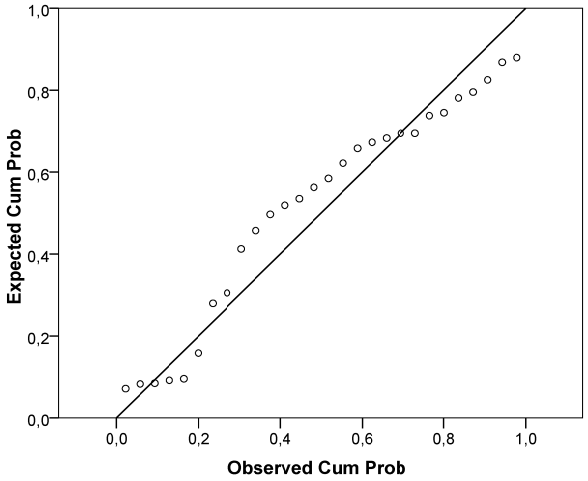


Figure D.4.: Normal P-P plot of the standardized residuals of the regression

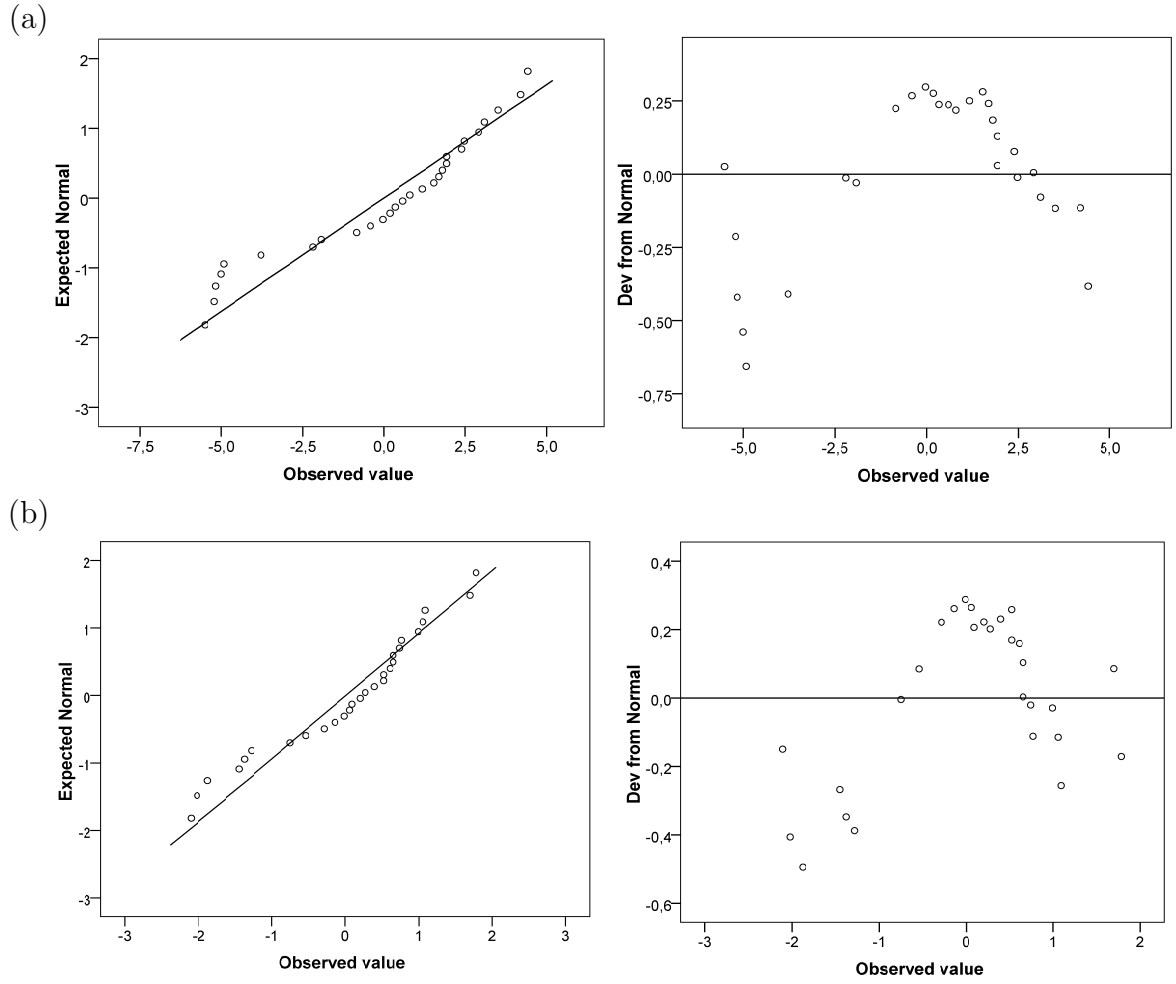


Figure D.5.: (a) Unstandardized residuals and (b) studentized residuals - Normal Q-Q plot (left) and detrended normal Q-Q plot (right)

Table D.5.: Tests of normality on residuals

Kolmogorov-Smirnov[a]			Shapiro-Wilk		
statistic	degrees of freedom	significance	statistic	degrees of freedom	significance
unstandardized					
,139	28	,177	,908	28	,018
studentized					
,135	28	,200[b]	,938	28	,097

[a]Lilliefors significance correction; [b]this is a lower bound of the true significance

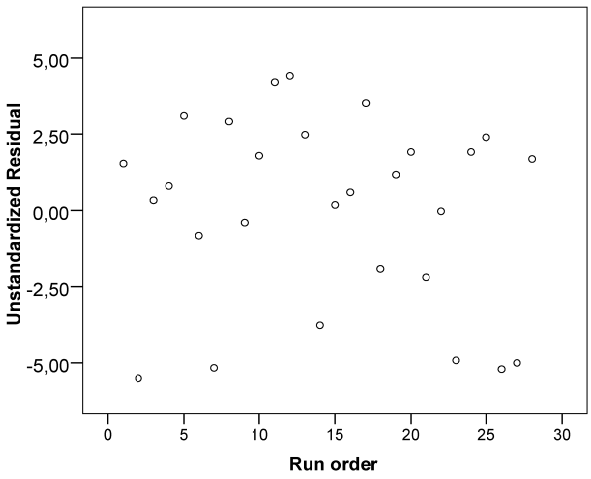
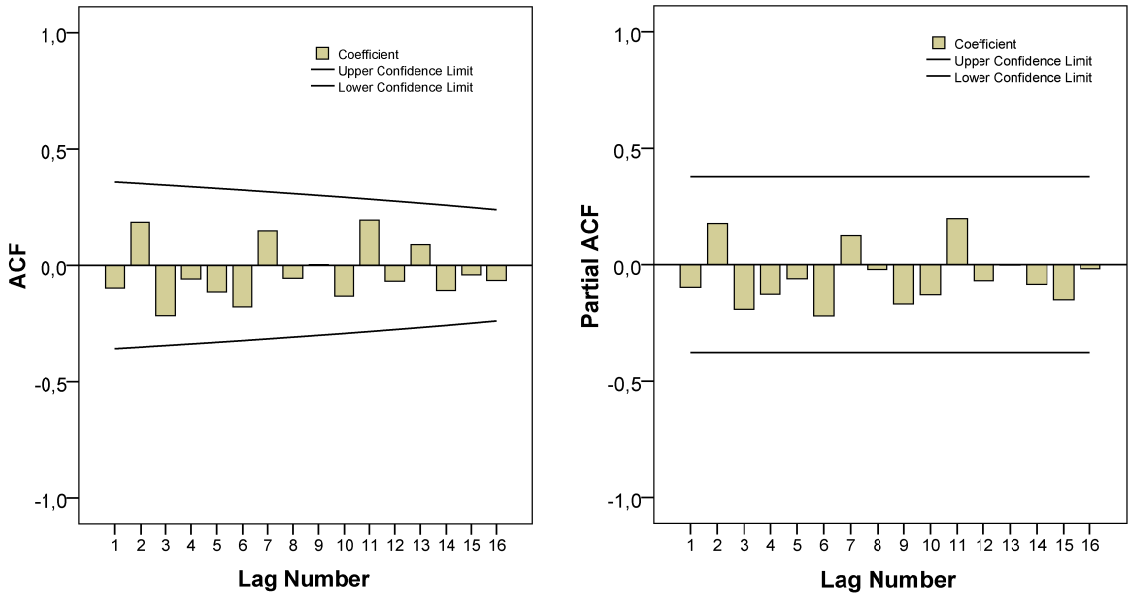


Figure D.6.: Unstandardized residuals against run order



(a) (b)

Figure D.7.: (a) Autocorrelation plot and (b) partial autocorrelation plot of unstandardized residuals

E. Mix proportions and test results

The mix proportions and test results of the mixes prepared for each experimental plan discussed in Chapters 5, 6 and 7 are presented in the following tables. In Tables E.1 to E.10 w_c, w_f, w_{sp},w_{wc}, w_{sd} represent the weight (by unit of mortar volume) of cement, limestone filler, superplasticizer, free water and sand (in dry state), respectively. In Tables E.15 to E.18 w_c, w_f, w_{Sp}, w_{wc}, w_{sd1}, w_{sd2} and w_{gd} represent the weight (by unit of concrete volume) of cement, limestone filler, superplasticizer, free water, sand 1, sand 2 and coarse aggregate (aggregates in dry state), respectively.

Table E.1.: Mix proportions and properties of fresh and hardened mortar specimens: CEM I 42,5 R (Cimpor-Alhandra) + V3000

Mix number	Ref.	w_c	w_f	w_{wc}	w_{Sp}	w_{sd}	Testing date	Dflow (mm)	Tfunnel (s)	fc,28 (MPa)
		(kg/m^3)								
1	C1	651,3	216,1	256,0	15,18	1157,4	18-01-2006	283	3,9	72,69
2	C2	651,3	216,1	256,0	15,18	1157,4	19-01-2006	278	3,7	71,06
3	C3	651,3	216,1	256,0	15,18	1157,4	20-01-2006	281	4,1	71,84
4	C4	651,3	216,1	256,0	15,18	1157,4	20-01-2006	278	4,1	68,14
5	F1	730,2	228,6	251,3	14,38	1093,1	20-01-2006	232	8,1	79,16
6	F2	821,4	63,1	284,1	13,27	1093,1	18-01-2006	256	3,6	72,91
7	F3	567,9	369,5	251,5	14,06	1093,1	19-01-2006	281	4,2	65,97
8	F4	638,9	221,6	284,4	12,91	1093,1	20-01-2006	310	1,9	69,64
9	F5	730,2	228,6	247,4	19,18	1093,1	18-01-2006	272	6,3	78,32
10	F6	821,4	63,1	280,5	17,69	1093,1	19-01-2006	286	3,3	75,50
11	F7	567,9	369,5	247,7	18,75	1093,1	20-01-2006	317	3,7	70,57
12	F8	638,9	221,6	280,9	17,21	1093,1	18-01-2006	336	1,8	76,67
13	F9	666,7	208,7	230,9	13,13	1221,7	18-01-2006	204	11,7	77,00
14	F10	750,0	57,6	260,9	12,11	1221,7	20-01-2006	225	5,5	74,15
15	F11	518,5	337,3	231,2	12,84	1221,7	19-01-2006	258	6,1	65,84
16	F12	583,3	202,3	261,2	11,78	1221,7	19-01-2006	290	2,8	69,13
17	F13	666,7	208,7	227,4	17,51	1221,7	20-01-2006	245	9,7	78,51
18	F14	750,0	57,6	257,6	16,15	1221,7	19-01-2006	260	4,6	76,71
19	F15	518,5	337,3	227,7	17,12	1221,7	19-01-2006	296	5,2	68,62
20	F16	583,3	202,3	258,0	15,71	1221,7	18-01-2006	321	2,4	70,57
21	CC1	720,2	81,9	284,5	14,04	1157,4	20-01-2006	308	2,0	69,72
22	CC2	566,2	382,0	220,8	16,59	1157,4	19-01-2006	263	10,0	73,28
23	CC3	521,1	329,2	256,3	14,88	1157,4	20-01-2006	318	2,4	61,27
24	CC4	868,4	27,6	255,6	15,68	1157,4	19-01-2006	197	10,5	76,16
25	CC5	651,3	216,1	252,5	19,52	1157,4	20-01-2006	314	3,0	75,59
26	CC6	651,3	216,1	259,6	10,84	1157,4	19-01-2006	231	4,8	74,26
27	CC7	592,1	196,5	234,3	13,80	1286,0	20-01-2006	262	5,8	75,31
28	CC8	710,5	235,8	277,7	16,56	1028,8	19-01-2006	308	2,7	70,56
29	([a])	468,3	374,5	207,7	14,49	1286,0	16-03-2006	248	10,3	64,41
30	([a])	601,1	346,5	221,9	17,62	1157,0	16-03-2006	258	9,6	72,48
31	([a])	654,3	335,0	227,8	18,70	1106,0	16-03-2006	254	10,1	74,10

[a] mixtures not used to derive the models

Table E.2.: Mix proportions and properties of fresh and hardened mortar specimens: CEM I 52,5 R (Cimpor-Alhandra) + V3000

Mix number	Ref.	w_c	w_f	w_{wc}	w_{Sp}	w_{sd}	Testing date	Dflow (mm)	Tfunnel (s)	fc,28 (MPa)
		(kg/m^3)								
1	C1	651,3	216,1	256,0	15,18	1157,4	16-01-2006	250	4,6	73,13
2	C2	651,3	216,1	256,0	15,18	1157,4	16-01-2006	250	4,6	75,72
3	C3	651,3	216,1	256,0	15,18	1157,4	17-01-2006	256	4,4	76,75
4	C4	651,3	216,1	256,0	15,18	1157,4	18-01-2006	254	4,1	76,34
5	F1	730,2	228,6	251,3	14,38	1093,1	16-01-2006	203	9,9	86,64
6	F2	821,4	63,1	284,1	13,27	1093,1	17-01-2006	220	4,3	78,97
7	F3	567,9	369,5	251,5	14,06	1093,1	16-01-2006	275	4,6	66,48
8	F4	638,9	221,6	284,4	12,91	1093,1	18-01-2006	293	2,0	70,37
9	F5	730,2	228,6	247,4	19,18	1093,1	16-01-2006	244	8,3	81,41
10	F6	821,4	63,1	280,5	17,69	1093,1	17-01-2006	250	3,4	76,77
11	F7	567,9	369,5	247,7	18,75	1093,1	17-01-2006	295	4,0	73,84
12	F8	638,9	221,6	280,9	17,21	1093,1	16-01-2006	311	2,0	79,54
13	F9	666,7	208,7	230,9	13,13	1221,7	16-01-2006	180	15,9	72,52
14	F10	750,0	57,6	260,9	12,11	1221,7	18-01-2006	201	6,1	76,59
15	F11	518,5	337,3	231,2	12,84	1221,7	17-01-2006	243	6,7	69,91
16	F12	583,3	202,3	261,2	11,78	1221,7	17-01-2006	262	3,1	74,46
17	F13	666,7	208,7	227,4	17,51	1221,7	17-01-2006	216	11,5	80,29
18	F14	750,0	57,6	257,6	16,15	1221,7	18-01-2006	233	5,3	71,90
19	F15	518,5	337,3	227,7	17,12	1221,7	16-01-2006	280	5,7	75,30
20	F16	583,3	202,3	258,0	15,71	1221,7	17-01-2006	300	2,6	69,05
21	CC1	720,2	81,9	284,5	14,04	1157,4	18-01-2006	276	2,2	78,11
22	CC2	566,2	382,0	220,8	16,59	1157,4	16-01-2006	241	10,4	77,13
23	CC3	521,1	329,2	256,3	14,88	1157,4	17-01-2006	303	2,7	68,29
24	CC4	868,4	27,6	255,6	15,68	1157,4	17-01-2006	168	14,4	86,24
25	CC5	651,3	216,1	252,5	19,52	1157,4	16-01-2006	286	3,8	71,38
26	CC6	651,3	216,1	259,6	10,84	1157,4	18-01-2006	222	5,3	76,53
27	CC7	592,1	196,5	234,3	13,80	1286,0	17-01-2006	235	6,5	71,67
28	CC8	710,5	235,8	277,7	16,56	1028,8	17-01-2006	277	3,1	77,52
29	([a])	466,5	378,3	205,6	16,06	1286,0	16-03-2006	255	9,4	67,64
30	([a])	494,8	373,0	207,3	17,23	1260,0	16-03-2006	250	10,3	71,37
31	([a])	532,5	379,3	211,3	18,68	1209,0	16-03-2006	251	10,0	73,40

[a] mixtures not used to derive the models

Table E.3.: Mix proportions and properties of fresh and hardened mortar specimens: CEM II/A-L 42,5 R (Cimpor-Alhandra) + V3000

Mix number	Ref.	w_c	w_f	w_{wc}	w_{Sp}	w_{sd}	Testing date	Dflow (mm)	Tfunnel (s)	fc,28 (MPa)
		(kg/m^3)								
1	C1	651,3	208,8	256,1	15,05	1157,4	11-01-2006	291	3,4	72,79
2	C2	651,3	208,8	256,1	15,05	1157,4	13-01-2006	286	3,4	75,47
3	C3	651,3	208,8	256,1	15,05	1157,4	13-01-2006	286	3,5	74,62
4	C4	651,3	208,8	256,1	15,05	1157,4	13-01-2006	290	3,3	73,93
5	F1	730,2	220,3	251,4	14,26	1093,1	11-01-2006	245	6,2	75,52
6	F2	821,4	53,8	284,2	13,13	1093,1	12-01-2006	268	2,7	77,43
7	F3	567,9	363,0	251,6	13,96	1093,1	12-01-2006	297	3,5	64,22
8	F4	638,9	214,4	284,5	12,80	1093,1	11-01-2006	322	1,7	69,57
9	F5	730,2	220,3	247,5	19,01	1093,1	12-01-2006	285	5,4	75,08
10	F6	821,4	53,8	280,7	17,50	1093,1	11-01-2006	300	2,5	81,23
11	F7	567,9	363,0	247,8	18,62	1093,1	12-01-2006	328	3,7	68,00
12	F8	638,9	214,4	281,0	17,06	1093,1	11-01-2006	349	1,7	66,07
13	F9	666,7	201,2	231,0	13,02	1221,7	11-01-2006	218	9,6	68,05
14	F10	750,0	49,1	261,0	11,99	1221,7	12-01-2006	244	4,1	74,68
15	F11	518,5	331,5	231,2	12,75	1221,7	13-01-2006	281	5,0	67,91
16	F12	583,3	195,7	261,3	11,69	1221,7	11-01-2006	295	2,5	62,52
17	F13	666,7	201,2	227,5	17,36	1221,7	11-01-2006	260	7,9	73,46
18	F14	750,0	49,1	257,8	15,98	1221,7	13-01-2006	276	3,7	78,93
19	F15	518,5	331,5	227,8	17,00	1221,7	12-01-2006	302	5,0	68,80
20	F16	583,3	195,7	258,1	15,58	1221,7	11-01-2006	317	2,2	64,99
21	CC1	720,2	73,7	284,6	13,89	1157,4	12-01-2006	311	1,9	72,97
22	CC2	566,2	375,6	220,9	16,48	1157,4	12-01-2006	266	8,8	67,42
23	CC3	521,1	323,3	256,4	14,78	1157,4	12-01-2006	321	2,4	64,36
24	CC4	868,4	17,8	255,8	15,51	1157,4	11-01-2006	215	8,0	85,50
25	CC5	651,3	208,8	252,6	19,35	1157,4	12-01-2006	321	2,8	72,18
26	CC6	651,3	208,8	259,6	10,75	1157,4	11-01-2006	260	3,8	69,00
27	CC7	592,1	189,8	234,4	13,68	1286,0	12-01-2006	268	5,0	69,76
28	CC8	710,5	227,7	277,8	16,42	1028,8	12-01-2006	311	2,3	73,57
29	([a])	464,6	376,9	206,9	13,33	1286,0	22-03-2006	255	8,6	60,50
30	([a])	618,6	323,1	222,7	17,22	1157,0	16-03-2006	258	8,6	65,15
31	([a])	751,9	288,8	239,1	19,64	1029,0	16-03-2006	256	8,6	69,12

[a] mixtures not used to derive the models

Table E.4.: Mix proportions and properties of fresh and hardened mortar specimens: CEM II/B-L 32,5 N (Cimpor-Alhandra) + V3000

Mix number	Ref.	w_c	w_f	w_{wc}	w_{Sp}	w_{sd}	Testing date	Dflow (mm)	Tfunnel (s)	fc,28 (MPa)
		(kg/m^3)								
1	C1	631,8	232,2	248,3	15,12	1157,4	23-01-2006	304	4,2	61,12
2	C2	631,8	232,2	248,3	15,12	1157,4	24-01-2006	298	4,7	61,17
3	C3	631,8	232,2	248,3	15,12	1157,4	25-01-2006	300	4,1	59,66
4	C4	631,8	232,2	248,3	15,12	1157,4	25-01-2006	295	4,6	60,11
5	F1	704,1	251,4	242,2	14,33	1093,1	24-01-2006	258	8,2	68,53
6	F2	800,4	73,4	276,9	13,11	1093,1	23-01-2006	276	3,4	66,25
7	F3	547,6	392,6	242,4	14,10	1093,1	25-01-2006	289	5,4	53,41
8	F4	622,5	234,0	277,1	12,85	1093,1	23-01-2006	317	2,3	53,74
9	F5	704,1	251,4	238,3	19,11	1093,1	24-01-2006	298	6,9	74,95
10	F6	800,4	73,4	273,3	17,48	1093,1	24-01-2006	312	2,8	67,70
11	F7	547,6	392,6	238,5	18,81	1093,1	24-01-2006	325	4,7	55,31
12	F8	622,5	234,0	273,6	17,13	1093,1	23-01-2006	346	1,9	54,98
13	F9	642,9	229,5	222,6	13,09	1221,7	23-01-2006	224	12,5	68,36
14	F10	730,8	67,0	254,3	11,97	1221,7	25-01-2006	255	4,7	68,25
15	F11	500,0	358,5	222,8	12,88	1221,7	24-01-2006	278	7,4	52,55
16	F12	568,4	213,7	254,5	11,73	1221,7	24-01-2006	298	3,2	48,24
17	F13	642,9	229,5	219,1	17,45	1221,7	24-01-2006	265	11,2	70,03
18	F14	730,8	67,0	251,1	15,96	1221,7	24-01-2006	290	4,4	70,22
19	F15	500,0	358,5	219,3	17,17	1221,7	24-01-2006	317	6,4	56,08
20	F16	568,4	213,7	251,3	15,64	1221,7	25-01-2006	317	2,8	52,56
21	CC1	704,3	88,4	278,3	13,87	1157,4	25-01-2006	318	2,0	60,04
22	CC2	541,7	410,9	211,0	16,67	1157,4	23-01-2006	273	12,0	60,03
23	CC3	505,4	346,3	248,4	14,91	1157,4	25-01-2006	318	3,1	47,32
24	CC4	842,3	42,1	248,0	15,48	1157,4	24-01-2006	256	7,4	80,29
25	CC5	631,8	232,2	244,7	19,44	1157,4	25-01-2006	330	3,7	58,25
26	CC6	631,8	232,2	251,8	10,80	1157,4	24-01-2006	259	5,2	61,40
27	CC7	574,3	211,1	227,3	13,75	1286,0	24-01-2006	271	6,7	61,92
28	CC8	689,2	253,3	269,2	16,49	1028,8	25-01-2006	316	3,2	59,83
29	([a])	466,9	361,0	208,8	12,36	1286,0	16-03-2006	260	10,5	49,78
30	([a])	572,7	349,3	225,7	13,76	1157,0	16-03-2006	263	8,7	58,14
31	([a])	714,1	300,3	245,3	14,31	1029,0	16-03-2006	258	8,4	67,17

[a] mixtures not used to derive the models

Table E.5.: Mix proportions and properties of fresh and hardened mortar specimens: CEM IV/B(V) 32,5 N (Cimpor-Alhandra) + V3000

Mix		w_c	w_f	w_{wc}	w_{Sp}	w_{sd}	Testing	Dflow	Tfunnel	fc,28
number	Ref.			(kg/m^3)			date	(mm)	(s)	(MPa)
1	C1	582,0	257,7	240,3	14,69	1157,4	26-01-2006	309	5,8	57,05
2	C2	582,0	257,7	240,3	14,69	1157,4	26-01-2006	312	6,1	55,16
3	C3	582,0	257,7	240,3	14,69	1157,4	27-01-2006	312	6,0	48,67
4	C4	582,0	257,7	240,3	14,69	1157,4	30-01-2006	300	6,1	54,54
5	F1	639,9	289,5	232,8	13,94	1093,1	27-01-2006	212	12,4	63,66
6	F2	736,1	99,6	269,6	12,54	1093,1	30-01-2006	250	5,6	56,59
7	F3	503,8	422,2	232,9	13,89	1093,1	26-01-2006	312	6,9	54,14
8	F4	579,5	252,2	269,6	12,48	1093,1	26-01-2006	336	2,8	50,55
9	F5	639,9	289,5	229,0	18,59	1093,1	27-01-2006	281	10,1	66,58
10	F6	736,1	99,6	266,2	16,71	1093,1	26-01-2006	301	5,1	64,04
11	F7	503,8	422,2	229,1	18,52	1093,1	30-01-2006	333	6,2	53,13
12	F8	579,5	252,2	266,2	16,63	1093,1	25-01-2006	360	2,8	56,45
13	F9	584,3	264,3	214,1	12,73	1221,7	25-01-2006	185	18,0	60,11
14	F10	672,1	90,9	247,7	11,45	1221,7	30-01-2006	227	7,0	57,50
15	F11	459,9	385,5	214,1	12,68	1221,7	26-01-2006	293	9,2	51,72
16	F12	529,1	230,3	247,7	11,39	1221,7	30-01-2006	309	4,2	46,92
17	F13	584,3	264,3	210,7	16,97	1221,7	30-01-2006	259	12,8	62,48
18	F14	672,1	90,9	244,6	15,26	1221,7	30-01-2006	277	6,5	64,09
19	F15	459,9	385,5	210,7	16,91	1221,7	30-01-2006	319	8,1	56,03
20	F16	529,1	230,3	244,6	15,19	1221,7	26-01-2006	340	3,7	53,66
21	CC1	654,8	104,3	272,0	13,28	1157,4	26-01-2006	315	2,9	59,13
22	CC2	491,1	449,5	200,7	16,46	1157,4	26-01-2006	269	15,7	57,80
23	CC3	470,1	366,8	240,4	14,65	1157,4	30-01-2006	338	4,2	47,54
24	CC4	763,9	80,4	240,3	14,78	1157,4	26-01-2006	190	12,7	64,57
25	CC5	582,0	257,7	236,9	18,89	1157,4	27-01-2006	334	5,4	64,74
26	CC6	582,0	257,7	243,8	10,50	1157,4	30-01-2006	248	7,4	52,65
27	CC7	529,1	234,3	220,1	13,36	1286,0	30-01-2006	281	7,8	55,65
28	CC8	634,9	281,1	260,6	16,03	1028,8	30-01-2006	321	5,0	61,58
29	([a])	479,7	326,5	215,4	11,09	1260,0	22-03-2006	234	11,6	47,45
30	([a])	576,6	300,3	227,1	13,97	1157,0	22-03-2006	254	9,8	54,31
31	([a])	729,0	220,6	247,3	18,26	1029,0	22-03-2006	282	8,4	72,12

[a] mixtures not used to derive the models

Table E.6.: Mix proportions and properties of fresh and hardened mortar specimens: CEM II/B-L 32,5 R (BR) (Cimpor[b]) + V3000

Mix number	Ref.	w_c	w_f	w_{wc}	w_{Sp}	w_{sd}	Testing date	Dflow (mm)	Tfunnel (s)	fc,28 (MPa)
		(kg/m^3)								
1	C1	596,0	331,7	224,9	11,60	1157,4	01-03-2006	311	6,0	68,69
2	C2	596,0	331,7	224,9	11,60	1157,4	01-03-2006	308	6,0	69,09
3	C3	596,0	331,7	224,9	11,60	1157,4	02-03-2006	318	6,0	72,38
4	C4	596,0	331,7	224,9	11,60	1157,4	03-03-2006	317	5,7	66,55
5	F1	653,4	376,3	214,7	10,30	1093,1	02-03-2006	251	12,3	73,58
6	F2	774,4	158,5	255,4	9,33	1093,1	02-03-2006	284	4,9	67,30
7	F3	501,5	514,4	214,8	10,16	1093,1	01-03-2006	286	8,6	55,00
8	F4	594,3	322,2	255,5	9,17	1093,1	01-03-2006	306	2,9	58,70
9	F5	653,4	376,3	210,5	15,45	1093,1	02-03-2006	312	8,5	80,19
10	F6	774,4	158,5	251,6	13,99	1093,1	01-03-2006	330	3,6	80,93
11	F7	501,5	514,4	210,6	15,24	1093,1	01-03-2006	322	7,1	61,07
12	F8	594,3	322,2	251,8	13,75	1093,1	01-02-2006	340	2,7	67,06
13	F9	596,6	343,6	197,5	9,40	1221,7	01-02-2006	218	19,6	77,69
14	F10	707,1	144,7	234,7	8,52	1221,7	02-03-2006	268	5,9	63,71
15	F11	457,8	469,7	197,6	9,28	1221,7	02-03-2006	258	12,2	58,88
16	F12	542,6	294,2	234,8	8,37	1221,7	01-02-2006	295	4,2	62,35
17	F13	596,6	343,6	193,7	14,10	1221,7	02-03-2006	298	11,3	80,63
18	F14	707,1	144,7	231,2	12,78	1221,7	01-03-2006	315	5,2	81,47
19	F15	457,8	469,7	193,8	13,91	1221,7	03-03-2006	307	9,2	61,54
20	F16	542,6	294,2	231,4	12,55	1221,7	03-03-2006	317	3,8	62,79
21	CC1	685,6	158,3	259,8	10,55	1157,4	01-03-2006	328[c]	1,9[c]	68,75[c]
22	CC2	482,5	551,4	180,7	12,92	1157,4	02-03-2006	242	21,5	68,61
23	CC3	471,8	444,6	225,0	11,46	1157,4	01-03-2006	310	4,9	52,08
24	CC4	808,8	138,2	224,7	11,84	1157,4	02-03-2006	295	8,5	87,08
25	CC5	596,0	331,7	221,1	16,23	1157,4	02-03-2006	330	5,2	81,38
26	CC6	596,0	331,7	228,7	6,96	1157,4	03-03-2006	184[c]	13,7[c]	60,15[c]
27	CC7	541,8	301,6	206,0	10,54	1286,0	03-03-2006	290	7,7	67,70
28	CC8	650,2	361,9	243,7	12,65	1028,8	01-03-2006	326	4,9	75,81
29	([a])	423,2	443,9	205,1	8,04	1260	15-03-2006	266	8,3	41,71
30	([a])	571,4	379,3	217,2	9,53	1157	15-03-2006	280	8,5	68,19
31	([a])	823,4	249,0	228,3	11,40	1029	15-03-2006	251	12,9	87,59

[a] mixtures not used to derive the models; [b]white cement was supplied by Cimpor but produced by Secil;
[c]these observations were identified as outliers and, consequently, were excluded from the data

Table E.7.: Mix proportions and properties of fresh and hardened mortar specimens: CEM I 42,5 R (Secil-Maceira) + V3000

Mix		w_c	w_f	w_{wc}	w_{Sp}	w_{sd}	Testing	Dflow	Tfunnel	fc,28
number	Ref.	(kg/m^3)					date	(mm)	(s)	(MPa)
1	C1	651,3	217,9	256,0	15,21	1157,4	11-01-2007	233	3,9	63,68
2	C2	651,3	217,9	256,0	15,21	1157,4	11-01-2007	234	4,1	60,76
3	C3	651,3	217,9	256,0	15,21	1157,4	17-01-2007	225	4,7	58,36
4	C4	651,3	217,9	256,0	15,21	1157,4	18-01-2007	241	4,3	62,07
5	F1	730,2	230,6	251,2	14,41	1093,1	11-01-2007	177	9,4	65,95
6	F2	821,4	65,4	284,1	13,30	1093,1	17-01-2007	209	3,6	62,73
7	F3	567,9	371,0	251,5	14,08	1093,1	18-01-2007	246	4,9	51,70
8	F4	638,9	223,4	284,4	12,93	1093,1	11-01-2007	266	2,1	60,58
9	F5	730,2	230,6	247,3	19,22	1093,1	18-01-2007	222	7,6	57,28
10	F6	821,4	65,4	280,5	17,74	1093,1	17-01-2007	243	3,4	62,28
11	F7	567,9	371,0	247,7	18,78	1093,1	18-01-2007	270	4,5	55,85
12	F8	638,9	223,4	280,9	17,25	1093,1	11-01-2007	291	1,8	60,11
13	F9	666,7	210,6	230,9	13,16	1221,7	11-01-2007	155	14,2	71,10
14	F10	750,0	59,7	260,9	12,15	1221,7	17-01-2007	192	5,2	64,73
15	F11	518,5	338,8	231,2	12,86	1221,7	11-01-2007	220	6,8	55,49
16	F12	583,3	203,9	261,2	11,81	1221,7	17-01-2007	242	2,9	49,03
17	F13	666,7	210,6	227,3	17,54	1221,7	11-01-2007	206	9,8	65,55
18	F14	750,0	59,7	257,6	16,19	1221,7	18-01-2007	226	4,5	59,81
19	F15	518,5	338,8	227,7	17,15	1221,7	17-01-2007	250	6,6	60,15
20	F16	583,3	203,9	258,0	15,75	1221,7	17-01-2007	272	2,6	55,20
21	CC1	720,2	83,9	284,5	14,07	1157,4	11-01-2007	259	2,0	64,30
22	CC2	566,2	383,6	220,8	16,62	1157,4	18-01-2007	211	11,4	65,27
23	CC3	521,1	330,7	256,2	14,91	1157,4	17-01-2006	284	2,7	49,36
24	CC4	868,4	30,1	255,6	15,72	1157,4	11-01-2007	165	10,3	63,18
25	CC5	651,3	217,9	252,5	19,56	1157,4	17-01-2007	266	4,0	63,23
26	CC6	651,3	217,9	259,5	10,87	1157,4	11-01-2007	192	5,3	62,55
27	CC7	592,1	198,1	234,3	13,83	1286,0	18-01-2007	224	6,3	55,37
28	CC8	710,5	237,8	277,7	16,59	1028,8	17-01-2007	250	3,1	62,69

Table E.8.: Mix proportions and properties of fresh and hardened mortar specimens: CEM I 42,5 R (Secil-Outão) + V3000

Mix number	Ref.	w_c (kg/m^3)	w_f (kg/m^3)	w_{wc} (kg/m^3)	w_{Sp} (kg/m^3)	w_{sd} (kg/m^3)	Testing date	Dflow (mm)	Tfunnel (s)	fc,28 (MPa)
1	C1	643,3	267,1	239,3	15,93	1157,4	23-01-2007	283	5,7	65,73
2	C2	643,3	267,1	239,3	15,93	1157,4	24-01-2007	283	5,6	68,16
3	C3	643,3	267,1	239,3	15,93	1157,4	24-01-2007	282	5,5	55,32
4	C4	643,3	267,1	239,3	15,93	1157,4	25-01-2006	279	5,9	60,67
5	F1	696,4	309,3	231,9	15,08	1093,1	23-01-2007	219	11,5	70,56
6	F2	801,1	122,3	268,5	13,85	1093,1	24-01-2007	236	4,8	61,54
7	F3	538,1	446,5	232,2	14,77	1093,1	23-01-2007	312	6,1	59,70
8	F4	619,0	280,2	268,8	13,49	1093,1	24-01-2007	317	2,5	65,29
9	F5	696,4	309,3	227,8	20,11	1093,1	23-01-2007	261	9,3	78,86
10	F6	801,1	122,3	264,8	18,47	1093,1	23-01-2007	284	4,2	72,27
11	F7	538,1	446,5	228,1	19,69	1093,1	24-01-2007	348	5,5	61,93
12	F8	619,0	280,2	265,1	17,98	1093,1	23-01-2007	366	2,4	64,00
13	F9	635,8	282,4	213,3	13,77	1221,7	22-01-2007	188	18,4	60,23
14	F10	731,4	111,7	246,7	12,65	1221,7	24-01-2007	216	6,3	67,05
15	F11	491,3	407,7	213,5	13,49	1221,7	23-01-2007	280	9,2	59,55
16	F12	565,2	255,8	247,0	12,32	1221,7	24-01-2007	309	3,7	62,86
17	F13	635,8	282,4	209,5	18,36	1221,7	23-01-2007	243	13,6	63,37
18	F14	731,4	111,7	243,2	16,86	1221,7	25-01-2007	261	5,3	63,68
19	F15	491,3	407,7	209,8	17,98	1221,7	24-01-2006	329	7,7	63,61
20	F16	565,2	255,8	243,6	16,42	1221,7	23-01-2007	352	2,7	60,68
21	CC1	723,7	114,8	270,9	14,67	1157,4	24-01-2007	156	16,7	68,47
22	CC2	542,8	457,4	199,9	17,50	1157,4	23-01-2007	258	15,1	61,85
23	CC3	488,9	401,0	239,6	15,57	1157,4	24-01-2007	352	4,0	55,76
24	CC4	814,8	118,3	239,0	16,33	1157,4	23-01-2007	202	11,5	60,12
25	CC5	643,3	267,1	235,6	20,48	1157,4	24-01-2006	320	5,1	74,62
26	CC6	643,3	267,1	243,0	11,38	1157,4	25-01-2007	231	7,0	65,49
27	CC7	584,8	242,8	219,2	14,48	1286,0	23-01-2007	254	8,6	58,40
28	CC8	701,8	291,3	259,5	17,38	1028,8	25-01-2007	295	4,7	64,50

Table E.9.: Mix proportions and properties of fresh and hardened mortar specimens: CEM I 42,5 R (Cimpor-Souselas) + V3000

Mix number	Ref.	w_c	w_f	w_{wc}	w_{Sp}	w_{sd}	Testing date	Dflow (mm)	Tfunnel (s)	fc,28 (MPa)
		(kg/m^3)								
1	C1	685,6	186,9	256,0	15,27	1157,4	06-02-2007	256	4,5	48,10
2	C2	685,6	186,9	256,0	15,27	1157,4	08-02-2007	252	4,8	52,73
3	C3	685,6	186,9	256,0	15,27	1157,4	08-02-2007	274	4,5	51,34
4	C4	685,6	186,9	256,0	15,27	1157,4	09-02-2007	270	4,7	49,64
5	F1	751,6	210,6	251,2	14,43	1093,1	08-02-2007	207	8,9	54,45
6	F2	845,6	42,8	284,1	13,33	1093,1	09-02-2007	276	4,0	54,51
7	F3	580,8	358,7	251,5	14,09	1093,1	06-02-2007	259	4,9	50,57
8	F4	653,4	209,5	284,4	12,94	1093,1	09-02-2007	316	2,3	50,05
9	F5	751,6	210,6	247,3	19,24	1093,1	08-02-2007	250	7,4	57,75
10	F6	845,6	42,8	280,5	17,77	1093,1	08-02-2007	292	2,9	52,08
11	F7	580,8	358,7	247,7	18,79	1093,1	09-02-2007	320	4,8	48,69
12	F8	653,4	209,5	280,9	17,26	1093,1	06-02-2007	309	2,0	48,88
13	F9	686,3	192,3	230,9	13,18	1221,7	06-02-2007	182	16,5	55,30
14	F10	772,1	39,1	260,9	12,17	1221,7	09-02-2007	222	5,6	46,51
15	F11	530,3	327,6	231,2	12,87	1221,7	06-02-2007	238	7,0	49,56
16	F12	596,6	191,3	261,2	11,82	1221,7	09-02-2007	275	2,9	45,71
17	F13	686,3	192,3	227,3	17,57	1221,7	06-02-2007	228	11,2	55,37
18	F14	772,1	39,1	257,6	16,22	1221,7	09-02-2007	264	5,0	50,05
19	F15	530,3	327,6	227,7	17,16	1221,7	08-02-2007	267	6,3	46,36
20	F16	596,6	191,3	258,0	15,76	1221,7	08-02-2007	298	2,9	50,89
21	CC1	758,1	49,6	284,4	14,14	1157,4	09-02-2007	292	2,3	48,88
22	CC2	596,0	356,6	220,8	16,67	1157,4	06-02-2007	226	12,6	51,22
23	CC3	521,1	329,7	256,3	14,89	1157,4	09-02-2007	305	2,9	45,62
24	CC4	868,4	28,4	255,6	15,69	1157,4	08-02-2007	196	9,4	54,60
25	CC5	685,6	186,9	252,4	19,63	1157,4	08-02-2007	282	4,1	57,38
26	CC6	685,6	186,9	259,5	10,91	1157,4	09-02-2007	217	5,2	47,72
27	CC7	623,3	169,9	234,3	13,88	1286,0	06-02-2007	226	7,0	49,00
28	CC8	747,9	203,9	277,6	16,66	1028,8	08-02-2007	302	3,1	52,68

Table E.10.: Mix proportions and properties of fresh and hardened mortar specimens: CEM I 52,5 R (Cimpor-Alhandra) + V3005

Mix number	Ref.	w_c	w_f	w_{wc}	w_{Sp}	w_{sd}	Testing date	Dflow (mm)	Tfunnel (s)	fc,28 (MPa)
		(kg/m^3)								
1	C1	611,1	294,5	246,4	7,92	1157,4	07-06-2006	272	6,64	67,50
2	C2	611,1	294,5	246,4	7,92	1157,4	08-06-2006	274	6,9	79,57
3	C3	611,1	294,5	246,4	7,92	1157,4	09-06-2006	277	6,1	71,47
4	C4	611,1	294,5	246,4	7,92	1157,4	12-06-2006	269	6,3	77,50
5	F1	676,5	325,9	238,6	7,52	1093,1	07-06-2006	178	15,9	81,60
6	F2	778,2	141,5	274,7	6,90	1093,1	09-06-2006	230	6,2	80,86
7	F3	526,1	456,5	238,7	7,37	1093,1	08-06-2006	258	7,3	70,56
8	F4	605,3	291,6	274,8	6,73	1093,1	12-06-2006	295	3,0	76,63
9	F5	676,5	325,9	236,7	10,02	1093,1	09-06-2006	254	10,6	76,95
10	F6	778,2	141,5	272,9	9,20	1093,1	08-06-2006	279	5,1	82,34
11	F7	526,1	456,5	236,9	9,83	1093,1	12-06-2006	329	6,4	76,01
12	F8	605,3	291,6	273,1	8,97	1093,1	07-06-2006	350	2,3	73,68
13	F9	617,6	297,6	219,4	6,86	1221,7	07-06-2006	143	28,4	82,37
14	F10	710,5	129,2	252,3	6,30	1221,7	12-06-2006	190	8,9	77,10
15	F11	480,4	416,8	219,5	6,73	1221,7	08-06-2006	216	12,0	73,56
16	F12	552,6	266,3	252,4	6,14	1221,7	09-06-2006	258	5,1	66,10
17	F13	617,6	297,6	217,7	9,15	1221,7	08-06-2006	2178	14,9	85,95
18	F14	710,5	129,2	250,7	8,40	1221,7	12-06-2006	253	6,7	77,08
19	F15	480,4	416,8	217,8	8,97	1221,7	08-06-2006	303	9,3	78,44
20	F16	552,6	266,3	250,9	8,19	1221,7	08-06-2006	332	3,8	74,49
21	CC1	687,5	145,6	277,4	7,29	1157,4	07-06-2006	296	3,0	71,10
22	CC2	515,6	480,5	207,6	8,72	1157,4	12-06-2006	187	21,1	81,39
23	CC3	488,9	400,6	246,5	7,78	1157,4	08-06-2006	327	4,2	67,95
24	CC4	814,8	117,6	246,2	8,16	1157,4	09-06-2006	169	16,8	84,50
25	CC5	611,1	294,5	244,7	10,19	1157,4	08-06-2006	318	5,5	77,03
26	CC6	611,1	294,5	248,1	5,66	1157,4	09-06-2006	196	9,5	77,64
27	CC7	555,6	267,7	225,6	7,20	1286,0	12-06-2006	230	10,2	81,14
28	CC8	666,7	321,2	267,2	8,64	1028,8	08-06-2006	301	4,8	80,19

Table E.11.: Properties of mortars and corresponding pastes incorporating CEM I 52,5 R (Cimpor-Alhandra) from different deliveries

Mix / cement delivery	Dflow[a] (mm)	Tfunnel[a] (s)	fc,28[a] (MPa)	Dflow[b] (mm)	Tflow[b] (s)	fc,28[b] (MPa)	PD[b]	w_{free}[b] (kg/m^3)	σ_0[b] (Pa)	η_{pl}[b] (Pa.s)	Temp. initial[b] (°C)	Time acceler.[b] (h)	Time peak[b] (h)	Temp. peak[b] (°C)
A/1st	255	9,4	67,64	–	–	–	–	–	–	–	–	–	–	–
A/2nd	237	10,9	72,42	144	43,6	80,27	0,650	66,58	1,218	0,545	22,8	6,4	12,3	37,1
A/3rd	259	9,4	71,49	160	36,7	88,14	0,653	71,56	0,577	0,357	23,0	6,6	12,7	37,5
A/4th	246	10,0	70,11	143	37,9	83,59	0,653	71,67	1,833	0,567	23,3	6,8	12,4	38,6
A/5th	262	8,9	68,68	160	36,6	88,44	0,654	72,50	0,643	0,410	23,3	6,5	12,4	36,8
A/6th	254	9,7	76,01	148	36,6	73,83	0,653	71,42	1,120	0,508	25,6	6,1	11,8	38,4
A/7th	242	10,2	59,08	146	35,2	73,88	0,652	70,42	1,297	0,564	27,2	5,9	11,0	38,7
A/8th	240	11,1	69,38	148	59,4	77,15	0,645	60,42	0,889	0,614	24,9	5,6	11,4	37,9
B/1st	250	10,3	71,37	–	–	–	–	–	–	–	–	–	–	–
B/2nd	240	10,3	74,41	140	54,2	86,40	0,651	62,33	1,278	0,626	22,5	7,3	12,9	37,7
B/3rd	261	9,1	75,28	154	39,6	88,55	0,656	70,00	0,649	0,399	23,0	7,6	12,8	38,2
B/4th	252	9,4	73,62	140	44,4	88,55	0,655	68,83	2,185	0,639	23,3	7,0	12,5	39,3
B/5th	267	8,8	74,36	153	44,0	87,63	0,656	69,92	0,698	0,461	23,0	7,3	13,0	37,6
B/6th	260	9,0	69,97	143	42,7	80,32	0,655	68,50	1,227	0,568	25,1	6,8	12,2	38,3
B/7th	247	9,3	66,18	140	41,6	73,37	0,655	67,75	1,520	0,625	27,4	6,0	11,5	39,3
B/8th	252	10,0	75,83	144	67,9	82,36	0,649	59,08	1,000	0,679	24,9	6,1	11,6	39,2
C/1st	251	10,0	73,40	–	–	–	–	–	–	–	–	–	–	–
C/2nd	246	10,3	85,52	136	66,1	86,20	0,655	57,67	1,486	0,694	22,5	7,3	12,8	38,14
C/3rd	273	8,1	80,68	152	48,7	93,09	0,659	64,00	0,685	0,424	23,0	7,6	13,0	37,71
C/4th	252	9,7	74,19	132	62,4	87,27	0,659	63,58	2,450	0,734	23,3	7,2	12,8	39,51
C/5th	266	9,0	73,34	148	54,1	88,70	0,659	63,92	0,851	0,511	23,0	7,3	13,4	37,45
C/6th	262	8,6	77,72	140	60,1	83,03	0,657	61,83	1,186	0,664	25,1	7,4	13,0	38,05
C/7th	246	9,5	75,50	133	72,7	80,01	0,655	58,83	1,376	0,761	27,4	6,7	12,3	39,33
C/8th	255	10,1	71,14	138	84,2	84,05	0,652	54,17	1,027	0,662	24,9	6,2	11,9	38,29

[a]mortar test results; [b]paste test results; Mix A: w/c=0,45; Sp/p=1,90%; V_w/V_p=0,724;V_s/V_m=0,50;
Mix B: w/c=0,43; Sp/p=1,99%; V_w/V_p=0,716 ;V_s/V_m=0,49; Mix C: w/c=0,41; Sp/p=2,05%; V_w/V_p=0,700;V_s/V_m=0,47

Table E.12.: Properties of mortars and corresponding pastes incorporating CEM I 42,5 R (Cimpor-Alhandra) from different deliveries

Mix / cement delivery	Dflow[a] (mm)	Tfunnel[a] (s)	fc,28[a] (MPa)	Dflow[b] (mm)	Tflow[b] (s)	fc,28[b] (MPa)	PD[b]	$w_{free}{}^{b}$ (kg/m^3)	$\sigma_0{}^{b}$ (Pa)	$\eta_{pl}{}^{b}$ (Pa.s)	Temp. initial[b] (°C)	Time acceler.[b] (h)	Time peak[b] (h)	Temp. peak[b] (°C)
A/1st	248	10,3	64,41	–	–	–	–	–	–	–	–	–	–	–
A/2nd	262	9,5	63,55	164	19,9	71,89	0,655	81,00	0,478	0,334	21,5	7,4	14,7	31,7
A/3rd	278	8,2	58,84	182	19,1	70,41	0,656	81,58	0,310	0,333	23,1	7,4	14,2	33,0
A/4th	275	8,7	56,68	166	22,1	65,20	0,655	81,08	0,567	0,360	23,1	6,5	13,2	33,4
A/5th	256	8,9	59,52	162	20,8	65,81	0,656	82,25	0,653	0,386	25,6	7,1	13,3	33,7
A/6th	264	8,6	56,77	163	21,7	71,58	0,656	82,50	0,598	0,383	22,7	6,8	13,2	33,8
A/7th	270	8,3	54,21	168	18,4	59,47	0,657	83,42	0,293	0,329	26,7	6,7	12,9	34,3
A/8th	265	9,1	51,13	170	21,7	63,05	0,655	80,67	0,510	0,344	24,5	6,7	13,3	33,0
B/1st	258	9,6	72,48	–	–	–	–	–	–	–	–	–	–	–
B/2nd	265	9,7	68,60	150	40,4	79,60	0,657	69,67	0,895	0,553	21,5	8,8	16,3	33,3
B/3rd	284	7,5	69,62	157	34,5	78,53	0,658	71,92	0,691	0,526	23,1	9,2	15,4	34,9
B/4th	273	8,1	71,46	150	38,1	71,63	0,657	69,67	0,928	0,545	22,9	8,0	13,8	35,1
B/5th	264	8,1	64,74	145	39,1	73,73	0,657	70,50	1,034	0,603	25,1	8,4	14,4	34,9
B/6th	275	7,8	63,31	150	40,4	73,22	0,657	70,50	0,877	0,586	23,1	7,8	14,4	35,6
B/7th	282	6,9	59,20	155	33,8	65,04	0,660	73,83	0,545	0,509	26,3	8,2	14,4	35,5
B/8th	280	7,6	62,53	144	36,0	69,90	0,657	70,75	0,978	0,548	24,2	7,3	14,2	34,6
C/1st	254	10,1	74,10	–	–	–	–	–	–	–	–	–	–	–
C/2nd	267	9,1	70,95	142	48,1	81,19	0,657	66,11	1,168	0,592	21,5	8,8	16,3	33,32
C/3rd	294	7,3	70,36	154	40,5	81,03	0,658	67,89	0,718	0,560	23,1	9,2	15,7	34,66
C/4th	273	8,3	70,03	146	51,8	77,87	0,657	66,11	1,055	0,619	22,8	8,0	14,2	36,23
C/5th	266	7,4	67,03	134	57,0	77,71	0,656	64,42	1,222	0,624	25,1	8,4	14,6	36,47
C/6th	278	7,7	64,06	147	50,3	83,54	0,657	66,11	0,958	0,642	24,2	8,1	15,0	35,58
C/7th	278	7,3	61,30	153	42,8	67,04	0,659	69,44	0,589	0,561	26,3	8,4	14,9	35,92
C/8th	270	8,0	67,24	139	56,4	72,91	0,657	66,11	1,023	0,612	23,9	7,8	14,8	34,08

[a]mortar test results; [b]paste test results; Mix A: w/c=0,45; Sp/p=1,72%; V_w/V_p=0,728;V_s/V_m=0,50;
Mix B: w/c=0,38; Sp/p=1,86%; V_w/V_p=0,710 ;V_s/V_m=0,45; Mix C: w/c=0,36; Sp/p=1,89%; V_w/V_p=0,704;V_s/V_m=0,43

Table E.13.: Properties of mortars and corresponding pastes incorporating CEM II/A-L 42,5 R (Cimpor-Alhandra) from different deliveries

Mix / cement delivery	Dflow[a] (mm)	Tfunnel[a] (s)	fc,28[a] (MPa)	Dflow[b] (mm)	Tflow[b] (s)	fc,28[b] (MPa)	PD[b]	w_{free}[b] (kg/m^3)	σ_0[b] (Pa)	η_{pl}[b] (Pa.s)	Temp. initial[b] (°C)	Time acceler.[b] (h)	Time peak[b] (h)	Temp. peak[b] (°C)
A/1st	255	8,6	60,50	–	–	–	–	–	–	–	–	–	–	–
A/2nd	259	9,2	59,74	159	22,8	73,78	0,657	81,50	0,532	0,269	21,3	6,4	13,0	32,8
A/3rd	260	8,8	61,01	158	24,3	63,00	0,654	77,33	0,703	0,352	22,2	6,4	14,0	30,7
A/4th	235	9,6	59,06	148	24,9	61,98	0,653	75,25	0,728	0,224	23,6	5,3	11,2	33,5
A/5th	262	8,6	56,97	166	24,4	69,33	0,656	79,50	0,516	0,281	23,7	5,9	12,8	32,8
A/6th	254	8,7	51,48	158	22,0	61,57	0,657	81,75	0,873	0,409	25,6	5,8	13,4	31,6
A/7th	257	8,5	58,32	157	21,7	63,31	0,656	80,42	0,982	0,413	25,1	5,4	12,0	33,9
A/8th	251	9,9	61,11	154	32,7	63,61	0,650	71,75	1,133	0,497	25,2	5,0	11,5	33,8
B/1st	258	8,6	65,15	–	–	–	–	–	–	–	–	–	–	–
B/2nd	264	7,8	69,64	148	34,7	83,03	0,656	71,67	0,846	0,458	21,9	7,6	14,2	35,2
B/3rd	269	7,4	67,79	148	39,4	77,30	0,655	69,25	1,246	0,545	22,0	7,6	15,0	32,6
B/4th	244	8,4	60,91	138	46,0	73,01	0,654	68,17	0,737	0,401	23,3	7,1	12,8	35,4
B/5th	275	7,9	70,09	151	40,0	79,04	0,656	71,08	0,703	0,451	23,5	6,9	13,9	36,0
B/6th	260	7,2	65,92	142	43,1	73,68	0,655	69,75	1,057	0,583	25,4	7,4	15,1	33,2
B/7th	267	7,3	64,13	141	44,9	75,41	0,655	69,58	1,293	0,613	24,9	6,6	13,4	36,7
B/8th	262	8,0	65,48	140	62,5	73,73	0,650	62,17	1,125	0,685	25,2	6,3	13,2	35,9
C/1st	256	8,6	69,12	–	–	–	–	–	–	–	–	–	–	–
C/2nd	266	7,9	71,18	134	62,9	87,88	0,655	63,33	1,315	0,606	22,1	7,6	14,5	36,19
C/3rd	260	7,6	70,92	128	64,5	82,87	0,656	64,75	1,813	0,672	22,4	7,7	15,0	34,71
C/4th	238	8,3	71,42	127	76,2	78,68	0,652	59,25	1,142	0,505	23,5	7,1	13,0	37,10
C/5th	272	7,1	76,41	137	67,7	85,38	0,654	62,92	0,982	0,568	23,5	7,4	14,6	36,52
C/6th	259	7,1	65,88	134	64,7	78,38	0,654	62,67	1,437	0,697	25,4	7,6	15,2	34,85
C/7th	256	7,3	64,83	140	77,6	81,03	0,653	61,50	1,229	0,652	24,8	7,0	14,0	37,14
C/8th	251	8,3	71,20	125	96,5	82,62	0,649	55,17	1,905	0,780	25,2	6,1	12,7	37,03

[a]mortar test results; [b]paste test results; Mix A: w/c=0,45; Sp/p=1,58%; V_w/V_p=0,719;V_s/V_m=0,50;
Mix B: w/c=0,37; Sp/p=1,83%; V_w/V_p=0,713 ;V_s/V_m=0,45; Mix C: w/c=0,33; Sp/p=1,89%; V_w/V_p=0,705;V_s/V_m=0,40

Table E.14.: Properties of mortars and corresponding pastes incorporating CEM II/B-L 32,5 N (Cimpor-Alhandra) from different deliveries

Mix / cement delivery	Dflow[a] (mm)	Tfunnel[a] (s)	fc,28[a] (MPa)	Dflow[b] (mm)	Tflow[b] (s)	fc,28[b] (MPa)	PD[b]	w_{free}[b] (kg/m^3)	σ_0[b] (Pa)	η_{pl}[b] (Pa.s)	Temp. initial[b] (°C)	Time acceler.[b] (h)	Time peak[b] (h)	Temp. peak[b] (°C)
A/1st	260	10,5	49,78	–	–	–	–	–	–	–	–	–	–	–
A/2nd	290	7,9	45,71	184	19,0	49,61	0,656	85,58	0,157	0,225	21,9	5,9	13,8	23,9
A/3rd	289	6,8	46,98	177	14,8	47,11	0,660	90,75	0,243	0,179	22,9	4,9	14,0	26,0
A/4th	288	6,6	45,90	180	16,2	46,80	0,658	88,67	0,492	0,284	23,1	5,3	15,9	27,0
A/5th	276	7,3	44,55	169	15,4	47,93	0,659	89,33	0,383	0,209	24,5	5,3	15,7	26,5
A/6th	286	6,6	43,12	178	16,4	44,81	0,658	88,50	0,352	0,261	24,4	5,0	11,1	26,1
A/7th	280	7,2	41,84	161	17,3	45,32	0,657	86,67	0,359	0,311	26,7	4,8	10,8	26,3
A/8th	275	10,3	37,09	174	20,4	44,25	0,655	84,08	0,307	0,320	24,5	4,9	11,7	26,5
B/1st	263	8,7	58,14	-	–	–	–	–	–	–	–	–	–	–
B/2nd	292	6,8	53,56	172	24,4	56,41	0,656	79,08	0,235	0,265	21,4	5,9	13,7	24,7
B/3rd	290	5,3	53,87	171	18,3	56,61	0,660	85,50	0,301	0,207	22,6	5,1	14,6	26,3
B/4th	294	5,6	53,76	167	20,5	54,11	0,658	82,83	0,669	0,352	22,9	5,2	15,4	27,7
B/5th	287	5,6	50,98	162	19,8	51,60	0,658	82,17	0,515	0,252	24,5	5,4	15,2	27,1
B/6th	292	5,5	51,34	165	19,2	53,50	0,658	82,67	0,508	0,283	24,0	5,0	11,3	26,4
B/7th	286	5,7	48,09	157	23,9	50,58	0,656	79,75	0,535	0,369	26,2	5,1	10,9	26,5
B/8th	299	5,8	45,92	166	27,2	50,94	0,656	78,83	0,433	0,377	23,6	4,8	11,7	26,6
C/1st	258	8,4	67,17	–	–	–	–	–	–	–	–	–	–	–
C/2nd	289	6,1	62,52	163	31,1	65,71	0,651	73,33	0,354	0,339	21,3	5,2	12,9	25,3
C/3rd	282	5,3	57,96	154	23,8	65,76	0,654	78,25	0,593	0,259	22,9	5,0	13,8	27,8
C/4th	284	5,2	56,92	150	26,5	61,98	0,653	77,00	0,938	0,421	22,9	5,0	14,4	28,9
C/5th	272	5,2	60,68	148	25,1	62,44	0,653	76,83	0,826	0,300	24,5	5,0	14,0	28,5
C/6th	277	5,2	60,34	148	28,9	60,85	0,652	75,33	0,755	0,372	24,0	4,9	11,0	27,7
C/7th	275	5,3	55,28	144	32,4	58,91	0,650	72,75	0,767	0,440	26,2	4,7	10,6	27,4
C/8th	293	5,1	50,69	146	33,9	58,91	0,650	72,67	0,643	0,443	23,5	4,7	11,2	27,7

[a]mortar test results; [b]paste test results; Mix A: w/c=0,45; Sp/p=1,49%; V_w/V_p=0,725;V_s/V_m=0,50;
Mix B: w/c=0,4; Sp/p=1,49%; V_w/V_p=0,714 ;V_s/V_m=0,45; Mix C: w/c=0,35; Sp/p=1,41%; V_w/V_p=0,714;V_s/V_m=0,40

Table E.15.: Mix proportions and properties of fresh and hardened concrete specimens used in the experimental design (BACPOR, Maprel, Rio Maior)

Mix number	Ref.	w_c	w_f	w_{Sp}	w_{wc}	w_{sd1}	w_{sd2}	w_{gd}	Testing date	Dflow (mm)	T50 (s)	Tfunnel (s)	H (mm)	fc,28 (MPa)
		(kg/m^3)												
0	C1	380	193	13,23	165	600	202	810	08-03-05	645	3,0	10,9	320	64,79
0	C2	380	193	13,23	165	600	202	810	09-03-05	665	2,8	10,5	335	62,16
0	C3	380	193	13,23	165	600	202	810	10-03-05	658	2,4	9,3	340	62,01
0	C4	380	193	13,23	165	600	202	810	11-03-05	650	2,7	10,0	337	62,16
1	F1	400	188	12,56	157	534	260	830	08-03-05	525	6,2	21,2	305	62,39
2	F2	382	180	11,99	174	547	266	789	10-03-05	692	1,8	8,2	340	59,70
3	F3	388	212	12,79	160	547	266	789	11-03-05	585	3,6	13,5	325	57,48
4	F4	354	193	11,66	170	534	260	830	11-03-05	650	2,2	8,4	327	57,46
5	F5	410	193	14,94	160	547	266	789	08-03-05	588	5,2	19,9	323	66,77
6	F6	374	176	13,62	170	534	260	830	10-03-05	693	2,1	9,0	338	60,98
7	F7	379	207	14,52	157	534	260	830	09-03-05	590	4,2	16,8	318	62,39
8	F8	362	198	13,87	174	547	266	789	10-03-05	743	1,5	6,9	330	58,86
9	F9	410	193	12,85	160	667	144	789	09-03-05	600	3,5	14,0	325	62,54
10	F10	374	176	11,72	170	652	141	830	14-03-05	660	2,6	7,7	338	58,66
11	F11	379	207	12,49	157	652	141	830	09-03-05	552	6,3	19,1	305	65,80
12	F12	362	198	11,93	174	667	144	789	11-03-05	695	1,8	8,4	340	57,56
13	F13	400	188	14,59	157	652	141	830	14-03-05	610	3,5	15,2	327	66,35
14	F14	382	180	13,94	174	667	144	789	11-03-05	708	1,7	7,4	340	67,34
15	F15	388	212	14,86	160	667	144	789	11-03-05	620	3,5	14,1	330	67,10
16	F16	354	193	13,55	170	652	141	830	14-03-05	748	1,5	6,6	340	57,47

(continues in next page →)

Table E.16.: Mix proportions and properties of fresh and hardened concrete specimens used in the experimental design (BACPOR, Maprel, Rio Maior)

Mix number	Ref.	w_c	w_f	w_{Sp}	w_{wc}	w_{sd1}	w_{sd2}	w_{gd}	Testing date	Dflow (mm)	T50 (s)	Tfunnel (s)	H (mm)	fc,28 (MPa)
		(kg/m^3)												
17	CC1	356	181	12,37	178	600	202	810	11-04-05	750	1,8	6,7	335	52,20
18	CC2	409	207	14,21	151	600	202	810	11-04-05	505	14,4[a]	28,5	305	75,31
19	CC3	360	210	13,16	165	600	202	810	12-04-05	685	2,4	10,2	340	62,01
20	CC4	403	174	13,30	165	600	202	810	12-04-05	640	2,7	11,8	337	65,03
21	CC5	380	193	15,21	165	600	202	810	12-04-05	708	2,5	9,4	340	61,91
22	CC6	380	193	11,24	165	600	202	810	12-04-05	595	4,4	11,8	327	59,81
23	CC7	380	193	13,23	165	719	82	810	11-04-05	640	3,9	10,5	337	66,17
24	CC8	380	193	13,23	165	481	323	810	11-04-05	650	3,1	9,9	337	59,42
25	CC9	371	189	12,92	162	586	198	850	11-04-05	650	2,8	10,9	325	54,09
26	CC10	389	198	13,53	169	614	207	769	11-04-05	650	3,2	10,6	340	59,25

[a] this observation was identified as an outlier

Table E.17.: Mix proportions and properties of fresh and hardened concrete specimens used in the experimental design (POCI/ECM/61649/2004)

Mix		w_c	w_f	w_{wc}	w_{Sp}	w_{sd1}	w_{sd2}	w_{gd}	Testing	Dflow	T50	Tfunnel	H2/H1	fc,28
number	Ref.	(kg/m^3)							date	(mm)	(s)	(s)	(mm)	(MPa)
0	C1	374	260	166	11,10	361	361	808	16-10-2006	730	1,6	10,4	0,81	57,75
0	C2	374	260	166	11,10	361	361	808	18-10-2006	778	1,4	10,3	0,89	54,96
0	C3	374	260	166	11,10	361	361	808	19-10-2006	730	1,2	10,8	0,86	60,11
0	C4	374	260	166	11,10	361	361	808	25-10-2006	715	1,8	10,8	0,88	60,69
0	C5	374	260	166	11,10	361	361	808	16-10-2006	709	1,3	10,4	0,84	55,78
0	C6	374	260	166	11,10	361	361	808	25-10-2006	751	1,6	10,6	0,87	59,54
1	F1	423	170	164	8,89	343	419	885	16-10-2006	510	5,5	28,4	0,00	59,83
2	F2	351	359	175	14,20	322	394	767	23-10-2006	808	1,4	7,4	0,93	53,26
3	F3	458	250	174	10,62	384	314	750	18-10-2006	682	1,8	10,4	0,80	59,29
4	F4	332	275	167	12,13	358	438	750	20-10-2006	782	1,0	7,7	0,88	49,78
5	F5	389	213	149	12,03	335	410	865	23-10-2006	488	∞	35,6	0,00	62,60
6	F6	341	283	173	12,49	295	360	865	16-10-2006	875	1,0	29,6[a]	0,86	53,83
7	F7	292	298	151	8,85	335	410	865	23-10-2006	595	3,7	22,8	0,55	51,18
8	F8	416	227	157	12,86	436	357	750	18-10-2006	590	3,5	20,8	0,63	60,72
9	F9	365	303	185	10,01	315	385	750	20-10-2006	790	1,1	5,2	0,93	47,90
10	F10	310	257	160	8,51	408	334	865	23-10-2006	680	1,4	12,7	0,70	51,02
11	F11	312	319	159	9,46	436	357	750	18-10-2006	700	2,1	13,3	0,86	49,05
12	F12	292	298	149	11,80	408	334	865	23-10-2006	688	2,2	18,7	0,72	53,84
13	F13	428	234	162	13,25	359	294	865	19-10-2006	670	2,2	17,9	0,71	64,02
14	F14	365	303	183	13,35	315	385	750	19-10-2006	870	0,6	4,9	0,88	53,08
15	F15	442	178	169	9,30	436	357	750	23-10-2006	582	5,0	14,0	0,67	68,93[b]

(continues in next page →)

Table E.18.: Mix proportions and properties of fresh and hardened concrete specimens used in the experimental design (POCI/ECM/61649/2004) (cont.)

Mix number	Ref.	w_c	w_f	w_{wc}	w_{Sp}	w_{sd1}	w_{sd2}	w_{gd}	Testing date	Dflow (mm)	T50 (s)	Tfunnel (s)	H2/H1 (mm)	fc,28 (MPa)
		(kg/m^3)												
16	F16	321	328	165	9,74	359	294	865	19-10-2006	722	1,4	10,7	0,88	54,44
17	F17	487	196	182	13,65	315	385	750	20-10-2006	762	1,7	6,6	0,96	60,35
18	F18	428	234	165	9,94	295	360	865	23-10-2006	588	2,0	18,7	0,52	63,97
19	F19	416	227	159	9,65	358	438	750	20-10-2006	448	∞	26,7	0,18	53,15
20	F20	413	166	158	11,60	408	334	865	19-10-2006	605	2,6	18,9	0,54	62,99
21	F21	365	303	182	13,35	384	314	750	24-10-2006	838	0,7	5,0	0,94	52,18
22	F22	455	183	175	9,57	359	294	865	19-10-2006	585	2,5	12,5	0,70	61,84
23	CC1	482	165	166	11,32	361	361	808	24-10-2006	635	1,5	13,0	0,80	63,24
24	CC2	306	320	166	10,95	361	361	808	24-10-2006	795	1,2	8,7	0,90	48,87
25	CC3	374	260	168	8,62	361	361	808	24-10-2006	590	1,8	13,8	0,67	47,80
26	CC4	374	260	164	13,58	361	361	808	24-10-2006	768	1,2	9,3	0,92	57,13
27	CC5	355	298	158	11,44	361	361	808	24-10-2006	730	1,7	12,1	0,82	62,96
28	CC6	391	225	174	10,78	361	361	808	24-10-2006	738	0,7	7,5	0,86	55,31
29	CC7	402	280	178	11,93	325	325	808	25-10-2006	770	0,7	7,0	0,89	53,39
30	CC8	346	241	155	10,26	398	398	808	25-10-2006	590	3,0	19,3	0,63	51,91
31	CC9	374	260	166	11,10	306	419	808	25-10-2006	710	1,4	11,6	0,81	57,68
32	CC10	374	260	166	11,10	417	304	808	25-10-2006	715	1,0	10,5	0,85	56,65
33	CC11	394	274	173	11,68	380	380	717	25-10-2006	772	0,9	8,8	0,90	54,47
34	CC12	354	247	159	10,52	342	342	898	25-10-2006	632	2,4	16,8	0,68	58,04

[a] this observation was excluded from data because this high value of Tfunnel was due to the occurrence of segregation and blocking of aggregates near the exit section of the funnel; [b] this observation was identified as an outlier and excluded from the data used to model fc,28